

Fall 2014

Development of Highly Active Ligands for Copper Catalyzed Atom Transfer Radical Processes

Aman Kaur

Follow this and additional works at: <https://dsc.duq.edu/etd>

Recommended Citation

Kaur, A. (2014). Development of Highly Active Ligands for Copper Catalyzed Atom Transfer Radical Processes (Doctoral dissertation, Duquesne University). Retrieved from <https://dsc.duq.edu/etd/734>

This Immediate Access is brought to you for free and open access by Duquesne Scholarship Collection. It has been accepted for inclusion in Electronic Theses and Dissertations by an authorized administrator of Duquesne Scholarship Collection. For more information, please contact phillips@duq.edu.

DEVELOPMENT OF HIGHLY ACTIVE LIGANDS FOR COPPER CATALYZED ATOM
TRANSFER RADICAL PROCESSES

A Dissertation

Submitted to the Bayer School of Natural and Environmental Sciences

Duquesne University

In partial fulfillment of the requirements for
the degree of Doctor of Philosophy

By

Aman Kaur

Master in Science (Honors School), Panjab University

December 2014

Copyright by

Aman Kaur

2014

DEVELOPMENT OF HIGHLY ACTIVE LIGANDS FOR COPPER CATALYZED ATOM
TRANSFER RADICAL PROCESSES

By

Aman Kaur

Approved November 6th, 2014

Dr. Tomislav Pintauer
Assistant Professor of Chemistry and
Biochemistry
(Committee Chair)

Dr. Ralph Wheeler
Professor of Chemistry and Biochemistry
(Committee Member)

Dr. Jennifer Aitken
Professor of Chemistry and Biochemistry
(Committee Member)

Dr. Rinaldo Poli
Professor, CNRS, LCC (Laboratoire de
Chimie de Coordination)
(External Reviewer)

Dr. Philip Reeder
Dean, Bayer School of Natural and
Environmental Sciences

Dr. Ralph Wheeler
Chair, Professor of Chemistry and
Biochemistry

ABSTRACT

DEVELOPMENT OF HIGHLY ACTIVE LIGANDS FOR COPPER CATALYZED ATOM TRANSFER RADICAL PROCESSES

By

Aman Kaur

December 2014

Dissertation supervised by Dr. Tomislav Pintauer

This dissertation focuses on the ligand design for atom transfer radical processes and direct reduction method. Atom transfer radical processes such as addition (ATRA), polymerization (ATRP) and cyclization (ATRC) are the fundamental organic reactions in which addition of alkyl halide via free radical means results in the formation of monoadducts or polymers. We have designed tris(2-pyridylmethyl)amine based ligands for ATRP, where systematic addition of the electron donating groups on the pyridine rings of TPMA, resulted in formation of three ligands; TPMA^{*1}, TPMA^{*2} and TPMA^{*3}. As indicated by electrochemical studies, a nearly stepwise decrease ($\Delta E \sim 60$ mV) of $E_{1/2}$ values on going from [Cu^{II}(TPMA)Br][Br] to [Cu^{II}(TPMA^{*3})Br][Br], confirming that the presence of electron donating groups increased the reducing ability of the corresponding copper(I) complexes. The complexes were utilized for Activator Regenerated by Electron Transfer (ARGET) ATRP, the preliminary

results indicated that the TPMA^{*2} ligand could have a higher future potential in copper catalyzed ATRP than TPMA^{*1} and TPMA^{*3}.

Secondly, a series of mononuclear mixed ligand copper(II) complexes with deprotonated L-amino acids (aa = glycine, alanine, phenylalanine and proline) and bidentate N-based ligands (NN = 1,10-phenanthroline, 2,2'-bipyridine), [Cu^{II}(aa)(NN)Cl] were originally designed for ATRA. However, these complexes were successfully utilized as precursors for the synthesis of copper(I) cyanide (CuCN) coordination polymers via direct reduction method. This method has provided an efficient alternative to traditionally used solvo- and hydrothermal methods, where [Cu^{II}(aa)(NN)Cl] complexes activated the cyanide functionality of the diazo radical initiator, 2,2'-azobis(2-methylpropionitrile) (AIBN) to synthesize multi-dimensional CuCN polymers. We observed that the dimensionality of the polymers was dependent on the structure of the ligand. One-dimensional (1D) polymers were exclusively formed with the aromatic N-based ligands whereas two- (2D) and three-dimensional (3D) frameworks were synthesized with aliphatic amines. We have observed that the ligand design has successfully regulated the size of the pores along with dimensionality. The work in this dissertation provided a significant contribution in two different fields; homogenous catalysis and material synthesis. With the help of the ligand design, we were able to understand as well as regulate the atom transfer radical processes and direct reduction method.

DEDICATION

Dedicated to my family

ACKNOWLEDGEMENT

With immense gratitude, I would like to acknowledge my mentor, Dr. Tomislav Pintauer. I am very grateful that he accepted me into his lab. I am even more grateful that he shared his primary love for metal chemistry. I have enjoyed all my projects and working with him. I am really thankful for the atmosphere Tom fosters in the lab – fun and at the same time challenging to make us a better scientist. I am glad to have been mentored by him. I am also thankful for the financial support from the Department of Chemistry and Biochemistry at Duquesne University as well as from the National Science Foundation.

Next, I would like to acknowledge my committee members, Dr. Jennifer Aitken, Dr. Ralph Wheeler and Dr. Rinaldo Poli. I appreciate their patience and their interest in my research. Their questions and advice has immensely helped me to think critically of my research and helped me to develop as a scientist. I am extremely thankful for their support especially, Dr. Rinaldo Poli for agreeing to be my external reviewer.

I am extremely grateful to Dr. William Eckenhoff for taking me under his wings during my initial days in laboratory. I have enjoyed our many discussions about my research and many other aspects of our work. I absolutely enjoyed his enthusiasm, which is extremely contagious and I have learnt a lot from him. I had an amazing experience in Pintauer's lab, which is attributed to extremely talented graduate students I have worked with in last few years. I would like to thank Dr. Marielle Balili, Dr. Carolynne Ricardo, Gabby Pros and Mike Novak for keeping the lab's environment very constructive as well as fun.

I had a great opportunity to work with some talented undergraduates, Matthew Wilding, Ashley Biernesser, Sean Noonan, Tom Ribelli, Elizabeth Roeske, Allison Jansto, Evan Perez, Erin Gorse, Jesse Martin and Meghan Wasson. I wish them luck for their future endeavors.

I am also very grateful to the instrumentation staff, Dan Bodnar, Lance Crosby and Ben Lauterbach for troubleshooting and ordering new equipments. I am also thankful to very amicable administrative staff, Amy Stroyne, Heather Costello, Maggie Cowburn and Michele Janosko for assisting and managing all the paper work.

As per my personal acknowledgements, I would like to thank my good friends that I have made here in Pittsburgh: Dr. Tushar Gupta, Tushar Koshaley, Nagi, Victor, Kim, Chelsea, Carol, Riyaz, Divay, Vishwas Pathak, Shikha and Seema. I am very grateful to have these friends along my side, otherwise I may not have been able to accomplish this goal. I appreciate their support and understanding.

Finally, I would like to thank my family for their unwavering support and patience especially my mother. She is constant source of inspiration and energy and is a pillar of my strength. My dad always wanted me to get good education and become an independent woman. I think along with me, he has also accomplished his goal. Thank you Mom and Dad for all the love and support! Last but not the least, I would like to thank my brother and his beautiful family. I must remark my brother for pushing me to pursue my education in the United States. I want to thank my niece, Itratt and my nephew, Shahbaaz for giving me the reason to smile and cherish every single day.

TABLE OF CONTENTS

	Page
Abstract.....	iv
Dedication.....	vi
Acknowledgement.....	vii
List of Tables.....	xii
List of Figures.....	xviii
List of Abbreviations.....	xxix
Chapter 1.....	1
1.1. Introduction.....	1
1.2. History and Background.....	2
1.3. Aspects of Atom Transfer Radical Processes.....	23
1.4. Structural Features of Tetradentate N-based ligands in copper catalyzed ATRA.....	31
1.5. Application.....	47
1.6. Conclusion.....	52
Chapter 2.....	72
2.1. Introduction and Background.....	73
2.2. Results and Discussion.....	78
2.3. Conclusions.....	102
2.4. Experimental Section.....	104
Chapter 3.....	118
3.1. Introduction.....	118

3.2. Background.....	120
3.3. One Dimensional Copper Cyanide (CuCN) Coordination Polymer.....	124
3.4. Two- and Three- Dimensional Copper Cyanide Coordination Polymer.....	131
3.5. Copper based Mixed Metal-Cyanide Coordination Polymer.....	137
3.6. Synthesis of Copper Cyanide Polymers.....	140
3.7. Characterization of Copper Cyanide Polymer.....	154
3.8. Properties of Copper Cyanide Polymers.....	158
3.9. Conclusion.....	162
Chapter 4.....	168
4.1. Introduction and Background.....	168
4.2. Results and Discussion.....	172
4.3. Conclusions.....	180
4.4. Experimental Section.....	180
Chapter 5.....	196
5.1. Introduction and Background.....	196
5.2. Results and Discussion.....	204
5.3 Role of ligand on dimensionality and pore size in CuCN polymer.....	219
5.3. Conclusions.....	211
5.4. Experimental Section.....	212
Chapter 6.....	219
6.1. Introduction and Background.....	220

6.2. Results and Discussion.....	225
6.3. Conclusions.....	240
6.4. Experimental Section.....	241
Appendix A.....	249
Appendix B.....	265
Appendix C.....	281
Appendix D.....	307

LIST OF TABLES

	Page
Table 1.2.1. ATRA of polyhalogenated alkanes to alkenes at 60 °C in the presence of AIBN.....	12
Table 1.2.2. Propagation rate constants ($M^{-1} s^{-1}$) of free radical polymerization.....	16
Table 1.2.3. Photoinitiated copper catalyzed ATRA of CCl_4 and CBr_4 to active alkenes at ambient temperature in the presence of AIBN.....	17
Table 1.2.4. ATRA of CBr_4 to alkenes at 60 °C in the presence of V-70.....	18
Table 1.2.5. ATRA of CBr_4 to alkenes at 60 °C in the presence of Ascorbic acid.....	20
Table 1.2.6. ATRC of bromoacetamides catalyzed by copper complexes with TPMA in the presence of AIBN as reducing agent.....	22
Table 1.3.1. Chain Transfer Constants for CCl_4 in free-radical polymerization at 60 °C.....	25
Table 1.3.2. Electrode potential and activation rate constant of different tridentate nitrogen based ligands utilized in copper catalyzed ATRP.....	29
Table 1.4.1. ATRA of CCl_4 to various alkenes with $[Cu^{II}(Me_6TREN)Cl][Cl]$ in the presence of AIBN as reducing agent.....	35
Table 1.4.2. ATRA of CCl_4 to alkenes with $[Cu^{II}(TDAPA)Cl][Y]$ ($Y = Cl^-, BF_4^-, BPH_4^-$) in the presence of AIBN as reducing agent.....	38
Table 1.4.3. Selected bond lengths [\AA] and angles [$^\circ$] for Cu(II) complexes with TPMA.....	43

Table 1.4.4. Selected bond distances (\AA) and angles ($^\circ$) for complexes $[\text{Cu}^{\text{II}}(\text{Me}_6\text{TREN})\text{Cl}][\text{Cl}]$ and $[\text{Cu}^{\text{II}}(\text{Me}_6\text{TREN})\text{Br}][\text{Br}]$	44
Table 1.5.1. ATRA reaction of p-nitrobenzyl bromide and styrene.....	49
Table 1.5.2. Utilization of monoadduct for the synthesis of tetrahydroquinoline.....	49
Table 2.2.1. Structural Comparison of Copper(I) Complexes with Substituted TPMA Ligands.....	80
Table 2.2.2. Structural Comparison of Copper(II) Complexes with Substituted TPMA Ligands.....	90
Table 2.2.3. Summary of λ_{max} and ϵ_{max} Values in Acetonitrile for $\text{Cu}^{\text{II}}\text{Br}_2$ Complexes with TPMA, TPMA ^{*1} , TPMA ^{*2} and TPMA ^{*3} Ligands.....	94
Table 2.2.4. Cyclic Voltammetry Data for Copper Complexes with TPMA Based Ligands in Acetonitrile.....	96
Table 2.2.5. Stability Constants for Copper Triflate Complexes with TPMA Based Ligands in Dimethylformamide at 25 $^\circ\text{C}$	100
Table 2.2.6. Polymerization Results for ARGET ATRP of <i>n</i> -Butyl Acrylate Catalyzed by 10 ppm of Copper Complexes with TPMA Based Ligands.....	102
Table 3.6.1: Synthesis of 1D coordination polymer under different conditions.....	141
Table 3.6.2. List of hydrothermal reactions using different cyanide sources.....	144
Table 3.6.3. List of coordination polymer through sulfur transfer method.....	147
Table 3.6.4. List of coordination polymers via direct reduction method.....	150
Table 3.6.5. Reaction conditions for the synthesis of the crystalline coordination polymers through slow diffusion and evaporation.....	153

Table 4.2.1. Experimental data for the synthesis of copper(I)-cyanide frameworks.....	175
Table 5.2.1. Experimental data for the synthesis of copper(I)-cyanide frameworks.....	200
Table 5.3.1. List of the polymers with dimensionality and total void volume.....	211
Table 6.2.1. Structural comparison between glycine complexes ($[\text{Cu}^{\text{II}}(\text{gly})(\text{phen})\text{Cl}]$ and $[\text{Cu}^{\text{II}}(\text{gly})(\text{bpy})\text{Cl}]$) and alanine complexes ($[\text{Cu}^{\text{II}}(\text{ala})(\text{phen})\text{Cl}]$ and $[\text{Cu}^{\text{II}}(\text{ala})(\text{bpy})\text{Cl}]$).....	230
Table 6.2.2. Structural comparison between glycine complexes ($[\text{Cu}^{\text{II}}(\text{pro})(\text{phen})\text{Cl}]$ and $[\text{Cu}^{\text{II}}(\text{pro})(\text{bpy})\text{Cl}]$) and alanine complexes ($[\text{Cu}^{\text{II}}(\text{phe})(\text{phen})\text{Cl}](\mathbf{1,2})$ and $[\text{Cu}^{\text{II}}(\text{phe})(\text{bpy})\text{Cl}]$).....	234
Table 6.2.3. Cyclic voltammetry data for in acetonitrile of $[\text{Cu}^{\text{II}}(\text{aa})(\text{NN})\text{Cl}]$ in DMSO.....	237
Table 6.2.4. Summary of λ_{max} and ϵ_{max} Values in methanol for $[\text{Cu}^{\text{II}}(\text{aa})(\text{NN})\text{Cl}]$ complex.....	239

LIST OF SCHEMES

Page

Scheme 1.2.1. Kharasch addition of halogenated alkane, CX_4 (X= halide, pseudohalide; R= H, alkyl, phenyl etc) to alkene initiated by organic peroxide.....	2
Scheme 1.2.2. Iron catalyzed ATRA of CCl_4 with acrylonitrile.....	3
Scheme 1.2.3. Proposed Catalytic Cycle of TMC ATRA.....	4
Scheme 1.2.4. Proposed catalytic cycle for copper catalyzed ATRC.....	5
Scheme 1.2.5. Proposed mechanism of copper catalyzed ATRP (L_m = ligand; X= Cl, Br).....	6
Scheme 1.2.6. Kharasch Addition of carbon tetrabromide with 1-alkene in the presence of the reducing agent, AIBN.....	11
Scheme 1.2.7. Decomposition of V-70 at room temperature.....	18
Scheme 1.2.8. Proposed mechanism for the reduction of $Cu^{II}LX$ (L= ligand; X = Cl, Br) complex with ascorbic acid.....	20
Scheme 1.2.9. Proposed mechanism for atom transfer radical cascade reaction catalyzed by $[Cu^{II}(TPMA)X][X]$ (X= Cl, Br) in the presence of reducing agent on different dienes.....	23
Scheme 1.4.1. Possible pathways during the activation of R-X via ISET in $[Cu^I(TPMA)Y]$ (Y= Cl, Br).....	35
Scheme 1.5.1. Schematic representation for ATRA of p-nitrobenzyl bromide and styrene.....	48
Scheme 1.5.2. Synthesis of tetrahydroquinolines from the precursors synthesized via ATRA.....	49
Scheme 1.5.3. Synthesis of initiators for the polymerization using copper catalyzed ATRA (1) followed by ATRP (2).....	50

Scheme 1.5.4. Synthetic route for the synthesis of (\pm)tylophorine utilizing ATRA.	51
Scheme 2.1.1. Representation of ATRP Equilibrium.....	74
Scheme 2.1.2. Substituted tris(2-pyridylmethyl)amine ligands investigated in the present study.....	78
Scheme 3.6.1. Decomposition of diaminomalonitrile to generate cyanide ligands.....	145
Scheme 3.6.2: Schematic representation of sulfur transfer from copper(I) thiocyanate to methanol.....	146
Scheme 3.8.1. Schematic representation of fluorescence and phosphorescence, where S = spin quantum number.....	158
Scheme 4.1.1. Bridging modes in metal-cyanide complexes.....	169
Scheme 4.2.1. Copper(II)/amino acid complexes used in the study.....	171
Scheme 4.2.2. Proposed reaction steps leading to the formation of Cu ^I (NN) cyanide coordination frameworks.	174
Scheme 5.1.1 Different metal cyanide binding modes (a) terminal, (b) μ -2, C,N , (c) μ 3-C,N,N and (d). bridging μ 3-C,C,N.	197
Scheme 5.2.1. Different N-based ligands used in the direct reduction method (a) 1,4-dibenzylpiperazine, (b) 1,4-bis(2,2-diphenylmethyl)piperazine, (c) Imidazole, (d) N,N,N',N'-Tetramethylethylene diamine (e) N,N,N',N,N''-Pentamethyldiethylenetriamine and (f) Tris(2-(dimethylamino)ethyl)amine.....	201
Scheme 6.1.1. Schematic representation of copper catalyzed ATRA in the presence of reducing agent, AIBN.....	221

Scheme 6.1.2. Schematic representation of the $[\text{Cu}^{\text{II}}(\text{aa})(\text{NN})\text{Cl}]$ complexes.....222

Scheme 6.1.3. Schematic representation of thermal or photodecomposition of AIBN to 2-cyanoprop-2-yl radicals.....224

Scheme 6.2.1. Schematic representation of CYCLAM and its derivative, where R=H, alkyl and phenyl.....226

LIST OF FIGURES

	Page
Figure 1.2.1. Different transition metals tethered to solid support utilized during ATRA and ATRC.....	8
Figure 1.2.2. Perfluorinated analogues of ligands PMDETA and Me ₆ TREN utilized in ATRC.....	9
Figure 1.2.3. Various reducing agents utilized in atom transfer radical processes.....	10
Figure 1.2.4. Different concentration of catalyst, [Cu ^{II} (TPMA)Br][Br] (a) 0.002, b) 0.01, c) 0.05, d) 0.1, e) 1.0, and f) 10 mol% utilized for the ATRA of 1- hexene. All these catalyst loadings, 100 % conversion and the yield of monoadduct > 93 % was achieved.....	19
Figure 1.3.1. Different alkyl halides utilized in atom transfer radical processes.....	24
Figure 1.3.2. Values of k _a (M ⁻¹ s ⁻¹) for different initiators with Cu ^I X/PMDETA (X = Cl, Br or I) measured in acetonitrile at 35 °C.....	24
Figure 1.3.3. Different alkenes typically utilized in atom transfer radical processes (R = H, alkyl).....	25
Figure 1.3.4. Substituted bipyridines utilized for ATRP.....	28
Figure 1.3.5. The electrode potential (mV vs SCE) of copper complexes with various N-based ligands.....	30
Figure 1.4.1. Tetradentate N-based ligands used for atom transfer radical processes.	
Figure 1.4.2. Variable temperature ¹ H NMR of [Cu ^I (TPMA)Br] in acetone-d ⁶	33
Figure 1.4.3. ¹ H NMR spectra (400 MHz, (CD ₃) ₂ CO) of [Cu ^I (TPMA)Br] at 180K (a), [Cu ^I (TPMA)][ClO ₄] at 298K (b), and [Cu ^I (TPMA)] ₂ [ClO ₄] ₂ at 185K (c).....	34

Figure 1.4.4. Variable temperature ^1H NMR of $[\text{Cu}^{\text{I}}(\text{Me}_6\text{TREN})\text{BPh}_4]$ in acetone- d^637

Figure 1.4.5. Molecular structure of A. $[\text{Cu}^{\text{II}}(\text{TPMA})\text{Br}][\text{Br}]$ (Br is excluded for clarity) B. $[\text{Cu}^{\text{I}}(\text{TPMA})\text{Br}]$. Selected distances [\AA] and angles [$^\circ$]: Cu1-N1 2.040(3), Cu1-N2 2.073(2), Cu1-Br1 2.3836(6), N1-Cu1-N2 80.86(5), N2-Cu1- N2i 117.53(3), N1-Cu1-Br1 180.00(5). Selected distances [\AA] and angles [$^\circ$]: Cu1-N1 2.4397(14), Cu1-N2 2.1024(15), Cu1-N3 2.0753(15), Cu1-N4 2.0709(15), Cu1-Br1 2.5088(3), N4-Cu1-N3 120.51(6), N4-Cu1-N2 112.40(6), N3-Cu1- N2 107.61(6), N4-Cu1-N1 75.37(5), N3-Cu1-N1 74.86(5), N2-Cu1-N1 74.80(5), N1- Cu1-Br1 179.14(3).....39

Figure 1.4.6. Molecular structure of A. $[\text{Cu}^{\text{I}}(\text{TPMA})\text{CH}_3\text{CN}][\text{BPh}_4]$ B. $[\text{Cu}^{\text{I}}(\text{TPMA})\text{PPh}_3][\text{BPh}_4]$ and at 150K, shown with 50% probability displacement ellipsoids. H-atoms and counter anion have been omitted for clarity. Selected distances [\AA] and angles [$^\circ$] for **A** : Cu1-N1 2.4109(10), Cu1-N2 2.1031(10), Cu1-N3 2.1114(11), Cu-N4 2.0624(10), Cu1-N5 1.9914(11), N1-Cu1-N2 74.47(4), N1-Cu1-N3 74.04(4), N1-Cu1-N4 76.08(3), N1-Cu1-N5 175.94(4), N2-Cu1- N3 109.44(4), N2-Cu1-N4 115.97(4), N2-Cu1-N5 104.02(5), N3-Cu1-N4 114.92(4), N3- Cu1-N5 103.19(5), N4-Cu1-N5 107.90(5). **B** Selected distances [\AA] and angles [$^\circ$]: Cu1-N1 2.214(3), Cu1-N2 2.073(3), Cu1-N3 2.114(3), Cu1-P1 2.1853(12), N1-Cu1-N2 80.81(12), N1-Cu1-N3 78.63(13), N2-Cu1-N3 117.13(13), N1-Cu1-P1 141.65(9), P1-Cu1-N2 119.74(10), P1-Cu1-N3 112.79(10) (Ref¹⁵³).....40

Figure 1.4.7. Molecular structure of $[\text{Cu}^{\text{I}}(\text{TPMA})][\text{BPh}_4]$ at 150K, shown with 50% probability displacement ellipsoids. H-atoms and counter anion have been omitted for clarity. Selected distances [\AA] and angles [$^\circ$]: Cu1-N1 2.211(3), Cu1-N2 2.042(4), Cu1- N3 2.037(4), Cu1-N4 2.036(4), Cu1-Cu2 2.8323(12), N1-Cu1-N2 80.73(13), N1-Cu1-N3 82.08(14), N1-Cu1-N4

81.39(14), N2-Cu1-N3 117.83(15), N2-Cu1-N4 117.49(14), N3- Cu1-N4 118.10(15), Cu1-Cu2-N5 177.73(10).....41

Figure 1.4.8. Molecular structure of $[\text{Cu}^{\text{I}}(\text{TPMA})_2][\text{ClO}_4]_2$ (**4**) at 150K, shown with 50% probability displacement ellipsoids. H-atoms, counter anions, and solvent molecules have been omitted for clarity. Selected distances [\AA] and angles [$^\circ$]: Cu1-N1 2.2590(13), Cu1-N2 1.9909(12), Cu1-N3 2.2213(16), Cu1-N4 1.9593(13), N1-Cu1-N2 81.87(5), N1- Cu1-N3 75.63(5), N1-Cu1-N4 123.01(5), N2-Cu1-N3 95.25(5), N2-Cu1-N4 150.49(6), N3-Cu1-N4 105.68(6) (Ref ¹⁵³).....42

Figure 1.4.9. Molecular structure of $[\text{Cu}^{\text{I}}(\text{Me}_6\text{TREN})][\text{BPh}_4]$ H-atoms and BPh_4^- are omitted for clarity. Selected bond distances [\AA] and angles [$^\circ$]: Cu-N1 2.153, Cu-N2 2.106, Cu-N2 2.105 , Cu-N2 2.115 N1-Cu-N2 119.19 N2-Cu-N3 119.191(11) N4-Cu-N2, N1-Cu-N4 180.00(4).....44

Figure 1.4.10. Molecular structure of **A.** $[\text{Cu}^{\text{I}}(\text{Me}_6\text{TREN})\text{PPh}_3][\text{BPh}_4]$ **B.** $[\text{Cu}^{\text{II}}(\text{Me}_6\text{TREN})\text{Br}][\text{Br}]$ collected at 150K shown with 50% probability displacement ellipsoids. H-atoms omitted for clarity. Selected bond distances [\AA] and angles [$^\circ$]: For $[\text{Cu}^{\text{I}}(\text{Me}_6\text{TREN})\text{PPh}_3][\text{BPh}_4]$ Cu1-N1 2.1450(14), Cu1-N2 2.1753(17), Cu1-N3 2.1865(18), Cu1-P1 2.1910(5), N1-Cu1-N2 85.79(6), N1-Cu1-N3 83.87(6), N2- Cu1-N3 113.40(8), N1-Cu1-P1 136.92(4), N2-Cu1-P1 111.80(6), N3-Cu1-P1 119.80(4) For $[\text{Cu}^{\text{II}}(\text{Me}_6\text{TREN})\text{Br}][\text{Br}]$, Cu-N1 2.046(2), Cu-N2 2.1527(13) Cu-Br2.4016(4), N1-Cu-N2 84.81(4) N2-Cu-X 95.19(4) N2-Cu-N2i 119.191(11) N1-Cu-X 180.00(4).....45

Figure 1.4.11. Molecular structure of **A.** $[\text{Cu}^{\text{II}}(\text{TDAPA})\text{Cl}][\text{BF}_4]$ **B.** $[\text{Cu}^{\text{I}}(\text{TDAPA})\text{CH}_3\text{CN}][\text{ClO}_4]$ with H and BF_4 , ClO_4^- atoms omitted for clarity. Selected bond distances for **A** [\AA] and angles [$^\circ$]:

Cu1-N1 22.052, Cu1-N2 2.160, Cu1-N3 2.140, Cu1- N4 2.131, Cu1-Cl1 2.212, N1-Cu1-Cl1 180, N2-Cu1-N3 118.33, N3-Cu1-N4 115.59, N2-Cu1-N4 113.40(9), N3- Cu1-N4 112.57(9), N2-Cu1-N5 121.48. Selected bond distances for **B** [Å] and angles[°]: Cu1-N1 2.372(2), Cu1-N2 2.234(2), Cu1-N3 2.267(3), Cu1- N4 2.206(2), Cu1-N5 1.953(3), N1-Cu1-N2 75.69(8), N1-Cu1-N3 75.03(8), N1-Cu1-N4 75.77(8), N1-Cu1-N5 175.49(11), N2-Cu1-N3 115.86(9), N2-Cu1-N4 113.40(9), N3- Cu1-N4 112.57(9), N2-Cu1-N5 103.09(12), N3-Cu1-N5 101.90(12), N4-Cu1-N5 108.60(11).....47

Figure 2.1.1. Correlations between K_{ATRP} , redox potential ($E_{1/2}$) and stability constants (β^{I} and β^{II}) for copper complexes with neutral nitrogen based ligands commonly used in ATRP. Generally, more reducing copper(I) complexes have higher values for K_{ATRP} and $\beta^{\text{II}}/\beta^{\text{I}}$ ratio, as a result of greater ligand stabilization towards copper(II) oxidation state.....76

Figure 2.2.1. Molecular structures of $\text{Cu}^{\text{I}}(\text{TPMA}^{*1})\text{Br}$ (a), $\text{Cu}^{\text{I}}(\text{TPMA}^{*2})\text{Br}$ (b) and $\text{Cu}^{\text{I}}(\text{TPMA}^{*3})\text{Br}$ (c) shown with 30% probability displacement ellipsoids. H-atoms have been omitted for clarity.....82

Figure 2.2.2. Space filling models (bottom view) of $\text{Cu}^{\text{I}}(\text{TPMA})\text{Br}$ (a) and $\text{Cu}^{\text{I}}(\text{TPMA}^{*3})\text{Br}$ (b) indicating twisting of 4-methoxy-3,5-dimethyl substituted pyridine arms. H-atoms have been omitted for clarity.....84

Figure 2.2.3. Variable temperature ^1H NMR spectra (400 MHz, $(\text{CD}_3)_2\text{CO}$) of $\text{Cu}^{\text{I}}(\text{TPMA}^{*1})\text{Br}$ complex in the aromatic and methylene regions.....85

Figure 2.2.4. Variable temperature ^1H NMR spectra (400 MHz, $(\text{CD}_3)_2\text{CO}$) of $\text{Cu}^{\text{I}}(\text{TPMA}^{*2})\text{Br}$ complex in the aromatic region.....87

Figure 2.2.5. Variable temperature ^1H NMR spectra (400 MHz, $(\text{CD}_3)_2\text{CO}$) of $\text{Cu}^{\text{I}}(\text{TPMA}^{*3})\text{Br}$ complex in the aromatic and methylene regions.....	88
Figure 2.2.6. Molecular structures of $[\text{Cu}^{\text{II}}(\text{TPMA}^{*1})\text{Br}][\text{Br}]$ (a), $[\text{Cu}^{\text{II}}(\text{TPMA}^{*2})\text{Br}][\text{Br}]$ (b) and $[\text{Cu}^{\text{II}}(\text{TPMA}^{*3})\text{Br}][\text{Br}]$ (c) shown with 30% probability displacement ellipsoids. H-atoms and bromide counterion have been omitted for clarity.....	90
Figure 2.2.7. Space filling models (top view) of $[\text{Cu}^{\text{II}}(\text{TPMA})\text{Br}][\text{Br}]$ (a), $[\text{Cu}^{\text{II}}(\text{TPMA}^{*1})\text{Br}][\text{Br}]$ (b), $[\text{Cu}^{\text{II}}(\text{TPMA}^{*2})\text{Br}][\text{Br}]$ (c) and $[\text{Cu}^{\text{II}}(\text{TPMA}^{*3})\text{Br}][\text{Br}]$ (d) indicating twisting of 4-methoxy-3,5-dimethyl substituted pyridine arms. H-atoms and bromide counterion have been omitted for clarity.....	93
Figure 2.2.8 Absorption spectra (Vis/NIR) of $\text{Cu}^{\text{II}}\text{Br}_2$ complexes with TPMA, TPMA^{*1} , TPMA^{*2} and TPMA^{*3} ligands in acetonitrile at ambient temperature ($[\text{Cu}^{\text{II}}]_0=5.0\times 10^{-3}$ M).....	95
Figure 2.2.9. Cyclic voltammograms of $\text{Cu}^{\text{II}}\text{Br}_2$ complexes with TPMA^{*1} , TPMA^{*2} and TPMA^{*3} ligands at 25 °C. All measurements were conducted in acetonitrile with 0.1 M TBAPF ₆ as a supporting electrolyte at a scan rate of 100 mV/s, $[\text{Cu}^{\text{II}}\text{Br}_2]_0:[\text{L}]_0=1:1$, $[\text{Cu}^{\text{II}}\text{Br}_2]_0=1.0$ mM.....	97
Figure 3.1.1. Different dimensionalities found in a coordination polymer: (a). 1D (b). 2D (c). 3D.....	119
Figure 3.1.2. The hydrogen-bonded network formed by the PtII complex.....	119
Figure 3.2.1. Molecular structure of (a) Prussian Blue and (b) Hofmann Clathrate.....	121
Figure 3.2.2. HOMO and LUMO orbitals of cyanide ligands involved in the sigma donation (top) and back bonding with metal (M) orbitals (bottom).....	121

Figure 3.2.3. Different binding modes of (a) cyanide, (b) carbonyl, (c) azide and (d) binding modes of the cyanide with copper metal.....	122
Figure 3.3.1. (a) Zigzag conformation of 1D coordination polymer (b).1D chain of $[\text{Cu}^{\text{I}}(4,4'\text{-dCO}_2\text{Et bpy})_{0.5}(\text{CN})]_n$	123
Figure 3.3.2. Packing of the CuCN chains in (a) $[\text{Cu}^{\text{I}}(4,4\text{-dCO}_2\text{Me-bpy})(\text{CN})]_n$, 1 and (b) $[\text{Cu}^{\text{I}}(4,4'\text{-dCO}_2\text{Et-bpy})_{0.5}(\text{CN})]_n$, 2	124
Figure 3.3.3. Packing structure of $[\text{Cu}^{\text{I}}_2(\text{CN})_2(\text{biquin})]_n$	125
Figure 3.3.4. (a) Zigzag Chain and packing of $[\text{Cu}^{\text{I}}_5(\text{pylpy})_2(\text{CN})_5]_n$ (b); (c) packing of $[\text{Cu}^{\text{I}}_5(\text{bpy})_2(\text{CN})_5]_n$	125
Figure 3.3.5. (a) 1D helical chain (b) π - π stacking of ligands from the adjoining CuCN chains during packing (c) H-bonding between guest molecule, methanol and cyanide incase of $[\text{Cu}^{\text{I}}(\text{phen})(\text{CN})\cdot\text{CH}_3\text{OH}]_n$	128
Figure 3.3.6. (a) Ladder shaped 1D topology, (b) $[\text{Cu}_2(\text{CN})_2(3\text{-PyHBIm})]_n$ and (c) $[\text{Cu}_2(\text{SCN})(\text{tpt})]_n$	130
Figure 3.4.1. The different CuCN conformations found in 2- and 3D copper cyanide networks (a) $[\text{Cu}_2(\text{CN})_3]^-$ (b) $[\text{Cu}_3(\text{CN})_4]^-$ (c) $[\text{Cu}_2(\text{CN})_4]^-$	131
Figure 3.4.2: (a) Linker and nodes in the network $[\text{Cu}_3(\text{CN})_4]^-$ (b) Geometry of square planar and tetrahedral nodes.....	134
Figure 3.4.3. Pillared 3D network of $[\text{Cu}^{\text{I}}_2(\text{CN})_3\cdot 0.5\text{TMEDA-H}_2]_n$ intercalated with positively charged TMEDA ligand.....	135
Figure 3.4.4. 2D coorugated sheets in $[\text{Cu}_3\text{CN}_3(\text{TMEDA})]_n$ representing the interdigitation by Cu center with TMEDA ligand.....	136

Figure 3.4.5. In $[(\text{Cu}(\mu\text{-CN}))_2(\mu\text{-Me}_4\text{-pyz})\text{-dioxane}]_n$, (a) Perpendicular growth of two cyanide chains and non planar ligand molecule (b) Interpenetrable 3D network (pink and purple) with hexagonal and rectangular channels and (c) chains interpenetrated through the helical chain of ligand.....	136
Figure 3.5.1. Lattice structure of (a) $[\text{Cu}(\text{pn})_2][\text{Cu}_3(\text{CN})_4]_n$ and (b) $[\text{Cu}_2(\text{CN})_3](\text{dmen})_n$	137
Figure 3.5.2. Asymmetric unit and 3D network of $[\text{Fe}(3\text{-Clpy})_2][\text{Cu}(3\text{-Clpy})_2(\text{CN})_2]_n$	138
Figure 3.5.3. 3D network and vapochromic behavior shown by $\text{Cu}(\text{DMSO})_2[\text{Au}(\text{CN})_2]_2$	139
Figure 3.6.1: (a) $\pi\text{-}\pi$ stacking in the $[\text{Cu}^{\text{I}}_3(4,4'\text{-dMe-bpy})_2(\text{CN})_3]_n$ (b) Packing diagram of $[\text{Cu}^{\text{I}}_3(4,4'\text{-dMe-bpy})_2(\text{CN})_3]_n$	151
Figure 3.6.2. Different tubes used for the growing the crystals of coordination polymers.....	154
Figure 3.7.1. (a) IR spectrum of $[\text{Cu}^{\text{I}}_2(\text{CN})_3 \cdot 0.5\text{TMEDA-H}_2]_n$ (b) XRPD pattern (calculated = red; black = experimental) of $[\text{Cu}^{\text{I}}_2(\text{phen})_2(\text{CN})_2 \cdot \text{CH}_3\text{OH}]_n$	156
Figure 3.7.2. TGA spectrum of $[\text{Cu}(\text{CN})_3(\text{Bzpip})_2]_n$	157
Figure 3.7.3. Excitation (black) and emission (red) spectra of copper cyanide polymer.....	157
Figure 3.8.2. (a) Excitation and Emission spectra of $[(\text{CuCN})_2(\text{Ph}_2\text{CHPIP})]_n$ (b) Color change at 298 K, 77K and 4K of the $[(\text{CuCN})_2(\text{Ph}_2\text{CHPIP})]_n$ (right to left).....	161
Figure 3.8.3. Reversible luminescence of CuCN adducts at 254nm A: Piperadine, B: N-N-methylpiperadine, C: N-ethylpiperadine, D: N-methylpyrrolidine E: dimethyl-N-cyclohexane F:	

triethylamine G: N-methylmorpholine H: N-methylpiperazine I: N,N'-Dimethylpiperazine) J: pyridine K: 2-methylpyridine L: 3-methylpyridine M: 4-methylpyridine, N: 2-ethylpyridine O: 3-Ethyl Pyridine, P: 4-Ethyl Pyridine, Q: 4-t-butylpyridine.....162

Figure 4.2.1. Molecular structure of $\text{Cu}^{\text{II}}(\text{ala})(\text{phen})\text{Cl}\cdot\text{CH}_3\text{OH}$ at 150 K, shown with 30% probability displacement ellipsoids. H-atoms and solvent molecules have been omitted for clarity. Selected bond distances [\AA] and angles[$^\circ$]: Cu1-O1 1.9258(18), Cu1-N1 2.0082(19), Cu1-N2 2.0260(19), Cu1-N3 2.007(2), Cu1-Cl1 2.5920(6), O1-Cu1-N3 84.10(8), O1-Cu1-N1 91.99(8), N3-Cu1-N1 160.26(9), O1-Cu1-N2 170.13(9), N4 Cu1 N2 99.20(8), N1 Cu1 N2 81.76(8), O1 Cu1 Cl1 95.76(7), N4 Cu1 Cl1 98.02(7), N1 Cu1 Cl1 101.63(6), N2 Cu1 Cl1 92.99(6).....172

Figure 4.2.2. One-dimensional helical chains (a), π - π stacking interactions (3.493(4) \AA) (b) and hydrogen bonding associated with guest MeOH molecules (2.464(4)-2.603(2) \AA) in $[\text{Cu}^{\text{I}}_2(\text{phen})_2(\text{CN})_2\cdot\text{CH}_3\text{OH}]_n$. Orange=Cu, blue=N, black=C, red=oxygen.....173

Figure 4.2.3. FT-IR spectra of $[\text{Cu}^{\text{I}}_2(\text{phen})_2(\text{CN})_2\cdot\text{CH}_3\text{OH}]_n$ synthesized from $\text{Cu}^{\text{II}}(\text{phe})(\text{phen})\text{Cl}$, $\text{Cu}^{\text{II}}(\text{gly})(\text{phen})\text{Cl}$, $\text{Cu}^{\text{II}}(\text{leu})(\text{phen})\text{Cl}$ and $\text{Cu}^{\text{II}}(\text{pro})(\text{phen})\text{Cl}$ complexes at 80 $^\circ$176

Figure 4.2.4. Crystal structures of $[\text{Cu}^{\text{I}}_3(4,4'\text{-dMe-bpy})_2(\text{CN})_3]_n$ (a), $[\text{Cu}^{\text{I}}(4,4'\text{-dCO}_2\text{Et-bpy})_{0.5}(\text{CN})]_n$ (b), $[\text{Cu}^{\text{I}}(4,4'\text{-dCO}_2\text{Me-bpy})(\text{CN})]_n$ (c) and $[\text{Cu}^{\text{I}}_5(\text{pylpy})_2(\text{CN})_5]_n$ (d). Hydrogen atoms have been omitted for clarity. Dark blue=Cu, light blue=N, black=C and red=O.....177

Figure 4.2.5. Three-dimensional framework of $[\text{Cu}^{\text{I}}_2(\text{CN})_3\cdot 0.5\text{TMEDA-H}_2]_n$ viewed along the *a* (a), *b* (b), and *c* (c) axes. Guest TMEDA-H₂ molecules have been removed for clarity. Dark blue=Cu, black=C or N.....179

Figure 5.1.1. The different CuCN conformations found in 2- and 3D copper cyanide networks (a) $[\text{Cu}_2(\text{CN})_3]^-$ (b) $[\text{Cu}_3(\text{CN})_4]^-$ (c) $[\text{Cu}_2(\text{CN})_4]^-$	198
Figure 5.1.2. Pillared 3D network of $[\text{Cu}_2^{\text{I}}(\text{CN})_3 \cdot 0.5\text{TMEDA-H}_2]_n$ intercalated with positively charged TMEDA ligand (blue=Cu; black= C,N and yellow=TMEDA).....	224
Figure 5.2.1 Crystal lattice of intercalated 2D polymer, $[\text{Cu}_4\text{CN}_6(\text{dbzpip-H}_2)]_n$ (blue=Cu; black= C,N and yellow=ligand).....	202
Figure 5.2.2. (a) Orientation of benzyl side groups of ligand. (b) Alternate orientation of the piperazine rings in the (6,3) nets.....	203
Figure 5.2.3. (a) Intercalated bdpmpip in the (6,3) net and (b) crystal packing along <i>c</i> axis in $[\text{Cu}_2\text{CN}_3(\text{bdpmpip-H})]_n$ (blue=Cu; black= C,N and yellow=ligand).....	204
Figure 5.2.4. (a) Intercalated imidazole in (6,3) net (b) and (c) Cuprophilic interactions along <i>a</i> and <i>b</i> axes in $[\text{Cu}_2\text{CN}_3 \cdot (\text{Im-H})]_n$ (blue=Cu; black= C,N and yellow=imidazole, (N=red)).....	206
Figure 5.2.5. Intercalated PMDETA ligand in the CuCN network of $[\text{Cu}_3(\text{CN})_5 \cdot (\text{PMDETA-H}_2)]_n$ (blue=Cu; black= C,N and yellow=PMDETA, (N=red)).....	207
Figure 5.2.6. (a) Pillared layered 3D network (<i>a</i> axis) (b) Biporous (6,4) nets (<i>c</i> axis) of $[\text{Cu}_7\text{CN}_{12} \cdot (\text{Me}_6\text{TREN-H}_3)_2]_n$ (blue=Cu; black= C,N and yellow= Me_6TREN).....	209
Figure 5.3.1. Large void of CuCN network of (a) $[\text{Cu}_2^{\text{I}}(\text{CN})_3 \cdot 0.5\text{TMEDA-H}_2]_n$ (b) $[\text{Cu}_3(\text{CN})_5 \cdot (\text{PMDETA-H}_2)]_n$ and (c) $[\text{Cu}_7\text{CN}_{10} \cdot (\text{Me}_6\text{TREN-H}_3)]_n$ (dark blue=Cu; black= C and light blue=N).....	210

Figure 6.1.1. (a) Synthesis of $[\text{Cu}^{\text{I}}_2(\text{phen})_2(\text{CN})_2 \cdot \text{CH}_3\text{OH}]_n$ under direct reduction reaction conditions. **(b)** Molecular structures of $[\text{Cu}^{\text{I}}_2(\text{phen})_2(\text{CN})_2 \cdot \text{CH}_3\text{OH}]_n$ shown with 30% probability displacement ellipsoids. H-atoms and methanol counterion have been omitted for clarity.....223

Figure 6.2.1. Molecular structures of a) $[\text{Cu}^{\text{II}}(\text{gly})(\text{phen})\text{Cl}]$ and b) $[\text{Cu}^{\text{II}}(\text{gly})(\text{bpy})\text{Cl}]$ shown with 30% probability displacement ellipsoids. H-atoms have been omitted for clarity.....226

Figure 6.2.2. Crystal lattice of $[\text{Cu}^{\text{II}}(\text{ala})(\text{phen})\text{Cl}]$ shown with 30% probability displacement ellipsoids showing π - π stacking and H-bonding intermolecular interactions.....229

Figure 6.2.3. Molecular structures of $[\text{Cu}^{\text{II}}(\text{ala})(\text{bpy})\text{Cl}]$ shown with 30% probability displacement ellipsoids. H-atoms have been omitted for clarity.....231

Figure 6.2.4. Molecular structures of $[\text{Cu}^{\text{II}}(\text{pro})(\text{phen})\text{Cl}]$ and $[\text{Cu}^{\text{II}}(\text{pro})(\text{bpy})\text{Cl}]$ shown with 30% probability displacement ellipsoids. H-atoms have been omitted for clarity.....232

Figure 6.2.5. Molecular structures of (a) $[\text{Cu}^{\text{II}}(\text{phe})(\text{phen})\text{Cl}]$ (b) $[\text{Cu}^{\text{II}}(\text{phe})(\text{bpy})\text{Cl}]$ shown with 30% probability displacement ellipsoids. H-atoms have been omitted for clarity.....233

Figure 6.7.6. Molecular structure of $[\text{Cu}^{\text{II}}(\text{gly})(\text{phen})]$ shown with 30% probability displacement ellipsoids. H-atoms and perchlorate counterion have been omitted for clarity.....236

Figure 6.2.7. Cyclic voltammograms of $[\text{Cu}^{\text{II}}(\text{pro})(\text{phen})\text{Cl}]$ and $[\text{Cu}^{\text{II}}(\text{pro})(\text{bpy})\text{Cl}]$ at 25 °C. All measurements were conducted in DMSO with 0.1 M TBABr vs Fc/Fc⁺ as a supporting electrolyte at a scan rate of 50 mV/s, $[\text{Cu}^{\text{II}}]_0=1.0 \text{ mM}$237

Figure 6.2.8. Absorption spectra of $[\text{Cu}^{\text{II}}(\text{aa})(\text{NN})\text{Cl}]$ complexes in methanol at ambient temperature ($[\text{Cu}^{\text{II}}]_0=5.0 \times 10^{-3} \text{ M}$).....238

LIST OF ABBREVIATIONS

ala	alanine
aa	amino acid
ATRA	atom transfer radical addition
ATRC	atom transfer radical cyclization
ATRP	atom transfer radical polymerization
AIBN	2,2'-azobis(isobutyronitrile)
bpy	2,2'-bipyridine
CP	Coordination polymer
CuCN	Copper cyanide coordination polymer
CBr ₄	carbon tetrabromide
CCl ₄	carbon tetrachloride
CHBr ₃	bromoform
CHCl ₃	chloroform
CH ₃ CN/ACN	acetonitrile
DMCBCy	1,4,8,11-tetraazacyclotetradecane
DMF	dimethylformamide
EtBriB	ethyl-2-bromoisobutyrate
gly	glycine
HMTETA	1,1,4,7,10,10-hexamethyltriethylenetetramine
ICAR	initiators for continuous activator regeneration
Imi	imidazole
ISET	inner sphere electron transfer

Me ₄ CYLAM	1,4,8,11-tetraaza-1,4,8,11-tetramethylcyclotetradecane
MeOH/CH ₃ OH	methanol
Me ₆ TREN	tris[2-(dimethyl)aminoethyl]amine <i>N</i> -alkyl-2-pyridylmethanimine
NAIkPMI	<i>N</i> -alkyl-2- pyridylmethanimine
NMR	nuclear magnetic resonance
OSET	Outer sphere electron sphere
PMDETA	N,N',N'',N''',N''''-pentamethyldiethyltriamine
phen	1,10-phenanthroline
phe	phenylalanine
pro	proline
TDAPA	tris(2-(dimethylamino)phenyl)amine
TEMPO	2,2,6,6-tetramethylpiperidin-1-oxyl
TPMA	tris(2-pyridylmethyl)amine
TPMA ^{*1}	1-(4-methoxy-3,5-dimethylpyridin-2-yl)- <i>N,N</i> -bis(pyridin-2-ylmethyl)methanamine
TPMA ^{*2}	1-(4-methoxy-3,5-dimethylpyridin-2-yl)- <i>N</i> -((4-methoxy-3,5-dimethylpyridin-2-yl)methyl)- <i>N</i> -(pyridin-2-ylmethyl)methanamine
TPMA ^{*3}	tris((4-methoxy-3,5-dimethylpyridin-2-yl)methyl)amine
TMEDA	Tetramethylethylenediamine
Tpx	trispyrazolyl borate
UV-Vis	ultraviolet-visible spectroscopy
V-70	2,2'-azobis(4-methoxy-2,4-dimethylvaleronitrile)

Chapter 1

Copper Catalyzed Atom Transfer Radical Processes

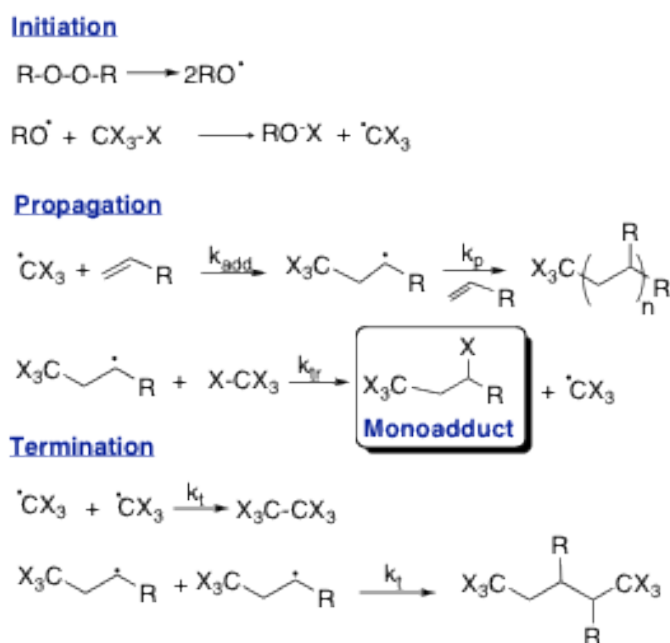
1.1. Introduction

Various radical processes have been successfully catalyzed with a wide variety of transition metal complexes based on copper, ruthenium, iron, or nickel.¹⁻²⁹ Among these metals, copper has been tremendously used as a catalytic candidate due to its ease in attaining different oxidation states (0-2), high binding affinity to the various functional groups, low toxicity, and relative cost. Different nitrogen-based ligands complexed with copper have been successfully used to catalyze atom transfer radical processes such as addition (ATRA), cyclization (ATRC) and polymerization (ATRP).³⁰⁻³⁵ These processes are synthetic tools used for the formation of C-C and C-X (X = halide, pseudohalide) bonds. Through these techniques, synthetically attractive small molecules or polymers with different topologies and functionalities have been tailored. In the past few years, numerous structural, kinetic and mechanistic studies had established the prerequisites for the catalytic candidates for ATRA, ATRC and ATRP, as well as developed a large library of the copper complexes with different ligands. These studies have clearly shown that the ligand design is a major component to tune the reactivity, efficiency and product selectivity for these radical processes. This chapter provides a detailed discussion on the effect of ligand design on the catalysis and the applications of atom transfer radical processes.

1.2. History and Background

In 1937, Kharasch and his coworkers discovered the *peroxide effect* involving the anti-Markovnikov addition of hydrogen bromide (HBr) to unsymmetrical alkenes in the presence of

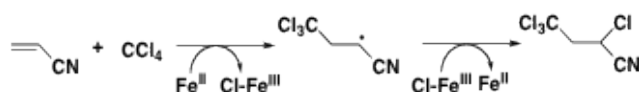
organic peroxide.^{36, 37} The proposed free radical based mechanism involved three major steps, namely initiation, propagation and termination, as outlined in **Scheme 1.2.1**. Following this discovery, various substrates such as hydrocarbons, polyhalogenated alkanes, alcohols, ethers, amines, aldehydes, ketones, aliphatic acids, esters and compounds of sulfur, phosphorus, silicon, tin and germanium have been activated to add across the double bond of alkenes in a similar fashion.^{8, 38-42}



Scheme 1.2.1. Kharasch addition of halogenated alkane, CX_4 ($X =$ halide, pseudohalide; $R =$ H, alkyl, phenyl etc) to alkene initiated by organic peroxide.

This process mediated in the presence of a radical initiator or light is now widely known as atom transfer radical addition (ATRA) or Kharasch addition. High yields were obtained with α -olefins (1-hexene, 1-octene and 1-decene) in comparison to the highly active alkenes such as styrenes, acrylates, vinyl acetate.^{42, 43} The solution to this problem was discovered accidentally by Minisci and his coworkers while attempting to polymerize acrylonitrile with carbon tetrachloride

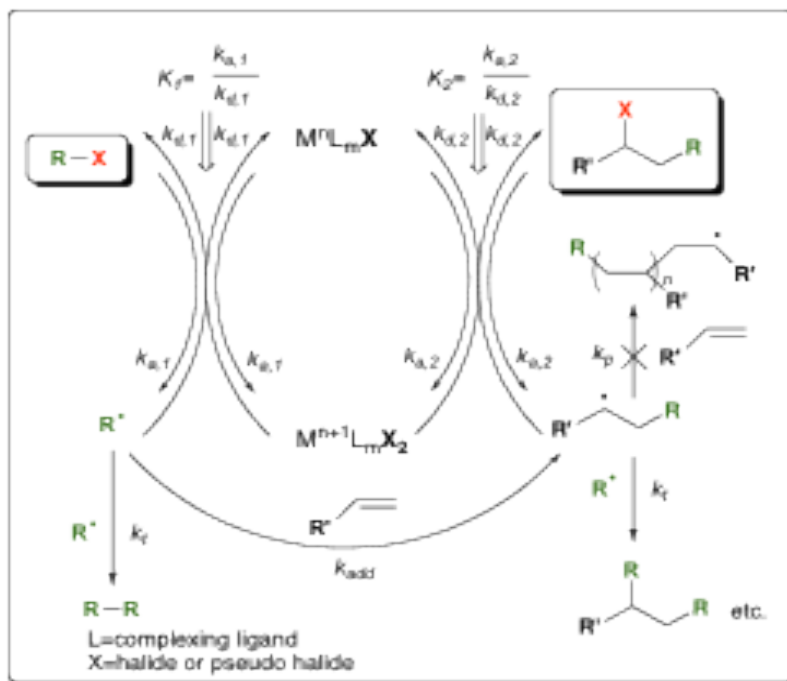
(CCl₄) in chloroform (CHCl₃) as the solvent using steel autoclave.⁴⁴ Surprisingly, higher yields of the monoadduct were obtained instead of polymers. The formation of the monoadduct was highly unexpected due to the high propagation rate constant (k_p) of acrylonitrile and low chain transfer constants (k_{tr}) of CCl₄ and CHCl₃, which favored the polymerization process. In 1961, it was concluded that the iron(III) chloride (FeCl₃), generated from the corrosion of the steel autoclave, acted as an efficient halogen transfer agent (**Scheme 1.2.2**).⁴⁵ This reaction marked the beginning of transition metal catalyzed (TMC) ATRA.⁴⁵⁻⁴⁸



Scheme 1.2.2. Iron catalyzed ATRA of CCl₄ with acrylonitrile.

After this discovery, different transition metals such as copper (Cu),^{1, 49-51} iron (Fe),¹⁸ ruthenium (Ru)⁵²⁻⁶² and nickel (Ni)^{6, 8, 9} have been used to catalyze these reactions with various alkenes and halogenated alkanes. The accepted mechanism for ATRA involves free radical intermediates (**Scheme 1.2.3**).^{31, 63-65} In this mechanism, the reaction is catalyzed by two different redox active states of the metal, Mt^nL_m and $Mt^{n+1}L_mX$ (Mt = metal; L_m = ligand). The catalytic cycle starts with the homolytic cleavage of the C-X bond of the alkyl halide (R-X) by metal in the lower oxidation state, (Mt^nL_m), acting as an activator. This step is accompanied by the oxidation of the metal center to $Mt^{n+1}L_mX$ and generates an alkyl radical (R[•]). This radical can react via three main pathways: it can add across the double bond of the alkene, terminate via radical-radical termination/coupling or can generate the starting material by abstracting the

halogen from the metal center. When the radical entered the desired pathway that is the addition to the double bond of an alkene, it generates another secondary radical (**Scheme 1.2.3**).



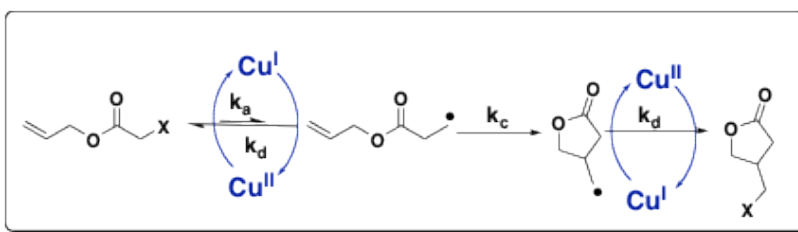
Scheme 1.2.3. Proposed Catalytic Cycle of TMC ATRA.

This secondary radical can further be deactivated by metal in the higher oxidation state, $M^{n+1}L_mX$ acting as a deactivator to form a desired product, monoadduct. The chemoselectivity of the monoadduct is governed by three main guidelines:

1. Rate constant of activation ($k_{a,1}$) should be much lower than the rate constant of deactivation ($k_{d,2}$) in order to keep the radical concentration low to suppress the radical-radical termination reactions.
2. Further activation of monoadduct should be avoided ($k_{a,1} \gg k_{a,2}$, ideally $k_{a,1} = 0$).

3. The rate of deactivation should be larger than the rate of propagation in order to suppress the formation of oligomers or polymers, ($k_{d,2}[\text{Mt}] \gg k_p[\text{alkene}]$).

Intramolecular ATRA or atom transfer radical cyclization (ATRC) is another attractive technique to synthesize cyclized monoadducts.⁶⁵⁻⁶⁸ In this process, bifunctional precursor containing alkene and halogen functionalities is used.⁶⁵⁻⁷⁰ As seen in ATRA (**Scheme 1.2.4**), the activator generates the alkyl radical by activating the C-X (X = halogen) bond, which undergoes cyclization to produce a cyclized radical.

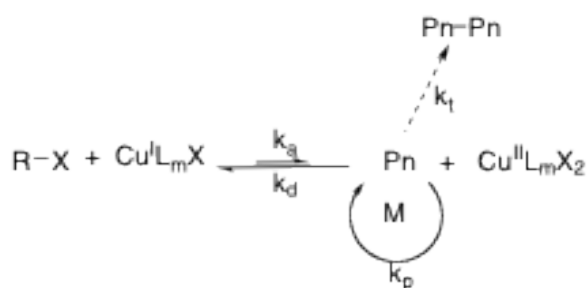


Scheme 1.2.4. Proposed catalytic cycle for copper catalyzed ATRC.

This radical is deactivated by the Cu(II) species in the catalytic cycle to form a cyclized monoadduct. The monoadducts produced via ATRA and ATRC have high commercial value. The halide functionality in these molecules can be easily reduced, eliminated, displaced, converted to a Grignard reagent or used as initiator for polymerization.⁶⁹⁻⁸¹

Another process, atom transfer radical polymerization (ATRP), which was discovered in 1995 simultaneously by the group of Matyjaszewski and Sawamoto.⁸²⁻⁸⁶ This methodology is a very versatile tool to synthesize of the macromolecules with well-defined composition, architecture and functionality. ATRP has been successfully catalyzed by a number of transition metal complexes such as titanium, molybdenum, rhenium, iron, ruthenium, osmium, rhodium,

cobalt, nickel, palladium and copper.^{15, 52, 87-111} Similar to the copper catalyzed ATRA and ATRC, the catalytic step starts with the activation of carbon halogen bond of the alkyl halide, also known as initiator, mediated by the Cu^I metal center, Cu^IL_mX (L_m = ligand; X = halogen, pseudohalide) (**Scheme 1.2.5**). The resulting alkyl radical can initiate the polymerization by successive addition to the double bond of the alkene or terminate by coupling or reversibly deactivated by Cu^{II} complex.^{91, 94, 112, 113}



Scheme 1.2.5. Proposed mechanism of copper catalyzed ATRP (L_m = ligand; X = Cl, Br).

The equilibrium ($K_{ATRP} = k_a/k_d$) between the activation and deactivation favors the deactivation processes, which minimized the radical termination reactions and aids the formation of a polymer with predetermined molecular weight with narrow molecular weight distributions. Copper catalyzed ATRP has been successfully used to synthesize polymers with different architectures such as branched, hyperbranched, dendritic, star- and comb-like polymers.^{88, 95, 98, 99, 106, 110, 111, 114-116}

In atom transfer radical processes, the concentration of deactivator increases with time due to unavoidable and often diffusion controlled radical-radical termination reactions, which results in the lowering of the concentration of the activator species, which slows down the process and decreases the selectivity.^{65, 68, 105, 112, 113, 117} Therefore, 5 to 30 mol-% of metal complex

is required to achieve high selectivity and yield, which makes these processes highly environmentally unfriendly and expensive. Furthermore, the isolation of the product that is contaminated with the metal can be problematic and increases the cost. Various approaches have been proposed to address these challenges and to make these processes highly efficient.

1.2.1. Solid Supported Catalysts

Solid support catalysts have always been economically advantageous for the large-scale synthesis because the catalysts can be easily reused and recovered from the product. Thus, such approach can be very beneficial for ATRA and ATRC systems. However, the application of solid-state catalysis for ATRP can be quite tedious because the diffusion of growing large polymeric chains to the active metal center to get deactivated would be difficult.^{15, 118-126} Different solid supports have been investigated such as cross-linked silica, cross-linked polystyrene and jandajel containing different metal centers like copper, nickel and ruthenium (**Figure 1.2.1**).^{118, 119} In one example, ligand N-propyl-2-pyridyl amine was tethered to silica and complexed to copper chloride (CuCl) and copper bromide (CuBr) salts. This solid support was used to catalyze the ATRC of various 2-haloacetamides with excellent yields (75 to 96%).¹¹⁸

In a similar manner, a copper based catalyst was used to generate nitrogen-based heterocycles in quantitative yields via ATRC.¹¹⁹ Even though high yields were obtained, the catalyst decomposed with each run as observed by a color change from brown Cu(I) to green corresponding to the oxidation to Cu(II).

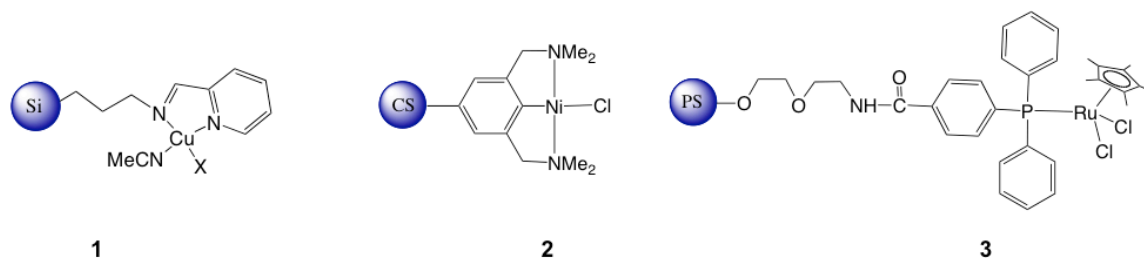


Figure 1.2.1. Different transition metals tethered to solid support utilized during ATRA and ATRC.

1.2.2. Biphasic Systems

In biphasic system, the two immiscible phases are utilized to recover or reuse the catalyst. The metal complexes are generally present in the aqueous phase.^{127, 128} A major limitation to this method is that these reactions are confined to water stable materials. Horvath and Rabai solved the problem by replacing water with the perfluoro solvents, which have very low solubility in the hydrocarbon-based solvents.¹²⁹ In order to increase the solubility of the metal complexes in perfluoro phase, metal centers were complexed to the fluorinated ligands. At higher temperature and pressure, the two phases become miscible and the reaction proceeds under homogenous conditions. On cooling, the phases separate out and the final product as well as the catalyst is recovered. This approach was successfully used for the ATRC of pent-4-enyl trichloroacetates in the presence of copper complex with perfluorinated analogue of ligands, N,N,N',N',N''-pentamethyldiethylenetriamine (PMDETA) and tris[2-(dimethylamino)ethyl]amine (Me₆TREN) (**Figure 1.2.2**) to obtain the product in 34 to 99 % yield.¹³⁰ The catalyst was regenerated and reused 4 times without any significant loss of the activity.

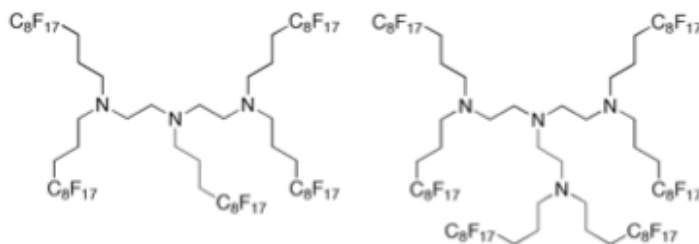


Figure 1.2.2. Perfluorinated analogues of ligands PMDETA and Me₆TREN utilized in ATRC.¹³⁰

1.2.3. Catalyst Regeneration

The catalyst regeneration technique was initially developed for copper catalyzed ATRP, where the activator was continuously regenerated from the deactivator in the catalytic cycle with the help of a reducing agent.¹³¹ Reducing agents such as phenol, glucose, ascorbic acid, hydrazine, tin(II) ethyl hexanoate, magnesium and free radical initiators like 2,2'-azobis(isobutyronitrile) (AIBN) and 2,2'-azobis(4-methoxy-2,4-dimethyl valeronitrile) (V-70) have been successfully used in various atom transfer radical processes, which lowered the metal concentration from 30 mol-% to mere ppm levels (**Figure 1.2.3**).^{18, 31, 50, 51, 105, 115, 132-136}

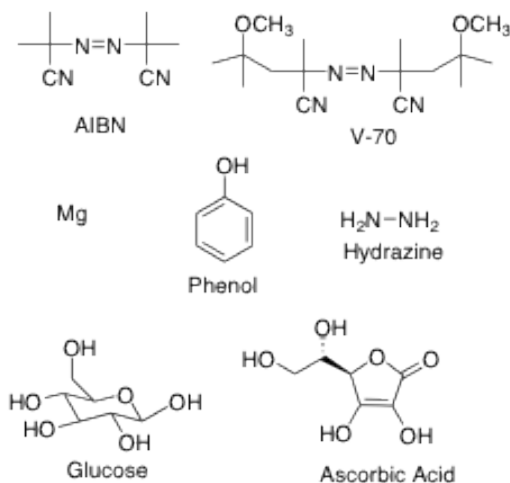
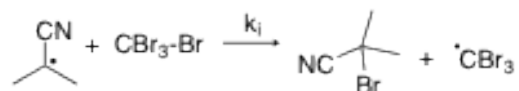
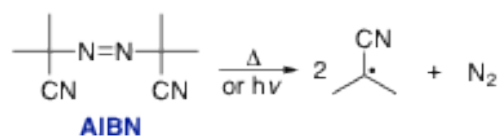


Figure 1.2.3. Various reducing agents utilized in atom transfer radical processes.

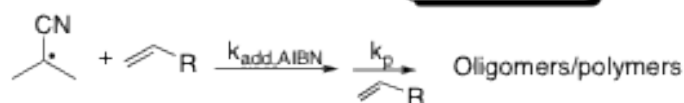
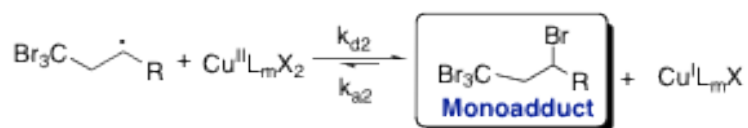
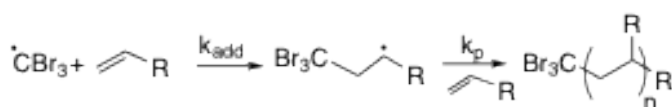
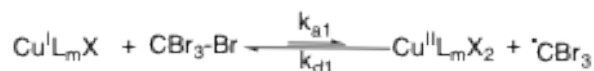
In one of the examples, the diazo-based reducing agent, AIBN was used during copper catalyzed ATRA where the turn-over number (TON) was increased from 0.1 and 10 to 160,000 under similar reaction conditions.⁵¹ This is the highest TON ever achieved in the ATRA reaction. The other main advantage of catalyst regeneration is that the reaction can be started with air- and moisture-stable metal complexes in the higher oxidation state.

In the presence of AIBN, the initiation step involved the slow decomposition of AIBN at higher temperature to give radicals, which reduced the Cu(II) to Cu(I) (**Scheme 1.2.6**). When the reaction was conducted in the absence of the AIBN, only 2 and 3 % conversion (conv) was achieved in case of 1-hexene and 1-octene respectively with CCl_4 with the catalyst, $[\text{Cu}^{\text{II}}(\text{TPMA})\text{Cl}][\text{Cl}]$ (**Table 1.2.1**).⁵⁰ This indicated that the reaction stopped after the activator, $[\text{Cu}^{\text{I}}(\text{TPMA})\text{Cl}]$ was completely converted to the deactivator $[\text{Cu}^{\text{II}}(\text{TPMA})\text{Cl}][\text{Cl}]$ due to unavoidable termination reactions. Similar poor results were obtained in the absence of the catalyst. When the reactions were conducted in the presence of catalyst and reducing agent, dramatic increase in the conv. and yield was observed (**Table 1.2.1**). At catalyst loadings of 0.005 mol-% w.r.t 1-alkene, higher yields of 98% and 87% with 1-hexene and 1-octene were obtained, respectively.

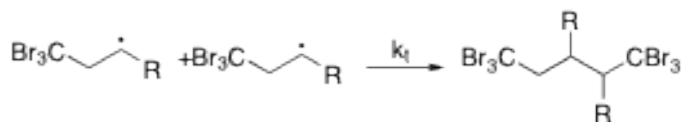
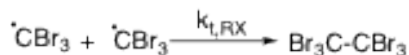
Initiation



Propagation



Termination



Scheme 1.2.6. Kharasch Addition of carbon tetrabromide with 1-alkene in the presence of the reducing agent, AIBN.

The yield decreased to 72% (1-hexene) and 67% (1-octene), when the concentration of the catalyst was halved. Chloroform and bromoform showed low activity in comparison to tetrahalogenated analogues (CCl_4 and CBr_4). This trend was attributed to higher C-X bond dissociation energy in trihalogenated alkanes in comparison to tetrahalogenated alkanes.^{50,51}

For active alkenes, styrene and methyl acrylate (**Table 1.2.1**, Entry **8-18**), high yields of monoadducts were obtained only at highest catalyst loadings. At lower catalyst loadings, these active alkenes were 100% consumed but the yields were significantly decreased. The yield of the monoadduct was lowered due to the side reactions such as oligomerization and polymerization initiated by isopropylcyano radicals generated during the thermal decomposition of AIBN.^{50,51}

Table 1.2.1. ATRA of polyhalogenated alkanes to alkenes at 60 °C in the presence of AIBN.^{50,51}

Entry ^(a)	Alkene	Alkyl Halide	Catalyst Loading	Conv/Yield	TON
1	1-hexene	CHBr ₃	10,000:1	67/61	6.1 x10 ³
		CHCl ₃	1000:1	56/56	560
		CCl ₄	5,000:1	98/98	4900
2			10,000:1	72/72	7200
4	1-octene	CHBr ₃	10,000:1	75/69	6.9 x10 ³
		CCl ₄	5000:1	87/87	4350
			10,000:1	67/67	6700
7	1-decene	CHBr ₃	10,000:1	74/63	6.3 x10 ³
8		CBr ₄	10,000:1	99/95	9.9 x10 ⁴
9			20,000:1	100/95	1.9 x10 ⁵
10	Styrene	CHBr ₃	1,000:1	100/92	9.2 x10 ²
			5,000:1	100/72	3.9 x10 ³
		CCl ₄	250:1	100/85	212
13		CBr ₄	10,000:1	100/94	9.4 x10 ⁴
14			20,000:1	100/82	1.6 x10 ⁵
15	Methyl Acrylate	CHBr ₃	500:1	100/92	3.3 x10 ²
			1,000:1	100/77	5.2 x10 ²
			5,000:1	100/66	1.1 x10 ³
18		CCl ₄	1000:1	100/60	600

^(a)All reactions were performed in CH₃CN at 60 °C for 24 with [R-Br]₀:[alkene]₀: [AIBN]₀=4:1:0.05, catalyst= [Cu^{II}(TPMA)Br][Br]. ^(b)Yield is based on the formation of monoadduct and was determined using ¹H NMR spectroscopy (relative errors are ±10%).

Kinetics of ATRA in the Presence of a Reducing Agent

The use of reducing agent has increased the mechanistic and kinetic complexity of the atom transfer radical processes. In the absence of the reducing agent, rate of alkene consumption is dependent on four different factors and depicted in equation (Eq) 1: ^{64, 137, 138}

- (a) Equilibrium constant ($K_{ATRA} = k_a/k_d$)
- (b) Concentration of the alkyl halide and the alkene
- (c) Rate constant for the alkene addition (k_{add})
- (d) Ratio of concentration of activator to deactivator $[Cu^I L_m X]/[Cu^{II} L_m X_2]$

$$-\frac{d[alkene]}{dt} = \frac{k_{a,1} k_{add} [Cu^I L_m X][RX][alkene]}{k_{d,1} [Cu^{II} L_m X_2]} = \frac{K_{ATRA} k_{add} [Cu^I L_m X][RX][alkene]}{[Cu^{II} L_m X_2]} \quad [1]$$

$$[R^*] = \frac{k_{a,1} [Cu^I L_m X][RX]}{k_{d,1} [Cu^{II} L_m X_2]} \quad [2]$$

The slope of a straight line obtained from the plot of $\ln(alkene)_0/(alkene)_t$ vs time gives the apparent equilibrium constant. The straight line in the plot also indicates the constant concentration of the radicals generated during the reaction (Eq 2). In the presence of a reducing agent such as AIBN, the number of reaction steps increased as outlined below and depicted in

Scheme 1.2.6.

1. Thermal or photodecomposition of AIBN to generate the radicals during initiation step.
2. Regeneration step involving the reduction of the Cu(II) to Cu(I) complex.
3. Free radical polymerization initiated by radicals generated by AIBN.

So, the rate of alkene consumption can be expressed in equation 3:

$$-\frac{d[\text{alkene}]}{dt} = k_{\text{add}}[R^*][\text{alkene}] + k_{\text{add,AIBN}}[I^*][\text{alkene}] + k_p[I-\text{Alk}^*][\text{alkene}] \quad [3]$$

In equation 3, the first term corresponds to the ATRA whereas second and the third term referred to the free radical polymerization initiated by AIBN. The second term can be neglected due to small concentration of radical, $[I^*]$ generated by AIBN. So, the rate of free-radical polymerization can only be expressed with the third term, where $[I-\text{Alk}^*]$ corresponds to the concentration of the radical generated by addition of (I) to alkene (Eq 4).

$$-\frac{d[\text{alkene}]}{dt} = k_{\text{add}}[R^*][\text{alkene}] + k_p[I^*][\text{alkene}] \quad [4]$$

The radical concentration can be easily derived by combining the equilibrium constant, activation and deactivation of the alkyl halide (Eq 5).

$$\begin{aligned} \frac{[Cu^I L_n X][I-X]}{[Cu^{II} L_n X_2][I^*]} &= \frac{k_{d,AIBN}}{k_{a,AIBN}} = \frac{1}{K_{ATRA,AIBN}} \\ \frac{[Cu^{II} L_n X_2][R^*]}{[Cu^I L_n X][R-X]} &= \frac{k_{a,I}}{k_{d,I}} = K_{ATRA,RX} \\ [R^*] &= \frac{K_{ATRA,RX}}{K_{ATRA,AIBN}} \frac{[R-X]}{[I-X]} [I^*] \end{aligned} \quad [5]$$

Applying the steady state approximation under the assumption that the rate of initiation is equal to the rate of termination, the concentration of radical species can be derived (Eq 5). Based on the final equation, we can see that the rate depends on many different factors including concentration of the alkene, alkyl halide, and I-X, equilibrium constants ($K_{ATRA,RX}$, $K_{ATRA,AIBN}$), k_{add} , k_p , decomposition (k_{dc}), and termination (k_t) rate constant.

$$\begin{aligned} \frac{d[I^*]}{dt} &= 2k_{dc}[AIBN] - 2k_t[I^*]^2 = 0 \\ [I^*] &= \sqrt{\frac{k_{dc}}{k_t}[AIBN]} \end{aligned}$$

$$-\frac{d[\text{alkene}]}{dt} = \sqrt{\frac{k_{dc}}{k_t} [\text{AIBN}]} \left(k_{add} \frac{K_{ATRA,RX}}{K_{ATRA,AIBN}} \frac{[R-X]}{[I-X]} + k_p \right) [\text{alkene}]$$

However, the rate of reaction was found to be fully independent of the concentration and nature of the copper complex (Eq 6). The results from different experiments were found to be consistent with the derived rate equation in the presence of a reducing agent (Eq 6). In ICAR (initiator for continuous activator regeneration) ATRP of styrene catalyzed by CuBr₂ complexes with different ligands in presence of AIBN showed that the ratio of $K_{ATRP,RX}/K_{ATRP,AIBN}$ remained constant and was not correlated with the nature or the concentration of the copper complex.¹³¹ Similar trends were obtained during ATRA with CCl₄ and different alkenes such as 1-octene, styrene and methyl acrylate at different catalytic loading of [Cu^{II}(TPMA)Cl][Cl].¹³⁸

The product selectivity is another important aspect, which is found to be dependent on the concentration and the nature of the Cu(II) complex. As stated before, in order to obtain the high yields of monoadduct, the rate of deactivation should be higher than the polymerization ($k_d[\text{Cu}^{\text{II}}] \ll k_p[\text{alkene}]$). Therefore, the active alkenes with high propagation rate constant (k_p) generate monoadduct in good yields under high catalyst loading. The k_p of the alkene is dependent on the temperature and can be regulated by changing the reaction conditions. For instance, the value of the k_p can be decreased to an order of $3.0 \times 10^2 \text{ M}^{-1} \text{ s}^{-1}$ at 25 °C $< k_p > 1.8 \times 10^3 \text{ M}^{-1} \text{ s}^{-1}$ at 60 °C, almost becomes comparable to the rate of deactivation or halogen transfer, $1.8 \times 10^3 \text{ s}^{-1} < k_{d,2}[\text{Cu}^{\text{II}}] > 1.8 \times 10^5 \text{ s}^{-1}$. The k_p values for different monomers are shown in **Table 1.2.2**.¹³⁹ So, the product selectivity can be easily modulated towards the monoadduct over polymer at lower temperatures.

Table 1.2.2. Propagation rate constants ($M^{-1} s^{-1}$) of free radical polymerization.

Alkene	k_p (60 °C)	k_p (25 °C)
Methyl acrylate	2.8×10^4	1.4×10^4
Butyl acrylate	3.1×10^4	1.5×10^4
Vinyl acetate	7.9×10^3	3.4×10^3
Styrene	3.6×10^3	87
Methyl methacrylate	8.2×10^2	3.2×10^2

ATRA of various alkenes and alkyl halides was conducted at ambient temperature in order to control the product selectivity and favors the formation of monoadducts over polymers.¹³³ These reactions were performed in the presence of AIBN, which can photo-initiate upon irradiation with UV light (**Table 3**). The photolysis of AIBN is established to be the first-order with a rate constant of $k = 1.2 \times 10^{-5} s^{-1}$ at 25 °C, which is similar to the thermal decomposition at 60 °C ($1.5 \times 10^{-5} s^{-1}$).^{133, 138} No conversion and monoadduct was obtained in the absence of AIBN or Cu(II) complex.¹³³

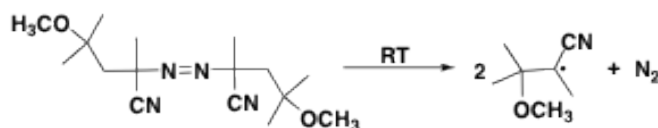
Table 1.2.3. Photoinitiated copper catalyzed ATRA of CCl_4 and CBr_4 to active alkenes at ambient temperature in the presence of AIBN.¹³³

Entry ^(a)	Alkene	Alkyl Halide	Catalyst Loading	Conv/Yield
1			1000:1	100/47 ^(c)
2			100:1	100/100
3		CCl_4	500:1	100/99
4	Methyl acrylate		1000:1	100/85
5			2000:1	100/84
6		CBr_4	500:1	100/100
7			10000:1	100/76
8	Methyl methacrylate	CCl_4	1000:1	100/48 ^(c)
9			100:1	100/100
10			500:1	100/99
11			1000:1	100/91
12		CBr_4	500:1	100/100
13			1000:1	100/73
14	Acrylonitrile	CCl_4	1000:1	99/88 ^(c)
15			100:1	100/98
16			500:1	100/84
17			1000:1	100/75

18			2000:1	96/65
19		CBr ₄	500:1	100/96
20			10000:1	95/87
21	Styrene	CCl ₄	100:1	99/96
22			500:1	50/46
23			1000:1	32/29
24			2000:1	27/22
25		CBr ₄	500:1	77/75
26			10000:1	60/51

^(a)All reactions were performed in CH₃CN in light for 24 h. Reaction temperature was maintained at 23 ± 2° C, [alkene]₀: [AIBN]₀ = 1:0.05, [alkene]₀ = 0.75M, catalyst = [Cu^{II}(TPMA)X][X] (X = Cl, Br). ^(b)Yield is based on the formation of monoadduct and was determined using ¹H NMR spectroscopy (relative errors are ±10%). ^(c)AIBN decomposition by heating at 60 °C.

As seen in **Table 1.2.3**, the yield of monoadduct was dramatically increased for the active alkenes indicating successful deactivation of the secondary radicals. When the reaction was conducted at 60 °C, only 47 (entry **1**) and 48 (entry **8**) % yield was obtained in case of methyl acrylate and methyl methacrylate with CCl₄, respectively. The yield almost doubled up to 85 (methyl acrylate) and 91 (methyl methacrylate) at ambient temperature. Similar significant improvements were observed in case of acrylonitrile whereas styrene did not show any such trend. The poor activity of the styrene can be attributed to the low addition rate constant (k_{add}). Another diazo based reducing agent, V-70, decomposes at room temperature to generate free radicals. (**Scheme 1.2.7**) This reducing agent has also been successfully used for the ATRA, ATRC and cascade reactions with different alkenes (**Table 1.2.4**).



Scheme 1.2.7. Decomposition of V-70 at room temperature.

Table 1.2.4. ATRA of CBr₄ to alkenes at 60 °C in the presence of V-70.³¹

Entry ^(a)	Alkene	Alkyl Halide	Catalyst Loading	% Yield	TON
1	1-hexene	CCl ₄	1000:1	93	930
2			2000:1	80	1600
3		CBr ₄	10000:1	100	4600
4			50000:1	88	17500
5	1-octene	CCl ₄	1000:1	97	970
6			2000:1	84	1680
7		CBr ₄	10000:1	100	4400
8			50000:1	93	18500
9	1-decene	CCl ₄	1000:1	96	960
10			2000:1	85	1750
11		CBr ₄	10000:1	98	3400
12			50000:1	93	14500
13	Styrene	CCl ₄	500:1	51	255
14		CBr ₄	200:1	91	124
15			2000:1	57	560
16		CHBr ₃	1000:1	70	700
17	Methyl Acrylate	CCl ₄	1000:1	84	840
18			2000:1	62	1240
19		CBr ₄	10000:1	82	330
20			50000:1	63	4400
21		CHBr ₃	1000:1	48	480
22	Methyl methacrylate	CCl ₄	1000:1	66	660
23			2000:1	44	880
24		CBr ₄	10000:1	63	6300
25			20000:1	62	7200
26	Vinyl Acetate	CCl ₄	1000:1	94	780
27			2000:1	70	1220
28		CBr ₄	5000:1	84	2500
29		CHBr ₃	1000:1	61	610

^(a)All reactions were performed in CH₃CN in light for 24 h. Reaction temperature was maintained at 22 ± 2° C, $[R-X]_0:[alkene]_0:[V-70]_0 = 1:1:0.05$, catalyst = [Cu^{II}(TPMA)X][X] (X = Cl, Br). ^(b)Yield is based on the formation of monoadduct and was determined using ¹H NMR spectroscopy (relative errors are ±10%).

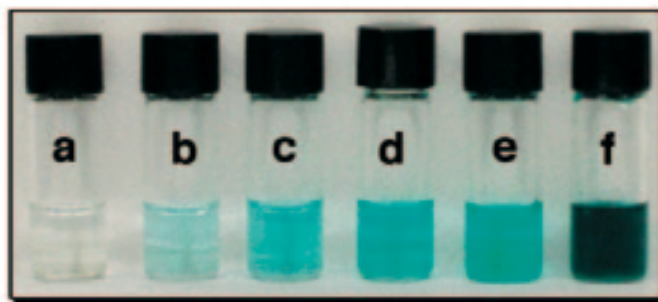
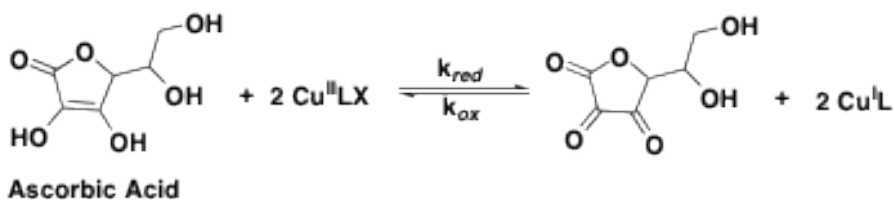


Figure 1.2.4. Different concentration of catalyst, $[\text{Cu}^{\text{II}}(\text{TPMA})\text{Br}][\text{Br}]$ (a) 0.002, b) 0.01, c) 0.05, d) 0.1, e) 1.0, and f) 10 mol% utilized for the ATRA of 1-hexene. For all these catalyst loadings, 100 % conversion and monoadduct yields of > 93 % were achieved.³¹

The results obtained by using V-70 as reducing agent were comparable with photo-initiated AIBN reactions (**Table 1.2.5**). In case of 1-hexene, a quantitative yield was obtained with the catalyst loading as low as 0.002 mol% (**Figure 1.2.4**). As expected, styrene showed poor results whereas methyl acrylate, methyl methacrylate and vinyl acetate showed high conversions as well as high yields.

A non-radical reducing agent, ascorbic acid has also been employed for atom transfer radical processes.^{105, 115} This reducing agent does not participate or initiate free radical polymerization unlike the radicals generated via decomposition of diazo based reducing agents so the high yields of the monoadduct was obtained at 60 °C even in case of active alkenes (**Scheme 1.2.8**). High turn over numbers (TONs) of 15,200 and 11,800 were obtained for 1-hexene and acrylonitrile, respectively at very low concentration of ascorbic acid (7 mol-% w.r.t alkene) (**Table 1.2.5**). Also, on the other hand, the other main advantage is complete elimination of the the deoxygenation step, which is necessary during ATRA in the presence of the diazo reducing agents. Thus, these reactions can be performed on bench top without any use of purging techniques.



Scheme 1.2.8. Proposed mechanism for the reduction of $\text{Cu}^{\text{II}}\text{LX}$ (L= ligand; X = Cl, Br) complex with ascorbic acid.

Table 1.2.5. ATRA of CBr_4 to alkenes at 60 °C in the presence of Ascorbic acid.¹¹⁵

Entry ^(a)	Alkene	Alkyl Halide	Catalyst Loading	% Conv/% Yield
1		CBr_4	5000:1	90/90
2	1-octene		10000:1	85/85
3			20000:1	76/76
4		CCl_4	500:1	90/90
5			1000:1	69/69
6		CBr_4	1000:1	100/100
7	Methyl Acrylate		5000:1	98/85
8			10000:1	99/64
9			20000:1	90/53
10		CCl_4	100:1	67/65
11			250:1	43/39
12		CBr_4	1000:1	100/99
13	Acrylonitrile		5000:1	98/88
14			10000:1	94/80
15			20000:1	80/59
16	Styrene	CCl_4	100:1	100/99
17			250:1	98/81
18		CBr_4	1000:1	100/100
19	Methyl methacrylate		5000:1	100/86
20			10000:1	69/57
21			20000:1	50/32
22		CCl_4	100:1	67/65
23			250:1	43/39

^(a)All reactions were performed in CH_3CN in light for 24 h. Reaction temperature was maintained at $22 \pm 2^\circ \text{C}$, $[\text{R-X}]_0 : [\text{alkene}]_0 : [\text{Ascorbic Acid}]_0 = 1:1:0.07$, catalyst = $[\text{Cu}^{\text{II}}(\text{TPMA})\text{X}][\text{X}]$ (X = Cl, Br). ^(b)Yield is based on the formation of monoadduct and was determined using ^1H NMR spectroscopy (relative errors are $\pm 10\%$).

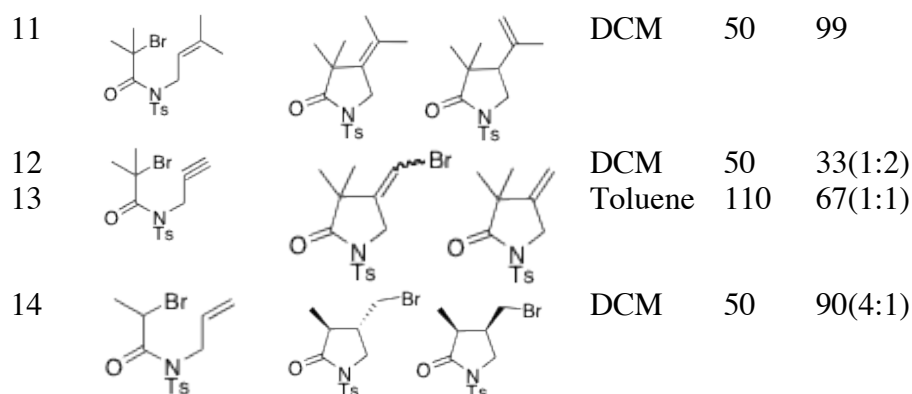
The copper complexes with tris-pyrazolylborate ligands have shown to be effective in ATRA without the use of any reducing agent at low catalysts concentrations (0.33-0.02 mol%). These reactions were conducted in the presence of small amounts of acetonitrile. The coordinating ability of the acetonitrile was able to saturate the coordination sphere of copper for

alkyl halide cleavage. This would result in lowering of the concentration of radicals and hence, prevent the accumulation of copper(II).¹⁴⁰

Along with extensive usage of catalyst regeneration in ATRA, this methodology has been successfully employed to ATRC and cascade reactions.^{31, 50, 64, 115, 135, 139} As shown in **Table 1.2.6**, ATRC was performed in the presence of AIBN as reducing agent with a number of bromoacetamides to yield 5-membered cyclic lactams in two different solvents, dichloromethane (DCM) and toluene. These reactions were conducted at 50 °C for DCM and 110 °C for the toluene for 24 h. Excellent to moderate yields of highly functionalized cyclized products were obtained.

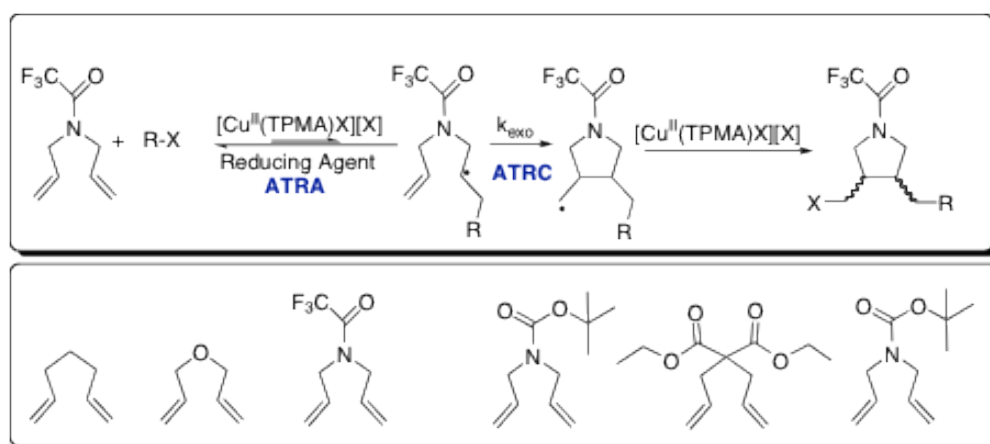
Table 1.2.6. ATRC of bromoacetamides catalyzed by copper complexes with TPMA in the presence of AIBN as reducing agent.

Entry	Substrate	Product	Solvent	T °C	Yield
1			DCM	50	84
2				50	97
3			Toluene	110	87
4			DCM	50	13 ^b
5			Toluene	110	88 ^b (1:2)
6			DCM	50	30(3:2)
7			Toluene	110	67(1:1)
8			DCM	50	95
9			DCM	50	100
10			DCM	50	99



^(a)Reactions were performed with [Substrate]₀: [Cu^I/Cu^{II}]₀: AIBN 1:0.01:0.1 for 24h

Cascade reactions are also very attractive synthetic routes to synthesize functionalized precursors similar to ATRA and ATRC (**Scheme 1.2.9**).^{31, 115} During the cascade reaction, different 1,4-, 1,5- and 1,6-dienes are utilized. As shown in **Scheme 1.2.9**, the C-X bond is activated via ATRA and generates the alkyl radical. This radical adds across the double bond of the diene to form a secondary radical.^{132, 141} In second step, the secondary radical undergoes cyclization through ATRC, which is followed by deactivation and thus, generates the final product. Quantitative yield of the final cyclized products has been obtained using different reducing agents such as AIBN, V-70 and ascorbic acid.^{132, 141}



Scheme 1.2.9. Proposed mechanism for atom transfer radical cascade reaction catalyzed by [Cu^{II}(TPMA)X][X] (X= Cl, Br) in the presence of reducing agent on different dienes.

1.2.4. Development of Highly Active Catalysts

Highly active catalysts tailored through the ligand design can potentially decrease the concentration of the metal in atom transfer radical processes. Various studies have shown that the metal complexes with high reducing ability can reduce the accumulation of the deactivator by continuous regeneration of the activator in the catalytic cycle.

1.3. Aspects of Atom Transfer Radical Reactions

1.3.1. Alkenes and Alkyl Halide

Alkenes and alkyl halides are the two main constituents in the atom transfer radical reactions. In case of ATRC, the alkene and alkyl halide are functional groups present in the same molecule. The alkyl halides, also known as initiators are generally polyhalogenated alkanes, benzylic halides,^{63, 142, 143} *N*-haloamines,⁶³ 1-halonitriles,^{144, 145} 1-haloacetates^{49, 146, 147} 1-haloaldehydes^{50,147,148} or alkylsulfonyl halides^{26,149-152} (**Figure 1.3.1**).

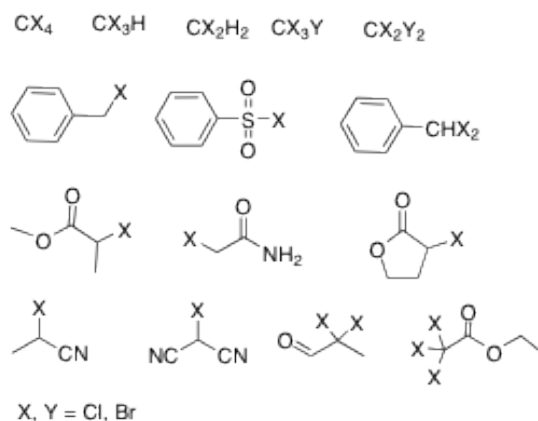


Figure 1.3.1. Different alkyl halides utilized in atom transfer radical processes.

The structure of the alkyl halide dictates the reactivity and hence, the activation processes in atom transfer radical processes. The reactivity of these molecules is dependent on the bond

dissociation energy (BDE), which is further correlated to different factors mentioned below: ⁶⁴.

94,147

1. Degree of substitution (primary < secondary < tertiary)

2. Leaving ability of the halide (Cl < Br < I)

3. Radical stabilizing group (-Ph≈C(O)OR<<CN)

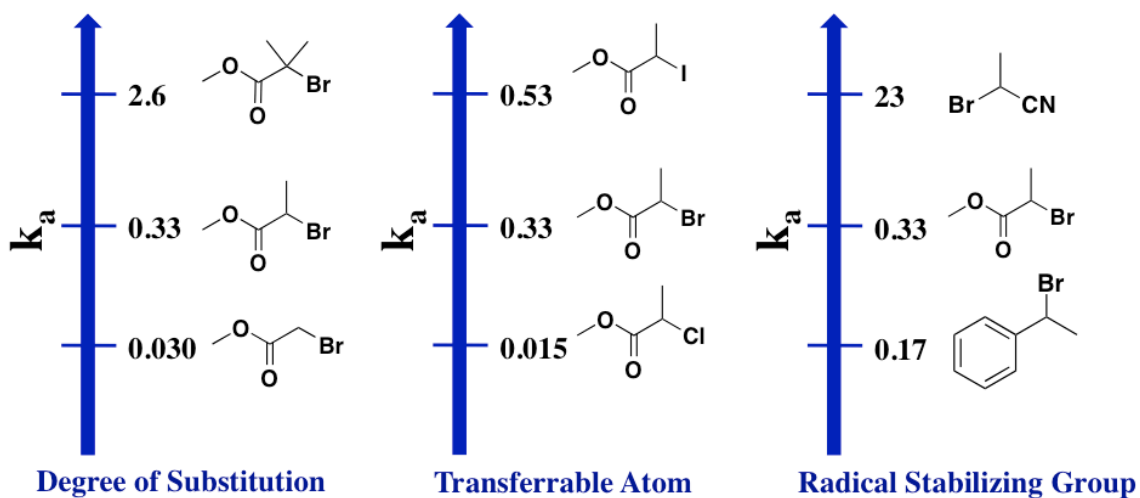


Figure 1.3.2. Values of k_a ($M^{-1}s^{-1}$) for different initiators with $Cu^I X/PMDETA$ ($X = Cl, Br$ or I) measured in acetonitrile at $35\text{ }^\circ C$. ^{64,94}

As mentioned in previous sections, the product selectivity in atom transfer radical processes is strongly dependent on the nature of the alkenes (**Figure 1.3.3**). The α -olefins (1-octene, 1-hexene and 1-decene) favor the formation of the monoadduct over polymers whereas the highly active alkenes such as styrenes, acrylates and acrylonitrile have high k_p and low k_{tr} values and tend to polymerize over monoadduct formation in the presence of the free radicals (**Table 1.3.1**).

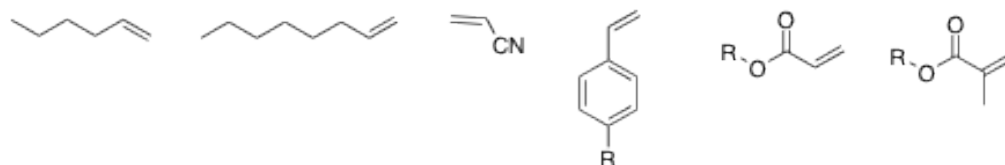


Figure 1.3.3. Different alkenes typically utilized in atom transfer radical processes (R = H, alkyl).

Table 1.3.1. Chain Transfer Constants for CCl_4 in free-radical polymerization at 60 °C.

Alkene	Chain Transfer Constant (k_t/k_p)
Ethylene	16.2
1-Hexene	14.5
Vinyl Acetate	1.04
Styrene	0.0109
Methyl acrylate	0.000124
Acrylonitrile	0.0000865

1.3.2. Ligand

Ligands play a pivotal role in the transition metal catalyzed atom transfer radical reactions by dictating the electronic and steric environment of the metal center. In these reactions, ligand influences the activation (k_a), deactivation rate constant (k_d), thereby controlling the equilibrium constant ($K_{ATRA/ATRP} = k_a/k_d$).^{64, 65, 92, 153-157}

The activation of the C-X bond is the rate-determining step. Therefore, the measurement of the activation rate constant is highly desirable in order to screen the catalytic candidates and also, for the optimization of the reactions. Typically, the copper (I) complex is reacted with the alkyl halide in the presence of the radical trapping agent, 2,2,6,6-tetramethylpiperidin-1-oxyl (TEMPO).^{50, 155, 158, 159} The rate of disappearance of alkyl halide or the appearance of Cu(II) species is monitored spectroscopically under pseudo first order conditions. The slope of plot of $\ln[\text{RX}]_0/[\text{RX}]_t$ vs time (t) gives the activation rate constant (slope = $-k_a[\text{Cu}^I]$).^{50, 155, 158, 159}

Based on various structural and kinetic studies, activation rate constant has found to be dependent on the structural features of the complexing ligand as listed below:

1. Core around the metal center: cyclic \approx linear < branched
2. Nature of chelating nitrogen: Aryl amine < aryl imine < alkyl amine < pyridine
3. Steric bulkiness around metal center decreases the activation rate constant
4. Linking unit around the nitrogen atom: (C4 << C3 < C2)
5. Denticity of the N-based ligand (tetradentate > tridentate > bidentate > monodentate)

The activity of the catalytic candidates can also be probed by cyclic voltammetry studies where electrode potential (E) is directly correlated to the equilibrium rate constant (**K**) and thus, correlated to the activation rate constant provided that the halidophilicity remains constant.

$$\ln K_{eq} = nFE/RT$$

$$K_{eq} = k_a/k_d$$

The complexes with high reducing abilities have been shown to be highly active in atom transfer radical processes. The reducing ability of the copper complex can be easily increased by increasing the electron density around the metal center, which increases the activation rate constant. As shown in **Figure 1.3.4**, a range of electron donating and electron withdrawing groups (-N(Me)₂, -OMe, Me, H, Cl) were substituted at 4 and 4' position of 2,2'-bipyridines to test the effect of the electron density on the catalytic activity during of ATRP of acrylates.¹⁶⁰ As predicted, the reducing ability of the complex increased with electron donating substituents in comparison to unsubstituted and electron withdrawing groups. Along with the increase in the electrode potential, activity of these complexes was significantly altered with these side groups. Complexes with (-N(Me)₂)₂-bpy and (-OMe)₂-bpy have been found to be approximately 400 and 100 times more active than with simple bipyridine ones respectively. High conversion of butylacrylate was observed with ligands with the electron donating group; 80 % of the monomer was converted in less than 0.5 hr in case of (N(Me)₂)₂-bpy while simple pyridine took almost 24

hr to achieve 40 % conv. Even with this high conversion, less control over the polymerization was observed due to the high concentration of radicals generated during activation process in the catalytic cycle by highly active complexes.

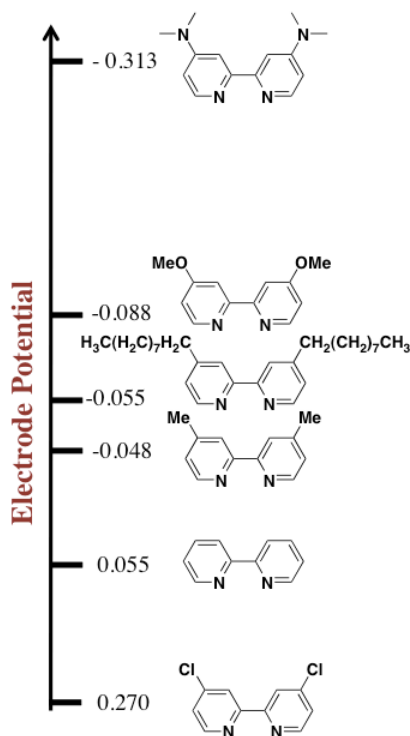


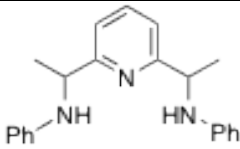
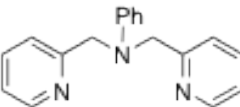
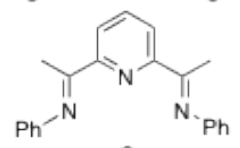
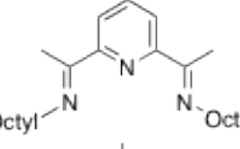
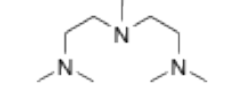
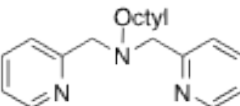
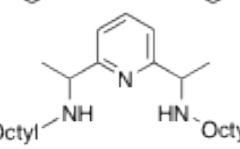
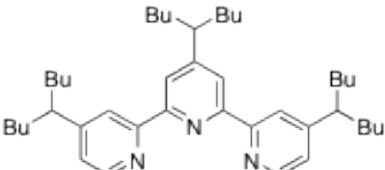
Figure 1.3.4. Substituted bipyridines utilized for ATRP.¹⁶⁰

A similar structure-activity study was conducted on the tridentate N-based ligands in copper catalyzed ATRP (**Table 1.3.2**).⁹² Different structural features of ligand around copper center have found to strongly dictate the electrode potential and activation rate constant. The aryl amine N-based ligands (Entry **1**) were less electron donating due to participation in the resonance and hence less reducing. The reducing nature was increased by replacing the aryl amines with pyridine (Entry **2** and **3**). The electrode potential was further dropped to -110 mV by introducing the alkyl imines with electron donating *n*-octyl linear chains. The alkyl based amines in entry **4-7**

with electron donating groups such as n-butyl (Bu) on terpyridine ligand increased the reducing character significantly.

The effect of the reducing ability was observed in activation rate constant in ATRP.

Table 1.3.2. Electrode potential and activation rate constant of different tridentate nitrogen based ligands utilized in copper catalyzed ATRP.⁹²

Entry	Ligand	Electrode Potential (mV)	k_a ($M^{-1}s^{-1}$)
1		200	2.0×10^{-6}
2		70	1.4×10^{-3}
3		65	4.0×10^{-4}
4		-110	1.4×10^{-2}
5		-155	1.1×10^{-1}
6		-175	6.6×10^{-1}
7		-220	5.0×10^{-2}
8		-240	4.2×10^{-1}

Another way to increase the electron density around metal center is by increasing the denticity of the complexing ligands. The tetradentate ligands were found to be far more reducing

than tridentate and bidentate ligands (**Figure 1.3.5**). This trend can also be seen in the magnitude of activation rate constant. The tetradentate ligands, TPMA and Me₆TREN showed the k_a value of 62 and 450 M⁻¹s⁻¹, respectively whereas bidentate ligand, bpy and tridentate ligand, PMDETA showed a significant decrease, 0.0066 and 2.7 M⁻¹s⁻¹, respectively.¹¹²

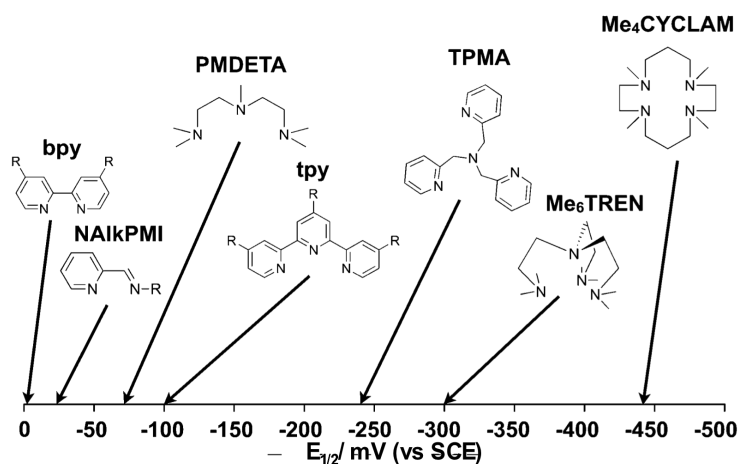


Figure 1.3.5. The electrode potential (mV vs SCE) of copper complexes with various N-based ligands.¹¹²

Deactivation Rate Constant (k_d)

The deactivation rate constant has typical magnitudes of 10⁸-10⁹M⁻¹s⁻¹ for copper complexes with N-based ligands. Unlike the activation process, the deactivation is a very fast process and hence, could not be probed using the simple spectroscopic techniques. However, it can be indirectly derived by measuring k_a and equilibrium constant for atom transfer ($K=k_a/k_d$). Other method, pulse laser photolysis has been successfully utilized to calculate the k_d .^{93, 155, 159} The structure of the Cu(II) species effects the k_d of the process. However, no direct correlation has been established between the Cu-Br bond length and k_d , but complexes with longer Cu^{II}-Br bond lengths have been found to have a smaller deactivation rate constant.¹³⁹ This was attributed to the relative bond strength of the Cu-Br bond.

1.4. Structural Features of Tetradentate N-based Ligands in Copper Catalyzed Atom Transfer Radical Processes

In this section the structural features of Cu(I/II) complexes with tripodal tetradentate ligands TPMA, Me₆TREN and TDAPA are discussed. The analysis of the catalyst structure in solution and solid-state provided an insight into the mechanistic and kinetic aspects of copper catalyzed atom transfer radical processes (**Figure 1.4.1**).

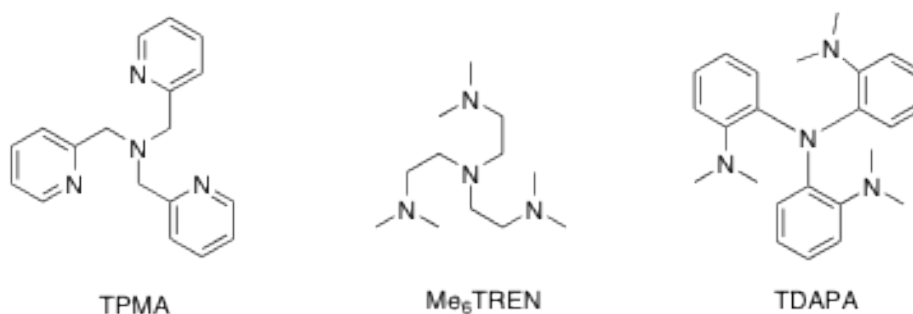


Figure 1.4.1. Tetradentate N-based ligands used for atom transfer radical processes.

A. Solution State Structural Studies

It is very imperative to study the structure of a catalyst in the solution because of the close resemblance with the homogenous experimental conditions. In copper based systems, solution studies can only be conducted on the Cu(I) species by ¹H NMR spectroscopy due to its diamagnetic nature. In past few years, our laboratory has extensively explored the structural features of copper complexes with different tetradentate N-based ligands. These studies have greatly aided in the understanding of the intricate details of the mechanism and also, established

the properties of an active catalytic system for atom transfer radical processes. On coordination of the ligand, to the Cu(I) center, the resonances of the ligand closer to metal shifted downfield w.r.t ^1H NMR of pure ligand. This downfield shift is caused by donation of electron density of ligand to the metal center. At room temperature, the peaks are broad due to fluxionality caused by dissociation of the ligand arm or halide anion from the copper center. On cooling to low temperature, the resonances are resolved to show the geometry of the complex in solution.

[Cu^I(TPMA)Br]

In the ^1H spectrum of [Cu^I(TPMA)Br], the resonances at 298K appeared very broad and shifted downfield in acetone- d_6 (**Figure 1.4.2**).⁵¹ The broadness at higher temperature was due to the association or dissociation of one of the TPMA arm or bromide anion causing the fluxionality in the system. This lability of the arm or bromide anion will facilitate the formation of coordinatively unsaturated copper center. This feature is very crucial during catalysis to promote the entrance of alkyl halide in the coordination sphere of copper to initiate the activation via inner sphere electron transfer (ISET).

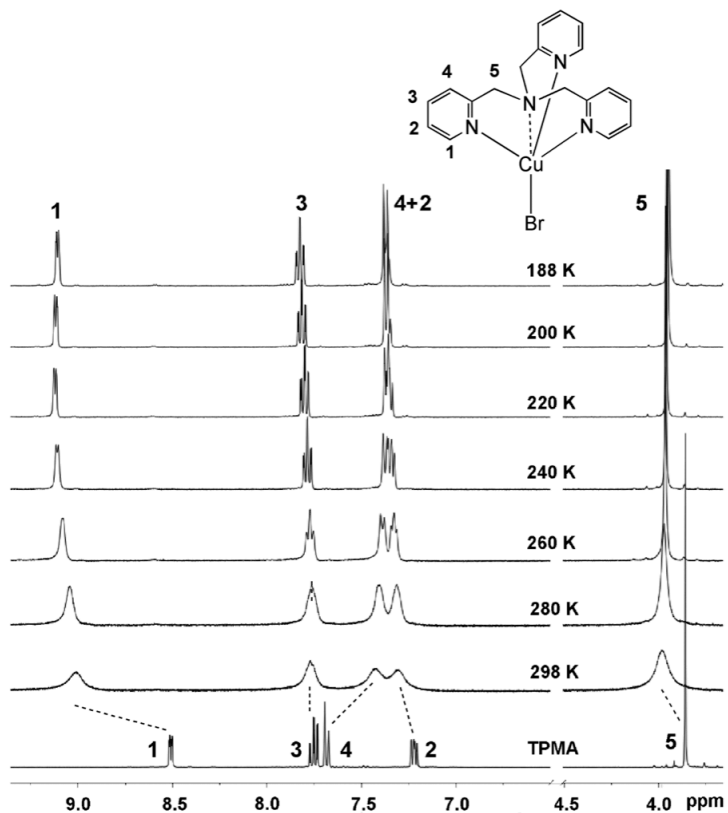


Figure 1.4.2. Variable temperature ^1H NMR of $[\text{Cu}^{\text{I}}(\text{TPMA})\text{Br}]$ in acetone- d^6 .⁵¹

The resonances were resolved as the monomeric Cu(I) species with 3-fold symmetry at 220K, due to absence of any extra peaks in the aromatic region. Generally, tripodal ligands with copper center show the dimerization in the solution state with bulky counter anions (ClO_4^- , BPh_4^-). When Cu(I)/TPMA complex was synthesized with bulky counter anions, the ^1H NMR showed the predicted dimerization, also, confirmed by crystal structure.

At 298 K, the $[\text{Cu}^{\text{I}}(\text{TPMA})][\text{ClO}_4^-]$ showed the resonances corresponding to the monomeric species but on further cooling to 180 K, peaks resolved and showed the dimeric complex (**Figure 1.4.3**). On dissolution of this complex in the strong coordinating solvent, acetonitrile- d^3 , the dimeric species changed into the monomeric ones. The similar effect was observed when copper center was complexed with strong coordinating ligand,

triphenylphosphine (PPh₃). The PPh₃ tends to coordinate with copper center strongly through back bonding.¹⁶¹

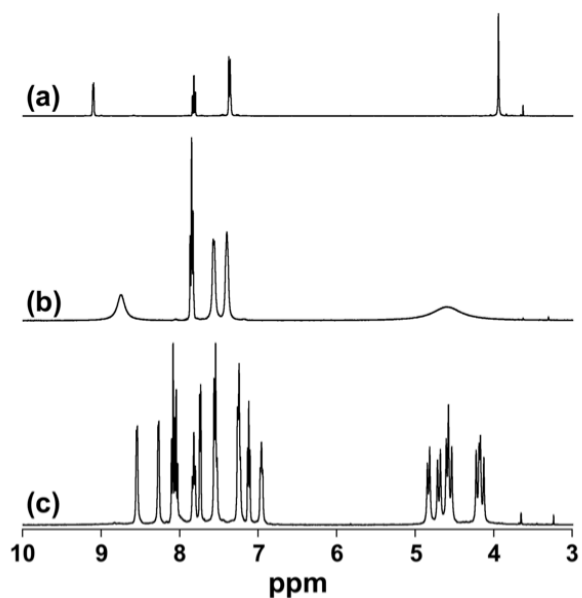
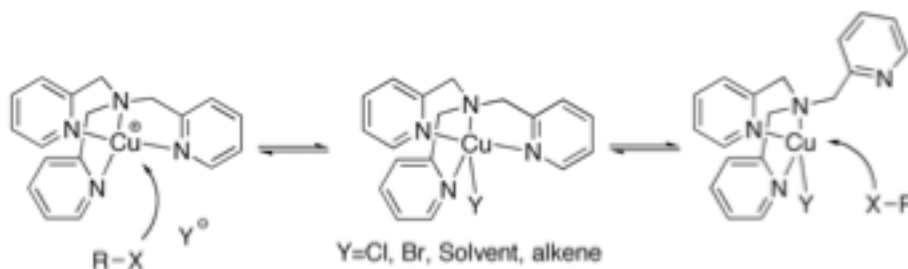


Figure 1.4.3. ¹H NMR spectra (400 MHz, (CD₃)₂CO) of [Cu^I(TPMA)Br] at 180K (a), [Cu^I(TPMA)][ClO₄] at 298K (b), and [Cu^I(TPMA)]₂[ClO₄]₂ at 185K (c).

The ¹H NMR spectrum of [Cu^I(TPMA)Br] with one extra equivalent of the TPMA ligand was recorded in acetone-d₆ to probe the lability of the pyridine arms in the complex. The excess of ligand would push the equilibrium towards the association of the pyridine arms and dissociation of the bromide anion. On further cooling, it was found that the peaks from the excess ligand resolved separately at lower temperature without any relevant association with the copper center. Based on these studies, it was concluded that lability of the TPMA arms was facilitated in the catalytic cycle via dissociation from the copper center as indicated in **Scheme 1.4.1.**¹⁶²



Scheme 1.4.1. Possible pathways during the activation of R-X via ISET in $[\text{Cu}^{\text{I}}(\text{TPMA})\text{Y}]$ (Y= Cl, Br).

$[\text{Cu}^{\text{I}}(\text{Me}_6\text{TREN})\text{Br}]$

The alkyl based tetradentate ligand, Me_6TREN forms an active catalytic system with copper for atom transfer radical processes.^{135, 163} The alkyl-based core of the ligand has increased the reducing ability and lability of the arms in comparison to TPMA. Irrespective of these structural advantages, the $[\text{Cu}^{\text{II}}(\text{Me}_6\text{TREN})\text{Cl}][\text{Cl}]$ complex has shown comparable catalytic activity as $[\text{Cu}^{\text{II}}(\text{TPMA})\text{Cl}][\text{Cl}]$ in the presence of reducing agent due to possible degradation during catalysis .

Table 1.4.1. ATRA of CCl_4 to various alkenes with $[\text{Cu}^{\text{II}}(\text{Me}_6\text{TREN})\text{Cl}][\text{Cl}]$ in the presence of AIBN as reducing agent.¹³⁵

Entry	Alkene ^[a]	Catalyst Loading	Conv/Yield
1	1-Hexene	1000:1	100/100
2	1-Hexene	2500:1	89/89
3	1-Octene	1000:1	99/99
4	<i>cis</i> -cyclooctene	1000:1	95/95
5	<i>cis</i> -cyclooctene	2500:1	85/85
6	Methyl acrylate	250:1	100/67

^[a]Reactions performed at 60°C in acetonitrile, $[\text{alkene}]_0:[\text{CCl}_4]:[\text{AIBN}]_0:[\text{Cu}]_0=1:1.1:0.05$. Conversion and yield were calculated by ¹H NMR spectroscopy.

As shown in **Table 1.4.1**, high catalytic activity was observed for ATRA with α -olefins and CCl_4 at high catalyst loading whereas moderate yield was obtained in case of methyl

acrylate. In order to probe further, variable temperature NMR study was conducted on $[\text{Cu}^{\text{I}}(\text{Me}_6\text{TREN})\text{PPh}_3][\text{BPh}_4]$ complex. Copper (I) complexes with Me_6TREN ligand have high propensity towards the disproportionation in solution. In order to stabilize the complex, triphenyl phosphine (PPh_3) was used to stabilize Cu(I) center in order to prevent disproportionation. Resonances of the ligand in aliphatic region shifted downfield, which indicated that the complexation with copper center was occurred, $[\text{Cu}^{\text{I}}(\text{Me}_6\text{TREN})(\text{PPh}_3)][\text{BPh}_4]$ (**Figure 1.4.4**). The methylene protons (**1**) appeared broad at room temperature whereas sharp singlet was observed for the methyl protons (**2**) attached to nitrogens.¹³⁵ On further cooling, resonances of **1** coalesced, indicating the rapid association and dissociation of the arms. Similar behavior was observed with methyl protons (**2**). However, no significant change in the peaks corresponding to PPh_3 (7.57-7.55 ppm and 7.49-7.44 ppm) and BPh_4^- (7.33, 6.92, and 6.77 ppm) was observed. Despite the rapid exchange between the alkyl arms, the Cu(I) center appeared to have symmetrical and monomeric geometry.

$[\text{Cu}^{\text{I}}(\text{TDAPA})\text{Br}]$

The tetradentate ligand, TDAPA has rigid structure skeleton than Me_6TREN and TPMA due to the phenyl rings (**Figure 1.4.1**). The ^1H spectrum of $[\text{Cu}^{\text{I}}(\text{TDAPA})\text{Br}]$ displayed protons corresponding to the phenyl rings shifted downfield whereas the methyl protons shifted upfield.¹⁶²

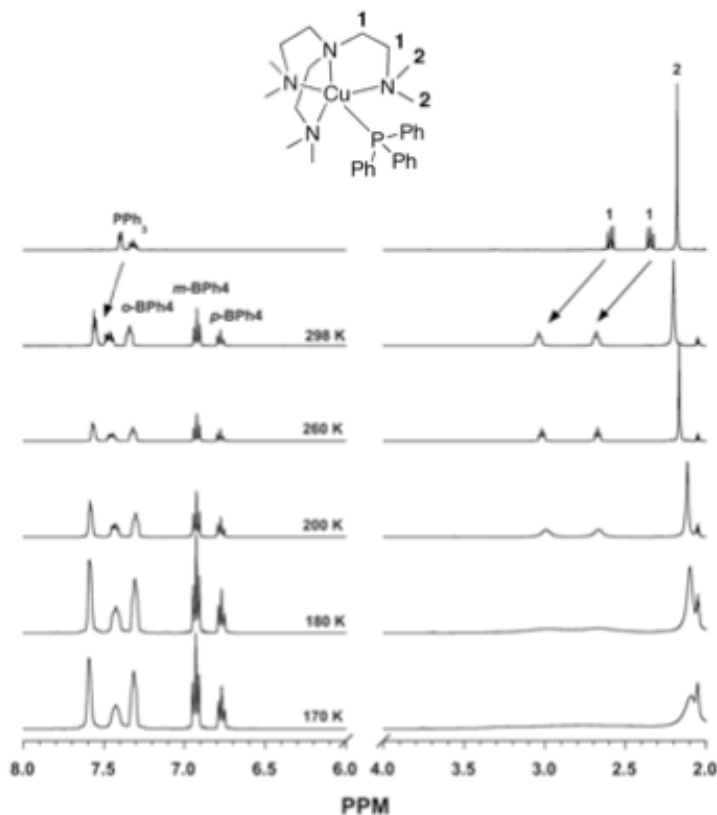


Figure 1.4.4. Variable temperature ^1H NMR of $[\text{Cu}^{\text{I}}(\text{Me}_6\text{TREN})\text{BPh}_4]$ in acetone- d^6 .¹⁶²

This discrepancy in the positions of the resonances indicated that the arms of the ligands were not labile.¹⁶² This behavior was further confirmed by the low catalytic activity in ATRA (**Table 1.4.2**) in comparison to the copper complexes with Me_6TREN and TPMA ligands. Poor yield was obtained for α -olefins as well as for active alkenes with CCl_4 in the presence of AIBN as reducing agent.¹⁶² This fact was further supported by the significant increase in the yield of the monoadduct when the ATRA was conducted with the $\text{Cu}(\text{II})/\text{TDAPA}$ complex with bulky non-coordinating counter anions, tetrafluoroborate (BF_4^-) or tetraphenyl borate (BPh_4^-)¹⁶² This significant change can be attributed to the open coordination site on the copper center necessary for the activation of C-X bond.¹⁶²

Table 1.4.2. ATRA of CCl_4 to alkenes with $[\text{Cu}^{\text{II}}(\text{TDAPA})\text{Cl}][\text{Y}]$ ($\text{Y}^- = \text{Cl}^-, \text{BF}_4^-, \text{BPh}_4^-$) in the presence of AIBN as reducing agent.¹⁶²

Entry	Alkene ^[a]	Catalyst	Conv/Yield
1	1-Hexene		24/24
2	1-Octene	[Cu ^{II} (TDAPA)Cl][Cl]	25/25
3	Styrene		41/7
4	Methyl Acrylate		100/1
5	1-Hexene		49/49
6	1-Octene	[Cu ^{II} (TDAPA)Cl][BF ₄]	59/59
7	Styrene		50/35
8	Methyl Acrylate		100/10
9	1-Hexene	[Cu ^{II} (TDAPA)Cl][BPh ₄]	60/60
10	1-Octene		45/45

^[a]Reactions performed at 60°C in acetonitrile, [alkene]₀: [CCl₄]: [AIBN]₀: [Cu]₀ = 250:250:12.5:1. Conversion and yield were calculated by ¹H NMR spectroscopy.

Based on the solution studies on different Cu(I) complexes, the ligand arm or halide anion has to continuously associate and dissociate from the copper center in order to provide room for incoming alkyl halide and start the catalytic cycle by activation process.

B. Solid-State Structural Studies

Single crystal X-ray crystallography is typically employed to characterize the copper(I/II) complexes in the solid-state to establish the structure-reactivity relationship of the catalytic systems in atom transfer radical processes. In comparison to Cu(II) species, isolation of Cu(I) complexes is quite difficult due to their high moisture and oxidative instability. Therefore, the crystallizations are conducted under the inert atmosphere with dry solvents. In this section, structural features of Cu(I/II) complexes with the tetradentate N-based ligands are discussed.

Tris(2-pyridyl methyl)amine (TPMA)

Tripodal TPMA ligand binds to Cu (I) and (II) centers in tetradentate fashion with 3-fold symmetry (**Figure 1.4.5**).^{50, 51} The pseudo-pentaco-ordinated copper center in [Cu^I(TPMA)Br]

complex adopted the distorted tetrahedral geometry. The bond length of Cu(I) and axial nitrogen (Cu1-N1) was found to be exceptionally long ($\text{Cu-N}_{\text{ax}} = 2.4397 \text{ \AA}$) in comparison to equatorial nitrogen ($(\text{Cu-N}_{\text{eq}})_{\text{average}} = 2.091 \text{ \AA}$).

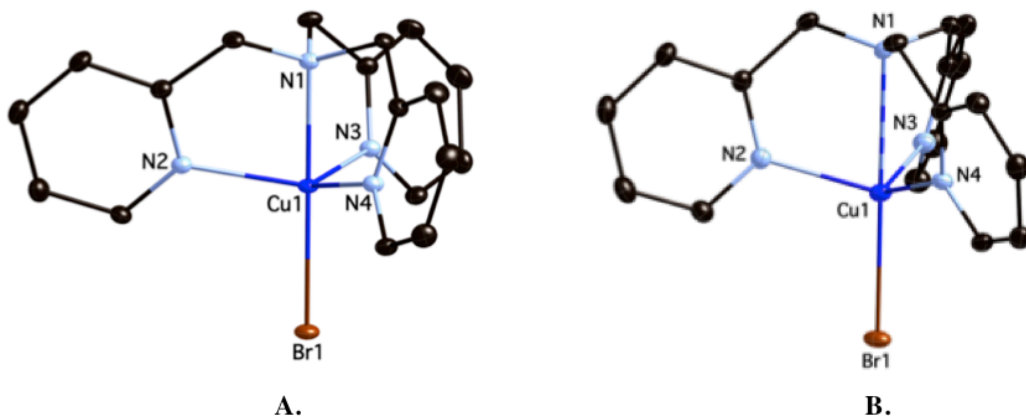


Figure 1.4.5. Molecular structure of A. $[\text{Cu}^{\text{I}}(\text{TPMA})\text{Br}][\text{Br}]$ (Br is excluded for clarity) B. $[\text{Cu}^{\text{I}}(\text{TPMA})\text{Br}]$. Selected distances [\AA] and angles [$^{\circ}$]: Cu1-N1 2.040(3), Cu1-N2 2.073(2), Cu1-Br1 2.3836(6), N1-Cu1-N2 80.86(5), N2-Cu1-N2i 117.53(3), N1-Cu1-Br1 180.00(5). Selected distances [\AA] and angles [$^{\circ}$]: Cu1-N1 2.4397(14), Cu1-N2 2.1024(15), Cu1-N3 2.0753(15), Cu1-N4 2.0709(15), Cu1-Br1 2.5088(3), N4-Cu1-N3 120.51(6), N4-Cu1-N2 112.40(6), N3-Cu1-N2 107.61(6), N4-Cu1-N1 75.37(5), N3-Cu1-N1 74.86(5), N2-Cu1-N1 74.80(5), N1-Cu1-Br1 179.14(3).

The axial bond elongation indicated that the Cu(I) center lacks any bonding interaction with the axial nitrogen, which was attributed to the preferred tetraco-ordinated geometry of the Cu(I) centers and ligand rigidity (**Figure 1.4.5**). The corresponding chloride complex, $[\text{Cu}^{\text{I}}(\text{TPMA})\text{Cl}]$ shared similar structural attributes except the axial bond length was slightly longer ($\text{Cu-N}_{\text{ax}} = 2.466 \text{ \AA}$) and Cu-Cl bond length was shorter (2.3976 \AA) than bromide analog ($\text{Cu-Br} = 2.5088 \text{ \AA}$). The change in the magnitude of bond lengths indicated the relative strengths of bonds in chloride and bromide complexes.

Various Cu(I)/TPMA complexes with the bulky counter anion (ClO_4^- , BPh_4^-) have also been isolated.¹⁵³ And as mentioned in the previous section, a strong coordinating solvent such as

acetonitrile or the ligand, favored the formation of a monomeric over the dimeric Cu(I) complex. The salt metathesis of the $[\text{Cu}^{\text{I}}(\text{TPMA})\text{Br}]$ with sodium tetraphenyl borate (NaBPh_4), yielded a pseudo pentacoordinated complex, $[\text{Cu}^{\text{I}}(\text{TPMA})\text{CH}_3\text{CN}][\text{BPh}_4]$ in presence of acetonitrile (**Figure 1.4.6**). The fifth axial site in this complex was occupied by the acetonitrile molecule.

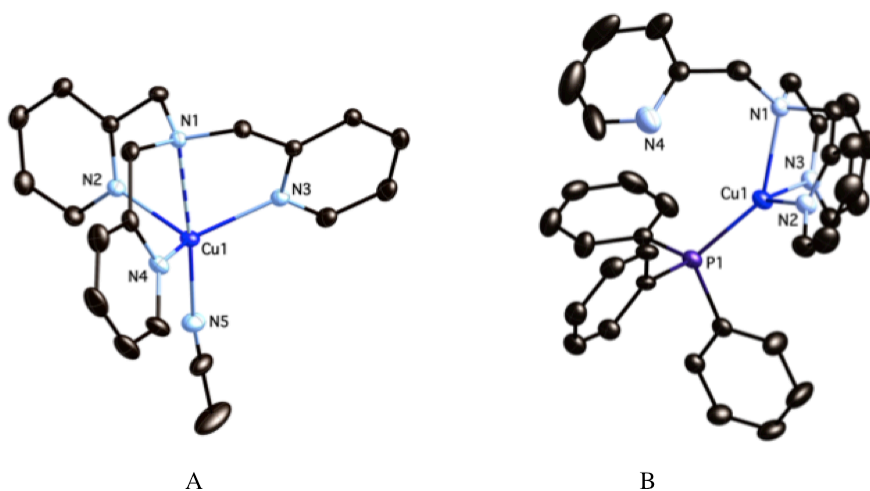


Figure 1.4.6. Molecular structure of A. $[\text{Cu}^{\text{I}}(\text{TPMA})\text{CH}_3\text{CN}][\text{BPh}_4]$ B. $[\text{Cu}^{\text{I}}(\text{TPMA})\text{PPh}_3][\text{BPh}_4]$ and at 150K, shown with 50% probability displacement ellipsoids. H-atoms and counter anion have been omitted for clarity. Selected distances [\AA] and angles [$^\circ$] for **A** : Cu1-N1 2.4109(10), Cu1-N2 2.1031(10), Cu1-N3 2.1114(11), Cu-N4 2.0624(10), Cu1-N5 1.9914(11), N1-Cu1-N2 74.47(4), N1-Cu1-N3 74.04(4), N1-Cu1-N4 76.08(3), N1-Cu1-N5 175.94(4), N2-Cu1-N3 109.44(4), N2-Cu1-N4 115.97(4), N2-Cu1-N5 104.02(5), N3-Cu1-N4 114.92(4), N3-Cu1-N5 103.19(5), N4-Cu1-N5 107.90(5). **B** Selected distances [\AA] and angles [$^\circ$]: Cu1-N1 2.214(3), Cu1-N2 2.073(3), Cu1-N3 2.114(3), Cu1-P1 2.1853(12), N1-Cu1-N2 80.81(12), N1-Cu1-N3 78.63(13), N2-Cu1-N3 117.13(13), N1-Cu1-P1 141.65(9), P1-Cu1-N2 119.74(10), P1-Cu1-N3 112.79(10) (Ref¹⁵³).

These monomeric complex shared their structural attributes with the chlorinated and brominated Cu(I) analogs with TPMA, $[\text{Cu}^{\text{I}}(\text{TPMA})\text{Cl}]$ and $[\text{Cu}^{\text{I}}(\text{TPMA})\text{Br}]$ (**Figure 1.4.5**).¹⁵³ In complex, $[\text{Cu}^{\text{I}}(\text{TPMA})\text{PPh}_3][\text{BPh}_4]$, the copper(I) center adopted tetrahedral geometry where one of the pyridyl arm moved out of the coordination sphere. Therefore, only small axial elongation ($\text{Cu-N}_{\text{ax}} = 2.214(3) \text{\AA}$) was observed.

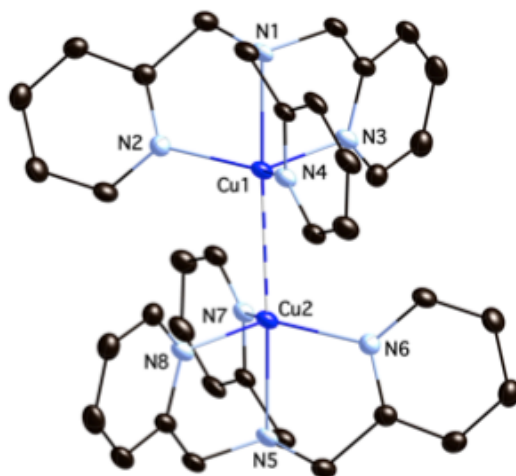


Figure 1.4.7. Molecular structure of $[\text{Cu}^{\text{I}}(\text{TPMA})][\text{BPh}_4]$ at 150K, shown with 50% probability displacement ellipsoids. H-atoms and counter anion have been omitted for clarity. Selected distances [Å] and angles [°]: Cu1-N1 2.211(3), Cu1-N2 2.042(4), Cu1-N3 2.037(4), Cu1-N4 2.036(4), Cu1-Cu2 2.8323(12), N1-Cu1-N2 80.73(13), N1-Cu1-N3 82.08(14), N1-Cu1-N4 81.39(14), N2-Cu1-N3 117.83(15), N2-Cu1-N4 117.49(14), N3-Cu1-N4 118.10(15), Cu1-Cu2-N5 177.73(10).¹⁵³

However, when the salt metathesis with was performed in methanol with NaBPh_4 , a dimeric complex, $[\text{Cu}^{\text{I}}(\text{TPMA})][\text{BPh}_4]$, with two copper centers showing cuprophilic interactions of Cu-Cu 2.8323(12) Å, was obtained (**Figure 1.4.7**). However, corresponding dimeric Cu(I) complex with perchlorate counter anion (ClO_4^-), $[\text{Cu}^{\text{I}}(\text{CH}_3\text{CN})_4][\text{ClO}_4]$, showed no cuprophilic interactions (**Figure 1.4.8**).¹⁵³ In this complex, each distorted tetrahedral copper center was bonded to four pyridyl arms through nitrogen with the bond lengths of 2.2590(13), 1.9909(12), 2.2213(16), and 1.9593(13) Å.

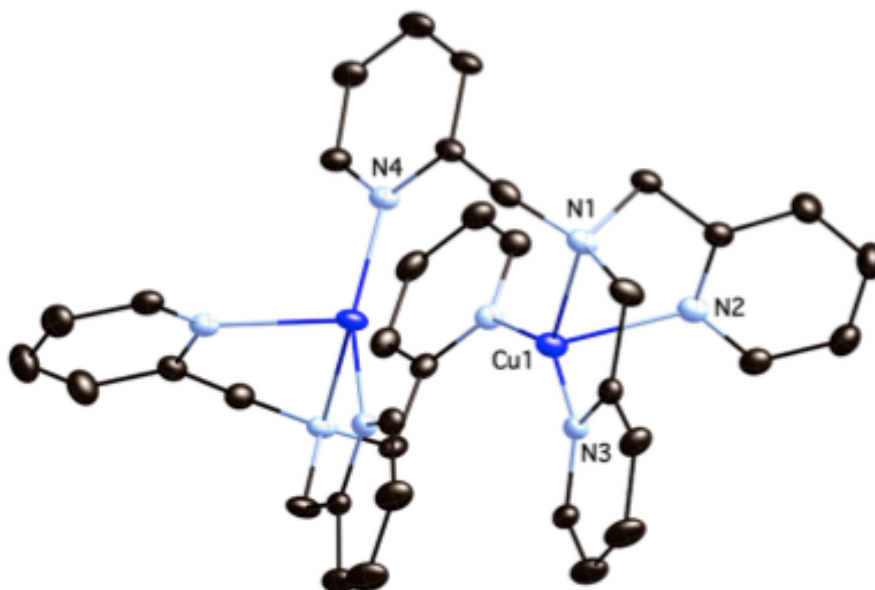


Figure 1.4.8. Molecular structure of $[\text{Cu}^{\text{I}}(\text{TPMA})_2][\text{ClO}_4]_2$ (**4**) at 150K, shown with 50% probability displacement ellipsoids. H-atoms, counter anions, and solvent molecules have been omitted for clarity. Selected distances [\AA] and angles [$^\circ$]: Cu1-N1 2.2590(13), Cu1-N2 1.9909(12), Cu1-N3 2.2213(16), Cu1-N4 1.9593(13), N1-Cu1-N2 81.87(5), N1-Cu1-N3 75.63(5), N1-Cu1-N4 123.01(5), N2-Cu1-N3 95.25(5), N2-Cu1-N4 150.49(6), N3-Cu1-N4 105.68(6) (Ref¹⁵³).

Various copper (II) complexes with TPMA and counter anions were also isolated. In $[\text{Cu}^{\text{II}}(\text{TPMA})\text{Cl}][\text{Cl}]$ ⁵⁰ and $[\text{Cu}^{\text{II}}(\text{TPMA})\text{Br}][\text{Br}]$ ⁵¹ complexes, pentacoordinate copper centers adopted trigonal bipyramidal geometry with 3-fold symmetry (**Figure 1.4.5**). Selected bond lengths [\AA] and angles [$^\circ$] for Cu(II) complexes with TPMA are outlined in **Table 1.4.3**. In $[\text{Cu}^{\text{II}}(\text{TPMA})\text{Br}][\text{Br}]$, the bond lengths ($\text{Cu}-\text{N}_{\text{eq}}$) were of same magnitude of 2.073 \AA while axial bond length ($\text{Cu}-\text{N}_{\text{ax}}$) was found to be 2.040 (3) \AA , nearly 0.400 \AA shorter than corresponding Cu(I) complex.

Table 1.4.3. Selected bond lengths [\AA] and angles [$^\circ$] for Cu(II) complexes with TPMA.

Complex	$[\text{Cu}^{\text{II}}(\text{TPMA})\text{Br}][\text{Br}]$	$[\text{Cu}^{\text{II}}(\text{TPMA})\text{Br}][\text{ClO}_4]$	$\text{Cu}^{\text{II}}(\text{TPMA})\text{Br}][\text{BPh}_4]$
Cu1-N1 _{ax}	2.040(3)	2.0387(17)	2.0534(11)
Cu1-N2 _{eq}	2.073(2)	2.0642(18)	2.0545(12)
Cu1-N3 _{eq}	2.073(2)	2.0515(17)	2.0328(12)
Cu1-N4 _{eq}	2.073(2)	2.1163(18)	2.0909(12)

Cu1-N _{eq}	2.073(2)	2.0773(31)	2.0594(21)
Cu1-Br1	2.3836(6)	2.3765(3)	2.3711(2)
N1-Cu1-N2	80.86(5)	80.36 (7)	82.32(5)
N1-Cu1-N3	80.86(5)	81.44(7)	81.55(5)
N1-Cu1-N4	80.86(5)	81.03(7)	80.98(5)
N2-Cu1-N3	117.53(3)	124.95(7)	128.21(5)
N3-Cu1-N4	117.53(3)	117.89(7)	115.28(5)
N4-Cu1-N2	117.53(3)	109.80(7)	110.17(5)
Br1-Cu1-N2	99.14(5)	100.44(5)	97.55(3)
Br1-Cu1-N3	99.14(5)	97.76(5)	98.68(3)
Br1-Cu1-N4	99.14(5)	99.03(5)	98.89(4)
Br1-Cu1-N1	180.00(5)	179.11(5)	179.77(3)

Similarly the equatorial bond lengths (Cu-N_{eq}) were found to be 0.0100 Å shortened than Cu(I) complex. The copper center, Cu(II) lied 0.329 Å below the least square plane (LSP) created by three nitrogens of pyridine ring. Similar pattern was observed in case of corresponding chloride complex, where the Cu-Cl bond length was slightly shorter (2.2369 Å). Copper(I/II) complexes with one non-coordinating counter anions (ClO₄⁻ and BPh₄⁻) also shared similar structural traits with slightly distorted C-3 symmetry. The high activity of TPMA can be explained by the fact that the minimum entropic rearrangement was required during the catalytic cycle due to close resemblance of the geometries of Cu(I) and Cu(II) complexes.

Tris(2-dimethylaminoethyl)amine (Me₆TREN)

Only few examples of Cu(I) complexes with Me₆TREN have been reported so far because these compounds are difficult to isolate due to their high disposition towards disproportionation.^{135, 164} The Cu(I) complex with non-coordinating counter anion, BPh₄⁻ has been isolated with distorted tetrahedral geometry (**Figure 1.4.9**). The Cu-N_{ax} bond length was slighter longer, 2.153 Å than the equatorial bond lengths (Cu-N_{eq} = 2.115 Å, 2.105 Å and 2.106 Å). The

copper atom lied approximately 0.146 below the LSP created by three equatorial nitrogens with the bond angles of N(4)-Cu(1)-N(2) of 119.19, N(3)-Cu(1)-N(4) 120.03.¹³¹

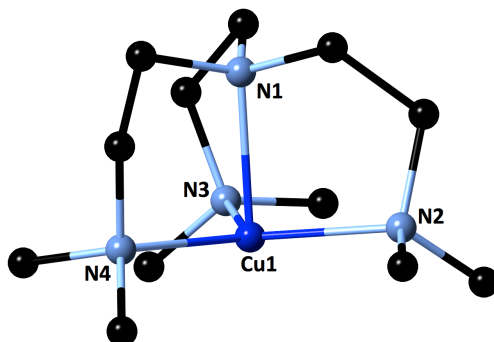


Figure 1.4.9. Molecular structure of $[\text{Cu}^{\text{I}}(\text{Me}_6\text{TREN})][\text{BPh}_4]$ H-atoms and BPh_4^- are omitted for clarity. Selected bond distances [\AA] and angles [$^\circ$]: Cu-N1 2.153, Cu-N2 2.106, Cu-N2 2.105, Cu-N2 2.115 N1-Cu-N2 119.19 N2-Cu-N3 119.191(11) N4-Cu-N2, N1-Cu-N4 180.00(4).

Similarly to Cu(I)/TPMA complex with the bulky and strong co-ordinating PPh_3 , copper center adopted tetrahedral geometry and one of the ligand arm was displaced out of the coordination sphere (**Figure 1.4.10**). The bond lengths and bond angles were found to be comparable with the corresponding TPMA complex (**Table 1.4.4**).¹⁰⁴

In $[\text{Cu}^{\text{II}}(\text{Me}_6\text{TREN})\text{Br}][\text{Br}]$, the copper center adopted the distorted trigonal bipyramidal geometry with C₃-symmetry. The tetradentate ligand coordinated to copper center through equatorially with the average bond length of 2.15 \AA whereas with the axial nitrogen, the bond length ($\text{Cu-N}_{\text{ax}} = 2.04 \text{ \AA}$) was found to be slightly shorter. The first bromide was attached to copper center axially with the bond length of 2.4016 \AA .

Table 1.4.4. Selected bond distances (\AA) and angles ($^\circ$) for complexes $[\text{Cu}^{\text{II}}(\text{Me}_6\text{TREN})\text{Cl}][\text{Cl}]$ and $[\text{Cu}^{\text{II}}(\text{Me}_6\text{TREN})\text{Br}][\text{Br}]$.

Complex	$[\text{Cu}^{\text{II}}(\text{Me}_6\text{TREN})\text{Cl}][\text{Cl}]$	$[\text{Cu}^{\text{II}}(\text{Me}_6\text{TREN})\text{Br}][\text{Br}]$
Cu-N1	2.0545(15)	2.046(2)
Cu-N2	2.1489(9)	2.1527(13)

Cu-X	2.2589(5)	2.4016(4)
N1-Cu-N2	84.62(3)	84.81(4)
N2-Cu-X	95.38(3)	95.19(4)
N2-Cu-N2 ⁱ	119.132(8)	119.191(11)
N1-Cu-X	180.00(2)	180.00(4)

The second bromide anion was non-coordinating and located outside the coordination sphere. The corresponding chloride complex showed similar structural features except the shorter Cu-Cl bond length (2.2589(5) Å) (**Table 1.4.4**). Similar to TPMA, Me₆TREN resulted in the formation of highly active catalytic candidates, which can be attributed to the minimum entropic rearrangement required in the catalytic cycle.

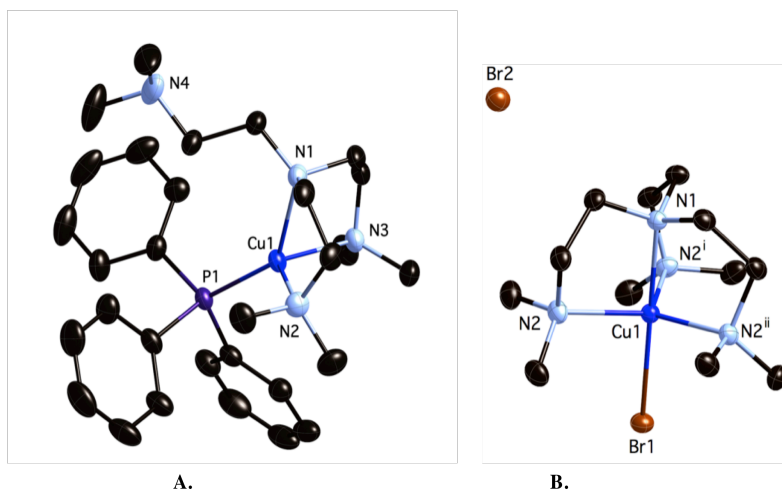


Figure 1.4.10. Molecular structure of **A.** [Cu^I(Me₆TREN)PPh₃][BPh₄] **B.** [Cu^{II}(Me₆TREN)Br][Br] collected at 150K shown with 50% probability displacement ellipsoids. H-atoms omitted for clarity. Selected bond distances [Å] and angles [°]: For [Cu^I(Me₆TREN)PPh₃][BPh₄] Cu1-N1 2.1450(14), Cu1-N2 2.1753(17), Cu1-N3 2.1865(18), Cu1-P1 2.1910(5), N1-Cu1-N2 85.79(6), N1-Cu1-N3 83.87(6), N2-Cu1-N3 113.40(8), N1-Cu1-P1 136.92(4), N2-Cu1-P1 111.80(6), N3-Cu1-P1 119.80(4) For [Cu^{II}(Me₆TREN)Br][Br], Cu-N1 2.046(2), Cu-N2 2.1527(13) Cu-Br 2.4016(4), N1-Cu-N2 84.81(4) N2-Cu-X 95.19(4) N2-Cu-N2ⁱ 119.191(11) N1-Cu-X 180.00(4).^{135, 164}

Tris(2-(dimethylamino)phenyl)amine (TDAPA)

The copper complex with tetradentate ligand, tris(2-(dimethylamino)phenyl)amine (TDAPA), showed poor catalytic activity in the ATRA.^{162, 165} In order to establish the structure-reactivity relationship, Cu(I) and Cu(II) complexes were characterized by single crystal X-ray crystallography. The molecular structure of Cu(I) complex, [Cu^I(TDAPA)CH₃CN][ClO₄] showed similar structural features found in TPMA and Me₆TREN complexes, where the pseudopentacoordinated Cu(I) center adopted the distorted tetrahedral geometry (**Figure 1.4.11**). The axial bond length (Cu-N_{ax} = 2.372 Å) was slightly elongated than the corresponding TPMA complex. Similarly, the bond lengths between equatorial nitrogens N2, N3, N4 and N5 and copper (Cu-N_{eq}) were elongated. The Cu(II) complex with counter anion, [Cu^{II}(TDAPA)Cl][BF₄] (BF₄⁻ = tetrafluoroborate) also shared similar structural features with corresponding TPMA based complexes. In this complex, copper(II) center adopted trigonal bipyramidal geometry with 3-fold symmetry. The copper center lied 0.258 Å below the LSP created by three equatorial nitrogen atoms. The small structural discrepancy was found in Cu-Cl bond length (2.212 Å), which was smaller than 2.2589(5) Å and 2.3976 Å in case of [Cu^{II}(TPMA)Cl][Cl] and [Cu^{II}(Me₆TREN)Cl][Cl], respectively. As mentioned in previous section, the Cu-X (X = Cl, Br) bond length strongly influenced the magnitude of deactivation rate constant (k_d). The shorter bond length lowered the k_d value and inefficiently deactivated the radicals in the catalytic cycle. Therefore, the low catalytic activity can be explained in terms of small k_d value along with the poor lability of the ligand arm necessary during catalysis as shown by NMR studies.

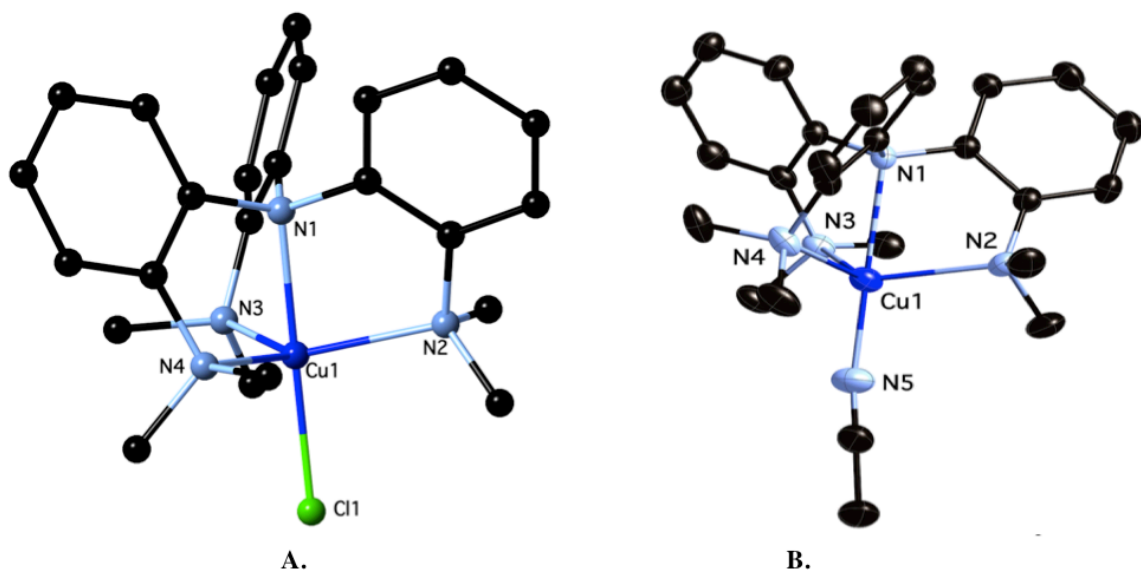
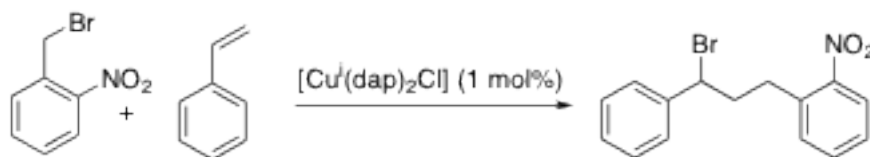


Figure 1.4.11. Molecular structure of A. $[\text{Cu}^{\text{II}}(\text{TDAPA})\text{Cl}][\text{BF}_4]$ B. $[\text{Cu}^{\text{I}}(\text{TDAPA})\text{CH}_3\text{CN}][\text{ClO}_4]$ with H and BF_4 , ClO_4^- atoms omitted for clarity. Selected bond distances for **A** [\AA] and angles $^\circ$: Cu1-N1 22.052, Cu1-N2 2.160, Cu1-N3 2.140, Cu1-N4 2.131, Cu1-Cl1 2.212, N1-Cu1-Cl1 180, N2-Cu1-N3 118.33, N3-Cu1-N4 115.59, N2-Cu1-N4 113.40(9), N3-Cu1-N4 112.57(9), N2-Cu1-N5 121.48. Selected bond distances for **B** [\AA] and angles $^\circ$: Cu1-N1 2.372(2), Cu1-N2 2.234(2), Cu1-N3 2.267(3), Cu1-N4 2.206(2), Cu1-N5 1.953(3), N1-Cu1-N2 75.69(8), N1-Cu1-N3 75.03(8), N1-Cu1-N4 75.77(8), N1-Cu1-N5 175.49(11), N2-Cu1-N3 115.86(9), N2-Cu1-N4 113.40(9), N3-Cu1-N4 112.57(9), N2-Cu1-N5 103.09(12), N3-Cu1-N5 101.90(12), N4-Cu1-N5 108.60(11).^{162, 165}

1.5. Applications of Atom Transfer Radical Reactions

Nearly 50% of commercially used polymers are produced through free-radical polymerization.¹⁶⁶ And, ATRP has played a key role in these free radical polymerizations to synthesize polymers with predefined topologies and functionalities. Three major advantages of ATRP are efficiency, high tolerance to other functional groups and less stringent reaction conditions. The importance and synthetic utility of ATRP has been highlighted in many published reviews and seminal studies.^{94, 114, 166-170} Therefore, in this section the applications of ATRA and ATRC will be discussed.

Reiser and his coworkers employed the copper (I) complex, $[\text{Cu}^{\text{I}}(\text{dap})_2\text{Cl}]$ ($\text{dap} = 2,9$ -bis(*p*-anisyl)-1,10-phenanthroline) to activate the C-X ($\text{X} = \text{Cl}, \text{Br}$) bond of benzylic halide in the presence of green LED visible light (530 nm) (**Scheme 1.5.1**).⁸⁰ Various substituted benzylic halides and styrene were used to synthesize the functionalized monoadducts (**Table 1.5.1**). No product was isolated in the absence of light or Cu(I) complex. When 1 mol% of $[\text{Cu}^{\text{I}}(\text{dap})_2\text{Cl}]$ was used during ATRA of *p*-nitrobenzyl bromide with styrene, 85% of yield was obtained in the presence of light. Similar transformations have also been successfully mediated by iridium complex, *fac*- $\text{Ir}(\text{ppy})_3$ ($\text{ppy} = 2$ -phenylpyridine) along with the electron rich species, triethyl amine, in the presence of visible light.⁸⁰ Another iridium complex, $[\text{Ir}(\text{ppy})_2(\text{dtbbpy})](\text{PF}_6)$ ($\text{dtbbpy} = 4,4'$ -di-*tert*-butyl-2,2'-bipyridyl)¹⁷¹ was successful in reproducing these results. However, a ruthenium based complex, $[\text{Ru}(\text{bpy})_3\text{Cl}_2]$ ($\text{bpy} = \text{bipyridine}$) produced a moderate yield of monoadduct (64 %) under same reaction conditions.¹⁷²



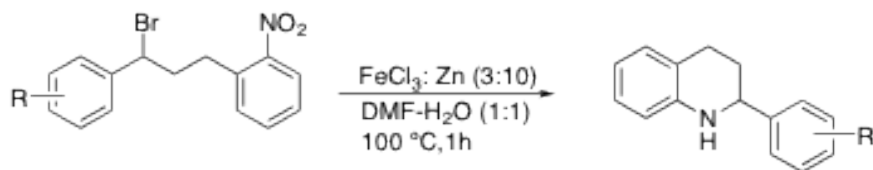
Scheme 1.5.1. Schematic representation for ATRA of *p*-nitrobenzyl bromide and styrene.⁸⁰

Table 1.5.1. ATRA reaction of *p*-nitrobenzyl bromide and styrene.⁸⁰

Entry	Catalyst	Yield ^[c]
1 ^[a]	$[\text{Cu}^{\text{I}}(\text{dap})_2\text{Cl}]$	60
2 ^[a]	$[\text{Cu}^{\text{I}}(\text{dap})_2\text{Cl}]$	85
3 ^[b]	$[\text{Cu}^{\text{I}}(\text{dap})_2\text{Cl}]$	85
4 ^[b]	$[\text{Ir}(\text{ppy})_2(\text{dtbbpy})](\text{PF}_6)$	85
5 ^[b]	$[\text{Ru}(\text{bpy})_3\text{Cl}_2]$	69
6 ^[b]	No catalyst	No reaction
7 ^[b]	No visible light	No reaction

^[a] Reaction Conditions: [*p*-nitrobenzyl bromide]: [styrene]:1:10; reaction was conducted for 24 h in dichloromethane (entry 1) and acetonitrile (entry 2) ^[b] [*p*-nitrobenzyl bromide]: [styrene]:1:5; reaction was conducted for 12 h in acetonitrile ^[c] Isolated yield after purification on silica gel.

Final product, monoadducts were isolated and used as precursors for the synthesis of tetrahydroquinoline, catalyzed by FeCl₃/Zn (3:10) (**Scheme 1.5.2** and **Table 1.5.2**). Tetrahydroquinolines are highly sought-after molecules and have been extensively used for synthesis of various drug molecules.¹⁷³⁻¹⁷⁸



Scheme 1.5.2. Synthesis of tetrahydroquinolines from the precursors synthesized via ATRA.

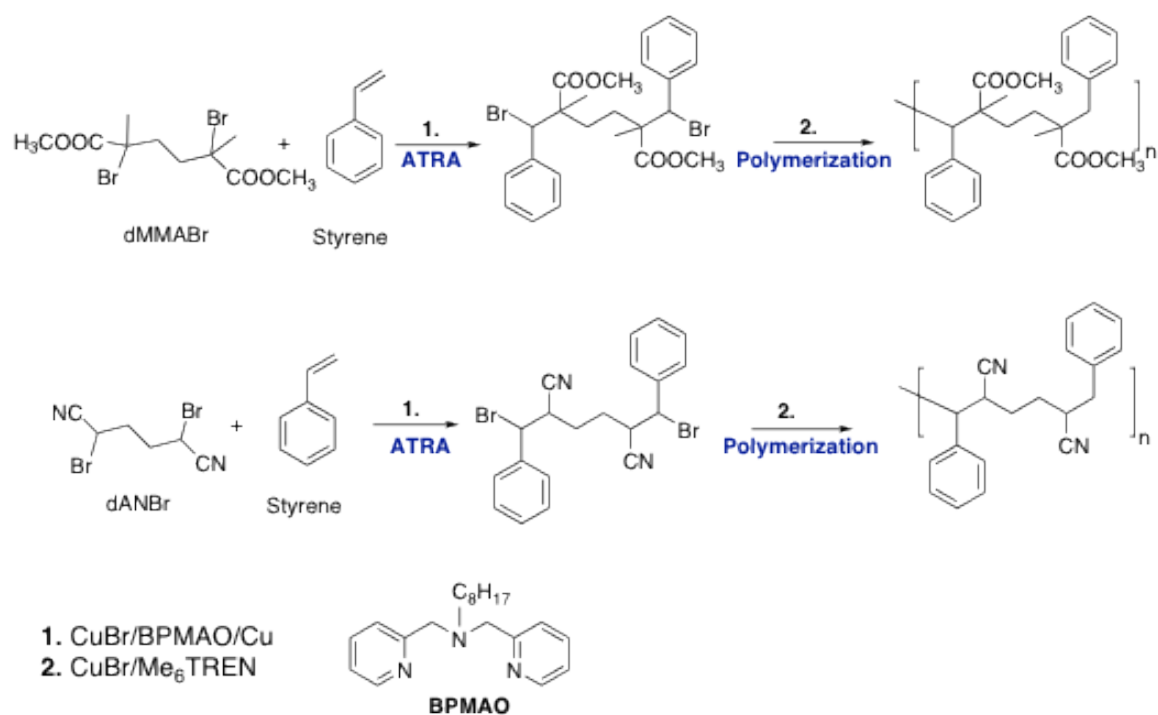
Table 1.5.2. Utilization of monoadduct for the synthesis of tetrahydroquinoline.⁸⁰

Entry	Monoadduct	Product	Yield ^(a)
1			75
2			72
3			70

^(a) Reaction conditions: Reaction was conducted in solvent= DMF:H₂O (1:1) at 100 °C for 1hr catalyzed by FeCl₃/Zn (3:10).

Monoadducts derived from ATRA and ATRC, contain halogen functionality and therefore, can be used as monomers or initiators for the polymerization. This synthetic route can prove to be highly advantageous as the properties of the polymers is dependent on the structure

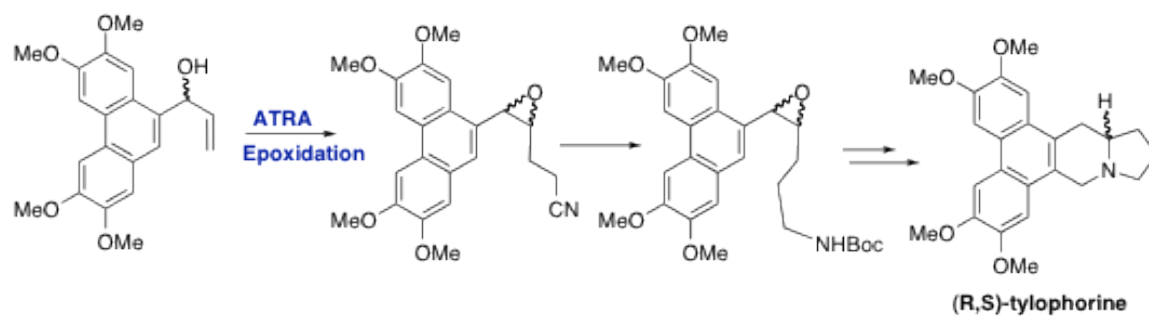
of the monomers. Chen-Li et. al. performed two step synthesis to control the polymerization and generate vinyl based copolymers with high molecular weight (**Scheme 1.5.3**).¹⁷⁹ In first step, ATRA was conducted on styrene with 2,5-dibromo-2,5-dimethylhexanedioate (dMMABr) and 2,5-dibromohexane dinitrile (dANBr), catalyzed by CuBr/BPMAO (BPMAO = *N,N*-bis(pyridin-2-ylmethyl)octan-1-amine) in the presence of Cu(0). In second step, the monoadduct was isolated to conduct polymerization in acetonitrile, catalyzed by Cu^IBr/Me₆TREN (**Scheme 1.5.3**).¹⁷⁹



Scheme 1.5.3. Synthesis of initiators for the polymerization using copper catalyzed ATRA (1) followed by ATRP (2).¹⁷⁹

The phenanthroindolizidine based alkaloid, (\pm)tylophorine is known to have anti-inflammatory and anti-tumor properties.^{178, 180} This compound is extracted from the plant, *Tylophora indica*. A number of synthetic approaches such as Friedel–Crafts-type acylation of an

aminoester,¹⁸¹ a 1,3-dipolar cycloaddition,¹⁸² *N*-acyldihydropyridones,¹⁸³ a nitrile stabilized ammonium ylide,¹⁸⁴ a Suzuki cross-coupling,¹⁸⁵ a palladium-catalyzed carboamination,¹⁸⁶⁻¹⁸⁸ a cobalt-catalyzed C–C bond formation,¹⁸⁸ or a free-radical cyclization⁸¹ have been used to synthesize this molecule in moderate yield. Recently, the (±)tylophorine was synthesized via ATRA as the key step in a good yield. The reaction was conducted on the allyl alcohol with idoacetonitrile in the presence of a radical initiator, lauroyl peroxide (**Scheme 1.5.4**). This step was followed by epoxidation via addition of 1,8-(diazabicyclo[5.4.0]undec-7-ene) (DBU). A good yield of epoxide (60%) was obtained followed by two more subsequent steps, a racemic mixture of (±)tylophorine was obtained.⁸¹



Scheme 1.5.4. Synthetic route for the synthesis of (±)tylophorine utilizing ATRA.⁸¹

These three examples highlighted the main uses of functionalized monoadducts obtained via ATRA and ATRC in natural product synthesis, pharmaceuticals as well as for materials.

1.6. Conclusion and Outlook

In conclusion, atom transfer radical processes are versatile tools to synthesize a range of small-functionalized molecules via ATRA and ATRC to polymers through ATRP. The copper

complexes with nitrogen-based ligands have proved to be the successful catalytic candidates for these processes. Different structural, kinetic and mechanistic studies have dramatically improved the efficiency and scope of these techniques. Along with these studies, ligand design and catalyst regeneration strategies have paved the way to make these processes atom-economical and environmentally friendly. The given examples have clearly demonstrated the synthetic utility in different areas, which might have implications in the research and industrial sectors.

References.

1. Ciampolini, M.; Nardi, N., Five-coordinated high-spin complexes of bivalent cobalt, nickel, and copper with tris(2-dimethylaminoethyl)amine. . *Inorg. Chem.* **1966**, *5*, (1), 41-44.
2. Sacconi, L.; Bertini, I., Five-Coordinate Nickel(II) Complexes with Nitrogen-Phosphorus and Nitrogen-Arsenic Tetradentate Ligands. *J. Am. Chem. Soc.* **1967**, *89*, (9), 2235-2236.
3. Di Vaira, M.; Orioli, P. L., Crystal structure of tris(2-dimethylaminoethyl)amine nickel(II) and copper(II) bromides. *Acta Cryst. Sec. B.* **1968**, *24*, (4), 595-599.
4. Mani, F.; Scapacci, G., Iron(II), cobalt(II) and nickel(II) complexes with the tripod ligand tris(3,5-dimethyl-1-pyrazolylmethyl)amine. Ferromagnetic exchange coupling in hexacoordinated dimeric nickel(II) complexes. . *Inorg. Chim. Acta* **1980**, *38*, (2), 151-155.
5. Ram, M. S.; Bakac, A.; Espenson, J. H., Free Radical Pathways to Alkyl Ccomplexes of a Nickel Tetraaza Macrocyclic. *Inorg. Chem.* **1986**, *25*, 3267-3272.
6. Grove, D. M.; van Koten, G.; Verschuuren, A. H. M., New Homogeneous Catalysts in the Addition of Polyhaloalkanes to Olefins; Organonickel(II) Complexes $[\text{Ni}\{\text{C}_6\text{H}_3(\text{CH}_2\text{NMe}_2)_{2-o,o'}\}\text{X}]$ (X = Chlorine, Bromine, Iodine). *J. Mol. Catal.* **1988**, *45*, 169-174.
7. Uegaki, H.; Kotani, Y.; Kamigaito, M.; Sawamoto, M., Nickel Mediated Living Radical Polymerization of Methyl Methacrylate. *Macromolecules* **1997**, *30*, (2249-2253).

8. van de Kuil, L. A.; Grove, D. M.; Gossage, R. A.; Zwikker, J. W.; Jenneskens, L. W.; Drenth, W.; van Koten, G., Mechanistic Aspects of the Kharasch Addition Reaction Catalyzed by Organonickel(II) Complexes Containing the Monoanionic Terdentate Aryldiamine Ligand System [C₆H₂(CH₂NMe₂)₂-2,6-R-4]-, *Organometallics* **1997**, *16*, (23), 4985-4994.
9. Gossage, R. A.; Van De Kuil, L. A.; Van Koten, G., Diaminoarylnickel(II) "Pincer" Complexes: Mechanistic Considerations in the Kharasch Addition Reaction, Controlled polymerization, and Dendrimeric Transition Metal Catalysts. *Acc. Chem. Res.* **1998**, *31*, (7), 423-431.
10. O. Fritsky, I.; Kozlowski, H.; J. Sadler, P.; P. Yefetova, O.; Swatek-Kozlowska, J.; A. Kalibabchuk, V.; Glowiak, T., Template synthesis of square-planar nickel(II) and copper(III) complexes based on hydrazide ligands. *Journal of the Chemical Society, Dalton Transactions* **1998**, (19), 3269-3274.
11. Kleij, A. W.; Gossage, R. A.; Gebbink, R. J. M.; Brinkmann, N.; Reijerse, E. J.; Kragl, U.; Lutz, M.; Spek, A. L.; van Koten, G., A "Dendritic Effect" in Homogeneous Catalysis with Carbosilane-Supported Arylnickel(II) Catalysts: Observation of Active-Site Proximity Effects in Atom-Transfer Radical Addition. *J. Am. Chem. Soc.* **2000**, *122*, (49), 12112-12124.
12. Kleij, A. W.; Gossage, R. A.; Jastrzebski, J. T. B. H.; Boersma, J.; van Koten, G., The "Dendritic Effect" in Homogeneous Catalysis with Carbosilane-Supported Arylnickel(II) Catalysts: Observation of Active-Site Proximity Effects in Atom-Transfer Radical Addition (p 176-178). *Angew. Chem. Int. Ed.* **2000**, *39*, (1), 176-178.
13. Yiunkin, T. R.; Connor, E. F.; Henderson, J. I.; Friedrich, S. K.; Grubbs, R. H.; Bansleben, D. A., Neutral, Single-Component Nickel(II) Polyolefin Catalysts that Tolerate Heteroatoms. *Science* **2000**, *287*, 460-462.
14. Schofield, M. H.; Halpern, J., Kinetics and Mechanism of Decomposition of Nickel Benzyl Complexes and Determination of Nickel Benzyl Bond Dissociation Energies. *Inorg. Chim. Acta* **2003**, *345*, 353-358.
15. Duquesne, E.; Habimana, J.; Degee, P.; Dubois, P., Nickel-Catalyzed Supported ATRP of Methyl Methacrylate Using Crosslinked Polystyrene Triphenylphosphine as Ligand. *Macromolecules* **2005**, *38*, (24), 9999-10006.

16. Yang, H.; Gao, H.; Wang, K.; Zhang, Z., Preparation, crystal structures and oxidation activity of two novel nickel(II) complexes of tripodal ligand containing coordinated solvent molecules. *Trans. Met. Chem.* **2006**, *31*, (7), 958-963.
17. Spasyuk, D. M.; Zargarian, D.; van der Est, A., New POCN-Type Pincer Complexes of Nickel(II) and Nickel(III). *Organometallics* **2009**, *28*, 6531-6540.
18. Eckenhoff, W. T.; Biernesser, A. B.; Pintauer, T., Structural characterization and investigation of iron(III) complexes with nitrogen and phosphorus based ligands in atom transfer radical addition (ATRA). *Inorganica Chimica Acta* **2012**, *382*, (0), 84-95.
19. Minisci, F.; Galli, R., Addition of N-Chloroamines to Styrene and Butadiene, Catalyzed by Iron and Copper Salts. *Chim. Ind. (Milan)* **1963**, *45*, (11), 1400-1401.
20. Brault, D.; Neta, P., Reactions of iron porphyrins with methyl radicals. *J. Am. Chem. Soc.* **1981**, *103*, (10), 2705-2710.
21. De Montellano, P. O.; Kunze, K. L.; Augusto, O., Hemoprotein Destruction. Iron-Nitrogen Shift of a Phenyl Group in a Porphyrin Complex. *J. Am. Chem. Soc.* **1982**, *104*, 3545-3546.
22. Ogoshi, H.; Sugimoto, H.; Yoshida, Z. I.; Kobayashi, Synthesis and Magnetic Properties of Aryliron(III) Complexes of Octaethylporphyrins. *J. Organomet. Chem.* **1982**, *234*, (2), 185-195.
23. Matsumoto, H.; Nakano, T.; Nagai, Y., Radical reactions in the coordination sphere. I. Addition of carbon tetrachloride and chloroform to 1-olefins catalyzed by ruthenium(II) complexes. *Tetrahedron Lett.* **1973**, (51), 5147-5150.
24. Matsumoto, H.; Nikaido, T.; Nagai, Y., Radical reactions in the Coordination Sphere. Reactions of Dichloro- and Trichloroacetic Acid Esters with 1-Olefins Catalyzed by Dichlorotris(triphenylphosphine)ruthenium(II). *J. Org. Chem.* **1976**, *41*, (2), 396-398.
25. Matsumoto, H.; Nakano, T.; Takasu, K.; Nagai, Y., Radical reactions in the coordination sphere. 4. Addition of carbon tetrachloride to cis-cyclooctene catalyzed by dichlorotris(triphenylphosphine)ruthenium(II). *J. Org. Chem.* **1978**, *43*, (9), 1734-1736.
26. Kamigata, N.; Sawada, H.; Kobayashi, M., Reactions of Arenesulfonyl Chlorides with Olefins Catalyzed by a Ruthenium(II) Complex. *J. Org. Chem.* **1983**, *48*, 3793-3796.

27. Nagashima, H.; Wakamatsu, H.; Itoh, K., A Novel Preparative Method for 1-Butyrolactams via Carbon-Carbon bond Formation: Copper or Ruthenium Catalyzed Cyclization of N-Allyl Trichloroacetimides. *J. Chem. Soc.* **1984**, (10), 652-653.
28. Nagashima, H.; Ara, K.; Wakamatsu, H.; Itoh, K., Stereoselective Preparation of Bicyclic Lactams by Copper or Ruthenium Catalyzed Cyclization of N-Allyltricholoacetamides: A Novel Entry to Pyrrolidine Alkaloid Skeletons. *Chem. Comm.* **1985**, (8), 518-519.
29. Ishibashi, H.; Nakatani, H.; Iwami, S.; Sato, T.; Nakamura, N.; Ikeda, M., Ruthenium~catalysed Atom-transfer Cyclisation of N-(Cyclohex-2-enyl)-a-chloro-a-(phenylthio)acetamides. A Formal Total Synthesis of (±)-Haemanthidine and (±)-Pretazettine *Chem. Comm.* **1989**, 1767-1769.
30. Ricardo, C.; Pintauer, T., Synthesis, characterization, and the role of counterion in cyclopropanation of styrene catalyzed by $[\text{Cu}^{\text{I}}(2,2'\text{-bpy})(\text{p-CH}_2=\text{CHC}_6\text{H}_5)][\text{A}]$ ($\text{A}=\text{ClO}_4^-$; PF_6^- and CF_3SO_3^- complexes. *J. Organomet. Chem.* **2007**, 692, 5165-5172.
31. Pintauer, T.; Eckenhoff, W. T.; Ricardo, C.; Balili, M. N. C.; Biernesser, A. B.; Noonan, S. T.; Taylor, M. J. W., Highly Efficient Ambient-Temperature Copper-Catalyzed Atom-Transfer Radical Addition (ATRA) in the Presence of Free-Radical Initiator (V-70) as a Reducing Agent *Chem. Eur. J.* **2009**, 15, (1), 38-41.
32. Pintauer, T.; Eckenhoff, W. T.; Ricardo, C.; Balili, M. N. C.; Biernesser, A. B.; Noonan, S. T.; Taylor, M. T., Highly Efficient Ambient-Temperature Copper-Catalyzed Atom-Transfer Radical Addition (ATRA) in the Presence of Free-Radical Initiator (V-70) as a Reducing Agent *Chem. Eur. J.* **2009**, 15, (1), 38-41.
33. Ricardo, C.; Pintauer, T., Copper catalyzed atom transfer radical cascade reactions in the presence of free-radical diazo initiators as reducing agents. *Chem. Comm.* **2009**, 21, 3029-3031.
34. Ricardo, C.; Pintauer, T., Copper catalyzed atom transfer radical cascade reactions in the presence of free-radical diazo initiators as reducing agents. *Chem. Comm.* **2009**, (21), 3029-3031.
35. Ricardo, C. L.; Pintauer, T., Synthesis of Functionalized Polytriazoles via One-Pot Sequential Copper-Catalyzed Azide-Alkyne [3+2] Cycloaddition and Atom Transfer Radical Addition (ATRA). *Isr. J. Chem.* **2012**, 52, (3-4), 320-327.

36. Magenau, A. J. D.; Kwak, Y.; Schröder, K.; Matyjaszewski, K., Highly Active Bipyridine-Based Ligands for Atom Transfer Radical Polymerization. *ACS Macro Letters* **2012**, *1*, (4), 508-512.
37. Kharasch, M. S.; Mayo, F. R., The Peroxide Effect in the Addition of Reagents to Unsaturated Compounds. I. The Addition of Hydrogen Bromide to Allyl Bromide. *J. Am. Chem. Soc.* **1933**, *55*, (6), 2468-2496.
38. Kharasch, M. S.; Engelmann, H.; Mayo, F. R., The Peroxide Effect in the Addition of Reagents to Unsaturated Compounds. XV. The Addition of Hydrogen Bromide to 1- and 2-Bromo- and Chloropropenes. *J. Org. Chem.* **1937**, *02*, (3), 288-302.
39. Kharasch, M. S.; Jensen, E. V.; Urry, W. H., Addition of Derivatives of Chlorinated Acetic Acid to Olefins. *J. Am. Chem. Soc.* **1945**, *67*, (9), 1626.
40. Kharasch, M. S.; Jensen, E. V.; Urry, W. H., Addition of Carbon Tetrachloride and Chloroform to Olefins. *Science* **1945**, *102*, (2640), 128.
41. Kharasch, M. S.; Jensen, E. V.; Urry, W. H., Addition of Carbon Tetrabromide and Bromoform to Olefins. *J. Am. Chem. Soc.* **1946**, *68*, (1), 154-155.
42. Kharasch, M. S.; Jensen, E. V.; Urry, W. H., Reactions of atoms and free radicals in solution. X. The addition of polyhalomethanes to olefins. *J. Am. Chem. Soc.* **1947**, *69*, (5), 1100-1105.
43. Kharasch, M. S.; Skell, P. S.; Fisher, P., Reactions of Atoms and Free Radicals in Solution. XII. The Addition of Bromo Esters to Olefins. *J. Am. Chem. Soc.* **1948**, *70*, (3), 1055-1059.
44. Lee, G. M.; Parvez, M.; Weinreb, S. M., Intramolecular metal catalyzed kharasch cyclizations of olefinic α -halo esters and acids. *Tetrahedron* **1988**, *44*, (15), 4671-4678.
45. De Malde, M.; Minisci, F.; Pallini, U.; Volterra, E.; Quilico, A., Reactions between acrylonitriles and aliphatic halogen derivatives. *Chim. Ind. (Milan)* **1956**, *38*, 371-382.
46. Minisci, F., Radical Reactions in Solution. Dipolar Character of Free Radicals from Decomposition of Organic Peroxides. *Gazz. Chim. Ital.* **1961**, *91*, 386-389.

47. Minisci, F.; Pallini, U., Radical Reactions in Solution. Haloalkylation of Acrylic Acid Derivatives. *Gazz. Chim. Ital.* **1961**, *91*, 1030-1036.
48. Minisci, F.; Galli, R., Influence of the Electrophilic Character on the Reactivity of Free Radicals in Solution. Reactivity of Alkoxy, Hydroxy, Alkyl, and Azido Radicals in the Presence of Olefins. *Tetrahedron Lett.* **1962**, *12*, 533-538.
49. Minisci, F.; Cecere, M.; Galli, R., Oxidation of Carbon Free Radicals in the Presence of Cu and Fe Salts. New Synthesis of Nitro Derivatives and Nitric Esters. *Gazz. Chim. Ital.* **1963**, *93*, 1288-1294.
50. Murai, S.; Sonoda, N.; Tsutsumi, S., Copper Salts Induced Addition of Ethyl Trichloroacetate to Olefins. *J. Org. Chem.* **1964**, *31*, (9), 3000-3003.
51. Eckenhoff, W. T.; Pintauer, T., Atom Transfer Radical Addition in the Presence of Catalytic Amounts of Copper(I/II) Complexes with Tris(2-pyridylmethyl)amine *Inorg. Chem.* **2007**, *46*, (15), 5844-5846.
52. Eckenhoff, W. T.; Garrity, S. T.; Pintauer, T., Highly Efficient Copper-Mediated Atom Transfer Radical Addition (ATRA) in the Presence of a Reducing Agent. *Eur. J. Inorg. Chem.* **2008**, *2008*, (4), 563-571.
53. Simal, F.; Demonceau, A.; Noels, A. F., Kharasch Addition and Controlled Atom Transfer Radical Polymerisation (ATRP) of Vinyl Monomers Catalyzed by Grubbs' Ruthenium-Carbene Complexes. *Tetrahedron Lett.* **1999**, *40*, (31), 5689-5693.
54. Simal, F.; Sebille, S.; Demonceau, A.; Noels, A. F.; Nunez, R.; Abad, M.; Teixidor, F.; Vinas, C., Radical Reactions Catalyzed by Ruthenium(II) Complexes with Anionic Carborane Phosphine Ligands: Kharasch Addition to Olefins and Controlled Polymerisation. *Tetrahedron Lett.* **2000**, *41*, (28), 5347-5351.
55. Tutusaus, O.; Delfosse, S.; Demonceau, A.; Noels, A. F.; Vinas, C.; Teixidor, F., Kharasch Addition Catalysed by Half-Sandwich Ruthenium Complexes. Enhanced Activity of Ruthenacarboranes. *Tetrahedron Lett.* **2003**, *44*, 8421-8425.
56. Motoyama, Y.; Gondo, M.; Masuda, S.; Iwashita, Y.; Nagashima, H., A Cationic Diruthenium Amidinate, $[(\eta^5\text{-C}_5\text{Me}_5)\text{Ru}(\mu_2\text{-i-PrN=C(Me)Ni-Pr})\text{Ru}(\eta^5\text{-C}_5\text{Me}_5)]^+$, as an Efficient Catalyst for the Atom-Transfer Radical Reactions. *Chem. Lett.* **2004**, *33*, 442-443.

57. Nagashima, H., Ruthenium in Organic Synthesis. In *Ruthenium in Organic Synthesis*, Murahashi, S.-I., Ed. Wiley-VCH: Weinheim, 2004; pp 333-343.
58. Motoyama, Y.; Hanada, S.; Niibayashi, S.; Shimamoto, K.; Takaoka, K.; Nagashima, H., Atom-transfer radical reactions catalyzed by a coordinatively unsaturated diruthenium amidinate, $[(\eta^5\text{-C}_5\text{Me}_5)\text{Ru}(\mu_2\text{-i-PrN double bond; length as m-dashC(Me)Ni-Pr})\text{Ru}(\eta^5\text{-C}_5\text{Me}_5)]^+$. *Tetrahedron* **2005**, *61*, (10216), 10216-10226.
59. Quebatte, L.; Solai, E.; Scopelliti, R.; Severin, K., A Bimetallic Ruthenium Ethylene Complex as a Catalyst Precursor for the Kharasch Reaction. *Organometallics* **2005**, *24*, (7), 1404-1406.
60. Seigal, B. A.; Fajardo, C.; Snapper, M. L., Tandem Catalysis: Generating Multiple Contiguous Carbon-Carbon Bonds through a Ruthenium-Catalyzed Ring-Closing Metathesis/Kharasch Addition. *J. Am. Chem. Soc.* **2005**, *127*, (46), 16329-16332.
61. Seigal, B. A.; Fajardo, C.; Snapper, M. L., Tandem Catalysis: Generating Multiple Contiguous Carbon-Carbon Bonds through a Ruthenium-Catalyzed Ring-Closing Metathesis/Kharasch Addition. *J. Am. Chem. Soc.* **2005**, *127*, (46), 16329-16332.
62. Severin, K., Ruthenium Catalysts for the Kharasch Reaction. *Curr. Org. Chem.* **2006**, *10*, 217-224.
63. Borguet, Y.; Richel, A.; Delfosse, S.; Leclerc, A.; Delaude, L.; Demonceau, A., Microwave-Enhanced Ruthenium-Catalysed Atom Transfer Radical Additions. *Tetrahedron Lett.* **2007**, *48*, 6334-6338.
64. Minisci, F., Free-Radical Additions to Olefins in the Presence of Redox Systems. *Acc. Chem. Res.* **1975**, *8*, (5), 165-171.
65. Eckenhoff, W. T.; Pintauer, T., Copper Catalyzed Atom Transfer Radical Addition (ATRA) and Cyclization (ATRC) Reactions in the Presence of Reducing Agents. *Cat. Rev. - Sci. Eng.* **2009**, *51*, 1-59.
66. Pintauer, T., "Greening" of copper catalyzed atom transfer radical addition (ATRA) and cyclization (ATRC) reactions. *ACS Symposium Series* **2009**, *1023*, 63-84.
67. Giese, B., Syntheses with radicals. Carbon-carbon coupling via organotin and -mercury compounds. *Angew. Chem. Int. Ed.* **1985**, *97*, (7), 555-567.

68. Giese, B.; Kopping, B.; Chatgililoglu, C., Tris(trimethylsilyl)silane as mediator in organic synthesis via radicals. *Tet. Lett.* **1989**, *30*, (6), 681-684.
69. Pintauer, T., Catalyst Regeneration in Transition-Metal-Mediated Atom-Transfer Radical Addition (ATRA) and Cyclization (ATRC) Reactions *Eur. J. Inorg. Chem.* **2010**, *17*, 2449-2460.
70. Curran, D. P., The Design and Application of Free Radical Chain Reactions in Organic Synthesis. Part 2. *Synthesis* **1988**, (7), 489-513.
71. Curran, D. P., The Design and Application of Free Radical Chain Reactions in Organic Synthesis. Part 1. *Synthesis* **1988**, (6), 417-439.
72. Balog, A.; Curran, D. P., Ring-Enlarging Annulations. A One-Step Conversion of Cyclic Silyl Acyloins and ω -Alkynyl Acetals to Polycyclic Enediones. *J. Org. Chem.* **1995**, *60*, 337-344.
73. Curran, D. P., *Comprehensive Organic Synthesis*. Pergamon: New York, 1992; p 715.
74. Curran, D. P.; Chen, M., *Tetrahedron Lett.* **1985**, *26*, 4991.
75. Curran, D. P.; Chen, M.-H., Radical-initiated polyolefinic cyclizations in condensed cyclopentanoid synthesis. Total synthesis of (\pm)- C_{19} (12)-capnellene. *Tetrahedron Letters* **1985**, *26*, (41), 4991-4994.
76. Curran, D. P.; Pakiewicz, D. M., Radical-Initiated Polyolefinic Cyclizations in Linear Triquinane Synthesis. Model Studies and Total Synthesis of (\pm)-Hirsutene. *Tetrahedron* **1985**, *41*, 3943-3958.
77. Curran, D. P.; Seong, C. M., Atom Transfer Addition and Annulation Reactions of Propargyldomalnonitrile. *Tetrahedron* **1992**, *48*, 2157-2174.
78. Jasperse, C. P.; Curran, D. P.; Fevig, T. L., Radical Reactions in Natural Product Synthesis. *Chem. Rev.* **1991**, *91*, 1237-1286.
79. Bernhardt, P. V., N-methylation of diamino-substituted macrocyclic complexes: intermolecular reactions. *Journal of the Chemical Society, Dalton Trans.* **1996**, (23), 4319-4324.

80. Laurent, B. A.; Grayson, S. M., An Efficient Route to Well-Defined Macrocyclic Polymers via "Click" Cyclization. *J. Am. Chem. Soc.* **2006**, *128*, (13), 4238-4239.
81. Paria, S.; Pirtsch, M.; Kais, V.; Reiser, O., Visible-Light-Induced Intermolecular Atom-Transfer Radical Addition of Benzyl Halides to Olefins: Facile Synthesis of Tetrahydroquinolines. *Synthesis* **2013**, *45*, (19), 2689-2698.
82. Ble-Gonzalez, E. A.; Porcel, S.; Cordero-Vargas, A., A Formal Synthesis of (\mp)-Tylophorine Based on an Atom Transfer Radical Addition Reaction. *Synlett* **2013**, *24*, (16), 2073-2076.
83. Wang, J.-S.; Matyjaszewski, K., Controlled/"living" radical polymerization. atom transfer radical polymerization in the presence of transition-metal complexes. *J. Am. Chem. Soc.* **1995**, *117*, (20), 5614-5615.
84. Wang, J. S.; Matyjaszewski, K., Controlled/"Living" Radical Polymerization. Atom Transfer Radical Polymerization in the Presence of Transition-Metal Complexes. *J. Am. Chem. Soc.* **1995**, *117*, (20), 5614-5615.
85. Wang, J. S.; Matyjaszewski, K., "Living"/Controlled Radical Polymerization. Transition-Metal-Catalyzed Atom Transfer Radical Polymerization in the Presence of a Conventional Radical Initiator. *Macromolecules* **1995**, *28*, (22), 7572-7573.
86. Wang, J. S.; Matyjaszewski, K., Controlled/"Living" Radical Polymerization. Halogen Atom Transfer Radical Polymerization Promoted by a Cu(I)/Cu(II) Redox Process. *Macromolecules* **1995**, *28*, (23), 7901-7910.
87. Kato, M.; Kamigaito, M.; Sawamoto, M.; Higashimura, T., Polymerization of Methyl Methacrylate with the Carbon Tetrachloride/Dichlorotris-(triphenylphosphine)ruthenium(II)/Methylaluminum Bis(2,6-di-tert-butylphenoxide) Initiating System: Possibility of Living Radical Polymerization. *Macromolecules* **1995**, *28*, (5), 1721-1723.
88. Ohno, K.; Goto, A.; Fukuda, T.; Xia, J.; Matyjaszewski, K., Kinetic Studies on the Activation Process in an ATRP. *Macromolecules* **1998**, *31*, 2699-2701.
89. Coessens, V.; Matyjaszewski, K., End Group Transformation of Polymers Prepared by ATRP, Substitutions to Azides. *J.M.S. Pure Appl. Chem.* **1999**, *A36*, (5&6), 667-679.

90. Kickelbick, G.; Matyjaszewski, K., 4,4',4''-Tris(5-nonyl)-2,2':6',2''-terpyridine as Ligand in Atom Transfer Radical Polymerization (ATRP). *Macromol. Rapid Commun.* **1999**, *20*, 341-346.
91. Gobelt, B.; Matyjaszewski, K., Diimino- and diaminopyridine complexes of CuBr and FeBr₂ as catalysts in atom transfer radical polymerization (ATRP) *Macromol. Chem. Phys.* **2000**, *201*, 1619-1624.
92. Matyjaszewski, K., *Controlled/Living Radical Polymerization. Progress in ATRP, NMP and RAFT*. ACS: Washington, DC., 2000; Vol. 768, p 484.
93. Matyjaszewski, K.; Gobelt, B.; Paik, H. J.; Horwitz, C. P., Tridentate Nitrogen-Based Ligands in Cu-Based ATRP: A Structure-Activity Study. *Macromolecules* **2001**, *34*, (3), 430-440.
94. Gromada, J.; Matyjaszewski, K., Measurement of Initial Degree of Polymerization without Reactivation as a New Method To Estimate Rate Constants of Deactivation in ATRP *Macromolecules* **2002**, *35*, 6167-6173.
95. Matyjaszewski, K., From Atom Transfer Radical Addition to Atom Transfer Radical Polymerization. *Curr. Org. Chem.* **2002**, *6*, (2), 67-82.
96. Min, K.; Gao, H.; Matyjaszewski, K., Preparation of Homopolymers and Block Copolymers in Miniemulsion by ATRP Using Activators Generated by Electron Transfer. *J. Am. Chem. Soc.* **2005**, *127*, 3825-3830.
97. Sumerlin, B. S.; Tsarevsky, N. V.; Louche, G.; Lee, R. Y.; Matyjaszewski, K., Highly efficient "click" functionalization of poly (3-azidopropyl methacrylate) prepared by ATRP. *Macromolecules* **2005**, *38*, (18), 7540-7545.
98. Golas, P. L.; Tsarevsky, N. V.; Sumerlin, B. S.; Matyjaszewski, K., Catalyst Performance in Click Coupling Reactions of Polymers Prepared by ATRP: Ligand and Metal Effects. *Macromolecules* **2006**, *39*, (19), 6451-6457.
99. Min, K.; Jakubowski, W.; Matyjaszewski, K., AGET ATRP in the Presence of Air in Miniemulsion and in Bulk. *Macromol. Rapid Commun.* **2006**, *27*, (8), 594-598.

100. Oh, J. K.; Tang, C.; Gao, H.; Tsarevsky, N. V.; Matyjaszewski, K., Inverse Miniemulsion ATRP: A New Method for Synthesis and Functionalization of Well-Defined Water-Soluble/Crosslinked Polymeric Particles. *J. Am. Chem. Soc.* **2006**, *128*, 5578-5584.
101. Tang, W.; Matyjaszewski, K., Effect of Ligand Structure on Activation Rate Constants in ATRP. *Macromolecules* **2006**, *39*, (15), 4953-4959.
102. Tsarevsky, N. V.; Braunecker, W. A.; Samuel, J. B.; Matyjaszewski, K., Rational Selection of Initiating/Catalytic Systems for the Copper Mediated Atom Transfer Radical Polymerization of Basic Monomers in Protic Media: ATRP of 4-Vinylpyridine. *Macromolecules* **2006**, *39*, (20), 6817-6824.
103. Tsarevsky, N. V.; Braunecker, W. A.; Tang, W.; Brook, S. J.; Matyjaszewski, K.; Weismann, G. R., Copper Based ATRP Catalysts of Very High Activity Derived from Dimethyl Crossbridged Cyclam. *J. Mol. Catal. A: Chem* **2006**, *257*, 132-140.
104. Golas, P., L.; Matyjaszewski, K., Click Chemistry and ATRP: A Beneficial Union for the Preparation of Functional Materials. *QSAR Comb. Sci.* **2007**, *26*, (11-12), 1116-1134.
105. Matyjaszewski, K.; Dong, H.; Jakubowski, W.; Pietrasik, J.; Kusumo, A., Grafting from Surfaces for "Everyone": ARGET ATRP in the Presence of Air. *Langmuir* **2007**, *23*, (8), 4528-4531.
106. Min, K.; Gao, H.; Matyjaszewski, K., Use of Ascorbic Acid as Reducing Agent for Synthesis of Well-Defined Polymers by ARGET ATRP. *Macromolecules* **2007**, *40*, 1789-1791.
107. Mueller, L.; Jakubowski, W.; Tang, W.; Matyjaszewski, K., Successful Chain Extension of Polyacrylate and Polystyrene Macroinitiators with Methacrylates in an ARGET and ICAR ATRP. *Macromolecules* **2007**, *40*, (18), 6464-6472.
108. Rosen, B. M.; Percec, V., A Density Functional Theory Computational Study of the Role of Ligand on the Stability of CuI and CuII Species Associated with ATRP and SET-LRP. *J. Polym. Sci. Part A: Polym. Chem.* **2007**, *45*, 4950.
109. Tang, W.; Matyjaszewski, K., Effects of Initiator Structure on Activation Rate Constants in ATRP. *Macromolecules* **2007**, *40*, (6), 1858-1863.

110. Tsarevsky, N.; Braunecker, W. A.; Vacca, A.; Gans, P.; Matyjaszewski, K., Competitive Equilibria in Atom Transfer Radical Polymerization. *Macromol. Symp.* **2007**, *248*, 60-70.
111. Chan, N.; Cunningham, M. F.; Hutchinson, R. A., ARGET ATRP of Methacrylates and Acrylates with Stoichiometric Ratios of Ligand to Copper. *Macromol. Chem. Phys.* **2008**, *209*, (17), 1797-1805.
112. Munoz-Bonilla, A.; Haddleton, D. M.; Cerrada, M. L.; Fernandez-Garcia, M., Synthesis of Poly(di[methylamine]ethyl methacrylate)-b-poly(cyclohexyl methacrylate)-b-poly(di[methylamine] ethyl methacrylate) Amphiphilic Triblock Copolymers by ATRP: Condensed-Phase and Solution Properties. *J. Polym. Sci. Part A: Polym. Chem.* **2008**, *46*, (1).
113. Pintauer, T.; Matyjaszewski, K., Structural and Mechanistic Aspects of Copper Catalyzed Atom Transfer Radical Polymerization. *Top. Organomet. Chem.* **2009**, *26*, 221-251.
114. Pintauer, T.; McKenzie, B.; Matyjaszewski, K., Toward structural and mechanistic understanding of transition metal-catalyzed atom transfer radical processes. *ACS Symp. Ser.* **2003**, *854*, 130-147.
115. Matyjaszewski, K.; Sumerlin, B.; Tsarevsk, V. N., Progress in Controlled Radical Polymerization: Materials and Applications. *American Chemical Society, D.C.* **2012**, ISBN: 978-0-8412-2756-9.
116. Taylor, M. J. W.; Eckenhoff, W. T.; Pintauer, T., Copper-catalyzed atom transfer radical addition (ATRA) and cyclization (ATRC) reactions in the presence of environmentally benign ascorbic acid as a reducing agent. *Dalton Trans.* **2010**, *39*, (47), 11475-11482.
117. Paterson, S. M.; Brown, D. H.; Chirila, T. V.; Keen, I.; Whittaker, A. K.; Baker, M. V., The synthesis of water-soluble PHEMA via ARGET ATRP in protic media *J. Polym. Sci. A: Polym. Chem.* **2010**, *48*, (18), 4084-4092.
118. Pintauer, T.; Matyjaszewski, K., Atom transfer radical addition and polymerization reactions catalyzed by ppm amounts of copper complexes. *Chem. Soc. Rev.* **2008**, *37*, (6), 1087-1097.
119. Clark, A. J.; Filik, R. P.; Haddleton, D. M.; Radigue, A.; Sanders, C. J., Solid Supported Catalysts for Atom Transfer Radical Cyclization of 2-Haloacetamides. *J. Org. Chem.* **1999**, *64*, (24), 8954-8957.

120. Clark, A. J.; Geden, J. V.; Thom, S., Solid Support Copper Catalysts for Atom Transfer Radical Cyclizations: Assessment of Support Type and Ligand Structure on Catalyst Performance in the Synthesis of Nitrogen Heterocycles. *J. Org. Chem.* **2006**, *71*, (4), 1471-1479.
121. Konak, C.; Ganchev, B.; Teodorescu, M.; Matyjaszewski, K.; Kopeckova, P.; Kopecek, J., Poly[N-(2-hydroxypropyl)methacrylamide-block-n-butyl acrylate] micelles in water/DMF mixed solvents. *Polymer* **2002**, *43*, (13), 3735-3741.
122. Tsarevsky, N. V.; Matyjaszewski, K., "Green" Atom Transfer Radical Polymerization: From Process Design to Preparation of Well-Defined Environmentally Friendly Polymeric Materials. *Chem. Rev.* **2007**, *107*, (6), 2270-2299.
123. Kickelbick, G.; Paik, H.-j.; Matyjaszewski, K., Immobilization of the Copper Catalyst in Atom Transfer Radical Polymerization. *Macromolecules* **1999**, *32*, (9), 2941-2947.
124. Haddleton, D. M.; Duncalf, D. J.; Kukulj, D.; Radigue, A. P., 3-Aminopropyl Silica Supported Living Radical Polymerization of Methyl Methacrylate: Dichlorotris(triphenylphosphine)ruthenium(II) Mediated Atom Transfer Polymerization *Macromolecules* **1999**, *32*, 4769-4775.
125. Shen, Y.; Zhu, S.; Zeng, F.; Pelton, R. H., Supported Atom Transfer Radical Polymerization of Methyl Methacrylate Mediated by CuBr-Tetraethyl Diethylenetriamine Grafted onto Silica Gel. *J. Polym. Sci. Part A: Polym. Chem.* **2001**, *39*, 1051-1059.
126. Shen, Y.; Zhu, S.; Pelton, R. H., Packed Column Reactor for Continuous Atom Transfer Radical Polymerization: Methyl Methacrylate Polymerization Using Silica Gel Supported Catalyst. *Macromol. Rapid Commun.* **2000**, *21*, 956-959.
127. Sasaki, T.; Zhong, C.; Tada, M.; Iwasawa, Y., Immobilized Metal Ion-Containing Ionic Liquids: Preparation, Structure, and Catalytic Performance in Kharasch Addition Reaction. *Chem. Comm.* **2005**, *19*, 2506-2508.
128. Joo, F.; Toth, Z., Catalysis by Water-Soluble Phosphine Complexes of Transition Metal Ions in Aqueous and Two-Phase Media. *J. Mol. Cat.* **1980**, *8*, 369-383.
129. Herrmann, W. A.; Kohlpaintner, C. W., Water-Soluble Ligands, Metal Complexes, and Catalysts: Synergism of Homogeneous and Heterogeneous Catalysis. *Angew. Chem. Int. Ed.* **1993**, *32*, (11), 1524-1544.

130. Horvath, I. T.; Rabai, J., Facile Catalyst Separation Without Water: Fluorous Biphasic Hydroformylation of Olefins. *Science* **1994**, *266*, (5182), 72-75.
131. Haddleton, D. M.; Jackson, S. G.; Bon, S. A. F., Copper(I)-Mediated Living Radical Polymerization under Fluorous Biphasic Conditions. *J. Am. Chem. Soc.* **2000**, *122*, 1542.
132. Matyjaszewski, K.; Jakubowski, W.; Min, K.; Tang, W.; Huang, J.; Braunecker, W.; Tsarevsky, N., Diminishing Catalyst Concentration in Atom Transfer Radical Polymerization with Reducing Agents. *Proc. Nat. Acad. Sci.* **2006**, *103*, (42), 15309-15314.
133. Thommes, K.; Icli, B.; Scopelliti, R.; Severin, K., Atom Transfer Radical Addition (ATRA) and Cyclization (ATRC) Reactions Catalyzed by a Mixture of [RuCl₂Cp*(PPh₃)] and Magnesium. *Chem. Eur. J.* **2007**, *13*, (24), 6899-6907.
134. Balili, M. N. C.; Pintauer, T., Photoinitiated ambient temperature copper-catalyzed atom transfer radical addition (ATRA) and cyclization (ATRC) reactions in the presence of free-radical diazo initiator (AIBN). *Dalton Transactions* **2011**, *40*, (12), 3060-3066.
135. Clark, A. J.; Wilson, P., Copper mediated atom transfer radical cyclisations with AIBN. *Tetrahedron Lett.* **2008**, *49*, 4848-4850.
136. Eckenhoff, W. T.; Pintauer, T., Atom transfer radical addition (ATRA) catalyzed by copper complexes with tris[2-(dimethylamino)ethyl]amine (Me₆TREN) ligand in the presence of free-radical diazo initiator AIBN. *Dalton Transactions* **2011**, *40*, (18), 4909-4917.
137. Eckenhoff, W. T.; Pintauer, T., New Tetradentate Ligand Tris-((3,5-Dimethyl-1H-pyrazol-1-yl)methyl)amine (TDPMA) for Atom Transfer Radical Addition (ATRA) *Polym. Prepr. (Am. Chem. Soc. Div. Polym. Chem.)* **2008**, *49*, (2), 213-214.
138. Balili, M. N. C.; Pintauer, T., Persistent Radical Effect in Action: Kinetic Studies of Copper-Catalyzed Atom Transfer Radical Addition in the Presence of Free-Radical Diazo Initiators as Reducing Agents. *Inorg. Chem.* **2009**, *48*, (18), 9018-9026.
139. Balili, M. N. C.; Pintauer, T., Kinetic Studies of the Initiation Step in Copper Catalyzed Atom Transfer Radical Addition (ATRA) in the Presence of Free Radical Diazo Initiators as Reducing Agents *Inorg. Chem.* **2010**, *49*, (12), 5642-5649.

140. Eckenhoff, W. T.; Pintauer, T., Copper Catalyzed Atom Transfer Radical Addition (ATRA) and Cyclization (ATRC) Reactions in the Presence of Reducing Agents. *Cat. Rev. Sci. Eng.* **2010**, *51*, (1), 1-59.
141. Munoz-Molina, J. M.; Belderrain, T. R.; Perez, P. J., An Efficient, Selective, and Reducing Agent-Free Copper Catalyst for the Atom-Transfer Radical Addition of Halo Compounds to Activated Olefins *Inorg. Chem.* **2010**, *49*, (2), 642-645.
142. Bull, J. A.; Hutchings, M. G.; Luján, C.; Quayle, P., New Reactivity Patterns of Copper(I) and Other Transition Metal NHC Complexes: Application to ATRC and Related Reactions *Tet. Lett.* **2008**, *49*, (8), 1352-1356.
143. Forti, L.; Ghelfi, F.; Pagnoni, U. M., Fe⁰ Initiated Halogen Atom Transfer Radical Addition of Methyl 2-Br-2-Cl-Carboxylates to Olefins. *Tetrahedron Lett.* **1996**, *37*, (12), 2077-2078.
144. Caronna, T.; Citterio, A.; Ghirardini, M.; Minisci, F., Nucleophilic Character of Alkyl Radicals. XIII. Absolute Rate Constants for the Addition of Alkyl Radicals to Acrylonitrile and Methyl Acrylate. *Tetrahedron* **1977**, *33*, 793-796.
145. Miniote, H. G.; Hubert, A. J.; Teyssie, P., The Role of Copper(I) Complexes in the Selective Formation of Oxazoles from Unsaturated Nitriles and Diazoesters. *J. Organomet. Chem.* **1975**, *88*, 115-120.
146. Julia, M.; Sasussine, L.; Thuillier, G. I., Addition du Chloroacetate de Methyle sur les Olefines. *J. Organomet. Chem.* **1979**, *174*, 359-366.
147. Fabre, J. L.; Julia, M.; Mansour, B.; Saussine, L., Addition en Catalyse Redox D'Halogenures Benzyliques sur les Double Liaisons. *J. Organomet. Chem.* **1979**, *177*, 221-229.
148. Steiner, E.; Martin, P.; Bellius, D., Metal-Catalyzed Radical Addition of Polyhalogenated Compounds to Olefins. Part 2. A New Simple Synthesis of 2,3,5-Trichloropyridine. *Helv. Chim. Acta* **1982**, *65*, 983-985.
149. Pierre, M.; Eginhard, S.; Streith, J.; Winkler, T.; Bellus, D., Metal-Catalyzed Additions of Organic Polyhalides to Olefins. 4. Convenient Approaches to Heterocycles via Copper-Catalyzed Additions of Organic Polyhalides to Activated Olefins. *Tetrahedron* **1985**, *41*, (19), 4057-4078.

150. Asscher, M.; Vosfsi, D., Chlorine Activation by Redox-transfer. Part I. The Reaction Between Aliphatic Amines and Carbon Tetrachloride. *J. Chem. Soc.* **1961**, 2261-2264.
151. Sinnreich, J.; Asscher, M., Redox-Transfer. VII. Addition of Ethylene and Butadiene to Functionally Substituted Aromatic Sulfonyl Chlorides. *J. Chem. Soc. Perkin Trans. 1*, **1972**, 1, 1543-1545.
152. Amiel, Y., The Thermal and the Copper-Catalyzed Addition of Sulfonyl Bromides to Phenylacetylene. *J. Org. Chem.* **1974**, *39*, 3867-3870.
153. Truce, W. E.; Wolf, G. C., Adducts of Sulfonyl Iodides with Acetylenes. *J. Org. Chem.* **1971**, *36*, 1727-1732.
154. Eckenhoff, W. T.; Pintauer, T., Structural Comparison of Copper(I) and Copper(II) Complexes with Tris(2-pyridylmethyl)amine Ligand in Atom Transfer Radical Addition. *Inorg. Chem.* **2010**, *49*, (22), 10617-10626.
155. Kickelbick, G.; Pintauer, T.; Matyjaszewski, K., Structural comparison of CuII complexes in atom transfer radical polymerization. *New J. Chem.* **2002**, *26*, (4), 462-468.
156. Pintauer, T.; Zhou, P.; Matyjaszewski, K., General Method for Determination of the Activation, Deactivation, and Initiation Rate Constants in Transition Metal Catalyzed Atom Transfer Radical Processes. *J. Am. Chem. Soc.* **2002**, *124*, 8196-8197.
157. Cohen, N. A.; Tillman, E. S.; Thakur, S.; Smith, J. R.; Eckenhoff, W. T.; Pintauer, T., Effect of the Ligand in Atom Transfer Radical Polymerization Reactions Initiated by Photodimers of 9-bromoanthracene. *Macromol. Chem. Phys.* **2009**, *210*, (3-4), 263-268.
158. Pintauer, T.; Matyjaszewski, K., Structural Aspects of Copper Catalyzed Atom Transfer Radical Polymerization. *Coord. Chem. Rev.* **2005**, *249*, ((11-12)), 1155-1184.
159. Pintauer, T.; Braunecker, W. A.; Collange, E.; Poli, R.; Matyjaszewski, K., Determination of Rate Constants for the Activation Step in Atom Transfer Radical Polymerization Using the Stopped-Flow Technique. *Macromolecules* **2004**, *37*, 2679-2682.
160. Matyjaszewski, K.; Paik, H.; Zhou, P.; Diamanti, S. J., Determination of Activation and Deactivation Rate Constants of Model Compounds in Atom Transfer Radical Polymerization. *Macromolecules* **2001**, *34*, (15), 5125-5131.

161. Eckenhoff, W. T.; Pintauer, T., Structural Comparison of Copper(i) Complexes with Tris(2-pyridylmethyl)amine in Atom Transfer Radical Addition (ATRA). *Polym. Prepr. (Am. Chem. Soc. Div. Polym. Chem.)* **2008**, *49*, (2), 282-283.
162. Eckenhoff, W. T.; Biernesser, A. B.; Pintauer, T., Kinetic and Mechanistic Aspects of Atom Transfer Radical Addition (ATRA) Catalyzed by Copper Complexes with Tris(2-pyridylmethyl)amine. *Inorg. Chem.* **2012**, *51*, (21), 11917-11929.
163. Queffelec, J.; Gaynor, S. G.; Matyjaszewski, K., Optimization of Atom Transfer Radical Polymerization Using Cu(I)/Tris(2-(dimethylamino)ethyl)amine as a Catalyst. *Macromolecules* **2000**, *33*, (23), 8629-8639.
164. Wurtele, C.; Sander, O.; Lutz, V.; Waitz, T.; Tucek, F.; Schindler, S., Aliphatic C-H Bond Oxidation of Toluene Using Copper Peroxo Complexes That Are Stable at Room Temperature. *J. Am. Chem. Soc.* **2009**, *131*, (22), 7544-7545.
165. Chu, L.; Hardcastle, K. I.; MacBeth, C. E., Transition Metal Complexes Supported by a Neutral Tetraamine Ligand Containing N,N-dimethylaniline Units. *Inorg. Chem.* **2010**, *49*, (16), 7521-7529.
166. Matyjaszewski, K.; Davis, T. P., *Handbook of Radical Polymerization*. Wiley: Hoboken, 2002.
167. Matyjaszewski, K.; Tsarevsky, N. V., Macromolecular Engineering by Atom Transfer Radical Polymerization. *J. Am. Chem. Soc.* **136**, (18), 6513-6533.
168. Patten, T. E.; Matyjaszewski, K., Copper(I)-Catalyzed Atom Transfer Radical Polymerization. *Acc. Chem. Res.* **1999**, *32*, (10), 895-903.
169. Shipp, D. A.; Matyjaszewski, K., Kinetic Analysis of Controlled/Living Radical Polymerizations by Simulations. 1. The Importance of Diffusion-Controlled Reactions. *Macromolecules* **1999**, *32*, (9), 2948-2955.
170. Matyjaszewski, K.; Xia, J., Atom Transfer Radical Polymerization. *Chem. Rev.* **2001**, *101*, (9), 2921-2990.
171. Shih, H.-W.; Vander Wal, M. N.; Grange, R. L.; MacMillan, D. W. C., Enantioselective C_{\pm} -Benzoylation of Aldehydes via Photoredox Organocatalysis. *J. Am. Chem. Soc.* **2010**, *132*, (39), 13600-13603.

172. Nguyen, J. D.; Tucker, J. W.; Konieczynska, M. D.; Stephenson, C. R. J., Intermolecular Atom Transfer Radical Addition to Olefins Mediated by Oxidative Quenching of Photoredox Catalysts. *J. Am. Chem. Soc* **2011**, *133*, (12), 4160-4163.
173. Katritzky, A. R.; Rachwal, S.; Rachwal, B., Recent progress in the synthesis of 1,2,3,4,-tetrahydroquinolines. *Tetrahedron* **1996**, *52*, (48), 15031-15070.
174. Ramachary, D. B.; Shruthi, K. S., Asymmetric synthesis of tetrahydroquinolines through supramolecular organocatalysis. *Org. Biomol. Chem.* **2014**, *12*, (25), 4300-4304.
175. Luo, C.; Huang, Y., A Highly Diastereo- and Enantioselective Synthesis of Tetrahydroquinolines: Quaternary Stereogenic Center Inversion and Functionalization. *J. Am. Chem. Soc* **2013**, *135*, (22), 8193-8196.
176. Boldi, A. M., Libraries from natural product-like scaffolds. *Current Opinion in Chemical Biology* **2004**, *8*, (3), 281-286.
177. Gelb, M. H., Drug discovery for malaria: a very challenging and timely endeavor. *Current Opinion in Chemical Biology* **2007**, *11*, (4), 440-445.
178. Barbay, J. K.; Gong, Y.; Buntinx, M.; Li, J.; Claes, C.; Hornby, P. J.; Van Lommen, G.; Van Wauwe, J.; He, W., Synthesis and characterization of 5,6,7,8-tetrahydroquinoline C5a receptor antagonists. *Bioorg. Med. Chem. Lett.* **2008**, *18*, (8), 2544-2548.
179. Wang, C.-H.; Song, Z.-Y.; Deng, X.-X.; Zhang, L.-J.; Du, F.-S.; Li, Z.-C., Combination of ATRA and ATRC for the Synthesis of Periodic Vinyl Copolymers. *Macromol. Rapid Commun* **2013**, *35*, (4), 474-478.
180. Gopalakrishnan C; Shankaranarayanan D; Nazimudeen SK; L, K., Effect of tylophorine, a major alkaloid of *Tylophora indica*, on immunopathological and inflammatory reactions. *Indian J Med Res* **1980**, *71*, 940-948.
181. Dumoulin, D.; Lebrun, S.; Couture, A.; Deniau, E.; Grandclaudeon, P., First Asymmetric Synthesis of Boehmeriasin A. *Eur. J. of Org. Chem.* **2010**, (10), 1943-1950.
182. Iida, H.; Watanabe, Y.; Tanaka, M.; Kibayashi, C., General synthesis of phenanthroindolizidine, phenanthroquinolizidine, and related alkaloids: preparation of (\pm)-tylophorine, (\pm)-cryptopleurine, (\pm)-septicine, and (\pm)-julandine. *J. Org. Chem.* **1984**, *49*, (13), 2412-2418.

183. Comins, D. L.; Chen, X.; Morgan, L. A., Enantiopure N-Acyldihydropyridones as Synthetic Intermediates: Asymmetric Synthesis of (±)-Septicine and (±)-Tylophorine. *J. Org. Chem.* **1997**, *62*, (21), 7435-7438.
184. Lahm, G.; Stoye, A.; Opatz, T., A Five-Step Synthesis of (±)-Tylophorine via a Nitrile-Stabilized Ammonium Ylide. *J. Org. Chem.* **2012**, *77*, (15), 6620-6623.
185. Fürstner, A.; Kennedy, J. W. J., Total Syntheses of the Tylophora Alkaloids Cryptopleurine, (-)-Antofine, (-)-Tylophorine, and (-)-Ficuseptine C. *Chem. Eur. J.* **2006**, *12*, (28), 7398-7410.
186. Rossiter, L. M.; Slater, M. L.; Giessert, R. E.; Sakwa, S. A.; Herr, R. J., A Concise Palladium-Catalyzed Carboamination Route to (±)-Tylophorine. *J. Org. Chem.* **2009**, *74*, (24), 9554-9557.
187. Mai, D. N.; Wolfe, J. P., Asymmetric Palladium-Catalyzed Carboamination Reactions for the Synthesis of Enantiomerically Enriched 2-(Arylmethyl)- and 2-(Alkenylmethyl)pyrrolidines. *J. Am. Chem. Soc.* **2010**, *132*, (35), 12157-12159.
188. Hsu, S.-F.; Ko, C.-W.; Wu, Y.-T., Cobalt-Catalyzed Carbon-Carbon Bond Formation: Synthesis and Applications of Enantiopure Pyrrolidine Derivatives[1]. *Adv. Syn. Catal.* **2011**, *353*, (10), 1756-1762.

Chapter 2

Structure Reactivity Studies in ATRP Reactions Catalyzed by Copper Complexes with Substituted Tris(2-pyridylmethyl)amine Based Ligands

ABSTRACT

Synthesis, characterization, electrochemical studies and ATRP activity of a series of novel copper(I and II) complexes with TPMA based ligands containing 4-methoxy-3,5-dimethyl substituted pyridine arms were reported. In the solid state, $\text{Cu}^{\text{I}}(\text{TPMA}^{*1})\text{Br}$, $\text{Cu}^{\text{I}}(\text{TPMA}^{*2})\text{Br}$ and $\text{Cu}^{\text{I}}(\text{TPMA}^{*3})\text{Br}$ complexes were found to be distorted tetrahedral in geometry and contained coordinated bromide anions. Pseudo coordination of the aliphatic nitrogen atom to copper(I) center was observed in $\text{Cu}^{\text{I}}(\text{TPMA}^{*2})\text{Br}$ and $\text{Cu}^{\text{I}}(\text{TPMA}^{*3})\text{Br}$ complexes, whereas pyridine arm dissociation occurred in $\text{Cu}^{\text{I}}(\text{TPMA}^{*1})\text{Br}$. All copper(I) complexes with substituted TPMA ligands exhibited high degree of fluxionality in solution. At low temperature, $\text{Cu}^{\text{I}}(\text{TPMA}^{*1})\text{Br}$ was found to be symmetrical and monomeric, while dissociation of either unsubstituted pyridine and/or 4-methoxy-3,5-dimethyl substituted pyridine arms was observed in $\text{Cu}^{\text{I}}(\text{TPMA}^{*2})\text{Br}$ and $\text{Cu}^{\text{I}}(\text{TPMA}^{*3})\text{Br}$. On the other hand, the geometry of the copper(II) complexes in the solid state deviated from trigonal bipyramidal, as confirmed by a decrease in τ values ($[\text{Cu}^{\text{II}}(\text{TPMA}^{*1})\text{Br}][\text{Br}]$ ($\tau=0.92$) > $[\text{Cu}^{\text{II}}(\text{TPMA}^{*3})\text{Br}][\text{Br}]$ ($\tau=0.77$) > $[\text{Cu}^{\text{II}}(\text{TPMA}^{*2})\text{Br}][\text{Br}]$ ($\tau=0.72$)). Furthermore, cyclic voltammetry studies indicated a nearly stepwise decrease ($\Delta E \sim 60$ mV) of $E_{1/2}$ values (TPMA (-240 mV) > TPMA^{*1} (-310 mV) > TPMA^{*2} (-360 mV) > TPMA^{*3} (-420 mV)) on going from $[\text{Cu}^{\text{II}}(\text{TPMA})\text{Br}][\text{Br}]$ to $[\text{Cu}^{\text{II}}(\text{TPMA}^{*3})\text{Br}][\text{Br}]$, confirming that the presence of electron donating groups in the 4 (-OMe) and 3,5 (-Me) positions of the pyridine

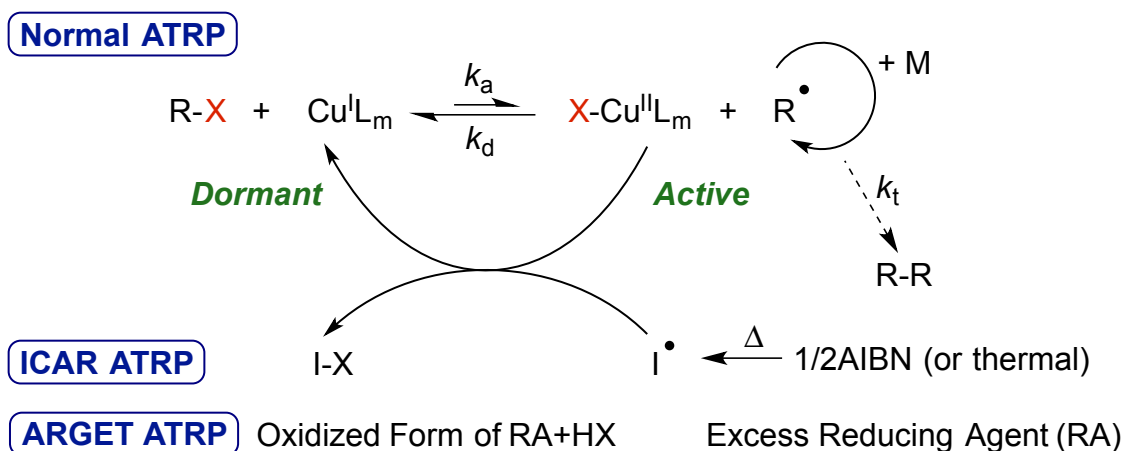
rings in TPMA increases the reducing ability of the corresponding copper(I) complexes. This increase was mostly the result of a stronger influence of substituted TPMA ligands towards stabilization of the copper(II) oxidation state ($\log\beta^I=13.4\pm 0.2$, $\log\beta^{II}=19.3$ (TPMA^{*1}), 20.5 (TPMA^{*2}) and 21.5 (TPMA^{*3})). Lastly, based on the straightforward synthesis and a large value for K_{ATRP} , the results indicate that TPMA^{*2} could have a higher future potential in copper catalyzed ATRP than previously reported TPMA^{*3}.

2.1. INTRODUCTION AND BACKGROUND

Tris(2-pyridylmethyl)amine (TPMA or TPA)^{1,2} is a widely used neutral tripodal nitrogen based ligand that has been complexed to a wide variety of transition metals. Currently, the Cambridge Crystallographic Database contains over 360 structures of TPMA complexes with metals spanning from group 1 to 13 of the periodic table, including many cases from the lanthanide and actinide series. TPMA contains both σ -donating tertiary amine and π -accepting pyridyl groups and is an excellent chelator that typically coordinates to a metal center in a tetradentate fashion.³⁻⁵ However, in some cases, tridentate coordination resulting from pyridyl arm dissociation has also been observed.^{3,6,7}

Over the past two decades, TPMA has received a considerable attention as a ligand of choice for many transition metal catalyzed reactions. For example, it is widely used as a chelator in copper and/or iron complexes that mimic certain metalloenzymes of relevance to oxygen activation.^{5, 8-17} Furthermore, a number of metal complexes with TPMA have also been shown to be active in C-H and O-O activation of small molecules,^{6,7 20-24} as well as [3+2] azide-alkyne cycloaddition.²⁵⁻²⁹ Lastly, copper complexes with TPMA are currently among the most active catalysts in atom transfer radical addition (ATRA)⁸⁻¹⁰ and polymerization (ATRP) reactions.^{11,12}

Both processes originated from well known Kharasch addition in which polyhalogenated compounds were added to alkenes via free-radical means.⁸⁻¹⁰ Recent studies have also indicated that TPMA is a superior complexing ligand in ATRA^{25, 31, 32, 35-45} and ATRP¹³⁻¹⁷ that utilize reducing agents. The role of a reducing agent in both systems is to continuously regenerate the activator species (copper(I) complex) from the corresponding deactivator (copper(II) complex). The latter one accumulates in the system as a result of unavoidable and often diffusion controlled radical-radical termination reactions. As a result, both processes can be conducted very efficiently using ppm amounts of the catalyst.¹⁷



Scheme 2.1.1. Representation of ATRP Equilibrium.

As indicated in **Scheme 2.1.1**, the ATRP equilibrium ($K_{\text{ATRP}}=k_a/k_d$) is controlled by a fast and reversible homolytic cleavage of a C-(pseudo)halogen bond in a redox reaction with the copper(I) catalyst, yielding well-defined halogen-capped polymers. Consequently, ATRP provides a very versatile synthetic tool for the preparation of polymers with predefined functionalities, compositions and architectures.¹⁸⁻²¹

Electrochemical measurements are commonly used to predict the activity of copper complexes in atom transfer radical processes, namely ATRA and ATRP.^{4,20,22-27} Generally, for a given alkyl halide, the equilibrium constant for atom transfer ($K_{\text{ATRP}}=k_a/k_d$) can be directly correlated with $E_{1/2}$ values provided that the halidophilicity of the metal complex ($X^- + [\text{Cu}^{\text{II}}\text{L}_m]^{2+} \rightleftharpoons [\text{Cu}^{\text{II}}\text{L}_m\text{X}]^+$, K_X , $X=\text{Br}$ or Cl) remains constant. As a result, for copper complexes with neutral nitrogen based ligands commonly used in ATRA and ATRP, a linear correlation between $\ln(K_{\text{ATRP}})$ and $E_{1/2}$ values is typically observed.^{25,28,29} Another method of predicting the activity of copper catalysts in ATRP is to directly compare the stability constants of Cu^{II} and Cu^{I} complexes with the particular ligand (β^{II} and β^{I} , respectively, Eq [1]). Both β^{II} and β^{I} should be large in

$$\beta^m = \frac{[\text{Cu}^m\text{L}_n]}{[\text{Cu}^m][\text{L}]^n}; m=\text{I or II}, n=1 \text{ or } 2 \quad [1]$$

order to eliminate or suppress possible concurrent reactions such as coordination of monomer and/or polymer, which are typically present in large excess relative to the catalyst. Generally, a copper complex with a low reduction potential should be more stable in its oxidized form (i.e. Cu^{II} should be more stable than Cu^{I}) in order to achieve high catalytic activity.^{26,27} Indeed, as indicated in **Figure 2.1.1**, more reducing copper(I) complexes have higher values for both K_{ATRP} and the ratio of the stability constants ($\beta^{\text{II}}/\beta^{\text{I}}$). Furthermore, an increase in $\beta^{\text{II}}/\beta^{\text{I}}$ ratio for a particular ligand is mostly the result of an increase in the stability constant of the copper(II) relative to copper(I) complex.^{26,28-33}

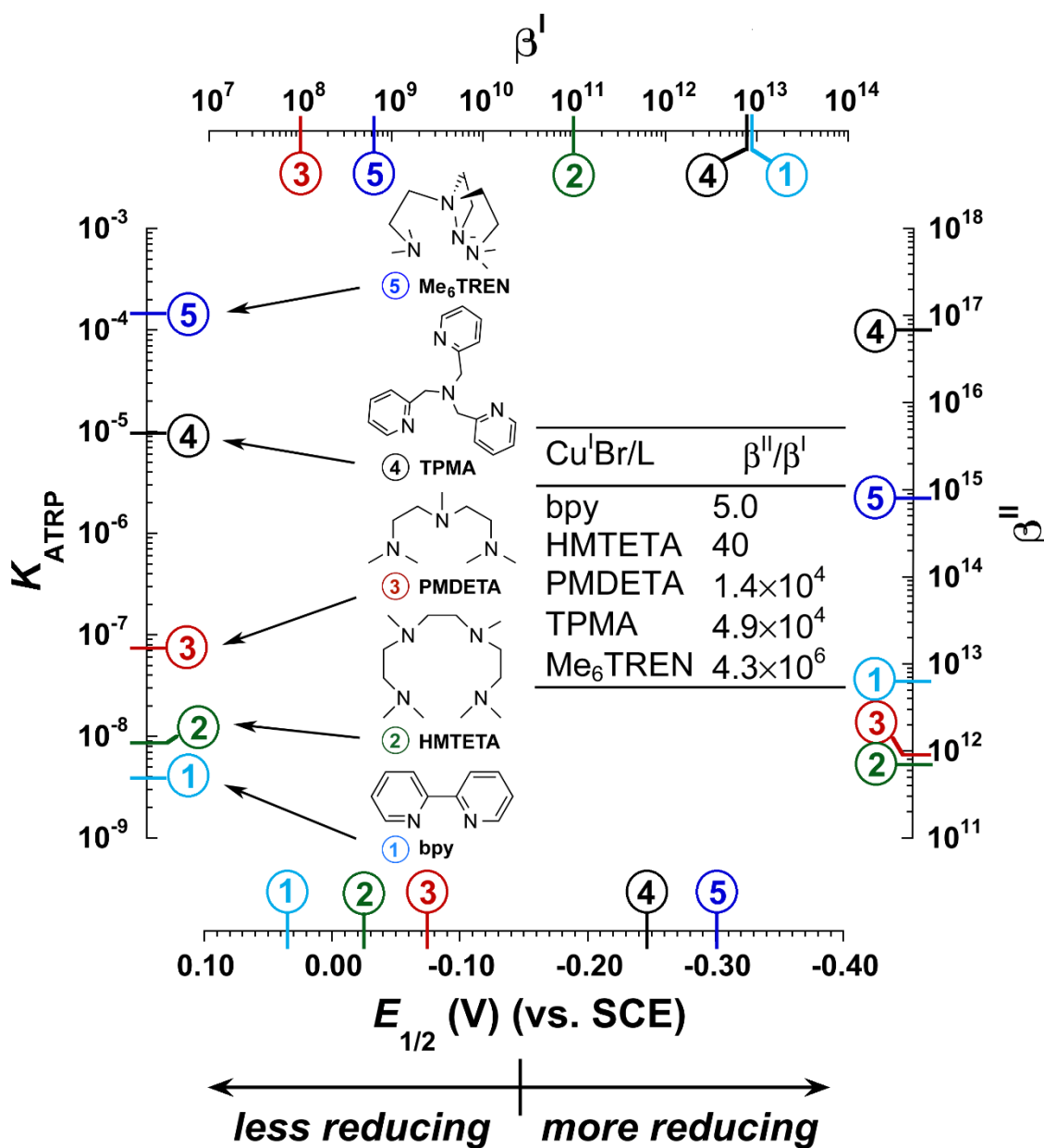
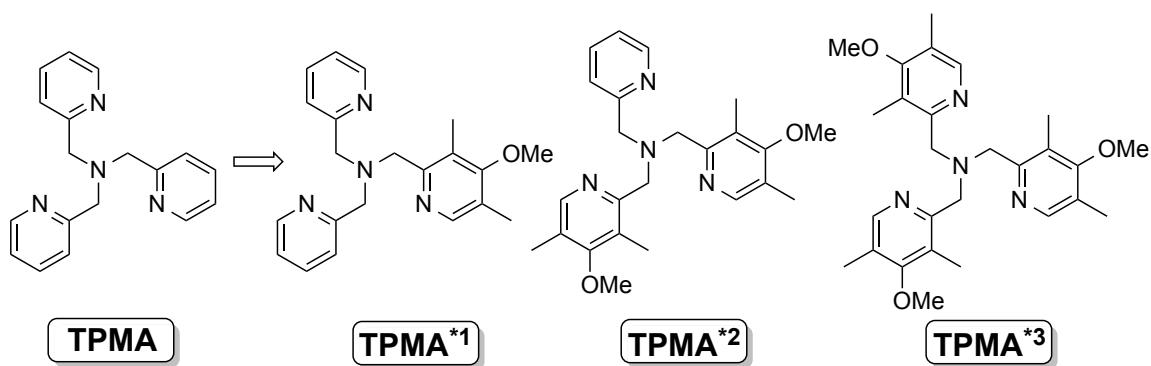


Figure 2.1.1. Correlations between K_{ATRP} , redox potential ($E_{1/2}$) and stability constants (β^I and β^{II}) for copper complexes with neutral nitrogen based ligands commonly used in ATRP. Generally, more reducing copper(I) complexes have higher values for K_{ATRP} and β^{II}/β^I ratio, as a result of greater ligand stabilization towards copper(II) oxidation state. All values were taken from Ref. ²⁶.

With the recent discovery indicating that the reducing agents can significantly reduce the amount of copper complexes in ATRP,¹⁷ a significant effort has been devoted towards development of more active catalysts that could be used at even lower concentrations, and

potentially enable controlled radical polymerization of α -olefins. The research in this area is significantly focused on ligand design, which can be used to tailor electronic properties of the copper(I) center. One way to increase the reduction potential of copper(I) complex is through systematic incorporation of electron donating groups (EDGs) to ligands that are already active in ATRP. This approach indeed seems to be justified, as demonstrated in a recent study which showed that EDGs in the *para*-substituted 2,2'-bipyridine ligands can significantly enhance catalytic activity in ATRP.³⁴ In a related work, inspired by the synthetic modifications of TPMA ligand for copper catalyzed oxygen activation³⁵ and iron mimicking site for methane monooxygenase,³⁶ even more active $\text{Cu}^{\text{II}}\text{X}_2/\text{TPMA}^{*3}$ (X=Br or Cl, TPMA^{*3} = tris((4-methoxy-3,5-dimethylpyridin-2-yl)methyl)amine) *in situ* system was discovered containing a total of nine EDGs.³⁷ This catalyst attained excellent polymerization results in photoATRP³⁸ of acrylates and emerged as one of the most active ATRP systems nowadays. Furthermore, it also elucidated the interplay between ATRP, organometallic mediated radical polymerization (OMRP) and catalytic termination pathways for the first time.³⁹

As evident from the discussion above, further development and catalytic activity of transition metal complexes containing modified TPMA ligands could provide invaluable and important information to various research fields ranging from inorganic, bioinorganic to organic/polymer chemistry. In this chapter, we report on the synthesis, characterization, electrochemical studies and ATRP activity of a series of novel copper(I and II) complexes with TPMA based ligands containing 4-methoxy-3,5-dimethyl substituted pyridine arms (**Scheme 2.1.2**).



Scheme 2.1.2. Substituted tris(2-pyridylmethyl)amine ligands investigated in the present study.

2.2. RESULTS AND DISCUSSION

Solid-State Structural Studies of Copper(I) Complexes. $\text{Cu}^{\text{I}}(\text{TPMA}^{\ast 1})\text{Br}$, $\text{Cu}^{\text{I}}(\text{TPMA}^{\ast 2})\text{Br}$ and $\text{Cu}^{\text{I}}(\text{TPMA}^{\ast 3})\text{Br}$ complexes were synthesized by reacting $\text{Cu}^{\text{I}}\text{Br}$ with the stoichiometric amounts of substituted TPMA based ligand (**Scheme 2.1.2**). Crystals suitable for X-ray analysis were obtained in acetone ($\text{Cu}^{\text{I}}(\text{TPMA}^{\ast 1})\text{Br}$) or methanol ($\text{Cu}^{\text{I}}(\text{TPMA}^{\ast 2})\text{Br}$ and $\text{Cu}^{\text{I}}(\text{TPMA}^{\ast 3})\text{Br}$) by slow diffusion of diethyl ether. The corresponding molecular structures are shown in **Figure 2.2.1**, with selected bond distances and angles summarized in **Table 2.2.1**. In the solid state, $\text{Cu}^{\text{I}}(\text{TPMA}^{\ast 1})\text{Br}$ complex was found to be distorted tetrahedral in geometry, with the complexation to the copper(I) center occurring through nitrogen atoms from both unsubstituted ($\text{Cu1-N2}=2.001(5)$ Å) and 4-methoxy-3,5-dimethyl substituted ($\text{Cu1-N1}=2.036$ Å) pyridine rings, aliphatic nitrogen atom ($\text{Cu-N4}=2.316(6)$ Å) and a bromine anion ($\text{Cu1-Br}=2.3511(10)$ Å). The remaining pyridine arm was dissociated from the copper(I) center ($\text{Cu1-N3}=3.494$ Å). In the case of previously isolated and structural characterized $\text{Cu}^{\text{I}}(\text{TPMA})\text{Br}$ ⁴⁰ and $\text{Cu}^{\text{I}}(\text{TPMA})\text{Cl}$ ⁴¹ complexes, ligand arm dissociation from TPMA was not observed in the solid state, unless bulky auxiliary ligands such as PPh_3 or 4,4'-bipyridine were used.³

In the latter two complexes, the distance between the copper(I) center and dissociated TPMA arm was much smaller than in $\text{Cu}^{\text{I}}(\text{TPMA}^{\ast 1})\text{Br}$ (3.258 and 2.523 Å, respectively). As indicated in **Table 2.2.1**, $\text{Cu}^{\text{I}}\text{-Br}$ and $\text{Cu}^{\text{I}}\text{-N}(\text{aliphatic})$ bonds in $\text{Cu}^{\text{I}}(\text{TPMA}^{\ast 1})\text{Br}$ complex were significantly longer ($\sim 0.313(6)$ Å) than the $\text{Cu}^{\text{I}}\text{-N}(\text{pyridine})$ ones. This is the primary reason for significant distortions from ideal tetrahedral geometry, as manifested in relevant bond angles ($\text{Br1-Cu1-N4}=132.36(13)^{\circ}$, and $\text{Br1-Cu1-N2}=125.68(15)^{\circ}$). Interestingly, $\text{Cu}^{\text{I}}\text{-N}$ bond lengths from substituted and unsubstituted pyridine arms were found to be very similar ($d(\text{Cu}^{\text{I}}\text{-N}_{\text{OMe,Me-py}})-d(\text{Cu}^{\text{I}}\text{-N}_{\text{py}})=0.035(8)$ Å). Lastly, the crystal structure of $\text{Cu}^{\text{I}}(\text{TPMA}^{\ast 1})\text{Br}$ was stabilized by a series of weak $\text{C-H}\cdots\text{C}$ (2.774(3)-3.039(5) Å) and dipole $\text{C-H}\cdots\text{Br}$ (3.021(3) Å) interactions. Additionally, $\pi\text{-}\pi$ stacking between 4-methoxy-3,5-dimethyl substituted pyridine rings (3.561(7) Å) was observed.

In the solid state, copper(I) halide complexes with TPMA ligand can be best described as formally being distorted tetrahedral in geometry, with the coordination to the copper(I) center occurring through a halide anion and three nitrogen atoms from pyridine rings.^{3,9,40,41} The remaining copper(I)-aliphatic nitrogen bond at approximately 2.4 Å is much more elongated when compared to typical $\text{Cu}^{\text{I}}\text{-N}$ bond length (2.0-2.1 Å).⁴ Similar structural features were also observed in $\text{Cu}^{\text{I}}(\text{TPMA}^{\ast 2})\text{Br}$ complex (**Figure 2.2.1b**).

Table 2.2.1. Structural Comparison of Copper(I) Complexes with Substituted TPMA Ligands.^a

Complex	[Cu ^I (TPMA)Br] ^b	[Cu ^I (TPMA ^{*1})Br] ^c	[Cu ^I (TPMA ^{*2})Br] ^c	[Cu ^I (TPMA ^{*3})Br] ^c
Cu1-N1	2.0709(15)	2.036(6)	2.0837(17)	2.092(3)
Cu1-N2	2.1024(15)	2.001(5)	2.0886(19)	2.116(3)
Cu1-N3	2.0753(15)	3.494	2.0452(17)	2.086(3)
Cu1-N4	2.4397(14)	2.316(6)	2.4190(19)	2.406(3)
Cu1-Br1	2.5088(3)	2.3511(10)	2.5025(3)	2.5045(6)
N1-Cu1-N2	112.40(6)	118.53(2)	114.40(7)	110.07(10)
N1-Cu1-N3	120.51(6)	/	122.31(7)	122.73(10)
N1-Cu1-N4	75.37(5)	79.24(19)	74.83(7)	75.76(10)
N2-Cu1-N3	107.61(6)	/	105.62(7)	108.22(10)
N3-Cu1-N4	74.84(5)	/	77.46(7)	75.29(10)
N4-Cu1-N2	74.80(5)	80.5(2)	75.39(6)	74.63(10)
Br1-Cu1-N1	105.25(4)	110.50(15)	101.59(5)	103.53(9)
Br1-Cu1-N2	105.43(4)	125.68(15)	103.06(5)	105.99(8)
Br1-Cu1-N3	104.28(4)	/	108.53(5)	104.91(7)
Br1-Cu1-N4	179.14(3)	132.36(13)	173.97(4)	179.22(7)
Cu1-LSP _{N_{Py}} ^d	0.538(3)	/	0.508(3)	0.534(8)

^aBond lengths are given in angstroms (Å) and angles in degrees (deg). ^bRef ⁴⁰. ^cN4 corresponds to aliphatic nitrogen atom in all complexes. Nitrogen atom in 4-methoxy-3,5-dimethyl substituted pyridine ring is labeled as N1 (Cu^I(TPMA^{*1})Br), N1 and N2 (Cu^I(TPMA^{*2})Br) and N1, N2 and N3 (Cu^I(TPMA^{*3})Br). ^dDistance between copper(I) atom and LSP derived from nitrogen atoms in pyridine rings.

The copper(I) center was coordinated by a nitrogen atom from unsubstituted pyridine arm (Cu1-N3=2.0452(17) Å), two nitrogen atoms from 4-methoxy-3,5-dimethyl substituted pyridine arms (Cu1-N1=2.0837(17) Å and Cu1-N2=2.0886(19) Å) and a bromine atom (2.5025(3) Å). The remaining Cu^I-N(aliphatic) bond distance (2.4190(19) Å) was slightly shorter than in Cu^I(TPMA)Br complex (2.4397(14) Å).⁴⁰

Furthermore, the copper(I) atom was positioned 0.508(3) Å below the least-squares plane derived from N1, N2 and N3 atoms towards the bromide anion, consistent with Cu^I preferring a tetrahedral geometry. The main Br1-Cu1-N4 axis (173.97(4)°) in Cu^I(TPMA^{*2})Br was slightly bent when compared to Cu^I(TPMA)Br (179.14(3)°). As a result, Cu^{II}(TPMA^{*2})Br complex does not possess near (non-crystallographic) three-fold symmetry with respect to Cu1-N4 vector and N1, N2 and N3 atoms. Lastly, the crystal structure of Cu^I(TPMA^{*2})Br was stabilized by weak C-H...C (2.800(2) Å) and dipole C-H...N (2.746(3) Å) and C-H...Br (2.892(7)-2.970(3) Å) interactions. The structural features of Cu^I(TPMA^{*3})Br complex (**Figure 2.2.1c**) were very similar to previously reported Cu^I(TPMA)Br.⁴⁰ The copper(I) center exhibited a distorted tetrahedral geometry and was coordinated by three nitrogen atoms from 4-methoxy-3,5-dimethyl substituted pyridine arms (Cu1-N1=2.093(3) Å, Cu1-N2=2.116(3) Å and Cu1-N3=2.086(3) Å) and a bromine atom (Cu1-Br1=2.5045(6) Å). Similarly to Cu^I(TPMA^{*2})Br, the remaining Cu^I-N(aliphatic) bond length (2.406(3) Å) was slightly shorter than in Cu^I(TPMA)Br complex (2.4397(14) Å).

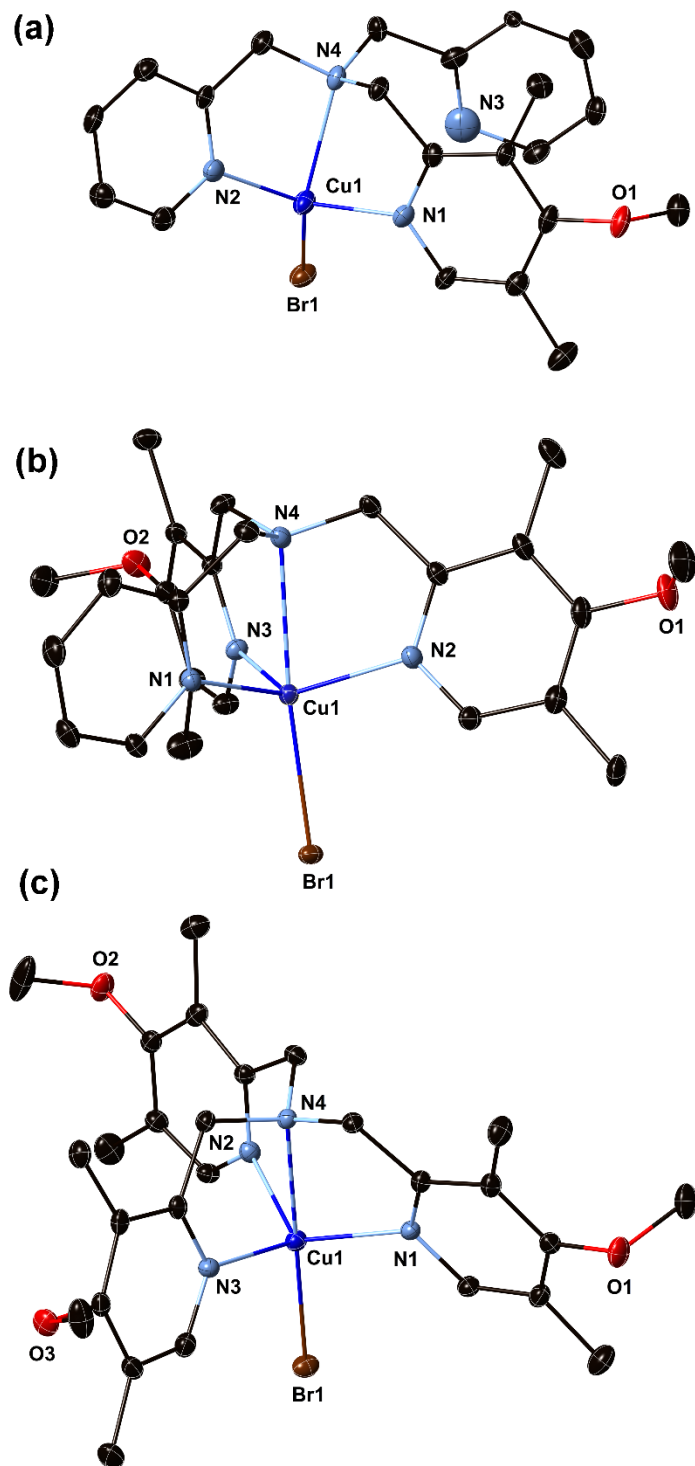


Figure 2.2.1. Molecular structures of $\text{Cu}^{\text{I}}(\text{TPMA}^{*1})\text{Br}$ (a), $\text{Cu}^{\text{I}}(\text{TPMA}^{*2})\text{Br}$ (b) and $\text{Cu}^{\text{I}}(\text{TPMA}^{*3})\text{Br}$ (c) shown with 30% probability displacement ellipsoids. H-atoms have been omitted for clarity.

The copper(I) atom was positioned 0.534(8) Å below the least-squares plane derived from N1, N2 and N3 atoms towards the bromide anion. With respect to Br1-Cu1-N4 vector and nitrogen atoms from substituted pyridine arms, Cu^I(TPMA^{*3})Br was nearly C₃-symmetric. However, as indicated in the space filling model (**Figure 2.2.2**), the presence of methoxy and methyl groups in the pyridine rings caused significant twisting of the ligand arms when compared to previously characterized Cu^I(TPMA)Br complex. Hence, viewing along Br1-Cu1-N4 axis, Cu^I(TPMA^{*3})Br appeared to be much closer to T-shaped rather than trigonal planar as observed in Cu^I(TPMA)Br. This cannot be attributed to the packing forces in the crystal structure because the only significant interactions in the unit cell were weak C-H---Br dipoles (2.780(4)-2.818(3) Å).

In summary, Cu^I(TPMA^{*1})Br, Cu^I(TPMA^{*2})Br and Cu^I(TPMA^{*3})Br complexes were found to be distorted tetrahedral in the solid state and contained coordinated bromide anions (Cu^I-Br=2.3511(10) Å, 2.5025(3) Å and 2.5045(6) Å, respectively). Pseudo coordination of the aliphatic nitrogen atom to copper(I) center was observed in Cu^I(TPMA^{*2})Br (Cu^I-N=2.4190(19) Å) and Cu^I(TPMA^{*3})Br (Cu^I-N=2.406(3) Å) complexes, similarly to previously isolated Cu^I(TPMA)Br (Cu^I-N=2.4397(14) Å).⁴⁰ On the other hand, pyridine arm dissociation occurred in Cu^I(TPMA^{*1})Br complex (Cu^I-N_{py}= 3.494(3)) Å). Regardless of the number of 4-methoxy-3,5-dimethyl substituted pyridine arms in TPMA^{*2} and TPMA^{*3} complexes, two of the Cu^I-N_{py} bonds were nearly identical (2.083±0.012 Å), whereas the third one either increased (TPMA^{*3}: Cu^I-N_{py}=2.116(3) Å) or decreased (TPMA^{*2}: Cu^I-N_{py}=2.0452(17) Å). Lastly, significant ligand arm twisting was observed in Cu^I(TPMA^{*3})Br complex when compared to Cu^I(TPMA)Br, which was found to be nearly C₃-symmetric in the solid state.

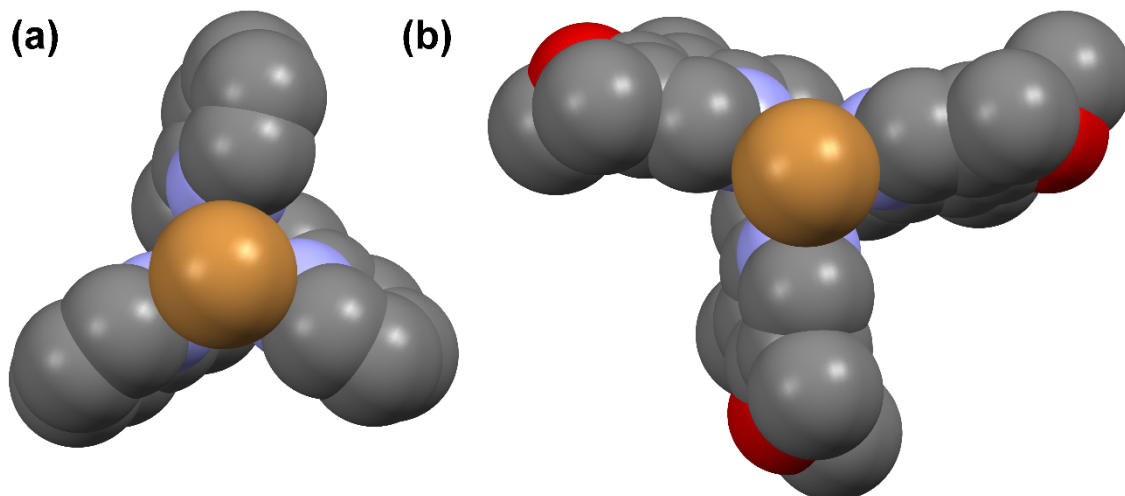


Figure 2.2.2. Space filling models (bottom view) of $\text{Cu}^{\text{I}}(\text{TPMA})\text{Br}$ (a) and $\text{Cu}^{\text{I}}(\text{TPMA}^{*3})\text{Br}$ (b) indicating twisting of 4-methoxy-3,5-dimethyl substituted pyridine arms. H-atoms have been omitted for clarity.

Solution Studies of Copper(I) Complexes. Variable temperature ^1H NMR spectroscopy was used to probe the structural features of copper(I) complexes with substituted TPMA based ligands in solution. Previously, this technique has been shown to be useful in examining structures of $\text{Cu}^{\text{I}}(\text{TPMA})\text{Br}$ ⁴⁰ and $\text{Cu}^{\text{I}}(\text{TPMA})\text{Cl}$ ^{41,42} complexes, which were found to be highly symmetrical and monomeric in solution, consistent with the solid-state studies. Shown in **Figure 2.2.3** are the aromatic and methylene regions of the variable temperature ^1H NMR spectra of $\text{Cu}^{\text{I}}(\text{TPMA}^{*1})\text{Br}$ complex in $(\text{CD}_3)_2\text{CO}$. The proton resonances at ambient temperature were very broad, indicating a fluxional system, very typical for d^{10} transition metal complexes containing neutral ligands.⁴³ However, on cooling to 220 K, the resonances due to the coordinated TPMA^{*1} became relatively well resolved. Only one set of resonances for the aromatic protons in TPMA^{*1} ligand were observed, which is not consistent with the solid-state structure of $\text{Cu}^{\text{I}}(\text{TPMA}^{*1})\text{Br}$ in which one pyridine arm was dissociated from the copper(I) center (vide supra).

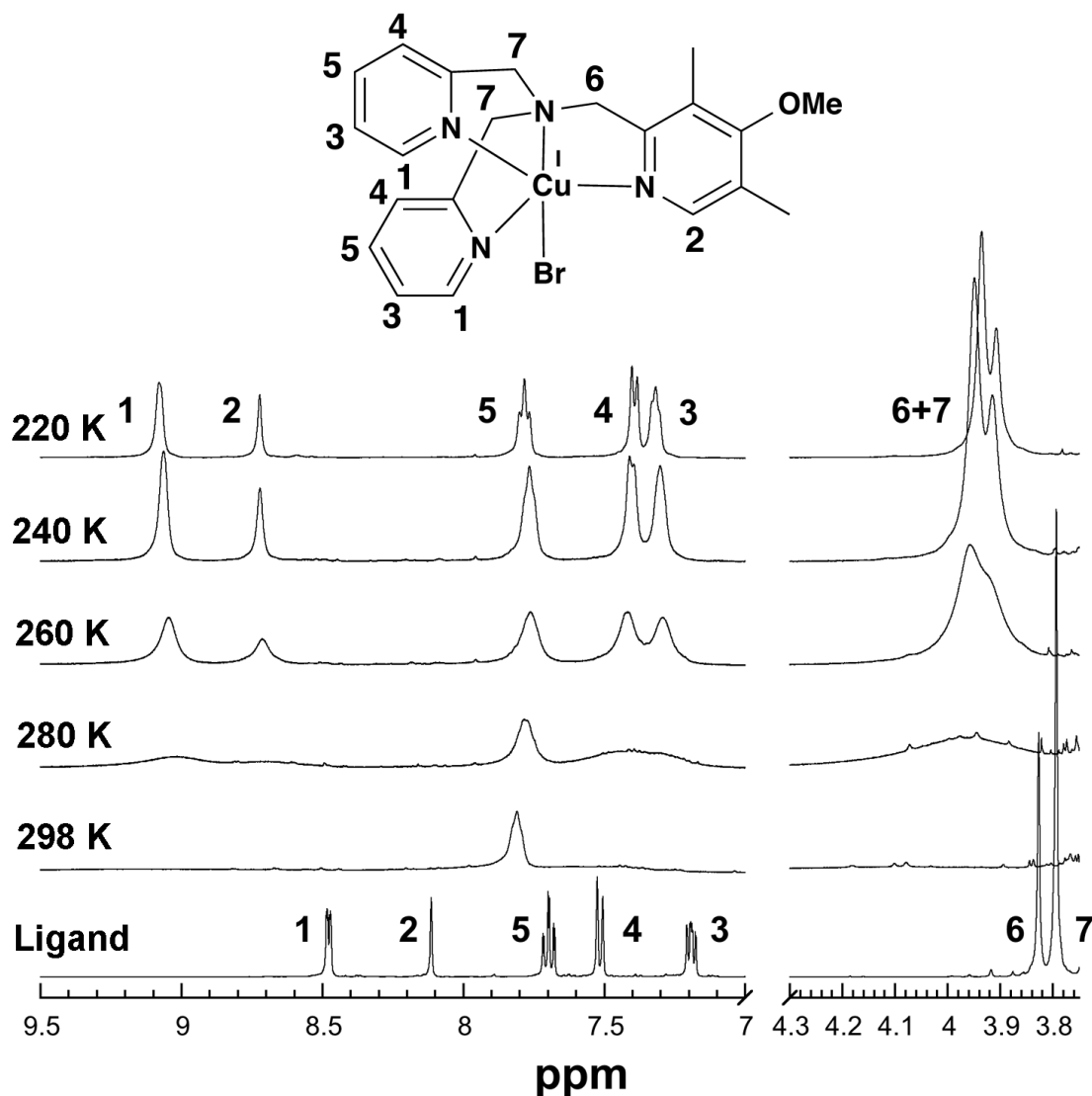


Figure 2.2.3. Variable temperature ^1H NMR spectra (400 MHz, $(\text{CD}_3)_2\text{CO}$) of $\text{Cu}^{\text{I}}(\text{TPMA}^{*1})\text{Br}$ complex in the aromatic and methylene regions.

The hydrogen atoms next to the nitrogen atoms in unsubstituted (H^1 , Figure 4) and 4-methoxy-3,5-dimethyl substituted (H^2 , Figure 4) pyridine arms at 220 K moved approximately 0.60 ppm downfield relative to free TPMA^{*1} . Such downfield shift between 0.50 and 0.70 ppm is typically observed in copper(I) complexes containing nitrogen-based ligands.⁷³⁻⁷⁶ Similarly, downfield shift for the methylene protons in TPMA^{*1} (H^6 and H^7 , **Figure 2.2.3**) by 0.10 ppm also indicated coordination. Much smaller shift for methylene protons (H^6 and H^7) in TPMA^{*1} , when

compared to pyridine protons (H^1 and H^2), clearly points to a weaker interaction between the aliphatic nitrogen atom and copper(I) center. Exactly the same trend was observed in previously characterized $Cu^I(TPMA)Br$ and $Cu^I(TPMA)Cl$.^{41,42} In latter complexes, TPMA was coordinated to the copper(I) center in a nearly C_3 -symmetric fashion with $Cu^I-N(\text{aliphatic})$ bond distance being on average 0.360 Å longer than the corresponding distances with nitrogen atoms from pyridine rings. Therefore, taking into account the presence of only one set of resonances for the aromatic protons in $TPMA^{*1}$ and similarity with the spectra of $Cu^I(TPMA)Br$ and $Cu^I(TPMA)Cl$, the structure of $Cu^I(TPMA^{*1})Br$ is most likely symmetrical and monomeric in solution as shown in **Figure 2.2.1**.

Similarly to $Cu^I(TPMA^{*1})Br$, the proton resonances in $Cu^I(TPMA^{*2})Br$ at room temperature were broad indicating highly fluxional system (**Figure 2.2.4**). On cooling to 188K, distinct resonances for protons associated with complexed unsubstituted (H^2 , $\delta 9.03$, $\delta - \delta_{\text{free}} = 0.59$ ppm) and 4-methoxy-3,5-dimethyl substituted (H^1 , $\delta 8.72$, $\delta - \delta_{\text{free}} = 0.53$ ppm) pyridine arms were observed. Interestingly, separate proton resonances for corresponding dissociated arms also appeared (pyridine: H^2 , $\delta 8.51$, $\delta - \delta_{\text{free}} = 0.07$ ppm and 4-methoxy-3,5-dimethyl pyridine: H^1 , $\delta 8.19$, $\delta - \delta_{\text{free}} = 0.06$ ppm). The spectrum was not consistent with commonly encountered dimerization that is easily observed by 1H NMR spectroscopy due to inequivalence of methylene protons,^{3,44} but rather the presence of two different complexes each containing uncomplexed pyridine and 4-methoxy-3,5-dimethyl substituted pyridine arms, respectively. Therefore, the proposed structures shown in **Figure 2.2.4** are not consistent with the solid state in which $TPMA^{*2}$ was coordinated to the copper(I) center through bromide anion and three nitrogen atoms from pyridine rings (vide supra).

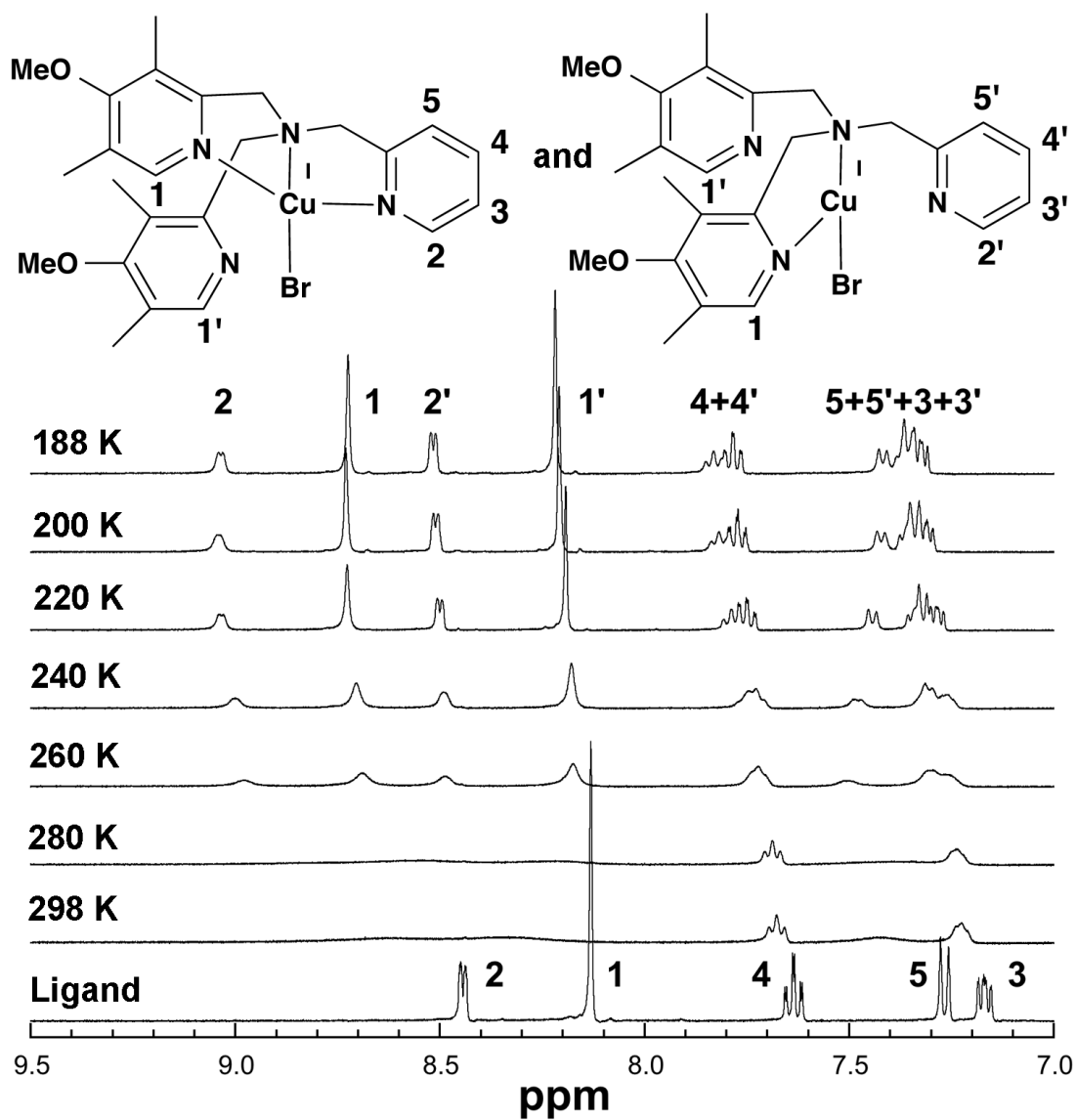


Figure 2.2.4. Variable temperature ^1H NMR spectra (400 MHz, $(\text{CD}_3)_2\text{CO}$) of $\text{Cu}^{\text{I}}(\text{TPMA}^{*2})\text{Br}$ complex in the aromatic region.

Lastly, ligand arm dissociation was also observed in $\text{Cu}^{\text{I}}(\text{TPMA}^{*3})\text{Br}$ complex (**Figure 2.2.5**). At 188 K, proton resonances for complexed and uncomplexed 4-methoxy-3,5-dimethyl substituted pyridine rings resolved in the integration ratio of 2:1.

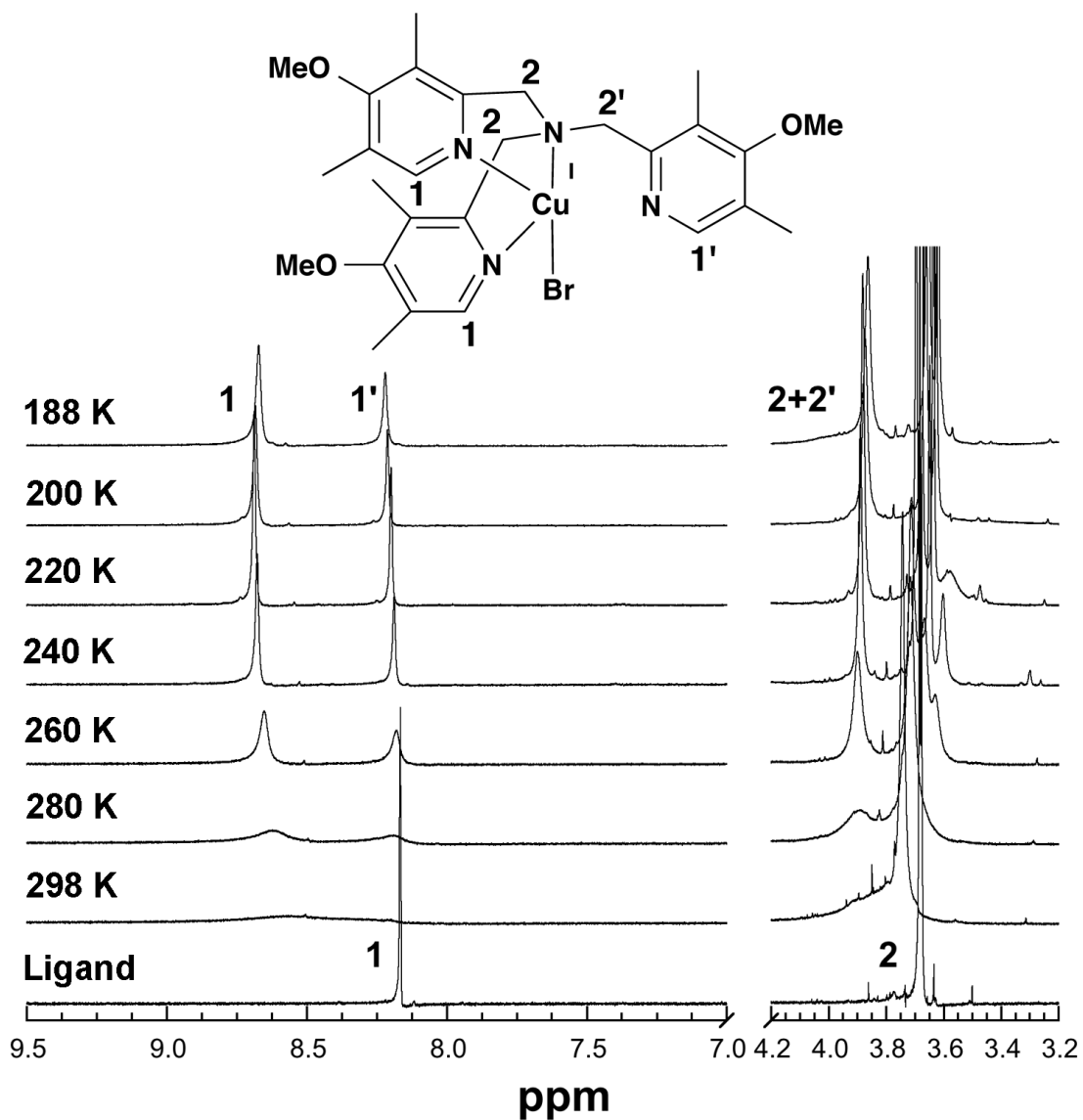


Figure 2.2.5. Variable temperature ^1H NMR spectra (400 MHz, $(\text{CD}_3)_2\text{CO}$) of $\text{Cu}^{\text{I}}(\text{TPMA}^{*3})\text{Br}$ complex in the aromatic and methylene regions.

This clearly indicates that $\text{Cu}^{\text{I}}(\text{TPMA}^{*3})\text{Br}$ adopts tetrahedral geometry in solution with copper(I) center being coordinated by two nitrogen atoms from pyridine arms, one aliphatic nitrogen atom, and a bromine atom. Therefore, the structure of $\text{Cu}^{\text{I}}(\text{TPMA}^{*3})\text{Br}$ in solution is not consistent with the solid state, but rather resembles $\text{Cu}^{\text{I}}(\text{TPMA}^{*1})\text{Br}$ discussed above (**Figure 2.2.1a**).

In summary, $\text{Cu}^{\text{I}}(\text{TPMA}^{*1})\text{Br}$, $\text{Cu}^{\text{I}}(\text{TPMA}^{*2})\text{Br}$ and $\text{Cu}^{\text{I}}(\text{TPMA}^{*3})\text{Br}$ complexes were found to be more fluxional in solution than previously investigated $\text{Cu}^{\text{I}}(\text{TPMA})\text{Br}$ and $\text{Cu}^{\text{I}}(\text{TPMA})\text{Cl}$.^{41,42} Furthermore, the structures of all three complexes were not consistent with the solid-state discussed above. At low temperature, $\text{Cu}^{\text{I}}(\text{TPMA}^{*1})\text{Br}$ was found to be symmetrical and monomeric. Lastly, dissociation of either unsubstituted pyridine and/or 4-methoxy-3,5-dimethyl substituted pyridine arms was observed in $\text{Cu}^{\text{I}}(\text{TPMA}^{*2})\text{Br}$ and $\text{Cu}^{\text{I}}(\text{TPMA}^{*3})\text{Br}$ complexes.

Solid-State Structural Studies of Copper(II) Complexes. Copper(II) complexes that are generated during ATRA and ATRP processes are essential for the deactivation step (i.e. reversible halogen atom abstraction from a copper(II) complex by radicals to generate dormant alkyl halide species and a copper(I) complex, **Scheme 2.1.1**).^{4,17,23} $[\text{Cu}^{\text{II}}(\text{TPMA}^{*1})\text{Br}][\text{Br}]$, $[\text{Cu}^{\text{II}}(\text{TPMA}^{*2})\text{Br}][\text{Br}]$ and $[\text{Cu}^{\text{II}}(\text{TPMA}^{*3})\text{Br}][\text{Br}]$ complexes were synthesized by reacting $\text{Cu}^{\text{II}}\text{Br}_2$ with the stoichiometric amounts of substituted TPMA based ligand. Crystals suitable for X-ray analysis were obtained in dichlorometane by slow diffusion of *n*-pentane. The corresponding molecular structures are shown in **Figure 2.2.6**, and selected bond distances and angles summarized in **Table 2.2.2**.

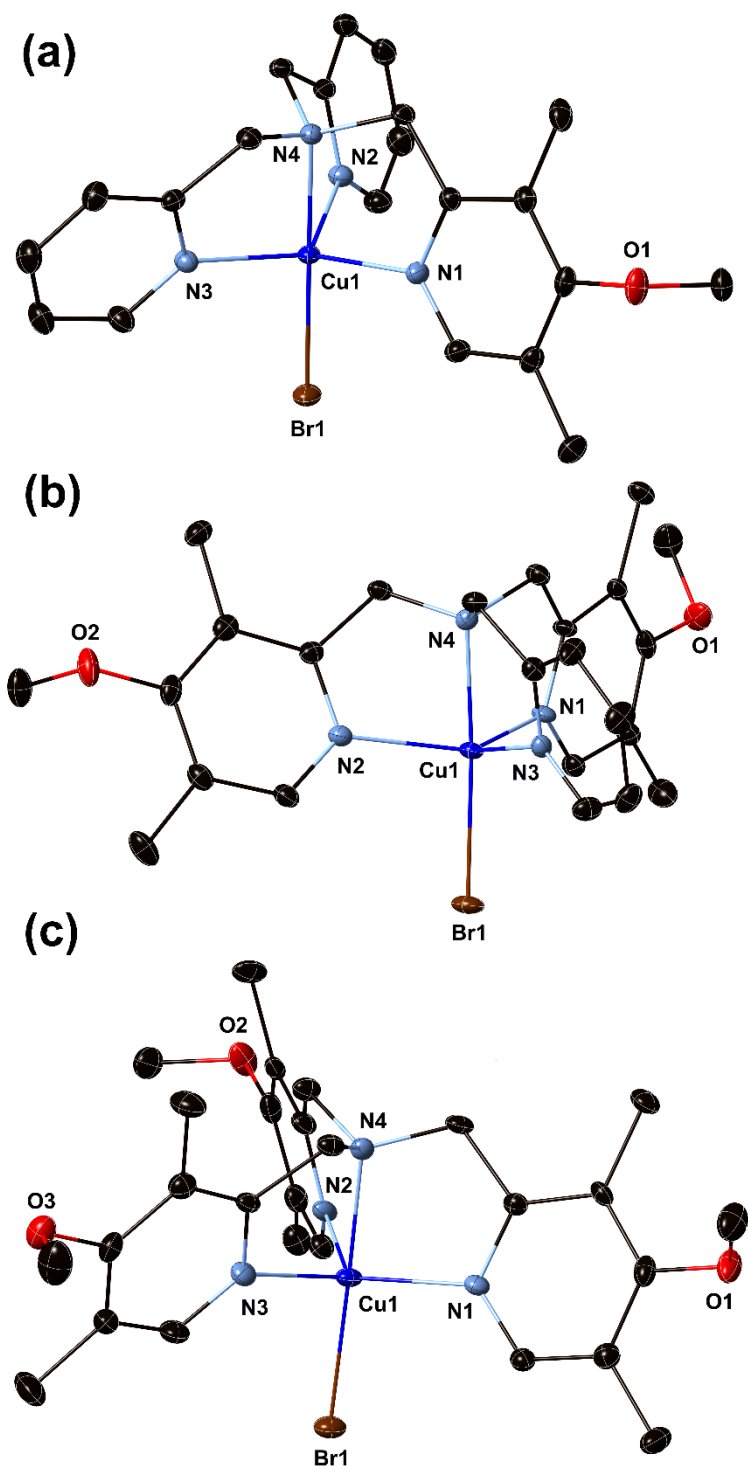


Figure 2.2.6. Molecular structures of $[\text{Cu}^{\text{II}}(\text{TPMA}^{*1})\text{Br}][\text{Br}]$ (a), $[\text{Cu}^{\text{II}}(\text{TPMA}^{*2})\text{Br}][\text{Br}]$ (b) and $[\text{Cu}^{\text{II}}(\text{TPMA}^{*3})\text{Br}][\text{Br}]$ (c) shown with 30% probability displacement ellipsoids. H-atoms and bromide counterion have been omitted for clarity.

Table 2.2.2. Structural Comparison of Copper(II) Complexes with Substituted TPMA Ligands.^a

Complex	[Cu ^{II} (TPMA)Br][Br] ^b	[Cu ^{II} (TPMA ^{*1})Br][Br] ^c	[Cu ^{II} (TPMA ^{*2})Br][Br] ^c	[Cu ^{II} (TPMA ^{*3})Br][Br] ^c
Cu1-N1 _{eq}	2.073(15)	2.062(2)	2.028(5)	2.059(3)
Cu1-N2 _{eq}	2.073(15)	2.0400(19)	2.072(5)	2.149(3)
Cu1-N3 _{eq}	2.073(15)	2.064(2)	2.136(4)	2.044(3)
Cu1-N4 _{ax}	2.040(3)	2.0411(19)	2.025(4)	2.028(3)
Cu1-Br1	2.3836(6)	2.3852(3)	2.3814(7)	2.3740(5)
N1-Cu1-N2	80.86(5)	117.74(8)	133.26(19)	115.63(12)
N1-Cu1-N3	80.86(5)	111.04(8)	114.07(18)	132.39(12)
N1-Cu1-N4	80.86(5)	80.61(8)	82.74(17)	81.07(12)
N2-Cu1-N3	117.53(3)	124.60(8)	105.58(18)	104.99(12)
N3-Cu1-N4	117.53(3)	81.01(8)	81.36(17)	82.81(12)
N4-Cu1-N2	117.53(3)	82.51(7)	79.66(18)	79.82(11)
Br1-Cu1-N1	99.14(5)	99.23(6)	98.72(12)	97.27(8)
Br1-Cu1-N2	99.14(5)	97.73(5)	97.19(12)	100.99(8)
Br1-Cu1-N3	99.14(5)	98.89(6)	100.71(12)	98.35(8)
Br1-Cu1-N4	180.00(5)	179.76(5)	176.64(13)	178.33(9)
Cu1-LSP _{N,Py} ^d	0.329	0.307	0.303	0.329
τ^e	1.0	0.92	0.72	0.77

^aBond lengths are given in angstroms (Å) and angles in degrees (deg). ^bRef ⁴⁰. ^cN4 corresponds to aliphatic nitrogen atom in all complexes. Nitrogen atom in 4-methoxy-3,5-dimethyl substituted pyridine ring is labeled as N1 ([Cu^{II}(TPMA^{*1})Br][Br]), N1 and N2 ([Cu^{II}(TPMA^{*2})Br][Br]) and N1, N2 and N3 ([Cu^{II}(TPMA^{*3})Br][Br]). ^dDistance between copper(I) atom and LSP derived from nitrogen atoms in pyridine rings. ^e τ parameter is calculated as $\tau=(\varphi_1-\varphi_2)/60$ where φ_1 and φ_2 are the largest and second largest N-Cu^{II}-N(Br) bond angles, $\tau=1$ (regular trigonal bipyramidal geometry) and $\tau=0$ (regular square pyramidal geometry).

All three complexes deviated from the ideal trigonal bipyramidal geometry observed in previously characterized $[\text{Cu}^{\text{II}}(\text{TPMA})\text{Br}][\text{Br}]$.⁴⁰ This can easily be seen from the corresponding τ values ($\tau=1$ for regular trigonal bipyramidal geometry and $\tau=0$ for regular square pyramidal geometry),^{45,46} which generally decreased in the order $[\text{Cu}^{\text{II}}(\text{TPMA})\text{Br}][\text{Br}]$ ($\tau=1$) > $[\text{Cu}^{\text{II}}(\text{TPMA}^{*1})\text{Br}][\text{Br}]$ ($\tau=0.92$) > $[\text{Cu}^{\text{II}}(\text{TPMA}^{*3})\text{Br}][\text{Br}]$ ($\tau=0.77$) > $[\text{Cu}^{\text{II}}(\text{TPMA}^{*2})\text{Br}][\text{Br}]$ ($\tau=0.72$). The average $\text{Cu}^{\text{II}}\text{-N}_{\text{eq}}$ bond distances increased on going from $[\text{Cu}^{\text{II}}(\text{TPMA}^{*1})\text{Br}][\text{Br}]$ (2.055(3) Å) to $[\text{Cu}^{\text{II}}(\text{TPMA}^{*2})\text{Br}][\text{Br}]$ (2.078(8) Å) and $[\text{Cu}^{\text{II}}(\text{TPMA}^{*3})\text{Br}][\text{Br}]$ (2.084(5) Å) complexes, and were not equal when compared to $[\text{Cu}^{\text{II}}(\text{TPMA})\text{Br}][\text{Br}]$ (2.073(15) Å). Generally, two $\text{Cu}^{\text{II}}\text{-N}_{\text{eq}}$ bond lengths were either longer (TPMA^{*1}: 2.063(3) Å v.s. 2.040(2) Å) or shorter (TPMA^{*2}: 2.050(7) Å v.s. 2.136(4) Å and TPMA^{*3}: 2.052(4) Å v.s. 2.149(3) Å). Furthermore, $\text{Cu}^{\text{II}}\text{-Br}$ bond length in $[\text{Cu}^{\text{II}}(\text{TPMA}^{*1})\text{Br}][\text{Br}]$ (2.3852(3) Å) and $[\text{Cu}^{\text{II}}(\text{TPMA}^{*2})\text{Br}][\text{Br}]$ (2.3814(7) Å) were similar to $[\text{Cu}^{\text{II}}(\text{TPMA})\text{Br}][\text{Br}]$ (2.3836(6) Å), but slightly decreased in $[\text{Cu}^{\text{II}}(\text{TPMA}^{*3})\text{Br}][\text{Br}]$ (2.3740(5) Å). Additionally, particularly in the case of $[\text{Cu}^{\text{II}}(\text{TPMA}^{*2})\text{Br}][\text{Br}]$ and $[\text{Cu}^{\text{II}}(\text{TPMA}^{*3})\text{Br}][\text{Br}]$, the presence of methoxy and methyl groups in the pyridine rings caused significant ligand arm twisting, as indicated in the space filling model (**Figure 2.2.7**). Lastly, the crystal structures of copper(II) complexes with

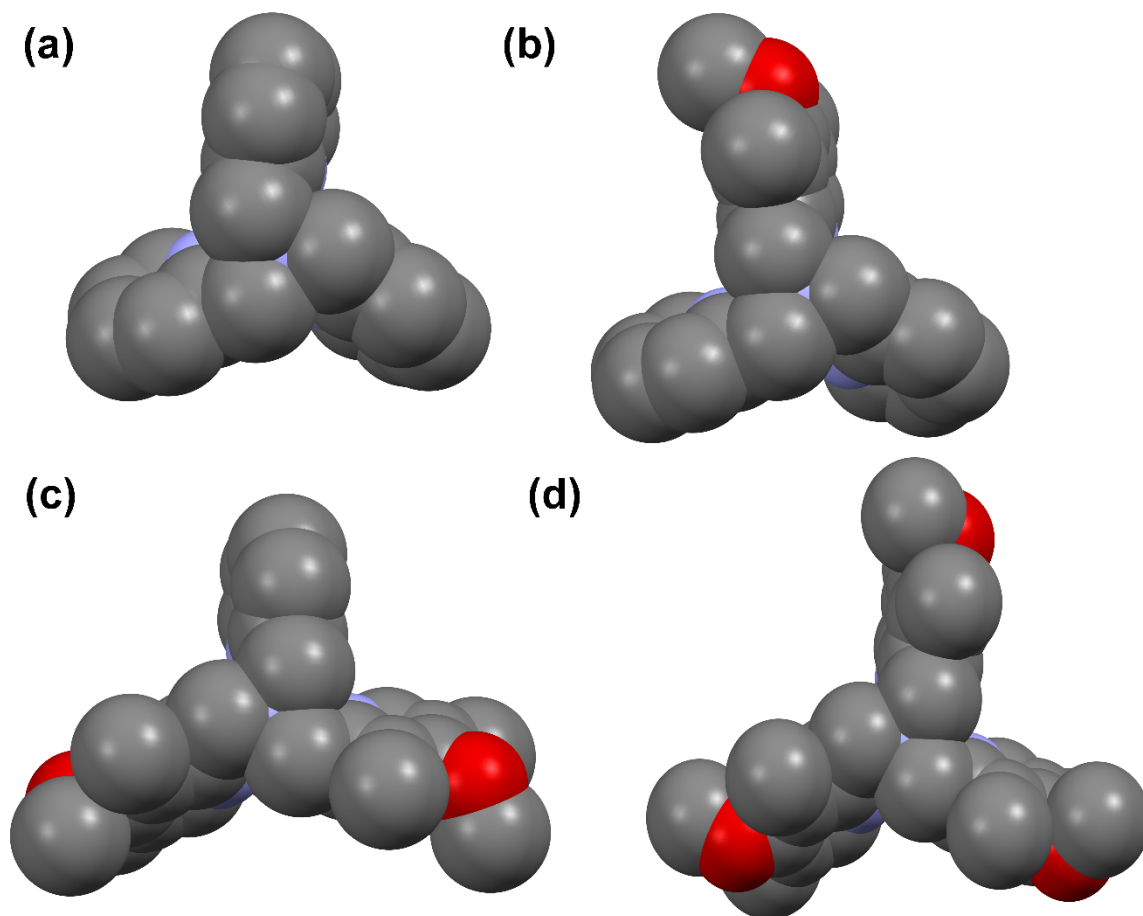


Figure 2.2.7. Space filling models (top view) of $[\text{Cu}^{\text{II}}(\text{TPMA})\text{Br}][\text{Br}]$ (a), $[\text{Cu}^{\text{II}}(\text{TPMA}^{*1})\text{Br}][\text{Br}]$ (b), $[\text{Cu}^{\text{II}}(\text{TPMA}^{*2})\text{Br}][\text{Br}]$ (c) and $[\text{Cu}^{\text{II}}(\text{TPMA}^{*3})\text{Br}][\text{Br}]$ (d) indicating twisting of 4-methoxy-3,5-dimethyl substituted pyridine arms. H-atoms and bromide counterion have been omitted for clarity.

substituted TPMA based ligands were stabilized by π - π stacking interactions between pyridine rings (TPMA^{*1}: 3.722(4) Å) and a series of weak C-H---C (TPMA^{*2}: 2.756(4) Å, TPMA^{*3}: 2.877*6) Å) and dipole C-H---O (TPMA^{*1}: 2.375(7) Å, TPMA^{*2}: 2.325(3)-2.674(5) Å, TPMA^{*3}: 2.657(2)-2.700(4) Å) and C-H---Br (TPMA^{*1}: 3.030(3)-3.042(3) Å, TPMA^{*2}: 2.882(4)-3.006(3) Å, TPMA^{*3}: 2.962(7)-3.020(5) Å) interactions.

With the exception of TPMA^{*1}, the structural feature of copper(I and II) complexes with TPMA^{*2} and TPMA^{*3} ligands appear to be rather similar. In $\text{Cu}^{\text{I}}(\text{TPMA}^{*2})\text{Br}$ and $\text{Cu}^{\text{I}}(\text{TPMA}^{*3})\text{Br}$ complexes, the average Cu-N_{eq} bond lengths are

0.0100 Å and 0.0140 Å longer than in [Cu^{II}(TPMA^{*2})Br][Br] and [Cu^{II}(TPMA^{*3})Br][Br], respectively. The N_{eq}-Cu-N_{aq} bond angles are very similar in both Cu^I and Cu^{II} complexes, while the average angle in the plane N_{eq}-Cu-N_{eq} is slightly larger in [Cu^{II}(TPMA^{*2})Br][Br] (117.63(2)°) and [Cu^{II}(TPMA^{*3})Br][Br] (117.67(2)°) when compared to Cu^I(TPMA^{*2})Br (114.11(12)°) and Cu^I(TPMA^{*3})Br (113.67(18)°), respectively. The only more pronounced difference in TPMA^{*2} and TPMA^{*3} coordination to the copper center can be seen in shortening of Cu-N_{ax} bond length by approximately 0.400 Å on going from Cu^I(TPMA^{*2} or ^{*3})Br to [Cu^{II}(TPMA^{*2} or ^{*3})Br][Br]. Similar conclusions were also reached in the case of previously isolated Cu^I(TPMA)Br and Cu^{II}(TPMA)Br][Br] complexes.⁴⁰

Solution Studies of Copper(II) Complexes. Apart from electrospray ionization mass spectrometry (ESI-MS), copper(II) complexes with substituted TPMA based ligands were also characterized in solution using UV-Vis spectroscopy (**Figure 2.2.8**). The corresponding λ_{\max} and ϵ_{\max} values are summarized in **Table 2.2.3**. Data for previously reported [Cu^{II}(TPMA)Br][Br],⁴⁰ [Cu^{II}(Me₆TREN)Br][Br]⁴⁷ (Me₆TREN=tris[2-(dimethylamino)ethyl]amine) and [Cu^{II}(bpy)₂Br][Br]^{4,48} (bpy=2,2'-bipyridine) complexes are included for comparison. The absorption spectra in the Vis/NIR region for copper(II) complexes with TPMA^{*1}, TPMA^{*2} and TPMA^{*3} ligands can be characterized in terms of

Table 2.2.3. Summary of λ_{\max} and ϵ_{\max} Values in Acetonitrile for Cu^{II}Br₂ Complexes with TPMA, TPMA^{*1}, TPMA^{*2} and TPMA^{*3} Ligands.

Complex	λ_{\max} (nm) / ϵ_{\max} (Lmol ⁻¹ cm ⁻¹)	Ref.
[Cu ^{II} (TPMA ^{*1})Br][Br]	983 (195), 754 (89)	this work
[Cu ^{II} (TPMA ^{*2})Br][Br]	982 (193), 754 (83)	this work
[Cu ^{II} (TPMA ^{*3})Br][Br]	979 (187), 756 (78)	this work
[Cu ^{II} (TPMA)Br][Br]	981 (178), 759 (75)	40
[Cu ^{II} (Me ₆ TREN)Br][Br]	973 (170), 757 (73)	47

the absorption bands centered around 754 and 980 nm. These bands are typically observed in [CuN₄X]⁺ (X=Br or Cl) chromophores that have trigonal bipyramidal geometry, and correspond to $d_{xz} \approx d_{yz} \rightarrow d_{z^2}$ and $d_{x^2-y^2} \approx d_{xy} \rightarrow d_{z^2}$ transitions, respectively.^{4,49-51} Furthermore, all spectra are consistent with previously characterized copper(II) complexes containing TPMA, Me₆TREN and bpy ligands, which were found to be trigonal bipyramidal in geometry. Therefore, solution structures of [Cu^{II}(TPMA^{*1})Br][Br], Cu^{II}(TPMA^{*2})Br][Br] and [Cu^{II}(TPMA^{*3})Br][Br] are consistent with the solid state discussed above.

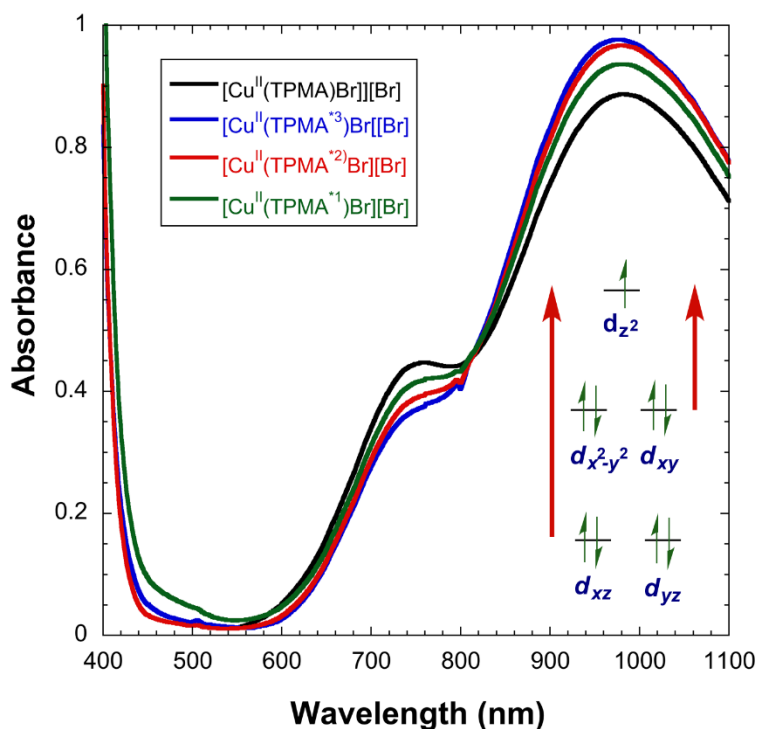


Figure 2.2.8. Absorption spectra (Vis/NIR) of Cu^{II}Br₂ complexes with TPMA, TPMA^{*1}, TPMA^{*2} and TPMA^{*3} ligands in acetonitrile at ambient temperature ([Cu^{II}]₀=5.0×10⁻³ M).

Electrochemical Studies. As mentioned in the introduction section, electrochemical measurements are commonly used to predict the activity of copper complexes in atom transfer radical processes, namely ATRA and ATRP.^{4,20,22-27} Generally, for a given alkyl halide, the equilibrium constant for atom transfer ($K_{\text{ATRP}}=k_a/k_d$) can be directly correlated with $E_{1/2}$ values provided that the halidophilicity of the metal complex ($X^- + [\text{Cu}^{\text{II}}\text{L}_m]^{2+} \rightleftharpoons [\text{Cu}^{\text{II}}\text{L}_m\text{X}]^+$, K_X , $X=\text{Br}$ or Cl) remains constant. As a result, for copper complexes with neutral nitrogen based ligands commonly used in ATRA or ATRP, a linear correlation between $\ln(K_{\text{ATRP}})$ and $E_{1/2}$ values is typically observed.^{25,28,29} The basic hypothesis behind this work was that the systematic incorporation of electron donating groups to pyridine rings in TPMA scaffold will result in more reducing and consequently more active ATRA/ATRP copper catalysts. Shown in Figure 10 are cyclic voltammograms of $[\text{Cu}^{\text{II}}(\text{TPMA}^{*1})\text{Br}][\text{Br}]$, $[\text{Cu}^{\text{II}}(\text{TPMA}^{*2})\text{Br}][\text{Br}]$ and $[\text{Cu}^{\text{II}}(\text{TPMA}^{*3})\text{Br}][\text{Br}]$ complexes in acetonitrile. The electrochemical data relative to SCE are given in **Table 2.2.4**. Values for previously reported $[\text{Cu}^{\text{II}}(\text{TPMA})\text{Br}][\text{Br}]$ ⁴⁰ and

Table 2.2.4. Cyclic Voltammetry Data for Copper Complexes with TPMA Based Ligands in Acetonitrile.

Complex ^a	$E_{1/2}$ (mV)	ΔE_p (mV)	i_{pa}/i_{pc}	Ref.
$[\text{Cu}^{\text{I}}(\text{TPMA}^{*1})\text{Br}][\text{Br}]$	-310	84	0.96	this work
$[\text{Cu}^{\text{I}}(\text{TPMA}^{*2})\text{Br}][\text{Br}]$	-360	86	0.95	this work
$[\text{Cu}^{\text{I}}(\text{TPMA}^{*3})\text{Br}][\text{Br}]$	-420	79	1.18	this work
$[\text{Cu}^{\text{I}}(\text{TPMA})\text{Br}][\text{Br}]$	-240	93	1.08	⁴⁰
$[\text{Cu}^{\text{I}}(\text{Me}_6\text{TREN})\text{Br}][\text{Br}]$	-300	115	0.72	²⁹

^aPotentials are reported relative to SCE and were measured under the same electrochemical cell conditions

$[\text{Cu}^{\text{II}}(\text{Me}_6\text{TREN})\text{Br}][\text{Br}]^{29}$ are included for comparison. All copper complexes displayed a single quasireversible redox behavior with $i_{\text{pa}}/i_{\text{pc}}$ varying from 0.95 to 1.18 and peak separations of less than 90 mV at a scan rate of 100 mV/s. Interestingly, a nearly stepwise decrease ($\Delta E \sim 60$ mV) of $E_{1/2}$ values (TPMA (-240 mV) > TPMA*1 (-310 mV) > TPMA*2 (-360 mV) > TPMA*3 (-420 mV)) was observed on going from $[\text{Cu}^{\text{II}}(\text{TPMA})\text{Br}][\text{Br}]$ to $[\text{Cu}^{\text{II}}(\text{TPMA}^*3)\text{Br}][\text{Br}]$, clearly indicating that the presence of electron donating groups in the 4 (-OMe) and 3,5 (-Me) positions of the pyridine rings in TPMA increases the reducing ability of the corresponding copper(I) complexes.

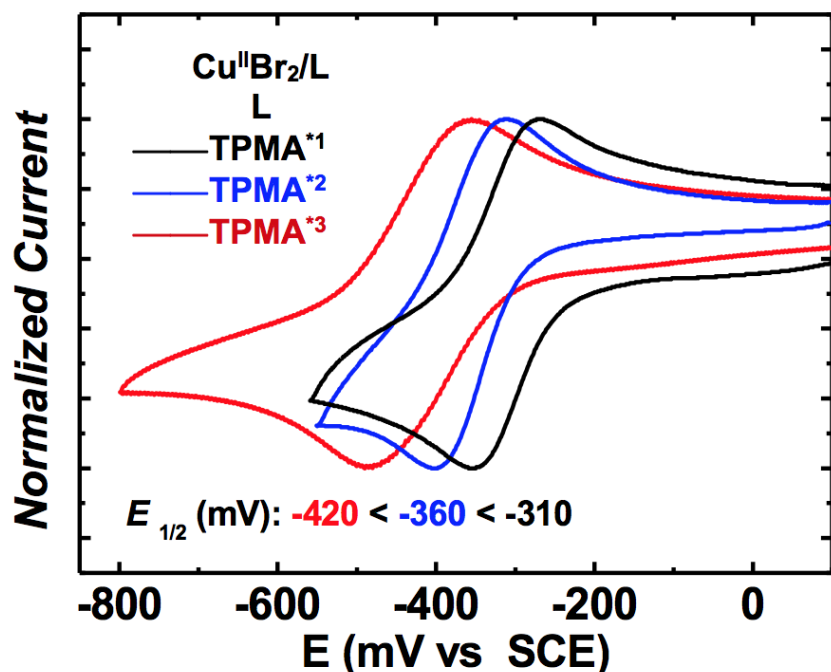


Figure 2.2.9. Cyclic voltammograms of $\text{Cu}^{\text{II}}\text{Br}_2$ complexes with TPMA*¹, TPMA*² and TPMA*³ ligands at 25 °C. All measurements were conducted in acetonitrile with 0.1 M TBAPF₆ as a supporting electrolyte at a scan rate of 100 mV/s, $[\text{Cu}^{\text{II}}\text{Br}_2]_0:[\text{L}]_0=1:1$, $[\text{Cu}^{\text{II}}\text{Br}_2]_0=1.0$ mM.

Similar trends were observed previously in the case of copper complexes containing tris-4-substituted (-^tBu, -Me, -MeO and -NMe₂) TPMA³⁵ and 4,4'-substituted (-Me, -MeO and

-NMe₂) bipyridine³⁴ based ligands. Furthermore, cyclic voltammograms for the copper(II) triflate complexes with substituted TPMA based ligands also followed the similar trend, with the exception that the $E_{1/2}$ values were less negative by ~250-275 mV. The diminished reducing potential originates from the differences in Cu^{II} stability constants as discussed below.^{31,32,40,52}

Another method for predicting the activity of copper catalysts in ATRP is to compare the stability constants of the Cu^{II} and Cu^I complexes with the particular ligand (β^{II} : Cu^{II}+mL \rightleftharpoons Cu^{II}L_m and β^I : Cu^I+mL \rightleftharpoons Cu^IL_m, respectively), since the equilibrium constant for atom transfer, K_{ATRP} , directly correlates with the ratio β^{II}/β^I . More importantly, β^{II} and β^I should be large in order to eliminate or suppress possible concurrent reactions such as coordination of monomer and/or polymer, which are typically present in large excess relative to the catalyst. Generally, more reducing copper complex should be more stable in its oxidized form (i.e. Cu^{II} should be more stable than Cu^I) in order to achieve high catalytic activity.²⁷ For the case of relatively stable 1:1 copper complexes, the ratio of the stability constants can be calculated from the readily available reduction potentials using Eq. [2], where $E_{\text{Cu}^{II}/\text{Cu}^I}^{o'}$ corresponds to a standard reduction potential for the Cu^{II}/Cu^I couple in the absence of a coordinating ligand.⁵³⁻⁵⁶

$$\ln \frac{\beta^{II}}{\beta^I} = \frac{F}{RT} (E_{\text{Cu}^{II}/\text{Cu}^I}^{o'} - E_{\text{Cu}^{II}L/\text{Cu}^IL}^{o'}) \quad [2]$$

Unfortunately, Eq. [2] only provides the ratio and not the specific stability constants for the respective oxidation states. While this ratio may increase with more active catalysts, it is not directly known whether this is a result of an increase in β^{II} or a decrease in β^I . However, another quantity, namely $\beta^{II}/(\beta^I)^2$ ratio, can be readily obtained from

disproportionation studies as previously reported in the literature.^{57,71} Utilizing the reaction between Cu^0 and $[\text{Cu}^{\text{II}}/\text{L}][\text{OTf}]_2$ (L=complexing ligand), the equilibrium constant, K_{disp} , can be determined and consequently $\beta^{\text{II}}/(\beta^{\text{I}})^2$. Finally, using these two experimentally determined ratios ($\beta^{\text{II}}/\beta^{\text{I}}$ and $\beta^{\text{II}}/(\beta^{\text{I}})^2$), the individual stability constants β^{I} and β^{II} can be calculated. It is important to note that both the electrochemical and disproportionation studies need to be conducted in the same solvent for more accurate and consistent results.

Using Eq. [1] and $E_{\text{Cu}^{\text{II}}/\text{Cu}^{\text{I}}}^{\circ}$ for CH_3CN , which was determined by potentiometry,⁵² the ratio of stability constants ($\beta_{\text{Br}}^{\text{II}} / \beta_{\text{Br}}^{\text{I}}$) for the coordination of Br^- anions to copper(I and II) complexes with TPMA^{*1}, TPMA^{*2} and TPMA^{*3} were determined to be 2.0×10^4 , 1.5×10^4 and 3.6×10^4 , respectively. These results were in excellent agreement with the previously reported value for TPMA (2.5×10^4),²⁵ and indicate that the degree of ligand arm substitution does not significantly affect halidophilicity. The stability constants ($\beta_{\text{L}}^{\text{II}}$ and $\beta_{\text{L}}^{\text{I}}$) for the complexation of TPMA, TPMA^{*1}, TPMA^{*2} and TPMA^{*3} ligands to copper(I and II) triflate complexes in dimethylformamide at 25 °C are summarized in **Table 2.2.5**. On going from TPMA to TPMA^{*3}, the stability constant β^{I} remains nearly constant, while β^{II} increases nearly 2300 times. Therefore, the trend observed in redox potentials discussed above clearly indicate that the TPMA based ligands induce a stronger influence towards the stabilization of the copper(II) oxidation state ($\log \beta^{\text{I}} = 13.4 \pm 0.2$, $\log \beta^{\text{II}} = 19.3$ (TPMA^{*1}), 20.5 (TPMA^{*2}) and 21.5 (TPMA^{*3})).

Electrochemical data, stability constants and previously established linear correlation between $\ln(K_{\text{ATRP}})$ and $E_{1/2}$ values^{23,29} indicate that copper complexes with

TPMA^{*1}, TPMA^{*2} and TPMA^{*3} ligands should have the equilibrium constant for atom transfer (K_{ATRP}) approximately 10, 100 and 1000 times larger than TPMA ($\Delta(E_2^0 - E_1^0) = 59 \text{ mV} \rightarrow K_2 / K_1 = 10$). Indeed, for $\text{Cu}^{\text{I}}(\text{TPMA}^{*3})\text{Br}$ complex, the equilibrium constant for atom transfer ($K_{\text{ATRP}} = k_a/k_d = 8400/2.0 \times 10^7 = 4.2 \times 10^{-4}$) was found to be nearly 1300 larger than for $\text{Cu}^{\text{I}}(\text{TPMA})\text{Br}$ ($K_{\text{ATRP}} = k_a/k_d = 3.8 \text{ M}^{-1}\text{s}^{-1}/1.2 \times 10^7 \text{ M}^{-1}\text{s}^{-1} = 3.2 \times 10^{-7}$). The large difference in K_{ATRP} values can be attributed mostly to an increase in the activation rate constant (k_a , $8400 \text{ M}^{-1}\text{s}^{-1}$ v.s. $3.8 \text{ M}^{-1}\text{s}^{-1}$), indicating that $\text{Cu}^{\text{I}}(\text{TPMA}^{*3})\text{Br}$ should be much more active in ATRP, as confirmed by recently published study.³⁷

Table 2.2.5. Stability Constants for Copper Triflate Complexes with TPMA Based Ligands in Dimethylformamide at 25 °C.

Ligand	β^{I}	β^{II}	$\log(\beta^{\text{II}}/\beta^{\text{I}})$
TPMA	1.3×10^{13}	1.3×10^{18}	5.0
TPMA ^{*1}	2.4×10^{13}	2.0×10^{19}	5.9
TPMA ^{*2}	1.6×10^{13}	3.0×10^{20}	7.3
TPMA ^{*3}	3.4×10^{13}	3.0×10^{21}	7.9

Application in Atom Transfer Radical Polymerization (ATRP).

TPMA is a widely used ligand for copper catalyzed ATRP methods ranging from conventional ATRP^{11,12,57} to improved protocols that require only ppm amounts of the catalyst.^{9,10,13-17,58} These enhanced synthetic procedures allow for the use of air stable Cu^{II} complexes, often eliminating the need for deoxygenation, and rely on the continuous reduction of Cu^{II} to Cu^{I} species within the polymerization process. Consequently, additional non-radical (e.g. tin(II) 2-ethylhexanoate = $\text{Sn}(\text{EH})_2$, ascorbic acid or

hydrazine) or radical (e.g. AIBN or V-70) reducing agents are employed. The selection of appropriate ATRP conditions is reliant on various factors such as monomer, initiator, ligand, solvent, etc.^{18,25} Large K_{ATRP} values require ATRP methods with constant regeneration of Cu^{I} complex due to early termination reactions that typical occur under normal ATRP conditions. Therefore, in the present study, activators regenerated by electron transfer (ARGET) ATRP⁵⁹ of *n*-butyl acrylate (*n*BA) was targeted utilizing low amounts of $\text{Sn}(\text{EH})_2$ as the reducing agent and only 10 ppm of the copper complexes with TPMA, TPMA^{*1}, TPMA^{*2} and TPMA^{*3} ligands. As indicated in Table 6, all catalysts showed excellent conversion and good correlation between experimental ($M_{n,\text{exp}}$) and theoretical molecular weights ($M_{n,\text{theo}}$). However, $[\text{Cu}^{\text{II}}(\text{TPMA}^{*2})\text{Cl}][\text{Cl}]$ and $[\text{Cu}^{\text{II}}(\text{TPMA}^{*3})\text{Cl}][\text{Cl}]$ showed a significantly narrower molecular weight distributions (M_w/M_n) than the corresponding copper(II) complexes with TPMA and TPMA^{*1} ligands, indicating better control in the polymerization system. Next, the kinetics were studied to further confirm reversible deactivation radical polymerization behavior. During the first 7h of the polymerization, a pseudo first order kinetic plot ($\ln([M]_0/[M]_t)$ v.s. t) was linear demonstrating constant radical concentration, which is one of the main criteria for a controlled ATRP. Additionally, a linear increase of experimentally determined molecular weight ($M_{n,\text{exp}}$) with monomer conversion was observed, as expected. However, $M_{n,\text{exp}}$ higher than the $M_{n,\text{theo}}$ values were obtained at the beginning of the polymerization, potentially indicating slow initiation. We are currently in the process of conducting detailed kinetic studies and further explore ATRP activity of copper complexes with substituted TPMA based ligands. Based on the straightforward synthesis and a large

value for K_{ATRP} , the preliminary results indicated that the TPMA^{*2} ligand could have a higher future potential in copper catalyzed ATRP than previously reported TPMA^{*3}.

Table 2.2.6. Polymerization Results for ARGET ATRP of *n*-Butyl Acrylate Catalyzed by 10 ppm of Copper Complexes with TPMA Based Ligands.

Complex ^a	Conv. (%)	$M_{n,\text{exp}}$	$M_{n,\text{theo}}$	M_w/M_n
[Cu ^{II} (TPMA)Cl][Cl]	90.5	19800	18800	2.01
[Cu ^{II} (TPMA ^{*1})Cl][Cl]	64.0	13500	13110	1.54
[Cu ^{II} (TPMA ^{*2})Cl][Cl]	90.0	19400	18700	1.46
[Cu ^{II} (TPMA ^{*3})Cl][Cl]	81.0	17800	16800	1.50

^aConditions: $[n\text{BA}]_0:[\text{EBiB}]_0:[\text{Sn}(\text{EH})_2]_0:[\text{TPMA}$ or TPMA^{*x}]₀:[Cu^{II}Cl₂]₀=160:1:0.1:0.03:0.016, EBiB=ethyl 2-bromoisobutyrate, $[n\text{BA}]_0=5.6$ M, 20% (v/v) anisole, $[\text{Cu}^{\text{II}}]_0=10$ ppm, $T=60$ °C, $t=24$ h. Monomer conversion was determined by ¹H NMR spectroscopy using anisole as an internal standard.

2.3. CONCLUSIONS

In summary, synthesis, characterization, electrochemical studies and ATRP activity of a series of novel copper(I and II) complexes with TPMA based ligands containing 4-methoxy-3,5-dimethyl substituted pyridine arms were reported. In the solid state, Cu^I(TPMA^{*1})Br, Cu^I(TPMA^{*2})Br and Cu^I(TPMA^{*3})Br complexes were found to be distorted tetrahedral in geometry and contained coordinated bromide anions (Cu^I-Br=2.3511(10) Å, 2.5025(3) Å and 2.5045(6) Å, respectively). Pseudo coordination of the aliphatic nitrogen atom to copper(I) center was observed in Cu^I(TPMA^{*2})Br (Cu^I-N=2.4190(19) Å) and Cu^I(TPMA^{*3})Br (Cu^I-N=2.406(3) Å) complexes, whereas pyridine arm dissociation occurred in Cu^I(TPMA^{*1})Br complex (Cu^I-N_{py}= 3.494(3)) Å). Regardless of the number of 4-methoxy-3,5-dimethyl substituted pyridine arms in

TPMA^{*2} and TPMA^{*3} complexes, two of the Cu^I-N_{py} bonds were nearly identical (2.083±0.012 Å), whereas the third one either increased (TPMA^{*3}: Cu^I-N_{py}=2.116(3) Å) or decreased (TPMA^{*2}: Cu^I-N_{py}=2.0452(17) Å). In solution, all copper(I) complexes with substituted TPMA ligands were found to be very fluxional. At low temperature, Cu^I(TPMA^{*1})Br was symmetrical and monomeric, while dissociation of either unsubstituted pyridine and/or 4-methoxy-3,5-dimethyl substituted pyridine arms was observed in Cu^I(TPMA^{*2})Br and Cu^I(TPMA^{*3})Br. On the other hand, the geometry of the copper(II) complexes in the solid state deviated from trigonal bipyramidal as confirmed by a decrease in τ values ([Cu^{II}(TPMA^{*1})Br][Br] ($\tau=0.92$) > [Cu^{II}(TPMA^{*3})Br][Br] ($\tau=0.77$) > [Cu^{II}(TPMA^{*2})Br][Br] ($\tau=0.72$)). Furthermore, cyclic voltammetry studies indicated a nearly stepwise decrease ($\Delta E \sim 60$ mV) of $E_{1/2}$ values (TPMA (-240 mV) > TPMA^{*1} (-310 mV) > TPMA^{*2} (-360 mV) > TPMA^{*3} (-420 mV)) on going from [Cu^{II}(TPMA)Br][Br] to [Cu^{II}(TPMA^{*3})Br][Br], confirming that the presence of electron donating groups in the 4 (-OMe) and 3,5 (-Me) positions of the pyridine rings in TPMA increases the reducing ability of the corresponding copper(I) complexes. This increase was mostly the result of a stronger influence of substituted TPMA ligands towards stabilization of the copper(II) oxidation state. Lastly, based on the straightforward synthesis and a large value for K_{ATRP} , the results indicate that TPMA^{*2} could have a higher future potential in copper catalyzed ATRP than previously reported TPMA^{*3}.

2.4. EXPERIMENTAL SECTION

General. All chemicals were purchased from commercial sources, and used as received if not stated otherwise. Tris(2-pyridylmethyl) amine (TPMA)¹⁴ and tris((4-methoxy-3,5-dimethylpyridin-2-yl)methyl)amine⁴⁰ were synthesized according to previously published literature procedures. Butyl acrylate (BA) was passed through a column filled with basic alumina to remove inhibitor prior to use. All procedures for atom transfer radical polymerizations and cyclic voltammetry were performed under argon or nitrogen. Solvents were degassed by at least three freeze-pump-thaw cycles. All manipulations involving copper(I) complexes were performed under argon in the drybox (<1.0 ppm O₂ and <0.5 ppm H₂O) or using standard Schlenk line techniques. Copper(II) complexes were synthesized under ambient conditions.

Instrumentation and Equipment. ¹H NMR spectra were obtained using Bruker Avance 300, 400 and/or 500 MHz spectrometers and chemical shifts are given in ppm relative to residual solvent peaks [CDCl₃ δ7.26 ppm; (CD₃)CO δ2.05 ppm; CD₃CN δ1.96 ppm]. iNMR and KaleidaGraph 4.1 software were used to generate images of NMR spectra. IR spectra were recorded in the solid state using Nicolet Smart Orbit 380 FT-IR spectrometer (Thermo Electron Corporation). Elemental analyses for C, H, and N were obtained from Midwest Microlabs, LLC. UV-Vis spectra were recorded using a Beckman DU-530 spectrometer in 1.0 cm path-length airtight quartz cuvettes. Mass spectra were recorded on a mass spectrometer with a Varian Saturn 2100T MS with 3900 GC using an EI source. In each case, characteristic fragments with their relative intensities in percentages are shown. Electrospray mass spectra were measured on a Thermo-Fisher

LCQ ESI/APCI Ion Trap containing a quadrupole field ion trap mass spectrometer with electrospray ionization (ESI). All cyclic voltammograms were measured at 25°C with a PARC 263A potentiostat. Solutions of CuBr₂ and Cu(OTf)₂ complexes with TPMA based ligands (1.0 mM) were prepared in dry acetonitrile containing 0.1 M NBu₄PF₆ as the supporting electrolyte. Measurements were carried out under N₂ atmosphere at a scanning rate (ν) of 0.1 Vs⁻¹, using a platinum disk and platinum mesh as the working and counter electrode, respectively. An Ag|AgIII⁻ reference electrode was used and potentials were measured relative to a ferrocenium/ferrocene couple ($E^{\circ}_{\text{Fc}^+/\text{Fc}}=0.391$ V vs SCE in CH₃CN),⁵⁹ which was used as an internal standard. This has allowed conversion of the potentials to the aqueous saturated calomel electrode (SCE) scale, to which all potentials are referenced. The stability constants for copper complexes (β^{I} and β^{II}) were determined using modified literature procedures,^{57,71}.

X-ray Crystal Structure Determination. The X-ray intensity data were collected at 150 K using graphite-monochromated Mo-K radiation (0.71073 Å) with a Bruker Smart Apex II CCD diffractometer. Data reduction included absorption corrections by the multi-scan method using SADABS.⁵² Structures were solved by direct methods and refined by full matrix least squares using SHELXTL 6.1 bundled software package.⁶⁰ The H-atoms were positioned geometrically (aromatic C-H 0.93, methylene C-H 0.97, and methyl C-H 0.96) and treated as riding atoms during subsequent refinement, with $U_{\text{iso}}(\text{H}) = 1.2U_{\text{eq}}(\text{C})$ or $1.5U_{\text{eq}}(\text{methyl C})$. The methyl groups were allowed to rotate about their local threefold axes. Crystal Maker 8.3 was used to generate molecular graphics.

Gel Permeation Chromatography (GPC). GPC was used to determine number average molecular weight (M_n) and M_w/M_n values. The GPC was conducted with a Waters 515 HPLC Pump and Waters 2414 Refractive Index Detector using PSS columns (Styrogel 102, 103, 105 Å) in tetrahydrofuran (THF) as an eluent at a flow rate of 1 mL/min at 35 °C. The column system was calibrated with 12 linear polystyrene (PSt, $M_n = 376\sim 2,570,000$) and 12 linear poly(methyl methacrylate) (PMMA, $M_n = 800 \sim 2,570,000$) standards. Diphenyl ether (DPE) was used as internal standard. Monomer conversion was determined by ^1H NMR spectroscopy.

Ligand Synthesis.

1-(4-methoxy-3,5-dimethylpyridin-2-yl)-N,N-bis(pyridin-2-ylmethyl)methanamine (TPMA^{*1}). A solution containing 2-chloromethyl-3,5-dimethyl-4-methoxypyridine•hydrochloride (100.0 mg, 0.450 mmol, 1.0 eq.), NaOH (36.0 mg, 0.900 mmol, 2.0 eq.) and 1.0 mL H₂O was added to bis(2-pyridylmethyl)amine (89.7 mg, 0.450 mmol, 1.0 eq.) dissolved in 1.0 mL of CH₂Cl₂ and heated in a pressure tube at 60 °C. After 24 hours, heterogeneous mixture was allowed to cool to room temperature, followed by the addition of 3.0 mL 1.0M NaOH solution. The aqueous layer was then extracted with CH₂Cl₂ (5x5.0 mL). The organic layers were combined and dried over MgSO₄. Following the filtration, yellow solution was concentrated under reduced pressure. Purification over alumina (MeOH/EtOAc, 5:95) yielded 120 mg (76%) of TPMA^{*1} as a yellowish oil. R_f : 0.47. ^1H NMR (400 MHz, CDCl₃, 298 K): δ 8.50 (d, $J=4.7$ Hz, 2H), δ 8.14 (s, 1H), δ 7.60 (td, $J=7.7, 1.9$ Hz, 2H), δ 7.43 (d, $J=7.8$ Hz, 2H), δ 7.11 (m, 2H), δ 3.83 (s, 6H), δ 3.69 (s, 3H), δ 2.18 (s, 3H), δ 2.12 (s, 3H). ^{13}C NMR (75 MHz,

CDCl₃, 298 K): δ164.1, 159.7, 157.0, 149.0, 148.7, 136.3, 126.4, 125.2, 123.7, 122.0, 60.5, 59.9, 59.3, 13.3, 10.9. MS (ESI) *m/z*: 349.2 [M+H]⁺.

1-(4-methoxy-3,5-dimethylpyridin-2-yl)-N-((4-methoxy-3,5-dimethylpyridin-2-yl)methyl)-N-(pyridin-2-ylmethyl)methanamine (TPMA*2). 2-Picolylamine (1.46 g, 13.5 mmol), 2-chloromethyl-4-methoxy-3,5-dimethylpyridine hydrochloride (6.00 g, 27.0 mmol) and Na₂CO₃ (7.25 g, 68.4 mmol) were placed in a pressure tube containing 200 mL of HPLC grade CH₃CN. Then, tetrabutylammonium bromide (3.0 mg, 9.3×10⁻³ mmol) was added to the stirred solution under nitrogen. The mixture was heated at 80 °C for 48 h, allowed to cool to room temperature, and poured into 150 mL 1.0 M NaOH. After extraction with CH₂Cl₂ (3×10.0 mL), the combined organic fractions were dried over Na₂SO₄, filtered, and the solvent evaporated under reduced pressure to give an orange/brown crude product. Purification over alumina (MeOH/EtOAc, 5:95) yielded 5.1 g (92%) of a yellowish, crystalline solid. *R_f*: 0.55. ¹H NMR (400 MHz, CDCl₃, 298 K): δ8.44 (d, *J*=4.7 Hz, 1H), δ8.15 (s, 2H), δ7.54 (td, *J*=7.8, 1.8 Hz, 1H), δ7.20 (d, *J*=7.8 Hz, 1H), δ7.09 (m, 1H), δ3.78 (s, 6H), δ3.68 (s, 6H), δ2.20 (s, 6H), δ1.91 (s, 6H). ¹³C NMR (75 MHz, CDCl₃, 298 K): δ164.1, 159.7, 157.2, 148.7, 148.5, 136.0, 126.5, 125.2, 124.4, 121.9, 60.5, 59.8, 59.3, 13.3, 10.5. MS (ESI) *m/z*: 407.2 [M+H]⁺.

Synthesis of Copper Complexes.

Cu^I(TPMA*1)Br. A solution of TPMA*1 (228 mg, 0.655 mmol) in 1.0 mL of methanol was added to a suspension of Cu^IBr (94.0 mg, 0.655 mmol) in 2.0 mL of methanol, resulting in the formation of a yellow solution. After stirring for 5 min at ambient

temperature, $\text{Cu}^{\text{I}}(\text{TPMA}^{*1})\text{Br}$ was precipitated as yellow powder by the slow addition of diethyl ether (yield=231 mg, 72%). X-ray quality crystals were obtained by crystallization in acetone via slow diffusion of diethyl ether. ^1H NMR ($(\text{CD}_3)_2\text{CO}$, 400 MHz, 220 K): δ 9.07 (s, 2H), δ 8.72 (s, 1H), δ 7.78 (pt, $J=7.5$ Hz, 2H), δ 7.39 (pd, $J=7.6$ Hz, 2H), δ 7.32 (m, 2H), δ 3.92 (m, 6H), δ 3.62 (s, 3H), δ 2.12 (s, 6H). Anal. Calcd. for $\text{C}_{21}\text{H}_{24}\text{BrCuN}_4\text{O}$ (491.89): C, 51.28; H, 4.92; N, 11.39. Found: C, 51.98; H, 4.99; N, 12.01.

$\text{Cu}^{\text{I}}(\text{TPMA}^{*2})\text{Br}$. The complex was prepared using the procedure for $\text{Cu}^{\text{I}}(\text{TPMA}^{*1})$ except that $\text{Cu}^{\text{I}}\text{Br}$ (94.0 mg, 0.655 mmol) and TPMA^{*2} (266 mg, 0.655 mmol) were used. Yield=331 mg (89%). X-ray quality crystals were obtained by crystallization in methanol via slow diffusion of diethyl ether. ^1H NMR ($(\text{CD}_3)_2\text{CO}$, 400 MHz, 188 K): δ 9.03 (m, 1H), δ 8.72 (s, 1H), δ 8.51 (m, 2H), δ 8.19 (s, 3H), δ 7.78 (m, 3H), δ 7.39 (m, 2H), δ 3.93(s, 2H), δ 3.90 (s, 1H), δ 3.67 (s, 6H), δ 2.19(s, 6H), δ 2.14(s, 6H) δ 1.80(s, 6H). Anal. Calcd. for $\text{C}_{24}\text{H}_{30}\text{BrCuN}_4\text{O}_2$ (549.97): C, 52.41; H, 5.50; N, 10.19. Found: C, 52.46; H, 5.47; N, 11.01.

$\text{Cu}^{\text{I}}(\text{TPMA}^{*3})\text{Br}$. The complex was prepared using the procedure for $\text{Cu}^{\text{I}}(\text{TPMA}^{*1})$ except that $\text{Cu}^{\text{I}}\text{Br}$ (94.0 mg, 0.655 mmol) and TPMA^{*3} (330 mg, 0.655 mmol) were used. Yield=331 mg (83%). X-ray quality crystals were obtained by crystallization in methanol via slow diffusion of diethyl ether. ^1H NMR ($(\text{CD}_3)_2\text{CO}$, 400 MHz, 188 K): δ 8.68 (s, 2H), δ 8.22 (s, 1H), δ 8.51 (m, 2H), δ 3.67(s, 4H), δ 3.61 (s, 2H), δ 3.67 (s, 6H), δ 2.19(s, 9H),

δ 2.14(s, 9H) δ 2.08(s, 9H). Anal. Calcd. for $C_{27}H_{36}BrCuN_4O_3$ (608.04): C, 53.33; H, 5.97; N, 9.21. Found: C, 53.42; H, 5.94; N, 9.41.

[Cu^{II}(TPMA^{*1})Br][Br]. A solution of TPMA^{*1} (425 mg, 1.21 mmol) in 5.0 mL of methylene chloride was added to a round-bottom flask containing Cu^{II}Br₂ (273 mg, 1.22 mmol). The reaction mixture was stirred at room temperature for 15 min and the product precipitated by the slow addition of *n*-pentane (ca. 20 mL). The supernatant liquid was decanted and the green powder was washed with 3×5.0 mL of *n*-pentane and dried under vacuum to yield 519 mg (75%) of [Cu^{II}(TPMA^{*1})Br][Br]. X-ray quality crystals were obtained by crystallization in dichloromethane via slow diffusion of *n*-pentane. UV-Vis (CH₃CN): λ_{max} = 983 nm, ϵ_{max} = 176.5 Lmol⁻¹cm⁻¹. FT-IR (solid): ν (cm⁻¹) = 3053(w), 2998(s), 1605(s) 1574(w), 1475.8(w), 1433(s), 1263(s), 1078(s), 733(s), 704(s), 610(s) Anal. Calcd. for $C_{21}H_{24}Br_2CuN_4O$ (571.79): C, 44.11; H, 4.23; N, 9.80. Found: C, 43.92; H, 4.29; N, 9.34.

[Cu^{II}(TPMA^{*2})Br][Br]. The complex was prepared using the procedure for [Cu^{II}(TPMA^{*1})Br][Br] except that Cu^{II}Br₂ (326 mg, 1.46 mmol) and TPMA^{*2} (593 mg, 1.46 mmol) were used. Yield=791 mg (86%). X-ray quality crystals were obtained by crystallization in dichloromethane via slow diffusion of *n*-pentane. UV-Vis (CH₃CN): λ_{max} = 980 nm, ϵ_{max} = 185 Lmol⁻¹cm⁻¹. FT-IR(Solid): ν (cm⁻¹) = 3053(w), 2998(w), 1600(s), 1578 (w), 1475(s), 1427(s), 1400(w), 1265(s), 1074(s), 994(s), 733(s), 704(s), 611(s). Anal. Calcd. for $C_{24}H_{30}Br_2CuN_4O_2$ (629.87): C, 45.76; H, 4.80; N, 8.89. Found: C, 45.38; H, 4.69; N, 8.02.

[Cu^{II}(TPMA^{*3})Br][Br]. The complex was prepared using the procedure for [Cu^{II}(TPMA^{*1})Br][Br] except that Cu^{II}Br₂ (326 mg, 1.46 mmol) and TPMA^{*3} (678 mg, 1.46 mmol) were used. Yield=844 mg (84%). X-ray quality crystals were obtained by crystallization in dichloromethane via slow diffusion of *n*-pentane. UV-Vis (CH₃CN): λ_{max} = 981 nm, ϵ_{max} = 191 Lmol⁻¹cm⁻¹. FT-IR(Solid): ν (cm⁻¹) = 3370(w), 2942(b), 1709(s) 1598(w), 1477(s), 1419(w), 1401(s), 1270(s), 1113(s), 1076(s), 997(s), 881(w). Anal. Calcd. for C₂₇H₃₆Br₂CuN₄O₃ (687.95): C, 47.14; H, 5.27; N, 8.14. Found: C, 45.52; H, 5.09; N, 8.02.

General Procedure for ARGET ATRP reactions. ATRP reactions were performed in 20 mL Schlenk flasks. In a typical experiment, butyl acrylate (BA) (22.5 mmol, 3.207 mL) and ethyl 2-bromoisobutyrate (EBiB) (0.141 mmol, 20.4 μ L) was dissolved in 70 μ L of anisole. After the addition of Cu^{II} complex, ([Cu^{II}Cl₂]₀: [TPMA^{*} ligand]₀) = 1:2; [Cu^{II}Cl₂]₀: [alkene]₀ = 10,000:1), the reaction mixture was degassed by three freeze pump thaw (FPT) cycles. The solution of tin(II) ethylhexanoate (0.03 M solution in anisole, 0.466 mL, 1.0 $\times 10^{-2}$ mmol) was also degassed using three FPT cycles, and then added to the reaction mixture under nitrogen atmosphere. The flask was placed in the oil bath at 60°C for 24 hrs. The conversion of the monomer was determined by ¹H NMR spectroscopy using anisole as the internal standard.

REFERENCES

1. Anderegg, G.; Wenk, F. *Helv. Chim. Acta* **1967**, *50*, 2330-2332.
2. Canary, J. W.; Yank, Y.; Roy, R.; Que, L. J.; Miyake, H. *Inorg. Synth.* **1998**, *32*, 70-75.

3. Eckenhoff, W. T.; Pintauer, T. *Inorg. Chem.* **2010**, *49*, 10617-10626.
4. Pintauer, T.; Matyjaszewski, K. *Coord. Chem. Rev.* **2005**, *249*, 1155-1184.
5. Karlin, K. D.; Zubieta, J. *Copper Coordination Chemistry: Biochemical and Inorganic Perspectives*; Adenine Press: New York, 1983.
6. Bjernemose, J.; Hazell, A.; McKenzie, C. J.; Mahon, M. F.; Nielsena, L. P.; Raithby, P. R.; Simonsen, O.; Toftlund, H.; Wolny, J. A. *Polyhedron* **2003**, *22*, 875-885.
7. Mandon, D.; Machkour, A.; Goetz, S.; Welter, R. *Inorg. Chem.* **2002**, *41*, 5364-5372.
8. Baldwin, M. J.; Ross, P. K.; Pate, J. E.; Tyeklar, Z.; Karlin, K. D.; Solomon, E. I. *J. Am. Chem. Soc.* **1991**, *113*, 8671-8679.
9. Fry, H. C.; Scaltrito, D. V.; Karlin, K. D.; Meyer, G. J. *J. Am. Chem. Soc.* **2003**, *125*, 11866-11871.
10. Karlin, K. D.; Hayes, J. C.; Juen, S.; Hutchinson, J. P.; Zubieta, J. *Inorg. Chem.* **1982**, *21*, 4106-4108.
11. Karlin, K. D.; Nanthakumar, A.; Fox, S.; Murthy, N. N.; Ravi, N.; Huynh, B. H.; Orosz, R. D.; Day, E. P. *J. Am. Chem. Soc.* **1994**, *116*, 4753-4763.
12. Karlin, K. D.; Wei, N.; Jung, B.; Kaderli, S.; Niklaus, P.; Zuberbuehler, A. D. *J. Am. Chem. Soc.* **1993**, *115*, 9506-9514.
13. Tyeklar, Z.; Jacobson, R. R.; Wei, N.; Murthy, N. N.; Zubieta, J.; Karlin, K. D. *J. Am. Chem. Soc.* **1993**, *115*, 2677-2689.
14. Wei, N.; Lee, D.; Murthy, N. N.; Tyeklar, Z.; Karlin, K. D.; Kaderli, S.; Jung, B.; Zuberbuehler, A. D. *Inorg. Chem.* **1994**, *33*, 4625-4626.

15. Wei, N.; Murthy, N. N.; Chen, Q.; Zubieta, J.; Karlin, K. D. *Inorg. Chem.* **1994**, *33*, 1953-1965.
16. Chishiro, T.; Shimazaki, Y.; Tani, F.; Naruta, Y. *Chem. Comm.* **2005**, 1078-1081.

17. Kim, E.; Helton, M. E.; Wasser, I. M.; Karlin, K. D.; Shen, L.; Hong-wei, H.; Moënné-Loccoz, P.; Incarvito, C. D.; Rheingold, A. L.; Honecker, M.; Kaderli, S.; Zuberbühler, A. D. *PNAS* **2003**, *100*, 3623-3628.

18. Company, A.; Lloret, J.; HGomez, L.; Costas, M. In *Alkane C-H Activation using Single Site Metal Catalysis*; Perez, P., Ed.; Springer: New York, 2012; Vol. 38, p 143.

19. Plietker, B. *Iron Catalysis in Organic Chemistry: Reactions and Applications*; Wiley-VCH: Weinheim, 2008.

20. Yamaguchi, M.; Kousaka, H.; Izawa, S.; Ichii, Y.; Kumano, T.; Masui, D.; Yamagishi, T. *Inorg. Chem.* **2006**, *45*, 8342-8354.

21. Jastrzebski, R.; Weckhuysen, B. M.; Bruijninx, P. C. A. *Chem. Comm.* **2013**, *49*, 6912-6914.

22. Kojima, T.; Matsuo, H.; Matsuda, Y. *Inorg. Chim. Acta* **2000**, *300-302*, 661-667.

23. Britovsek, G.; England, J.; White, A. *Inorg. Chem.* **2005**, *44*, 8125-8134.

24. Yoon Lee, J.; Peterson, R. L.; Ohkubo, K.; Garcia-Bosch, I.; JHimes, R. A.; Woertink, J.; Moore, C. D.; Solomon, E. I.; Fukuzumi, S.; Karlin, K. D. *J. Am. Chem. Soc.* **2014**, *136*, 9925-9937.

25. Ricardo, C.; Pintauer, T. *Chem. Commun.* **2009**, 3029-3031.

26. Ricardo, C.; Pintauer, T. *Eur. J. Inorg. Chem.* **2011**, 1292-1301.

27. Ricardo, C.; Pintauer, T. *Isr. J. Chem.* **2012**, *52*, 320-327.

28. Ricardo, C.; Pintauer, T. *ACS Symp. Ser.* **2012**, *1100*, 73-98.
29. Berg, R.; Straub, B. F. *Beilstein J. Org. Chem.* **2013**, *9*, 2715-2750.

30. Clark, A. J. *Chem. Soc. Rev.* **2002**, *31*, 1-11.

31. Eckenhoff, W. T.; Pintauer, T. *Cat. Rev. Sci. Eng.* **2010**, *52*, 1-59.

32. Pintauer, T. *Eur. J. Inorg. Chem.* **2010**, 2449-2460.

33. Matyjaszewski, K.; Xia, J. *Chem. Rev.* **2001**, *101*, 2921-2990.

34. Wang, J.-S.; Matyjaszewski, K. *J. Am. Chem. Soc.* **1995**, *117*, 5614-5615.

35. Balili, M. N. C.; Pintauer, T. *Inorg. Chem.* **2009**, *48*, 9018-9026.

36. Eckenhoff, W. T.; Garrity, S. T.; Pintauer, T. *Eur. J. Inorg. Chem.* **2008**, 563-571.

37. Eckenhoff, W. T.; Pintauer, T. *Inorg. Chem.* **2007**, *46*, 5844-5846.

38. Pintauer, T. *ACS Symp. Ser.* **2009**, *1023*, 63-84.

39. Pintauer, T.; Eckenhoff, W. T.; Ricardo, C.; Balili, M. N. C.; Biernesser, A. B.; Noonan, S. J.; Taylor, M. J. W. *Chem. Eur. J.* **2009**, *15*, 38-41.

40. Pintauer, T.; Matyjaszewski, K. *Chem. Soc. Rev.* **2008**, *37*, 1087-1097.

41. Pintauer, T.; Matyjaszewski, K. *Top. Organomet. Chem.* **2009**, *26*, 221-251.

42. Muñoz-Molina, J. M.; Belderraín, T. R.; Pérez, P. J. *Adv. Synth. Catal.* **2008**, *350*, 2365-2372.

43. Muñoz-Molina, J. M.; Belderraín, T. R.; Pérez, P. J. *Inorg. Chem.* **2010**, *49*, 642-645.
44. Muñoz-Molina, J. M.; Caballero, A.; Díaz-Requejo, M. M.; Trofimenko, S.; Belderraín, T. R.; Pérez, P. J. *Inorg. Chem.* **2007**, *46*, 7725-7730.
45. Balili, M. N. C.; Pintauer, T. *Inorg. Chem.* **2010**, *49*, 5642-5649.
46. Jakubowski, W.; Matyjaszewski, K. *Macromolecules* **2005**, *38*, 4139-4146.
47. Jakubowski, W.; Matyjaszewski, K. *Angew. Chem. Int. Ed.* **2006**, *45*, 4482-4486.
48. Jakubowski, W.; Min, K.; Matyjaszewski, K. *Macromolecules* **2006**, *39*, 39-45.
49. Matyjaszewski, K.; Jakubowski, W.; Min, K.; Tang, W.; Huang, J.; Braunecker, W. A.; Tsarevsky, N. V. *Proc. Natl. Acad. Sci. U.S.A.* **2006**, *103*, 15309-15314.
50. Matyjaszewski, K. *Macromolecules* **2012**, *45*, 4015-4039.
51. Coessens, V.; Pintauer, T.; Matyjaszewski, K. *Prog. Polym. Sci.* **2001**, *26*, 337.
52. Tsarevsky, N. V.; Matyjaszewski, K. *Chem. Rev.* **2007**, *107*, 2270-2299.
53. Matyjaszewski, K.; Tsarevsky, N. V. *Nat. Chem.* **2009**, *1*, 276-288.
54. Pintauer, T.; McKenzie, B.; Matyjaszewski, K. *ACS Symp. Ser.* **2003**, *854*, 130-147.
55. Braunecker, W. A.; Matyjaszewski, K. *Prog. Polym. Sci.* **2007**, *32*, 93-146.
56. Tang, W.; Kwak, Y.; Braunecker, W.; Tsarevsky, N. V.; Coote, M. L.; Matyjaszewski, K. *J. Am. Chem. Soc.* **2008**, *130*, 10702-10713.

57. Tsarevsky, N. V.; Braunecker, W. A.; Matyjaszewski, K. *J. Organomet. Chem.* **2007**, *692*, 3212-3222.
58. Tsarevsky, N. V.; Braunecker, W. A.; Vacca, A.; Gans, P.; Matyjaszewski, K. *Macromol. Symp.* **2007**, *248*, 60-70.
59. Tang, W.; Tsarevsky, N. V.; Matyjaszewski, K. *J. Am. Chem. Soc.* **2006**, *128*, 1598-1604.
60. Qiu, J.; Matyjaszewski, K.; Thounin, L.; Amatore, C. *Macromol. Chem. Phys.* **2000**, *201*, 1625-1631.
61. Navon, N.; Golub, G.; Cohen, H.; Paoletti, P.; Valtancoli, B.; Bencini, A.; Meyerstein, D. *Inorg. Chem.* **1999**, *38*, 3484-3488.
62. Ambundo, E. A.; Deydier, M. V.; Grall, A. J.; Aguera-Vega, N.; Dressel, L. T.; Copper, T. H.; Heeg, M. J.; Ochrymowycz, L. A.; Rorabacher, D. B. *Inorg. Chem.* **1999**, *38*, 4233-4242.
63. Golub, G.; Lashaz, A.; Cohen, A.; Paoletti, P.; Bencini, A.; Valtancoli, B.; Meyerstein, D. *Inorg. Chim. Acta* **1997**, *255*, 111-115.
64. Tsarevsky, N. V.; Tang, W.; Brooks, S. J.; Matyjaszewski, K. *ACS Symp. Ser.* **2006**, *944*, 56-70.
65. Magenau, A. J. D.; Kwak, Y.; Schröder, K.; Matyjaszewski, K. *ACS Macro Letters* **2012**, *1*, 508-512.
66. Zhang, C. X.; Kaderli, S.; Costas, M.; Kim, E.-I.; Neuhold, Y.-M.; Karlin, K. D.; Zuberbuhler, A. D. *Inorg. Chem.* **2003**, *42*, 1807-1824.
67. Xue, G.; Wang, D.; DeHont, R.; Fiedler, A. T.; Shan, Xiaopeng; Münck, E.; Que, L, Jr. *PNAS* **2007**, *104*, 20713-20718.
68. Schröder, K.; Mathers, R. T.; Buback, J.; Konkolewicz, D.; Magenau, A. J. D.; Matyjaszewski, K. *ACS Macro Letters* **2012**, *1*, 1037-1040.

69. Konkolewicz, D.; Schöder, K.; Buback, J.; Bernhard, S.; Matyjaszewski, K. *ACS Macro Letters* **2012**, *1*, 1219-1223.
70. Schröder, K.; Konkolewicz, D.; Poli, R.; Matyjaszewski, K. *Organometallics* **2012**, *31*, 7994-7999.
71. Bortolamei, N.; Isse, A. A.; Di Marco, V. B.; Gennaro, A.; Matyjaszewski, K. *Macromolecules* **2010**, *43*, 9257-9267.
72. Sheldrick, G. M. *SADABS Version 2.03*; University of Gottingen: Germany, 2002.
73. Sheldrick, G. M. *SHELXTL 6.1, Crystallographic Computing System*; Bruker Analytical X-Ray System: Madison, WI, 2000.
74. Hsu, S. C.; Chien, S. S.; Chen, H. H.; Chiang, M. Y. *Chin. Chem. Soc.* **2007**, *54*, 685-692.
75. Mason, J. *Chem. Rev.* **1987**, *87*, 1299-1312.
76. Kitagawa, S.; Munakata, M. *Inorg. Chem.* **1981**, *20*, 2261-2267.
77. Kitagawa, S.; Munakata, M.; Miyaji, N. *Inorg. Chem.* **1982**, *21*, 3842-3843.
78. Munakata, M.; Kitagawa, S.; Kosome, S.; Asahara, A. *Inorg. Chem.* **1986**, *25*, 2622-2627.
79. Thompson, J. S.; Swiatek, R. M. *Inorg. Chem.* **1985**, *24*, 110-113.
80. Eckenhoff, W. T.; Biernesser, A. B.; Pintauer, T. *Inorg. Chem.* **2012**, *51*, 11917-11929.
81. Addison, A. W.; Nageswara Rao, T.; Reedijk, J.; van Rijn, J.; Verschoor, G. C. *J. Chem. Soc. Dalton Trans.* **1984**, 1349-1356.

82. Harrison, W. D.; Kennedy, D. M.; Ray, N. J.; Sheahan, R.; Hathaway, B. J. *J. Chem. Soc. Dalton Trans.* **1981**, 1556-1564.
83. Eckenhoff, W. T.; Pintauer, T. *Dalton Trans.* **2011**, 40, 4909-4917.
84. Pintauer, T.; Qiu, J.; Kickelbick, G.; Matyjaszewski, K. *Inorg. Chem.* **2001**, 40, 2818-2824.
85. Hiskey, M. A.; Ruminski, R. R. *Inorg. Chim. Acta* **1986**, 112, 189-195.
86. McLachlan, G. A.; Fallon, G. D.; Martin, R. L.; Spiccia, L. *Inorg. Chem.* **1995**, 34, 254-261.
87. Hathaway, B. J. *Comprehensive Coordination Chemistry*; Pergamon Press: Oxford, England, 1987.
88. Buckingham, D. A.; Sargeson, A. M. In *Chelating Agents and Metal Chelates*; Dwyer, F. P., Mellor, D. P., Eds.; Academic Press: New York, 1964.
89. Lingane, J. J. *Chem. Rev.* **1941**, 29, 1.
90. Rossotti, F. J. C.; Rossotti, H. *The Determination of Stability Constants*; McGraw Hill: New York, 1961.
91. Vlcek, A. A. *Prog. Inorg. Chem.* **1963**, 5, 211.
92. Matyjaszewski, K.; Patten, T. E.; Xia, J. *J. Am. Chem. Soc.* **1997**, 119, 674-680.
93. Min, K.; Jakubowski, W.; Matyjaszewski, K. *Macromol. Rapid Commun.* **2006**, 27, 594-598.
94. Wang, Y.; Soerensen, N.; Zhong, M.; Schroeder, H.; Buback, M.; Matyjaszewski, K. *Macromolecules* **2013**, 46, 683-691.

Chapter 3

Copper Cyanide Coordination Polymers

3.1. Introduction

Inorganic-organic hybrid materials have gained popularity in the past few decades due to their unique properties such as electrical conductivity, magnetism, non-linear optics, molecular sensing, gas storage and zeolitic ability.¹⁻¹⁰ These properties are tunable and have potential to address today's energy and environmental issues, for example, storage of hydrogen, and methane gas, CO₂ sequestration, etc. The ability of the inorganic metal cations and organic ligands to self assemble in an infinite manner results in the formation of a coordination polymer. The structure and dimension of these polymers are determined by the various factors such as coordination and binding preferences of the metal, ligand flexibility, intermolecular forces in the polymeric framework such as H-bonding and π - π stacking. Using these structural directing elements, synthetic chemists can easily modulate the properties of the coordination polymer.

First row transition metals are the attractive starting materials due to their high stability and availability, and their chemistry has been extensively explored in comparison to second and third row elements. Generally metal salts such as halides, nitrates or with non-coordinating anions- perchlorates, triflates are used as precursors.^{6, 11-18} These metal salts coordinate to organic and/or inorganic ligands such as cyanide (CN⁻) and azide (N₃⁻) to form one- (1D), two- (2D) and three dimensional (3D) coordination polymers (**Figure 3.1.1**).

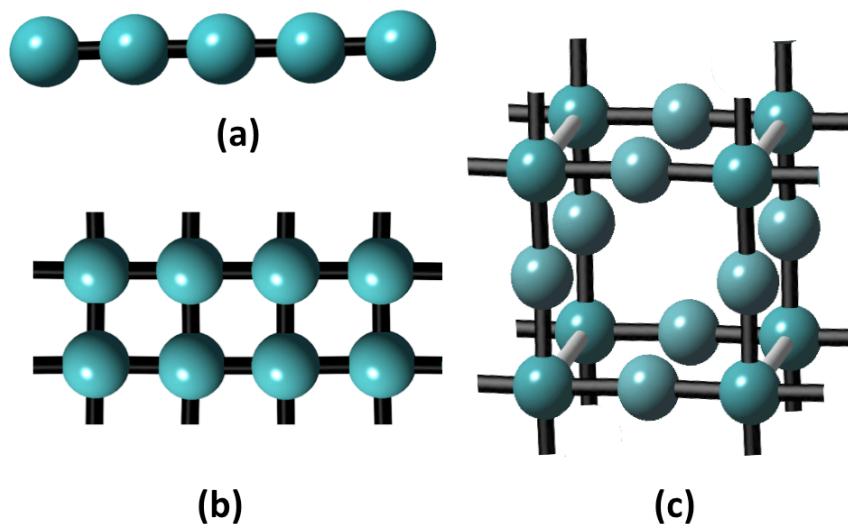


Figure 3.1.1. Different dimensionalities found in a coordination polymer: (a). 1D (b). 2D (c). 3D

Along with these two essential constituents, these polymers can also contain counter anions or guest molecules in the interstitial spaces. It is important to note that these polymers must extend in various dimensions via coordination bonding in order to be defined as a coordination polymer.

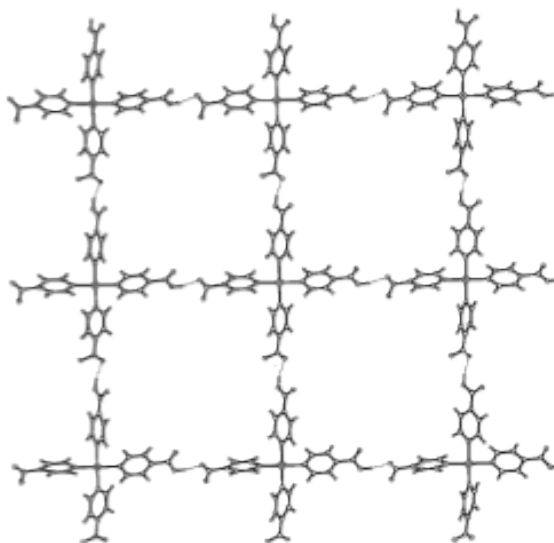


Figure 3.1.2. The hydrogen-bonded network formed by the Pt^{II} complex.^{1,14}

In **Figure 3.1.2**, a square planar platinum metal center, Pt(II) is coordinated to the four substituted pyridine ligands and is extended into 3D network via H-bonding. Because of this, the network can only be considered as a supramolecular compound rather than a 3D coordination polymer.¹⁴

3.2. Background

The first coordination polymer was discovered accidentally by Johann Diesbach, a German dyemaker during the synthesis of the cochineal red lake dye. Instead of a red color, the mixture turned blue upon mixing iron(II) sulfate with the cheap potash, later realized to be contaminated with ox blood. Not only was this the first example of coordination compound and a polymer, but also the first synthetic dye, known as prussian blue. In later years, this compound was commercially used and replaced very expensive lapis lazuli based blue dye.¹⁹ Even now, prussian blue and its analogs are extensively used as blue pigments in paints and also as antidote for heavy metal poisoning due to its strong metal affinity.

The structure of this dye was elucidated, 372 years after its discovery and found to be the iron based 3D coordination polymer with the formula, $[\text{Fe}_4(\text{Fe}(\text{CN})_6)_3 \cdot x\text{H}_2\text{O}]$ (**Figure 3.2.1, a**).^{20, 21} The crystal structure has a cubic framework made up of two iron species, Fe(II) and Fe(III) coordinated to each other via a cyanide ligand. Low spin (LS) Fe(II) and high spin (HS) Fe(III) sites have octahedral geometry and interstitial spaces are occupied by guest molecules, such as potassium ions (K^+) or water molecules.

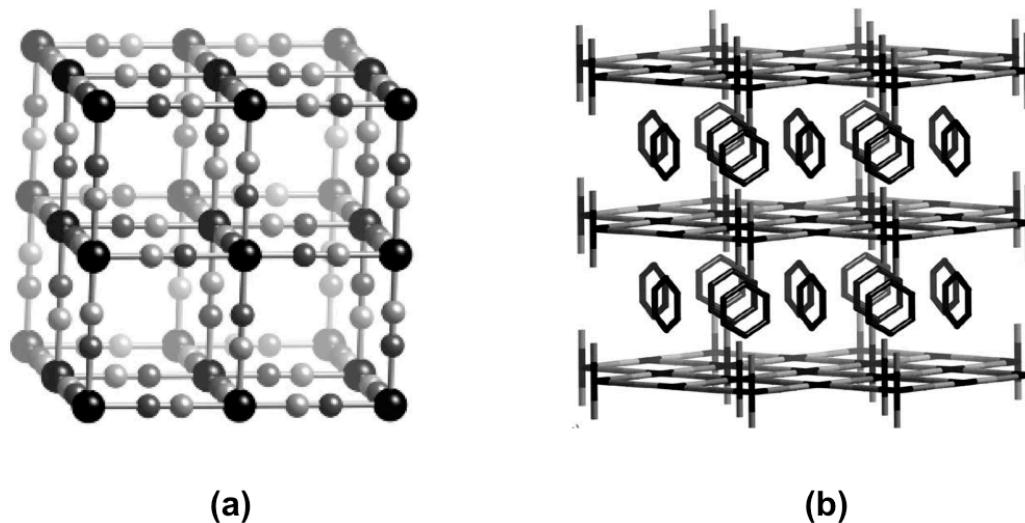


Figure 3.2.1. Molecular structure of (a) Prussian Blue and (b) Hofmann Clathrate.

Following this discovery, monomeric zinc ($\text{Zn}(\text{CN})_2$) and cadmium ($\text{Cd}(\text{CN})_2$) cyanometallate compounds were synthesized.^{22,23} In year 1949, Powell and Rayner synthesized and determined the structure of nickel based cyanide coordination polymer, $([\text{Ni}(\text{NH}_3)_2\text{Ni}(\text{CN})_4]_2\text{C}_6\text{H}_6)$, also known as hofmann clathrate (**Figure 3.2.1, b**).^{24,25} The research interests increased in this area due to the versatile nature of the cyanide ligand.^{26,27,28} This ambidentate nature monoanionic ligand can bind to a metal center through carbon as well as nitrogen via different binding modes (**Figure 3.2.3, a**). Through the carbon atom, the cyano group donates the electron pair from the HOMO to the metal's empty orbitals and can also, participate in back bonding by accepting the electrons from metal center to π^* orbitals (**Figure 3.2.2**).^{3,29,30}

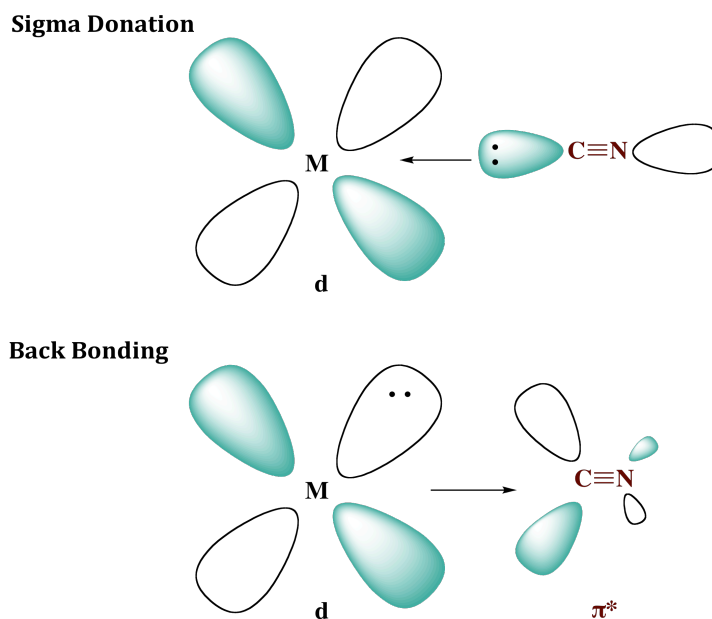


Figure 3.2.2. HOMO and LUMO orbitals of cyanide ligands involved in the sigma donation (top) and back bonding with metal (M) orbitals (bottom).

There are other small ligands such as isoelectronic carbonyl moiety ($-CO$) that tend to bind to the metal center in three different ways. Unlike the cyanide ligand, this ligand is regarded as an organic ligand because it binds to the metal center only via the carbon atom (**Figure 3.2.3, b**).

Another example, linear and inorganic azide ligand ($-N_3^-$) coordinate to the metal center in six different modes through nitrogen (**Figure 3.2.3, c**). The small and compact size of these ligands increases the stability and robustness of the inorganic or organometallic materials.^{1, 16, 29} In this chapter, the synthesis and properties of the copper based cyanide coordination polymers are discussed. Due to the high reducing nature of the cyanide ligand, only copper(I) compounds and polymers are known with the exception of some Cu(I/II) mixed polymers. Copper (I) center can bind to cyanide in four

different ways; terminal capping through C (**I**), bicoordinate (μ_2 -C,N) (**II**), tricoordinate (μ_3 -C,N,N) (**III**) and dimeric (μ_3 -C,C,N) (**IV**) fashion. 1D polymers are rich in **I**, **II** and **III** binding modes whereas 2D and 3D frameworks contain all four modes. (**Figure 3.2.3**).

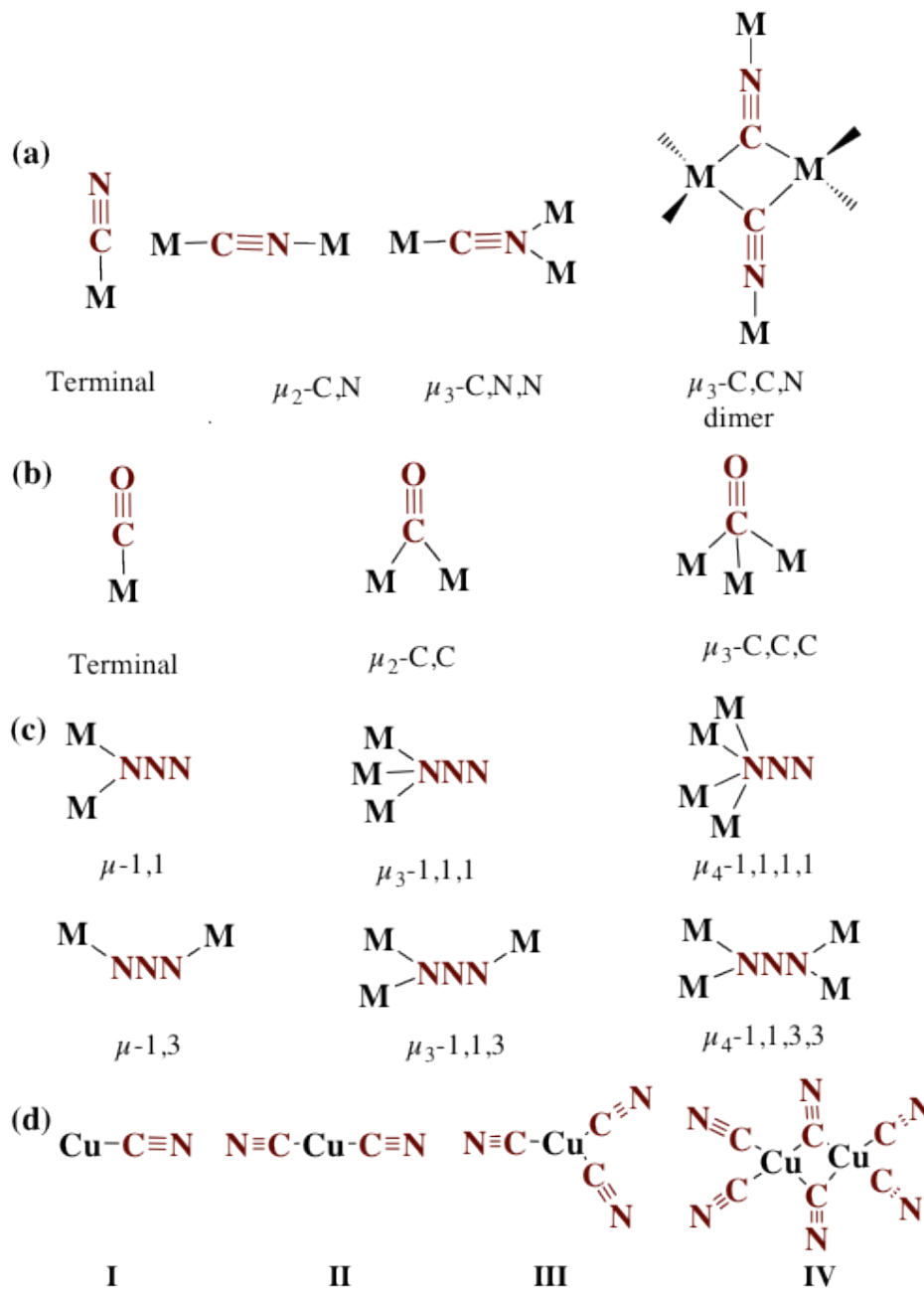


Figure 3.2.3. Different binding modes of (a) cyanide, (b) carbonyl, (c) azide and (d) binding modes of the cyanide with copper metal.

3.3. One Dimensional Copper Cyanide (CuCN) Coordination Polymer

1D polymers have a straightforward topology in comparison to 2D and 3D, and therefore, are considered to be less interesting. In spite of their simple architecture but predicting the final topology of the 1D polymer is quite difficult. Their structural features have been found to be dependent on many factors such as nature, and denticity of the organic ligand, packing and experimental conditions. Generally, a 1D polymer consists of an infinitely long CuCN chain, which is decorated by ligands. The structure of a 1D polymer is generally explained in terms of symbols **A**, **B** and **C** representing the connectivity or coordination environment around copper(I) sites in the main chain; where **A** = dicoordinated, **B** = tricoordinated and **C** = tetracoordinated copper center.

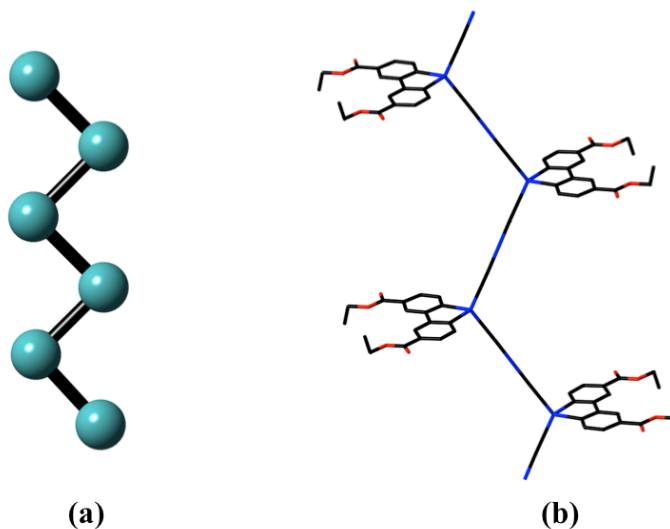


Figure 3.3.1. (a) Zigzag conformation of 1D coordination polymer (b), 1D chain of $[\text{Cu}^{\text{I}}(4,4'\text{-dCO}_2\text{Et-bpy})_{0.5}(\text{CN})]_n$.³¹

Zigzag conformation is the most common topology found in 1D CuCN polymers (Figure 3.3.1). The zigzag structure generally consists of an exoditopic ligand and a

tetrahedral copper (I) centers. The supramolecular interaction between these zigzags chains, such as π - π stacking and H-bonding increases the complexity of these structures. The structure of the ligand dictates the connectivity and packing of these $(\text{CuCN})_\infty$ chains in the lattice. In $[\text{Cu}^{\text{I}}(4,4\text{-dCO}_2\text{Me-bpy})(\text{CN})]_n$ (**1**), the ligand dimethyl 2,2'-bipyridine-4,4'-dicarboxylate (4,4-dCO₂Me-bpy) decorated the CuCN backbone in CCCC pattern. Interestingly, on changing the methyl with an ethyl side group in $[\text{Cu}^{\text{I}}(4,4'\text{-dCO}_2\text{Et-bpy})_{0.5}(\text{CN})]_n$ (**2**), the connectivity changed from CCCC to ACAC, which could be attributed to the bulkiness of the ethyl side group (**Figure 3.3.2**). The connectivity strongly affects the packing of these chains in the lattice; for instance, the pitch space, which is the distance between ligands oriented in the same direction doubled from 8.140 Å to 16.786 Å in **1** and **2**, respectively. In **1**, one molecule of the ligand from the neighboring chain was packed inside the pitch space while in case of **2**, two substituted bipyridines from two adjoining chains were accommodated inside one pitch space (**Figure 3.3.2**).³¹

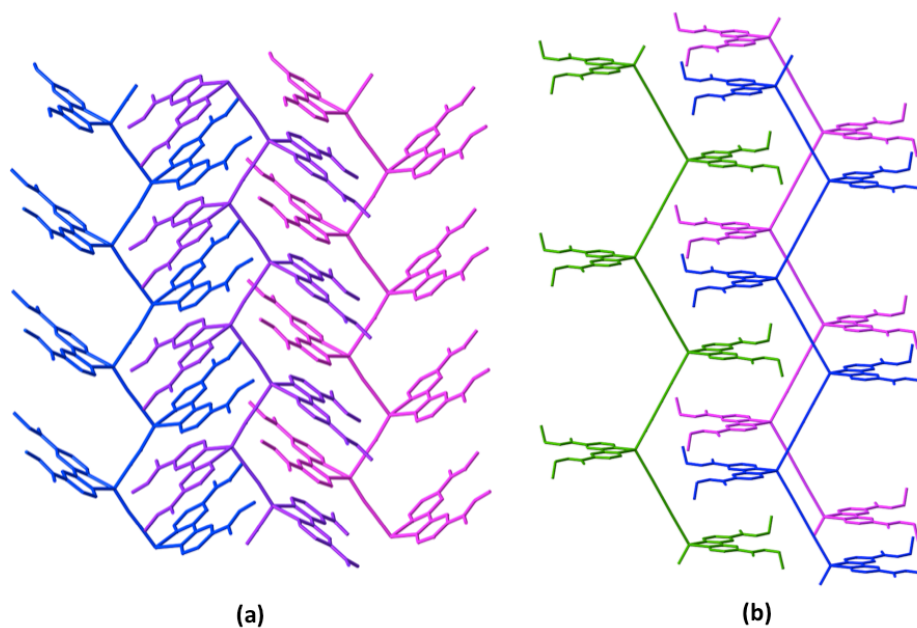


Figure 3.3.2. Packing of the CuCN chains in (a) $[\text{Cu}^{\text{I}}(4,4\text{-dCO}_2\text{Me-bpy})(\text{CN})]_n$, **1** and (b) $[\text{Cu}^{\text{I}}(4,4'\text{-dCO}_2\text{Et-bpy})_{0.5}(\text{CN})]_n$, **2**.³¹

Similar connectivity of ACAC was observed in coordination polymers, $[\text{Cu}_2^{\text{I}}(\text{CN})_2(\text{biquin})]_n$ and $[\text{Cu}^{\text{I}}(\text{CN})(\text{dpphen})]_n$ (biquin = 2,2'-biquinoline, dpphen = 4,7-diphenyl-1,10-phenanthroline) with bulky ligands.¹¹ The packing in these polymers was found to be similar to **1** where only one ligand was packed in the pitch space of the neighboring CuCN chain (**Figure 3.3.3**).

Some examples are reported where the zigzag chain adopted a wave like pattern; for example $[\text{Cu}_5^{\text{I}}(\text{pylpy})_2(\text{CN})_5]_n$ (pylpy = pyrazolyl pyridine) that was synthesized via direct reduction method (**Figure 3.3.4, a**). The decorating moiety or subunit, $[\text{Cu}_2^{\text{I}}(\text{pylpy})(\text{CN})]$ consisted of a copper center coordinated to the ligand, pylpy lying planar to the CuCN backbone with ACAC connectivity.³¹ Similar structure was also found in another 1D CuCN polymer, $[\text{Cu}_5^{\text{I}}(\text{bpy})_2(\text{CN})_5]_n$ where $[\text{CuCN}(\text{bpy})]$ (bpy = 4,4'-bipyridine) attached to a zigzag chain in a planar fashion, synthesized via hydrothermal treatment of CuCN, KCN and ligand in 25 % yield.¹¹ For the same ligand, helical shaped 1D polymers have been reported when different cyanide sources were employed in the synthesis. In the first case, potassium ferricyanide

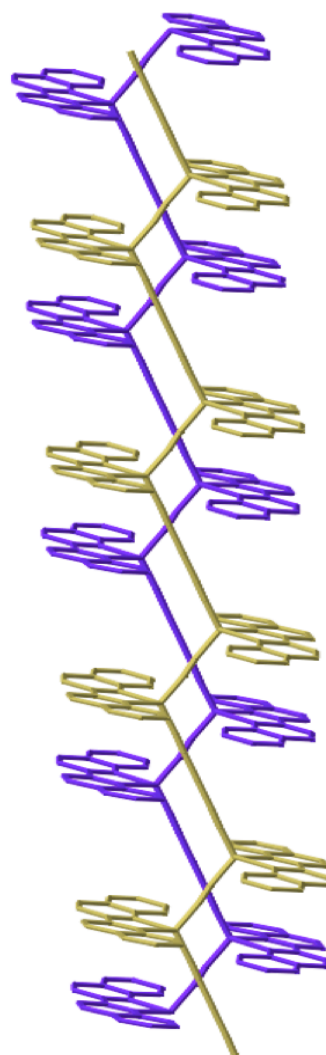


Figure 3.3.3. Packing structure of $[\text{Cu}_2^{\text{I}}(\text{CN})_2(\text{biquin})]_n$.¹¹

($K_3(Fe(CN)_6)$) was used under solvothermal reaction conditions to give 58% yield while in the second case, diazo based compound, 2,2'-azobis(isobutyronitrile) (AIBN) was used to generate the polymer in quantitative yields of 82% (80 °C) and 77 % (25±3 °C) through direct reduction method.³¹ Based on the yields, it can be speculated that the helical shaped polymers are more thermodynamically favored over the zigzag chained structure with 4,4'-bipyridine.

In the zigzag structure of $[Cu^I_5(bpy)_2(CN)_5]_n$, the decorating moiety was attached to the CuCN backbone at an angle of 112.95°. The Cu-C bond length in the subunit was 1.856 Å which was comparatively smaller than found in $(CuCN)_\infty$ chains (Cu-C=1.908 Å) (**Figure 3.3.4, a**). The opposite trend was found for Cu-N bond lengths (Cu-N_{subunit}=1.948 Å; Cu-N_{backbone}=1.925 Å).

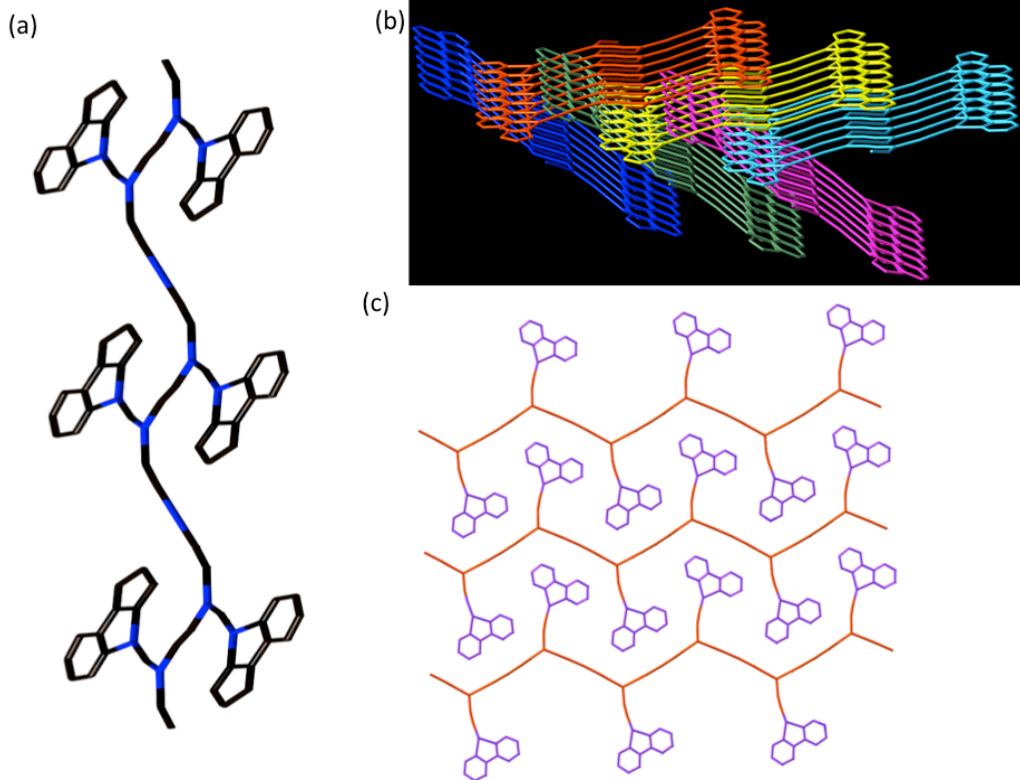


Figure 3.3.4. (a) Zigzag Chain and packing of $[\text{Cu}^{\text{I}}_5(\text{pylpy})_2(\text{CN})_5]_n$ (b); (c) packing of $[\text{Cu}^{\text{I}}_5(\text{bpy})_2(\text{CN})_5]_n$.^{11,31}

The zigzag shaped coordination polymer, $[\text{Cu}^{\text{I}}_5(\text{pylpy})_2(\text{CN})_5]_n$, exhibited the similar geometrical parameters. In the packing diagram, ribbon shaped CuCN chains were packed inside the interstitial spaces of the neighboring 1D chain, projected at 50°. This packing generates a complex 3D supramolecular network (**Figure 3.3.4, b**). While the $[\text{Cu}^{\text{I}}_5(\text{bpy})_2(\text{CN})_5]_n$ packed in different fashion where the 1D zigzag chains are arranged parallel to each other to form a 2D sheet. The subunit, $[\text{CuCN}(\text{Bpy})]$ of one 1D chain are inserted into the pitch space of the neighboring chains (**Figure 3.3.4, c**).

Other common topology found in the 1D polymer is helical shape. This topology is considered to be very interesting due to its similarities to some biological molecules. The chirality of the ligand dictates the distribution of left- and right-handed helices; whereas, an achiral ligand generally produce racemic mixtures of helical polymers.

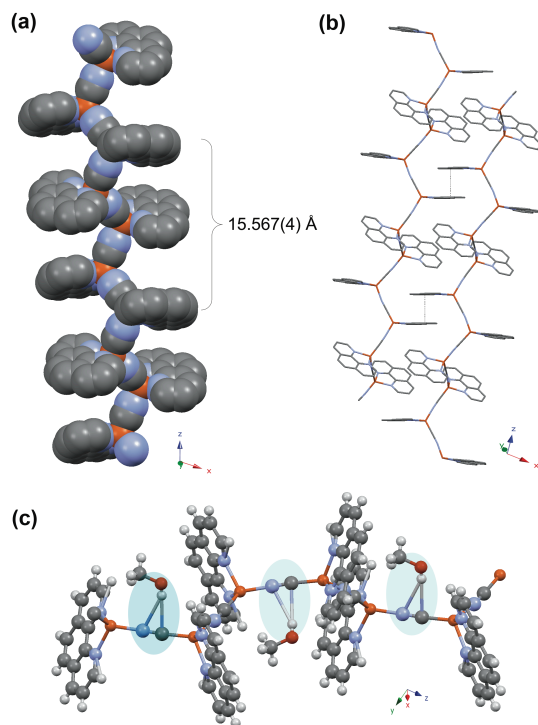


Figure 3.3.5. (a) 1D helical chain (b) π - π stacking of ligands from the adjoining CuCN chains during packing (c) H-bonding between guest molecule, methanol and cyanide in case of $[\text{Cu}^{\text{I}}(\text{phen})(\text{CN})\cdot\text{CH}_3\text{OH}]_n$.³¹

These polymers were packed by π - π stacking and H-bonding with the guest molecules encapsulated in the inter-chain spaces. For example, $[\text{Cu}^{\text{I}}(\text{phen})(\text{CN})\cdot\text{CH}_3\text{OH}]_n$ has a helical CuCN backbone with a pitch of 15.567 Å (**Figure 3.3.5, a**) and the chains were packed with the distance of 3.384 Å, indicating the presence of π - π stacking.³¹ This polymer was synthesized in methanol by the direct reduction method. Each asymmetric unit contained one molecule of methanol as a guest molecule, which interacted with the cyanide ligand of the CuCN backbone via H-bonding (**Figure 3.3.5, c**). When the synthesis was carried out in a mixture of ethanol and water (1:1) under solvothermal reaction conditions, half an equivalent of ethanol was crystallized in each asymmetric unit. Similar to the methanol analogue, the ethanol molecule extensively participated in the H-bonding. (**Table 3.3.1, Entry 4**).³²

The third topology is the ladder shaped 1D backbone, which is not commonly observed in cyanide-based polymers. In this architecture two parallel chains are attached to each other by a ligand to form a ladder (**Figure 3.3.6, a**). For example, the bidentate ligand, 2-(3-pyridyl)benzimidazole (3-PyHBIIm), bridged two CuCN chains to generate a ladder shaped topology.³³ Each chain consisted of a tricoordinated Cu(I) center attached to the nitrogen of the 3-PyHBIIm ligand with bond length of 2.073 Å ($\text{Cu}-\text{N}_{\text{lig}}$) and two cyanides with bond lengths of $\text{Cu}-\text{C}_{\text{CN}}$ 1.868 Å and $\text{Cu}-\text{N}_{\text{CN}}$ 1.889 Å, respectively. The copper center adopted a distorted trigonal planar geometry with angles, $\text{N}_{\text{lig}}-\text{Cu}-\text{C}_{\text{CN}}$ 116.43°, $\text{N}_{\text{lig}}-\text{Cu}-\text{N}_{\text{CN}}$ 103.50° and $\text{N}_{\text{CN}}-\text{Cu}-\text{C}_{\text{CN}}$ 139.88°. The aromatic rings of the ligands on the chains were found to be 3.602 Å apart, indicating presence of π - π stacking

(Figure 3.3.6, b). Another example of ladder 1D polymer, $[\text{Cu}_2(\text{SCN})(\text{tpt})]_n$ ($\text{tpt} = 2,4,5$ -tris(2-pyridyl)-1,3,5-triazine) synthesized via the sulfur transfer method, where two chains were bridged by thiocyanate functionality. The backbone consisted of two crystallographically distinct copper centers. The first copper (I) center has distorted square planar geometry, which lied 0.177 \AA below the least square plane (LSP) and was coordinated to two sulfur atoms with average bond distance of 2.457 \AA and two cyanide ligands through carbon and nitrogen. The second Cu(I) center adopted a pseudo-pentacoordinated geometry coordinated to three nitrogens of ligand, tpt and two sulfurs with bond lengths $\text{Cu-S}(1) 2.339 \text{ \AA}$ and $\text{Cu-S}(2) 2.295 \text{ \AA}$ (Figure 3.3.6, c). The Cu-S bond length in the bridging mode was larger than Cu-S in the 1D chains indicating the relative strengths of the Cu-S bond. The aromatic rings of the ligand, tpt lie parallel to each other along the a axis with a distance of 3.814 \AA indicating π - π stacking. Along the same axis, these 1D chains created hexagonal channels with dimension of $3.538 \text{ \AA} \times 3.702 \text{ \AA}$ (Figure 3.3.6, c).³⁴

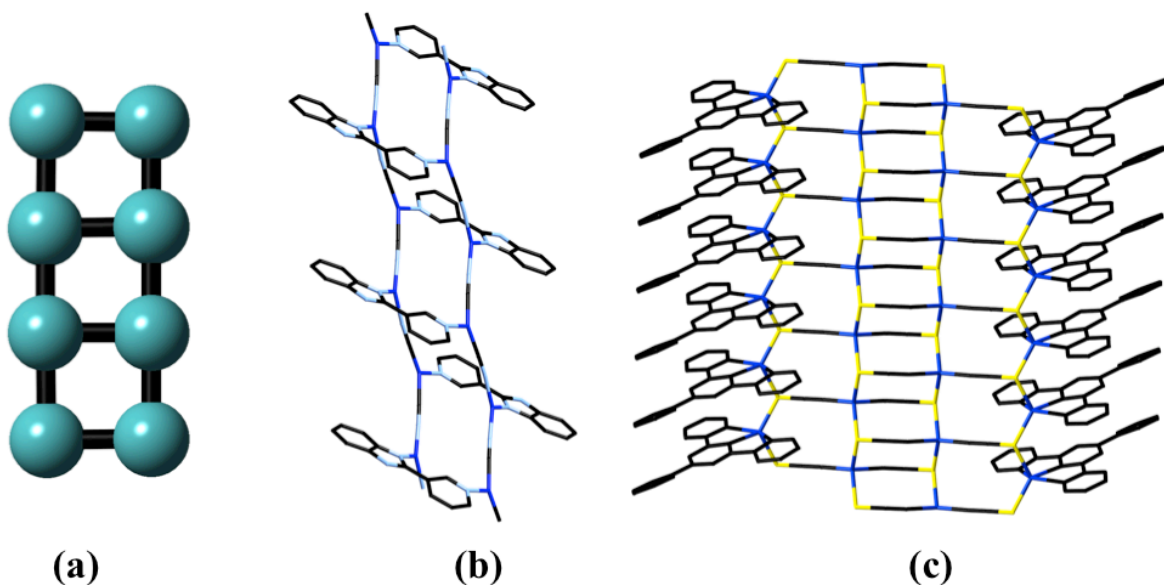


Figure 3.3.6. (a) Ladder shaped 1D topology, (b) $[\text{Cu}_2(\text{CN})_2(3\text{-PyHBIIm})]_n$ and (c) $[\text{Cu}_2(\text{SCN})(\text{tpt})]_n$.^{33,34}

3.4. Two- and Three- Dimensional Copper Cyanide Coordination Polymer

Due to the versatile nature of the cyanide ligand, a number of complex 2D and 3D networks are known. These polymeric CuCN networks are highly photoluminescent and generally anionic in nature represented with the general formulae, $[\text{Cu}_2(\text{CN})_3]^-$, $[\text{Cu}_3(\text{CN})_4]^-$ and $[\text{Cu}_2(\text{CN})_4]^-$ (**Figure 3.4.1**).²⁹ $[\text{Cu}_2(\text{CN})_3]^-$ is the most commonly found repeating unit in the $(\text{CuCN})_n$ chains, where all the copper centers are tricoordinate and generates hexagonal or honey combed shaped nets. The same hexagonal shape is retained by $[\text{Cu}_3(\text{CN})_4]^-$ with two extra CN-Cu-CN units are assimilated in the final network which has tricoordinated and dicoordinated copper centers. $[\text{Cu}_2(\text{CN})_4]^-$ has a diamondoid structure where the copper (I) sites have four coordinated rare conformations.²⁹

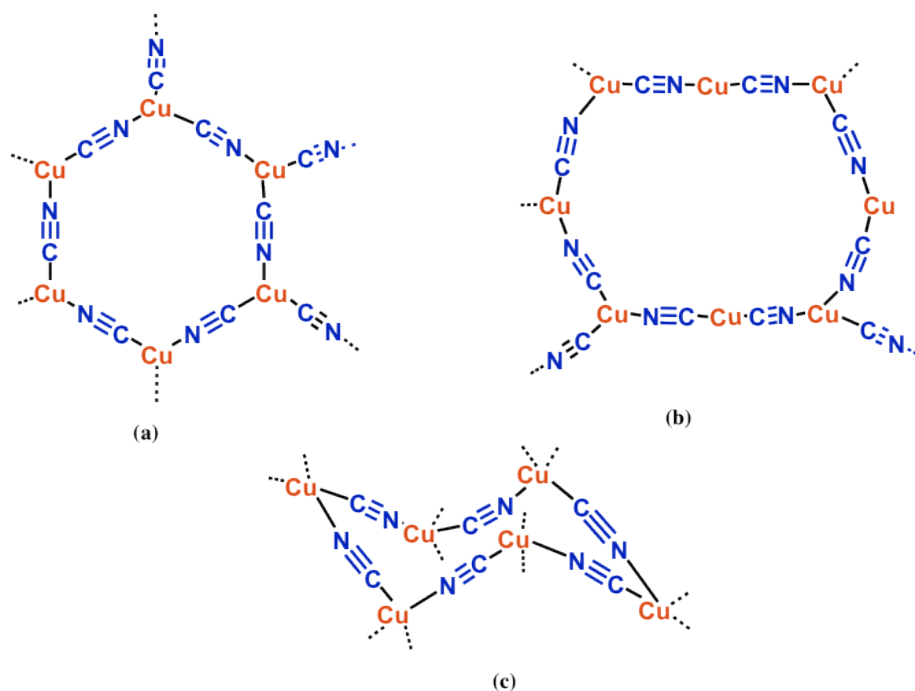


Figure 3.4.1. The different CuCN conformations found in 2- and 3D copper cyanide networks (a) $[\text{Cu}_2(\text{CN})_3]^-$ (b) $[\text{Cu}_3(\text{CN})_4]^-$ (c) $[\text{Cu}_2(\text{CN})_4]$.²⁹

In order to simplify the topology of 2D and 3D frameworks, A.F. Wells classified the complex structures into nets or networks.³⁵⁻³⁷ Each network is a polymer made up of nodes interconnected by linkers. A linker connects two nodes and each node is linked by three or more linkers.^{1, 38} In the example illustrated in **Figure 3.4.2(a)**, two different copper (I) sites are present in $(\text{CuCN})_\infty$, where a tricoordinated copper center is assigned as a node and another copper (I) site acts as a linker since it is attached to only two cyanide ligands. A network is defined by the symbol (n,p) , where n is the size of the shortest circuit and p is the connectivity of the nodes.¹ In **Figure 3.4.1**, networks (a) and (b) are assigned as $(6,3)$ while network (c) is defined as $(6,4)$.³⁹ In CuCN based polymers are either 3-connected or 4-connected nets contain tricoordinated and tetracoordinated nodes. It must be noted that networks do not define any geometrical environment of the atoms in the coordination polymer. In other words, the topology of the square planar and tetrahedral nodes is the same while their geometry is totally different (**Figure 3.4.2, b**).

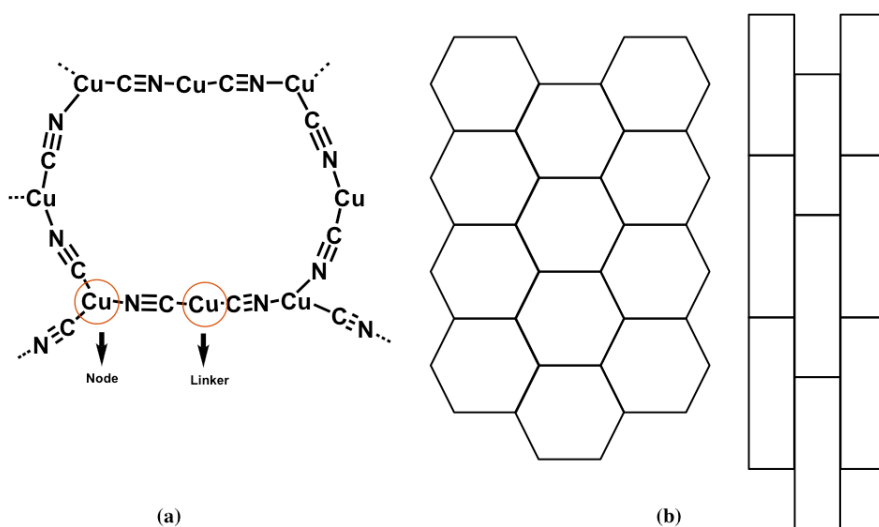


Figure 3.4.2: (a) Linker and nodes in the network $[\text{Cu}_3(\text{CN})_4]^-$ (b) Geometry of square planar and tetrahedral nodes.^{1,29}

Understanding the packing of the networks is another crucial structural aspect to design and analyze these multi-dimensional complex structures. These networks are tightly packed and generally no empty spaces are found and pores are occupied by metal cations, positively charged ligands or other guest molecules, such as solvents. These networks can further be divided into three main classes on the basis of the packing efficiency.³⁵⁻⁴¹

1. **Intercalation** – In this type of packing, the empty spaces or pores are occupied by guest molecules or ligand. For example, 3D network of $[\text{Cu}_2^+(\text{CN})_3 \cdot 0.5\text{TMEDA-H}_2]_n$ (TMEDA = tetramethyl ethylene diamine) contained protonated TMEDA encapsulated in the anionic CuCN networks.³¹ These networks were synthesized via direct reduction method. Similar structures were obtained, $[\text{Cu}(\text{pn})_2][\text{Cu}_3(\text{CN})_4]$ and $[\text{Cu}_2(\text{CN})_3][\text{NEt}_4]_n$ (pn = 1,3-propanediamine, NEt_4^+ = tetraethylammonium salt), where positively charged $[\text{Cu}(\text{pn})]^+$ and NEt_4^+ were trapped inside the anionic CuCN rings to form intercalated polymers (**Figure 3.4.3**). These 3D networks consisted of three nets (8,4), (7,4) and (6,4), which contain dimeric copper (I) sites. These networks are example of pillared 3D layers where 2D sheets are connected by pillars of cyanide ligands.³¹

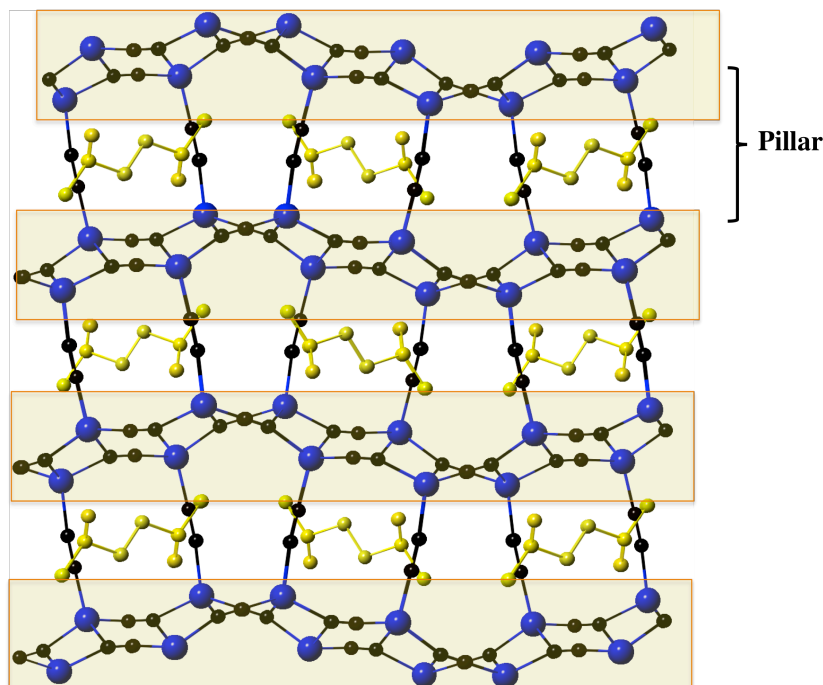


Figure 3.4.3. Pillared 3D network of $[\text{Cu}_2^{\text{I}}(\text{CN})_3 \cdot 0.5\text{TMEDA} \cdot \text{H}_2]_n$ intercalated with positively charged TMEDA ligand.³¹

2. **Interdigitation.** Interdigitation is the classification of materials that contain stacked layers held by weak intermolecular forces and the contour of the channels is outlined by these layers or ligands.^{1, 16, 38-41} The 2D networks interdigitated with TMEDA with the corrugated sheets with (8,4) nets. These networks were obtained by treatment of CuCN with the ligand in the presence of sodium sulfate pentahydrate. The nets created distorted hexagonal channels (**Figure 3.4.4**) interdigitated with copper sites coordinated with the TMEDA and cyanide ligands. A second trigonal planar Cu(I) site coordinated with three cyanide ligand through carbon and nitrogen with bond angles, N(1)-Cu-C(1) 129.95°, N(2)-Cu-C(1) 115.56° and N(1)-Cu-N(2) 114.49°.

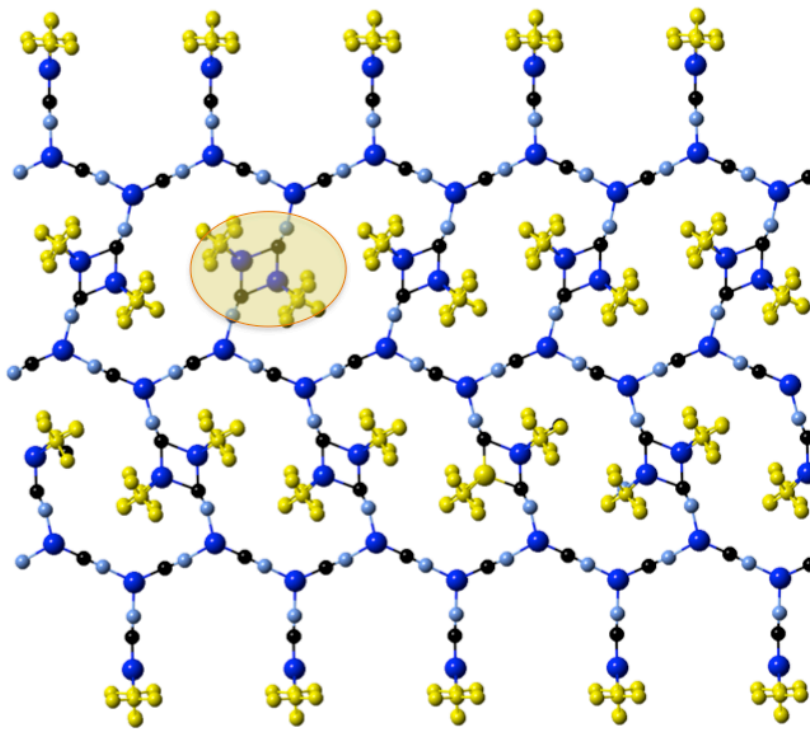


Figure 3.4.4. 2D coorugated sheets in $[\text{Cu}_3\text{CN}_3(\text{TMEDA})]_n$ representing the interdigitation by Cu center with TMEDA ligand. ³⁴

3. **Interpenetration.** When two or more nets are not connected to each other and cannot be separated without breaking any bonds, are known as interpenetrated networks. This was best illustrated by, $[(\text{Cu}(\mu\text{-CN}))_2(\mu\text{-Me}_4\text{-pyz})\text{-dioxane}]_n$ polymer ($\text{Me}_4\text{-pyz} = 1,2,4,5\text{-tetramethyl pyrazole}$), where copper(I) centers were tricoordinated to the carbon and nitrogen atoms of two cyanide ligands and the nitrogen of a ligand, $\text{Me}_4\text{-pyz}$ with bond length of 2.063 \AA .² Interestingly, aromatic ring of the space ligand, $\text{Me}_4\text{-pyz}$ lost its planarity and two of the nitrogen atoms (N1, N2) tilted out of the least square planes (LSP) created by four carbons by 0.224 \AA and -0.222 \AA in a chair conformation, respectively. The ligand was attached to two copper centers to generate a ribbon shaped 2D

structure. Due to steric or electronic strain caused by CuCN chains, Me₄-pyz lost its aromaticity. As shown in **Figure 3.4.5, a**, the CuCN chains were extended in an almost perpendicular fashion to give rise to a 3D interpenetrable network. These (8,3) nets were interpenetrated in the helical chain through the spacer ligand (**Figure 3.4.5, c**) and gave rise to two large channels. These channels have two structures: hexagonal shaped where the solvent molecule, dioxane was encapsulated and one rectangular formed from the helical chain of [CuCN(Me₄-pyz)]_n.

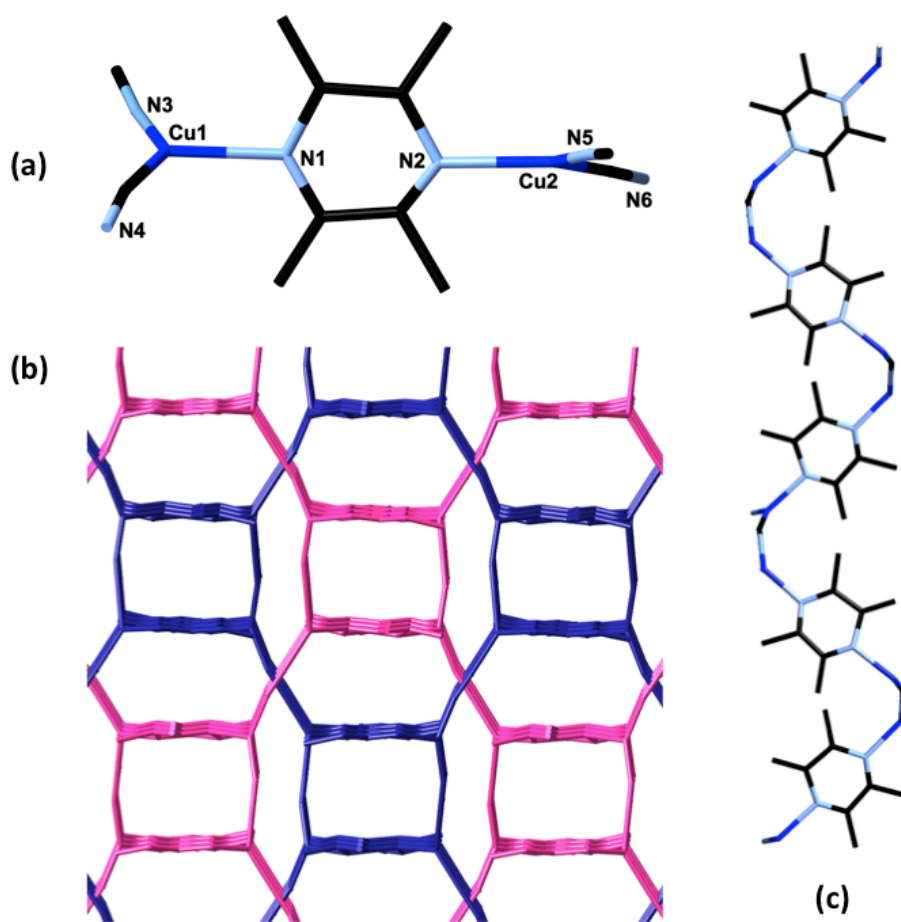


Figure 3.4.5: In [(Cu(μ -CN))₂(μ -Me₄-pyz)-dioxane]_n, (a) Perpendicular growth of two cyanide chains and non planar ligand molecule (b) Interpenetrable 3D network (pink and purple) with hexagonal and rectangular channels and (c) chains interpenetrated through the helical chain of the ligand.²

3.5. Copper based Mixed Metal-Cyanide Coordination Polymer

There are two possible types of mixed metal cyanide coordination polymer with copper. In one type copper centers have two different oxidation sites, Cu(I) and Cu(II).¹² These polymers are generally synthesized at lower temperature either by slow diffusion or evaporation techniques due to high reducing ability of CN⁻ anions. Cu(II) sites can either be encapsulated in the pores or assimilated in the main chain. For example, the 3D network of [Cu(pn)₂][Cu₃(CN)₄]_n (pn = 1,2-propanediamine), has a distorted Cu(II) square planar CuN₄ center, where [Cu^{II}(pn)₂]²⁺ was entrapped inside the anionic [Cu^I₃(CN)₄]⁻ networks (**Figure 3.5.1, a**).⁴²

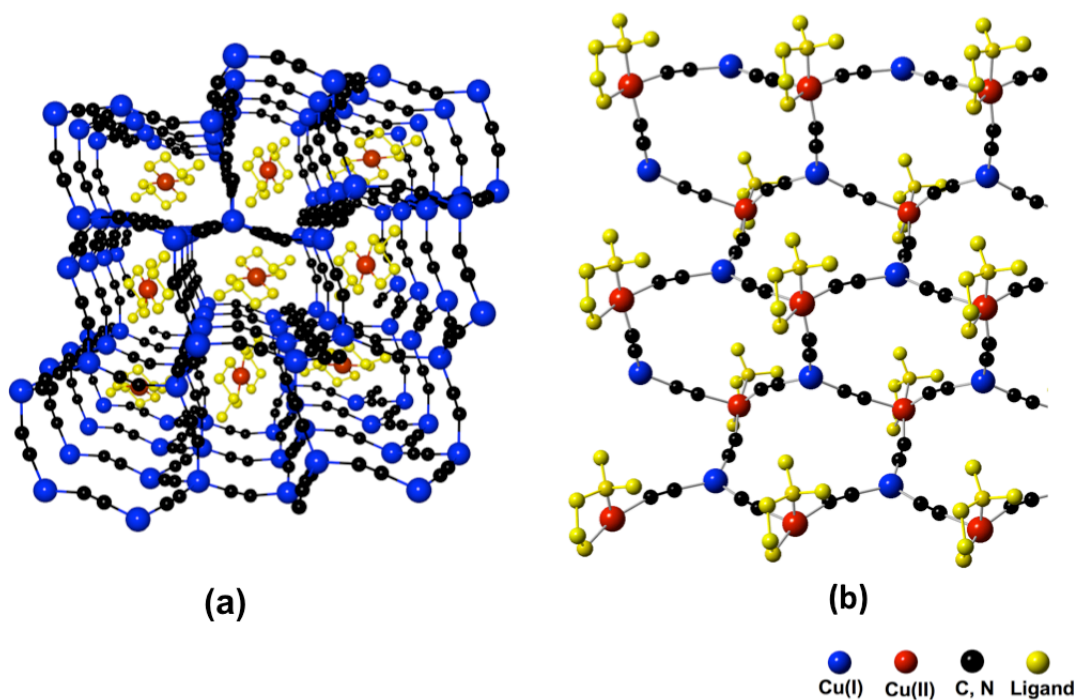


Figure 3.5.1. Lattice structure of (a) [Cu(pn)₂][Cu₃(CN)₄]_n and (b) [Cu₂(CN)₃](dmen)_n.

The strong sigma donor, diamine, coordinated exclusively to Cu(II) sites due to high affinity towards nitrogen based ligands (**Figure 3.5.1, a**).⁴² In another example,

Cu(II) sites were assimilated in the final corrugated 2D sheets, giving rise to alternating (6,5) nets. In the chain, Cu(II) center adopted the pentaco-ordinated distorted square pyramidal geometry with a tau value (τ) of 0.23, whereas the Cu(I) center was coordinated to three cyanide ligands with distorted trigonal planar geometry (**Figure 3.5.1, b**).⁴²

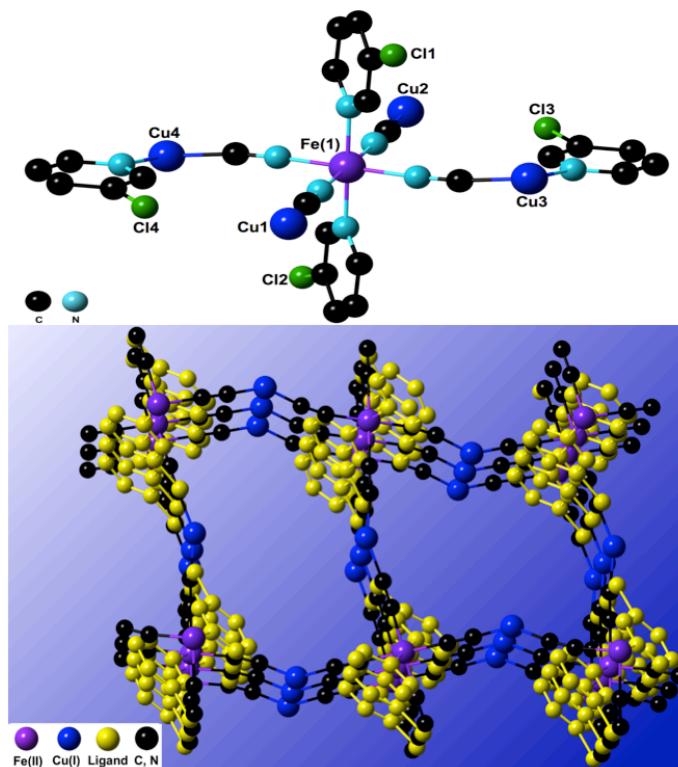


Figure 3.5.2. Asymmetric unit and 3D network of $[\text{Fe}(\text{3-Clpy})_2][\text{Cu}(\text{3-Clpy})_2(\text{CN})_2]_n$.⁴⁴

Another type of mixed coordination polymer are the bimetallic systems containing Cu(I) metal with other metals such as iron(II), silver(I) and gold(I). There are a number of iron(II)-copper(I) mixed cyanide polymers that have been reported where Fe(II) sites adopted an octahedral geometry bridged together through anionic $[\text{CuCN}_n]^{(n-1)-}$ chains.^{12, 43} Real and his coworkers synthesized Cu(I)-Fe(II) 1-3D heterobimetallic polymer with substituted pyridine (X-py; X= F, Cl, Br, I). In $[\text{Fe}(\text{3-Clpy})_2][\text{Cu}(\text{3-}$

$\text{Clpy})_2(\text{CN})_2]_n$ where 3-Clpy = 3-chloropyrazine), an octahedral Fe(II) center coordinated to two ligands, 3-Clpy and 4 cyano ligands and bridged to other Fe(II) sites by the distorted tetrahedral copper centers, $[\text{Cu}(3\text{-Clpy})(\text{CN})_2]^-$ (**Figure 3.5.2**). Paramagnetic Cu(II) and Fe(II) species altered the magnetic properties and spin crossover (SCO) behavior.⁴⁴

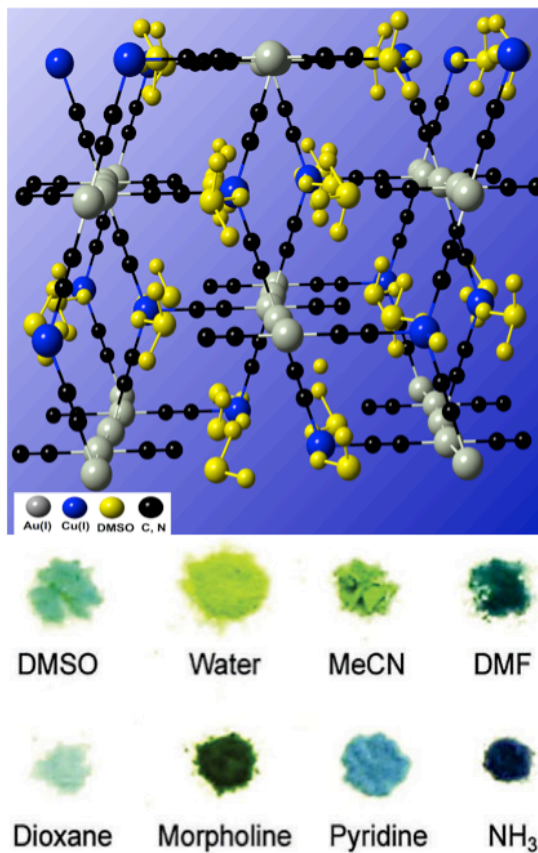


Figure 3.5.3. 3D network and vapochromic behavior shown by $\text{Cu}(\text{DMSO})_2[\text{Au}(\text{CN})_2]_2$.⁴⁵

Other examples of heterobimetallic polymers of Cu(I) with Ag(I) or Au(I) also showed unique properties. Reversible vapochromic behavior was shown by the series of Cu(I)-Au(I) cyanide coordination polymers (**Figure 3.5.3**). In polymer $\text{Cu}(\text{DMSO})_2[\text{Au}(\text{CN})_2]_2$, copper center was coordinated to two DMSO molecules and two

[Au(CN)₂]⁻ linkers to generate 2D sheets stacked by aurophilic interactions (Au---Au) of 3.426 Å to give 3D networks.⁴⁵ When the material was exposed to the vapors of different solvents, the blue color of the material changed into different colors (**Figure 3.5.3**). This behavior was found to be reversible as indicated by the color change and IR spectroscopy. Thermal treatment was required to regenerate the polymer when exposed to strongly coordinating ligands, such as ammonia and pyridine. Such vapochromic materials have huge potential as chemical sensors.

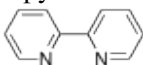
3.6. Synthesis of Copper Cyanide Polymers

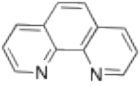
Knowledge of coordination chemistry of the metals and ligands are important aspects in the determination of the structure of coordination polymers. Temperature plays a significant role in hydrothermal and solvothermal reactions. These reactions are generally conducted in an autoclave under autogenous pressure well above the boiling point of the solvent and thus, changing the solvent property drastically. Viscosity of the solvent decreases, while the solubility of the precursors increases in the reaction medium. During the hydrothermal treatment of 1:1:2 stoichiometric ratio of CuCl₂·H₂O, [K₃(Fe(CN)₆)] and bipyridine has generated two products at different temperature. At 120 °C, mixed metal cyanide coordination polymer, [(Fe^{II}₂(bpy)(μ-CN)₄Cu^I₂(CN)₂·H₂O]_n was obtained in which octahedral iron was assimilated in the CuCN backbone (**Table 3.6.1; Entry 1**). When the temperature was increased, Fe(II) ions did not participate in the formation of the 1D polymer indicating higher temperature favors the copper rich compound, [Cu^I(μ-CN)(bpy)]_n.¹²

Pike and coworkers synthesized various multi-dimensional polymers by refluxing an acetonitrile solution of CuCN and potassium cyanide (KCN) with different nitrogen based ligands.^{46, 47} X-ray quality crystals were only obtained at higher temperature under solvothermal reaction conditions for prolonged reaction times. The direct reduction method successfully yielded 1D copper cyanide polymers at 80 °C as well as at room temperature upon irradiation with UV light in quantitative yields. In the case of the 3D polymer, the $[\text{Cu}^{\text{I}}_2(\text{CN})_3 \cdot 0.5\text{TMEDA-H}_2]_n$, product was only achieved at 80 °C indicating that a high temperature was necessary for the synthesis of a high dimensional compound.³¹

Copper-rich 1D chains were obtained after reacting CuCN with KCN in the presence of nitrogen based ligands, 4,4'-bipyridine and 1,10-phenanthroline in equimolar quantities in BABA and BAABAA connectivity respectively (**Table 3.6.1**, entry **4** and **8**). When the reactions were conducted with different cyanide sources such as potassium ferricyanide ($\text{K}_3[\text{Fe}(\text{CN})_6]$) or AIBN, a 1D polymer was obtained with a CCCC topology (**Table 3.6.1**, entry **3-7**).³³

Table 3.6.1: Synthesis of 1D coordination polymer under different conditions

Entry	Coordination Polymer	Ligand	Reaction Conditions	Dimensionality/Connectivity
1	$[(\text{Fe}^{\text{II}}_2(\text{bpy})(\mu\text{-CN})_4\text{Cu}^{\text{I}}_2(\text{CN})_2) \cdot \text{H}_2\text{O}]_n$	Bpy = 4,4'-bipyridine 	Hydrothermal Starting Material: CuCl ₂ ·H ₂ O: K ₃ [Fe(CN) ₆] ligand (1:1:2) Solvent: Water Experimental Conditions: 120°C for 1 week Yield	1D polymer ¹²
2	$[\text{Cu}^{\text{I}}(\mu\text{-CN})(\text{bpy})]_n$	Bpy = 4,4'-bipyridine	Hydrothermal Starting Material: CuCl ₂ ·H ₂ O:K ₃ [Fe(C	1D ¹² CCCC

			N) ₆]: Ligand (1:1:2) Solvent: Water Experimental Conditions: 160 °C for 1 week Yield 54 %	
3	[Cu ^I (μ-CN)(bpy)] _n	Bpy = 4,4'-bipyridine	Direct Reduction Method Starting Material: [Cu ^{II} (ala)(bpy)Cl]: AIBN: ascorbic acid (1:10:2) Solvent: Methanol Experimental Conditions: 80 °C and RT under UV irradiation in the presence Yield: 82% (80°C); 77% (RT)	1D CCCC
4	[Cu ^I ₃ (CN) ₃ (bpy)]·0.1H ₂ O _n	Bpy = 4,4'-bipyridine	Hydrothermal Starting Material: CuCN:KCN:ligand1, 2,4-triazole: (1:1:1:0.28) Solvent: water Experimental Conditions: 165°C for 190h Yield: 25%	1D ¹¹ BABA
5	[Cu ^I ₃ (μ-CN) ₃ (phen) ₃] _n	Phen = 1,10-phenanthroline 	Hydrothermal Starting Material: CuCl ₂ ·H ₂ O: K ₃ [Fe(CN) ₆] Phenanthroline (1:1:2) Experimental Conditions 160 °C for 1 week Yield: 67 %	1D ¹² CCCC
6	[Cu ^I (phen)(CN)·0.5 C ₂ H ₅ OH] _n ³¹	Phen = 1,10-phenanthroline	Solvothermal Starting Material: CuCN:1,10-phenanthroline (1:1) Solvent: water: ethanol (1:1) Experimental Conditions 140 °C for 48 h Yield: 58% based on	1D CCCC

			ligand	
7	$[\text{Cu}^{\text{I}}(\text{phen})(\text{CN})\cdot\text{CH}_3\text{OH}]_n$	Phen = 1,10-phenanthroline	Direct Reduction Method Starting Material: [Cu ^{II} (AA)(bpy)Cl]: AIBN: ascorbic acid (1:10:2) Solvent: Methanol Experimental Conditions: 80 °C and RT under UV irradiation in the presence Yield: 92 % (80 °C) 94 % (RT)	1D CCCC
8.	$[\text{Cu}_3(\text{CN})_3(\text{phen})]_n$	Phen = 1,10-phenanthroline	Hydrothermal Starting Material: CuCN:KCN:ligand (1:1:1) Solvent: water Experimental Conditions: 170°C for 96h Yield: 45%	1D BAABAA

Different synthetic approaches have been developed to synthesize copper cyanide coordination polymer with the most common ones are the solvo- and hydrothermal methods. Various cyanide sources such as CuCN, alkali metal cyanides (KCN, NaCN), ferricyanide salts, AIBN, diaminomaleonitrile and acetonitrile⁵ were employed with different copper salts to generate these polymers. Some methodologies are discussed briefly in the following sections.

Solvo/hydrothermal Methods

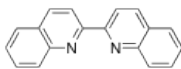
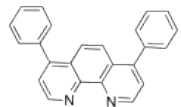
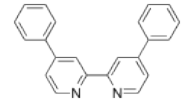
As mentioned above, these methods are commonly employed to synthesize CuCN polymers in different topologies and dimensionalities. In these methods, various copper salts such as halides, nitrates, thiocyanate, triflates, acetates and cyanide are dissolved in water (hydrothermal) or other solvent (solvothermal) along with the ligand and placed in

an autoclave under high temperature and pressure for prolonged reaction times.^{11, 18, 32, 34,}

43

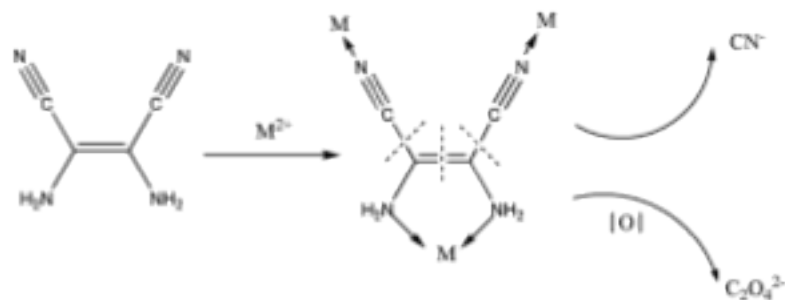
In some reactions, CuCN is employed as both a copper as well as a cyanide source, which resulted in the formation of a copper rich polymer with poor yield. In the following examples, copper(II) nitrate was used with CuCN and heated to 170 °C to give rise to coordination polymer in 10-20 % yield, (Table 3.6.2, Entry 1 and 2). Under similar reaction conditions, the yield was dramatically increased when potassium cyanide (KCN) was used as an additional cyanide source with ligand diphenyl bipyridine, Table 3.6.2, Entry 3.

Table 3.6.2. List of hydrothermal reactions using different cyanide sources.

Entry	Coordination Polymer/Products	Ligand	Reaction Conditions	Dimensionality/Connectivity
1	$[\text{Cu}^{\text{I}}_2(\text{CN})_2(\text{biquin})]_n$ ¹¹	Biquin = 2,2'-biquinoline 	Starting Material: CuCN:Cu(NO ₃) ₂ .2.5 H ₂ O: ligand (6:1:1) Solvent: Water Experimental Conditions: 170 °C for 85.6 h Yield: 20 %	1D ABAB ¹¹
2	$[\text{Cu}^{\text{I}}(\text{CN})(\text{dpphen})]_n$ ¹¹	Dpphen = 4,7-diphenyl-1,10-phenanthroline 	Starting Material: CuCN:Cu(NO ₃) ₂ .2.5 H ₂ O: ligand (4:1.4:1) Solvent: Water Experimental Conditions: 170 °C for 96 h Yield: 10%	1D CCCC ¹¹
3	$[\text{Cu}^{\text{I}}_2(\text{CN})_2(\text{dpbp})]_n$ ¹¹	Dpbp = 4,4'-Diphenyl-2,2'-bipyridine 	Starting Material: CuCN:KCN:ligand (4:1:1) Solvent: Water Experimental Conditions: 170 °C for 96 h Yield: 65%	1D ACCACC ¹¹
4	$[[\text{Cu}(\text{H}_2\text{O})(\text{NH}_3)_4][\text{Cu}$	Ammonia	Starting Material:	3D

	$3(\text{CN})_5] \cdot \text{H}_2\text{O}]_n^{48}$		<p>$\text{Cu}(\text{OH})_2\text{CuCO}_3$: diaminomaleonitrile (1:2) $\text{NH}_3 \cdot \text{H}_2\text{O}$ (25 mL) Solvent: Methanol Experimental Conditions: 110 °C for 48 h Yield: Poor</p>	
5	$[(\text{CH}_3)_4\text{N}[\text{Cu}(\text{H}_2\text{O})(\text{NH}_3)_4][\text{Cu}_4(\text{CN})_7]]_n^{48}$	$[(\text{CH}_3)_4\text{N}]^+$	<p>Starting Material: $\text{Cu}(\text{OH})_2\text{CuCO}_3$: diaminomaleonitrile: $[(\text{CH}_3)_4\text{N}]\text{Cl}$ (1:2:2) $\text{NH}_3 \cdot \text{H}_2\text{O}$ (25 mL) Solvent: Methanol Experimental Conditions: 110 °C for 48 h Yield: Poor</p>	3D
6	$[(\text{CH}_3\text{OH}_2)_2[\text{Cu}_2(\text{CN})_3]]_n$		<p>Starting Material: $\text{Cu}(\text{OH})_2\text{CuCO}_3$: diaminomaleonitrile: $\text{Eu}(\text{NO}_3)_2$ (1:2:0.5) $\text{NH}_3 \cdot \text{H}_2\text{O}$ (25 mL) Solvent: Methanol Experimental Conditions: 110 °C for 48 h Yield: Poor</p>	3D

Under solvothermal reaction conditions, Batten and his coworkers employed diaminomalonitrile as a cyanide source (**Scheme 3.6.1**). This method was used to synthesize three new coordination polymers starting with the mixture of copper salts, $\text{Cu}(\text{OH})_2$ and CuCO_3 in very poor yields (> 5 %). At high temperature, diaminomalonitrile decomposed to give two cyanide ligands that bonded to the copper to generate coordination polymers as shown in **Scheme 3.6.1**⁴⁸



Scheme 3.6.1. Decomposition of diaminomalonitrile to generate cyanide ligands.

This method provided a synthetic route to generate the mixed Cu(I/II) 3D networks (**Table 3.6.2**, entry **4** and **5**). Positively charged $[\text{Cu}(\text{H}_2\text{O})(\text{NH}_3)_4]^+$ and tetramethyl ammonium salt, $[(\text{CH}_3)_4\text{N}]^+$, acted as guest molecules and were encapsulated in the anionic CuCN networks. However, the polymer $[(\text{CH}_3\text{OH}_2)_2[\text{Cu}_2(\text{CN})_3]]$ (Entry **6**), has protonated methanol molecules encapsulated in the pores with accessible porosity of $390 \text{ m}^2\text{g}^{-1}$ as calculated by the Connolly algorithm.

In another method known as the sulfur transfer method, copper(I) thiocyanate (CuSCN) is used as a cyanide source. In this method, CuSCN decomposed to form $\text{Cu}(\text{I})\text{CN}$ and transferred sulfur either to a solvent or a ligand under solvothermal reaction conditions. Generally, acetonitrile or a mixture of the acetonitrile with different solvents such as methanol, ethanol, n-hexane, benzene and cyclohexane is used. Under these reaction conditions the solvent was found to have a dramatic effect on the structure of the coordination polymer. For example, a 3D polymer (**Table 3.6.3**, entry **1**) containing dodecanuclear copper(I) centers was coordinated by methyl mercaptide. Methyl mercaptide is thought to be the sulfur transfer product of methanol. In the absence of an alcoholic solvent along with acetonitrile, no product was formed.^{34,49}

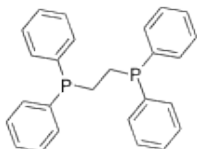
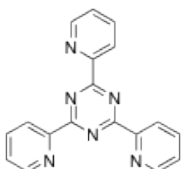


Scheme 3.6.2: Schematic representation of sulfur transfer from copper(I) thiocyanate to methanol.³⁴

Polymer $[(\text{CuCN})_2(\text{dppeS}_2)]_n$ (**Table 3.6.3**, entry **2**), contained tricoordinated copper(I) sites that bind to the sulfur atoms of dppeS_2 , and the carbon and nitrogen of two cyanide ligands in a distorted T shaped geometry. The final structure was a 2D ladder shaped coordination polymer (**Figure 3.5.2**). Unlike the $[(\text{CuCN})_2(\text{dppeS}_2)]_n$ coordination polymer, $[(\text{CuCN})_2(\text{tpt})]_n$ (**Table 3.6.3**, entry **3**) had four coordinated distorted Cu(I) center extending into three dimension via a tridentate ligand, 2,4,5-tris(2-pyridyl)-1,3,5-triazine (tpt). One of the nitrogen atoms of the tpt was not coordinated to the copper site, whereas the side product, dppeS_2 did not assimilate in the final structure. A similar copper and ligand coordination environment was found in $[\text{Cu}_2(\text{CN})_2(\text{tpt})]_n$ (**Table 3.6.3**, entry **4**), but the infinite CuCN chains were extended in only two directions to give a 2D coordination polymer. In the above-mentioned examples, we can clearly see the effect of the solvent system on the dimensionality (**Table 3.6.3**). The compound in entry **3** has been synthesized in pure acetonitrile giving rise to 3D polymers. While product in entry **4** was synthesized in a solvent mixture of acetonitrile and n-hexane to and resulted in the formation of a 2D polymer. Similar solvent effects were shown in entry **5**, where a mixture of acetonitrile and benzene or cyclohexane was used and the thiocyanate functionality was assimilated in the polymer, indicating that sulfur transfer was not efficient in these solvent systems. The backbone of the final product (entry **6**) consists of alternating CuSCN and CuCN and extends in the 2D networks. It was also observed that the higher temperature was necessary for the sulfur transfer; at 140 °C, none of CuSCN decomposed and was directly assimilated in the final triladder coordination polymer

along with the monocoordinated tpt ligand. This was further proved by the absence of the sulfur transfer product, dppeS₂.

Table 3.6.3. List of coordination polymer through sulfur transfer method.

Entry	Coordination Polymer/Products	Ligand	Reaction Conditions	Dimensionality
1	[Cu(μ ₃ -SCH ₃) ₂ (CN)] ₂ [Cu ₁₀ (μ ₃ -SCH ₃) ₄ (μ ₄ -SCH ₃) ₂] _n ³⁴	In situ generation of methyl mercaptide (-SCH ₃)	Starting Material: CuSCN Solvent: CH ₃ CN:CH ₃ OH (1:1) Reaction Conditions: 140 °C for 72 hr Yield: not reported	3D
2	[(CuCN) ₂ (dppeS ₂)] _n ⁴⁹	Dppe = 1,2-(diphenylphosphine) ethane 	Starting Material: CuSCN: dppe (1:2) Solvent: ACN:n-hexane (3:1) Experimental Conditions: 180 °C for 60 h Yield: 67%	2D
3	[(CuCN) ₂ (tpt)] _n + dppeS ₂ ⁴⁹	Tpt = 2,4,5-tris(2-pyridyl)-1,3,5-triazine 	Starting Material: CuSCN:dppe: tpt (2:1:1) Solvent: ACN Experimental Conditions: 180 °C for 60 h Yield: 60%	3D
4	[Cu ₂ (CN) ₂ (tpt)] _n + dppeS ₂ ⁴⁹	Tpt	Starting Material: CuSCN:dppe: tpt (2:1:1) Solvent: ACN:n-hexane (1:1 v/v) Reaction Conditions: 180 °C for 60 h Yield: 48%	2D
5	[Cu ₂ (SCN)(CN) ₂ (tpt)] _n + dppeS ₂ ⁴⁹	Tpt	Starting Material:	2D

			<p>CuSCN:dppe: tpt (2:1:1) Solvent: ACN:n-cyclohexane or ACN: benzene (1:1 v/v) Reaction Conditions: 180 °C for 60 h Yield: 56 %</p>	
6	$[\text{Cu}_2(\text{SCN})(\text{tpt})]_n^{49}$	Tpt	<p>Starting Material: CuSCN:dppe: tpt (2:1:1) Solvent: ACN:n-cyclohexane or ACN: benzene (1:1 v/v) Reaction Conditions: 140 °C for 60 h Yield: 47 %</p>	1D

Direct Reduction Method

The direct reduction method was discovered in our laboratory while conducting atom transfer radical addition (ATRA) in the presence of the diazo free radical initiator, AIBN. The reaction was catalyzed by the copper(II) complex, $[\text{Cu}^{\text{II}}(\text{ala})(\text{phen})\text{Cl}]$ (ala = alanine, phen = 1,10-phenanthroline). After 24 hr, red block crystals precipitated out of the reaction mixture; which were initially thought to be Cu(I) complexes.³¹

Upon further characterization of the crystals using single crystal X-ray diffraction, it was found that the red block crystals were 1D helical Cu(I) cyanide coordination polymer containing 1,10-phenanthroline (**Figure 3.3.5**). A similar product was obtained with different amino acids (glycine, phenylalanine and proline) at 80 °C, and even at room temperature upon the irradiation with UV light. Mechanistic studies showed that AIBN was activated on the copper center, which also acted as a source of the cyanide

ligand. To check the applicability of this method, reactions with various N-based ligands (**Scheme 3.6.3**) were conducted. Quantitative yields and good quality crystals were obtained at RT as well as 80 °C (**Table 3.6.4**).

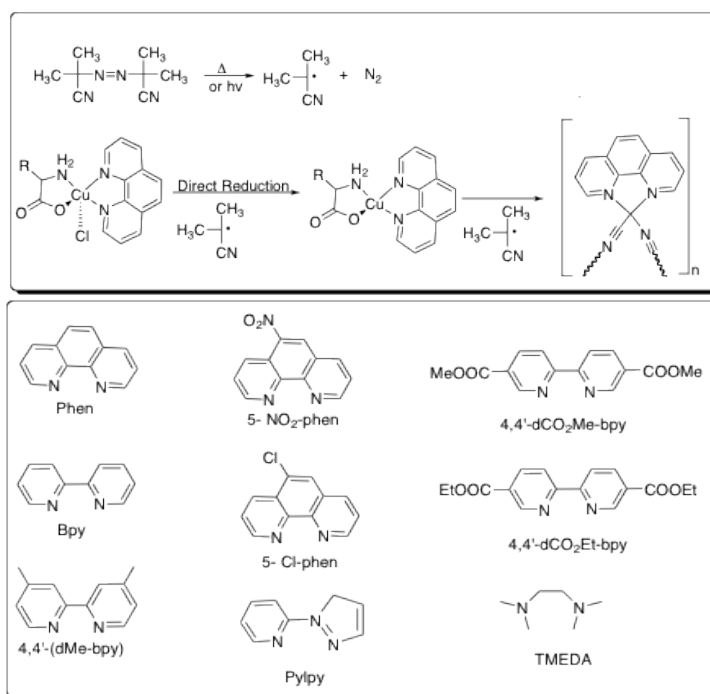
At higher temperature or under UV irradiation, AIBN decomposed and generated radicals that reduced the Cu(II) center into a Cu(I) species (**Scheme 3.6.3**). The cyanide functionality on the radical then activated by the Cu(I) center and generated polymers. These polymers were packed in different ways and participated in various intermolecular interactions, including π - π stacking and hydrogen bonding (**Scheme 3.3.5**).

Table 3.6.4. List of coordination polymers via direct reduction method.³¹

Entry	Coordination Polymer ^[a]	T (°C)	Yield (%)	$\nu(\text{CN})$ (cm ⁻¹)	Dimensionality/Connectivity
1	[Cu ^I ₂ (phen) ₂ (CN) ₂ *CH ₃ OH] _n	80	92	2102	1D
		RT	94	2102	CCCC
2	[Cu ^I (bpy)(CN)] _n	80	82	2106	1D
		RT	77	2106	CCCC
3	[Cu ^I (5-NO ₂ -phen)(CN)] _n	80	73	2100	1D*
		RT	63	2099	
4	[Cu ^I (5-Cl-phen)(CN)] _n	80	74	2104	1D*
		RT	72	2105	
5	[Cu ^I ₃ (4,4'-dMe-bpy) ₂ (CN) ₃] _n	80	89	2104	1D
		RT	76	2103	CCAC
6	[Cu ^I (4,4'-dCO ₂ Me-bpy)(CN)] _n	80	77	2113	1D
		RT	49	2114	CCCC
7	[Cu ^I (4,4'-dCO ₂ Et-bpy) _{0.5} (CN)] _n	80	83	2128	1D
		RT	53	2121	ACCA
8	[Cu ^I ₅ (pylpy) ₂ (CN) ₅] _n	80	77	2129	1D
		RT	89	2123	ABAB
9	[Cu ^I ₂ (CN) ₃ *0.5TMEDA-H ₂] _n	80	63	2126, 2089	Pillared 3D; intercalated with TMEDA-H ₂

^[a]All reactions were performed in CH₃OH using Cu^{II}(ala)(NN)Cl complexes (NN=bidentate nitrogen based ligand, Scheme 2). Yields were calculated based on copper after 24 h. [Cu^{II}]₀: [AIBN]₀: [ascorbic acid]₀=1:10:2, RT=22±2 °C. * No crystal structure was obtained.

In the 1D zigzag chains of $[\text{Cu}^{\text{I}}(4,4'\text{-dMe-bpy})_2(\text{CN})_3]_n$, two different copper sites were present. The first, a bicoordinated Cu(I) site was attached to the cyanide ligands through carbon and nitrogen at an angle of 180° and the second, a distorted tetrahedral Cu(I) center was coordinated to ligand, 4,4'-dMe-bpy and two cyanide ligand (**Figure 3.6.1**). The aromatic ligands of neighboring chains were interlocked by π - π stacking with distance of 3.697 \AA (**Figure 3.6.1**).³¹



Scheme 4.6.3. Schematic representation of direct reduction methodology where R= H(glycine), CH₃(alanine), -CH₂C₆H₅ (phenylalanine), -CH₂CH₂CH₂CH₂- (proline); Different ligands utilized in the generation of coordination polymer.

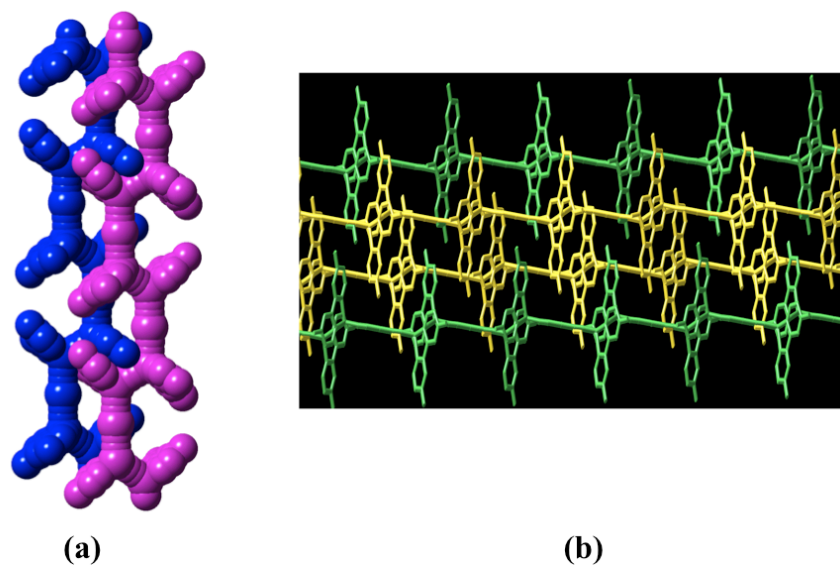


Figure 3.6.1: (a) π - π stacking in the $[\text{Cu}^{\text{I}}_3(4,4'\text{-dMe-bpy})_2(\text{CN})_3]_n$ (b) Packing diagram of $[\text{Cu}^{\text{I}}_3(4,4'\text{-dMe-bpy})_2(\text{CN})_3]_n$.

Another method was reported by Britton and his group, where a cyanide ligand was generated in situ by reacting ammonia and formaldehyde with copper(II) acetate in water in the presence of sodium thiosulfate pentahydrate. This methodology was tested on various alkyl amines to generate 1D, 2D and 3D polymers with poor to moderate yields.¹⁵

Among the synthetic challenges in this area, the ability to obtain high quality crystals in order to elucidate the polymer's structure is quite tedious. As these polymers are insoluble in many common solvents, recrystallization or the use of any spectroscopic technique is not possible. Some polymers are soluble in strongly coordinating solvent such as acetonitrile, which change the original structure by binding to the metal center. Therefore, it is imperative to get crystals directly from the reaction media.

Copper cyanide crystals are mainly derived from solvo/hydrothermal methods. Synthetic techniques that utilized the lower temperatures favor the formation of low

quality crystals or in amorphous form. However, the direct reduction method yields good quality crystals at room temperature under UV irradiation, or even at 80 °C. In addition the amount of the solvent employed had an effect on the quality of the crystals; 3 mL and 15 mL of methanol was found to be optimum for the formation of high quality crystals in microscale and macroscale synthesis, respectively.³¹

Another synthetic technique is slow diffusion, commonly utilized to generate crystals of metal organic frameworks. In this method, solution of ligand is diffused into solution of metal. Sometimes one solution is set as a gel with the gelling agent, tetramethoxy silane, and is then slowly diffused into the other solution to give crystals. Alternatively, a special type of vials or tubes (**Figure 3.6.2**) have been used to successfully crystallize the polymers.¹

Table 3.6.5. Reaction conditions for the synthesis of the crystalline coordination polymers through slow diffusion and evaporation.^{42,44}

Entry	Coordination Polymer	Ligand	Reaction Conditions	Dimensionality / Connectivity
1	$[\text{Cu}(\text{pn})_2][\text{Cu}_3(\text{CN})_4]_n$ ⁴²	pn = 1,2-propanediamine	Layering; Starting Material: Cu(NO ₃) ₂ ·3H ₂ O and KCN; ligand (1:4:3) in water. Product obtained after few days Yield: 70%	3D network by anionic Cu ^I CN and Cu ^{II} (pn) entrapped in the cavity
2	$[\text{Cu}_2(\text{CN})_3](\text{dmen})_n$ ⁴²	dmen = N,N'-dimethylethylenediamine	Layering; Starting Material: Cu(NO ₃) ₂ ·3H ₂ O and KCN; ligand (1:4:3) in water. Product obtained after	2D neutral sheets- Cu(I/II) center are assimilated in the chain

			few days Yield: 65 %	
3	$[\text{Cu}_3(\text{CN})_4(\text{tmen})]_n$ ⁴²	tmen = N,N,N',N'-tetramethylethylenediamine	Layering; Starting Material: Cu(NO ₃) ₂ ·3H ₂ O and KCN; ligand (1:4:3) in water. Product obtained after few days Yield: 60 %	3D star shaped network Cu(I/II) center are assimilated in the chain
4	$[\text{Cu}_2(\text{CN})_3][\text{NEt}_4]_n$ ⁴²	NEt ₄ PF ₆ = tetraethylammonium hexafluorophosphate	Slow evaporation; Starting Material: Cu(NO ₃) ₂ ·3H ₂ O : KCN (1:4) Yield: 65 %	Honeycomb 2D sheets.
5	$[\text{Fe}(3\text{-Xpy})_2[\text{Cu}(3\text{-Xpy})_2(\text{CN})_2]_2]_n$ where X= F(1), Cl(2), Br(3) ⁴⁴		Slow diffusion Yield: 35%(1), 30%(2), 25%(3)	

These crystallization methods generally require a lot of time on the order of weeks to months in addition to a constant supervision of the reaction tubes. This supervision is required because kinetically favored crystals can easily grow and redissolved back into the mother liquor whereas the thermodynamically favored crystals take a longer to grow. Thus, when left unattended for a longer period of time, two or more products can form. Elucidation of the structure of the polymer is as important as the synthesis. Structure elucidation enabled the prediction of the properties and possible applications of the coordination polymer. The different techniques used to characterize coordination polymers are discussed in detail in the following section.

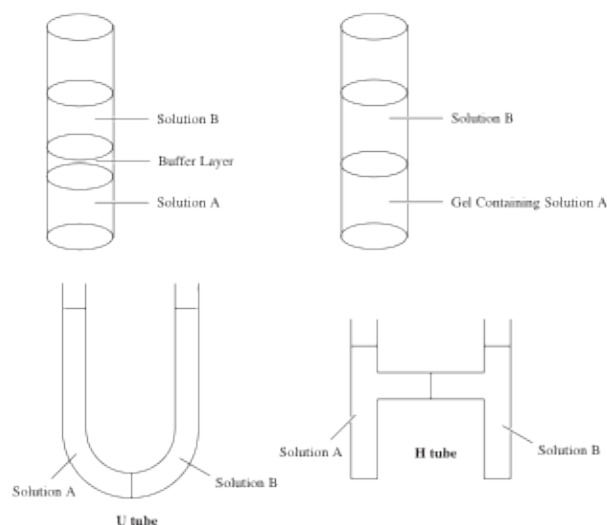


Figure 3.6.2. Different tubes used for the growing the crystals of coordination polymers.¹

3.7. Characterization of Copper Cyanide Polymers

Single X-ray Crystallography

Unlike organic polymers, coordination polymers can be characterized by single crystal X-ray crystallography. As mentioned in the previous section, obtaining good quality crystals is important for determining the structure of the final polymer. Due to the poor solubility in common solvents, spectroscopic techniques cannot be used for the characterization. Furthermore, since two or more products can result during the synthesis of coordination polymers and therefore, a single crystal might not represent the entire batch of sample. To correlate the crystal with the bulk material, we can characterize the sample with powder X-ray diffraction (PXRD).

Powder X-ray Diffraction

The PXRD technique has been successfully used for the identification of the phase purity of the bulk sample with data obtained by single crystal X-ray diffraction. In

Figure 3.7.1, a simulated XRPD pattern of $[\text{Cu}^{\text{I}}_2(\text{phen})_2(\text{CN})_2 \cdot \text{CH}_3\text{OH}]_n$ was generated by single crystal data (red) and matched with the sample synthesized at 80 °C (black).³¹ In some cases, the intensity of the peaks do not match due to preferred orientations caused by the sample preparation technique or due to the polymeric nature of the material. There are other less reliable techniques available such as IR and raman spectroscopy to characterize the bulk materials.

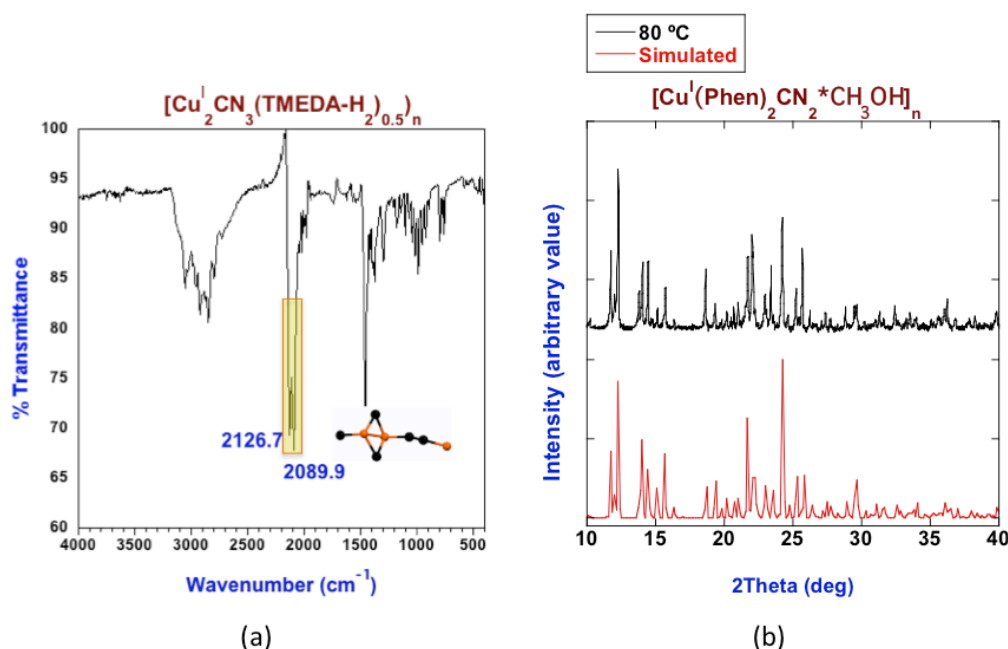


Figure 3.7.1. (a) IR spectrum of $[\text{Cu}^{\text{I}}_2(\text{CN})_3 \cdot 0.5\text{TMEDA-H}_2]_n$ (b) XRPD pattern (calculated = red; black = experimental) of $[\text{Cu}^{\text{I}}_2(\text{phen})_2(\text{CN})_2 \cdot \text{CH}_3\text{OH}]_n$.³¹

Infrared spectroscopy

Copper cyanide polymers exhibit very sharp peak at 2000-2300 cm⁻¹. This absorbance corresponds to a CN⁻ stretching. In comparison to the free nitrile peak at 2080 cm⁻¹, peaks appeared at higher frequency when bonded to the metal center due to strong sigma donation from the HOMO orbitals from the cyanide.^{7, 12, 29, 31} The effect of

the back bonding is less pronounced or not observed by IR spectroscopy. The position of the peak is strongly dependent on the nature of the bonding of the nitrile to the metal. In the IR spectrum of $[\text{Cu}^{\text{I}}_2(\text{CN})_3 \cdot 0.5\text{TMEDA-H}_2]_n$, two peaks were present in the cyanide region at 2126.7 and 2089.9 cm^{-1} , which correspond to the dimeric and monomeric cyanide coordination, respectively (**Figure 3.7.1**).³¹ However, in many cases such splitting is not observed.

Thermogravimetric Analysis (TGA)

To test the thermal stability of the CuCN networks at different temperatures thermogravimetric analysis can be used. The thermal analysis of the $[\text{CuCN}(\text{L})]_n$ (L= ligand) networks generally starts with the decomposition of the ligand at 150-200 °C followed by CuCN degradation at nearly 400 °C. This technique can also be used to predict the structure of the polymer. The TGA spectrum $[\text{Cu}(\text{CN})_3(\text{Bzpip})_2]_n$ exhibited two mass losses between 150-200 °C. This indicates the systematic loss of the two molecules of the ligand benzylpiperazine which is followed by decomposition of CuCN networks at around 400 °C (**Figure 3.7.2**).⁴⁷

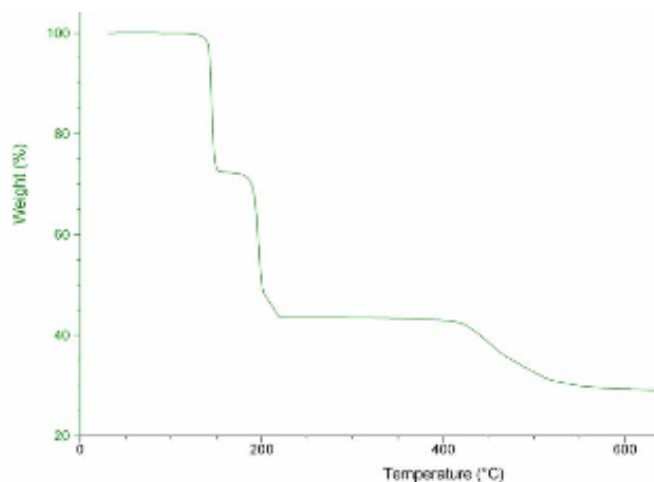
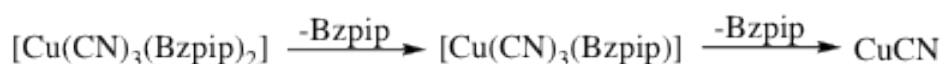
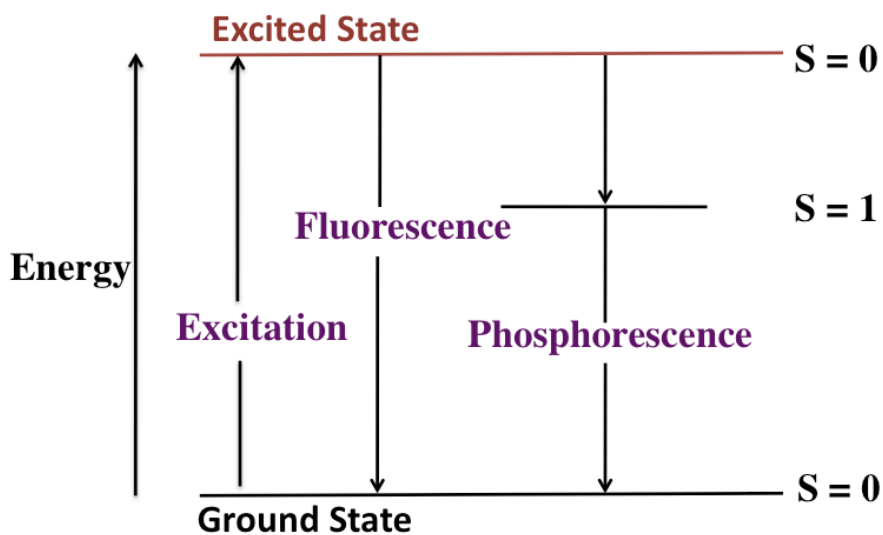


Figure 3.7.2. TGA spectrum of $[\text{Cu}(\text{CN})_3(\text{Bzpip})_2]_n$.⁴⁷

3.8. Properties of Copper Cyanide Polymers

Luminescence

Electronic transitions from excited to ground state after photoexcitation result in the emission of light, known as luminescence. There are two different types of luminescence depending on the nature of the excited state: fluorescence and phosphorescence. Fluorescence is carried out with rapid energy dissipation resulting in the loss of energy of emitted light in comparison to the absorbed light while in phosphorescence, energy dissipation is slow from excited triplet state to ground state (Scheme 3.8.1).



Scheme 3.8.1. Schematic representation of fluorescence and phosphorescence, where S = spin quantum number.

Phosphorescence causes materials to glow in the dark. Chromophoric ligands in metal complexes absorb the light and transfer the energy to metal center also known as ligand-to-metal charge-transfer (LMCT). In some cases, the energy can be transferred from the metal to the ligand causing metal to ligand charge transfer (MLCT) In some cases, the π - π^* transition in the ligand causes luminescence without any participation from the metal center.^{3, 29, 30, 46, 47}

Coordination polymers can amplify emission properties due to their physical attributes or couple with the guest molecules in comparison to the luminescent small molecules or organic polymers. In addition to these properties, coordination polymers are highly stable which make them potential candidates for sensor materials.

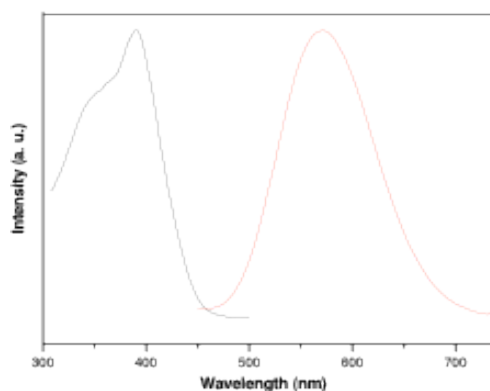


Figure 3.8.1. Excitation (black) and emission (red) spectra of copper cyanide polymer.³³

Lanthanide based polymers have been extensively studied due to their significant emissive properties and larger band gaps.⁵⁰ In some cases, luminescent behavior has been found to be strongly dependent on the guest molecules. In the absence of any guest molecule, no emission spectrum was observed in the case of europium-based polymer, (btc = benzene tricarboxylate). However, on addition of the solvent molecule, dimethyl

formamide (DMF) resulted in a significant increase in fluorescence while acetone quenched the luminescence.⁵⁰

The luminescent spectrum of pure CuCN showed the three peaks at 288, 307 and 345 nm. On coordination with ligands, the luminescence of the CuCN polymes can either be amplified or disappear depending on the nature of the ligand. These polymers generally absorb in the UV region and emit in the visible region, resulting in a bathochromic shift in emission spectrum (**Figure 3.8.2**). Upon excitation, electronic transition occur from the d^{10} orbital to the d^9s^1 or d^9p^1 or π^* orbitals of the ligand. However, in some cases these transitions are quenched due to π - π^* transitions in chromophoric aromatic ligands.

Luminescent behavior of these polymers is also found to be dependent on the temperature. The intensity and wavelength of the emission spectra changed dramatically in comparison on change from 298 K to 77 K. In case of $[(\text{CuCN})_2(\text{Ph}_2\text{CHPIP})]_n$, the intensity of high energy (HE) peaks increased while intensity of low energy (LE) peaks decreased at 77 K with respect to the peak intensities at 298 K (**Figure 3.8.2**).⁴⁷

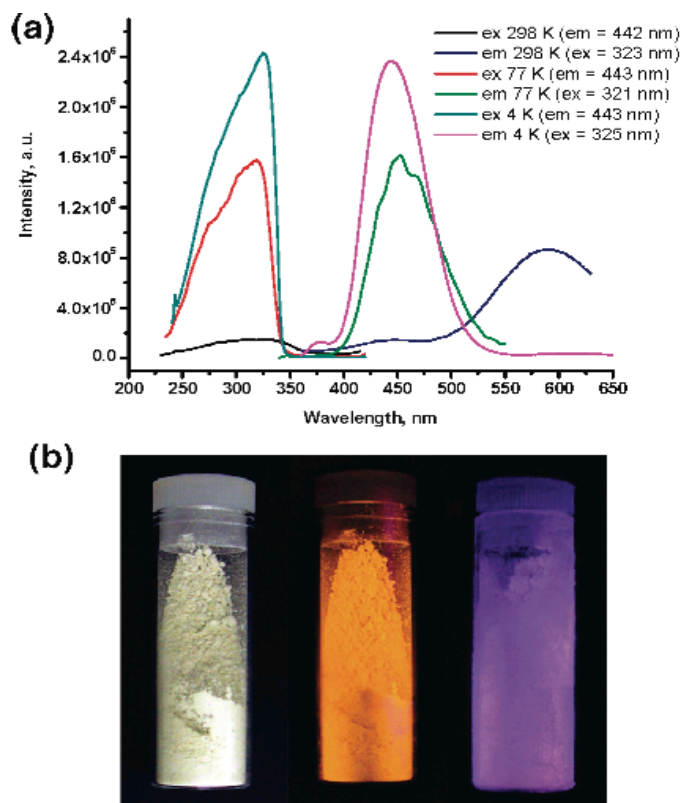


Figure 3.8.2. (a) Excitation and Emission spectra of $[(\text{CuCN})_2(\text{Ph}_2\text{CHPIP})]_n$ (b) Color change at 298 K, 77K and 4K of the $[(\text{CuCN})_2(\text{Ph}_2\text{CHPIP})]_n$ (right to left).

In other examples, CuCN showed reversible photoluminescence when it is exposed to the vapors of N-based ligands on excitation in the UV region at 254 nm. These adducts, formed by complexation of ligands with CuCN, emit different colors in the visible region and made these networks attractive candidates for chemical sensing (Figure 3.8.3).⁴⁷



Figure 3.8.3. Reversible luminescence of CuCN adducts at 254nm A: Piperadine, B: N-N-methylpiperadine, C: N-ethylpiperadine, D: N-methylpyrrolidine E: dimethyl-N-cyclohexane F: triethylamine G: N-methylmorpholine H: N-methylpiperazine I: N,N'-Dimethylpiperazine) J: pyridine K: 2-methylpyridine L: 3-methylpyridine M: 4-methylpyridine, N: 2-ethylpyridine O: 3-Ethyl Pyridine, P: 4-Ethyl Pyridine, Q: 4-t-butylpyridine.

Magnetism and Spin Crossover Behavior of Copper Cyanide Coordination Polymers

Competition between the spin pairing energy and the energy gap between the e_g and t_{2g} metal orbitals results in the spin crossover phenomenon (SCO) in transition metal ions. CuCN networks do not show this behavior due to the diamagnetic nature of the d^{10} Cu(I) center. When the paramagnetic centers, such as Fe(II), Co(II) or Cu(II) were introduced to the diamagnetic CuCN networks, a dramatic change in the magnetic properties and SCO behavior of the coordination polymers was observed.⁵¹⁻⁵⁴ Studies have been done on coordination polymers, $[\text{Fe}(\text{3-Clpy})_2[\text{Cu}(\text{3-Clpy})_2(\text{CN})_2]_2]_n$ displayed a

poorly resolved two-step spin conversion, $T_{c1} = 169$ K and $T_{c2} = 210$ K, indicated the presence of two distinct crystallographically Fe(II) sites.⁴⁴ Polymers with fluorinated pyridine ligand showed 81% of low-spin (LS) state compounds and 19% of the residual Fe^{II} ions in the high-spin (HS) state at 293 K and underwent an irreversible spin transition at $T_c = 356$ K. However, in the polymer with the brominated ligand, the Fe(II) centers were 100% high spin.⁴⁴ Coordination polymers with paramagnetic metal centers have potential to be used as molecular magnets.

3.9. Conclusion

The versatile binding modes of cyanide with Cu(I) makes it an ideal ligand to form complex and fascinating architecture of 1D, 2D and 3D networks. Various approaches have been reviewed for the synthesis of these robust copper-based cyanide polymers with different nitrogen-based ligands. The influence of structural and experimental factors on product distribution and yields has been discussed. These networks showed attractive properties such as photoluminescence via excitation of 3d electrons into the 4s or π^* orbitals of the ligands, color change in presence of solvents, spin crossover behavior. Due to such properties and the robust nature of the CuCN polymers, these frameworks can have potential application in different fields like chemical sensing, electronics, molecular storage and molecular magnets.

References:

1. Batten, S. R.; Neville, S. M.; Turner, D. R., Coordination Polymers - Design, Analysis and Application. In Royal Society of Chemistry, **2009**.
2. Etaiw, S.; Badr El-din, A., Assembly and Fluorescence Properties of 3D-Copper(I) Cyanide Coordination Polymers Based on Methylpyrazine and

- Tetramethylpyrazine in Presence of Me_3SnCl . *J. Inorg. Organomet. Polym.* **2011**, *21*, (1), 110-117.
3. Ley, A. N.; Dunaway, L. E.; Brewster, T. P.; Dembo, M. D.; Harris, T. D.; Baril-Robert, F.; Li, X.; Patterson, H. H.; Pike, R. D., Reversible luminescent reaction of amines with copper(i) cyanide. *Chem. Comm.* **2010**, *46*, (25), 4565-4567.
 4. Suh, M. P.; Park, H. J.; Prasad, T. K.; Lim, D.-W., Hydrogen Storage in Metal-Organic Frameworks. *Chem. Rev.* *112*, (2), 782-835.
 5. Yang, L.; Xin, L.; Tian, J.; Du, P.; Wei, X.; Liao, S.; Zhang, Y.; Lv, R.; Gu, W.; Liu, X., Synthesis of a rare 3D copper cyanide compound based on 3-(5-(pyridin-4-yl)-1H-1,2,4-triazol-3-yl)pyridine via the transformation of acetonitrile to inorganic cyanide. *J. Mol. Struct.* *1064*, (0), 1-5.
 6. Noro, S.-i.; Kitagawa, S.; Kondo, M.; Seki, K., A New, Methane Adsorbent, Porous Coordination Polymer [$\{\text{CuSiF}_6(4,4'\text{-bipyridine})_2\}_n$]. *Angew. Chem. Int. Ed.* **2000**, *39*, (12), 2081-2084.
 7. Xu, Y.; Ren, Z.-G.; Li, H.-X.; Zhang, W.-H.; Chen, J.-X.; Zhang, Y.; Lang, J.-P., Syntheses, crystal structures and luminescent properties of two one-dimensional coordination polymers $[\text{CuX}(\text{dmpzm})_n]$ ($\text{X}=\text{CN}$, NCS ; $\text{dmpzm}=\text{bis}(3,5\text{-dimethylpyrazolyl})\text{methane}$). *J. Mol. Struct.* **2006**, *782*, (3), 150-156.
 8. Estrader, M.; Diaz, C.; Ribas, J.; Solans, X.; Font-Bardoa, M., Synthesis, characterization and magnetic properties of six new copper(II) complexes with aminoacids as bridging ligand, exhibiting ferromagnetic coupling. *Inorg. Chim. Acta* **2008**, *361*, (15), 3963-3969.
 9. Agusti, G.; Munoz, M. C.; Gaspar, A. B.; Real, J. A., Spin-Crossover Behavior in Cyanide-Bridged Iron(II), Copper(I) Bimetallic 1,3D Metal-Organic Frameworks. *Inorg. Chem.* **2009**, *48*, (8), 3371-3381.
 10. Larionova, J.; Guari, Y.; Sangregorio, C.; Guerin, C., Cyano-bridged coordination polymer nanoparticles. *New. J. Chem.* **2009**, *33*, (6), 1177-1190.
 11. Chesnut, D. J.; Kusnetzow, A.; Birge, R.; Zubieta, J., Solid state coordination chemistry: ligand influences on the structures of one-dimensional copper(i) cyanide-organodiimine solids. *Dalton Trans.* **2001**, (18), 2581-2586.

12. Mao, H.; Zhang, C.; Xu, C.; Zhang, H.; Shen, X.; Wu, B.; Zhu, Y.; Wu, Q.; Wang, H., Self-assembly of three hetero- and homopolynuclear cyanide bridged complexes of FeII-CuI and CuI: hydrothermal syntheses, structural characterization and properties. *Inorg. Chim. Acta* **2005**, 358, (6), 1934-1942.
13. Park, K.-M.; Yoon, I.; Seo, J.; Lee, J.-E.; Kim, J.; Choi, K. S.; Jung, O.-S.; Lee, S. S., Two-Dimensional Square-Grid versus One-Dimensional Double-Stranded Networks: Counterion Regulation of the Formation of Macrocycle-Based Copper(I) Coordination Frameworks. *Crys. Growth Des.* **2005**, 5, (5), 1707-1709.
14. Aakeröy, C. B.; Beatty, A. M.; Leinen, D. S., A Versatile Route to Porous Solids: Organic-Inorganic Hybrid Materials Assembled through Hydrogen Bonds. *Angew. Chem. Int. Ed.* **1999**, 38, (12), 1815-1819.
15. Stocker, F. B.; Staeva, T. P.; Rienstra, C. M.; Britton, D., Crystal Structures of a Series of Complexes Produced by Reaction of Copper(I) Cyanide with Diamines. *Inorg. Chem.* **1999**, 38, (5), 984-991.
16. Batten, S. R., Coordination polymers. *Current Opinion in Solid State and Materials Science* **2001**, 5, (2-3), 107-114.
17. Khlobystov, A. N.; Blake, A. J.; Champness, N. R.; Lemenovskii, D. A.; Majouga, A. G.; Zyk, N. V.; Schröder, M., Supramolecular design of one-dimensional coordination polymers based on silver(I) complexes of aromatic nitrogen-donor ligands. *Coordination Chem. Rev.* **2001**, 222, (1), 155-192.
18. Pan, L.; Frydel, T.; Sander, M. B.; Huang, X.; Li, J., The Effect of pH on the Dimensionality of Coordination Polymers. *Inorg. Chem.* **2001**, 40, (6), 1271-1283.
19. Ball, P., Bright Earth: Art and Invention of Color. **2001**.
20. Herren, F.; Fischer, P.; Ludi, A.; Halg, W., *Inorg. Chem.* **1908**, 12.
21. Buser, H. J.; Schwarzenbach, D.; Petter, W.; Ludi, A., The crystal structure of Prussian Blue: $\text{Fe}_4[\text{Fe}(\text{CN})_6]_3 \cdot x\text{H}_2\text{O}$. *Inorg. Chem.* **1977**, 16, (11), 2704-2710.
22. Zhdanov, H., *C.R. Acad. Sci. USSR* **1941**, 31.

23. Shugam, F.; Zhdanov, H., *Acta Physiochim. USSR* **1945**, 20.
24. Powell, H. M.; Rayner, J. H., *Nature* **1949**, 163.
25. Rayner, J. H.; Powell, H. M., *J. Chem. Soc.* **1958**, 3412.
26. Iwamoto, T.; Nakano, T.; Morita, M.; Miyoshi, T.; Miyamoto, T.; Sasaki, Y., *Inorg. Chim. Acta.* **1968**, 2, 313.
27. Miyoshi, T.; Iwamoto, T.; Sasaki, Y., *Inorg. Nucl. Chem. Lett.* **1970**, 6.
28. Iwamoto, T., *Encyclopedia of Supramolecular Chemistry* ed. J.L. Atwood and J.W.Steed, Marcel Dekker, New York, **2004**.
29. Pike, R. D., Structure and Bonding in Copper(I) Carbonyl and Cyanide Complexes. *Organometallics* **2012**, 31, (22), 7647-7660.
30. Bayse, C. A.; Brewster, T. P.; Pike, R. D., Photoluminescence of 1-D Copper(I) Cyanide Chains: A Theoretical Description. *Inorg. Chem.* **2008**, 48, (1), 174-182.
31. Kaur, A.; Pintauer, T., Copper(I)–Cyanide Frameworks through Thermal or Photodecomposition of the Free Radical Diazo Initiator AIBN. *Eur. J. Inorg. Chem.* **2013**, 2013, (19), 3297-3301.
32. Nie, J.; Wang, J.; Dai, C., catena-Poly[[[(1,10-phenanthroline)copper(I)]- μ -cyanido] ethanol hemisolvate]. *Acta Crystallogr. Sect E* **2010**, 66, m1538-m1539.
33. Wang, H.; Li, M.-X.; Shao, M.; He, X., Syntheses, structures and luminescent properties of four copper(I) cyanide coordination polymers based on 2-(n-pyridyl)benzimidazole ligands *Polyhedron* **2007**, 26, (17), 5171-5176.
34. Li, D.; Wu, T., Transformation of Inorganic Sulfur into Organic Sulfur: A Novel Photoluminescent 3-D Polymeric Complex Involving Ligands in Situ Formation. *Inorg. Chem.* **2004**, 44, (5), 1175-1177.
35. Wells, A. F., Structural Inorganic Chemistry. *Oxford University Press* **1945**.

36. Wells, A. F., The geometrical basis of crystal chemistry. Part 1. *Acta Crystallogr.* **1954**, 7.
37. Wells, A. F., Three dimensional nets and polyhedra. *Wiley* **1977**.
38. Batten, S. R., Glorious uncertainty—challenges for network design. *J. Solid State Chem.* **2005**, 178, (8).
39. Batten, S. R.; Robson, R., Interpenetrating Nets: Ordered, Periodic Entanglement. *Angew. Chem. Int. Ed.* **1998**, 37, (11).
40. Batten, S. R.; Hoskins, B. F.; Robson, R., Interdigitation, Interpenetration and Intercalation in Layered Cuprous Tricyanomethanide Derivatives. *Chem. Euro. J.* **2000**, 6, (1), 156-161.
41. Batten, S. R., Topology of interpenetration. *Cryst. Eng. Comm.* **2001**, 3, (18).
42. Colacio, E.; Kivekšs, R.; Lloret, F.; Sunberg, M.; Suarez-Varela, J.; Bardajv, M.; Laguna, A., Architecture Dependence on the Steric Constrains of the Ligand in Cyano-Bridged Copper(I) and Copper(II), àíCopper(I) Mixed-Valence Polymer Compounds Containing Diamines:, Crystal Structures and Spectroscopic and Magnetic Properties. *Inorg. Chem* **2002**, 41, (20), 5141-5149.
43. Agusti, G.; Munoz, M. C.; Gaspar, A. B.; Real, J. A., Spin-Crossover Behavior in Cyanide-Bridged Iron(II),Copper(I) Bimetallic 1,3D Metal,Organic Frameworks. *Inorg. Chem.* **2009**, 48, (8), 3371-3381.
44. He, X.; Lu, C.-Z.; Yuan, D.-Q.; Chen, S.-M.; Chen, J.-T., Synthesis and Crystal Structures of Four Cyanide-Bridged Coordination Polymers. *Eur. J. of Inorg. Chem.* **2005**, 2005, (11), 2181-2188.
45. Lefebvre, J.; Batchelor, R. J.; Leznoff, D. B., Cu[Au(CN)₂]₂(DMSO)₂: Golden Polymorphs That Exhibit Vapochromic Behavior. *J. Am. Chem. Soc.* **2004**, 126, (49), 16117-16125.
46. Pike, R. D.; deKrafft, K. E.; Ley, A. N.; Tronic, T. A., Threaded structure and blue luminescence of (CuCN)₂₀(Piperazine)₇. *Chem. Comm.* **2007**, (36), 3732-3734.

47. Lim, M. J.; Murray, C. A.; Tronic, T. A.; deKrafft, K. E.; Ley, A. N.; deButts, J. C.; Pike, R. D.; Lu, H.; Patterson, H. H., Copper(I) Cyanide Networks: Synthesis, Structure, and Luminescence Behavior. Part 2. Piperazine Ligands and Hexamethylenetetramine(1). *Inorg. Chem.* **2008**, *47*, (15), 6931-6947.
48. Deng, H.; Qiu, Y.; Daiguebonne, C.; Kerbellec, N.; Guillou, O.; Zeller, M.; Batten, S. R., Synthesis of New Copper Cyanide complexes via the Transformation of Organonitrile to Inorganic Cyanide. *Inorg. Chem.* **2008**, *47*, (13), 5866-5872.
49. Zhou, X.-P.; Li, D.; Tao, W.; Xuanjun, Z., Syntheses of supramolecular CuCN complexes by decomposing CuSCN: a general route to CuCN coordination polymers? *Dalton Trans.* **2006**, 2435-2443.
50. Chen, B.; Yang, Y.; Zapata, F.; Lin, G.; Qian, G.; Lobkovsky, E. B., Luminescent Open Metal Sites within a Metal–Organic Framework for Sensing Small Molecules. *Advanced Materials* **2007**, *19*, (13), 1693-1696.
51. Visinescu, D.; Fabelo, O.; Ruiz-Perez, C.; Lloret, F.; Julve, M., Synthesis, crystal structure and magnetic properties of a new cyanide-bridged mixed-valence copper(I)/copper(II) clathrate. *Inorg. Chem. Comm.* **2013**, *35*, (0), 252-254.
52. Landee, C. P.; Wicholas, M.; Willett, R. D.; Wolford, T., Magnetic exchange in a one-dimensional polymeric chain containing cyanide-bridged copper(II). *Inorg. Chem.* **1979**, *18*, (8), 2317-2318.
53. Toma, L. M.; Delgado, F. S.; Ruiz-Perez, C.; Carrasco, R.; Cano, J.; Lloret, F.; Julve, M., Synthesis, crystal structures and magnetic properties of single and double cyanide-bridged bimetallic Fe²⁺/Cu²⁺ zigzag chains. *Dalton Trans.* **2004**, (18), 2836-2846.
54. Li, S.-T.; Zhao, C.-C.; Cui, A.-L.; Kou, H.-Z., Cyanide-bridged one-dimensional bimetallic complexes based on a tridentate copper(II) building block: synthesis, crystal structures and magnetic properties. *Transition Met. Chem.* **2014**, *39*, (4).

Chapter 4

Copper(I)-Cyanide Frameworks via Thermal or Photo- Decomposition of Free Radical Diazo Initiator (AIBN)[†]

Abstract

Thermal- or photodecomposition of classical free radical generating diazo reagent 2,2'-azobis(2-methylpropionitrile) (AIBN) was used as the source of cyanide anions in the synthesis of copper(I)-cyanide frameworks. The reported methodology utilized direct reduction of $\text{Cu}^{\text{II}}(\text{aa})(\text{NN})\text{X}$ (aa=deprotonated amino acid, NN=bidentate nitrogen based ligand, X=Cl or Br) complexes by AIBN/ascorbic acid to yield seven novel coordination networks. Aromatic amines were directly incorporated into one-dimensional $\text{Cu}^{\text{I}}\text{-CN}$ chains. In the case of aliphatic amine tetramethylethylenediamine (TMEDA), three-dimensional $\text{Cu}^{\text{I}}\text{-CN}$ framework was obtained. This novel procedure is mild, applicable to a variety of nitrogen-based ligands, and represents an efficient alternative to currently used hydrothermal or solvothermal methods.

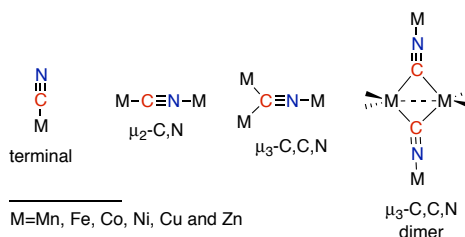
4.1. Introduction

During the past decade, metal-organic frameworks (MOFs) have attracted considerable interest due to their architectural diversity and potential applications in heterogeneous

[†] Reproduced in part with permission from Kaur, A.;Pintauer, T. *Eur. J. Inorg. Chem.* **2013**, (19), 3297-3301. Copyright 2008 Wiley-VCH Verlag GmbH & Co.

catalysis, photovoltaics, thin-film devices, membranes, biomedical imaging, and gas purification, separation and storage.⁶²⁻⁶⁴ Broadly defined, MOFs are crystalline compounds consisting of metal cations or clusters connected by multitopic organic “strut” or “linker” ions or molecules to form one-, two- and three-dimensional structures that can be porous.⁶⁰ Cyanide anions are among the most versatile “linker” ions due to not only their ability to coordinate to a wide range of metal centers, but also different bridging modes (**Scheme 4.1.1**).⁶⁵ Because of these properties, MOFs incorporating cyanide anions have been widely investigated, in particular for hydrogen storage,⁶⁶⁻⁶⁸ and are perhaps the oldest class of synthetic microporous materials.

Metal-cyanide frameworks are typically synthesized using solvothermal or hydrothermal methods that require high temperatures, pressures, prolonged reaction times, and highly toxic metal cyanide precursors.⁶⁹ Both methods generally lack the ability to predict the desired network geometry and have been known to be unselective, often leading to the formation of several products. For example, hydrothermal treatment of a mixture of $\text{Cu}^{\text{II}}\text{Cl}_2$, $\text{K}_3[\text{Fe}^{\text{III}}(\text{CN})_6]$, tetrazole and acetonitrile at 160 °C/170 °C yielded two polymorphs, $\text{H}_5\text{O}_2[\text{Cu}^{\text{I}}_2(\text{CN})_3]$, both of which contained hexagonal $[\text{Cu}^{\text{I}}_2(\text{CN})_3]^-$ layers but different supramolecular arrays.⁷⁰



Scheme 4.1.1. Bridging modes in metal-cyanide complexes.

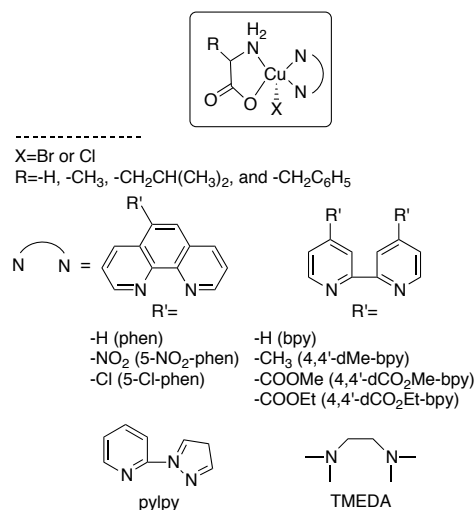
Various systematic methodologies have been developed to gain control over the network structure, and they mainly involve the interplay between using rigid ligands (e.g. 4,4'-bipyridine or hexamethylenetetramine) and anions with different coordinating abilities.⁷¹ Also, a significant progress has been made in controlling the interpenetration of polymer networks, which greatly influences the cavity size of the porous material.⁷²⁻⁷⁴ However, despite these advances, very little attention has been paid to the development of novel synthetic methodologies that can be used in the preparation of MOFs, in particular metal-cyanide networks.

In this chapter, we report that direct reduction of $\text{Cu}^{\text{II}}(\text{aa})(\text{NN})\text{X}$ (aa=deprotonated amino acid, NN=bidentate nitrogen based ligand, X=Cl or Br) complexes by free radicals generated from thermal- or photodecomposition of commonly used diazo reagents such as AIBN (2,2'-azobis(2-methylpropionitrile)) and/or ascorbic acid affords well-defined copper(I)-cyanide frameworks in excellent yields.⁷⁵ The reported procedure is mild, applicable to a variety of nitrogen-based ligands, and represents an efficient alternative to conventionally used hydrothermal or solvothermal methods.

4.2. Results and Discussion

Originally, neutral and distorted square pyramidal $\text{Cu}^{\text{II}}(\text{aa})(\text{NN})\text{X}$ (aa=deprotonated amino acid, NN=bidentate nitrogen based ligand, X=Cl or Br, **Scheme 4.2.1**) complexes were prepared for use as catalysts in atom transfer radical addition (ATRA). The representative molecular structure of $\text{Cu}^{\text{II}}(\text{ala})(\text{phen})\text{Cl}$ (ala=*L*-alanine, phen=1,10-phenanthroline) is shown in **Figure 4.2.1**. ATRA is the fundamental organic reaction for

the formation of C-C bonds utilizing alkyl halides and alkenes.^{11, 76} It is mechanistically similar to well-known atom transfer radical polymerization (ATRP), which is used to synthesize polymeric materials with well-controlled molecular weights and polydispersities.⁷⁷ These reactions typically utilize reducing agents, such as free radicals generated by thermal or photo-decomposition of diazo reagents (e.g. AIBN) or ascorbic acid, which are used to regenerate the activator or copper(I) complex.



Scheme 4.2.1. Copper(II)/amino acid complexes used in the study.

When $\text{Cu}^{\text{II}}(\text{ala})(\text{phen})\text{Cl}$ was utilized as catalyst under standard ATRA conditions ($[\text{1-octene}]_0 : [\text{CCl}_4]_0 : [\text{AIBN}]_0 : [\text{Cu}^{\text{II}}]_0 = 250 : 275 : 12.5 : 1$, solvent = CH_3OH , $T = 60\text{ }^\circ\text{C}$), we observed a relatively fast change in the color from blue to dark red, indicating that the reduction of $\text{Cu}^{\text{II}}(\text{ala})(\text{phen})\text{Cl}$ to $\text{Cu}^{\text{I}}(\text{ala})(\text{phen})$ took place. However, soon after, the red crystalline material began to precipitate from the reaction mixture. Originally, we thought that the problem was the solubility of $\text{Cu}^{\text{I}}(\text{ala})(\text{phen})$, but to the greatest surprise, single crystal X-ray analysis revealed the formation of $[\text{Cu}^{\text{I}}_2(\text{phen})_2(\text{CN})_2 \cdot \text{CH}_3\text{OH}]_n$ coordination polymer.

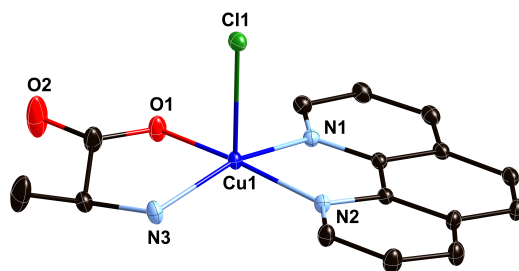


Figure 4.2.1. Molecular structure of $\text{Cu}^{\text{II}}(\text{ala})(\text{phen})\text{Cl}\cdot\text{CH}_3\text{OH}$ at 150 K, shown with 30% probability displacement ellipsoids. H-atoms and solvent molecules have been omitted for clarity. Selected bond distances [Å] and angles[°]: Cu1-O1 1.9258(18), Cu1-N1 2.0082(19), Cu1-N2 2.0260(19), Cu1-N3 2.007(2), Cu1-Cl1 2.5920(6), O1-Cu1-N3 84.10(8), O1-Cu1-N1 91.99(8), N3-Cu1-N1 160.26(9), O1-Cu1-N2 170.13(9), N4 Cu1 N2 99.20(8), N1 Cu1 N2 81.76(8), O1 Cu1 Cl1 95.76(7), N4 Cu1 Cl1 98.02(7), N1 Cu1 Cl1 101.63(6), N2 Cu1 Cl1 92.99(6).

Copper(I) atoms in the crystal structure of $[\text{Cu}^{\text{I}}_2(\text{phen})_2(\text{CN})_2\cdot\text{CH}_3\text{OH}]_n$ were coordinated by two cyanide ($\text{Cu}^{\text{I}}\text{-X}=1.911(2)\text{-}1.940(3)$ Å) and two nitrogen atoms from 1,10-phenanthroline ($\text{Cu}^{\text{I}}\text{-N}=2.094(2)\text{-}2.120(2)$ Å) to give a distorted tetrahedral environment. The cyanide ligands were linearly coordinated (C-N-Cu angles ranged from $175.3(2)^\circ$ to $178.1(2)^\circ$) and bridged adjacent Cu^{I} atoms to form a one-dimensional helical chains running along the *b* axis with a long pitch of 15.567(4) Å (**Figure 4.2.2a**). The intrachain $\text{Cu}^{\text{I}}\text{-Cu}^{\text{I}}$ distance across the cyanide bridges was determined to be 4.924(3) Å, whereas the shortest-interchain distance between copper centers was 6.617(2) Å. Additionally, crystal structure was stabilized by $\pi\text{-}\pi$ stacking interactions (3.493(4) Å, **Figure 4.2.2b**) between 1,10-phenanthroline ligands from two adjacent chains and O-H--N bonding (2.603(2)-2.464(4) Å, **Figure 4.2.2c**) due to methanol.

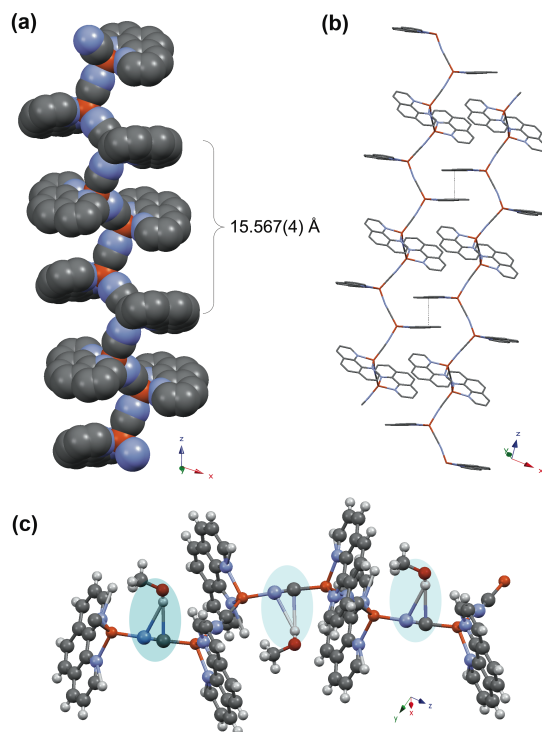
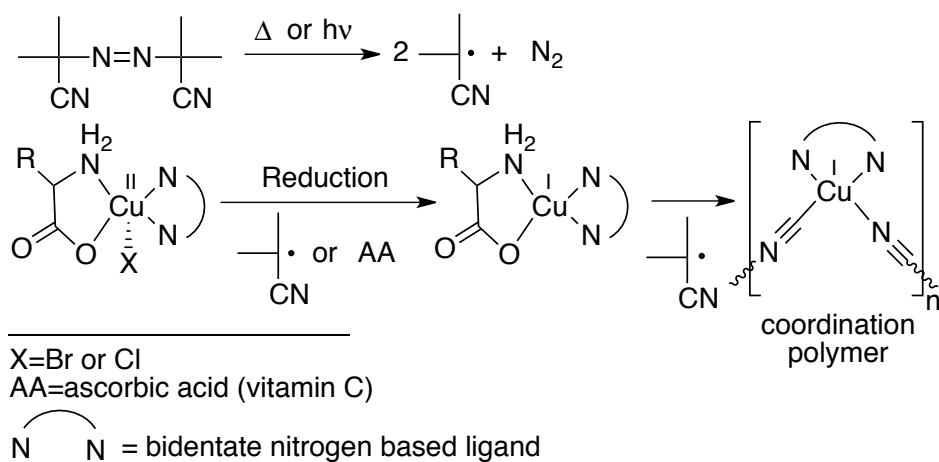


Figure 4.2.2. One-dimensional helical chains (a), π - π stacking interactions (3.493(4) Å) (b) and hydrogen bonding associated with guest MeOH molecules (2.464(4)-2.603(2) Å) in $[\text{Cu}^{\text{I}}_2(\text{phen})_2(\text{CN})_2 \cdot \text{CH}_3\text{OH}]_n$. Orange=Cu, blue=N, black=C, red=oxygen.

When the above reaction was repeated at 80°C using AIBN and ascorbic acid only ($[\text{Cu}^{\text{II}}]_0:[\text{AIBN}]_0:[\text{ascorbic acid}]_0=1:10:2$), the coordination polymer was isolated in 92% yield after 24 h (based on copper, **Table 4.2.1**). The ascorbic acid was added to the reaction mixture in order to accelerate the reduction process. Alternatively, nearly identical yield was obtained if the reaction was conducted with $\text{Cu}^{\text{I}}(\text{ala})(\text{phen})$ in the presence of AIBN, but absence of ascorbic acid. The main advantage of utilizing copper(II) complex is the elimination of otherwise necessary deoxygenation step. The starting copper(II) complex does not need to be isolated, but can be conveniently prepared in situ prior to the addition of AIBN and/or ascorbic acid. What is even more important to notice is that the yield of coordination polymer increased to 94% (based on

copper) when the reaction was conducted under ambient temperature using photodecomposition of AIBN (**Table 4.2.1**). Previously reported synthesis of $[\text{Cu}^{\text{I}}(\text{phen})(\text{CN})]_n$ by hydrothermal treatment of $\text{Cu}^{\text{II}}(\text{NO}_3)_2$, $\text{K}_3[\text{Fe}^{\text{III}}(\text{CN})_6]$ and 1,10-phenanthroline in H_2O at $150\text{ }^\circ\text{C}$ for 48 h yielded only 45% of the coordination polymer.¹⁸



Scheme 4.2.2. Proposed reaction steps leading to the formation of $\text{Cu}^{\text{I}}(\text{NN})$ cyanide coordination frameworks.

Before demonstrating the efficiency of this novel transformation with other nitrogen-based ligands, preliminary studies were conducted in order to gain insight into the mechanistic features of the process. The proposed reaction steps leading to the formation of $\text{Cu}^{\text{I}}\text{-CN}$ coordination polymers are illustrated in **Scheme 4.2.2**. Firstly, the yield and crystallinity of the resulting product is greatly dependent on the concentration of AIBN, with optimum amount of 10 eq. relative to copper(II). Also, the variety of amino acids can be used in the reaction. This was demonstrated in the case of 1,10-phenanthroline complex in which the yields of the product were determined to be 85% (alanine), 84% (glycine), 72% (phenylalanine) and 63% (proline) (**Figure 4.2.3**). The

absence of amino acid did not result in any polymer formation, indicating that the reaction is highly selective only when deprotonated amino acids were coordinated to the copper(II) center.

Table 4.2.1. Experimental data for the synthesis of copper(I)-cyanide frameworks.

Coordination Polymer ^[a]	T (°C)	Yield (%)	$\nu(\text{CN})$ (cm ⁻¹)
[Cu ^I ₂ (phen) ₂ (CN) ₂ *CH ₃ O	80	92	2102
H] _n	RT	94	2102
[Cu ^I (bpy)(CN)] _n	80	82	2106
	RT	77	2106
[Cu ^I (5-NO ₂ -phen)(CN)] _n	80	73	2100
	RT	63	2099
[Cu ^I (5-Cl-phen)(CN)] _n	80	74	2104
	RT	72	2105
[Cu ^I ₃ (4,4'-dMe-	80	89	2104
bpy) ₂ (CN) ₃] _n	RT	76	2103
[Cu ^I (4,4'-dCO ₂ Me-	80	77	2113
bpy)(CN)] _n	RT	49	2114
[Cu ^I (4,4'-dCO ₂ Et-	80	83	2128
bpy) _{0.5} (CN)] _n	RT	53	2121
[Cu ^I ₅ (pylpy) ₂ (CN) ₅] _n	80	77	2129
	RT	89	2123
[Cu ^I ₂ (CN) ₃ *0.5TMEDA-	80	63	2126, 2089
H ₂] _n			

^[a]All reactions were performed in CH₃OH using Cu^{II}(ala)(NN)Cl complexes (NN=bidentate nitrogen based ligand, Scheme 2). Yields were calculated based on copper after 24 h. [Cu^{II}]₀: [AIBN]₀: [ascorbic acid]₀=1:10:2, RT=22±2 °C.

The yields with other monoanionic ligands such as acetates or acetylacetonates were very low and the resulting materials were not crystalline. Furthermore, the radicals generated by thermal or photo-decomposition of AIBN were the source of cyanide anions because other non-diazo radical initiators such as peroxides were unsuccessful in the reaction.

Having demonstrated the successful synthesis of [Cu^I₂(phen)₂(CN)₂*CH₃OH]_n employing AIBN as the source of cyanide anions, additional experiments were performed utilizing various aromatic and aliphatic bidentate nitrogen based ligands. The results are

summarized in **Table 4.2.1**. For all substrates, excellent yields were obtained at 80 °C and ambient temperature (22±2 °C). The resulting polymers were fully characterized using powder X-ray diffraction, elemental analysis and IR spectroscopy.

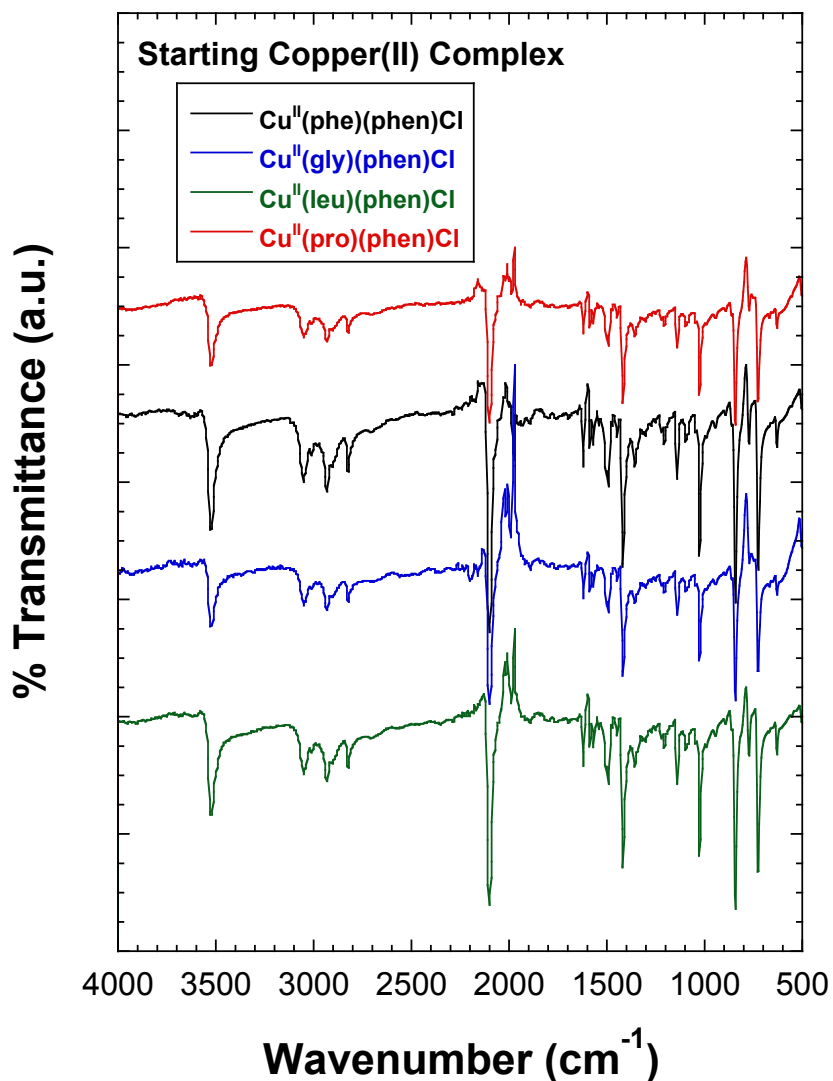


Figure 4.2.3. FT-IR spectra of $[\text{Cu}_2(\text{phen})_2(\text{CN})_2 \cdot \text{CH}_3\text{OH}]_n$ synthesized from $\text{Cu}^{\text{II}}(\text{phe})(\text{phen})\text{Cl}$, $\text{Cu}^{\text{II}}(\text{gly})(\text{phen})\text{Cl}$, $\text{Cu}^{\text{II}}(\text{leu})(\text{phen})\text{Cl}$ and $\text{Cu}^{\text{II}}(\text{pro})(\text{phen})\text{Cl}$ complexes at 80 °C.

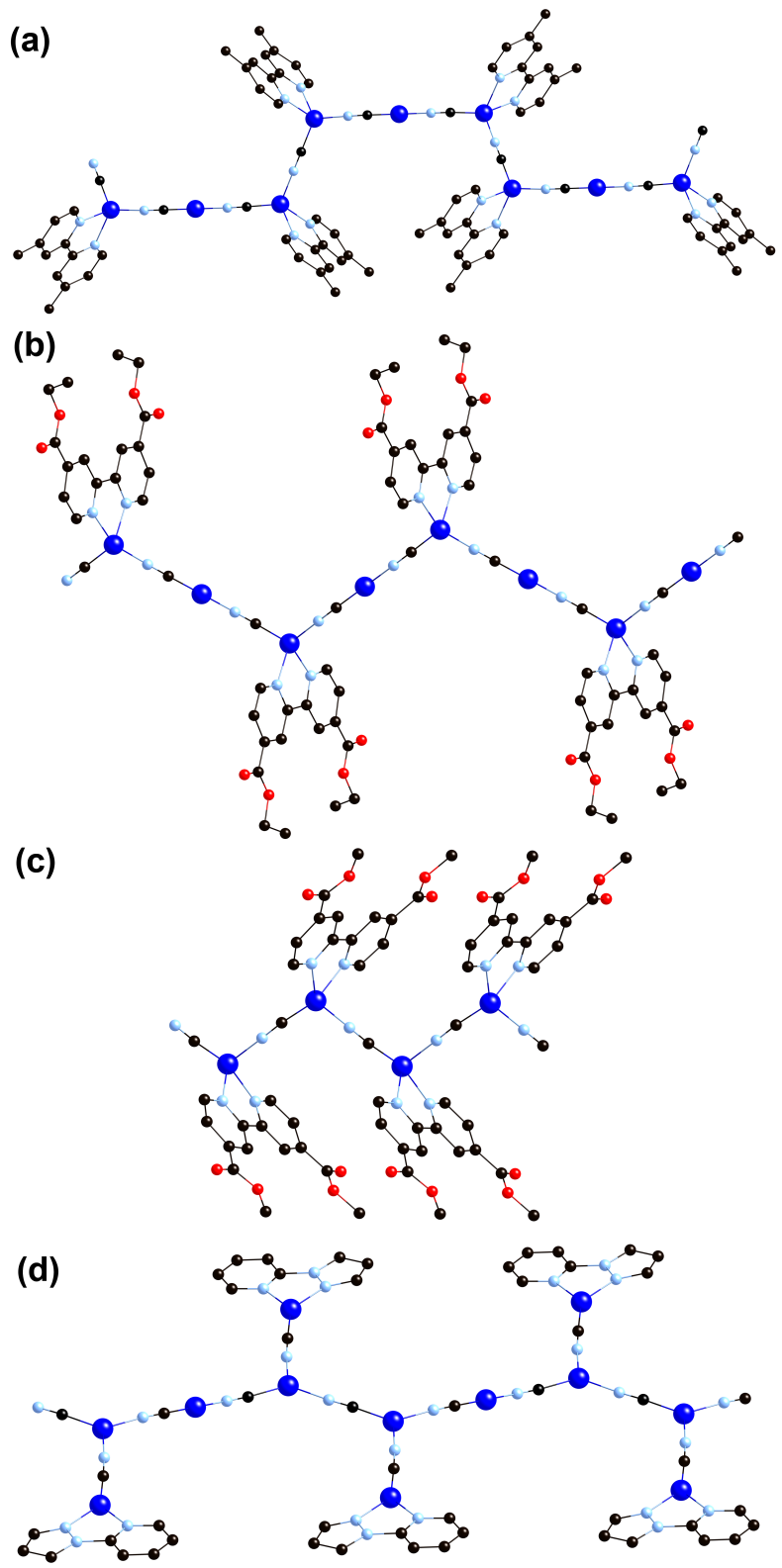


Figure 4.2.4. Crystal structures of $[\text{Cu}^{\text{I}}_3(4,4'\text{-dMe-bpy})_2(\text{CN})_3]_n$ (a), $[\text{Cu}^{\text{I}}(4,4'\text{-dCO}_2\text{Et-bpy})_{0.5}(\text{CN})]_n$ (b), $[\text{Cu}^{\text{I}}(4,4'\text{-dCO}_2\text{Me-bpy})(\text{CN})]_n$ (c) and $[\text{Cu}^{\text{I}}_5(\text{pylpy})_2(\text{CN})_5]_n$ (d). Hydrogen atoms have been omitted for clarity. Dark blue=Cu, light blue=N, black=C and red=O.

Additionally, in the case of bpy, 4,4'-dMe-bpy, 4,4'-dCO₂Me-bpy, 4,4'-dCO₂Et-bpy, pylpy and TMEDA, single crystal X-ray structures were determined. The representative examples for aromatic amines are shown in **Figure 4.2.4** (the structure of $[\text{Cu}^{\text{I}}(\text{bpy})(\text{CN})]_n$ has been published previously⁷⁸). Crystal structure of $[\text{Cu}^{\text{I}}_3(4,4'\text{-dMe-bpy})_2(\text{CN})]_n$ consisted of one-dimensional Cu^I-CN zigzag chains in which two- (A) and four- (C) coordinate copper(I) sites repeated in A-C-C-A pattern (**Figure 4.2.4a**). The four-coordinate copper(I) atoms exhibited highly distorted tetrahedral geometry through coordination to two cyano groups (Cu^I-X=1.913(2) Å and 1.943(2) Å) and the nitrogen donors of the 4,4'-dMe-bpy ligand (Cu^I-N=2.120(2) Å and 2.113(2) Å). As a consequence of this repeat pattern, the crystal structure was strongly stabilized by π-π stacking interactions (3.112(2) Å) between 4,4-dMe-bpy rings from two adjacent chains. $[\text{Cu}^{\text{I}}(4,4'\text{-dCO}_2\text{Et-bpy})(\text{CN})]_n$ still contained A and C coordinate copper(I) sites, but the repeat pattern changed to alternating A-C-A-C (**Figure 4.2.4b**). Interestingly, replacing ethyl by the methyl group in 4,4'-dCO₂Et-bpy resulted in the formation of $[\text{Cu}^{\text{I}}(4,4'\text{-dCO}_2\text{Me-bpy})(\text{CN})]_n$ in which the one-dimensional chains exhibited C-C-C-C pattern due to all copper(I) atoms being four-coordinate (**Figure 4.2.4c**). The tri-coordinate copper(I) atoms (B) were found along the Cu^I-N chains in the crystal structure of $[\text{Cu}^{\text{I}}_5(\text{pylpy})_2(\text{CN})_5]_n$ which showed A-B-B-A pattern (**Figure 4.2.4d**). However, unlike in the other three structures discussed above (**Figure 4.2.4a-c**), the coordinated complexing ligand was not directly attached to the main chain, but rather through an additional cyano bridge. As a result, pylpy rings were nearly parallel to the direction of

propagation of the zigzag Cu^I-CN chains. Finally, replacing aromatic with the aliphatic ligand such as TMEDA (*N,N,N',N'*-tetramethylethylenediamine) resulted in the formation of three-dimensional pillared-layered framework.

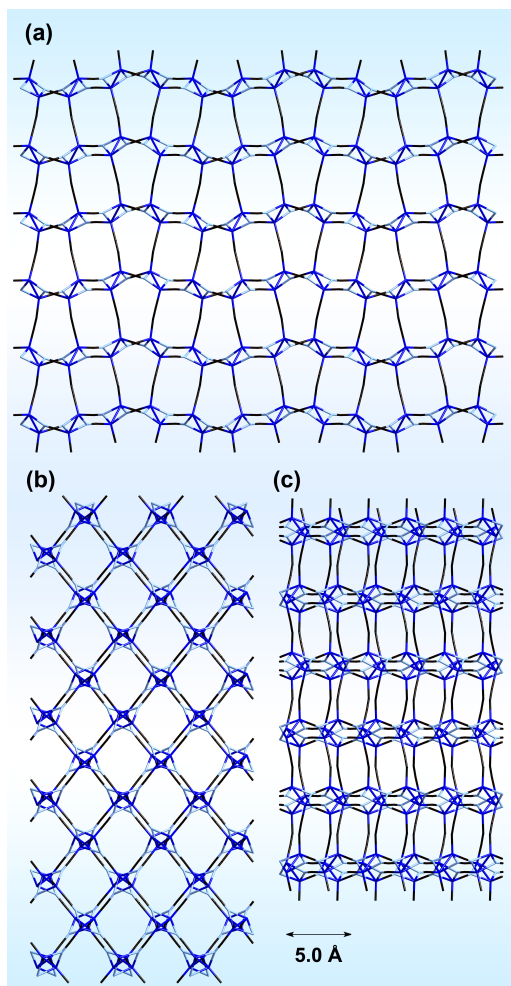


Figure 4.2.5. Three-dimensional framework of $[\text{Cu}_2(\text{CN})_3 \cdot 0.5\text{TMEDA-H}_2]_n$ viewed along the *a* (a), *b* (b), and *c* (c) axes. Guest TMEDA-H₂ molecules have been removed for clarity. Dark blue=Cu, black=C or N, light blue= μ_3 -C,C,N cyano bridging.

The crystal structure of $[\text{Cu}_2(\text{CN})_3 \cdot 0.5\text{TMEDA-H}_2]_n$ indicated that the network consisted of exclusively tetra- coordinate copper(I) atoms bridged by cyanide anions (**Figure 4.2.5**). The voids were partially occupied by guest TMEDA-H₂ molecules. The

total void volume without TMEDA-H₂ was estimated by PLATON to be 684.9 Å³, corresponding to 40.4% of the total unit cell volume. The Cu^I-CN framework contained only two penetrable channels due to μ₃-C,C,N cyano bridging (**Scheme 4.1.1** and **Figure 4.2.5c**) with approximate dimensions of 7.7×6.2 Å (**Figure 4.2.5a**) and 7.0×5.0 Å (**Figure 4.2.5b**).

4.3. Conclusions

In summary, direct reduction of Cu^{II}(aa)(NN)X (aa=deprotonated amino acid, NN=bidentate nitrogen based ligand, X=Cl or Br) complexes by free radicals generated from thermal or photo-decomposition of commonly used diazo compounds such as AIBN (2,2'-azobis(2-methylpropionitrile)) and/or ascorbic acid afforded well-defined copper(I)-cyanide frameworks in excellent yields. To the best of our knowledge, this is the first example in which a classical free radical generating organic reagents have been used as the source of cyanide anions in the synthesis of metal-cyanide frameworks. The reported procedure is mild, applicable to a variety of nitrogen based ligands, and represents an efficient alternative to currently used hydrothermal or solvothermal methods.

4.4. Experimental Section

General Procedures. All chemicals were purchased from commercial sources and used as received. Dimethyl-2,2'-bipyridine-4,4'-dicarboxylate (4,4'-dCO₂Me-bpy), diethyl-2,2'-bipyridine-4,4'-dicarboxylate (4,4'-dCO₂Et-bpy) (Maerker, G.; Case, F. H. *J. Am. Chem. Soc.* **1958**, *80*, 2745-2748) and pyrazolylpyridine (pylpy) (Zhang, H.; Cai, Q.; Ma, D. *J. Org. Chem.* **2005**, *70*, 5164-5173) were synthesized according to previously

published literature procedures. AIBN was recrystallized from cold methanol and dried at room temperature under a vacuum. All manipulations involving copper(I) complexes were performed under argon in the drybox (<1.0 ppm O₂ and <0.5 ppm H₂O) or using standard Schlenk line techniques.

Instrumentation and Equipment. ¹H NMR spectra were obtained using Bruker Avance 400 and 500 MHz spectrometers, and chemical shifts are given in ppm relative to residual solvent peaks (CDCl₃ δ7.26 ppm). IR spectra were recorded in the solid state using Nicolet Smart Orbit 380 FT-IR spectrometer (Thermo Electron Corporation). Elemental analyses for C, H, and N were obtained from Midwest Microlabs, LLC. UV-irradiation was carried out using a high-intensity UV curing lamp (Spectroline model SB-100PC, Spectronics Corporation, Westbury, NY, long wave UV (365 nm)), which was equipped with a 2F100C clear filter that reduces transmission of medium (UV-B) and short wave (UV-C) radiations to safe levels, while emitting a UV intensity of 27000 μWcm⁻² at a distance of 15.0 cm. The UV-lamp was typically placed 4.0 cm from the reaction mixture. KaleidaGraph 4.1 software was used to generate images of IR spectra and powder XRD patterns.

X-ray Crystal Structure Determination. The X-ray intensity data were collected at 150 K using graphite-monochromated Mo Kα radiation (λ=0.71073 Å) on a Bruker Smart Apex II CCD diffractometer. Data reduction included absorption corrections by the multiscan method using SADABS (Sheldrick, G. M. *SADABS Version 2.03*; University of Gottingen: Germany, 2002). Crystal data and experimental conditions are given in

Tables S1-S4. Structures were solved by direct methods and refined by full-matrix least squares using SHELXTL 6.1 bundled software package (Sheldrick, G. M. *SHELXTL 6.1, Crystallographic Computing System*; Bruker Analytical X-Ray System: Madison, WI, 2000). The H atoms were positioned geometrically (aromatic C-H=0.93 Å, methylene C-H=0.97 Å and methyl C-H=0.96 Å) and treated as riding atoms during subsequent refinement, with $U_{iso}(H)=1.2U_{eq}(C)$ or $1.5U_{eq}$ (methyl C). The methyl groups were allowed to rotate about their local 3-fold axes. Crystal Maker 8.3 was used to generate molecular graphics.

X-ray Powder Diffraction. Measurements were performed on a Panalytical X'Pert Pro MPD powder X-ray diffractometer using copper K_{α} radiation with a wavelength of 1.541871 Å and operating with a tube power of 45 kV 40 mA. Data were collected from 5° to 145° 2θ with a step size of 0.0083556° and scan rate of 0.010644 °/s. The incident beam optics were comprised of a 0.02 rad soller slit, a divergent slit of 1/4° and an anti-scatter slit of 1/2°; whereas, the diffracted beam optics were comprised of a 0.02 rad soller slit and an anti-scatter slit of 1/4°. The samples were prepared for analysis using a top fill method where the sample powder is added from bottom to top of a sample holder and spread out gently using a razor blade to minimize preferred orientation.

Synthesis of $Cu^{II}(aa)(NN)X$ (aa=deprotonated amino acid, NN=bidentate N-based ligand and X=Cl or Br). In a typical experiment, stoichiometric amounts of sodium hydroxide (1.00 mmol, 0.0400 g) and *L*-alanine (1.00 mmol, 0.0891 g) were dissolved in 4.0 mL of methanol and stirred at ambient temperature for 1 h. Sodium salt of *L*-alanine

was then added dropwise to $\text{Cu}^{\text{II}}\text{Cl}_2$ (1.00 mmol, 0.134 g) dissolved in 2.0 mL of methanol. After stirring for 10 min, sodium chloride was removed by filtration. The appropriate nitrogen based ligand (1.00 mmol, $m(\text{phen})=0.180$ g, $m(\text{bpy})=0.156$ g, $m(5\text{-NO}_2\text{-phen})=0.225$ g, $m(5\text{-Cl-phen})=0.215$ g, $m(4,4'\text{-dMe-bpy})=0.184$ g, $m(4,4\text{-dCO}_2\text{Me-bpy})=0.272$ g, $m(4,4'\text{-dCO}_2\text{Et-bpy})=0.300$ g, $m(\text{pylpy})=0.145$ g and $m(\text{TMEDA})=0.116$ g) dissolved in 2.0 mL of methanol was then added dropwise to the resulting solution. For ligand structures, refer to Scheme 2 in the manuscript. The final product was precipitated by the addition of 20 mL of diethyl ether, filtered, washed with diethyl ether/pentane, and dried under vacuum to yield $\text{Cu}^{\text{II}}(\text{ala})(\text{phen})\text{Cl}$ (0.249 g, 68%), $\text{Cu}^{\text{II}}(\text{ala})(\text{bpy})\text{Cl}$ (0.190 g, 56%), $\text{Cu}^{\text{II}}(\text{ala})(5\text{-NO}_2\text{-phen})\text{Cl}$ (0.249 g, 62%), $\text{Cu}^{\text{II}}(\text{ala})(5\text{-Cl-phen})\text{Cl}$ (0.276 g, 67%), $\text{Cu}^{\text{II}}(\text{ala})(4,4'\text{-dMe-bpy})\text{Cl}$ (0.230 g, 61%), $\text{Cu}^{\text{II}}(\text{ala})(4,4'\text{-dCOOMe-bpy})\text{Cl}$ (0.432 g, 62%), $\text{Cu}^{\text{II}}(\text{ala})(4,4'\text{-dCO}_2\text{Et-bpy})\text{Cl}$ (0.329 g, 64%), and $\text{Cu}^{\text{II}}(\text{ala})(\text{pylpy})\text{Cl}$ (0.239 g, 72%). $\text{Cu}^{\text{II}}(\text{ala})(\text{TMEDA})\text{Cl}$ was used in the synthesis of coordination polymers without prior isolation. The corresponding complexes with $\text{Cu}^{\text{II}}\text{Br}_2$ (1.00 mmol, 0.223 g) or $\text{Cu}^{\text{II}}\text{Cl}_2$ (1.00 mmol, 0.135) and different amino acids (1.00 mmol, $m(L\text{-alanine})=0.0891$ g, $m(\text{glycine})=0.0751$ g, $m(\text{phenylalanine})=0.165$ g, $m(\text{leucine})=0.131$ g and $m(\text{proline})=0.115$ g) were prepared analogously to the above procedure.

Synthesis of Copper(I)-Cyanide Frameworks Employing Thermal Decomposition of AIBN (2,2'-azobis(2-methylpropionitrile) at 80 °C. $\text{Cu}^{\text{I}}(\text{aa})(\text{NN})\text{X}$ (0.0608 mmol) and 10 equivalents of AIBN (0.608 mmol, 0.100 g) were dissolved in 3.0 mL of methanol in a glass tube (ethanol in the case of $\text{Cu}^{\text{I}}(4,4'\text{-dCO}_2\text{Et-bpy})\text{Cl}$). The reaction mixture was

flushed with argon for 30 seconds, followed by the addition of 2 equivalents of ascorbic acid relative to copper(II) complex (0.121 mmol, 0.0216 g). The tube was then immediately capped, sealed with teflon and electrical tape, and placed in an oil bath thermostated at 80 °C. After 24 h, the precipitate was filtered, thoroughly washed with water, methanol, acetone and dichloromethane, and dried under vacuum at ambient temperature. The crystalline material was characterized by elemental analysis, IR spectroscopy, single crystal X-ray crystallography and powder X-ray diffraction. The supporting data is reported in Appendix C.

[Cu^I₂(phen)₂(CN)₂*CH₃OH]_n. Dark brown crystals, yield=15.9 mg (92% based on copper). FT-IR (solid): $\nu(\text{CN})=2102$ (s) cm^{-1} . Anal. Calcd. for C₂₇H₂₀Cu₂N₆O (571.59): C, 56.74; H, 3.53; N, 14.70. Found: C, 56.52; H, 3.69; N, 14.39.

[Cu^I(bpy)(CN)]_n. Dark brown crystals, yield=12.2 mg (82% based on copper). FT-IR (solid): $\nu(\text{CN})=2106$ (s) cm^{-1} . Anal. Calcd. for C₁₁H₈CuN₃ (245.74): C, 53.76; H, 3.28, N, 17.10. Found: C, 53.67; H, 3.27; N, 17.07.

[Cu^I(5-NO₂-phen)(CN)]_n. Dark brown powder, yield=13.4 mg (73% based on copper). FT-IR (solid): $\nu(\text{CN})=2100$ (s) cm^{-1} . Anal. Calcd. for C₁₃H₇CuN₄O₂ (314.76): C, 49.60; H, 2.24; N, 17.80. Found: C, 48.97; H, 2.35; N, 16.84.

[Cu^I(5-Cl-phen)(CN)]_n. Dark brown powder, yield=13.6 mg (74% based on copper). FT-IR (solid): $\nu(\text{CN})=2104$ (s) cm^{-1} . Anal. Calcd. for $\text{C}_{13}\text{H}_7\text{CuN}_3\text{Cl}$ (304.21): C, 51.33; H, 2.32; N, 13.81. Found: C, 51.18; H, 2.50; N, 13.59.

[Cu^I₃(4,4'-dMe-bpy)₂(CN)₃]_n. Bright orange crystals, yield=11.4 mg (89% based on copper). FT-IR (solid): $\nu(\text{CN})=2104$ (s) cm^{-1} . Anal. Calcd. for $\text{C}_{27}\text{H}_{24}\text{Cu}_3\text{N}_7$ (637.18): C, 50.90; H, 3.80; N, 15.39. Found: C, 50.34; H, 3.99; N, 15.07.

[Cu^I(4,4'-dCO₂Me-bpy)(CN)]_n. Dark brown/black crystals, yield=16.9 mg (77% based on copper). FT-IR (solid): $\nu(\text{CN})=2113$ (s) cm^{-1} . Anal. Calcd. for $\text{C}_{15}\text{H}_{12}\text{CuN}_3\text{O}_4$ (361.83): C, 49.77; H, 3.34; N, 11.61. Found: C, 48.96; H, 3.44; N, 11.51.

[Cu^I(4,4'-dCO₂Et-bpy)_{0.5}(CN)]_n. Dark reddish brown crystals, yield=12.0 mg (83% based on copper). FT-IR (solid): $\nu(\text{CN})=2128$ (s) cm^{-1} . Anal. Calcd. for $\text{C}_9\text{H}_8\text{CuN}_2\text{O}_2$ (237.72): C, 45.09; H, 3.36; N, 11.69. Found: C, 44.62; H, 3.40; N, 11.72.

[Cu^I₅(pylpy)₂(CN)₅]_n. Colorless crystals, yield 7.0 mg (77% based on copper). FT-IR (solid): $\nu(\text{CN})=2129$ (s) cm^{-1} . Anal. Calcd. for $\text{C}_{21}\text{H}_{14}\text{Cu}_5\text{N}_{11}$ (738.18): C, 34.17; H, 1.91; N, 20.87. Found: C, 35.51; H, 2.18; N, 20.10.

[Cu^I₂(CN)₃*0.5TMEDA-H₂]_n. Colorless crystals, yield=5.0 mg (63% based on copper). FT-IR (solid): $\nu(\text{CN})=2126$ (s) cm^{-1} , 2089(s) cm^{-1} . Anal. Calcd. for $\text{C}_6\text{H}_5\text{Cu}_2\text{N}_4$ (264.27): C, 27.25; H, 3.43; N, 21.20. Found: C, 27.14; H, 3.68; N, 20.84.

Synthesis of Copper(I)-Cyanide Frameworks Employing Photodecomposition of AIBN (2,2'-azobis(2-methylpropionitrile) at Ambient Temperature. $\text{Cu}^{\text{II}}(\text{aa})(\text{NN})\text{X}$ (0.0608 mmol) and 10 equivalents of AIBN (0.608 mmol, 0.100 g) were dissolved in 3.0 mL of methanol in a glass tube (ethanol in the case of $\text{Cu}^{\text{II}}(4,4'\text{-dCO}_2\text{Et-bpy})\text{Cl}$). The reaction mixture was flushed with argon for 30 seconds, followed by the addition of 2 equivalents of ascorbic acid relative to copper(II) complex (0.121 mmol, 0.0216 g). The tube was then immediately capped, sealed with teflon and electrical tape, and placed under a UV lamp. A water bath was used to maintain the reaction temperature at 23 ± 2 °C. After 24 h, the precipitate was filtered, thoroughly washed with water, methanol, acetone and dichloromethane, and dried under vacuum at ambient temperature. The crystalline material was characterized by elemental analysis ($[\text{Cu}^{\text{I}}_2(\text{phen})_2(\text{CN})_2 \cdot \text{CH}_3\text{OH}]_n$), IR spectroscopy, single crystal X-ray crystallography and powder X-ray diffraction. The supporting data is reported in Appendix C.

$[\text{Cu}^{\text{I}}_2(\text{phen})_2(\text{CN})_2 \cdot \text{CH}_3\text{OH}]_n$. Dark brown crystals, yield=16.3 mg (94% based on copper). FT-IR (solid): $\nu(\text{CN})=2102(\text{s}) \text{ cm}^{-1}$. Anal. Calcd. for $\text{C}_{27}\text{H}_{20}\text{Cu}_2\text{N}_6\text{O}$ (571.59): C, 56.74; H, 3.53; N, 14.70. Found: C, 56.92; H, 3.52; N, 14.61.

$[\text{Cu}^{\text{I}}(\text{bpy})(\text{CN})]_n$. Dark brown crystals, yield=11.5 mg (77% based on copper). FT-IR (solid): $\nu(\text{CN})=2106(\text{s}) \text{ cm}^{-1}$.

$[\text{Cu}^{\text{I}}(5\text{-NO}_2\text{-phen})(\text{CN})]_n$. Brown powder, yield=11.5 mg (63% based on copper). FT-IR(solid): $\nu(\text{CN})=2099(\text{s}) \text{ cm}^{-1}$.

[Cu^I(5-Cl-phen)(CN)]_n. Dark brown powder, yield=13.3 mg (72% based on copper).

FT-IR (solid): $\nu(\text{CN})=2105(\text{s}) \text{ cm}^{-1}$.

[Cu^I₃(4,4'-dMe-bpy)₂(CN)₃]_n. Orange crystals, yield=9.7 mg (76% based on copper).

FT-IR (solid): $\nu(\text{CN})=2103(\text{s}) \text{ cm}^{-1}$.

[Cu^I(4,4'-dCO₂Me-bpy)(CN)]_n. Dark brown/black crystals, yield=10.4 mg (49% based on copper). FT-IR(solid): $\nu(\text{CN})=2114(\text{s}) \text{ cm}^{-1}$.

[Cu^I(4,4'-dCO₂Et-bpy)_{0.5}(CN)]_n. Dark reddish brown crystals, yield=7.7 mg (53% based on copper). FT-IR(solid): $\nu(\text{CN})=2121(\text{s}) \text{ cm}^{-1}$.

[Cu^I₅(pylpy)₂(CN)₅]_n. Colorless crystals, yield=8.0 mg (89% based on copper). FT-IR (solid): $\nu(\text{CN})=2123 (\text{s}) \text{ cm}^{-1}$.

Large Scale Synthesis of [Cu^I₂(phen)₂(CN)₂*CH₃OH]_n and [Cu^I(bpy)(CN)]_n

Cu^{II}(ala)(phen)Cl (0.608 mmol, 0.223 g) and 10 equivalents of AIBN (6.08 mmol, 1.00 g) were dissolved in 5.0 mL of methanol and placed in a steel autoclave. The reaction mixture was then purged with argon for 1-2 min, followed by the addition of 2.0 equivalents of ascorbic acid (1.21 mmol, 0.216 g) relative to copper(II) complex. The autoclave was sealed immediately after the addition of ascorbic acid and placed in an oven thermostated at 80°C. After 24 h, the crystalline material was filtered, thoroughly washed with water, methanol, acetone and dichloromethane, and dried under vacuum to

yield 149 mg (86% based on copper) of $[\text{Cu}^{\text{I}}_2(\text{phen})_2(\text{CN})_2 \cdot \text{CH}_3\text{OH}]_n$ (FT-IR (solid): $\nu(\text{CN})=2101(\text{s}) \text{ cm}^{-1}$). $[\text{Cu}^{\text{I}}(\text{bpy})(\text{CN})]_n$ was synthesized using identical procedure except that $\text{Cu}^{\text{II}}(\text{all})(\text{bpy})\text{Cl}$ was used instead of $\text{Cu}^{\text{II}}(\text{ala})(\text{phen})\text{Cl}$ (yield=80.6 mg, 54% based on copper, FT-IR (solid): $\nu(\text{CN})=2106(\text{s}) \text{ cm}^{-1}$).

References

1. Pintauer, T.; Matyjaszewski, K., Structural Aspects of Copper Catalyzed Atom Transfer Radical Polymerization. *Coord. Chem. Rev.* **2005**, *249*, ((11-12)), 1155-1184.
2. Anderegg, G.; Wenk, F., Synthesis of Tris(2-pyridylmethyl)amine. *Helv. Chim. Acta* **1967**, *50*, 2330-2332.
3. Canary, J. W.; Yank, Y.; Roy, R.; Que, L. J.; Miyake, H., *Inorg. Synth.* **1998**, *32*, 70-75.
4. Eckenhoff, W. T.; Pintauer, T., Structural Comparison of Copper(I) and Copper(II) Complexes with Tris(2-pyridylmethyl)amine Ligand. *Inorg. Chem.* **2010**, *49*, 10617-10626.
5. Pintauer, T.; Matyjaszewski, K., Structural Aspects of Copper Catalyzed Atom Transfer Radical Polymerization. *Coord. Chem. Rev.* **2005**, *249*, (11-12), 1155-1184.
6. Karlin, K. D.; Zubieta, J., *Copper Coordination Chemistry: Biochemical and Inorganic Perspectives*. Adenine Press: New York, 1983.
7. Company, A.; Lloret, J.; HGomez, L.; Costas, M., Alkane C-H Oxygenation Catalyzed by Transition Metal Complexes. In *Alkane C-H Activation using Single Site Metal Catalysis*, Perez, P., Ed. Springer: New York, 2012; 38, 143.
8. Plietker, B., *Iron Catalysis in Organic Chemistry: Reactions and Applications*. Wiley-VCH: Weinheim, 2008.

9. Clark, A. J., Atom Transfer Radical Cyclisation Reactions Mediated by Copper Complexes. *Chem. Soc. Rev.* **2002**, *31*, (1), 1-11.
10. Eckenhoff, W. T.; Pintauer, T., Copper Catalyzed Atom Transfer Radical Addition (ATRA) and Cyclization (ATRC) Reactions in the Presence of Reducing Agents. *Cat. Rev. Sci. Eng.* **2010**, *52*, 1-59.
11. Pintauer, T., Catalyst Regeneration in Transition-Metal-Mediated Atom-Transfer Radical Addition (ATRA) and Cyclization (ATRC) Reactions. *Eur. J. Inorg. Chem.* **2010**, 2449-2460.
12. Matyjaszewski, K.; Xia, J., Atom Transfer Radical Polymerization. *Chem. Rev.* **2001**, *101*, (9), 2921-2990.
13. Wang, J.-S.; Matyjaszewski, K., Controlled/"Living" Radical Polymerization. Atom Transfer Radical Polymerization in the Presence of Transition-Metal Complexes. *J. Am. Chem. Soc.* **1995**, *117*, (20), 5614-5615.
14. Jakubowski, W.; Matyjaszewski, K., Activators Generated by Electron Transfer for Atom Transfer Radical Polymerization. *Macromolecules* **2005**, *38*, 4139-4146.
15. Jakubowski, W.; Matyjaszewski, K., Activators Regenerated by Electron Transfer for Atom-Transfer Radical Polymerization of (Meth)acrylates and Related Block Copolymers. *Angew. Chem. Int. Ed.* **2006**, *45*, (27), 4482-4486.
16. Jakubowski, W.; Min, K.; Matyjaszewski, K., Activators Regenerated by Electron Transfer for Atom Transfer Radical Polymerization of Styrene *Macromolecules* **2006**, *39*, (1), 39-45.
17. Matyjaszewski, K.; Jakubowski, W.; Min, K.; Tang, W.; Huang, J.; Braunecker, W. A.; Tsarevsky, N. V., Diminishing Catalyst Concentration in Atom Transfer Radical Polymerization with Reducing Agents. *Proc. Natl. Acad. Sci. U.S.A.* **2006**, *103*, 15309-15314.
18. Pintauer, T.; Matyjaszewski, K., Atom Transfer Radical Addition and Polymerization Reactions Catalyzed by ppm Amounts of Copper Complexes. *Chem. Soc. Rev.* **2008**, *37*, 1087-1097.

19. Matyjaszewski, K., Atom Transfer Radical Polymerization (ATRP): Current Status and Future Perspectives. *Macromolecules* **2012**, *45*, (10), 4015-4039.
20. Coessens, V.; Pintauer, T.; Matyjaszewski, K., Functional Polymers by Atom Transfer Radical Polymerization. *Prog. Polym. Sci.* **2001**, *26*, 337.
21. Tsarevsky, N. V.; Matyjaszewski, K., "Green" Atom Transfer Radical Polymerization: From Process Design to Preparation of Well-Defined Environmentally Friendly Polymeric Materials. *Chem. Rev.* **2007**, *107*, 2270-2299.
22. Matyjaszewski, K.; Tsarevsky, N. V., *Nat. Chem.* **2009**, *1*, 276-288.
23. Pintauer, T.; McKenzie, B.; Matyjaszewski, K., Toward Structural and Mechanistic Understanding of Transition Metal-Catalyzed Atom Transfer Radical Processes *ACS Symp. Ser.* **2003**, *854*, 130-147.
24. Pintauer, T.; Matyjaszewski, K., Structural and Mechanistic Aspects of Copper Catalyzed Atom Transfer Radical Polymerization. *Top. Organomet. Chem.* **2009**, *26*, 221-251.
25. Braunecker, W. A.; Matyjaszewski, K., Controlled/Living Radical Polymerization: Features, Developments and Perspectives. *Prog. Polym. Sci.* **2007**, *32*, 93-146.
26. Tang, W.; Kwak, Y.; Braunecker, W.; Tsarevsky, N. V.; Coote, M. L.; Matyjaszewski, K., Understanding Atom Transfer Radical Polymerization: Effect of Ligand and Initiator Structures on the Equilibrium Constants *J. Am. Chem. Soc.* **2008**, *130*, (132), 10702-10713.
27. Tsarevsky, N. V.; Braunecker, W. A.; Matyjaszewski, K., Electron Transfer Reactions Relevant to Atom Transfer Radical Polymerization. *J. Organomet. Chem.* **2007**, *692*, 3212-3222.
28. Tsarevsky, N. V.; Braunecker, W. A.; Vacca, A.; Gans, P.; Matyjaszewski, K., Competitive Equilibria in Atom Transfer Radical Polymerization. *Macromol. Symp.* **2007**, *248*, 60-70.

29. Tang, W.; Tsarevsky, N. V.; Matyjaszewski, K., Determination of Equilibrium Constants for Atom Transfer Radical Polymerization. *J. Am. Chem. Soc.* **2006**, *128*, (5), 1598-1604.
30. Qiu, J.; Matyjaszewski, K.; Thounin, L.; Amatore, C., Cyclic Voltammetric Studies of Copper Complexes Catalyzing Atom Transfer Radical Polymerization. *Macromol. Chem. Phys.* **2000**, *201*, 1625-1631.
31. Navon, N.; Golub, G.; Cohen, H.; Paoletti, P.; Valtancoli, B.; Bencini, A.; Meyerstein, D., Design of Ligands That Stabilize Cu(I) and Shift the Reduction Potential of the CuII/I Couple Cathodically in Aqueous Solutions. *Inorg. Chem.* **1999**, *38*, 3484-3488.
32. Ambundo, E. A.; Deydier, M. V.; Grall, A. J.; Aguera-Vega, N.; Dressel, L. T.; Copper, T. H.; Heeg, M. J.; Ochrymowycz, L. A.; Rorabacher, D. B., *Inorg. Chem.* **1999**, *38*, 4233-4242.
33. Golub, G.; Lashaz, A.; Cohen, A.; Paoletti, P.; Bencini, A.; Valtancoli, B.; Meyerstein, D., *Inorg. Chim. Acta* **1997**, *255*, 111-115.
34. Tsarevsky, N. V.; Tang, W.; Brooks, S. J.; Matyjaszewski, K., Factors Determining the Performance of Copper-Based Atom Transfer Radical Polymerization Catalysts and Criteria for Rational Catalyst Selection. *ACS Symp. Ser.* **2006**, *944*, 56-70.
35. Magenau, A. J. D.; Kwak, Y.; Schröder, K.; Matyjaszewski, K., Highly Active Bipyridine-Based Ligands for Atom Transfer Radical Polymerization. *ACS Macro Letters* **2012**, *1*, 508-512.
36. Zhang, C. X.; Kaderli, S.; Costas, M.; Kim, E.-I.; Neuhold, Y.-M.; Karlin, K. D.; Zuberbuhler, A. D., Copper(I)-Dioxygen Reactivity of [(L)Cu^I]⁺ (L=Tris(2-pyridylmethyl)amine): Kinetic/Thermodynamic and Spectroscopic Studies Concerning the Formation of Cu-O₂ and Cu₂-O₂ Adducts as a Function of Solvent Medium and 4-Pyridyl Ligand Substituent Variations. *Inorg. Chem.* **2003**, *42*, 1807-1824.
37. Xue, G.; Wang, D.; DeHont, R.; Fiedler, A. T.; Shan, Xiaopeng; Münck, E.; Que, L, Jr., A synthetic precedent for the [Fe^{IV}₂(μ-O)₂]diamond core proposed for methane monooxygenase intermediate Q. *PNAS* **2007**, *104*, (52), 20713-20718.

38. Schröder, K.; Mathers, R. T.; Buback, J.; Konkolewicz, D.; Magenau, A. J. D.; Matyjaszewski, K., Substituted Tris(2-pyridylmethyl)amine Ligands for Highly Active ATRP Catalysts. *ACS Macro Letters* **2012**, *1*, (8), 1037-1040.
39. Konkolewicz, D.; Schöder, K.; Buback, J.; Bernhard, S.; Matyjaszewski, K., Visible Light and Sunlight Photoinduced ATRP with ppm of Cu Catalyst. *ACS Macro Letters* **2012**, *1*, 1219-1223.
40. Schröder, K.; Konkolewicz, D.; Poli, R.; Matyjaszewski, K., Formation and Possible Reactions of Organometallic Intermediates with Active Copper(I) Catalysts in ATRP *Organometallics* **2012**, *31*, 7994-7999.
41. Eckenhoff, W. T.; Garrity, S. T.; Pintauer, T., Highly Efficient Copper Mediated Atom Transfer Radical Addition (ATRA) in the Presence of Reducing Agent. *Eur. J. Inorg. Chem.* **2008**, 563-571.
42. Eckenhoff, W. T.; Pintauer, T., Atom Transfer Radical Addition in the Presence of Catalytic Amounts of Copper(I/II) Complexes with Tris(2-pyridylmethyl)amine. *Inorg. Chem.* **2007**, *46*, (15), 5844-5846.
43. Hsu, S. C.; Chien, S. S.; Chen, H. H.; Chiang, M. Y., Synthesis and Characterization of Copper(I) Complexes Containing Tri(2-Pyridylmethyl)Amine Ligand. *Chin. Chem. Soc.* **2007**, *54*, 685-692.
44. Mason, J., Patterns of Nuclear Magnetic Shielding of Transition-Metal Nuclei. *Chem. Rev.* **1987**, *87*, 1299-1312.
45. Eckenhoff, W. T.; Biernesser, A. B.; Pintauer, T., Kinetic and Mechanistic Aspects of Atom Transfer Radical Addition (ATRA) Catalyzed by Copper Complexes with Tris(2-pyridylmethyl)amine. *Inorg. Chem.* **2012**, *51*, 11917-11929.
46. Addison, A. W.; Nageswara Rao, T.; Reedijk, J.; van Rijn, J.; Verschoor, G. C., *J. Chem. Soc. Dalton Trans.* **1984**, 1349-1356.
47. Harrison, W. D.; Kennedy, D. M.; Ray, N. J.; Sheahan, R.; Hathaway, B. J., *J. Chem. Soc. Dalton Trans.* **1981**, 1556-1564.

48. Eckenhoff, W. T.; Pintauer, T., Atom Transfer Radical Addition (ATRA) Catalyzed by Copper Complexes with Tris[2-(dimethylamino)ethyl]amine (Me₆TREN) Ligand in the Presence of Free-Radical Diazo Initiator AIBN. *Dalton Trans.* **2011**, *40*, (18), 4909-4917.
49. Pintauer, T.; Qiu, J.; Kickelbick, G.; Matyjaszewski, K., Synthesis, Characterization, and Bromine Substitution by 4,4'-Di(5-nonyl)-2,2'-bipyridine in CuII(4,4'-di(5-nonyl)-2,2'-bipyridine)Br₂. *Inorg. Chem.* **2001**, *40*, (12), 2818-2824.
50. Hiskey, M. A.; Ruminski, R. R., *Inorg. Chim. Acta* **1986**, *112*, 189-195.
51. McLachlan, G. A.; Fallon, G. D.; Martin, R. L.; Spiccia, L., Synthesis, Structure and Properties of Five-Coordinate Copper(II) Complexes of Pentadentate Ligands with Pyridyl Pendant Arms. *Inorg. Chem.* **1995**, *34*, 254-261.
52. Hathaway, B. J., *Comprehensive Coordination Chemistry*. Pergamon Press: Oxford, England, 1987.
53. Bortolamei, N.; Isse, A. A.; Di Marco, V. B.; Gennaro, A.; Matyjaszewski, K., Thermodynamic Properties of Copper Complexes Used as Catalysts in Atom Transfer Radical Polymerization. *Macromolecules* **2010**, *43*, (22), 9257-9267.
54. Buckingham, D. A.; Sargeson, A. M., Chelating Agents and Metal Chelates. In *Chelating Agents and Metal Chelates*, Dwyer, F. P.; Mellor, D. P., Eds. Academic Press: New York, 1964.
55. Lingane, J. J., Interpretation of the Polarographic Waves of Complex Metal Ions. *Chem. Rev.* **1941**, *29*, 1.
56. Rossotti, F. J. C.; Rossotti, H., *The Determination of Stability Constants*. McGraw Hill: New York, 1961.
57. Vlcek, A. A., *Prog. Inorg. Chem.* **1963**, *5*, 211.
58. Matyjaszewski, K.; Patten, T. E.; Xia, J., Controlled/"living" Radical Polymerization. Kinetics of the Homogeneous Atom Transfer Radical Polymerization of Styrene. *J. Am. Chem. Soc.* **1997**, *119*, 674-680.

59. Min, K.; Jakubowski, W.; Matyjaszewski, K., AGET ATRP in the Presence of Air in Miniemulsion and in Bulk. *Macromol. Rapid Commun.* **2006**, *27*, (8), 594-598..
60. Sheldrick, G. M., *SADABS Version 2.03*. University of Gottingen: Germany, 2002.
61. Sheldrick, G. M., *SHELXTL 6.1, Crystallographic Computing System*. Bruker Analytical X-Ray System: Madison, WI, 2000.
62. Sumida, K.; Rogow, D. L.; Mason, J. A.; McDonald, T. M.; Bloch, E. D.; Hern, Z. R.; Bae, T.-H.; Long, J. R., Carbon Dioxide Capture in Metal-Organic Frameworks. *Chem. Rev.* **2012**, *112*, 724-781.
63. Stock, N.; Biswas, S., Synthesis of Metal-Organic Frameworks (MOFs): Routes to Various MOF Topologies, Morphologies, and Composites. *Chem. Rev.* **2012**, *112*, 933-969.
65. Kreno, L. E.; Leong, K.; Farha, O. K.; Allendorf, M.; Van Duyne, R. P.; Hupp, J. T., Metal-Organic Framework Materials as Chemical Sensors. *Chem. Rev.* **2012**, *112*, 1105-1125.
66. Pike, R. D., Structure and Bonding in Copper(I) Carbonyl and Cyanide Complexes. *Organometallics* **2012**, *31*, (22), 7647-7660.
67. Suh, M. P.; Park, H. J.; Prasad, T. K.; Lim, D.-W., Hydrogen Storage in Metal-Organic Frameworks. *Chem. Rev.* **2012**, *112*, 782-835.
68. Murray, L. J.; Dinca, M.; Long, J. R., Hydrogen Storage in Metal-Organic Frameworks. *Chem. Soc. Rev.* **2009**, *38*, 1294-1314.
69. Kaye, S. S.; Long, J. R., Hydrogen Storage in the Dehydrated Prussian Blue Analogues $M_3[Co(CN)_6]_2$ (M = Mn, Fe, Co, Ni, Cu, Zn). *J. Am. Chem. Soc.* **2005**, *127*, 9604-9605.
70. James, S. L., Metal-Organic Frameworks. *Chem. Soc. Rev.* **2003**, *32*, 276-288.
71. Zhang, X.-M.; Qing, Y.-L.; Wu, H.-S., Two Cuprous Cyanide Polymorphs: Diamond Net Versus 3,4-Connected Net. *Inorg. Chem.* **2008**, *47*, 2255-2257.

72. Withersby, M. A.; Blake, A. J.; Champness, N. R.; Hubberstey, P.; Li, W. S.; Schroder, M., Anion Control in Bipyridylsilver(I) Networks: A Helical Polymeric Array. *Angew. Chem. Int. Ed. Engl.* **1997**, *36*, 2327.
73. Hoskins, B. F.; Robson, R., Infinite Polymeric Frameworks Consisting of Three Dimensionally Linked Rod-Like Segments. *J. Am. Chem. Soc.* **1989**, *111*, 5962-5964.
74. Hoskins, B. F.; Robson, R., Design and Construction of a New Class of Scaffolding-Like Materials Comprising Infinite Polymeric Frameworks of 3D-Linked Molecular Rods. A Reappraisal of the Zinc Cyanide and Cadmium Cyanide Structures and the Synthesis and Structure of the Diamond-Related Frameworks $[\text{Ni}(\text{CH}_3)_4][\text{Cu}^{\text{I}}\text{Zn}^{\text{II}}(\text{CN})_4]$ and $\text{Cu}^{\text{I}}[4,4',4'',4'''-\text{Tetracyanotetraphenylmethane}]\text{BF}_4 \cdot x\text{C}_6\text{H}_5\text{NO}_2$. *J. Am. Chem. Soc.* **1990**, *112*, 1546-1554.
75. Abrahams, B. F.; Hoskins, B. F.; Michail, D. M.; Robson, R., Assembly of Porphyrin Building Blocks into Network Structures with Large Channels. *Nature* **1994**, *369*, 727-729.
76. Kaur, A.; Pintauer, T., Copper(I)-Cyanide Frameworks through Thermal or Photodecomposition of the Free Radical Diazo Initiator AIBN. *Eur. J. Inorg. Chem.* **2013**, (19), 3297-3301.
77. Thommes, K.; Kiefer, G.; Scopelliti, R.; Severin, K., Olefin Cyclopropanation by a Sequential Atom-Transfer Radical Addition and Dechlorination in the Presence of a Ruthenium Catalyst. *Angew. Chem. Int. Ed.* **2009**, *48*, (43), 8115-8119.
78. He, X.; Lu, C.-Z.; Yuan, D.-Q.; Chen, S.-M.; Chen, J.-T., Synthesis and Crystal Structures of Four Cyanide-Bridged Coordination Polymers. *Eur. J. Inorg. Chem.* **2005**, 2181-2188.

Chapter 5

Synthesis of Two-Dimensional and Three-Dimensional Copper(I) Cyanide Frameworks via Direct Reduction Method

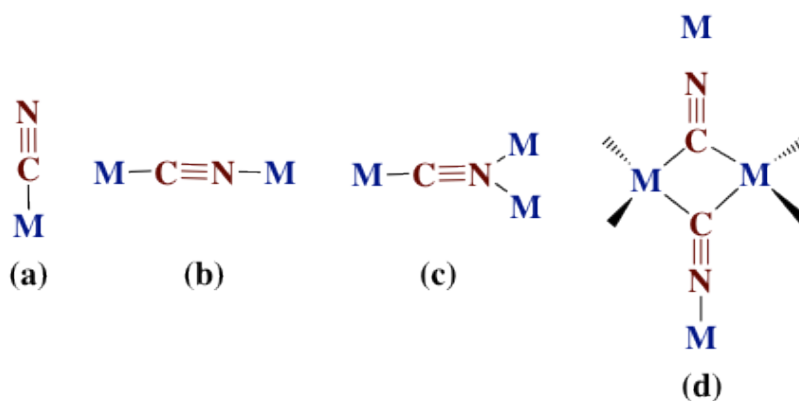
Abstract

The direct reduction methodology utilized 2-azoisobutyronitrile (AIBN) as a source of cyanide ligand as well as reducing agent used for the reduction of the precursor, $[\text{Cu}^{\text{II}}(\text{ala})(\text{NN})\text{Cl}]$ (ala=alanine and NN = nitrogen based ligands) to yield novel two-dimensional (2D) and three-dimensional (3D) copper(I) cyanide (CuCN) co-ordination polymers. The cavity size and the dimensionality of these CuCN networks were found to dependent on the nature and size of the ligand. In the case of rigid cyclic amines, 2D CuCN frameworks were obtained whereas the flexible alkyl amines generated 3D polymers. The X-ray analyses revealed that the polymers exhibited novel intercalated networks where positively charged alkamines acted as guest molecules. These polymers were characterized by IR spectroscopy, X-ray powder diffraction (XRPD) and single crystal X-ray crystallography.

5.1 Introduction

Coordination polymers consist of metal ions and ligands or linkers, and often contain neutral or charged guest molecules, intercalated inside the interstitial spaces. The variation in the structure and properties of the polymers are generally dependent on the nature of the ligand or linker.¹⁻⁴ The cyanide anions are the most versatile linkers due to

their ability to coordinate to a variety of metals in different coordination modes (**Scheme 5.1.1**) to yield one- (1D), two- (2D) and three-dimensional (3D) coordination polymers.⁵⁻⁷



Scheme 5.1.1 Different metal cyanide binding modes (a) terminal, (b) μ^2 -C,N, (c) μ^3 -C,N,N and (d). bridging μ^3 -C,C,N.

The 2D and 3D frameworks have attracted immense attention due to their potential applications in different fields related to their porosity.⁷⁻¹⁷ CuCN polymers have interesting properties such as exceptional robustness, luminescence, conductivity, high porosity, and thermal stability.⁵⁻¹⁷ These properties can potentially be translated into different applications such as single molecule magnet, molecular sensors and storage of reactive gases.⁷⁻¹⁷ Along with their wide applicability, these polymers have fascinating and complex architectures, which have made this field quite interesting as well as challenging.

The CuCN networks are generally anionic in nature represented with the general formulae, $[\text{Cu}_2(\text{CN})_3]^-$, $[\text{Cu}_3(\text{CN})_4]^-$ and $[\text{Cu}_2(\text{CN})_4]^-$ (**Figure 5.1.1**).¹⁸ $[\text{Cu}_2(\text{CN})_3]^-$ is the most commonly found repeating unit in the $(\text{CuCN})_n$ chains, where all the copper centers are tricoordinated and generate hexagonal or honey combed shaped nets. The same hexagonal shape is retained by $[\text{Cu}_3(\text{CN})_4]^-$ moiety where two extra CN-Cu-CN units are incorporated in the final network containing dicoordinated as well as tricoordinated

copper centers. The $[\text{Cu}_2(\text{CN})_4]^-$ stoichiometry is not commonly observed in CuCN networks where net has diamondoid type structure and Cu(I) sites adopted rare tetracoordinated conformation.¹⁸

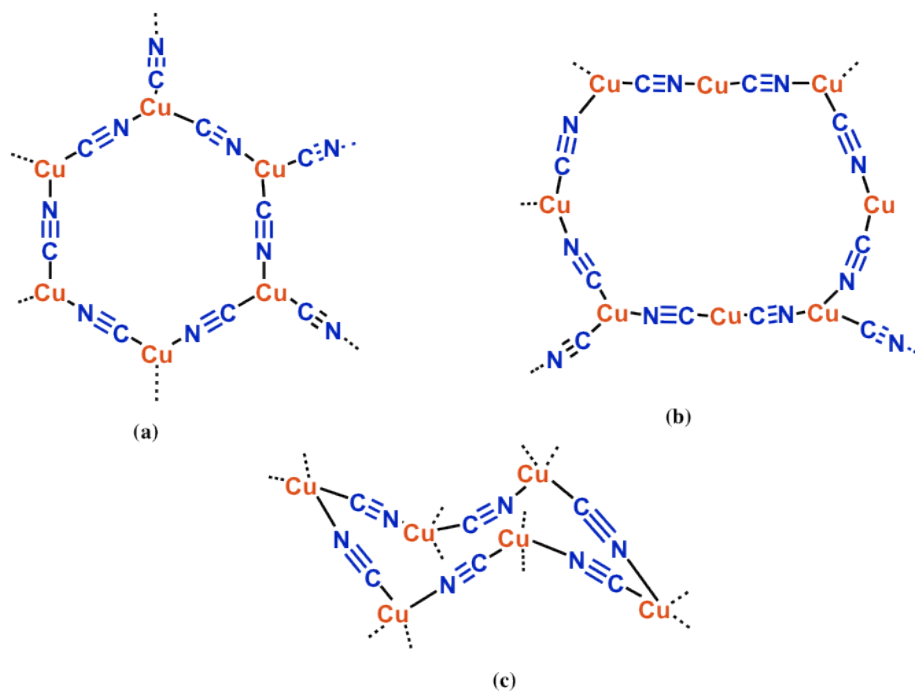


Figure 5.1.1. The different CuCN conformations found in 2- and 3D copper cyanide networks (a) $[\text{Cu}_2(\text{CN})_3]^-$ (b) $[\text{Cu}_3(\text{CN})_4]^-$ (c) $[\text{Cu}_2(\text{CN})_4]^-$.¹⁸

Conventionally, these polymers are synthesized using alkali or alkaline metal cyanide salts by solvothermal and hydrothermal methods at elevated temperature and pressure for a prolonged reaction time.^{6,7,19,20} Apart from the high time and energy expenditure, these reactions generally lack the control over the structure and phase purity of the final product, which has proved to be a major setback to this field. The final

structure of the product was found to be dependent on different physical parameters such as coordination nature of metal and ligand, nature and volume of the solvent, temperature, cyanide source, and relative concentration of metal to ligand.^{6, 21-24}

In this chapter, we focused on the synthesis of novel 2D and 3D coordination polymer by utilizing the organic cyanide source, AIBN, via direct reduction method in good yields. On thermal decomposition of AIBN, 2-cyanoprop-2-yl radicals are generated, which act as a source of the cyanide ligand. Another reducing agent, ascorbic acid was used along with AIBN to accelerate the reduction process. In previous studies, we demonstrated that the aromatic N-based ligands generated 1D polymers, whereas the alkyl based ligand tetramethyl ethylenediamine (TMEDA) resulted in the formation of pillared layer 3D polymer (**Figure 5.1.2**).²⁵

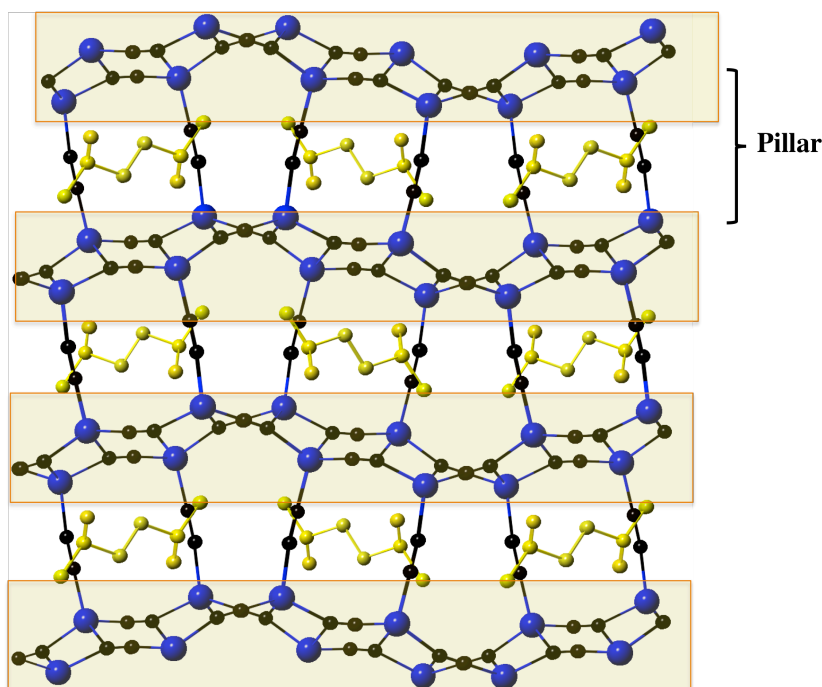


Figure 5.1.2. Pillared 3D network of $[\text{Cu}^{\text{I}}_2(\text{CN})_3 \cdot 0.5\text{TMEDA} \cdot \text{H}_2]_n$ intercalated with positively charged TMEDA ligand (blue=Cu; black= C,N and yellow=TMEDA).²⁵

The voids of the 3D polymer, $[\text{Cu}_2(\text{CN})_3 \cdot 0.5\text{TMEDA-H}_2]_n$ were found to be partially occupied with ligand, TMEDA-H₂.²⁵ In this chapter, we are extending the application of direct reduction method and utilized different aliphatic N-based ligands to regulate the dimensionality and pore size of the CuCN frameworks through the ligand design.

5.2 Results and Discussion.

5.2.1 Synthesis and characterization

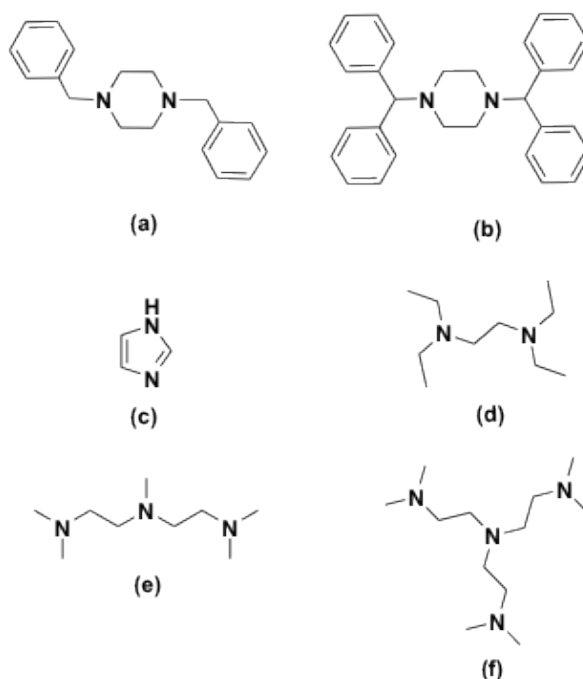
The 2D and 3D polymers were synthesized via the direct reduction method in good yields at 80 °C. The results are summarized in **Table 5.2.1**. Two different classes of aliphatic N-based ligands were used; cyclic alkanamines (1,4-dibenzylpiperazine (dbpip) and 1,4-bis(2,2-diphenylmethyl)piperazine (bdppip)) and alkyl amines (imidazole (imi), pentamethylethylenediamine (PMDETA) and tris(2-(dimethylamino)ethyl)amine (Me₆TREN)) (**Scheme 5.2.1**).

Table 5.2.1. Experimental data for the synthesis of copper(I)-cyanide frameworks.

Polymer	ν (-CN) stretching	% Yield (w.r.t Cu)
$[\text{Cu}_4\text{CN}_6 \cdot (\text{dbzpip-H}_2)]_n$	2088	82
$[\text{Cu}_2\text{CN}_3 \cdot (\text{bdppip-H})]_n$	2120, 2100	69
$[\text{Cu}_2\text{CN}_3 \cdot (\text{Im-H})]_n$	2088	91
$[\text{Cu}_2^{\text{I}}(\text{CN})_3 \cdot 0.5\text{TMEDA-H}_2]_n$ ^b	2126, 2089	63
$[\text{Cu}_3(\text{CN})_5 \cdot (\text{PMDETA-H}_2)]_n$	2103, 2086	72
$[\text{Cu}_7\text{CN}_{10} \cdot (\text{Me}_6\text{TREN-H}_3)]_n$	2110	69

^a All the reactions were performed in methanol at 80 °C. Yields were calculated on the basis of copper. $[\text{Cu}^{\text{II}}]_0 : [\text{AIBN}]_0 : [\text{Ascorbic acid}]_0 = 1 : 10 : 2$. ^b[Ref 2].

These polymers showed a strong –CN stretching peak in the range of 2080 to 2130 cm^{-1} in the IR spectra (**Table 5.2.1**). The crystallinity of these polymers was highly dependent on the concentration of the AIBN and on the solvent volume. Ten equivalents of AIBN w.r.t $[\text{Cu}^{\text{II}}]$ concentration and 3 mL of the methanol generated the good quality crystal. The crystalline material was characterized by single crystal X-ray crystallography and the phase purity of the bulk sample was analyzed by X-ray powder diffraction.



Scheme 5.2.1. Different N-based ligands used in the direct reduction method (a) 1,4-dibenzylpiperazine, (b) 1,4-bis(2,2-diphenylmethyl)piperazine, (c) Imidazole, (d) N,N,N',N'-Tetramethylethylenediamine (e) N,N,N',N',N''-Pentamethyldiethylenetriamine and (f) Tris(2-(dimethylamino)ethyl)amine.

5.2.2 Molecular Structures

$[\text{Cu}_4\text{CN}_6^*(\text{dbzpip-H}_2)]_n$ and $[\text{Cu}_2\text{CN}_3^*(\text{bdmpip-H})]_n$. Cyclic piperazine ligands resulted in the formation of 2D CuCN frameworks with (6,3) nets (**Figure 5.2.1** and **5.2.4**). The crystal structures of $[\text{Cu}_4\text{CN}_6^*(\text{dbzpip-H}_2)]_n$ and $[\text{Cu}_2\text{CN}_3^*(\text{bdmpip-H})]_n$ consisted of tricoordinated copper(I) atoms bridged via cyanide anions with the

stoichiometry of $[\text{Cu}_2(\text{CN})_3]$. Average Cu-C and Cu-N bond lengths of 1.87 Å and 1.93 Å was observed in these networks. The protonated ligands were intercalated inside the pores of the 2D CuCN sheets.

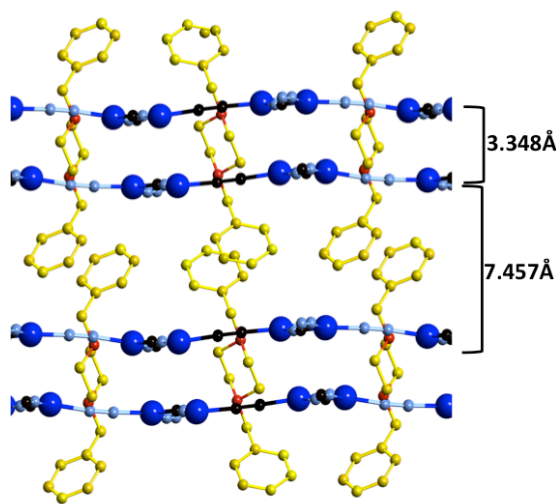


Figure 5.2.1 Crystal lattice of intercalated 2D polymer, $[\text{Cu}_4\text{CN}_6(\text{dbzpip-H}_2)]_n$ (blue=Cu; black= C,N and yellow=ligand).

In $[\text{Cu}_4\text{CN}_6(\text{dbzpip-H}_2)]_n$, 2D CuCN planar honey-combed shaped sheets were stacked on each other with an inter-chain distance of 3.348 Å. Between these two layers, the piperazine in chair shaped conformation was intercalated (Figure 5.2.1 and 5.2.2b). This stacking was further interrupted in order to accommodate the substituents benzyl rings and the inter-chain distance increased to 7.457 Å. Along the *b* axis, chair shaped piperazine molecules were oriented in alternating fashion in order to closely pack the substituents in the inter-chain space (Figure 5.2.2a).

Interestingly, the same ligand under solvothermal reaction conditions generated 3D network, where the copper center is chelated to 1,4-dibenzyl piperazine along with the cyanide ligand.²⁶ Different products were obtained depending on the stoichiometry of the ligand relative to CuCN.²⁶ When the reaction was conducted under direct reduction

reaction condition at different ligand ratios w.r.t. $[\text{Cu}^{\text{II}}]$, same product was obtained. However, the quality of the crystals was found to significantly increased with an increase in ligand concentration.

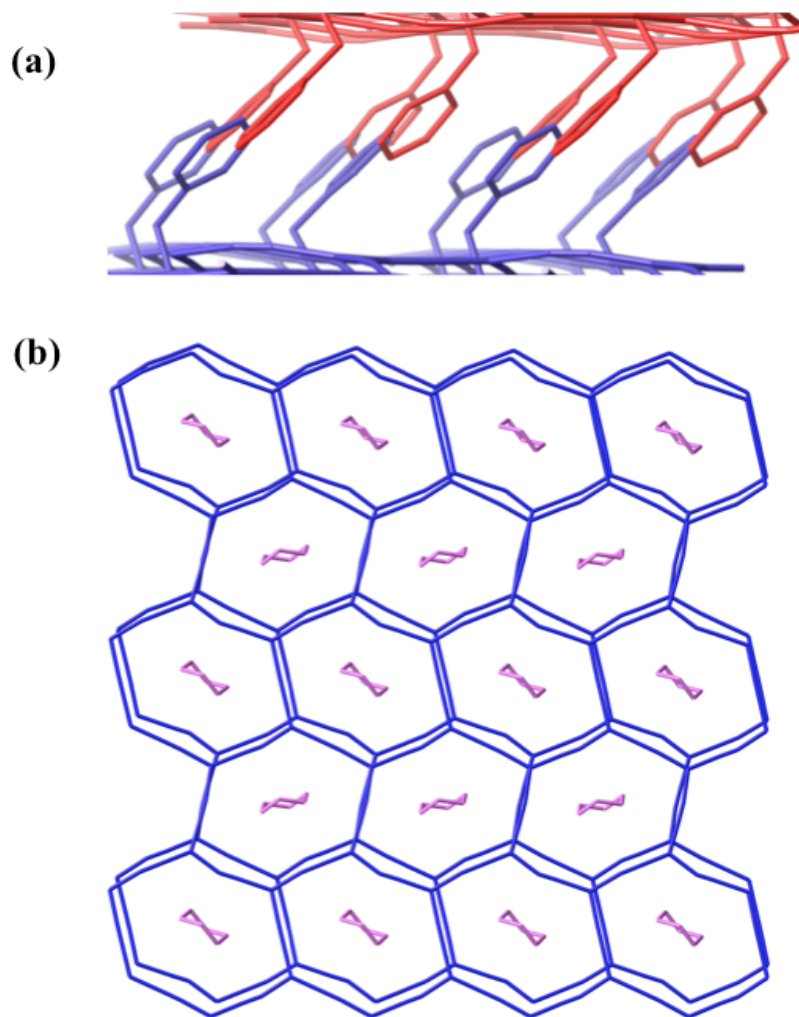


Figure 5.2.2. (a) Orientation of benzyl side groups of ligand. (b) Alternate orientation of the piperazine rings in the (6,3) nets.

The crystal structure of $[\text{Cu}_2\text{CN}_3(\text{bdpmpip-H})]_n$ polymer was found isomorphous to $[\text{Cu}_4\text{CN}_6(\text{dbzpip-H}_2)]_n$, except the 2D CuCN sheets attained a wave-like form (Figure

5.2.2b). Another distinct feature was that the only one of the nitrogen atom of the encapsulated piperazine ligand was protonated. The protonated nitrogen atom was found to be closer to the anionic CuCN nets than the neutral part of piperazine, which can be attributed to the electrostatic interaction between cationic ligand and anionic CuCN nets.

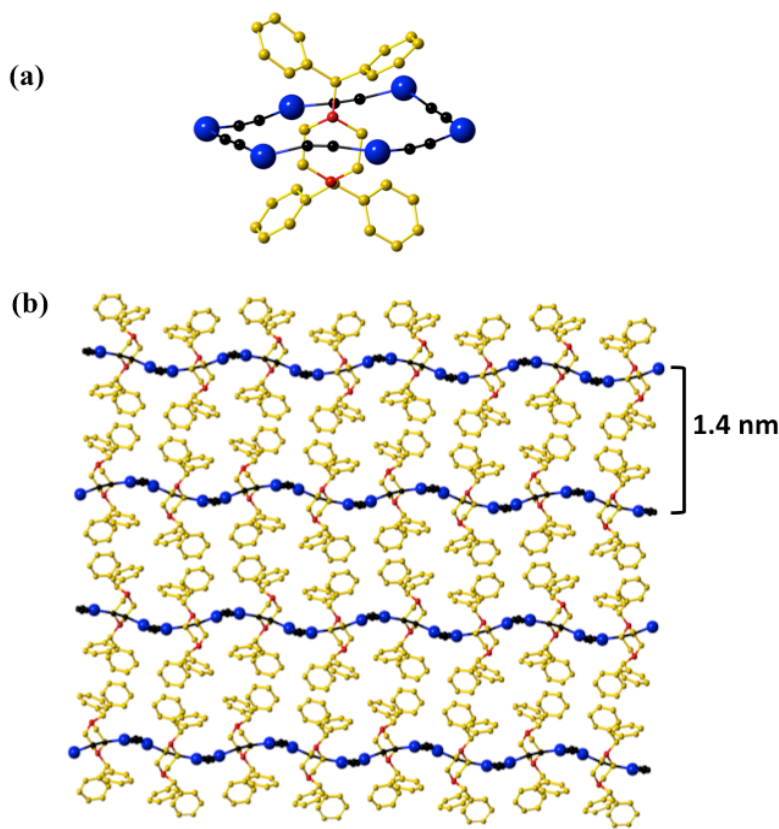


Figure 5.2.3. (a) Intercalated bdpmpip in the (6,3) net and (b) crystal packing along the *c* axis in $[\text{Cu}_2\text{CN}_3(\text{bdpmpip-H})]_n$ (blue=Cu; black= C,N and yellow=ligand).

In contrast to $[\text{Cu}_4\text{CN}_6(\text{dbzpip-H}_2)]_n$, ligand molecules were accommodated in only one 2D CuCN net along the *c* axis, which can be attributed to the bulky side group of 1,4-bis(2,2-diphenylmethyl)piperazine (**Figure 5.2.3**). In non-planar (6,3) nets, two crystallographic distinct trico-ordinated copper centers were present. The only difference between these two Cu(I) centers, is the Cu1-C1 bond length. In one of Cu(I) center, Cu1-C1 bond was slightly long. However, no distinct difference was observed in the Cu-N

bond lengths. This difference was reflected in the IR spectrum of the polymer, which showed two –CN stretching bands at 2120 and 2100 cm^{-1} . The small difference of 20 cm^{-1} between the two bands indicated that the cyanide functionalities were in similar coordination environments. The inter-chain distance between two CuCN sheets was found to be very large (1.4 nm), which can again be attributed to the bulky diphenylmethyl side groups (**Figure 5.2.3**).

$[\text{Cu}_2\text{CN}_3^*(\text{Im-H})]_n$

Imidazole is the planar five membered heterocycle, which generated a pseudo 3D pillared layer Cu(I)CN network along the *a* axis (**Figure 5.2.4**). Similar to the polymers with the piperazine-based ligands, the $[\text{Cu}_2\text{CN}_3^*(\text{Im-H})]_n$ consisted of (6,3) nets. In each net, the copper center adopted a distorted trigonal planar geometry. Each copper(I) atom was coordinated to the two nitrogen with a bond length of 2.005 and 1.956 Å, and to carbon with a bond distance of 1.919 Å.

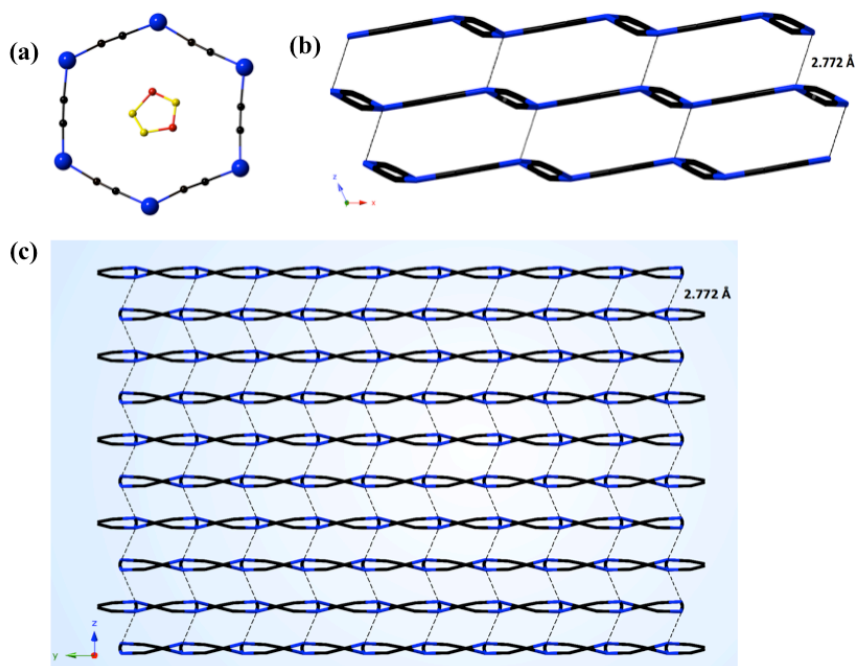


Figure 5.2.4. (a) Intercalated imidazole in (6,3) net (b) and (c) Cuprophilic interactions along the *a* and *b* axes in $[\text{Cu}_2\text{CN}_3^*(\text{Im-H})]_n$ (blue=Cu; black= C,N and yellow=imidazole, (N=red)).

The nets were stacked on each other with an inter-chain distance of 3.749 Å. The 2D CuCN nets were found to have cuprophilic interactions of 2.772 Å between stacked chains resulting in the formation of pseudo 3D networks. The guest molecule, (Im-H)⁺ was found to be intercalated in the pores of polymers and made the penetrable channels along the *a*-axis non penetrable.

$[\text{Cu}_3(\text{CN})_5^*(\text{PMDETA-H}_2)]_n$

The tridentate N-based ligand, PMDETA, results in the formation of a 3D pillared layer polymer, $[\text{Cu}_3(\text{CN})_5^*(\text{PMDETA-H}_2)]_n$. The crystal structure of $[\text{Cu}_3(\text{CN})_5^*(\text{PMDETA-H}_2)]_n$ consisted of two crystallographic distinct copper (I) center. Both the copper(I) centers were tetraordinated, where first copper center involved in the μ_3 -C,C,N cyano bridging (**Scheme 5.2.1**). On the other hand, the second copper(I) atom adopted distorted tetrahedral geometry and coordinated to four cyanide ligands. Two different cyanide stretching bands at 2103 and 2086 cm^{-1} were obtained in the IR spectrum corresponding to the cyanide with μ_3 -C,C,N and μ_2 -C,N binding modes, respectively. The large sized PMDETA-H₂ ligands penetrate into the voids and result in the formation of large (9,4) nets. The total void volume without PMDETA-H₂ was estimated by Platon to be 684.9 Å³, corresponding to 40.4% of the total unit cell volume. The Cu^I-CN framework contained only two penetrable channels due to μ_3 -C,C,N cyano bridging and (**Figure 5.2.5**) with approximate dimensions of 11.6×6.5 Å and 10.1×9.5 Å (**Figure 5.2.4a**) .

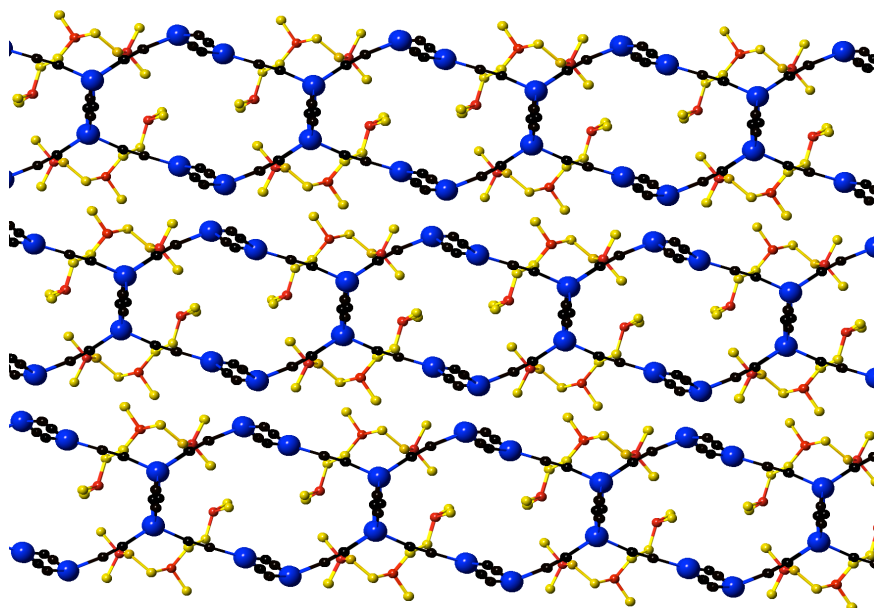
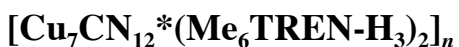


Figure 5.2.5. Intercalated PMDETA ligand in the CuCN network of $[\text{Cu}_3(\text{CN})_5^*(\text{PMDETA-H}_2)]_n$ (blue=Cu; black= C,N and yellow=PMDETA, (N=red)).



The tripodal Me_6TREN ligand generated a 3D pillared layer framework, $[\text{Cu}_7\text{CN}_{12}^*(\text{Me}_6\text{TREN-H}_3)_2]_n$, consist of two crystallographic unique tetraco-ordinated Cu(I) sites. One Cu(I) center adopted distorted tetrahedral geometry by co-ordinating to three cyanide anions in the μ_2 -C,N and one in a terminal fashion. The terminal copper cyanide bond was found to be distorted in the crystal structure. The second Cu(I) center bridged to the cyanide anions through μ_3 -C,C,N mode. Along the a axis, non-penetrable pillars were attached to each other via planar (6,3) CuCN nets acting as linkers (Figure 5.2.6a). These pillars and linkers generated very large channels with dimensions of

16.498x9.292 Å. These channels are made up of large sized nets (16,4) and contained two molecules of guest molecules i.e. protonated Me₆TREN ligand. Along the *c* axis, biporous channels made up of (6,3) nets with the dimensions of 8.250x6.608Å and 7.935x7.281Å were found. The large channels (8.250x6.608Å) were occupied by guest molecules. The total void volume without any guest molecules was estimated by PLATON to be 1800 Å³, corresponding to 68.8% of the total unit cell volume.

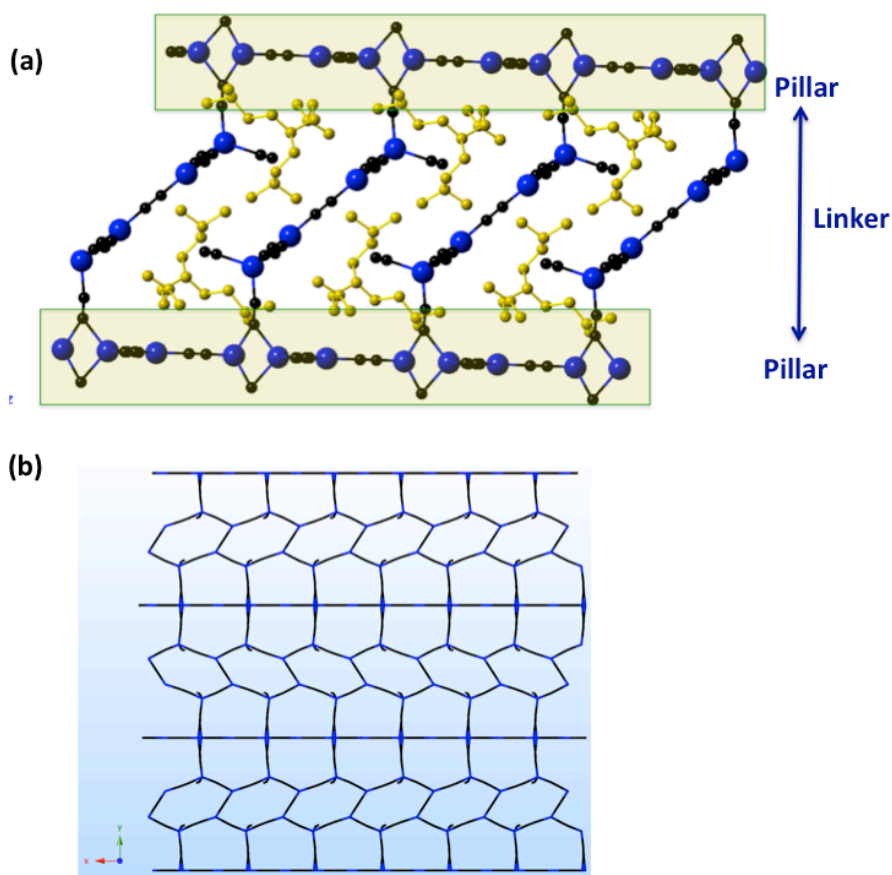


Figure 5.2.6. (a) Pillared layered 3D network (*a* axis) (b) Biporous (6,4) nets (*c* axis) of [Cu₇CN₁₂*(Me₆TREN-H₃)₂]_n (blue=Cu; black= C,N and yellow=Me₆TREN).

5.3 Role of ligand on the dimensionality and pore size in CuCN polymer

We observed that the structure of the ligand has dictated the dimensionality and the pore size in the CuCN frameworks. With the direct reduction method, the aromatic N-based ligands could be successfully synthesized the one-dimensional polymer whereas aliphatic amine, tetramethylethylenediamine (TMEDA) resulted in the formation of pillared layer 3D network. In this study, we have utilized two different categories of ligands; cyclic amines and aliphatic amines. The cyclic amines imparted flexibility between the aromatic N-based ligands and the aliphatic amines. The rigid backbone of the cyclic amines has limited the growth of the network to only 2 dimensions and thus resulted in the formation of 2D CuCN coordination polymers. In case of imidazole, the backbone was very rigid but due to its planar and small size, it allowed cuprophilic interactions and thus, resulted in the formation of *pseudo* 3D network. The flexible bidentate, tridentate and tetradentate N-based ligands enabled the growth of the polymer in all directions, and formed pillared layered 3D CuCN polymers.

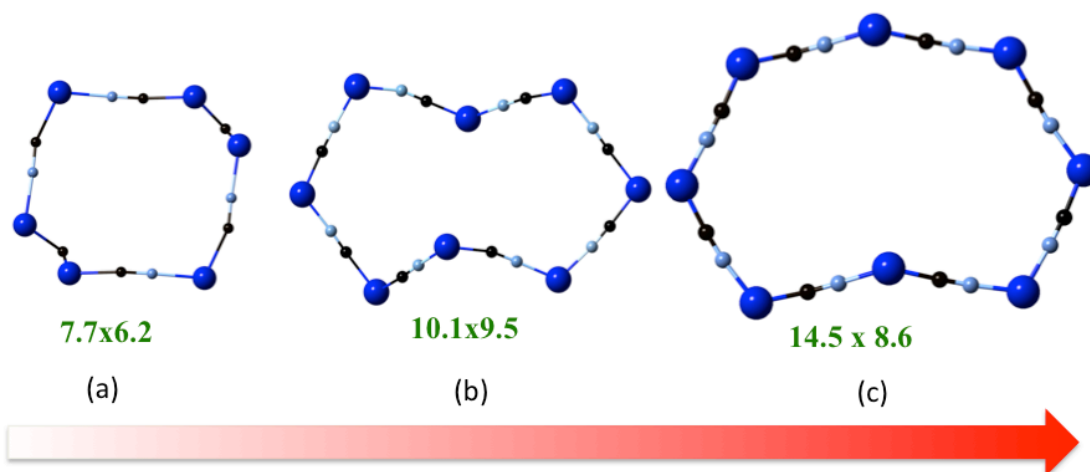


Figure 5.3.1. Large void of CuCN network of (a) $[\text{Cu}_2(\text{CN})_3 \cdot 0.5\text{TMEDA-H}_2]_n$ (b) $[\text{Cu}_3(\text{CN})_5 \cdot (\text{PMDETA-H}_2)]_n$ and (c) $[\text{Cu}_7\text{CN}_{10} \cdot (\text{Me}_6\text{TREN-H}_3)]_n$ (dark blue=Cu; black=C and light blue=N).

The size of the pore as well as of the channels of the polymers was also found to be dependent on the size of the ligand (**Figure 5.3.1**). The size of the channel increased from 7.7x6.2 in case of TMEDA to 10.1x9.5 for PMDETA. The same effect was observed with tetradentate ME₆TREN ligand and the size of the channel was found to be 14.5x8.6 Å. These pillared layer structures consist of different channels (the largest channel was used for the comparison). The results are summarized in **Table 5.3.1**.

Table 5.3.1. List of the polymers with dimensionality and total void volume.

Polymer	Dimensionality	Size of Channels (Å)	Void Volume (Å ³) ^b	Volume per unit cell (%) ^b
[Cu ₄ CN ₆ *(dbzpip-H ₂)] _n	2D	11.1x7.4	896.1	67.0
[Cu ₂ CN ₃ *(bdmpip-H)] _n	2D	10.3x7.4	2573.9	87.0
[Cu ₂ CN ₃ *(Im-H)] _n	Pseudo-3D	6.5x4.8 10.1x8.6		
[Cu ₂ (CN) ₃ *0.5TMEDA-H ₂] _n ^b	3D	7.7x6.2 7.0x5.0	684.9	40.4
[Cu ₃ (CN) ₅ *(PMDETA-H ₂)] _n	3D	11.6x6.5 9.5x10.1	2333.6	58.0
[Cu ₇ CN ₁₀ *(Me ₆ TREN-H ₃)] _n	3D	14.5x8.69 10.1x8.5	1800	68.8

^bVolume was calculated using PLATON software.

5.4. Conclusion

Different N-based ligands (cyclic amines and alkamines) were used to regulate the dimensionality and the pore size of the copper cyanide frameworks. The direct reduction method was used to synthesize novel 2D and 3D copper-cyanide frameworks (CuCN). The radicals generated via the thermal decomposition of AIBN (2,2'-azobis(2-methylpropionitrile)) along with reducing agent ascorbic acid reduced the Cu(II) complexes, [Cu^{II}(ala)(NN)Cl] (ala = alanine, NN= N-based ligand) and afforded the

CuCN frameworks in good yields. As expected, the structure of the N-based ligands influenced the dimensionality and the pore size of the frameworks. The cyclic N-based ligands, piperazine, results in the formation of 2D polymers whereas flexible alkamines generated the 3D frameworks. The size of the channels was found to be correlated to the size of the N-based ligands. The dimension of the pore and net was expanded as we increased the size of the substituents. These polymers showed strong –CN stretching peaks in the IR spectra and were characterized by the single crystal X-ray crystallography and by powder X-ray diffraction. In conclusion, we were successful in regulating the dimensionality and pore size in CuCN frameworks using direct reduction method through ligand design.

5.5. Experimental.

General Procedures. All chemicals were purchased from commercial sources and used as received. Tris(2-(dimethylamino)ethyl)amine (Me_6TREN)²⁷, 1,4-dibenzylpiperazine, 1,4-dibenzhyrlypiperazine and 1,4-bis(perfluorobenzyl)piperazine were synthesized according to previously published literature procedures²⁶. AIBN was recrystallized from cold methanol and dried at room temperature under vacuum.

Instrumentation and Equipment. ¹H NMR spectra were obtained using Bruker Avance 400 MHz spectrometers, and chemical shifts are given in ppm relative to residual solvent peaks (CDCl_3 , δ 7.26 ppm). IR spectra were recorded in the solid state using Nicolet Smart Orbit 380 FT-IR spectrometer (Thermo Electron Corporation). Elemental analyses for C, H, and N were obtained from Roberston Laboratories, NJ. KaleidaGraph 4.1 software

was used to generate images of IR spectra and powder XRD patterns.

X-ray Crystal Structure Determination. The X-ray intensity data was collected at 150 K using graphite-monochromated Mo $K\alpha$ radiation ($\lambda=0.71073$ Å) on a Bruker Smart Apex II CCD diffractometer. Data reduction included absorption corrections by the multiscan method using SADABS (Sheldrick, G. M. *SADABS Version 2.03*; University of Gottingen: Germany, 2002). Crystal data and experimental conditions are given in Tables S1-S4. Structures were solved by direct methods and refined by full-matrix least squares using SHELXTL 6.1 bundled software package (Sheldrick, G. M. *SHELXTL 6.1, Crystallographic Computing System*; Bruker Analytical X-Ray System: Madison, WI, 2000). The H atoms were positioned geometrically (aromatic C-H=0.93 Å, methylene C-H=0.97 Å and methyl C-H=0.96 Å) and treated as riding atoms during subsequent refinement, with $U_{iso}(H)=1.2U_{eq}(C)$ or $1.5U_{eq}$ (methyl C). The methyl groups were allowed to rotate about their local 3-fold axes. Crystal Maker 8.3 was used to generate molecular graphics.

X-ray Powder Diffraction. Measurements were performed on a Panalytical X'Pert Pro MPD powder X-ray diffractometer using copper $K\alpha$ radiation with a wavelength of 1.541871 Å and operating with a tube power of 45 kV 40 mA. Data were collected from 5° to 145° 2θ with a step size of 0.0083556° and scan rate of 0.010644 °/s. The incident beam optics were comprised of a 0.02 rad soller slit, a divergent slit of 1/4° and an anti-scatter slit of 1/2°; whereas, the diffracted beam optics were comprised of a 0.02 rad soller slit and an anti-scatter slit of 1/4°. The samples were prepared for analysis using a

top fill method where the sample powder is added from bottom to top of a sample holder and spread out gently using a razor blade to minimize preferred orientation.

Synthesis of $\text{Cu}^{\text{II}}(\text{ala})(\text{NN})\text{X}$ (aa=deprotonated amino acid, NN = N-based ligand and X=Cl). In a typical experiment, stoichiometric amounts of sodium hydroxide (1.00 mmol, 0.0400 g) and *L*-alanine (1.00 mmol, 0.0891 g) were dissolved in 4.0 mL of methanol and stirred at ambient temperature for 1 h. Sodium salt of *L*-alanine was then added dropwise to $\text{Cu}^{\text{II}}\text{Cl}_2$ (1.00 mmol, 0.134 g) dissolved in 2.0 mL of methanol. After stirring for 10 min, sodium chloride was removed by filtration. The appropriate nitrogen based ligand dissolved in 2.0 mL of methanol was then added dropwise to the resulting solution. For ligand structures, refer to **Scheme 5.2.1**. The copper(II) complexes were used in the synthesis of coordination polymers without prior isolation.

Synthesis of Copper(I)-Cyanide Frameworks Employing Thermal Decomposition of AIBN (2,2'-azobis(2-methylpropionitrile). $\text{Cu}^{\text{II}}(\text{ala})(\text{NN})\text{X}$ (0.0608 mmol) and 10 equivalents of AIBN (0.608 mmol, 0.100 g) were dissolved in 3.0 mL of methanol in a glass tube. The reaction mixture was flushed with argon for 30 seconds, followed by the addition of 2 equivalents of ascorbic acid relative to copper(II) complex (0.121 mmol, 0.0216 g). The tube was then immediately capped, sealed with teflon and electrical tape, and placed in an oil bath thermostated at 80 °C. After 24 h, the precipitate was filtered, thoroughly washed with water, methanol, acetone and dichloromethane, and dried under vacuum at ambient temperature. The crystalline material was characterized by IR spectroscopy, single crystal X-ray crystallography, and powder X-ray diffraction.

$[\text{Cu}_4\text{CN}_6(\text{dbzpip-H}_2)]_n$. Colorless crystals, yield= 11.2mg (82% based on copper). FT-IR (Solid) $\nu(\text{CN})=2088$ (s) cm^{-1} .

$[\text{Cu}_2\text{CN}_3(\text{bdmpip-H})]_n$. Colorless crystals, yield= 17.3mg (69% based on copper). FT-IR (Solid) $\nu(\text{CN})=2120, 2100$ (s) cm^{-1} .

$[\text{Cu}_2\text{CN}_3(\text{Im-H})]_n$. Colorless crystals, yield= 10.0mg (91% based on copper). FT-IR (Solid) $\nu(\text{CN})=2088$ (s) cm^{-1} .

$[\text{Cu}_3(\text{CN})_5(\text{PMDETA-H}_2)]_n$. Colorless crystals, yield= 7.2mg (72% based on copper). FT-IR (Solid) $\nu(\text{CN})=2103, 2086$ (s) cm^{-1} .

$[\text{Cu}_7\text{CN}_{12}(\text{Me}_6\text{TREN-H}_3)]_n$. Light brown crystals, Yield= 8.7mg (82% based on copper). FT-IR (Solid) $\nu(\text{CN})=2110$ (s) cm^{-1} .

References.

1. Batten, S. R.; Robson, R., Interpenetrating Nets: Ordered, Periodic Entanglement. *Ang. Chem. Int. Ed.* **1998**, *37*, (11).
2. Batten, S. R.; Hoskins, B. F.; Robson, R., Interdigitation, Interpenetration and Intercalation in Layered Cuprous Tricyanomethanide Derivatives. *Chem.Euro.J.* **2000**, *6*, (1), 156-161.
3. Batten, S. R., Coordination polymers. *Current Opinion in Solid State and Materials Science* **2001**, *5*, (2-3), 107-114.
4. Batten, S. R., Topology of interpenetration. *Cryst. Eng. Comm.* **2001**, *3*, (18).

5. Batten, S. R., Glorious uncertainty—challenges for network design. *Journal of Solid State Chemistry* **2005**, *178*, (8).
6. Deng, H.; Qiu, Y.; Daiguebonne, C.; Kerbellec, N.; Guillou, O.; Zeller, M.; Batten, S. R., Synthesis of New Copper Cyanide complexes via the Transformation of Organonitrile to Inorganic Cyanide. *Inorg. Chem.* **2008**, *47*, (13), 5866-5872.
7. Batten, S. R.; Neville, S. M.; Turner, D. R., Coordination Polymers - Design, Analysis and Application. In Royal Society of Chemistry: 2009.
8. Etaiw, S.; Badr El-din, A., Assembly and Fluorescence Properties of 3D-Copper(I) Cyanide Coordination Polymers Based on Methylpyrazine and Tetramethylpyrazine in Presence of Me₃SnCl. *Journal of Inorganic and Organometallic Polymers and Materials* *21*, (1), 110-117.
9. Ley, A. N.; Dunaway, L. E.; Brewster, T. P.; Dembo, M. D.; Harris, T. D.; Baril-Robert, F.; Li, X.; Patterson, H. H.; Pike, R. D., Reversible luminescent reaction of amines with copper(i) cyanide. *Chemical Communications* *46*, (25), 4565-4567.
10. Suh, M. P.; Park, H. J.; Prasad, T. K.; Lim, D.-W., Hydrogen Storage in Metal-Organic Frameworks. *Chemical Reviews* *112*, (2), 782-835.
11. Chen, B.; Yang, Y.; Zapata, F.; Lin, G.; Qian, G.; Lobkovsky, E. B., Luminescent Open Metal Sites within a Metal–Organic Framework for Sensing Small Molecules. *Advanced Materials* **2007**, *19*, (13), 1693-1696.
12. Noro, S.-i.; Kitagawa, S.; Kondo, M.; Seki, K., A New, Methane Adsorbent, Porous Coordination Polymer [$\{\text{CuSiF}_6(4,4'\text{-bipyridine})_2\}_n$]. *Angewandte Chemie International Edition* **2000**, *39*, (12), 2081-2084.
13. Xu, Y.; Ren, Z.-G.; Li, H.-X.; Zhang, W.-H.; Chen, J.-X.; Zhang, Y.; Lang, J.-P., Syntheses, crystal structures and luminescent properties of two one-dimensional coordination polymers $[\text{CuX}(\text{dmpzm})]_n$ (X=CN, NCS; dmpzm=bis(3,5-dimethylpyrazolyl)methane). *Journal of Molecular Structure* **2006**, *782*, (2,Äì3), 150-156.
14. Estrader, M.; Diaz, C.; Ribas, J.; Solans, X.; Font-Bardia, M., Synthesis, characterization and magnetic properties of six new copper(II) complexes with

- aminoacids as bridging ligand, exhibiting ferromagnetic coupling. *Inorganica Chimica Acta* **2008**, *361*, (145), 3963-3969.
15. Agusti, G.; Munoz, M. C.; Gaspar, A. B.; Real, J. A., Spin-Crossover Behavior in Cyanide-Bridged Iron(II),Copper(I) Bimetallic 1,3D Metal,Organic Frameworks. *Inorganic Chemistry* **2009**, *48*, (8), 3371-3381.
 16. Larionova, J.; Guari, Y.; Sangregorio, C.; Guerin, C., Cyano-bridged coordination polymer nanoparticles. *New Journal of Chemistry* **2009**, *33*, (6), 1177-1190.
 17. Murray, L. J.; Dinca, M.; Long, J. R., Hydrogen storage in metal-organic frameworks. *Chemical Society Reviews* **2009**, *38*, (5), 1294-1314.
 18. Pike, R. D., Structure and Bonding in Copper(I) Carbonyl and Cyanide Complexes. *Organometallics* **2012**, *31*, (22), 7647-7660.
 19. Park, K.-M.; Yoon, I.; Seo, J.; Lee, J.-E.; Kim, J.; Choi, K. S.; Jung, O.-S.; Lee, S. S., Two-Dimensional Square-Grid versus One-Dimensional Double-Stranded Networks: Counterion Regulation of the Formation of Macrocyclic-Based Copper(I) Coordination Frameworks. *Crystal Growth & Design* **2005**, *5*, (5), 1707-1709.
 20. Corma, A.; Garcia, H.; Llabris i Xamena, F. X., Engineering Metal Organic Frameworks for Heterogeneous Catalysis. *Chemical Reviews* **110**, (8), 4606-4655.
 21. Kitagawa, S.; Uemura, K., Dynamic porous properties of coordination polymers inspired by hydrogen bonds. *Chemical Society Reviews* **2005**, *34*, (2), 109-119.
 22. Pike, R. D.; deKrafft, K. E.; Ley, A. N.; Tronic, T. A., Threaded structure and blue luminescence of $(\text{CuCN})_{20}(\text{Piperazine})_7$. *Chemical Communications* **2007**, (36), 3732-3734.
 23. Li, D.; Wu, T., Transformation of Inorganic Sulfur into Organic Sulfur: A Novel Photoluminescent 3-D Polymeric Complex Involving Ligands in Situ Formation. *Inorganic Chemistry* **2004**, *44*, (5), 1175-1177.
 24. Colacio, E.; Kivekis, R.; Lloret, F.; Sunberg, M.; Suarez-Varela, J.; Bardaja, M.; Laguna, A., Architecture Dependence on the Steric Constraints of the Ligand in

- Cyano-Bridged Copper(I) and Copper(II),Copper(I) Mixed-Valence Polymer Compounds Containing Diamines;Crystal Structures and Spectroscopic and Magnetic Properties. *Inorganic Chemistry* **2002**, *41*, (20), 5141-5149.
25. Kaur, A.; Pintauer, T., Copper(I)–Cyanide Frameworks through Thermal or Photodecomposition of the Free Radical Diazo Initiator AIBN. *European Journal of Inorganic Chemistry* **2013**, (19), 3297-3301.
26. Lim, M. J.; Murray, C. A.; Tronic, T. A.; deKrafft, K. E.; Ley, A. N.; deButts, J. C.; Pike, R. D.; Lu, H.; Patterson, H. H., Copper(I) Cyanide Networks: Synthesis, Structure, and Luminescence Behavior. Part 2. Piperazine Ligands and Hexamethylenetetramine(1). *Inorganic Chemistry* **2008**, *47*, (15), 6931-6947.
27. Eckenhoff, W. T.; Pintauer, T., Atom transfer radical addition (ATRA) catalyzed by copper complexes with tris[2-(dimethylamino)ethyl]amine (Me₆TREN) ligand in the presence of free-radical diazo initiator AIBN. *Dalton Transactions* **2011**, *40*, (18), 4909-4917.

Chapter 6

Synthesis, Characterization and Structural Investigation of Mixed Ligand Copper(II) Complexes Utilized as Precursors in Direct Reduction Method

Abstract

A series of mononuclear mixed ligand copper(II) complexes with deprotonated L-amino acids (aa = glycine, alanine, phenylalanine and proline) and bidentate N-based ligands (NN = 1,10-phenanthroline, 2,2'-bipyridine), $[\text{Cu}^{\text{II}}(\text{aa})(\text{NN})\text{Cl}]$ were synthesized and characterized. These complexes were successfully utilized as precursors for the synthesis of copper(I) cyanide (CuCN) coordination polymers via direct reduction method. This method has provided an efficient alternative to traditionally used solvo- and hydrothermal methods, where $[\text{Cu}^{\text{II}}(\text{aa})(\text{NN})\text{Cl}]$ complexes activated the cyanide functionality of the diazo radical initiator, 2,2'-azobis(2-methylpropionitrile) (AIBN) to synthesize multi-dimensional CuCN polymers. In order to gain the mechanistic insight, the structural features of the Cu(II) complexes were investigated. All complexes adopted the square pyramidal geometry and interacted via different intermolecular forces such as H-bonding and π - π stacking in unit cell. These complexes showed equatorial compression, which resulted in the elongation of Cu-Cl bond length ranging from 2.464 Å ($[\text{Cu}^{\text{II}}(\text{pro})(\text{phen})\text{Cl}]$) to 2.600 Å ($[\text{Cu}^{\text{II}}(\text{gly})(\text{bpy})\text{Cl}]$) in comparison to the trigonal bipyramidal Cu(II) complexes with neutral N-based bidentate ligands. It was observed that the tetragonal compression and the elongation of Cu-Cl bond were more pronounced in case of complexes with tau value (τ) closer to zero. Depending on the orientation of

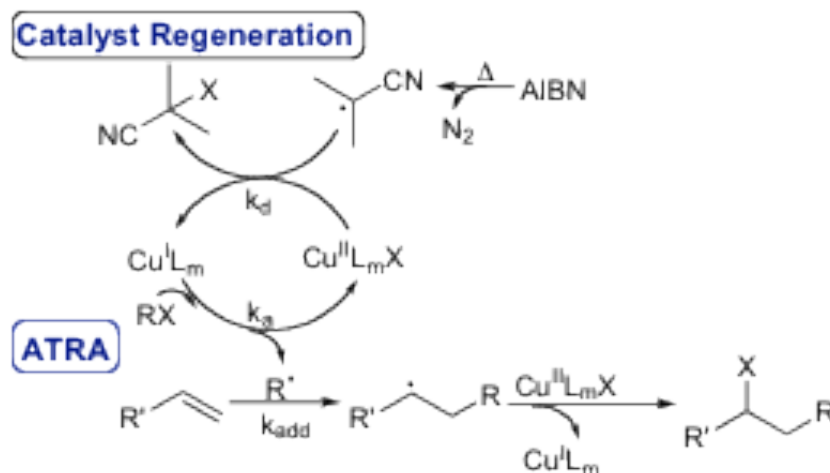
the substituent (-R) of the amino acid in $[\text{Cu}^{\text{II}}(\text{ala})(\text{bpy})\text{Cl}]$, $[\text{Cu}^{\text{II}}(\text{phe})(\text{phen})\text{Cl}]$ and $[\text{Cu}^{\text{II}}(\text{phe})(\text{bpy})\text{Cl}]$, two distinct Cu(II) complexes with different structural parameters were isolated in solid-state.

6.1. Introduction

In biological systems, amino acid residues of peptides regulate the electronic and steric environment of metals such as iron and copper in the active site of metalloenzymes.¹⁻¹⁰ These enzymes play an important role in almost all biological forms and participate in electron transfer (ET) processes, such as photosynthesis and respiration, crucial for sustaining life. The redox activity of the metal centers is largely found to be dependent on donor atoms (N,O and S) of the the amino acids and their side groups (-R).^{3, 10, 11} Therefore, the amino acids fine-tune the ET properties and reduction potentials of the metal centers.

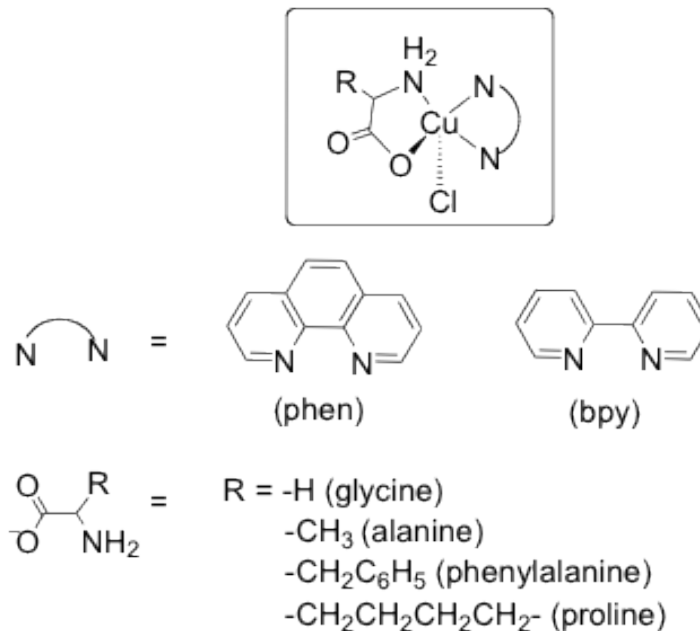
Along with the mimicking the active centers, amino acids and its derivatives have received attention as a ligand of choice in copper complexes due to their cytotoxic properties and potential use as anti-tumor chemotherapeutic agents.¹²⁻¹⁹ Also, on the other hand these complexes were used as precursors in direct reduction method for the synthesis of one- (1D), two- (2D) and three-dimensional (3D) copper(I) cyanide coordination polymers.¹² Originally, these complexes were designed as catalytic candidates for atom transfer radical addition (ATRA). ATRA is a synthetic technique used for the formation of C-C and C-X bond via the addition of polyhalogenated alkanes to alkenes.¹³⁻¹⁶ The reaction is typically conducted in the presence of reducing agent, to continuously regenerate the activator species (copper(I) complex) from the corresponding

deactivator (copper(II) complex). The latter one accumulates as a result of unavoidable radical-radical termination reactions (**Scheme 5.1.1**).¹⁵⁻¹⁸ This process is also known as catalyst regeneration and was developed in mechanistically similar atom transfer radical polymerization (ATRP).^{17,19}



Scheme 6.1.1. Schematic representation of copper catalyzed ATRA in the presence of reducing agent, AIBN.

In $[\text{Cu}^{\text{II}}(\text{aa})(\text{NN})\text{Cl}]$ complex, the deprotonated amino acid binds to the copper via N and O donor atoms (**Scheme 6.1.2**). The electronegative oxygen was expected to withdraw the electron density from the metal center, which might enhance the stability of electron rich activator species, Cu(I) complex. Therefore, these complexes were expected to be less active than Cu(II) coordinated to neutral N-based ligands. The versatility of these ligands was further increased due to availability of variety of electron donating and withdrawing side groups (-R). The neutral N,N-based ligand (1,10-phenanthroline, 2,2'-bipyridine) was used as second ligand to increase the solubility and stability of these complexes and also, to accommodate the halide in the fifth axial position.

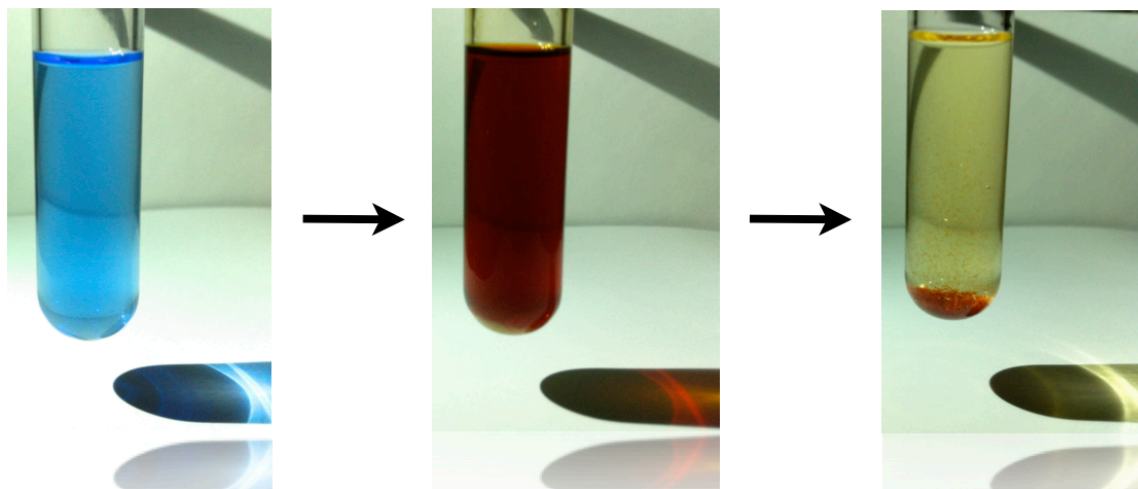


Scheme 6.1.2. Schematic representation of the $[\text{Cu}^{\text{II}}(\text{aa})(\text{NN})\text{Cl}]$ complexes.

The complex, $[\text{Cu}^{\text{II}}(\text{ala})(\text{phen})\text{Cl}]$ were used as catalysts for the ATRA with carbon tetrachloride (CCl_4) and α -olefins (1-octene and 1-hexene) in the presence of diazo based reducing agent, 2,2'-azobis(2-methylpropionitrile) (AIBN) in methanol at 80 °C. Surprisingly, the color of the solution was changed fast from the blue to dark red, indicating that the reduction of $[\text{Cu}^{\text{II}}(\text{ala})(\text{phen})\text{Cl}]$ to $[\text{Cu}^{\text{I}}(\text{ala})(\text{phen})]$.¹² However, the color change was accompanied by the precipitation of red crystalline material after 24 hours as shown in **Figure 6.1.1a**.

Initially, we assumed that the Cu(I) complex has poor solubility in the solvent, however, the single X-ray analysis revealed the formation of $[\text{Cu}^{\text{I}}(\text{phen})_2(\text{CN})_2 \cdot \text{CH}_3\text{OH}]_n$ coordination polymer, **Figure 6.1.1b**.

(a)



(b)

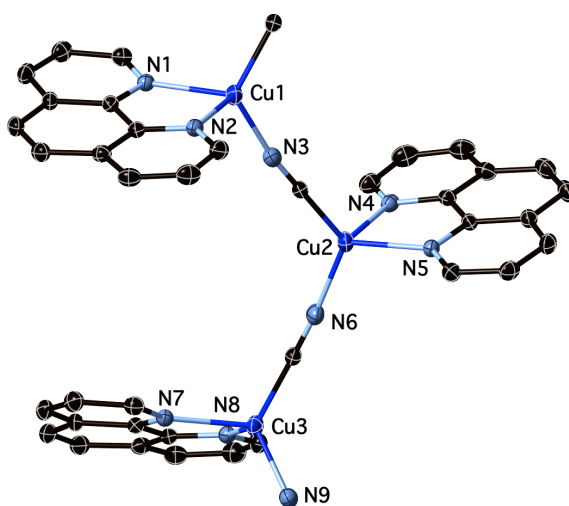
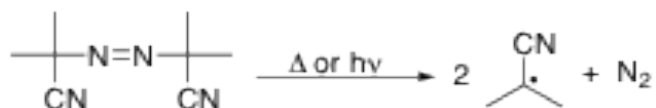


Figure 6.1.1. (a) Synthesis of $[\text{Cu}_2^{\text{I}}(\text{phen})_2(\text{CN})_2 \cdot \text{CH}_3\text{OH}]_n$ under direct reduction reaction conditions. (b) Molecular structures of $[\text{Cu}_2^{\text{I}}(\text{phen})_2(\text{CN})_2 \cdot \text{CH}_3\text{OH}]_n$ shown with 30% probability displacement ellipsoids. H-atoms and methanol counterion have been omitted for clarity.¹²

The quantitative yield of the polymer was obtained at 80 °C of 92% as well as under ambient reaction conditions upon UV irradiation (94%). The thermal- and

photodecomposition of AIBN generated the 2-cyanoprop-2-yl radicals, which acts as an source of cyanide anions (**Scheme 5.1.3**).



Scheme 6.1.3. Schematic representation of thermal or photodecomposition of AIBN to 2-cyanoprop-2-yl radicals.

Along with AIBN, another reducing agent, ascorbic acid was added to the mixture to accelerate the reaction ($[Cu^{II}]_0:[AIBN]_0:[ascorbic\ acid]_0 = 1:10:2$). When the reactions was conducted with corresponding Cu(I) complex, $[Cu^I(ala)(phen)]$ nearly identical yield of polymer was obtained. However, the main advantage of the utilizing Cu(II) complex is the elimination of necessary deoxygenation step. No polymer was isolated in the absence of the L-alanine, indicating that the reaction is highly selective and coordination of the deprotonated amino acid is crucial for the method. Surprisingly, the variety of the deprotonated amino acids successfully generated the same product with slightly different yields 84% (glycine), 72% (phenylalanine) and 63% (proline). After demonstration of successful synthesis, various bidentate aromatic and aliphatic N-based was employed to generate multi-dimensional CuCN polymers in quantative yields.¹²

Traditionally, CuCN polymers are synthesized using solvothermal or hydrothermal method, which require high temperature and pressure for prolonged reactions times. These methods utilized toxic metal salts as precursors and generally results in the formation of several products. In contrast, the direct reduction method is

mild, efficient and applicable to a variety of nitrogen-based ligands to generate multi-dimensional CuCN polymers. A significant effort is required to understand the mechanistic aspects of the direct reduction method. In this chapter, structural investigation of copper(II) complexes with a range of deprotonated amino acid and N-based ligands in the solid state and solution is examined (**Scheme 6.1.2**).

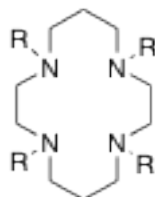
6.2. Results and Discussion

6.2.1. Solid-State Structural Studies of Copper(II) Complexes.

Cu(II) complexes were synthesized by reacting $\text{Cu}^{\text{II}}\text{Cl}_2$ with the stoichiometric amounts of N-based ligands and deprotonated amino acid. Crystals suitable for X-ray analysis were obtained in methanol by slow diffusion of diethyl ether. The molecular structures of the complexes are shown in **Figures 6.2.1-6.2.5** with selected bond distances and angles summarized in **Tables 6.2.1-6.2.3**.

The geometry of pentacoordinated copper(II) complexes is quite varied, ranging from trigonal bipyramidal to square pyramidal. The coordination environment of copper(II) center in these complexes, $[\text{Cu}^{\text{II}}(\text{aa})(\text{NN})\text{Cl}]$, is square pyramidal, where amino acid and bidentate N,N-ligand occupied the equatorial sites and chloride atom coordinated to metal axially. Due to steric constraints caused by these two in-plane ligands, the tetragonal elongation of axial bond was observed, making Cu-Cl bond quite long (**Table 2-4**) in comparison to the copper(II) chloride complexes with nitrogen based complexes.²⁰ However, similar structural characteristic were observed in pentacoordinated Cu(II) center with cyclic tetradentate ligand, 1,4,8,11-

tetraazacyclotetradecane (CYCLAM) and its derivatives (**Scheme 6.2.1**).²¹⁻²⁴ The Cu(II) center coordinated to four nitrogen atoms of the CYCLAM with the fifth site occupied by halogen anion.



Scheme 6.2.1. Schematic representation of CYCLAM and its derivative, where R=H, alkyl and phenyl.

CYCLAM and its derivatives typically enforces the square pyramidal geometry of Cu(II) center and Cu-X (X= Cl, Br) bond lengths were found to be elongated due to steric effects of macrocyclic ligand.²¹⁻²⁴ In copper catalyzed atom transfer radical processes, the Cu^{II}-Br bond length of the catalysts was found to correlated with the deactivation rate constant (k_d) (**Scheme 6.1.1**).²⁵ In the catalytic cycle, the Cu(II) complex reduced to the Cu(I) center along with the deactivation of the radicals with deactivation rate constant (k_d).²⁶⁻²⁸ The complexes with weaker or longer Cu^{II}-Br bond length were found to have low k_d value.^{20, 25} The value of k_d value was $2.0 \times 10^4 \text{ M}^{-1} \text{ s}^{-1}$ in $[\text{Cu}^{\text{II}}(\text{Me}_4\text{CYCLAM})\text{Br}][\text{Br}]$ with the bond distance of $2.8092(6) \text{ \AA}$ (Cu^{II}-Br), which is very low in comparison to active Cu(II) catalysts known in ATRA.²⁹ For instance, tetradentate ligand, tris[2-(dimethylamino)ethyl]amine (Me₆TREN) coordinates to copper(II) center in trigonal bipyramidal fashion with Cu^{II}-Br bond length of $2.393(3) \text{ \AA}$ and has very high k_d value of $1.4 \times 10^7 \text{ M}^{-1} \text{ s}^{-1}$.^{30, 31} However, no direct correlation has been established and k_d value is also dependent on other experimental factors. Based on Cu-Cl bond length, we can assume that these complexes might have lower k_d value and the axial Cu^{II}-X elongation is

predominately observed in square pyramidal complexes.³²⁻³⁴ When the two equivalents of neutral N-based ligands such as 2,2'-bipyridine and 1,10-phenanthroline were complexed to the Cu(II) center in pentacoordinated fashion. These complexes, $[\text{Cu}^{\text{II}}(\text{bpy})_2\text{Cl}][\text{ClO}_4]^{35}$ and $[\text{Cu}^{\text{II}}(\text{phen})_2\text{Cl}][\text{ClO}_4]^{36}$ were found to adopted the trigonal bipyramidal geometry. And, no axial elongation with quite short Cu-Cl bond lengths was not observed (in case of $[\text{Cu}^{\text{II}}(\text{bpy})_2\text{Cl}][\text{ClO}_4]$; Cu-Cl 2.263 Å and $[\text{Cu}^{\text{II}}(\text{phen})_2\text{Cl}][\text{ClO}_4]$; Cu-Cl 2.299 Å).^{35,36}

Glycine Complexes

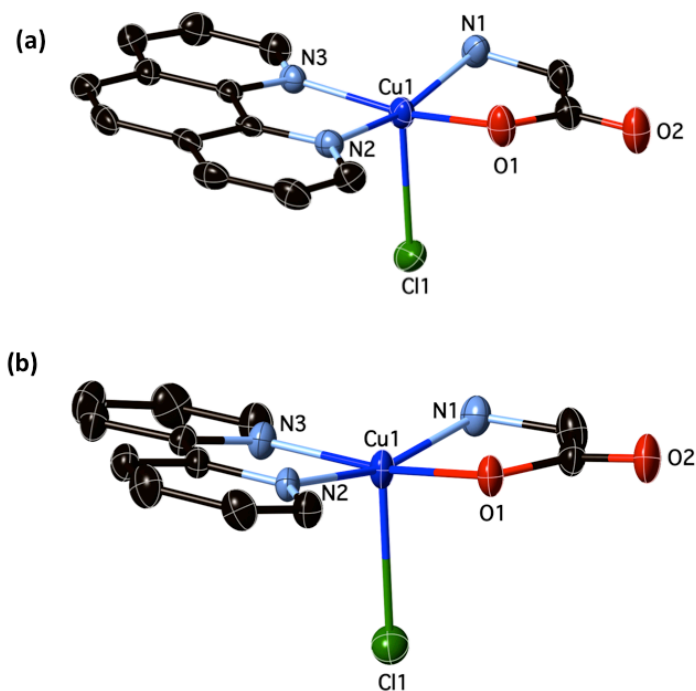


Figure 6.2.1. Molecular structures of a) $[\text{Cu}^{\text{II}}(\text{gly})(\text{phen})\text{Cl}]$ and b) $[\text{Cu}^{\text{II}}(\text{gly})(\text{bpy})\text{Cl}]$ shown with 30% probability displacement ellipsoids. H-atoms have been omitted for clarity.

The copper complexes with glycine, $[\text{Cu}^{\text{II}}(\text{gly})(\text{phen})\text{Cl}]$ and $[\text{Cu}^{\text{II}}(\text{gly})(\text{bpy})\text{Cl}]$, were structurally similar and adopted square pyramidal geometry with the τ value of 0.06

and 0.09, respectively (**Figure 6.2.1**). The Cu1-O1 bond lengths in both the complexes were almost similar. However, other equatorial bond lengths (Cu-N) in complex, [Cu^{II}(gly)(bpy)Cl], were shorter than the corresponding phenanthroline complex (**Table 6.2.1**).

Such equatorial compression resulted in the elongation of axial Cu-Cl bond length by 0.012 Å in bipyridine complex. In comparison to the complexes with alanine, proline and phenylalanine, the Cu-Cl bond lengths were the longest, which can be attributed to the in-plane coordination of the glycine. The bond angles and position of the copper center w.r.t equatorial plane were also found to be quite comparable. In case of [Cu^{II}(gly)(phen)Cl], the copper center lied 0.250 Å below the plane, almost 0.06 Å lower than the bipyridine complex. These complexes were participated intermolecular forces in the crystal lattice. In complex [Cu^{II}(gly)(phen)Cl], significant π - π stacking (3.384 Å) was found along with the H-bonding between the carbonyl oxygen (C=O) and the proton of the primary amine (N-H) of the deprotonated glycine (2.339 Å). In complex, [Cu^{II}(gly)(bpy)Cl], π - π stacking was not observed. However, two molecules of water were crystallized in each unit cell, which formed a complex network via H-bonding between the protons, and the nitrogen of the primary amines and chloride atom. The [Cu^{II}(gly)(bpy)Cl] without any water guest molecule has been reported with no H-bonding.³⁷

Alanine Complexes

Similar to [Cu^{II}(gly)(bpy)Cl], a solvent molecule, methanol was crystallized in the unit cell of the [Cu^{II}(ala)(phen)Cl]. The O-H group of the methanol participated

extensively in the H-bonding with the carbonyl oxygen of the alanine with the distance of (O-H...O(aa)) 2.303 Å (**Figure 6.2.2**).

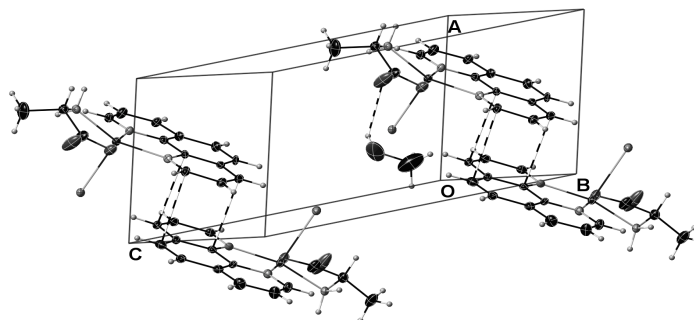


Figure 6.2.2. Crystal lattice of [Cu^{II}(ala)(phen)Cl] shown with 30% probability displacement ellipsoids showing π - π stacking and H-bonding intermolecular interactions.

The π - π stacking with the distance of 3.286 Å was observed between the phenanthroline rings (**Figure 6.2.2**). Apart with H-bonding, [Cu^{II}(ala)(phen)Cl] complex shared many geometrical features with [Cu^{II}(gly)(bpy)Cl]. Selected bond lengths and distances are summarized in **Table 6.2.1**. The Cu1-O1 bond was slightly short (1.926 Å) in comparison to the glycine complexes, leading to significant equatorial compression. The effect of the equatorial compression was clearly reflected on the bond distance between Cu1-Cl1 of 2.592 Å. Such Cu-O shortening distorted the square pyramidal geometry as indicated by the τ value of 0.16. The copper center lies almost 0.248 Å below the least square plane (LSP).

Table 6.2.1. Structural comparison between glycine complexes ([Cu^{II}(gly)(phen)Cl] and [Cu^{II}(gly)(bpy)Cl]) and alanine complexes ([Cu^{II}(ala)(phen)Cl] and [Cu^{II}(ala)(bpy)Cl]).^{a,b}

	[Cu ^{II} (gly)(phen)Cl]	[Cu ^{II} (gly)(bpy)Cl]	[Cu ^{II} (ala)(phen)Cl]	[Cu ^{II} (ala)(bpy)Cl]	
	/	/	/	1	2
Cu1-O1 _{aa}	1.951(2)	1.954(2)	1.926(1)	1.975(3)	1.955 (3)
Cu1-N1 _{aa}	2.016(2)	1.997(3)	2.009(1)	1.967(4)	1.985(4)
Cu1-N2 _{NN}	2.033(2)	1.998(3)	2.025(1)	2.039(4)	2.037(4)
Cu1-N3 _{NN}	2.023(2)	2.010(3)	2.002 (3)	1.978(4)	2.002(4)
Cu1-Cl1	2.579(1)	2.600(1)	2.592(6)	2.495(1)	2.476(1)
Cl1-Cu1-O1	94.92(8)	97.47(8)	95.77(7)	104.43(11)	104.4(1)
Cl1-Cu1-N1	98.99(9)	96.53(10)	101.63(5)	95.54(12)	101.5(1)
O1-Cu1-N1	83.62(9)	84.20(11)	91.95(8)	82.46(14)	83.49(15)
O1-Cu1-N2	167.34(9)	93.33(10)	170.14(8)	156.82(14)	156.34(16)
O1-Cu1-N3	92.72(9)	168.36(11)	84.12(8)	92.29(14)	91.44(14)
N1-Cu1-N2	98.24(9)	162.86(12)	81.79(7)	101.68(15)	99.76(16)
N1-Cu1-N3	163.37(9)	97.88(11)	160.17(8)	171.83(16)	166.6(1)
N2-Cu1-N3	81.92(9)	81.29(11)	99.19(8)	80.74(15)	80.05(1)
τ^c	0.06	0.09	0.16	0.25	0.2

^aBond
^d

lengths are given in angstroms (Å) and angles in degrees (deg). ^b aa = amino acid; NN= nitrogen-based ligand (1,10-phenanthroline or 2,2'-bipyridine) ^c τ parameter is calculated as $\tau = (\phi - \phi')/60$ where ϕ and ϕ' are the largest and second largest N-Cu^{II}-N(Cl) bond angles, $\tau=1$ (regular trigonal bipyramidal geometry) and $\tau=0$ (regular square pyramidal geometry).

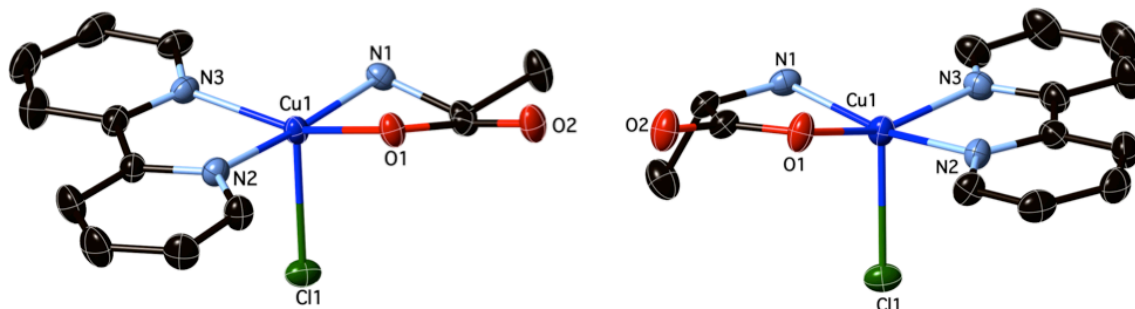


Figure 6.2.3. Molecular structures of $[\text{Cu}^{\text{II}}(\text{ala})(\text{bpy})\text{Cl}]$ shown with 30% probability displacement ellipsoids. H-atoms have been omitted for clarity.

Depending on the orientation of the side group ($\text{R} = -\text{CH}_3$) of alanine in $[\text{Cu}^{\text{II}}(\text{ala})(\text{bpy})\text{Cl}]$, the complex was isolated in two crystallographic distinct Cu(II) centers, **1** (in-plane) and **2** (out-plane) (**Figure 6.2.3**). These two complexes showed different structural features (**Table 6.2.1**). The Cu-Cl bond length in complex **1** was longer (2.495(1)) than in complex **2** (2.476(1)), which might be due to the strain imposed by in-plane methyl group. The lengthening of Cu-Cl bond was also accompanied by the distortion in the geometry of the Cu(II) center, indicated by the τ value of 0.25. The glycine has no substituents and therefore, these complexes tend to have τ value closer to 0 indicating near perfect square pyramidal geometry.

Proline Complexes.

In $[\text{Cu}^{\text{II}}(\text{pro})(\text{phen})\text{Cl}]$ complex, the cyclic ring of the proline was found to impose strain on the copper center and significantly distorted the geometry (**Figure 6.2.4**). The τ value of the complex was found to be 0.42, indicating the geometry is between the square pyramidal and trigonal bipyramidal. However, no such effect was found in bipyridine complex,

[Cu^{II}(pro)(bpy)Cl], where copper center adopted a square pyramidal geometry with the τ value of 0.03.

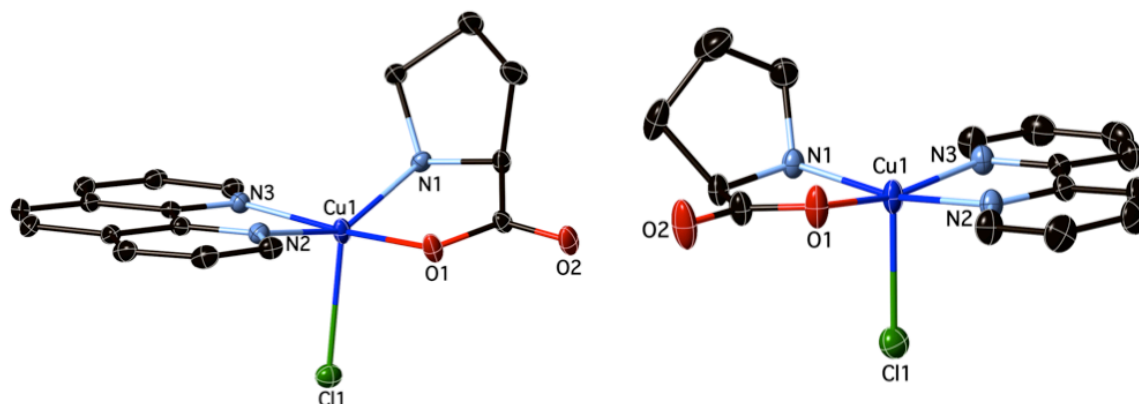


Figure 6.2.4. Molecular structures of [Cu^{II}(pro)(phen)Cl] and [Cu^{II}(pro)(bpy)Cl] shown with 30% probability displacement ellipsoids. H-atoms have been omitted for clarity.

The distortion of the geometry in [Cu^{II}(pro)(phen)Cl] influenced the Cu1-Cl bond length, which was 0.07 Å shorter than [Cu^{II}(pro)(bpy)Cl] complex. The Cu1-N1 bond length was 0.021 Å long in [Cu^{II}(pro)(phen)Cl] complex and copper center was found to be 0.355 Å below the equatorial plane. However, the square pyramid Cu(II) center in bipyridine complex lied 0.288 Å below the LSP. This discrepancy can be attributed to the significant deviation from the square pyramidal geometry of phenanthroline complex. Like other complexes, extensive π - π stacking was observed with the distance of 3.387 Å in [Cu^{II}(pro)(phen)Cl] and 3.332 Å in [Cu^{II}(pro)(bpy)Cl].

Phenylalanine Complexes.

The [Cu^{II}(phe)(phen)Cl] and [Cu^{II}(phe)(bpy)Cl] complexes crystallized in two different crystallographic distinct forms (**1** and **2**), depending on the orientation of the phenyl ring (**Figure 6.2.5, a and b**). In complex **1**, the phenyl ring rotated towards the Cu(II) center, whereas in **2**, the

ring oriented away from metal. This orientation of -R group greatly influenced the structural parameters of these complexes.

(a)

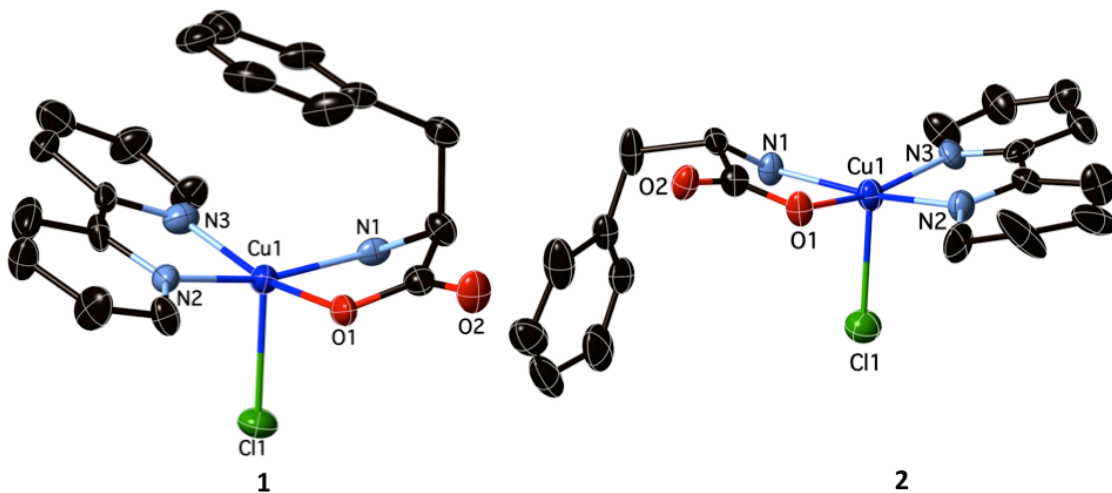
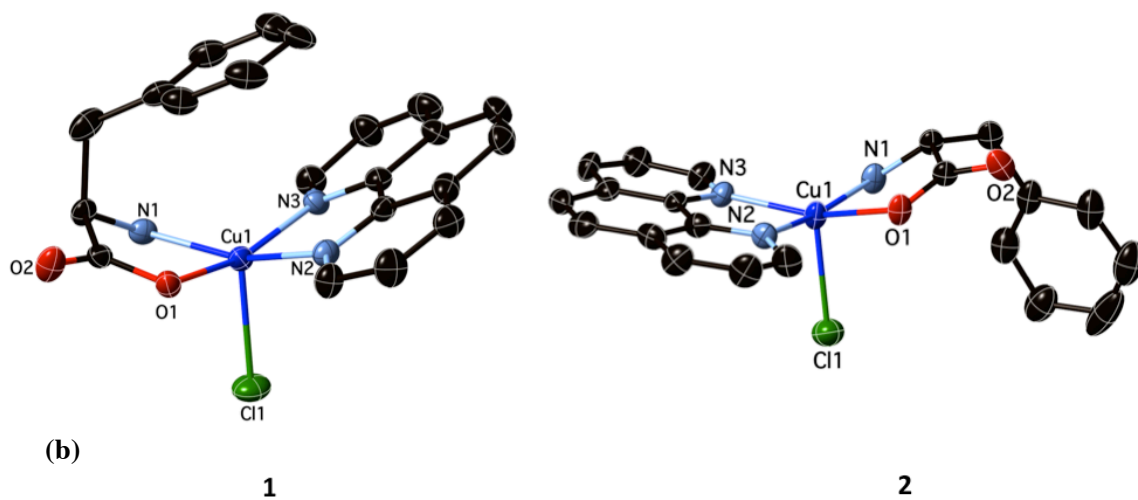


Figure 6.2.5. Molecular structures of (a) [Cu^{II}(phe)(phen)Cl] (b) [Cu^{II}(phe)(bpy)Cl] shown with 30% probability displacement ellipsoids. H-atoms have been omitted for clarity.

Table 6.2.2. Structural comparison between glycine complexes ([Cu^{II}(pro)(phen)Cl] and [Cu^{II}(pro)(bpy)Cl]) and alanine complexes ([Cu^{II}(phe)(phen)Cl](**1,2**) and [Cu^{II}(phe)(bpy)Cl])^{a,b}

	[Cu ^{II} (pro)(phe n)Cl]	[Cu ^{II} (pro)(bpy) Cl]	[Cu ^{II} (phe)(phen)Cl]	[Cu ^{II} (phe)(bpy)Cl]		
	/	/	1	2	1	2
Cu1-O1 _{AA}	1.931(1)	1.946(1)	1.959(3)	1.950(4)	1.885(18)	1.990(18)
Cu1-N1 _{AA}	2.015(2)	1.998(2)	2.033(4)	2.005(4)	2.00(1)	2.01(2)
Cu1-N2 _{NN}	2.019(2)	1.998(2)	2.003(4)	2.030(4)	2.01(3)	2.04(2)
Cu1-N3 _{NN}	2.024(2)	2.029(2)	1.992(4)	1.990(4)	2.08(2)	2.03(2)
Cu1-Cl1	2.464(7)	2.534(1)	2.482(1)	2.566(1)	2.561(7)	2.585(6)
Cl1-Cu1-O1	96.07(7)	101.85(10)	97.89(12)	99.49(14)	101.8(5)	99.9(7)
Cl1-Cu1-N1	89.84(6)	93.76(7)	94.57(13)	89.89(16)	103.4(10)	103.2(9)
O1-Cu1-N1	91.83(8)	85.02(8)	81.95(15)	81.20(16)	91.2(8)	92.2(10)
O1-Cu1-N2	85.40(8)	92.00(9)	90.50(16)	91.94(17)	84.2(7)	82.4(8)
O1-Cu1-N3	171.73(9)	165.04(12)	161.59(16)	161.76(18)	162.0(7)	163.2(9)
N1-Cu1-N2	146.07(9)	167.39(10)	159.77(16)	168.4(2)	172.3(9)	169.6(12)
N1-Cu1-N3	97.01(2)	99.35(9)	100.03(16)	102.29(17)	101.8(5)	101.8(8)
N2-Cu1-N3	81.82(9)	80.61(9)	81.45(16)	81.39(18)	80.9(8)	80.9(9)
τ	0.42	0.03	0.03	0.11	0.01	0.11

^aBond lengths are given in angstroms (Å) and angles in degrees (deg). ^b aa = amino acid; NN= nitrogen-based ligand (1,10-phenanthroline or 2,2'-bipyridine) ^c τ parameter is calculated as $\tau=(\phi - \phi)/60$ where ϕ and ϕ are the largest and second largest N-Cu^{II}-N(Cl) bond angles, $\tau=1$ (regular trigonal bipyramidal geometry) and $\tau=0$ (regular square pyramidal geometry).

The complexes **1** of $[\text{Cu}^{\text{II}}(\text{phe})(\text{phen})\text{Cl}]$ and $[\text{Cu}^{\text{II}}(\text{phe})(\text{bpy})\text{Cl}]$ showed less tetragonal compression in comparison to the isomer **2**. Therefore, Cu1-Cl1 bond length in **1** was 0.084 Å shorter in case of $[\text{Cu}^{\text{II}}(\text{phe})(\text{phen})\text{Cl}]$ and 0.092 Å in $[\text{Cu}^{\text{II}}(\text{phe})(\text{bpy})\text{Cl}]$ than complex, **2**. Such geometrical restraints were also accompanied with the deviation of the geometry from the square pyramidal geometry as indicated by the τ values ($[\text{Cu}^{\text{II}}(\text{phe})(\text{phen})\text{Cl}]$, $\tau = 0.03$ (**1**) and 0.11 (**2**) and $[\text{Cu}^{\text{II}}(\text{phe})(\text{bpy})\text{Cl}]$, $\tau = 0.01$ (**1**) and 0.11 (**2**)). Similar to other complexes, these isomers showed π - π stacking with the distance of 3.398 Å ($[\text{Cu}^{\text{II}}(\text{phe})(\text{phen})\text{Cl}]$) and ($[\text{Cu}^{\text{II}}(\text{phe})(\text{bpy})\text{Cl}]$) between the aromatic rings of phenanthroline and bipyridine. The H-bonding was also found present between N-H...O, with the distance of 3.000 Å in crystal packing diagram. Interestingly, the Cu(II) complexes with non coordinating anion maintained the square pyramidal geometry. The fifth axial site was occupied by the carbonyl oxygen of the other molecule and thus, making a one-dimensional polymer. These complexes were extensively studied and have cytotoxic properties.

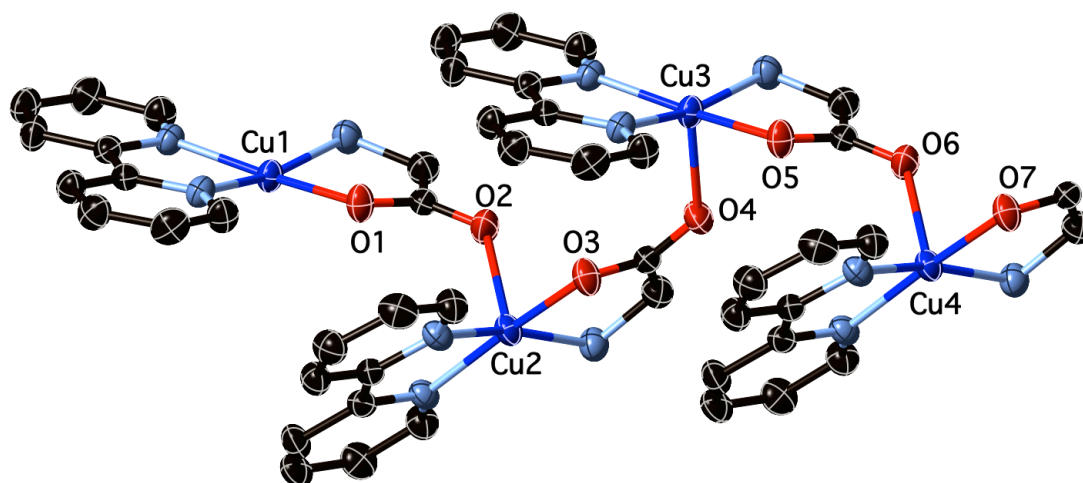


Figure 6.7.6. Molecular structure of $[\text{Cu}^{\text{II}}(\text{gly})(\text{phen})]$ shown with 30% probability displacement ellipsoids. H-atoms and perchlorate counterion have been omitted for clarity.

These complexes were also characterized by IR spectroscopy in the solid state. In [Cu^{II}(aa)(NNCl)] complex, the intensity of N-H stretching decreased upon complexation due to the electron donation to copper center. Other peaks shifted w.r.t pure ligands indicated the formation of Cu(II) complex.

Electrochemistry of the copper complexes

The complexes [Cu^{II}(aa)(NN)Cl], showed irreversible cycles except the proline based complexes in dimethyl sulfoxide (DMSO). The electrochemical data relative to ferrocenium couple is given in **Table 6.2.3**. The cathodic peak observed in all the complexes with the potential ranging from -420 mV to -786 mV, indicating the corresponding Cu(I) was not very stable.

The [Cu^{II}(pro)(phen)Cl] and [Cu^{II}(pro)(bpy)Cl] showed quasi-reversible redox cycle with i_{pa}/i_{pc} of 1.00 at a scan rate of 0.05 V/s with $E_{1/2}$ value of - 0.330 and -0.331 V, respectively (**Figure 6.2.7**). The peak separation (ΔE_p) was observed to be quite large in comparison to the copper(II) based complexes with the neutral nitrogen based ligands. The bipyridine based complexes showed slightly higher cathodic potential (E_c) than phenanthroline-based complexes.

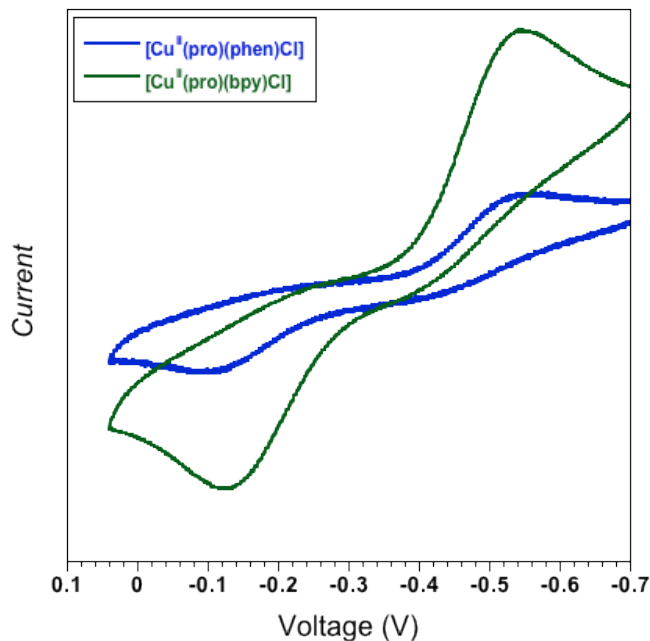


Figure 6.2.7. Cyclic voltammograms of $[\text{Cu}^{\text{II}}(\text{pro})(\text{phen})\text{Cl}]$ and $[\text{Cu}^{\text{II}}(\text{pro})(\text{bpy})\text{Cl}]$ at 25 °C. All measurements were conducted in DMSO with 0.1 M TBABr vs Fc/Fc^+ as a supporting electrolyte at a scan rate of 500 mV/s, $[\text{Cu}^{\text{II}}]_0=1.0$ mM.

Table 6.2.3. Cyclic voltammetry data for in acetonitrile of $[\text{Cu}^{\text{II}}(\text{aa})(\text{NN})\text{Cl}]$ in DMSO.

Complex	$E_c/E_{1/2}$	i_{pa}/i_{pc}	ΔE_p
$[\text{Cu}^{\text{II}}(\text{gly})(\text{phen})\text{Cl}]$	-0.782/-	-	-
$[\text{Cu}^{\text{II}}(\text{gly})(\text{bpy})\text{Cl}]$	-0.799/-	-	-
$[\text{Cu}^{\text{II}}(\text{ala})(\text{phen})\text{Cl}]$	-0.420/-	-	-
$[\text{Cu}^{\text{II}}(\text{ala})(\text{bpy})\text{Cl}]$	-0.573/-	-	-
$[\text{Cu}^{\text{II}}(\text{pro})(\text{phen})\text{Cl}]$	-0.533/-0.330	0.99	0.564
$[\text{Cu}^{\text{II}}(\text{pro})(\text{bpy})\text{Cl}]$	-0.550/-0.331	1.00	0.419
$[\text{Cu}^{\text{II}}(\text{phe})(\text{phen})\text{Cl}]$	-0.616/-	-	-
$[\text{Cu}^{\text{II}}(\text{phe})(\text{bpy})\text{Cl}]$	-0.657/-	-	-

Apart from electrochemical studies, copper(II) complexes were also characterized in solution using UV-Vis spectroscopy (Figure 10). The corresponding λ_{max} and ϵ_{max} values are

summarized in **Table 6.2.4**. The absorption spectra in the visible region for all the copper(II) complexes can be characterized in terms of absorption bands centered between 601-615 nm.

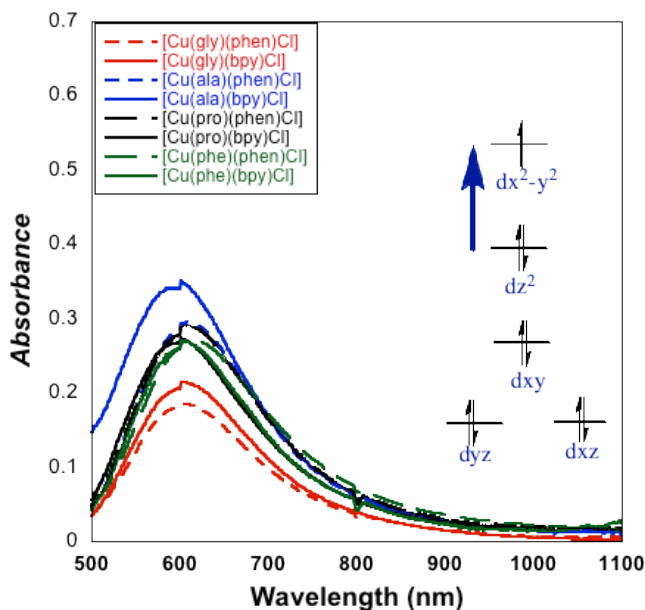


Figure 6.2.8. Absorption spectra of $[\text{Cu}^{\text{II}}(\text{aa})(\text{NN})\text{Cl}]$ complexes in methanol at ambient temperature ($[\text{Cu}^{\text{II}}]_0 = 5.0 \times 10^{-3} \text{ M}$).

This high energy band is generally observed in copper(II) complexes with square bipyramidal or octahedral geometry and corresponds to the transition between d_{z^2} to $d_{x^2-y^2}$, which is caused due to the unusual bite angle of the rigid aromatic amine ligands.^{35, 38, 39} However, the extinction coefficient is quite lower than observed in $[\text{CuN}_4\text{X}]^+$ ($\text{X}=\text{Br}$ or Cl) chromophores.^{19, 25,}
²⁶ Based on UV-Vis studies, the solutions structures of copper(II) complexes are consistent with the solid-state discussed in the previous section.

Table 6.2.4. Summary of λ_{\max} and ϵ_{\max} values in methanol for $[\text{Cu}^{\text{II}}(\text{aa})(\text{NN})\text{Cl}]$ complex.

Complex	ϵ	λ_{\max}
$[\text{Cu}^{\text{II}}(\text{gly})(\text{phen})\text{Cl}]$	43	603
$[\text{Cu}^{\text{II}}(\text{gly})(\text{bpy})\text{Cl}]$	36.5	605
$[\text{Cu}^{\text{II}}(\text{ala})(\text{phen})\text{Cl}]$	48.6	608
$[\text{Cu}^{\text{II}}(\text{ala})(\text{bpy})\text{Cl}]$	54	601
$[\text{Cu}^{\text{II}}(\text{pro})(\text{phen})\text{Cl}]$	44.5	605
$[\text{Cu}^{\text{II}}(\text{pro})(\text{bpy})\text{Cl}]$	53	601
$[\text{Cu}^{\text{II}}(\text{phe})(\text{phen})\text{Cl}]$	59	615
$[\text{Cu}^{\text{II}}(\text{phe})(\text{bpy})\text{Cl}]$	57.5	603

Effect of Amino Acids on the structure of Copper(II) Complexes

The solution and solid state structure of $[\text{Cu}^{\text{II}}(\text{aa})(\text{NN})\text{Cl}]$ showed very unique structural features in comparison to $[\text{CuN}_4]^{2+}$ complexes.^{19, 25, 26} We observed that the oxygen based monoanionic ligands strongly influenced the bonding and geometry of the Cu(II) centers in $[\text{CuN}_3\text{O}]^+$ complexes. On the contrary to the complexes with bidentate neutral N-based ligands, Cu(II) centers adopted the square pyramidal geometry. The shortening of Cu1-O1_{aa} bond length was expected due to the ionic nature of the bonding. However, the Cu1-N_{aa}/Cu1-N_{NN} showed significant compression of the core and elongation of the axial Cu-Cl bond length. Similar features were observed in the copper (II) complexes with sterically encumbered macrocyclic ligand, CYCLAM. The weak/longer Cu-Cl bond length in these complexes would result in the rapid reduction of Cu(II) to Cu(I) complex in the presence of reducing agent. This fact was further supported by the instantaneous color change from blue (Cu(II)) to red Cu(I) on addition of ascorbic acid under direct reduction condition. The electrochemical studies showed irreversible cycle with no anodic electrochemical peak indicating that the corresponding Cu(I) complexes, $[\text{Cu}^{\text{I}}(\text{aa})(\text{NN})]$ are unstable in nature. Several attempts to isolate Cu(I) species have failed so far and no structure has been reported in the literature. Therefore, more mechanistic studies are required in order to understand the mechanism of direct reduction method. The side

group(-R) of the amino acid was also found to influence the geometry of the Cu(II) center. The in-plane orientation of R w.r.t Cu(II) center increased the tetragonal distortion and thus, distorted the geometry of the complex in comparison to out of plane orientation of substituent.

6.3. Conclusion

In summary, synthesis, characterization and electrochemical studies of copper(II) complexes with amino acids and neutral N-based ligands were reported. In the solid state, these complexes showed square pyramidal geometry and participated in various intermolecular forces such as H-bonding and π - π stacking. However, the $[\text{Cu}^{\text{II}}(\text{pro})(\text{phen})\text{Cl}]$ showed large deviation in geometry as indicated by the tau value of 0.49. Such deviation from the perfect geometry greatly influenced other structural features such as bond shortening of Cu-Cl and small compression of the copper core was observed. Interestingly, the orientation of the R group in case of $[\text{Cu}^{\text{II}}(\text{ala})(\text{bpy})\text{Cl}]$, $[\text{Cu}^{\text{II}}(\text{phe})(\text{phen})\text{Cl}]$ and $[\text{Cu}^{\text{II}}(\text{phe})(\text{bpy})\text{Cl}]$ complexes, two distinct crystallographic Cu(II) centers were isolated. In solution state, UV-Vis spectroscopy supported the square pyramidal geometry of these complexes in the methanol. The proline based ($[\text{Cu}^{\text{II}}(\text{pro})(\text{phen})\text{Cl}]$ and $[\text{Cu}^{\text{II}}(\text{pro})(\text{bpy})\text{Cl}]$) complexes were able to show quasi-reversible cycles whereas other complexes showed an irreversible reduction cycle w.r.t Fc/Fc⁺ couple. The bipyridine complexes showed slightly higher cathodic potential (E_c) than the phenanthroline-based complexes. However, no distinct trend was observed in the electrochemical studies. During ATRA reactions, these complexes unexpectedly yielded Cu(I) cyanide coordination polymer in quantitative yields via activation of the nitrile bond of the reducing agent, AIBN. This synthetic route, also known as direct reduction method, was found to be applicable to various N-based ligands and generated multi-dimensional CuCN frameworks in excellent yields.

6.5. Experimental Part

General Procedures – All chemicals were purchased from the commercial sources and used as received. Copper(II) complexes were synthesized according to the published procedure under ambient conditions

Instrumentation.

UV-Vis spectroscopy - UV-vis spectra were recorded using Beckman DU-530 spectro- meter

IR spectroscopy - IR spectra were recorded in the solid state using Nicolet Smart Orbit 380 FT-IR spectrometer (Thermo Electron Corporation).

Elemental Analysis for C, H, and N - Elemental analyses for C, H, and N were obtained from Midwest Microlabs, LLC and Robertson Microlabs, NJ.

X-ray Crystal Structure Determination- The X-ray intensity data was collected at 150 K using graphite-monochromated Mo-K radiation (0.71073 Å) with a Bruker Smart Apex II CCD diffractometer. Data reduction included absorption corrections by the multi-scan method using SADABS.⁴⁰ Structures were solved by direct methods and refined by full matrix least squares using SHELXTL 6.1 bundled software package.⁴¹ The H-atoms were positioned geometrically (aromatic C-H 0.93, methylene C-H 0.97, and methyl C-H 0.96) and treated as riding atoms during subsequent refinement, with $U_{iso}(\text{H}) = 1.2U_{eq}(\text{C})$ or $1.5U_{eq}(\text{methyl C})$. The methyl groups were allowed to rotate about their local threefold axes. Crystal Maker 8.3 was used to generate molecular graphics. For detailed crystallographic data tables refer to supporting information.

Cyclic voltammetry - Electrochemical measurements were carried out using Bioanalytical Systems (BAS) model CV-50W in a dry box. Cyclic voltammograms were recorded with a standard three-electrode system consisting of a Pt-wire working electrode, a standard calomel reference electrode, and a Pt-wire auxiliary electrode. Tetrabutylammonium perchlorate (TBA-ClO₄) and tetrabutylammonium chloride (TBA-Cl) were used as the supporting electrolyte, and all voltammograms were externally referenced to ferrocene. As such, the potentials are reported with respect to Fc/Fc⁺ couple, without junction correction. All cyclic voltammograms were simulated digitally to obtain the half-wave potentials.

Synthesis of [Cu^{II}(aa)(NN)Cl] (aa=deprotonated amino acid, NN=bidentate N-based ligand) complexes.

[Cu^{II}(ala)(phen)Cl]. The stoichiometric amounts of sodium hydroxide (1.00 mmol, 0.0400 g) and *L*-alanine (1.00 mmol, 0.0891 g) were dissolved in 4.0 mL of methanol and stirred at ambient temperature for 1 h. Sodium salt of *L*-alanine was then added dropwise to Cu^{II}Cl₂ (1.00 mmol, 0.134 g) dissolved in 2.0 mL of methanol. After stirring for 10 min, sodium chloride was removed by filtration. The nitrogen based ligand, 1,10-phenanthroline (1.00 mmol, phen=0.180 g) dissolved in 2.0 mL of methanol was then added dropwise to the resulting solution. The final product was precipitated by the addition of 20 mL of diethyl ether, filtered, washed with diethyl ether and dried under vacuum to yield [Cu^{II}(ala)(phen)Cl]. Yield=0.236g (68 %). UV-Vis (CH₃OH): λ_{max} = 608 nm, ϵ_{max} = 48.6 Lmol⁻¹cm⁻¹. FT-IR (solid): ν (cm⁻¹), 3205m, 3118m, 3038w, 1659s, 1519m, 1431m, 1382m, 1347m, 1279 m, 1183 m, 1142w, 854s, 732s, 563w. Anal. Calcd. for C₁₅H₁₄ClCuN₃O₂ (347.29): C,49.05; H, 3.84; N, 11.44; Found: C, 48.65; H, 3.84 ; N,

11.30.

[Cu^{II}(ala)(bpy)Cl]. The complex was prepared using the similar procedure used for [Cu^{II}(ala)(phen)Cl]. Yield=0.253 g (73%). UV-Vis (CH₃OH): λ_{max} = 601 nm, ϵ_{max} = 78 Lmol⁻¹cm⁻¹. FT-IR (solid): ν (cm⁻¹), 3272m, 3194w, 3110s, 3019w, 1634s, 1389s, 1289s, 1244s, 1187m, 1120m 856m, 832m, 677w, 564m, 519s. Anal. Calcd. for C₁₃H₁₉ClCuN₃O₂ (347.29): C,43.26; H, 4.46; N, 11.63; Found: C, 43.54 ; H, 3.85; N,10.91.

[Cu^{II}(gly)(phen)Cl]. The complex was prepared using the similar procedure used for [Cu^{II}(ala)(phen)Cl]. Yield= (72%). UV-Vis (CH₃OH): λ_{max} = 603 nm, ϵ_{max} = 43 Lmol⁻¹cm⁻¹. FT-IR (solid): ν (cm⁻¹), 3272m, 3192w, 3109s, 3017w, 1634s, 1555w, 1492w, 1448w, 1389s, 1289m, 1186m, 1119m, 1025s, 920m, 856m, 831m, 675w, 563w, 469w, 431w. Anal. Calcd. for C₁₄H₁₄ClCuN₃O₃ (353.26): C, 45.29; H, 3.80; N, 11.32; Found C, 45.61; H, 3.52 ; N, 11.23.

[Cu^{II}(gly)(bpy)Cl]. The complex was prepared using the similar procedure used for [Cu^{II}(ala)(phen)Cl]. Yield= (78%). UV-Vis (CH₃OH): λ_{max} = 605 nm, ϵ_{max} = 36.5 Lmol⁻¹cm⁻¹. FT-IR (solid): ν (cm⁻¹), 3234m, 3200w, 2051m, 2029s, 2008m, 1641s, 1602s, 1434w, 1320s, 1135, 1389s, 1242m, 782m, 669w, 545w, 421w, 418w. Anal. Calcd. for C₁₂H₁₂ClCuN₃O₂ (329.24): C, 43.78; H, 3.67;N, 12.76; Found C, ; H, ; N, .

[Cu^{II}(pro)(phen)Cl]. The complex was prepared using the similar procedure used for [Cu^{II}(ala)(phen)Cl]. Yield=0.322g (82%). UV-Vis (CH₃OH): λ_{max} = 605 nm, ϵ_{max} = 44.5 Lmol⁻¹cm⁻¹. FT-IR (solid): ν (cm⁻¹), 3425m, 3170w, 2982s, 2876w, 1649s, 1561s, 1425s, 1369s, 1141m,

1074m, 928m, 850s, 722s, 645m, 461s. Anal. Calcd. for $C_{17}H_{16}ClCuN_3O_2$ (393.32): C, 51.91; H, 4.10; N, 10.68; Found: C,47.20 ; H, 4.42; N,10.29 .

[Cu^{II}(pro)(bpy)Cl]. The complex was prepared using the similar procedure used for [Cu^{II}(ala)(phen)Cl]. Yield= 0.291g (79%). UV-Vis (CH₃OH): λ_{max} = 601 nm, ϵ_{max} = 53 Lmol⁻¹cm⁻¹. The complex was prepared using the procedure for [Cu^{II}(ala)(phen)Cl] FT-IR (solid): ν (cm⁻¹), 3233m, 3060w, 2978s, 2944w, 1621s, 1475s, 1447s, 1369s, 1315m, 1047m, 921m, 852s, 782s, 692m, 520m. Anal. Calcd. for $C_{15}H_{16}ClCuN_3O_2$ (369.30): C, 48.78; H, 4.37; N, 11.38; Found: C,47.41; H, 3.91; N,11.45.

[Cu^{II}(phe)(phen)Cl]. The complex was prepared using the similar procedure used for [Cu^{II}(ala)(phen)Cl]. Yield= 0.332g (75%). UV-Vis (CH₃OH): λ_{max} = 615 nm, ϵ_{max} = 59 Lmol⁻¹cm⁻¹. FT-IR (solid): ν (cm⁻¹), 3450m, 3223w, 3116s, 1610s, 1519(w), 1454(w), 1430(s), 1398(s), 1324 (s), 1107 (s), 875 (s), 852 (s), 720(s) , 641m, 598w. $C_{21}H_{18}ClCuN_3O_2$ (443.38) C, 57.89; H, 4.09; N, 9.48; Found: C, 59.02; H, 4.00; N, 9.14.

[Cu^{II}(phe)(bpy)Cl]. The complex was prepared using the similar procedure used for [Cu^{II}(ala)(phen)Cl]. Yield= 0.331g (79%). UV-Vis (CH₃OH): λ_{max} = 603 nm, ϵ_{max} = 57.5 Lmol⁻¹cm⁻¹. FT-IR (solid): ν (cm⁻¹) 3228(w), 3130(w), 3023 (s), 2920(w) 1621 (s), 1494(w), 1474(w), 1441(s), 1391 (s), 1315 (s), 1123 (s), 772 (s), 697 (s), 600 (s) Anal. Calcd. for $C_{19}H_{18}ClCuN_3O_2$ (419.36) C, 54.42; H, 4.33; N, 10.02; Found C, 54.68 ; H, 4.18 ; N, 8.99.

Reference

1. Cusanovich, M. A.; Meyer, T. E., Heme Proteins; . *Elsevier* **1988**, 4.
2. Adman, E. T., A comparison of the structures of electron transfer proteins. (0006-3002).
3. Bertrand, P.; Mbarki, O.; Asso, M.; Blanchard, L.; Guerlesquin, F.; Tegoni, M., Control of the redox potential in c-type cytochromes: importance of the entropic contribution. *Biochemistry* **1995**, 34, (35), 11071-11079.
4. Liu, J.; Chakraborty, S.; Hosseinzadeh, P.; Yu, Y.; Tian, S.; Petrik, I.; Bhagi, A.; Lu, Y., Metalloproteins Containing Cytochrome, Iron-Sulfur, or Copper Redox Centers. *Chemical Reviews* **2014**, 114, (8), 4366-4469.
5. Chamorovsky, S. K.; Zakharova, N. I.; Remennikov, S. M.; Sabo, Y.; Rubin, A. B., The cytochrome subunit structure in the photosynthetic reaction center of *Chromatium minutissimum*. *FEBS Letters* **1998**, 422, (2), 231-234.
6. Malkin, R.; Rabinowitz, J. C., Nonheme iron electron-transfer proteins. (1545-4509).
7. Bowler, B. E.; Raphael, A. L.; Gray, H. B., Long-Range Electron Transfer in Donor(Spacer)Acceptor Molecules and Proteins. *Prog. Inorg. Chem* **1990**, 38.
8. Blondin, G.; Girerd, J. J., Interplay of electron exchange and electron transfer in metal polynuclear complexes in proteins or chemical models. *Chemical Reviews* **1990**, 90, (8), 1359-1376.
9. Malmstrom, B. G.; Wittung-Stafshede, P., Effects of protein folding on metalloprotein redox-active sites; electron-transfer properties of blue and purple copper proteins. **1999**, 185, 127-140.
10. Cordes, M.; Giese, B., Electron transfer in peptides and proteins. (0306-0012).
11. Wherland, S.; Gray, H. B., In Biological Aspects of Inorganic Chemistry; . *Dolphin, D., Ed.; John Wiley: New York*, **1977**.

12. Kaur, A.; Pintauer, T., Copper(I)–Cyanide Frameworks through Thermal or Photodecomposition of the Free Radical Diazo Initiator AIBN. *European Journal of Inorganic Chemistry* **2013**, 2013, (19), 3297-3301.
13. Eckenhoff, W. T.; Garrity, S. T.; Pintauer, T., Highly Efficient Copper-Mediated Atom Transfer Radical Addition (ATRA) in the Presence of a Reducing Agent. *Eur. J. Inorg. Chem.* **2008**, 2008, (4), 563-571.
14. Eckenhoff, W. T.; Pintauer, T., Atom Transfer Radical Addition in the Presence of Catalytic Amounts of Copper(I/II) Complexes with Tris(2-pyridylmethyl)amine *Inorg. Chem.* **2007**, 46, (15), 5844-5846.
15. Pintauer, T., "Greening" of copper catalyzed atom transfer radical addition (ATRA) and cyclization (ATRC) reactions. *ACS Symposium Series* **2009**, 1023, 63-84.
16. Pintauer, T., Catalyst Regeneration in Transition-Metal-Mediated Atom-Transfer Radical Addition (ATRA) and Cyclization (ATRC) Reactions *Eur. J. Inorg. Chem.* **2010**, 17, 2449-2460.
17. Pintauer, T.; Matyjaszewski, K., Atom transfer radical addition and polymerization reactions catalyzed by ppm amounts of copper complexes. *Chem. Soc. Rev.* **2008**, 37, (6), 1087-1097.
18. Ricardo, C.; Pintauer, T., Copper catalyzed atom transfer radical cascade reactions in the presence of free-radical diazo initiators as reducing agents. *Chem. Comm.* **2009**, 21, 3029-3031.
19. Pintauer, T.; McKenzie, B.; Matyjaszewski, K., Toward structural and mechanistic understanding of transition metal-catalyzed atom transfer radical processes. *ACS Symp. Ser.* **2003**, 854, 130-147.
20. Eckenhoff, W. T.; Pintauer, T., Copper Catalyzed Atom Transfer Radical Addition (ATRA) and Cyclization (ATRC) Reactions in the Presence of Reducing Agents. *Cat. Rev. Sci. Eng.* **2009**, 51, 1-59.
21. Donnelly, P. S.; Harrowfield, J. M.; Skelton, B. W.; White, A. H., Carboxymethylated Cage Amines: Coordination and Lactamization. *Inorganic Chemistry* **2001**, 40, (22), 5645-5652.
22. Bernhardt, P. V.; Sharpe, P. C., New Stereoselective Routes to Macrocyclic Ligands. *Inorganic Chemistry* **1998**, 37, (7), 1629-1636.

23. Khan, A.; Silversides, J. D.; Madden, L.; Greenman, J.; Archibald, S. J., Fluorescent CXCR4 chemokine receptor antagonists: metal activated binding. *Chem. Comm.* **2007**, 0, 416-418.

24. Bernhardt, P. V., N-methylation of diamino-substituted macrocyclic complexes: intermolecular reactions. *Journal of the Chemical Society, Dalton Transactions* **1996**, (23), 4319-4324.

25. Pintauer, T.; Matyjaszewski, K., Structural Aspects of Copper Catalyzed Atom Transfer Radical Polymerization. *Coord. Chem. Rev.* **2005**, 249, (11-12), 1155-1184.

26. Balili, M. N. C.; Pintauer, T., Kinetic Studies of the Initiation Step in Copper Catalyzed Atom Transfer Radical Addition (ATRA) in the Presence of Free Radical Diazo Initiators as Reducing Agents *Inorg. Chem.* **2010**, 49, (12), 5642-5649.

27. Matyjaszewski, K., From Atom Transfer Radical Addition to Atom Transfer Radical Polymerization. *Curr. Org. Chem.* **2002**, 6, (2), 67-82.

28. Pintauer, T.; Matyjaszewski, K., Structural and Mechanistic Aspects of Copper Catalyzed Atom Transfer Radical Polymerization. *Top. Organomet. Chem.* **2009**, 26, 221-251.

29. Gromada, J.; Matyjaszewski, K., Measurement of Initial Degree of Polymerization without Reactivation as a New Method To Estimate Rate Constants of Deactivation in ATRP *Macromolecules* **2002**, 35, 6167-6173.

30. Matyjaszewski, K.; Paik, H.; Zhou, P.; Diamanti, S. J., Determination of Activation and Deactivation Rate Constants of Model Compounds in Atom Transfer Radical Polymerization. *Macromolecules* **2001**, 34, (15), 5125-5131.

31. Eckenhoff, W. T.; Pintauer, T., Atom transfer radical addition (ATRA) catalyzed by copper complexes with tris[2-(dimethylamino)ethyl]amine (Me6TREN) ligand in the presence of free-radical diazo initiator AIBN. *Dalton Transactions* **2011**, 40, (18), 4909-4917.

32. Balili, M. N. C.; Pintauer, T., Persistent Radical Effect in Action: Kinetic Studies of Copper-Catalyzed Atom Transfer Radical Addition in the Presence of Free-Radical Diazo Initiators as Reducing Agents. *Inorg. Chem.* **2009**, 48, (18), 9018-9026.

33. Pintauer, T.; Braunecker, W. A.; Collange, E.; Poli, R.; Matyjaszewski, K., Determination of Rate Constants for the Activation Step in Atom Transfer Radical Polymerization Using the Stopped-Flow Technique. *Macromolecules* **2004**, *37*, 2679-2682.
34. Pintauer, T.; Zhou, P.; Matyjaszewski, K., General Method for Determination of the Activation, Deactivation, and Initiation Rate Constants in Transition Metal Catalyzed Atom Transfer Radical Processes. *J. Am. Chem. Soc.* **2002**, *124*, 8196-8197.
35. Harrison, W. D.; Kennedy, D. M.; Power, M.; Sheahan, R.; Hathaway, B. J., *Dalton Transactions* **1981**, 1556.
36. Boys, D.; Escobar, C.; Martinez-Carrera, S., The structure of chlorobis(1,10-phenanthroline)copper(II) perchlorate. *Acta Crystallographica Section B* **1981**, *37*, (2), 7408.
37. Mohamed, M. S.; Shoukry Fau Ali, A. G.; Ali, A. G., Synthesis and structural characterization of ternary Cu (II) complexes of glycine with 2,2'-bipyridine and 2,2'-dipyridylamine. The DNA-binding studies and biological activity. (1873-3557).
38. Foley, J.; Tyagi, S.; Hathaway, B. J., Crystal Structure of [CuI(bpy)₂][PF₆]. *J. Chem. Soc., Dalton Trans.* **1984**, 1-5.
39. Hathaway, B. J., Copper. *Coordination Chemistry Reviews* **1981**, *35*, (0), 211-252.
40. Sheldrick, G. M., *SADABS Version 2.03*. University of Gottingen: Germany, 2002.
41. Sheldrick, G. M., *SHELXTL 6.1, Crystallographic Computing System*. Bruker Analytical X-Ray System: Madison, WI, 2000.

Appendix A

A.1. Crystallographic Tables

Table A.1.1 Crystallographic data for [Cu^I(TPMA^{*1})Br] and [Cu^I(TPMA^{*2})Br].

	[Cu ^I (TPMA ^{*1})Br]	[Cu ^I (TPMA ^{*2})Br]
Formula	C ₂₁ H ₂₄ BrCuN ₄ O	C ₂₄ H ₃₀ BrCuN ₄ O ₂
Color	Yellow	Orange
Shape	Plate	Rod
Formula Weight	491.89	549.97
Crystal System	Triclinic	Monoclinic
Space Group	P-1	Cc
Temp (K)	150	150
Cell Constants		
a, Å	9.8318 (14)	8.3336 (2)
b, Å	10.1915 (12)	21.0561 (5)
c, Å	11.5258 (14)	14.0166 (3)
α, deg	108.248 (9)	90
β, deg	102.053 (9)	100.040 (1)
γ, deg	101.989 (9)	90
V, Å ³	1025.2 (2)	2421.87 (10)
Formula units/unit cell	2	4
D _{cal'd} , gcm ⁻³	1.594	1.517
Absorption coefficient, mm ⁻¹	3.03	2.58
F(000)	588	1164
Diffractometer	Bruker Smart ApexII	Bruker Smart ApexII
Radiation, graphite monochr.	Mo Kλ (λ = 0.71073 Å)	Mo Kλ (λ = 0.71073 Å)
Crystal size, mm	0.22 × 0.10 × 0.03	0.81 × 0.12 × 0.12
θ range, deg	2.4 < θ < 32.50	1.9 < θ < 31.31
Range of h,k,l	±11, ±11, ±30	±12, ±31, ±20
Reflections collected/unique	10829/3394	20434/7836
Refinement Method	multi-scan	multi-scan
Data/Restraints/Parameters	3395/0/256	7836/2/295
GOF on F ₂	0.87	0.57
R _{int}	0.078	0.028
Final R indices [I > 2σ(I)]	0.048	0.025
R indices (all data)	0.150	0.079
Max. Resid. Peaks (e ⁻ Å ⁻³)	0.55 and -0.59	0.34 and -0.39

Table A.2.2 Crystallographic data for [Cu^I(TPMA^{*3})Br] and [Cu^{II}(TPMA^{*1})Br][Br].

	[Cu ^I (TPMA ^{*3})Br]	[Cu ^{II} (TPMA ^{*1})Br][Br]
Formula	C ₂₇ H ₃₆ BrCuN ₄ O ₃	C ₂₁ H ₂₄ BrCuN ₄ O·Br
Color	Brown	Green
Shape	Cubic	Cubic
Formula Weight	608.05	571.79
Crystal System	Monoclinic	Monoclinic
Space Group	P2 ₁ /n	P2 ₁ /c
Temp (K)	150	150
Cell Constants		
a, Å	8.3019 (2)	15.2862 (4)
b, Å	21.5474 (5)	9.7907 (2)
c, Å	16.0245 (4)	16.3026 (4)
α, deg	90	90
β, deg	104.688 (2)	104.372 (1)
γ, deg	90	90
V, Å ³	2772.86 (12)	2363.53 (10)
Formula units/unit cell	4	4
D _{cal'd} , gcm ⁻³	1.457	1.607
Absorption coefficient, mm ⁻¹	2.26	4.32
F(000)	1256	1140
Diffractometer	Bruker Smart ApexII	Bruker Smart ApexII
Radiation, graphite monochr.	Mo Kλ(λ =0.71073 Å)	Mo Kλ (λ =0.71073 Å)
Crystal size, mm	0.21 × 0.07 × 0.05	0.51 × 0.08 × 0.06
θ range, deg	2.3 < θ < 26.5	2.5 < θ < 27.7
Range of h,k,l	±10, ±27, ±20	±21, ±19, ±12
Reflections collected/unique	29684/5297	32121/5540
Refinement Method	multi-scan	multi-scan
Data/Restraints/Parameters	5297/0/334	5540/0/265
GOF on F ₂	0.61	0.83
R _{int}	0.071	0.029
Final R indices [I>2σ(I)]	0.036	0.028
R indices (all data)	0.115	0.105
Max. Resid. Peaks (e ⁻ ·Å ⁻³)	0.39 and -0.31	1.19 and -0.59

Table A.2.3 Crystallographic data for [Cu^{II}(TPMA^{*2})Br][Br] and [Cu^{II}(TPMA^{*3})Br][Br].

	[Cu ^{II} (TPMA ^{*2})Br][Br]	[Cu ^{II} (TPMA ^{*3})Br][Br]
Formula	C ₂₄ H ₃₀ BrCuN ₄ O ₂ ·Br	C ₂₇ H ₃₆ BrCuN ₄ O ₃ ·Br
Color	Green	Green
Shape	Cubic	Cubic
Formula Weight	629.87	687.95
Crystal System	Monoclinic	Triclinic
Space Group	Pc	P-1
Temp (K)	150	150
Cell Constants		
a, Å	16.4808 (3)	14.8434 (4)
b, Å	8.8546 (1)	16.5774 (5)
c, Å	18.6534 (3)	17.2306 (5)
α, deg	90	115.218 (2)
β, deg	98.448 (1)	111.733 (2)
γ, deg	90	94.596 (2)
V, Å ³	2692.57 (7)	3417.37 (17)
Formula units/unit cell	4	4
D _{cal'd} , gcm ⁻³	1.554	1.337
Absorption coefficient, mm ⁻¹	3.81	3.01
F(000)	976	2040
Diffractometer	Bruker Smart ApexII	Bruker Smart ApexII
Radiation, graphite monochr.	Mo Kλ (λ =0.71073 Å)	Mo Kλ (λ =0.71073 Å)
Crystal size, mm	0.37 × 0.34 × 0.27	0.35 × 0.09 × 0.05
θ range, deg	2.2 < θ < 33.3	1.5 < θ < 25.1
Range of h,k,l	±24, ±12, ±27	±21, ±19, ±12
Reflections collected/unique	45615/17287	39285/9706
Refinement Method	multi-scan	multi-scan
Data/Restraints/Parameters	17287/2/607	12114/0/685
GOF on F ₂	1.06	0.96
R _{int}	0.028	0.034
Final R indices [I > 2σ(I)]	0.057	0.037
R indices (all data)	0.175	0.133
Max. Resid. Peaks (e ⁻ ·Å ⁻³)	5.54 and -0.74	1.15 and -0.65

A.2. FT-IR Spectroscopy

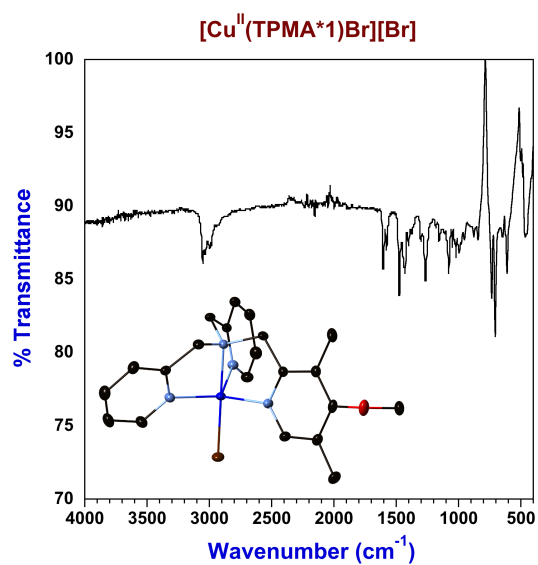


Figure S11. Solid state ATR FT-IR of $[\text{Cu}^{\text{II}}(\text{TPMA}^{\ast 1})\text{Br}][\text{Br}]$.

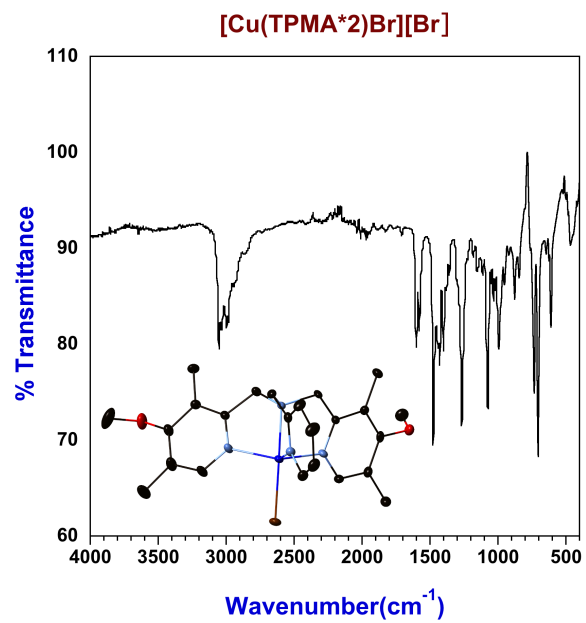


Figure S2. Solid state ATR FT-IR of [Cu^{II}(TPMA*₂)Br][Br].

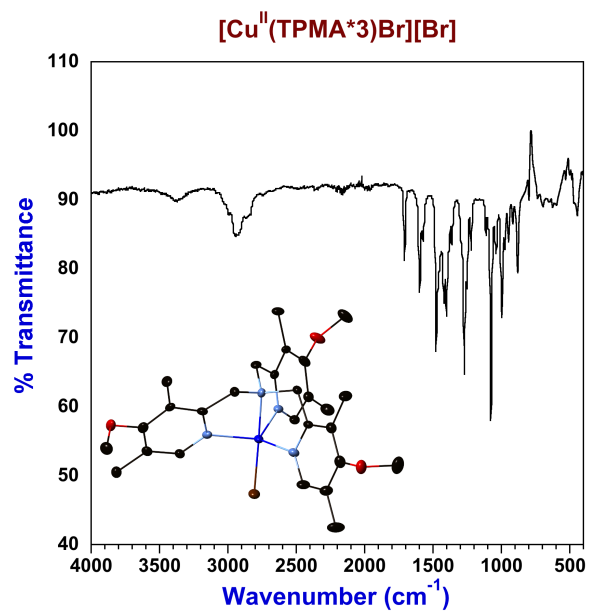


Figure S3. Solid state ATR FT-IR of [Cu^{II}(TPMA*3)Br][Br].

A.3. Ligand and Complex Characterization

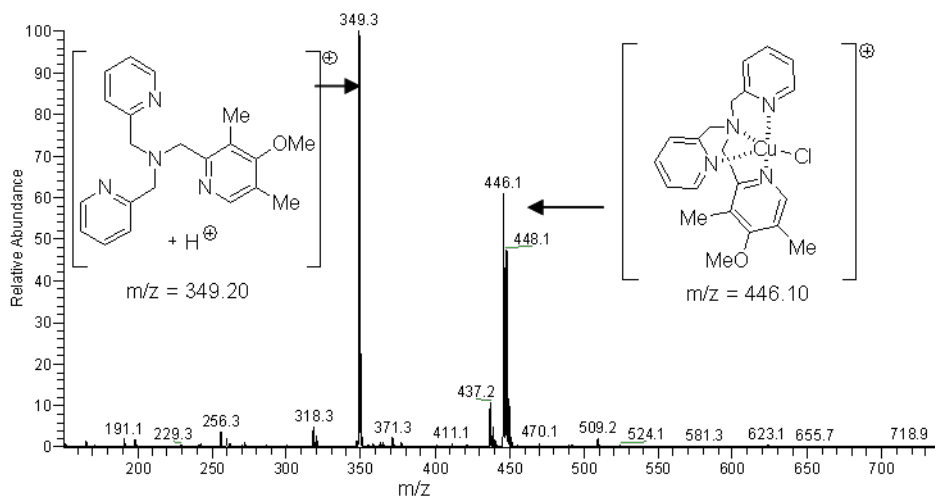


Figure A.3.1 ESI-MS spectra of $[\text{Cu}^{\text{II}}(\text{TPMA}^*1)\text{Cl}][\text{Cl}] = 1:2$ in MeCN.

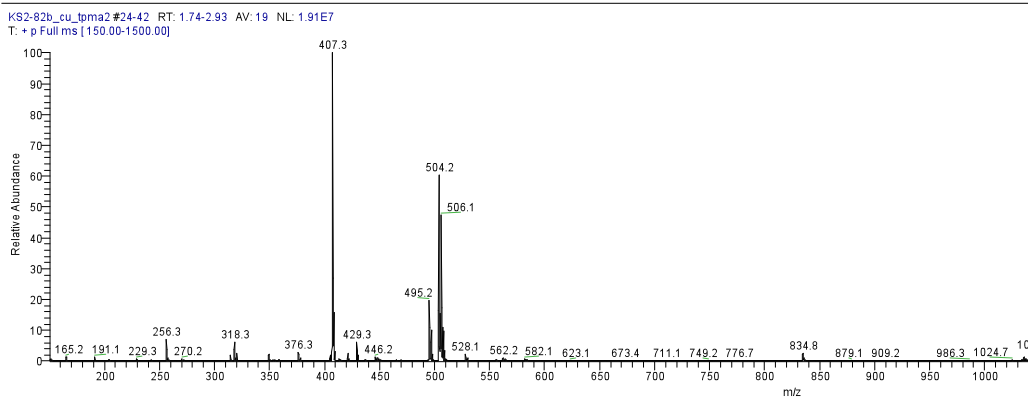


Figure A.3.2. ESI-MS for Cu/TPMA*-2 (m/z): $[\text{TPMA}^*-2 + \text{H}]^+ = 407.3$; $[\text{CuTPMA}^*-2\text{Cl}]^+ = 504.2$.

KS1-58Aredo#84-105 RT: 4.35-5.32 AV: 22 SB: 80 0.01-4.04 NL: 3.60E7
T: + p Full ms [150.00-1000.00]

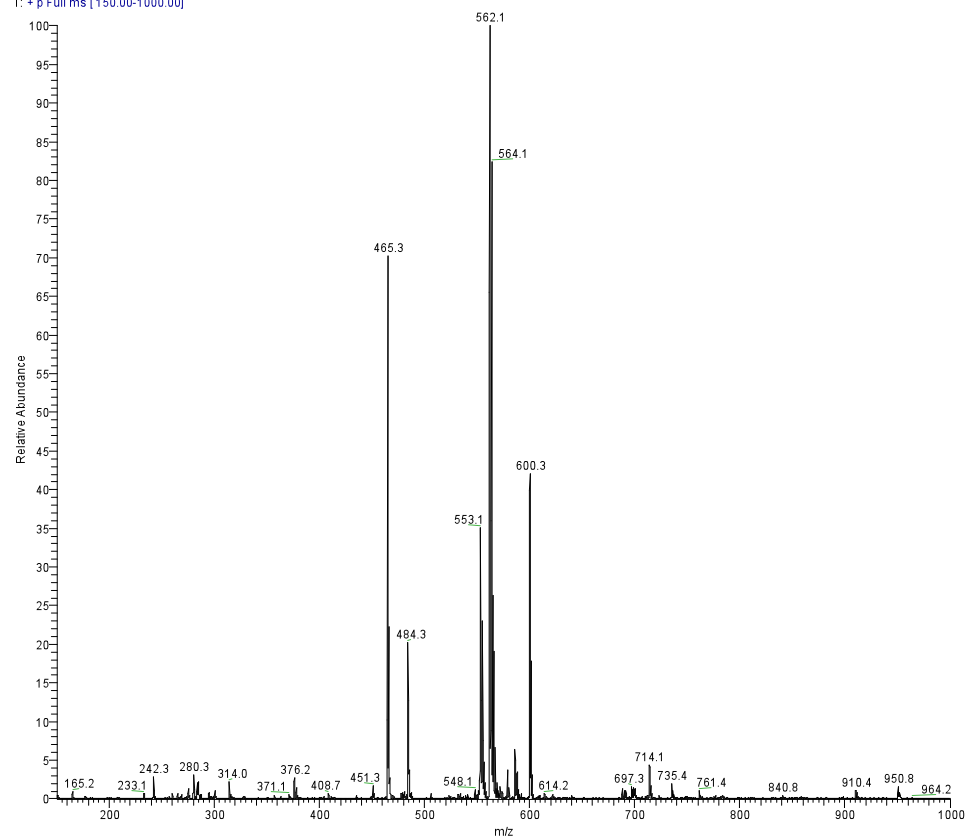


Figure A.3.3. ESI-MS for $\text{CuCl}_2/\text{TPMA}^*-3$

A4. ^1H NMR spectroscopy

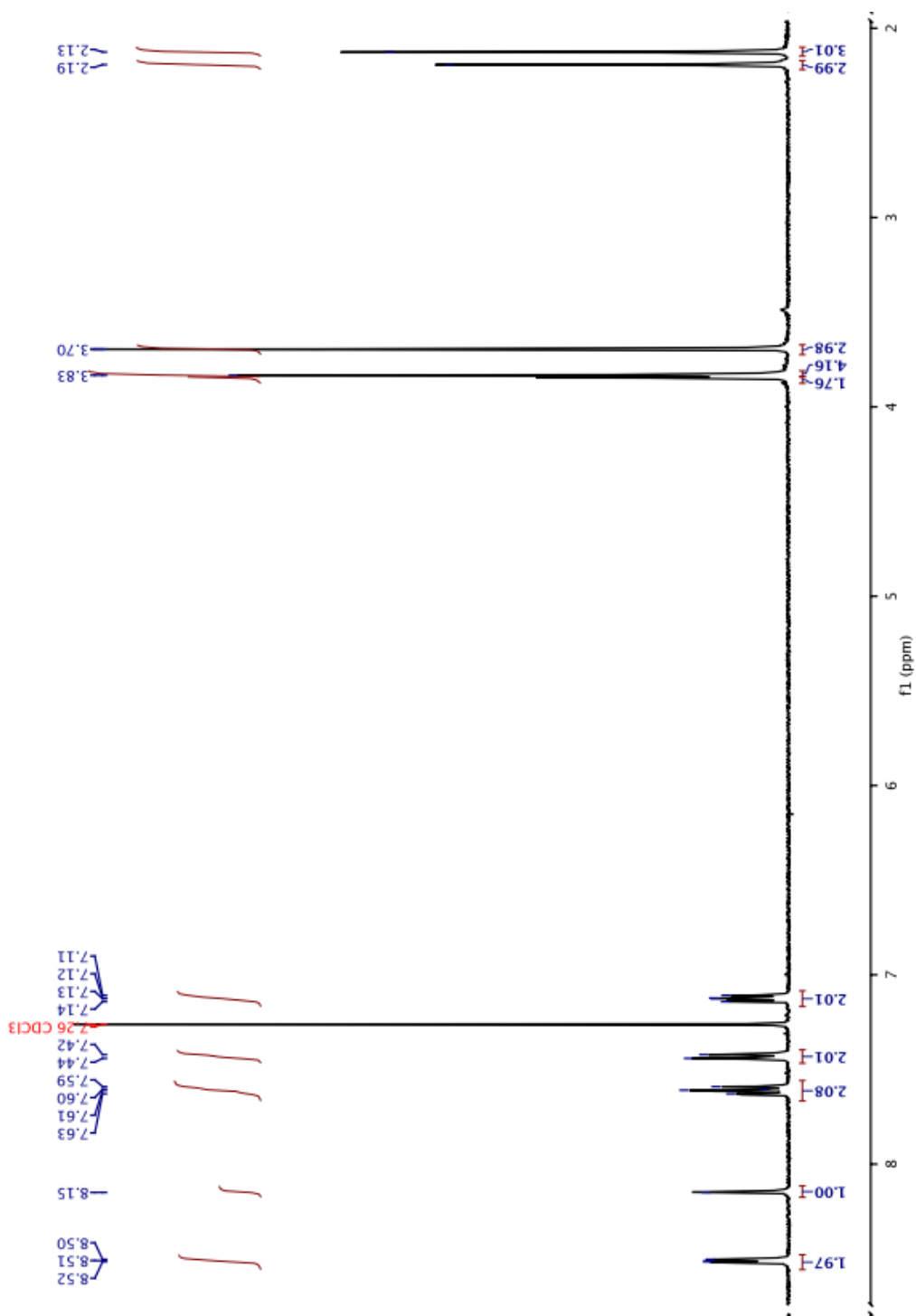


Figure A.4.1. ^1H NMR (400 MHz, CDCl_3 , 298 K) spectrum of TPMA*1.

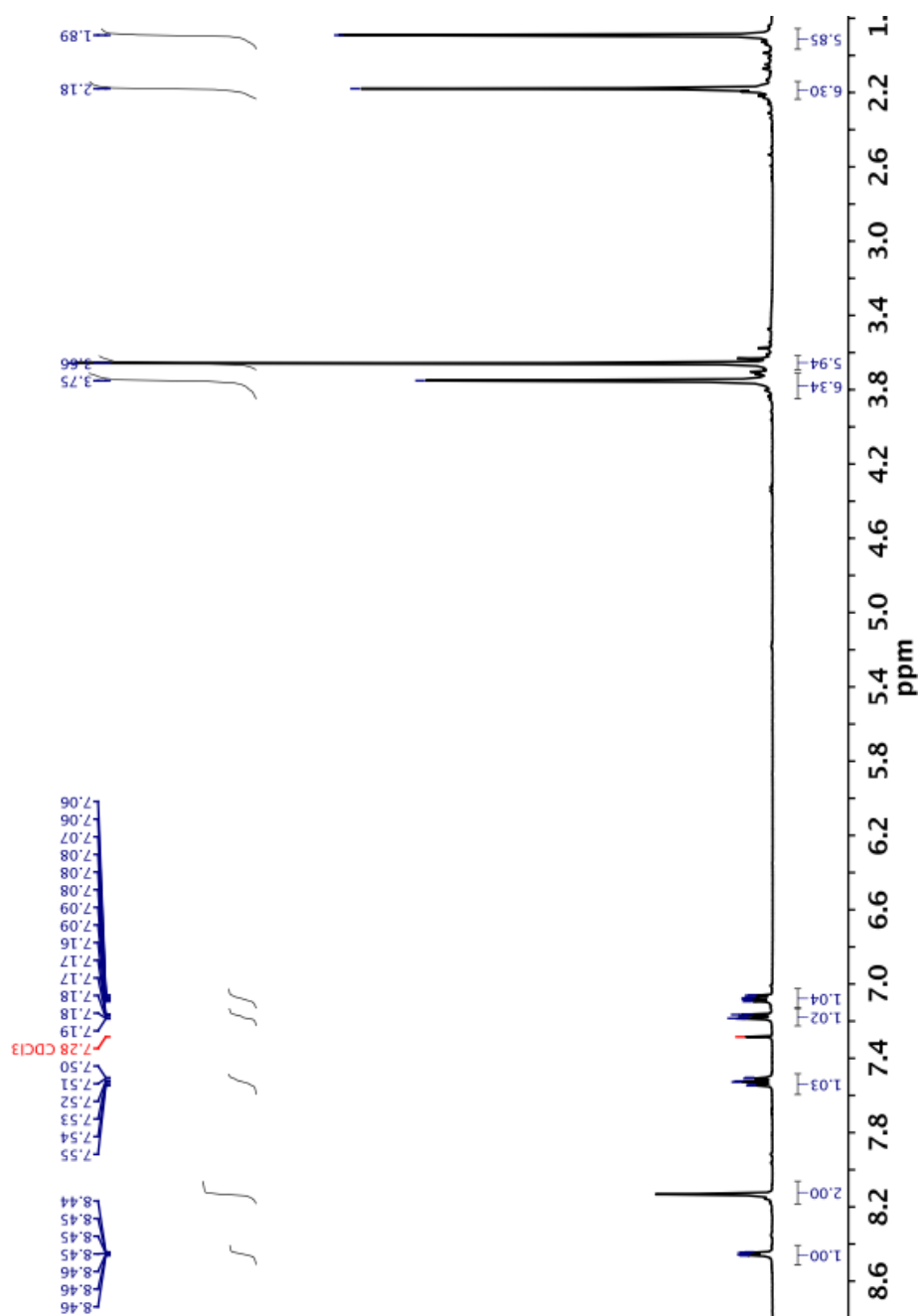


Figure A.4.2 ¹H NMR (400 MHz, CDCl₃, 298 K) spectrum of TPMA*2.

A.5. Crystal Packing Diagrams

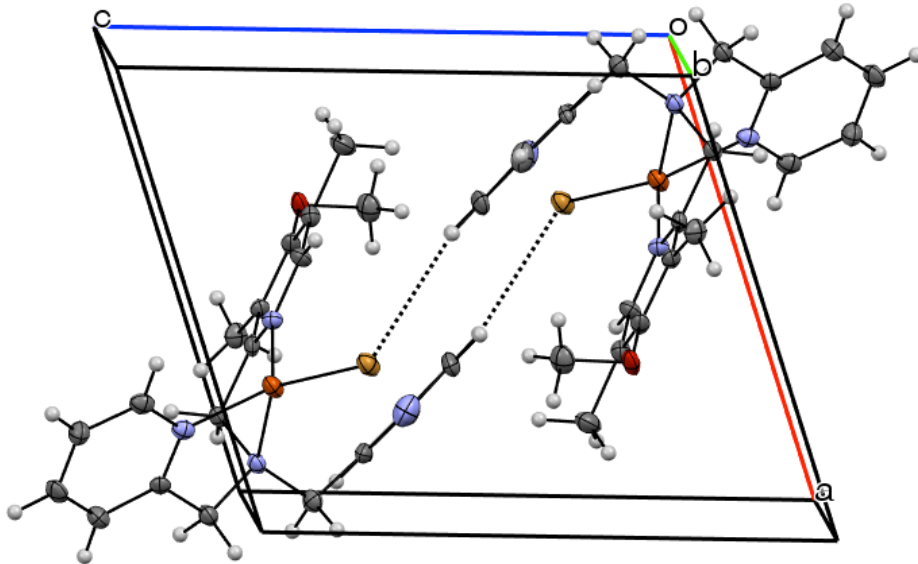


Figure A.5.1 Crystal packing diagram of [Cu^I(TPMA^{*})Br] showing weak C-H...Br interactions.

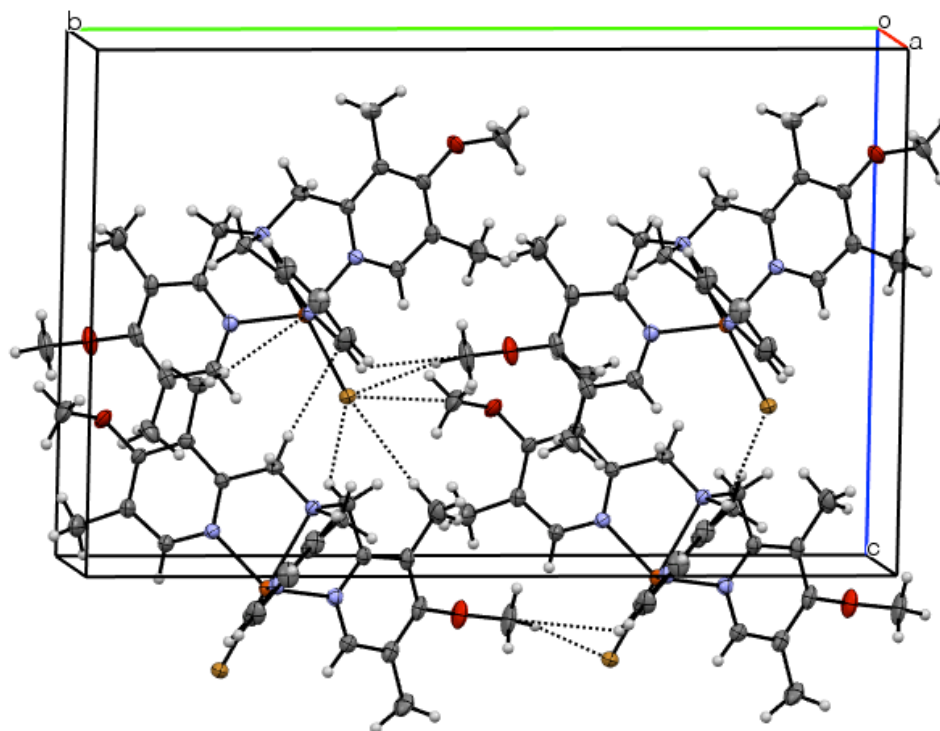


Figure A.5.2. Crystal packing diagram of [Cu^I(TPMA^{*2})Br] showing weak C-H...Br interactions.

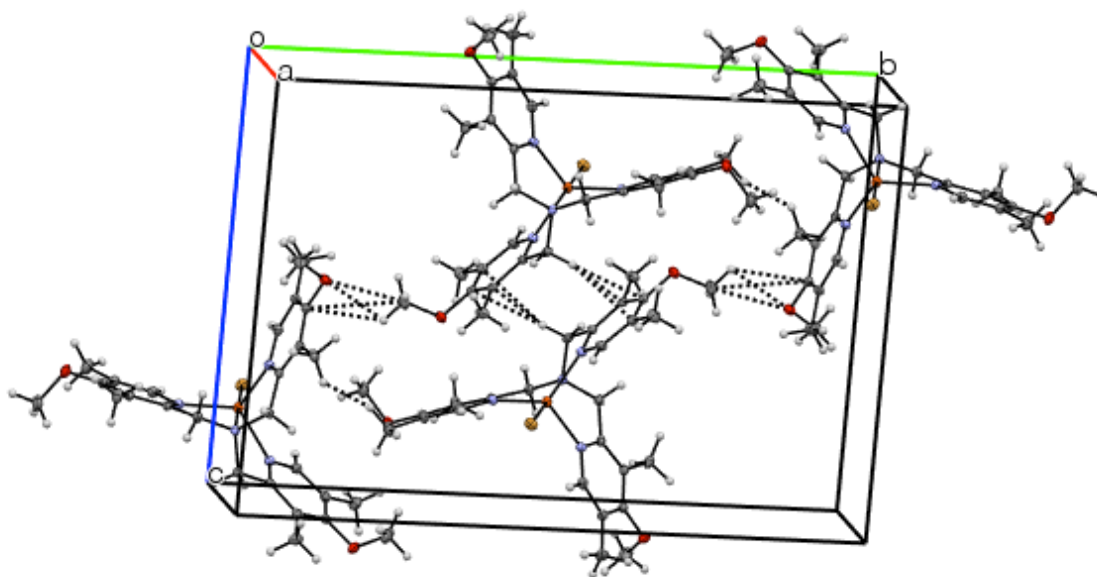


Figure A.5.3. Crystal packing diagram of $[\text{Cu}^{\text{I}}(\text{TPMA}^{*3})\text{Br}]$, showing weak C-H...O interactions, as well as short C-H...C contacts.

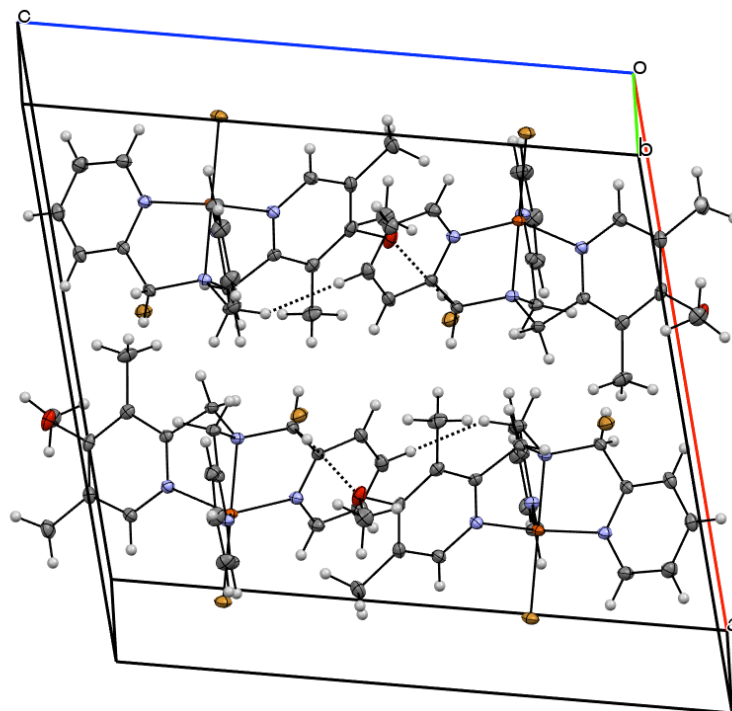


Figure A.5.4. Crystal packing diagram of [Cu^{II}(TPMA*1)Br][Br], showing weak C-H...O interactions, as well as short C-H...C contacts.

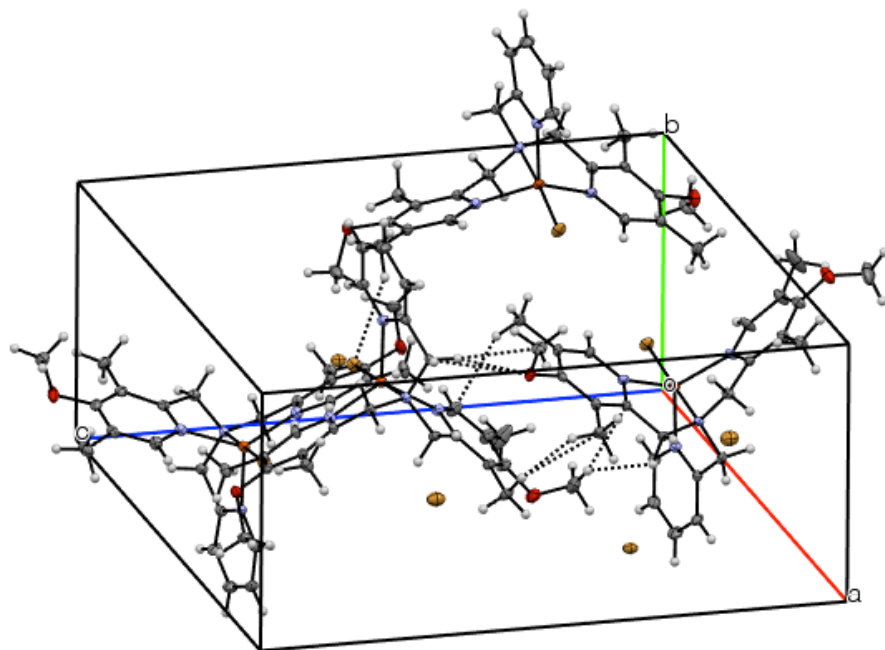


Figure A.5.5. Crystal packing diagram of $[\text{Cu}^{\text{II}}(\text{TPMA}^{*2})\text{Br}][\text{Br}]$, showing weak C-H...O interactions, as well as short C-H...C contacts.

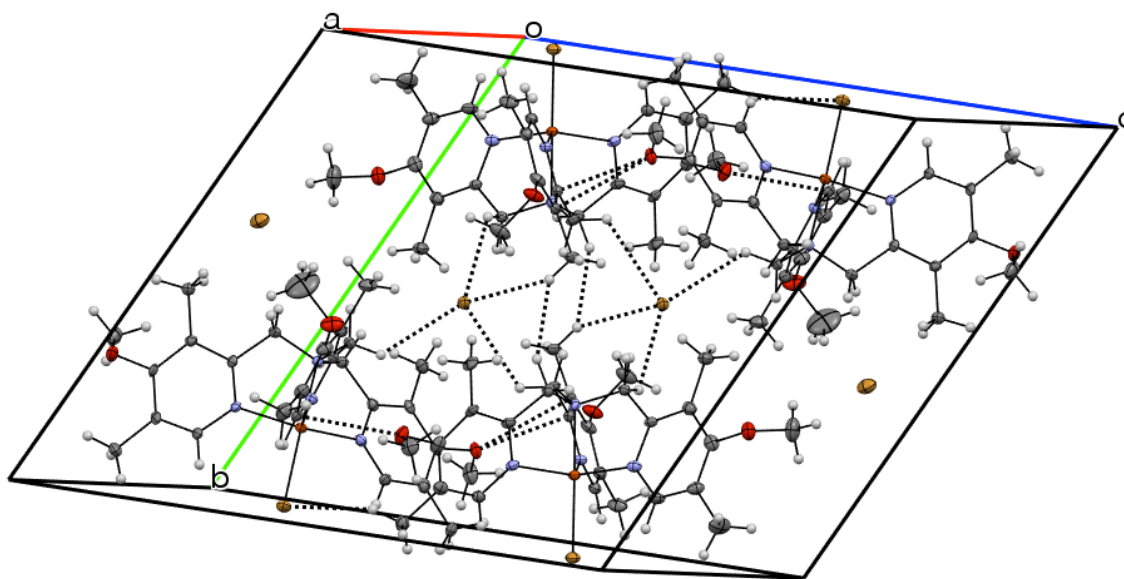


Figure A.5.6. Crystal packing diagram of $[\text{Cu}^{\text{II}}(\text{TPMA}^{*3})\text{Br}][\text{Br}]$, showing weak C-H...O, C-H...Br interactions, as well as short C-H...C contacts.

Appendix B

B.1. Crystallographic Tables

Table. B.1.1. Crystallographic Table for [Cu^{II}(gly)(phen)Cl] and [Cu^{II}(gly)(bpy)Cl].

	[Cu(gly)(phen)Cl]	[Cu(gly)(bpy)Cl]
Formula	C ₁₄ H ₁₂ ClCuN ₃ O ₂	C ₁₂ H ₁₂ ClCuN ₃ O ₂ ·H ₂ O
Color	Blue	Blue
Shape	Cubic	Cubic
Formula Weight	353.27	347.26
Crystal System	Monoclinic	Monoclinic
Space Group	<i>P2₁/n</i>	<i>P21/c</i>
Temp (K)	150	150
Cell Constants		
a, Å	6.988 (4)	10.463(3)
b, Å	12.284 (7)	18.278(6)
c, Å	20.375 (12)	7.684(2)
α, deg	90	90
β, deg	95.110 (9)	104.36(4)
γ, deg	90	90
V, Å³	1741.9 (18)	1423.5(7)
Formula units/unit cell	4	4
Dcal'd, gcm⁻³	1.347	1.654
Absorption coefficient, mm⁻¹	1.41	1.73
F(000)	716	804
Diffractometer	Bruker Smart ApexII	Bruker Smart ApexII
Radiation, graphite monochr.	Mo Kλ (λ =0.71073 Å)	Mo K λ(λ =0.71073 Å)
Crystal size, mm	0.36x0.28x0.24	0.42x0.23x0.14
θ range, deg	1.9 < θ < 28.4	1.8 < θ < 25.5
Range of h,k,l	±9, ±12, ±29	±8, ±11, ±28
Reflections collected/unique	4736/3077	18973/2944
Rint	0.042	0.040
Refinement Method	Full Matrix Least-Squares on F ₂	Full Matrix Least-Squares on F ₂
Data/Restraints/Parameters	4294/0/190	2944/0/221
GOF on F₂	0.86	1.02
R indices (all data)	0.130	R1=0.055 wR2=0.190
Max. Resid. Peaks (e⁻Å⁻³)	0.48 and -0.39	0.25 and -0.42

[Cu^{II}(ala)(bpy)Cl]	
Formula	C ₁₃ H ₁₄ ClCuN ₃ O ₂
Color	Blue
Shape	Cubic
Formula Weight	343.27
Crystal System	Monoclinic
Space Group	<i>P</i> 2 ₁
Temp (K)	296
Cell Constants	
a, Å	8.5043 (5)
b, Å	14.8340 (9)
c, Å	11.5372 (7)
α, deg	90
β, deg	99.262 (1)
γ, deg	90
V, Å³	1436.47 (15)
Formula units/unit cell	4
Dcal'd, gcm⁻³	1.587
Absorption coefficient, mm⁻¹	1.74
F(000)	700
Diffractometer	Bruker Smart ApexII
Radiation, graphite monochr.	Mo Kλ (λ =0.71073 Å)
Crystal size, mm	0.43 × 0.12 × 0.12
θ range, deg	1.92 < θ < 32.61
Range of h,k,l	±11, ±19, ±15
Reflections collected/unique	7018/5897
Rint	0.028
Refinement Method	Full Matrix Least-Squares on F ²
Data/Restraints/Parameters	7018/1/363
GOF on F₂	0.064
Final R indices [I>2σ(I)]	R1=0.031 wR2=0.095
Max. Resid. Peaks (e*Å⁻³)	1.169 and -1.153

Table. B.1.2. Crystallographic Table for [Cu^{II}(pro)(phen)Cl] and [Cu^{II}(pro)(bpy)Cl].

	[Cu ^{II} (pro)(phen)Cl]	[Cu ^{II} (pro)(bpy)Cl]
Formula	C ₁₇ H ₁₆ ClCuN ₃ O ₂	C ₁₅ H ₁₆ ClCuN ₃ O ₂
Color	Blue	Blue
Shape	Cubic	Cubic
Formula Weight	393.33	369.31
Crystal System	Orthorhombic	Orthorhombic
Space Group	<i>P</i> 2 ₁ 2 ₁ 2 ₁	<i>P</i> 2 ₁ 2 ₁ 2 ₁
Temp (K)	150	150
Cell Constants		
a, Å	6.9820 (1)	6.6121 (7)
b, Å	9.7401 (1)	9.8561 (10)
c, Å	23.2192 (3)	23.308 (2)
α, deg	90	90
β, deg	90	90
γ, deg	90	90
V, Å³	1579.03 (3)	1519.0 (3)
Formula units/unit cell	4	4
Dcal'd, gcm⁻³	1.654	1.615
Absorption coefficient, mm⁻¹	1.57	1.62
F(000)	804	756
Diffractometer	Bruker Smart ApexII	Bruker Smart ApexII
Radiation, graphite monochr.	Mo Kλ (λ=0.71073 Å)	Mo Kλ (λ =0.71073 Å)
Crystal size, mm	0.18x0.16x0.10	0.56 × 0.49 × 0.42
θ range, deg	1.8 < θ < 25.5	1.8 < θ < 25.5
Range of h,k,l	±8, ±11, ±28	±8, ±11, ±28
Reflections collected/unique	18973/2944	19852/5322
R_{int}	0.040	0.023
Refinement Method	Full Matrix Least-Squares on F ₂	Full Matrix Least-Squares on F ₂
Data/Restraints/Parameters	2944/0/221	5322/0/199
GOF on F₂	1.02	0.72
R indices (all data)	0.022 and 0.060	0.031 and 0.104
Max. Resid. Peaks (e*Å⁻³)	0.28 and -0.28	0.25 and -0.42

Table. B.1.3. Crystallographic Table for [Cu^{II}(phe)(phen)Cl] and [Cu^{II}(phe)(bpy)Cl].

	[Cu ^{II} (phe)(phen)Cl]	[Cu ^{II} (phe)(bpy)Cl]
Formula	C ₂₁ H ₁₈ ClCuN ₃ O ₂	C ₂₉ H ₂₃ ClCuN ₄ O ₃
Color	Blue	Blue
Shape	Plate	Plate
Formula Weight	443.38	574.50
Crystal System	Monoclinic	Monoclinic
Space Group	<i>P</i> 2 ₁	<i>P</i> 2 ₁
Temp (K)	296	296
Cell Constants		
a, Å	11.6685 (11)	11.744 (6)
b, Å	16.2658 (16)	25.004 (12)
c, Å	11.7482 (11)	12.347 (6)
α, deg	90	90
β, deg	101.303 (2)	90
γ, deg	90	90
V, Å³	2186.5 (4)	3626 (3)
Formula units/unit cell	4	4
Dcal'd, gcm⁻³	1.347	1.052
Absorption coefficient, mm⁻¹	1.14	0.77
F(000)	908	1180
Diffractometer	Bruker Smart ApexII	Bruker Smart ApexII
Radiation, graphite monochr.	Mo Kλ (λ = 0.71073 Å)	Mo Kλ (λ = 0.71073 Å)
Crystal size, mm	0.90 × 0.61 × 0.12	0.33 × 0.19 × 0.16
θ range, deg	1.8 < θ < 31.7	1.6 < θ < 33.0
Range of h,k,l	±17, ±23, ±17	±15, ±37, ±17
Reflections collected/unique	11666/6772	33873/8665
R_{int}	0.0	0.068
Refinement Method	Full Matrix Least-Squares on F ₂	Full Matrix Least-Squares on F ₂
Data/Restraints/Parameters	11166/1/505	21550/1/939
GOF on F₂	0.92	1.15
R indices (all data)	0.060 and 0.164	0.114 and 0.301
Max. Resid. Peaks (e*Å⁻³)	0.82 and -0.40	0.55 and -0.42

B.2. FT-IR Spectra of Copper(II)-aminoacid complexes

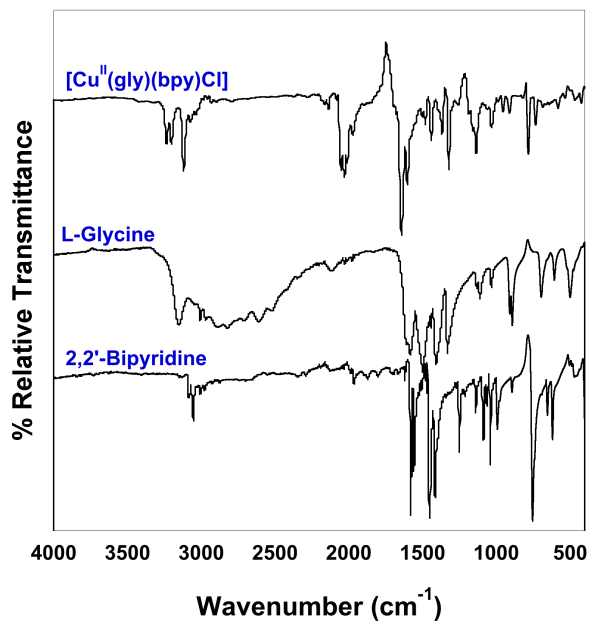
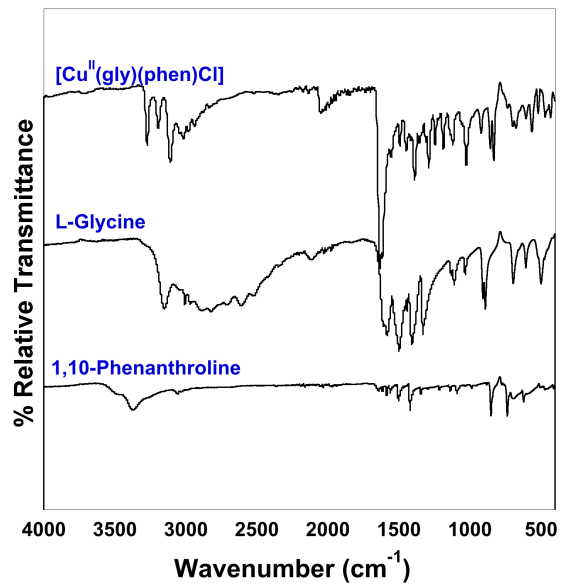


Figure B.2.1 FT-IR spectra of glycine complexes, [Cu^{II}(gly)(bpy)Cl] and [Cu^{II}(gly)(phen)Cl]

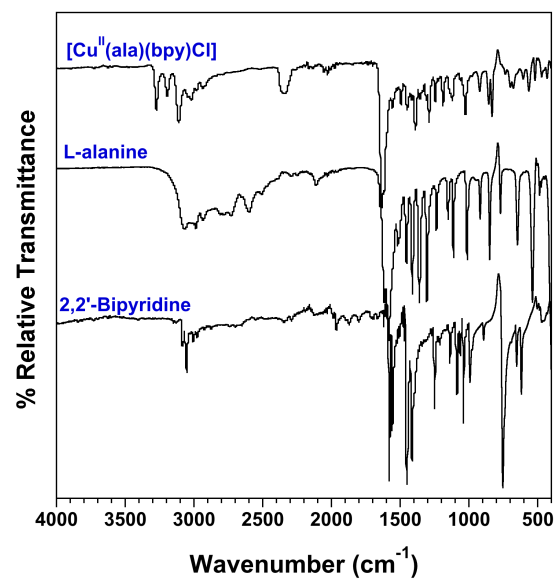


Figure B.2.2 FT-IR spectra of [Cu^{II}(ala)(bpy)Cl]

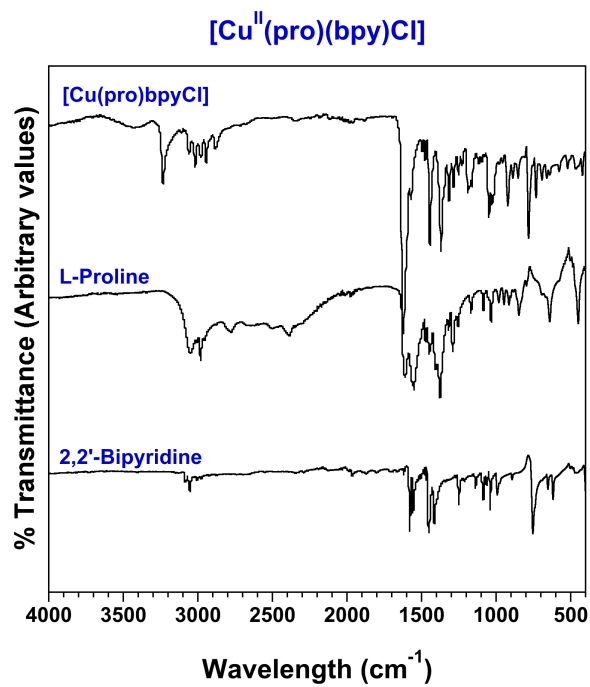
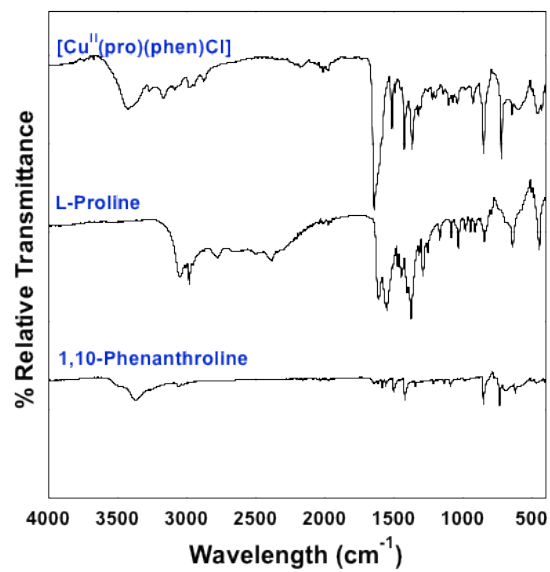


Figure B.2.3. FT-IR spectra of proline complexes, $[\text{Cu}^{\text{II}}(\text{pro})(\text{phen})\text{Cl}]$ and $[\text{Cu}^{\text{II}}(\text{pro})(\text{bpy})\text{Cl}]$

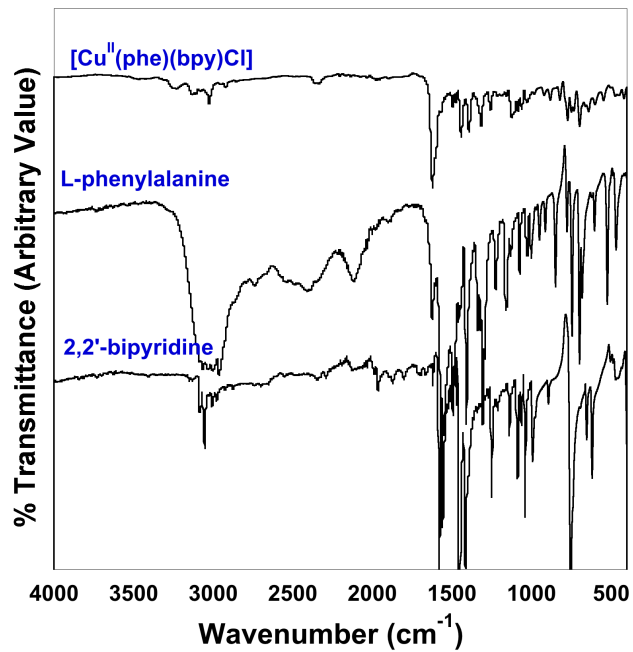


Figure B.2.4 FT-IR spectra of [Cu^{II}(phe)(phen)Cl] and [Cu^{II}(phe)(bpy)Cl]

B.3. Crystal packing structures of $[\text{Cu}^{\text{II}}(\text{aa})(\text{NN})\text{Cl}]$

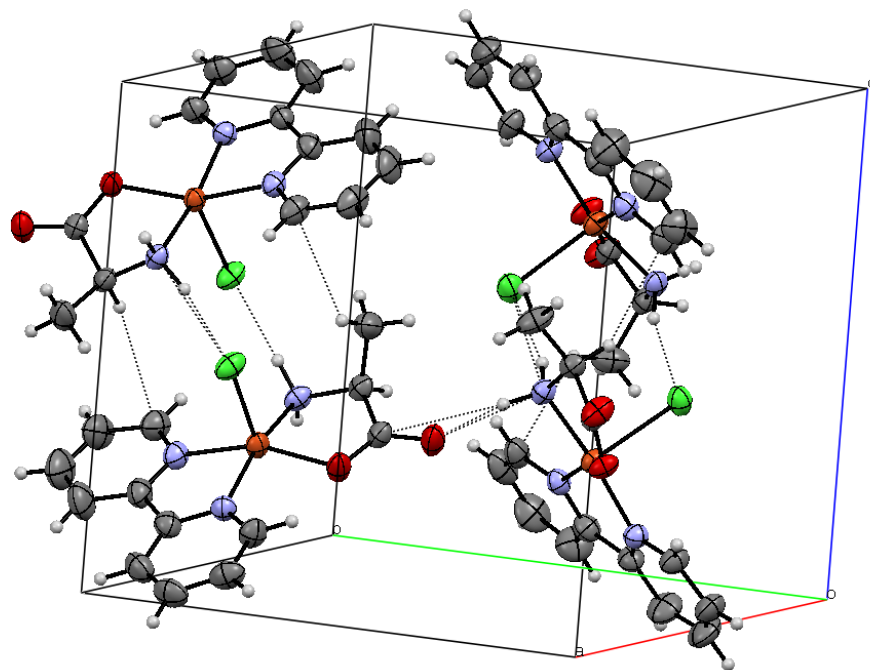


Figure B.3.1. Crystal packing diagram of $[\text{Cu}^{\text{II}}(\text{ala})(\text{bpy})\text{Cl}]$ with 30% probability ellipsoids, showing N-H...Cl, N-H...O interactions.

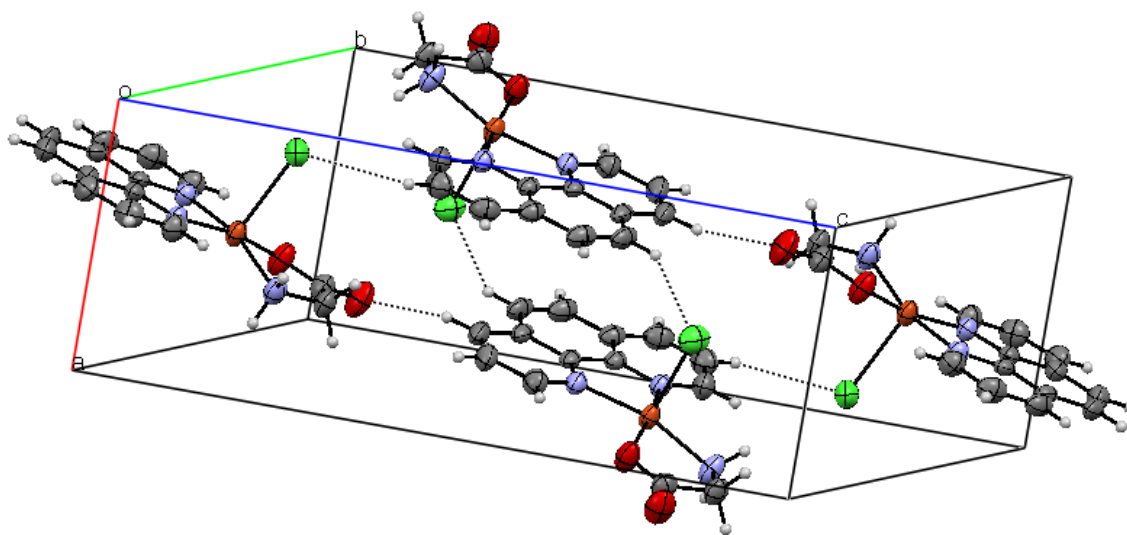


Figure B.3.2. Crystal packing diagram of [Cu^{II}(gly)(phen)Cl] with 30% probability ellipsoids, showing C-H...Cl interactions.

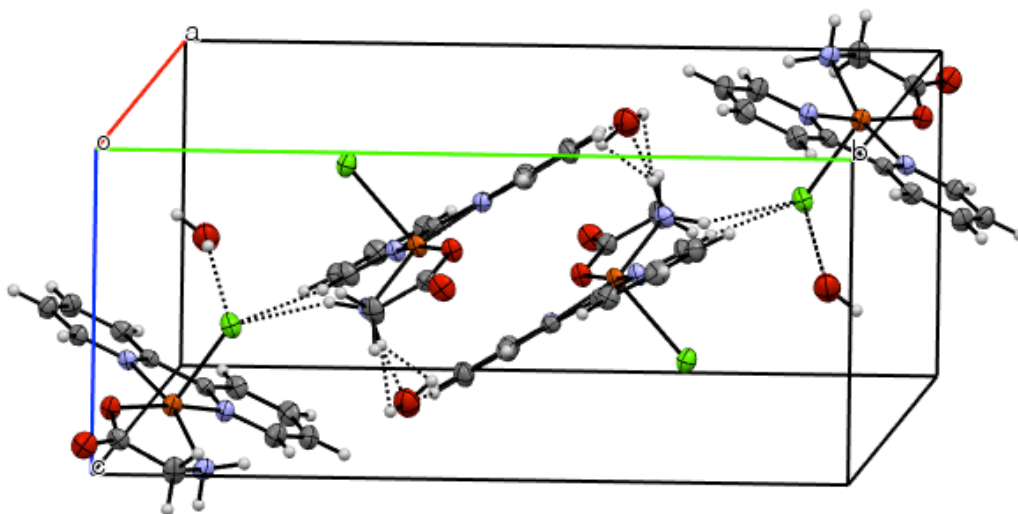


Figure B.3.3. Crystal packing diagram of [Cu^{II}(gly)(bpy)Cl] with 30% probability ellipsoids, showing N-H...O, N...O, Cl...H-C, π-π stacking interactions.

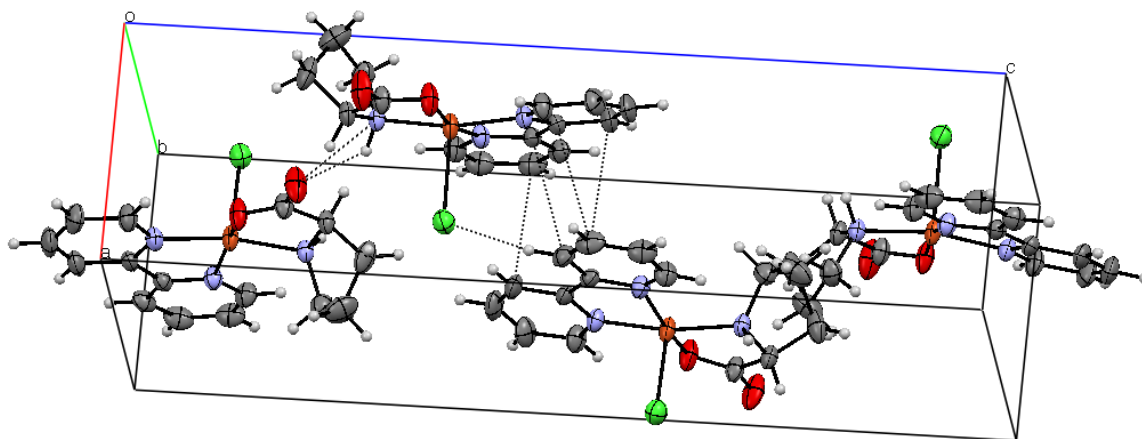


Figure B.3.4. Crystal packing diagram of [Cu^{II}(pro)(bpy)Cl] with 30% probability ellipsoids, showing N-H...O, N...O, Cl...H-C, π - π stacking interactions.

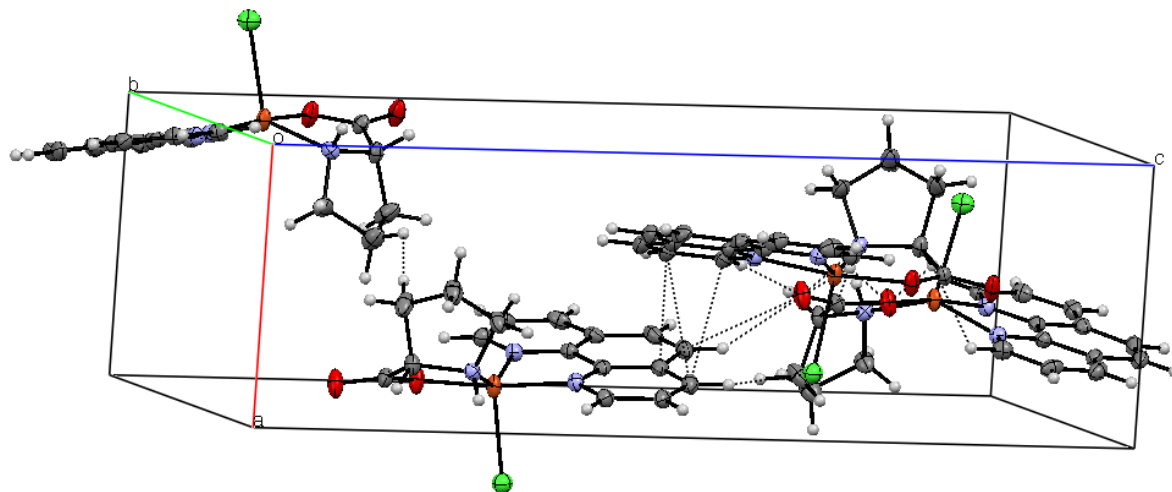


Figure B.3.5. Crystal packing diagram of [Cu^{II}(pro)(phen)Cl] with 30% probability ellipsoids, showing N-H...O, N...O, Cl...H-C, π - π stacking interactions.

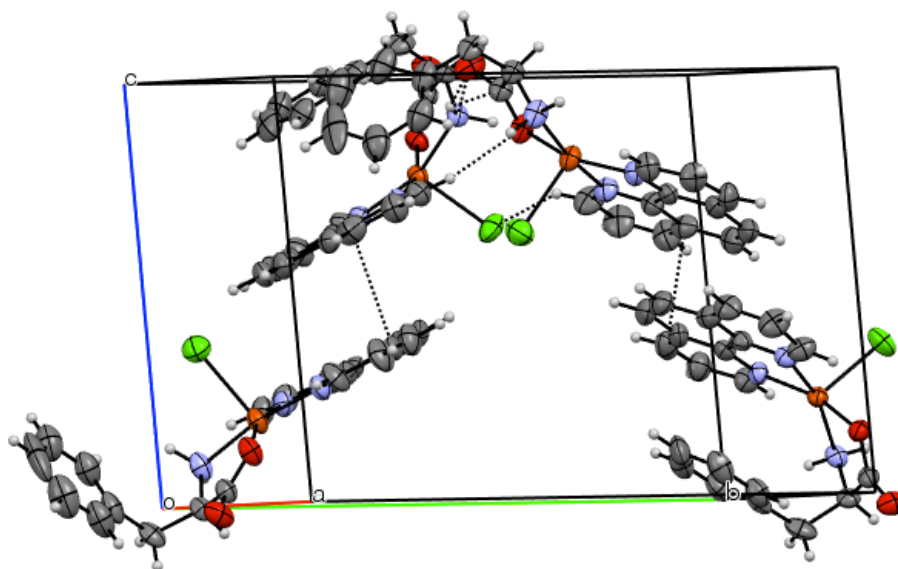


Figure B.3.6. Crystal packing diagram of [Cu^{II}(phe)(phen)Cl] with 30% probability ellipsoids, showing N-H...O, N...O, Cl...H-C, π - π stacking interactions.

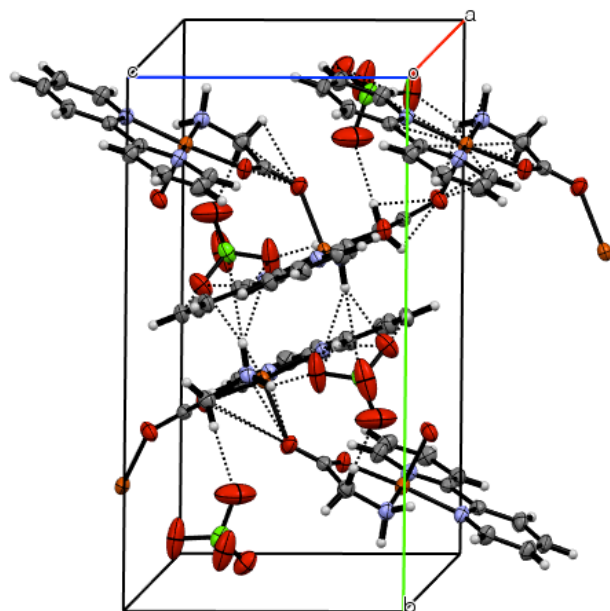


Figure B.3.7. Crystal packing diagram of [Cu^{II}(gly)(bpy)][ClO₄] with 30% probability ellipsoids, showing N-H...O, N...O, Cl...H-C, π - π stacking interactions.

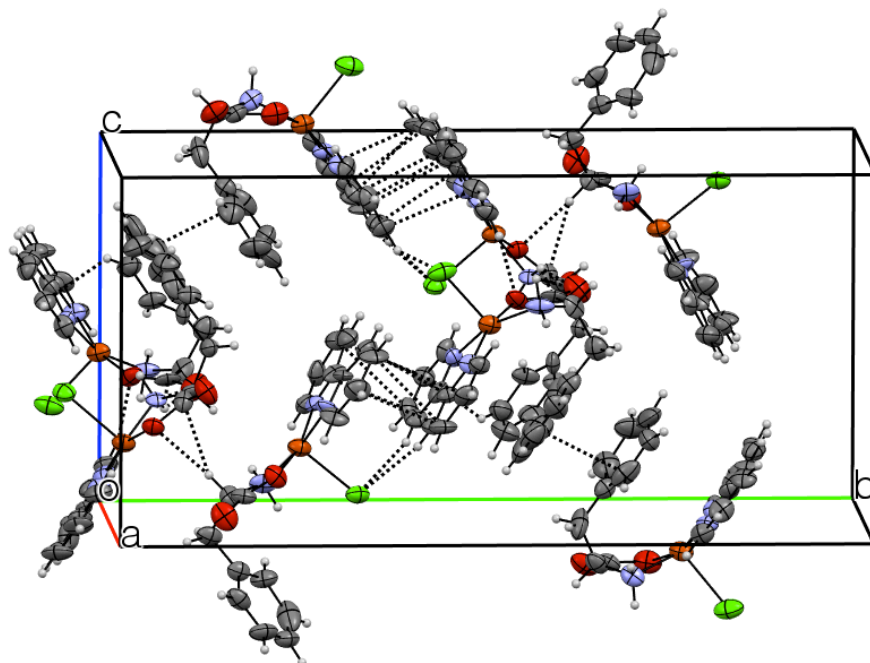


Figure B.3.8. Crystal packing diagram of [Cu^{II}(phe)(bpy)Cl] with 30% probability ellipsoids, showing N-H...O, N...O, Cl...H-C, π - π stacking interactions.

Appendix C.

C.1 Crystallographic Data Tables

Table C.1.1 Crystallographic data for $\text{Cu}^{\text{II}}(\text{ala})(\text{phen})\text{Cl}$ and $[\text{Cu}^{\text{I}}_2(\text{phen})_2(\text{CN})_2 \cdot \text{CH}_3\text{OH}]_n$.

	$\text{Cu}^{\text{II}}(\text{ala})(\text{phen})\text{Cl}$	$[\text{Cu}^{\text{I}}_2(\text{phen})_2(\text{CN})_2 \cdot \text{CH}_3\text{OH}]_n$
Formula	$\text{C}_{16}\text{H}_{18}\text{Cl Cu N}_3\text{O}_3$	$\text{C}_{27}\text{H}_{20}\text{Cu}_2\text{N}_6\text{O}$
Color	blue	brown
Shape	rhomboid	cubic
Formula Weight	399.32	571.59
Crystal System	Triclinic	Monoclinic
Space Group	P-1	P 21/c
Temp (K)	150	296
Cell Constants		
a, Å	6.9308	18.368(4)
b, Å	11.7430(6)	8.3102(17)
c, Å	11.8558(6)	16.414(3)
α, deg	107.4360(10)	90
β, deg	106.2740(10)	110.08(10)
γ, deg	98.8790(10)	90
V, Å³	3697.6(6)	2353.3(8)
Formula units/unit cell	2	4
Dcal'd, gcm⁻³	1.554	1.613
Absorption coefficient, mm⁻¹	1.455	1.841
F(000)	408.6	1160
Diffractometer	Bruker Smart ApexII	Bruker Smart ApexII
Radiation, graphite monochr.	Mo K λ ($\lambda=0.71073$ Å)	Mo K λ ($\lambda=0.71073$ Å)
Crystal size, mm	0.55 x 0.45 x 0.44	0.28 x 0.20 x 0.12
θ range, deg	1.92 < θ < 32.61	1.18 < θ < 32.65
Range of h,k,l	$\pm 10, \pm 17, \pm 17$	$\pm 27, \pm 12, \pm 24$
Reflections collected/unique	10878/6228	38085 / 8119
R_{int}	0.0161	0.0331
Refinement Method	Full Matrix Least-Squares on F ²	Full Matrix Least-Squares on F ²
Data/Restraints/Parameters	5649/0/232	8119 / 0 / 329
GOF on F²	1.129	0.754
Final R indices [I > 2σ(I)]	R ₁ =0.0448 wR ₂ =0.1206	R ₁ = 0.0446, wR ₂ = 0.1296
R indices (all data)	R ₁ =0.0485 wR ₂ =0.1223	R ₁ = 0.0647, wR ₂ = 0.1483
Max. Resid. Peaks (e⁻Å⁻³)	1.169 and -1.153	2.209 and -0.457

Table C.1.2 Crystallographic data for $[\text{Cu}^{\text{I}}_3(4,4'\text{-dMe-bpy})_2(\text{CN})_3]_n$ and $[\text{Cu}^{\text{I}}(4,4'\text{-dCO}_2\text{Me-bpy})(\text{CN})]_n$.

	$[\text{Cu}^{\text{I}}_3(4,4'\text{-dMe-bpy})_2(\text{CN})_3]_n$	$[\text{Cu}^{\text{I}}(4,4'\text{-dCO}_2\text{Me-bpy})(\text{CN})]_n$
Formula	$\text{C}_{27}\text{H}_{24}\text{Cu}_3\text{N}_7$	$\text{C}_{15}\text{H}_{12}\text{CuN}_3\text{O}_4$
Color	orange	brown
Shape	rhomboid	cubic
Formula Weight	637.18	361.83
Crystal System	Monoclinic	Orthorhombic
Space Group	C 2/c	Cmca
Temp (K)	150	150
Cell Constants		
a, Å	10.7314(2)	22.0906(5)
b, Å	12.4074(2)	8.4465(2)
c, Å	20.8852(3)	15.4257(4)
α, deg	90	90
β, deg	100.1220(10)	90
γ, deg	90	90
V, Å³	2737.56(8)	2878.25(12)
Formula units/unit cell	4	8
Dcal'd, gcm⁻³	1.546	1.578
Absorption coefficient, mm⁻¹	2.338	1.538
F(000)	1288	1400
Diffractometer	Bruker Smart ApexII	Bruker Smart ApexII
Radiation, graphite monochr.	Mo K λ ($\lambda=0.71073$ Å)	Mo K λ ($\lambda=0.71073$ Å)
Crystal size, mm	0.24 x 0.15 x 0.09	0.26 x 0.19 x 0.06
θ range, deg	2.27 < θ < 32.42	1.84 < θ < 29.94
Range of h,k,l	$\pm 14, \pm 16, \pm 28$	$\pm 30, \pm 11, \pm 21$
Reflections collected/unique	20620 / 3620	22146 / 2139
R_{int}	0.0225	0.0297
Refinement Method	Full Matrix Least-Squares on F ²	Full Matrix Least-Squares on F ²
Data/Restraints/Parameters		
rs	3620 / 0 / 172	2139 / 0 / 112
GOF on F²	1.027	1.053
Final R indices [I > 2σ(I)]	R ₁ = 0.0289, wR ₂ = 0.0803	R ₁ = 0.0267, wR ₂ = 0.0750
R indices (all data)	R ₁ = 0.0410, wR ₂ = 0.0862	R ₁ = 0.0326, wR ₂ = 0.0787
Max. Resid. Peaks (e*Å⁻³)	0.352 and -0.357	0.572 and -0.428

Table C.1.3. Crystallographic data for $[\text{Cu}^{\text{I}}(4,4'\text{-dCO}_2\text{Et-bpy})_{0.5}(\text{CN})_n]$ and $[\text{Cu}^{\text{I}}_5(\text{pylpy})_2(\text{CN})_5]_n$.

	$[\text{Cu}^{\text{I}}(4,4'\text{-dCO}_2\text{Et-bpy})_{0.5}(\text{CN})_n]$	$[\text{Cu}^{\text{I}}_5(\text{pylpy})_2(\text{CN})_5]_n$
Formula	$\text{C}_{10} \text{H}_8 \text{Cu} \text{N} \text{O}_2$	$\text{C}_{21} \text{H}_{14} \text{Cu}_5 \text{N}_{11}$
Color	brown	colorless
Shape	plates	plates
Formula Weight	237.72	738.18
Crystal System	Monoclinic	Monoclinic
Space Group	C 2/c	P 21/n
Temp (K)	296	296
Cell Constants		
a, Å	5.8362(3)	10.3461(7)
b, Å	24.3364(12)	9.2983(6)
c, Å	13.8996(7)	12.6572(8)
α, deg	90	90
β, deg	96.559(3)	99.046(5)
γ, deg	90	90
V, Å³	1961.27(17)	1202.49(14)
Formula units/unit cell	8	2
Dcal'd, gcm⁻³	1.61	2.039
Absorption coefficient, mm⁻¹	2.196	4.385
F(000)	960	724
Diffractometer	Bruker Smart ApexII	Bruker Smart ApexII
Radiation, graphite monochr.	Mo K λ ($\lambda=0.71073$ Å)	Mo K λ ($\lambda=0.71073$ Å)
Crystal size, mm	0.15 x 0.31 x 0.04	0.09 x 0.07 x 0.05
θ range, deg	1.67 < θ < 29.55	2.37 < θ < 24.42
Range of h,k,l	$\pm 8, \pm 33, \pm 19$	$\pm 12, \pm 10, \pm 11$
Reflections collected/unique	15201/2747	12708 / 1981
R_{int}	0.0356	0.0417
Refinement Method	Full Matrix Least-Squares on F ²	Full Matrix Least-Squares on F ²
Data/Restraints/Parameter s	2733 / 0 / 130	1981 / 0 / 170
GOF on F²	1.061	1.045
Final R indices [I > 2σ(I)]	R ₁ = 0.0395, wR ₂ = 0.1322	R ₁ = 0.0417, wR ₂ = 0.0844
R indices (all data)	R ₁ = 0.0601, wR ₂ = 0.1520	R ₁ = 0.0731, wR ₂ = 0.0987
Max. Resid. Peaks (e⁻Å⁻³)	0.512 and -0.516	0.734 and -0.373

Table C.1.4. Crystallographic data for $[\text{Cu}_2(\text{CN})_3 \cdot 0.5\text{TMEDA} \cdot \text{H}_2]_n$.

	$[\text{Cu}_2(\text{CN})_3 \cdot 0.5\text{TMEDA} \cdot \text{H}_2]_n$
Formula	$\text{C}_6\text{H}_9 \text{Cu}_2 \text{N}_4$
Color	colorless
Shape	plates
Formula Weight	264.27
Crystal System	Orthorhombic
Space Group	Pbca
Temp (K)	150
Cell Constants	
a, Å	7.6458(5)
b, Å	13.5219(8)
c, Å	16.3845(10)
α, deg	90
β, deg	90
γ, deg	90
V, Å³	1693.92(18)
Formula units/unit cell	4
Dcal'd, gm⁻³	0.52
Absorption coefficient, mm⁻¹	1.242
F(000)	262
Diffractometer	Bruker Smart ApexII
Radiation, graphite monochr.	$\text{Mo K}\lambda$ ($\lambda=0.71073$ Å)
Crystal size, mm	0.60 x 0.11 x 0.05
θ range, deg	$2.49 < \theta < 32.51$
Range of h,k,l	$\pm 11, \pm 20, \pm 25$
Reflections collected/unique	19738 / 2953
R_{int}	0.0236
Refinement Method	Full Matrix Least-Squares on F ²
Data/Restraints/Parameters	2953 / 0 / 114
GOF on F²	1.052
Final R indices [I>2σ(I)]	$R_1 = 0.0311, wR_2 = 0.1005$
R indices (all data)	$R_1 = 0.0346, wR_2 = 0.1029$
Max. Resid. Peaks (e⁻Å⁻³)	1.252 and -1.021

C.2. FT-IR Spectra of Copper(I)-Cyanide Frameworks

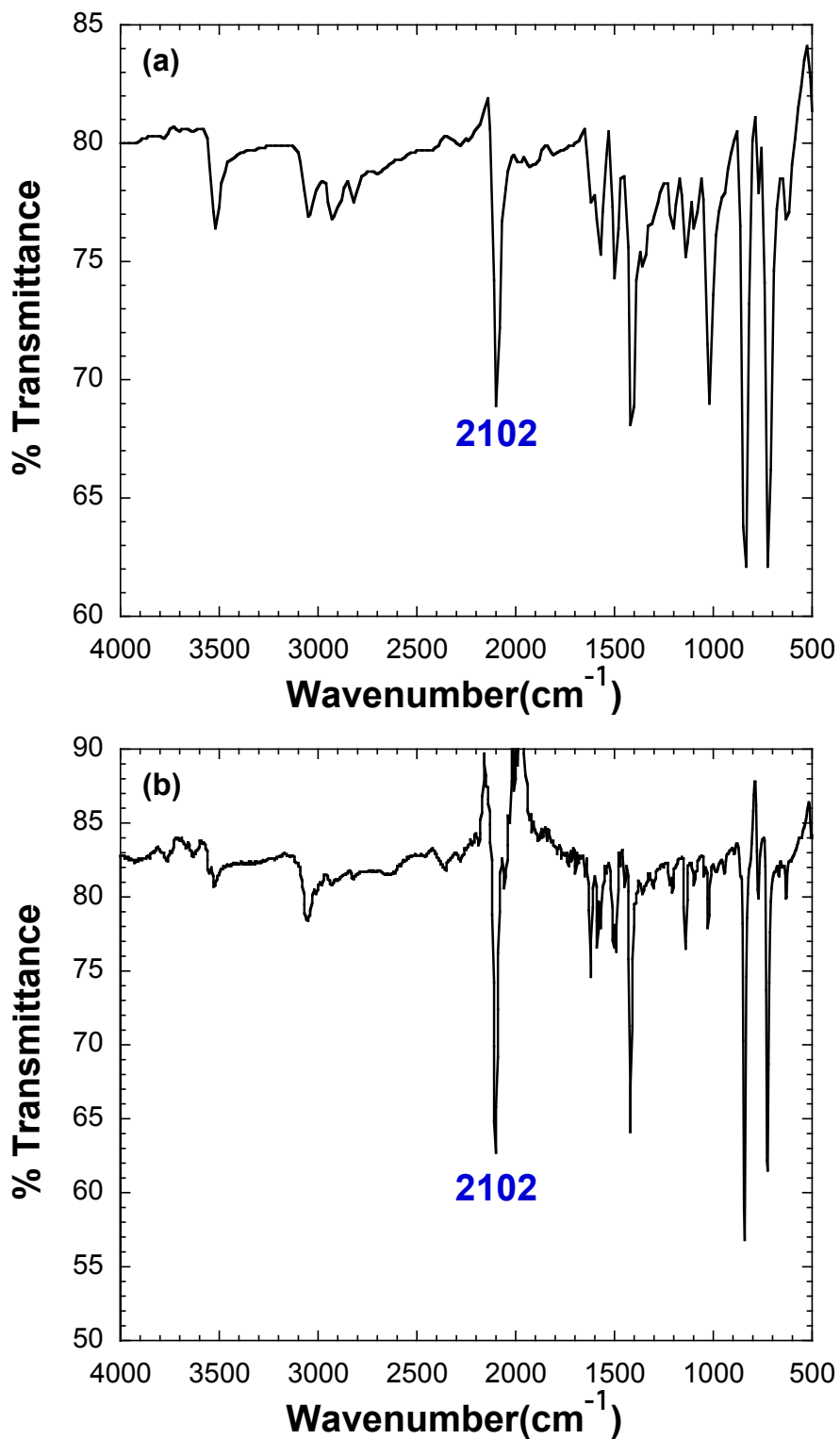


Figure C.2.1. FT-IR spectra of [Cu^I₂(phen)₂(CN)₂*CH₃OH]_n synthesized at 80 °C (a) and ambient temperature (b).

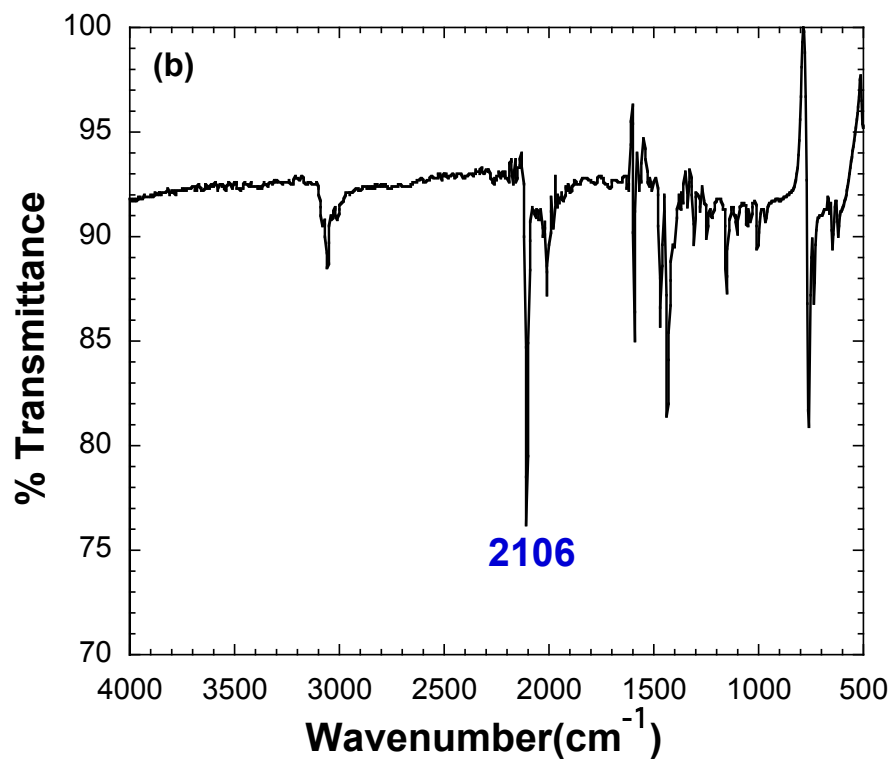
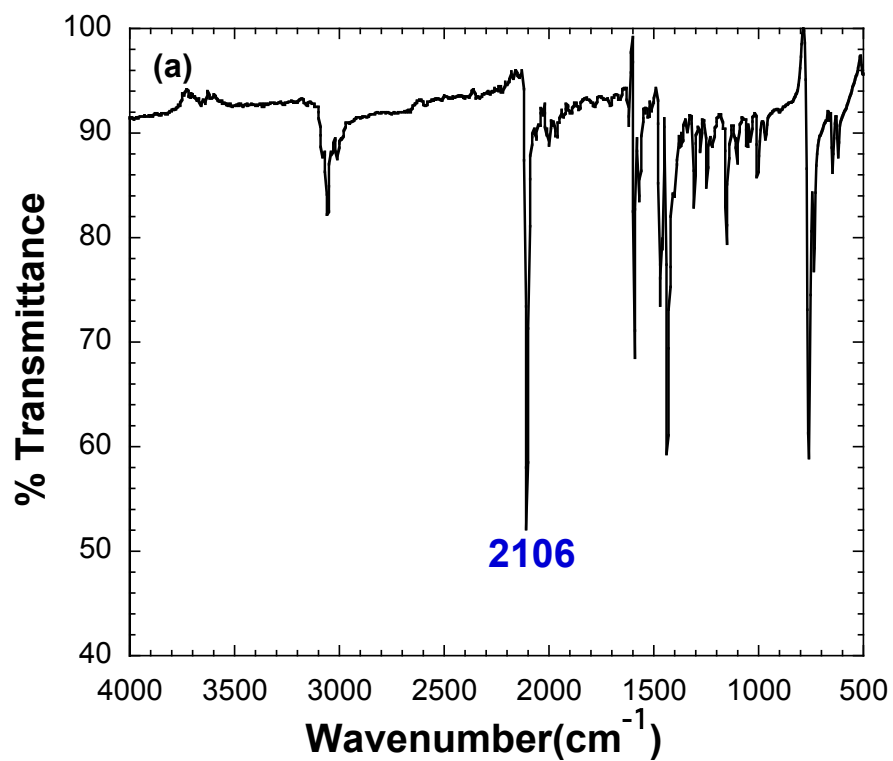


Figure C.2.2. FT-IR spectra of $[\text{Cu}^{\text{I}}(\text{bpy})(\text{CN})]_n$ synthesized at 80 °C (a) and ambient temperature (b).

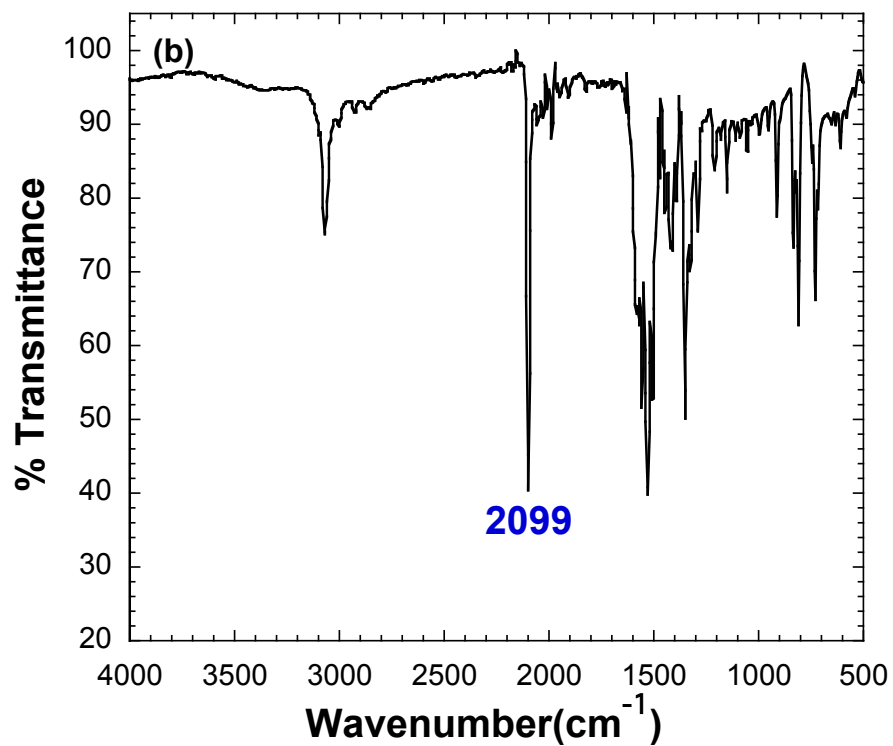
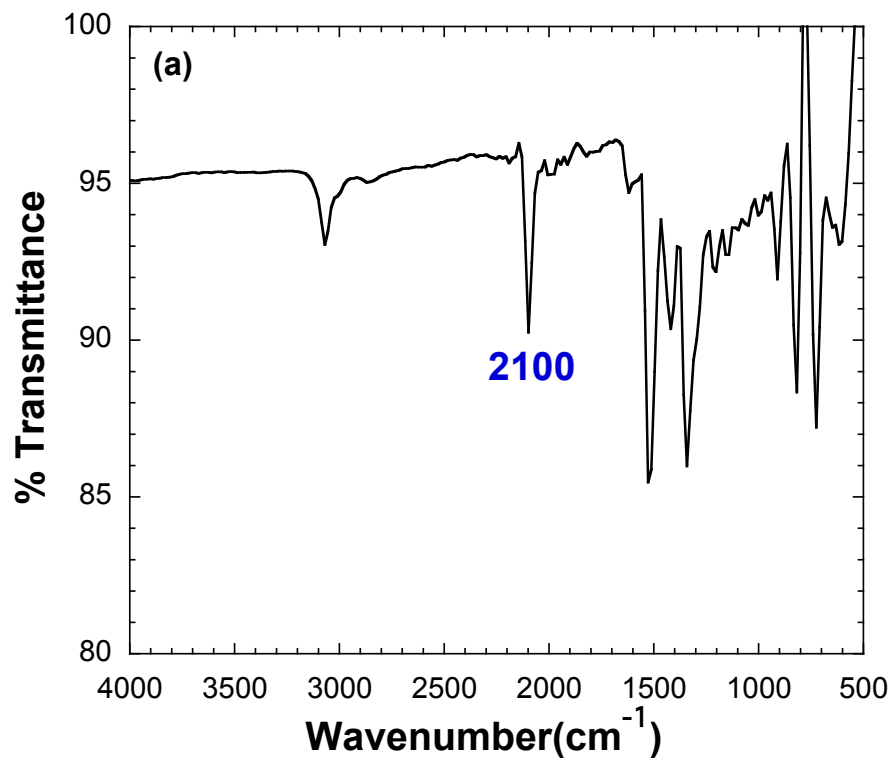


Figure C.2.3. FT-IR spectra of $[\text{Cu}^{\text{I}}(5\text{-NO}_2\text{-phen})(\text{CN})]_n$ synthesized at 80 °C (a) and ambient temperature (b).

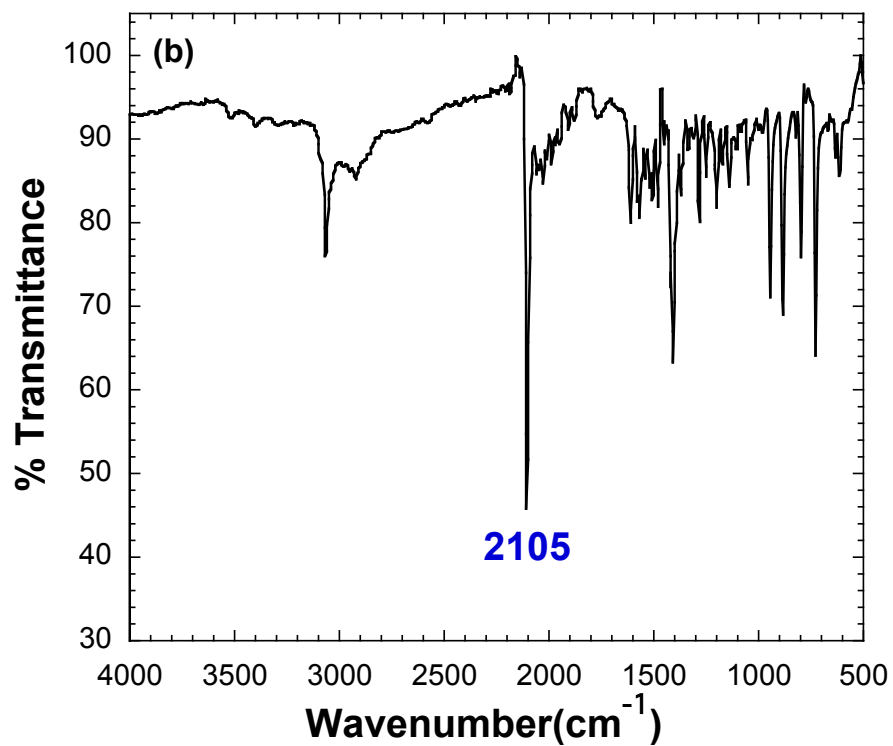
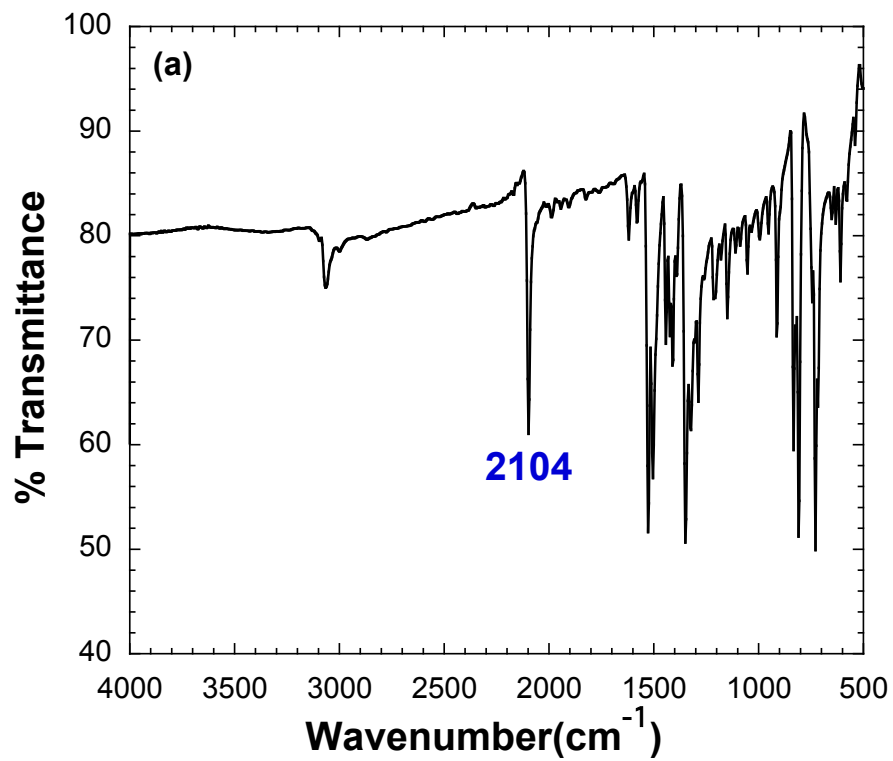


Figure C.2.4. FT-IR spectra of $[\text{Cu}^{\text{I}}(5\text{-Cl-phen})(\text{CN})]_n$ synthesized at $80\text{ }^\circ\text{C}$ (a) and ambient temperature (b).

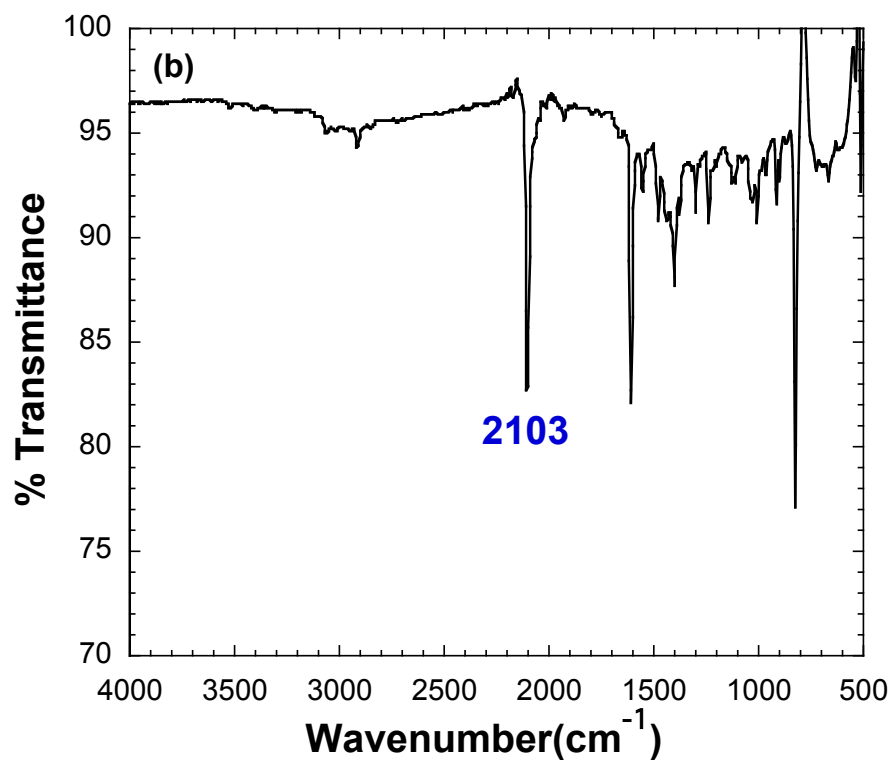
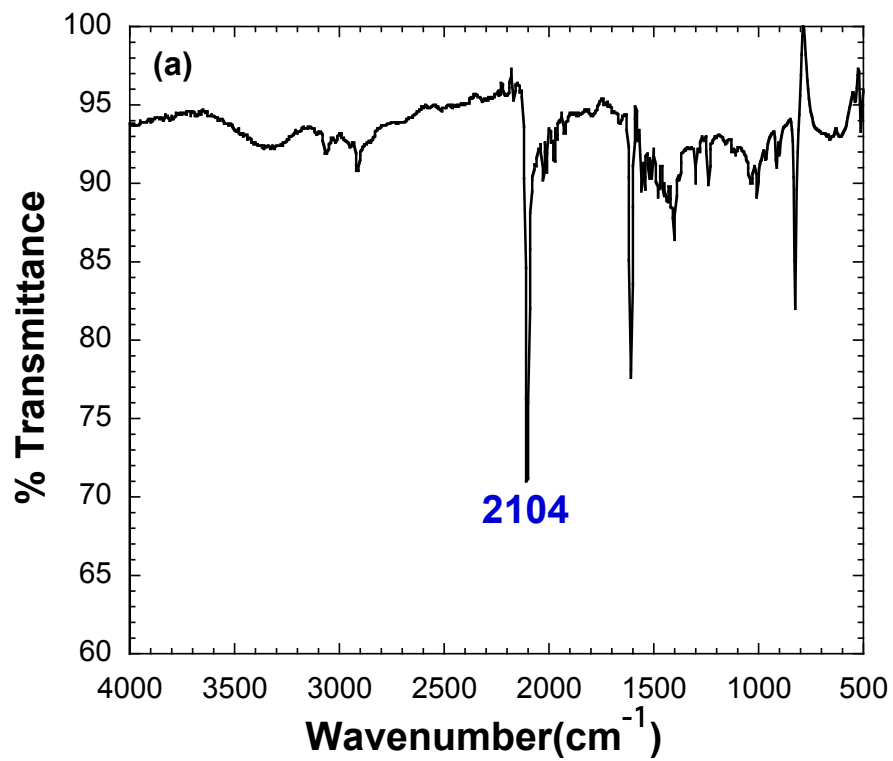


Figure C.2.5. FT-IR spectra of $[\text{Cu}^{\text{I}}_3(4,4'\text{-dMe-bpy})_2(\text{CN})_3]_n$ synthesized at 80 °C (a) and ambient temperature (b).

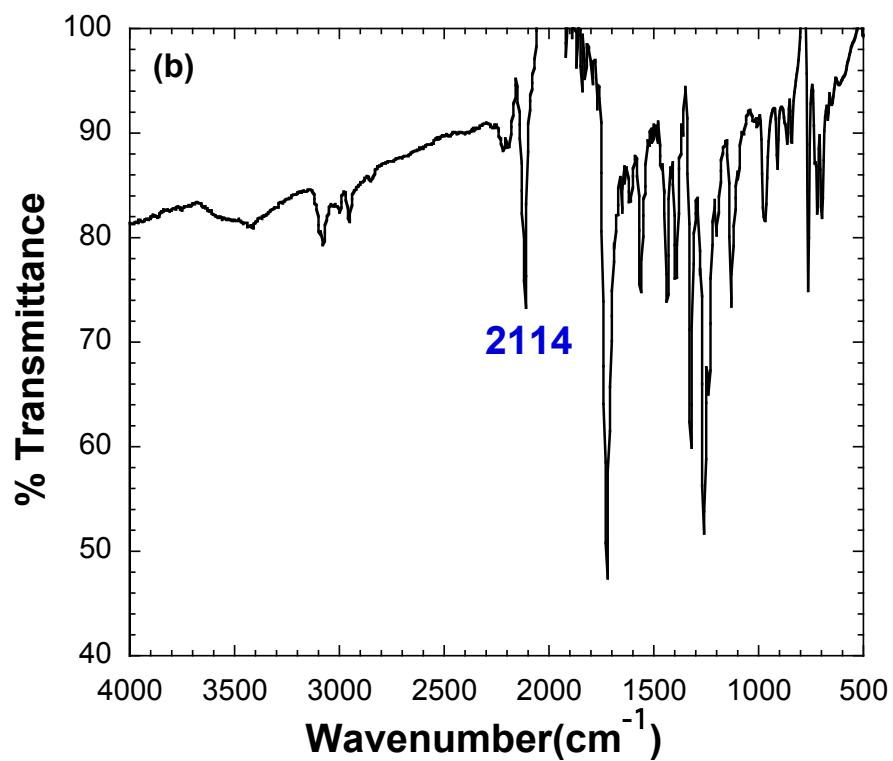
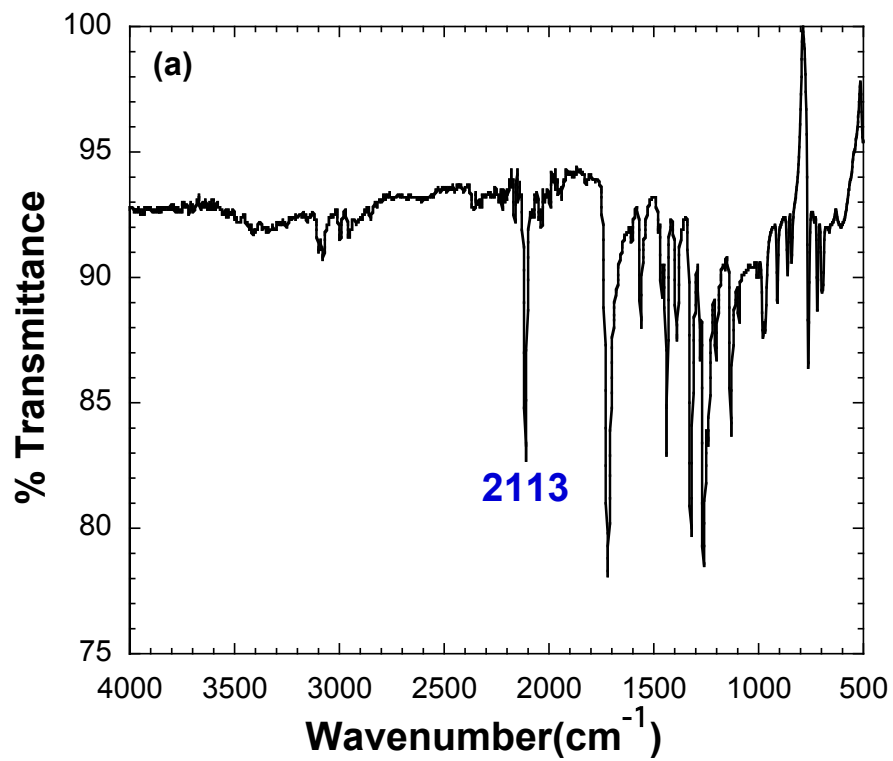


Figure C.2.6. FT-IR spectra of $[\text{Cu}^{\text{I}}(4,4'\text{-dCO}_2\text{Me-bpy})(\text{CN})]_n$ synthesized at 80 °C (a) and ambient temperature (b).

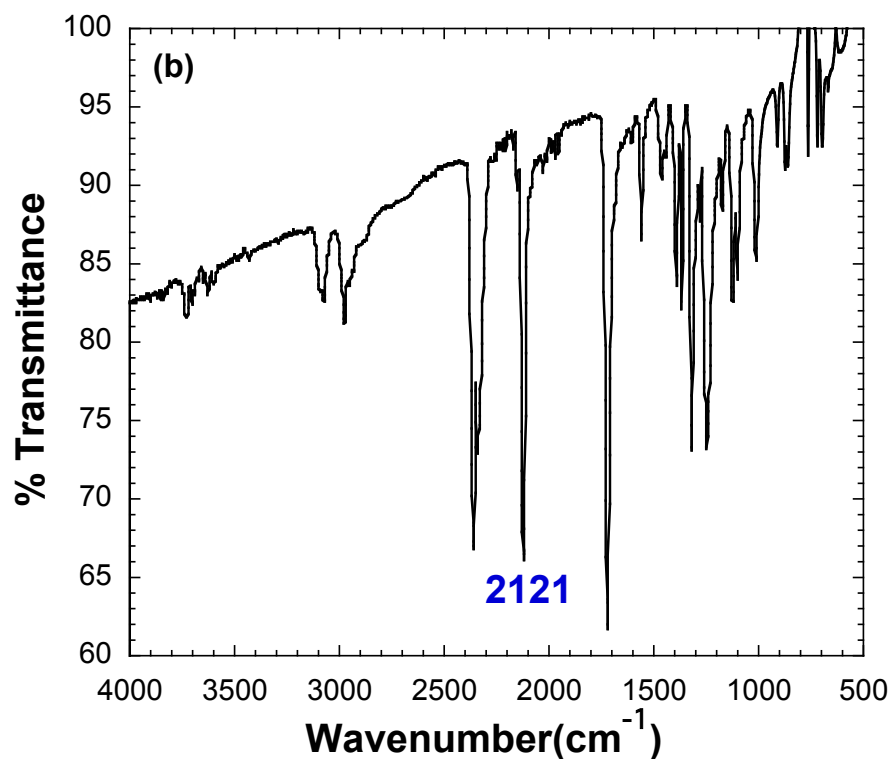
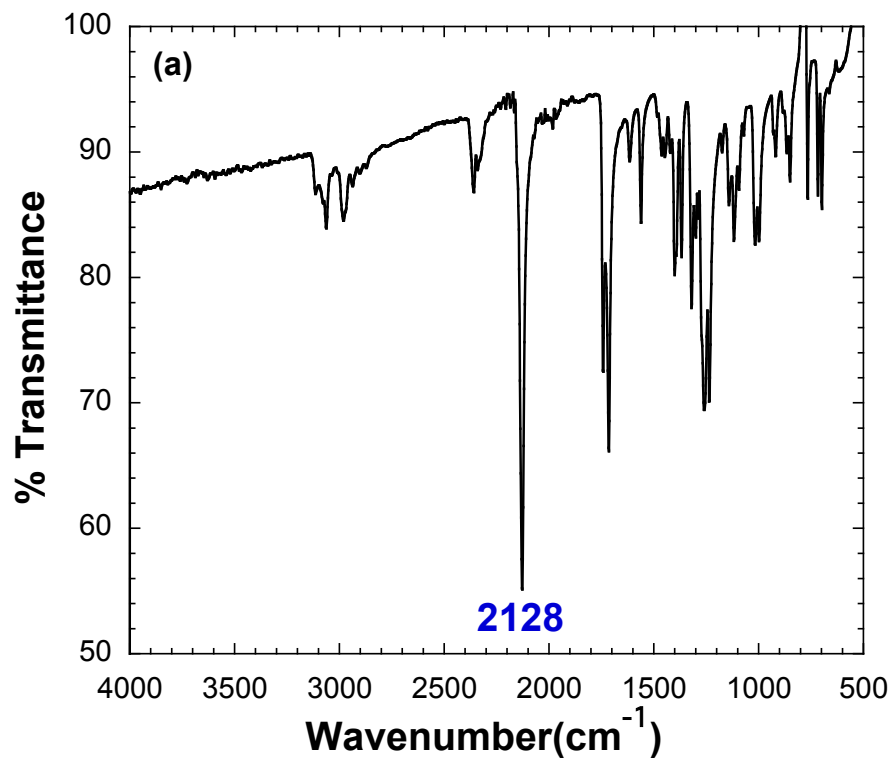


Figure C.2.7. FT-IR spectra of $[\text{Cu}^{\text{I}}(4,4'\text{-dCO}_2\text{Et-bpy})_{0.5}(\text{CN})]_n$ synthesized at 80 °C (a) and ambient temperature (b).

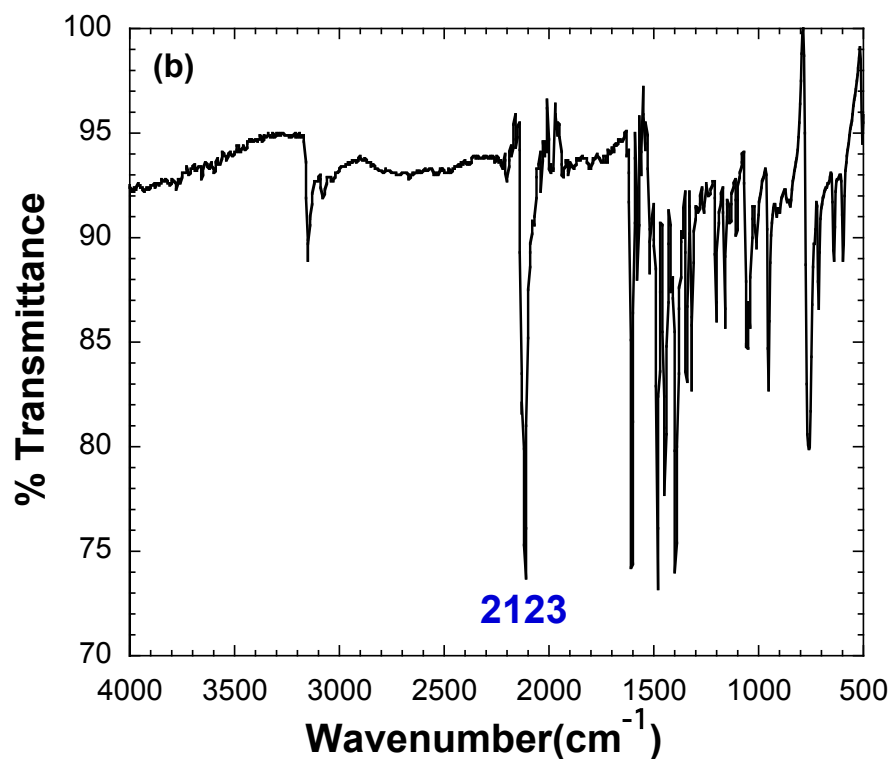
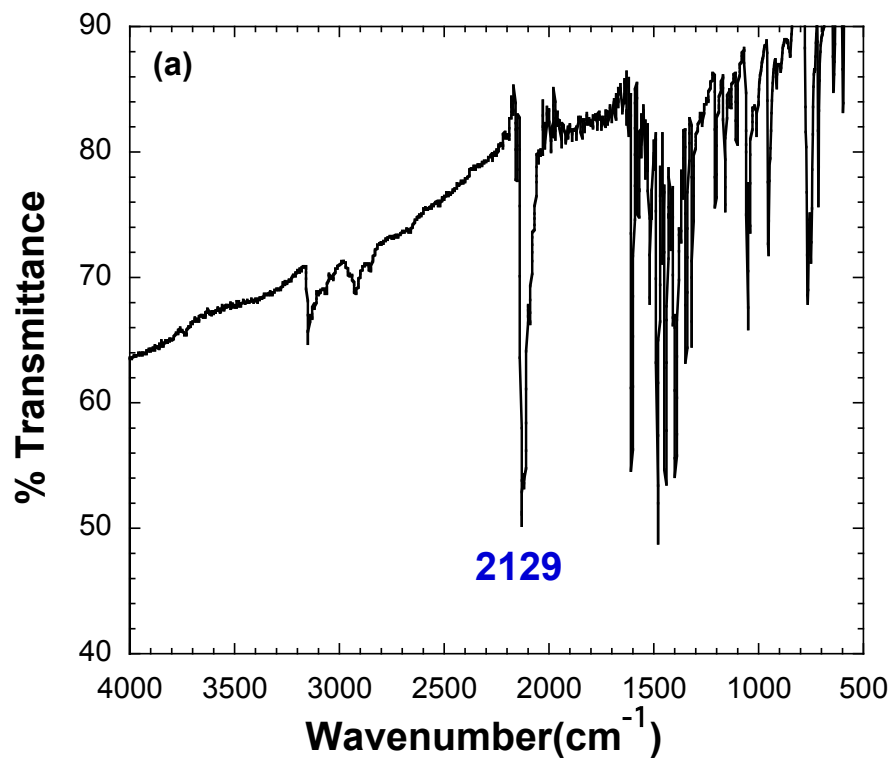


Figure C.2.8. FT-IR spectra of $[\text{Cu}^{\text{I}}(\text{pyIpy})_2(\text{CN})_5]_n$ synthesized at 80 °C (a) and ambient temperature (b).

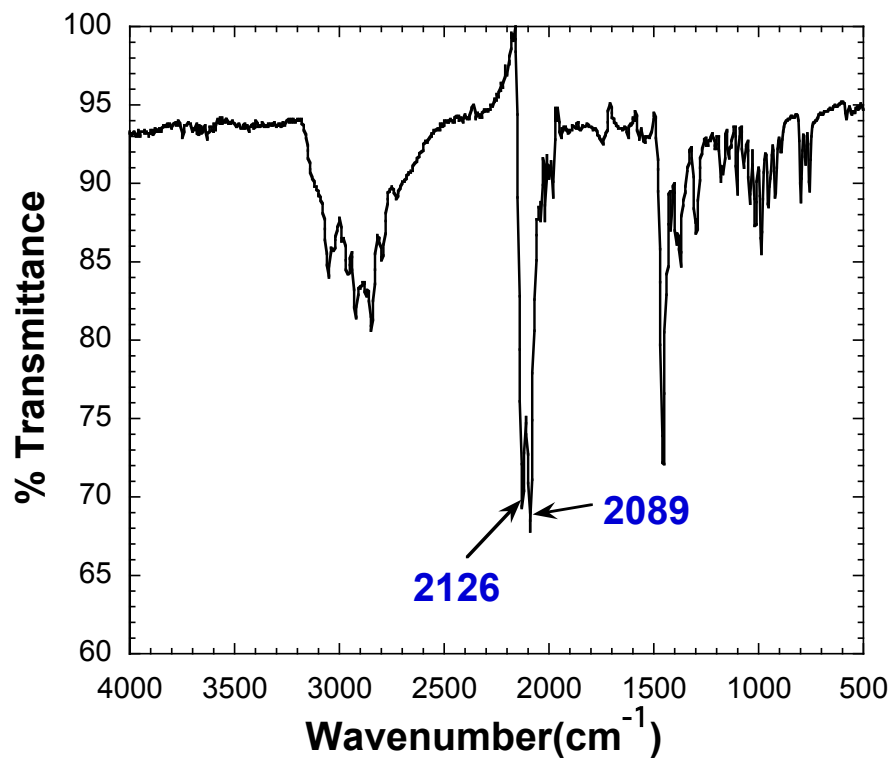


Figure C.2.9. FT-IR spectrum of $[\text{Cu}_2(\text{CN})_3 \cdot 0.5\text{TMEDA} \cdot \text{H}_2]_n$ synthesized at 80 °C.

C.3. Powder X-Ray Diffraction Patterns for Copper(I)-Cyanide Frameworks

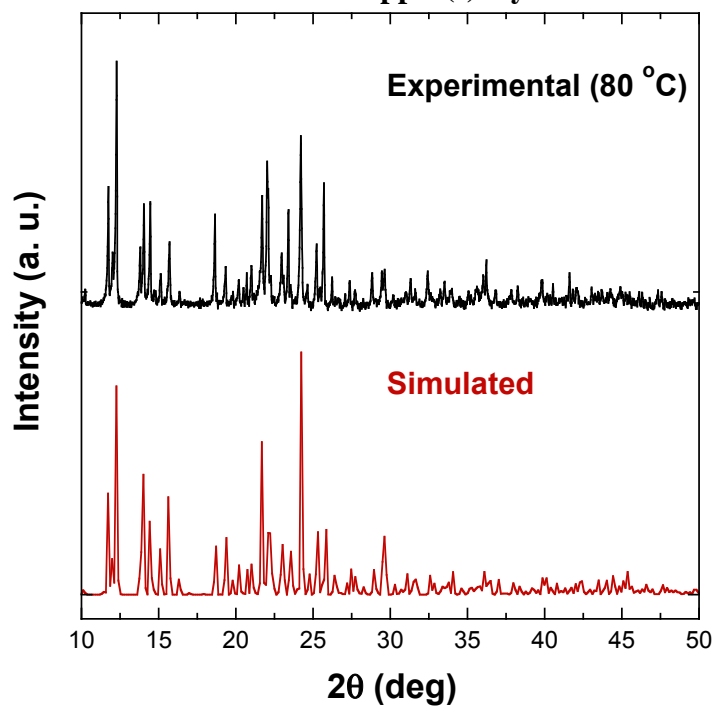


Figure C.3.1. Experimental and simulated powder X-ray diffraction pattern of $[\text{Cu}^1_2(\text{phen})_2(\text{CN})_2 \cdot \text{CH}_3\text{OH}]_n$ synthesized at 80 °C

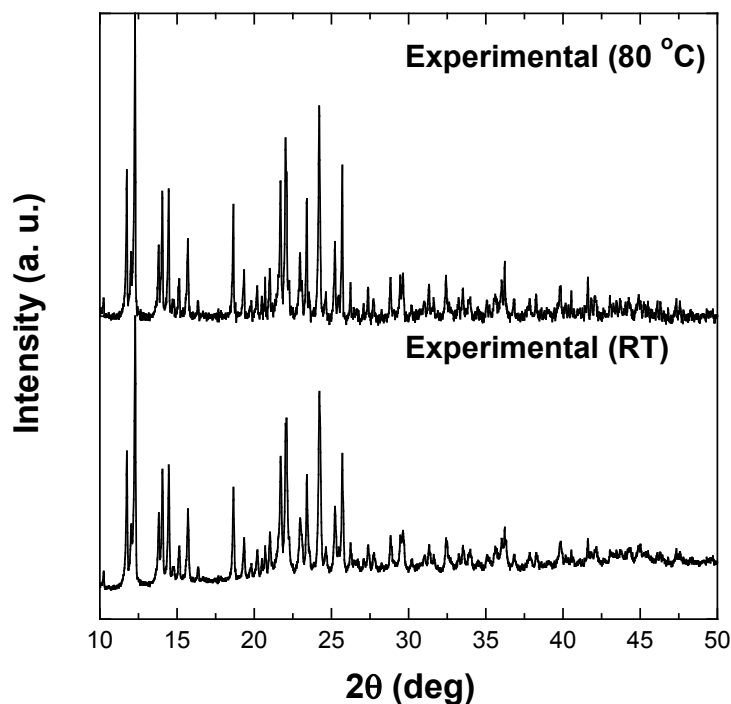


Figure C.3.2. Experimental powder X-ray diffraction pattern of $[\text{Cu}^1_2(\text{phen})_2(\text{CN})_2 \cdot \text{CH}_3\text{OH}]_n$ synthesized at 80 °C and ambient temperature.

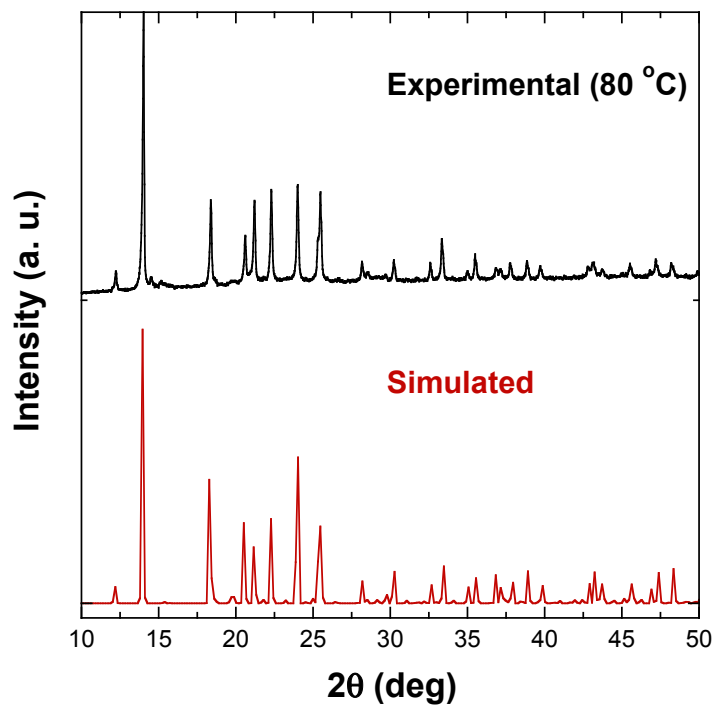


Figure C.3.3. Experimental and simulated powder X-ray diffraction pattern of $[\text{Cu}^{\text{I}}(\text{bpy})(\text{CN})]_n$ synthesized at 80 °C.

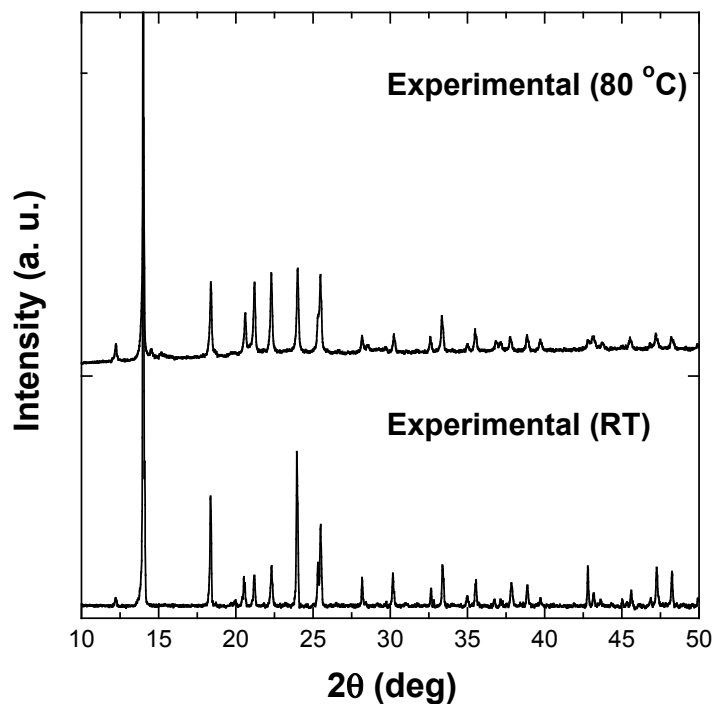


Figure C.3.4. Experimental powder X-ray diffraction pattern of $[\text{Cu}^{\text{I}}(\text{bpy})(\text{CN})]_n$ synthesized at 80 °C and ambient temperature.

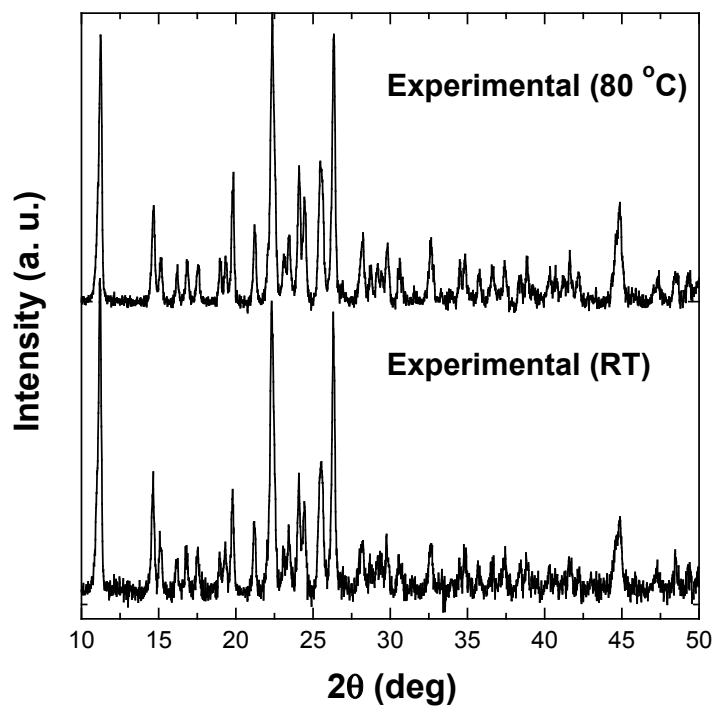


Figure C.3.5. Experimental powder X-ray diffraction pattern of $[\text{Cu}^{\text{I}}(5\text{-NO}_2\text{-phen})(\text{CN})]_n$ synthesized at 80 °C and ambient temperature.

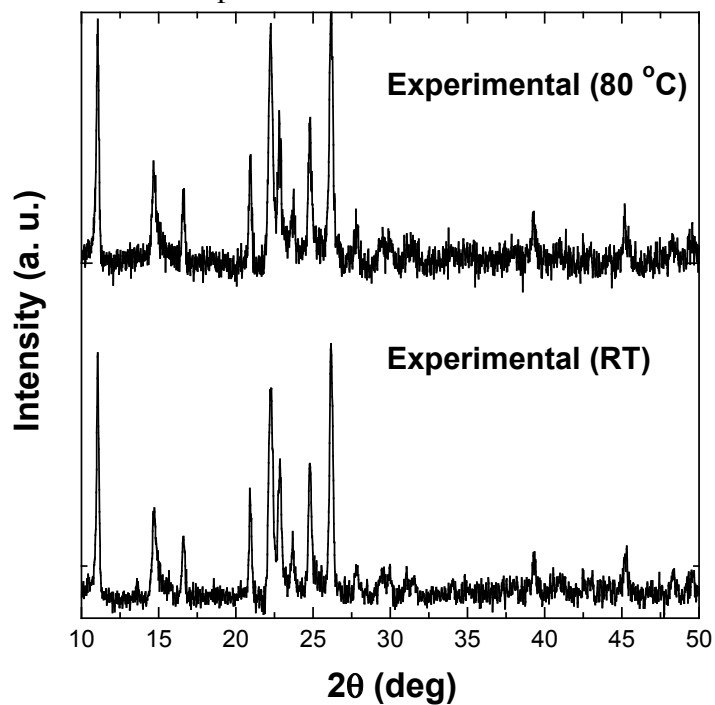


Figure C.3.6. Experimental powder X-ray diffraction pattern of $[\text{Cu}^{\text{I}}(5\text{-Cl-phen})(\text{CN})]_n$ synthesized at 80 °C and ambient temperature.

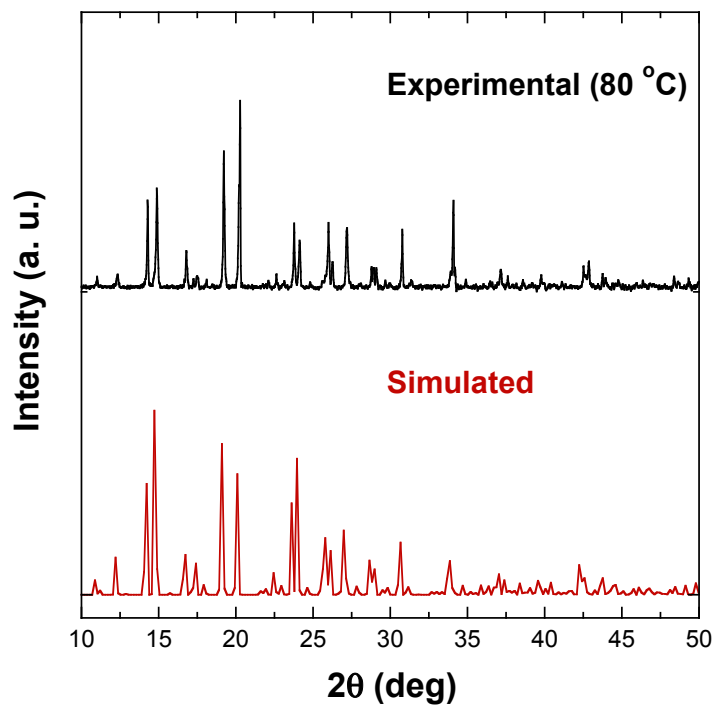


Figure C.3.7. Experimental and simulated powder X-ray diffraction pattern of $[\text{Cu}^{\text{I}}_3(4,4'\text{-dMe-bpy})_2(\text{CN})_3]_n$ synthesized at 80 °C.

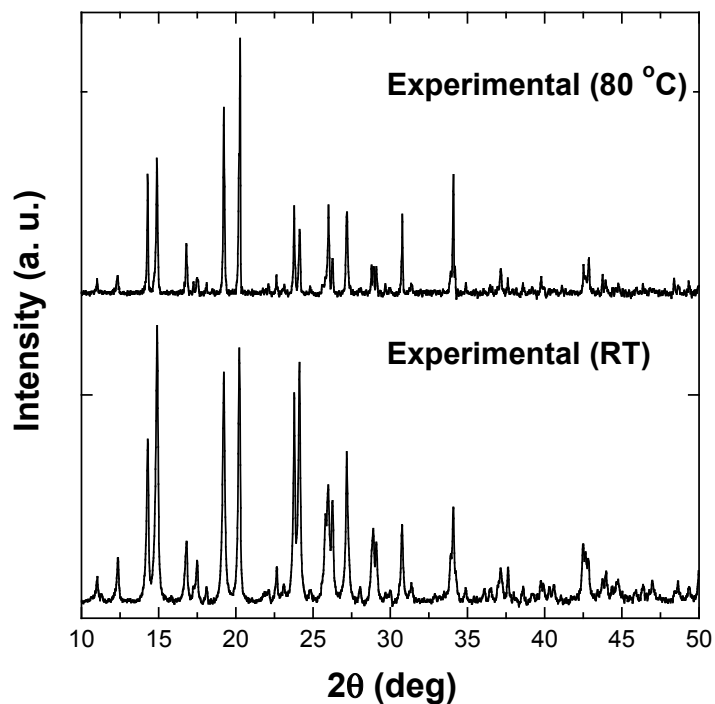


Figure C.3.8. Experimental powder X-ray diffraction pattern of $[\text{Cu}^{\text{I}}_3(4,4'\text{-dMe-bpy})_2(\text{CN})_3]_n$ synthesized at 80 °C and ambient temperature.

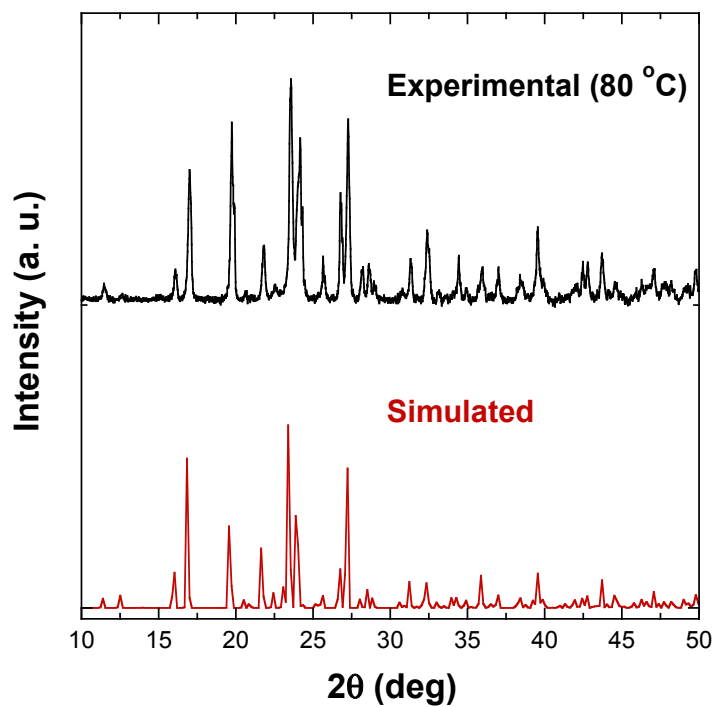


Figure C.3.9. Experimental and simulated powder X-ray diffraction pattern of $[\text{Cu}^{\text{I}}(4,4'\text{-dCO}_2\text{Me-bpy})(\text{CN})]_n$ synthesized at $80\text{ }^\circ\text{C}$.

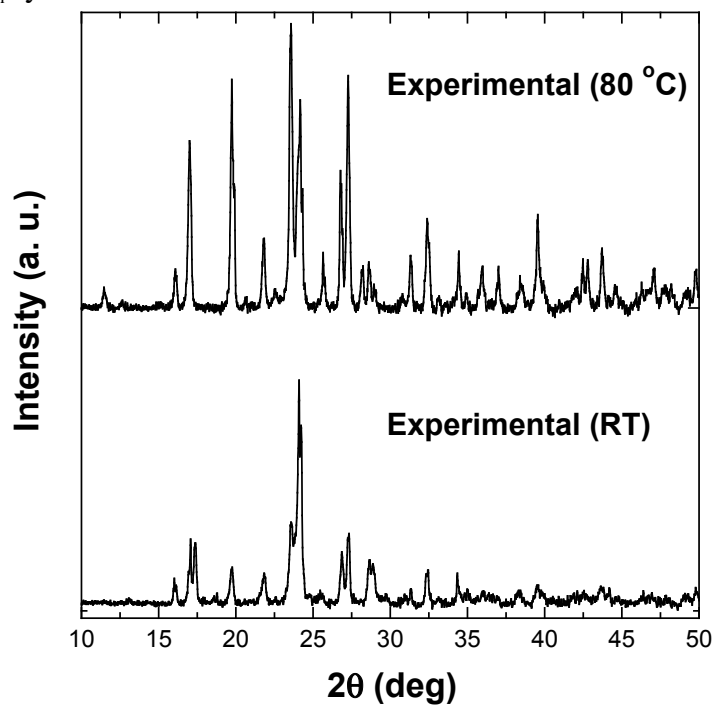


Figure C.3.10 Experimental powder X-ray diffraction pattern of $[\text{Cu}^{\text{I}}(4,4'\text{-dCO}_2\text{Me-bpy})(\text{CN})]_n$ synthesized at $80\text{ }^\circ\text{C}$ and ambient temperature.

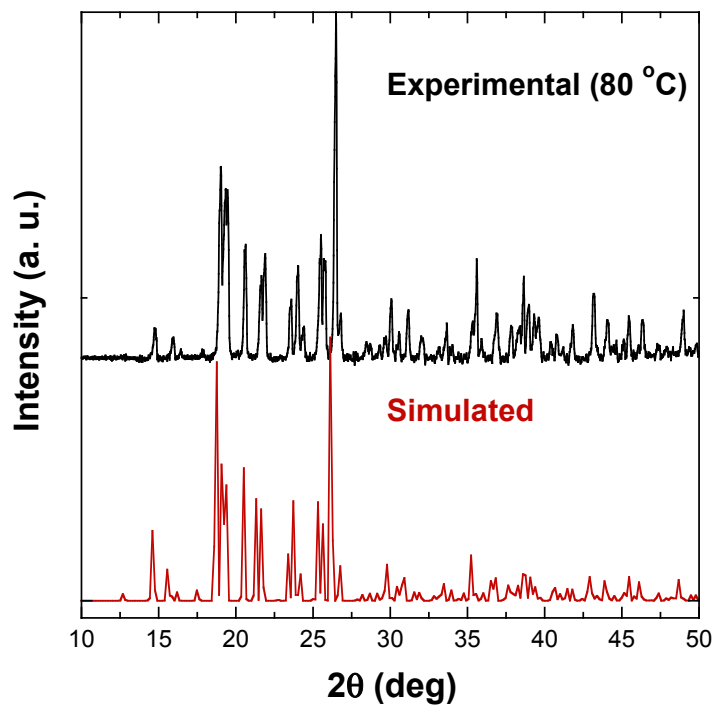


Figure C.3.11. Experimental and simulated powder X-ray diffraction pattern of $[\text{Cu}^{\text{I}}(4,4'\text{-dCO}_2\text{Et-bpy})_{0.5}(\text{CN})]_n$ synthesized at 80 °C.

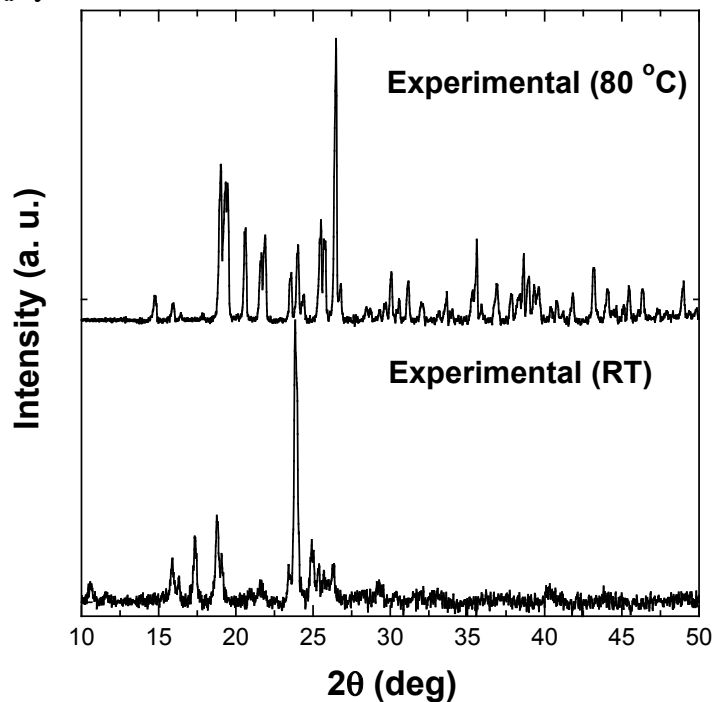


Figure C.3.12. Experimental powder X-ray diffraction pattern of $[\text{Cu}^{\text{I}}(4,4'\text{-dCO}_2\text{Et-bpy})_{0.5}(\text{CN})]_n$ synthesized at 80 °C and ambient temperature.

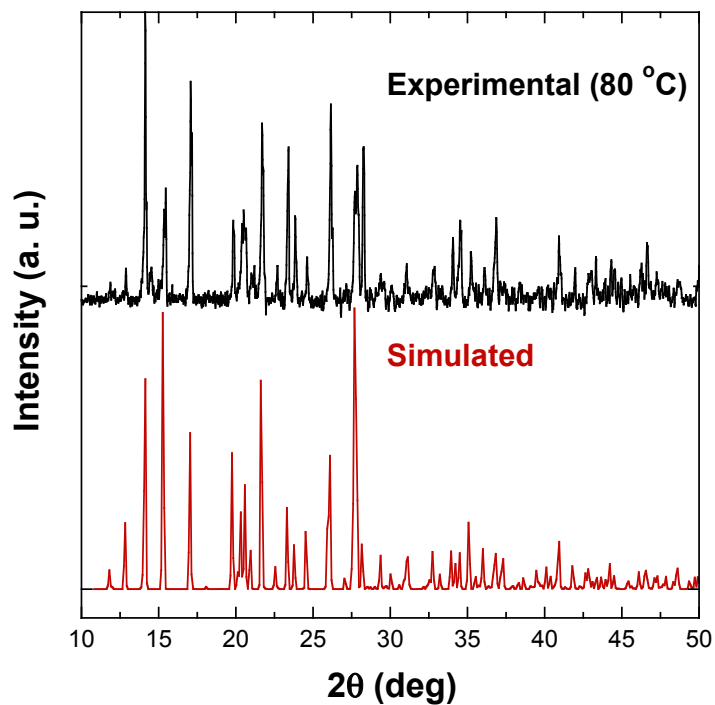


Figure C.3.13. Experimental and simulated powder X-ray diffraction pattern of $[\text{Cu}^{\text{I}}(\text{pylpy})_2(\text{CN})_5]_n$ synthesized at 80 °C.

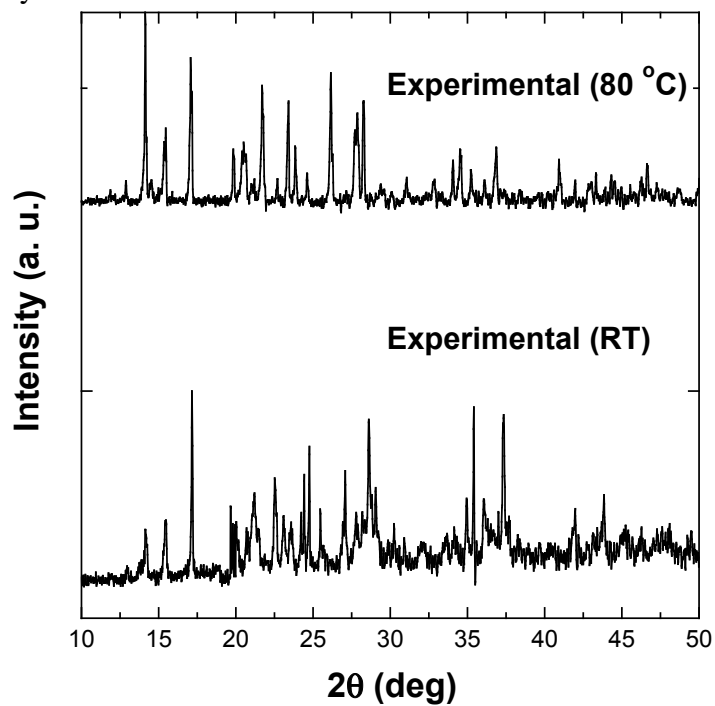


Figure C.3.14. Experimental powder X-ray diffraction pattern of $[\text{Cu}^{\text{I}}(\text{pylpy})_2(\text{CN})_5]_n$ synthesized at 80 °C and ambient temperature.

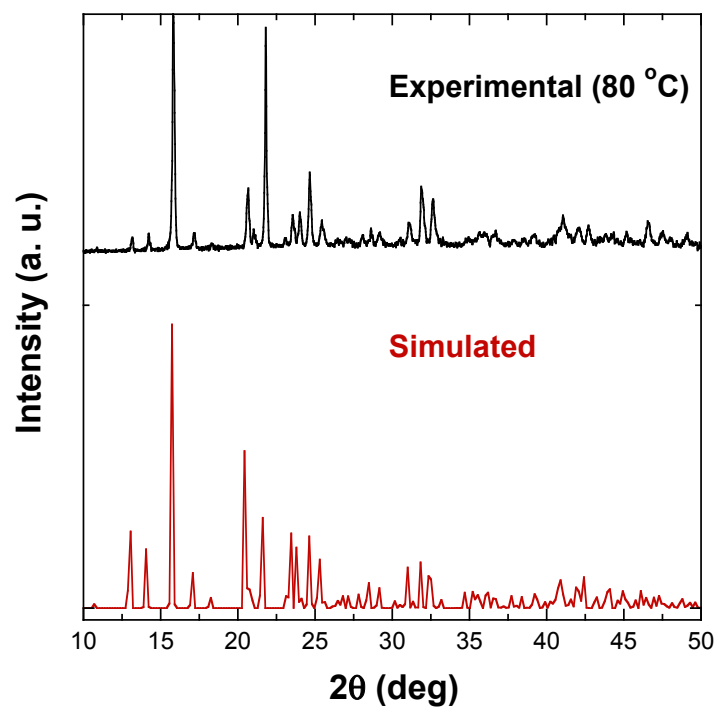


Figure C.3.15. Experimental and simulated powder X-ray diffraction pattern of $[\text{Cu}_2(\text{CN})_3 \cdot 0.5\text{TMEDA-H}_2]_n$ synthesized at 80 °C.

C.4 Packing Diagrams for Copper(I)-Cyanide Frameworks

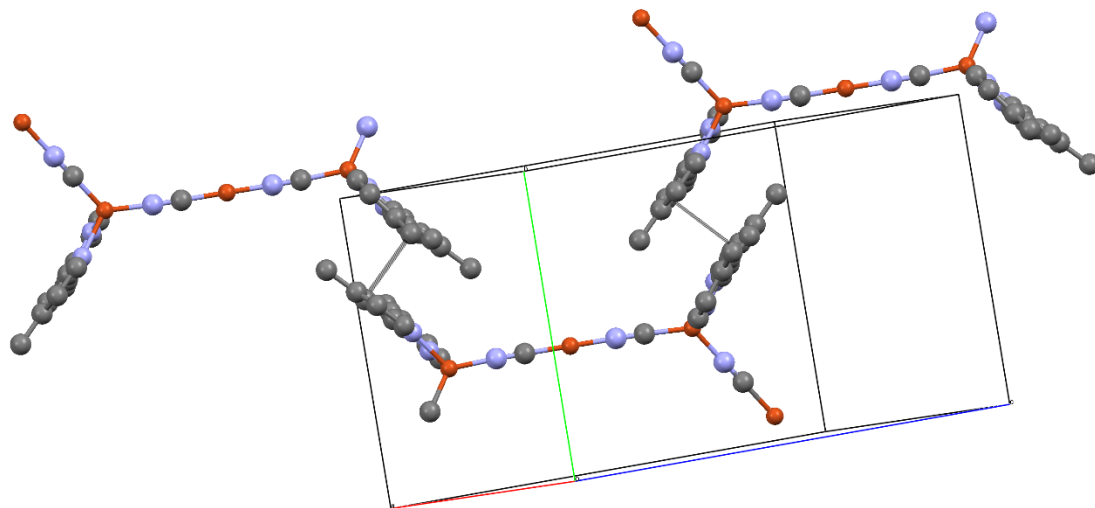


Figure C.4.1. Partial packing diagram of $[\text{Cu}^{\text{I}}_3(4,4'\text{-dMe-bpy})_2(\text{CN})_3]_n$ showing π - π stacking interactions (3.112(2) Å) between 4,4'-dMe-bpy ligands.

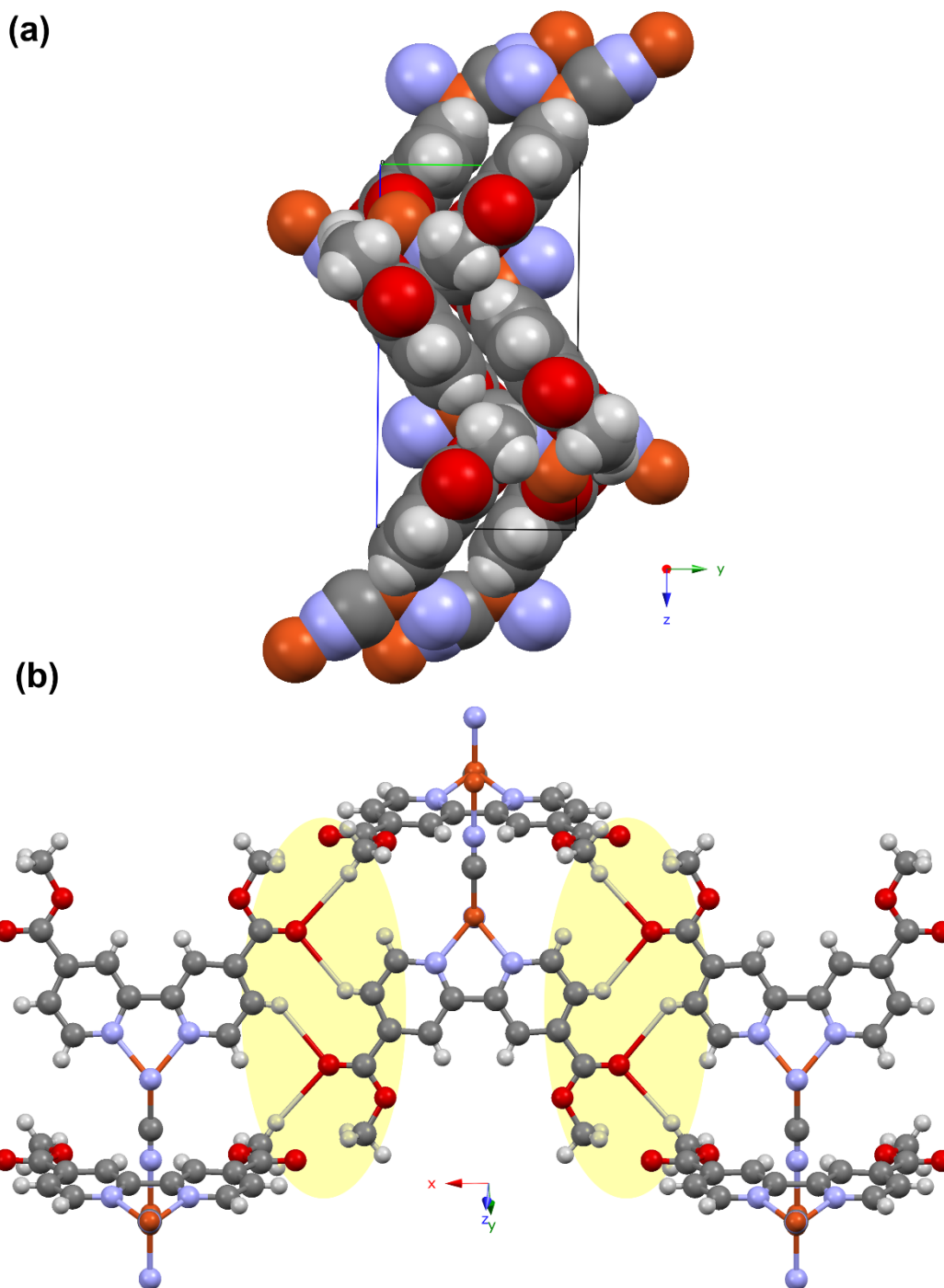


Figure C.4.2. Partial packing diagram of $[\text{Cu}^{\text{I}}(4,4'\text{-dCO}_2\text{Me-bpy})(\text{CN})]_n$ showing one-dimensional zigzag chains and layering of 4,4'-dCO₂Me-bpy ligands (a) and weak intermolecular C-H...O (2.641(3)-2.677(2) Å) interactions.

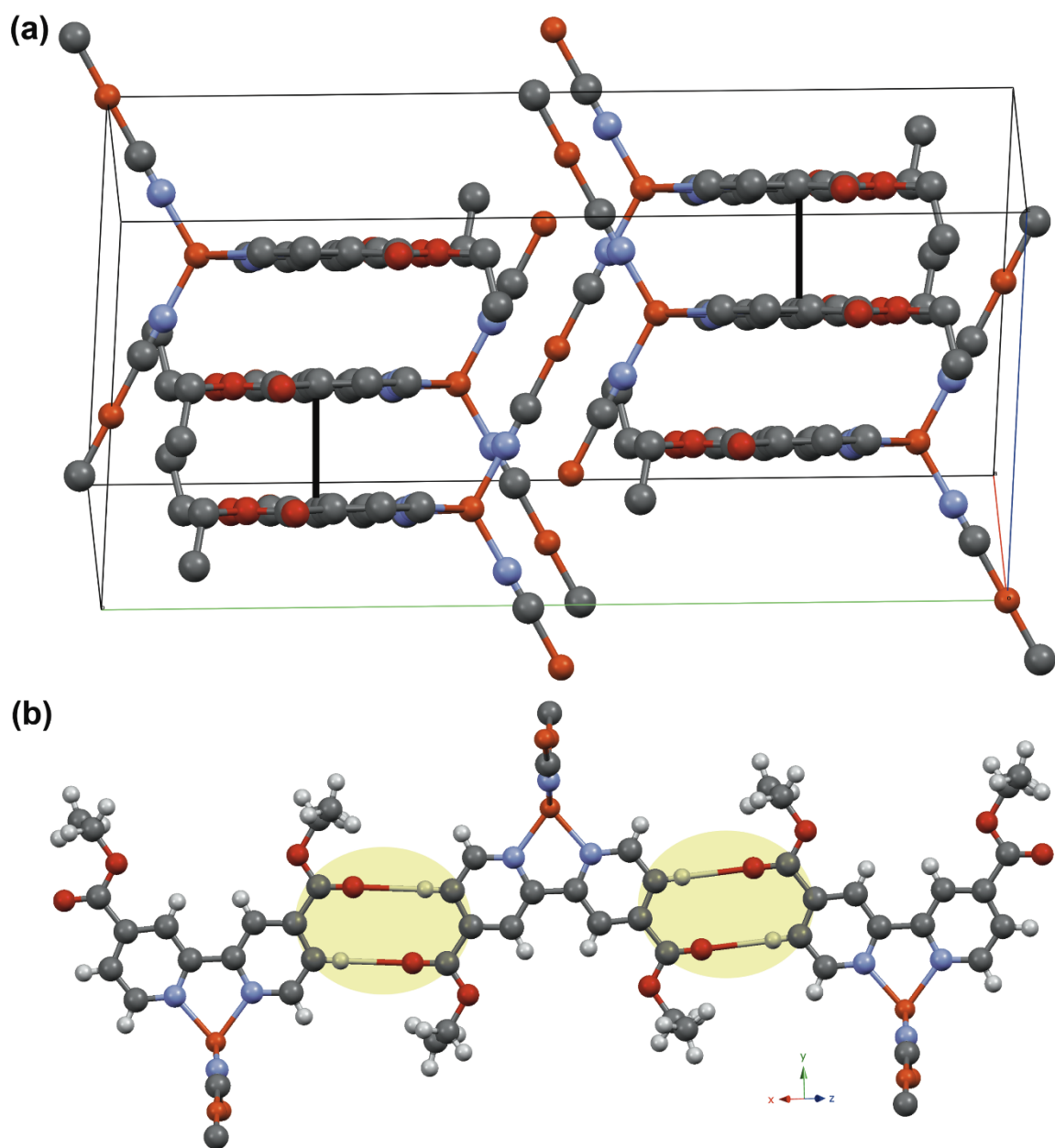


Figure C.4.3. Partial packing diagram of $[\text{Cu}^{\text{I}}(4,4'\text{-dCO}_2\text{Et-bpy})_{0.5}(\text{CN})]_n$ showing π - π stacking interactions (3.526(3) Å) between 4,4'-dCO₂Et-bpy ligands (a) and weak intermolecular C-H...O (2.463(4) Å) contacts.

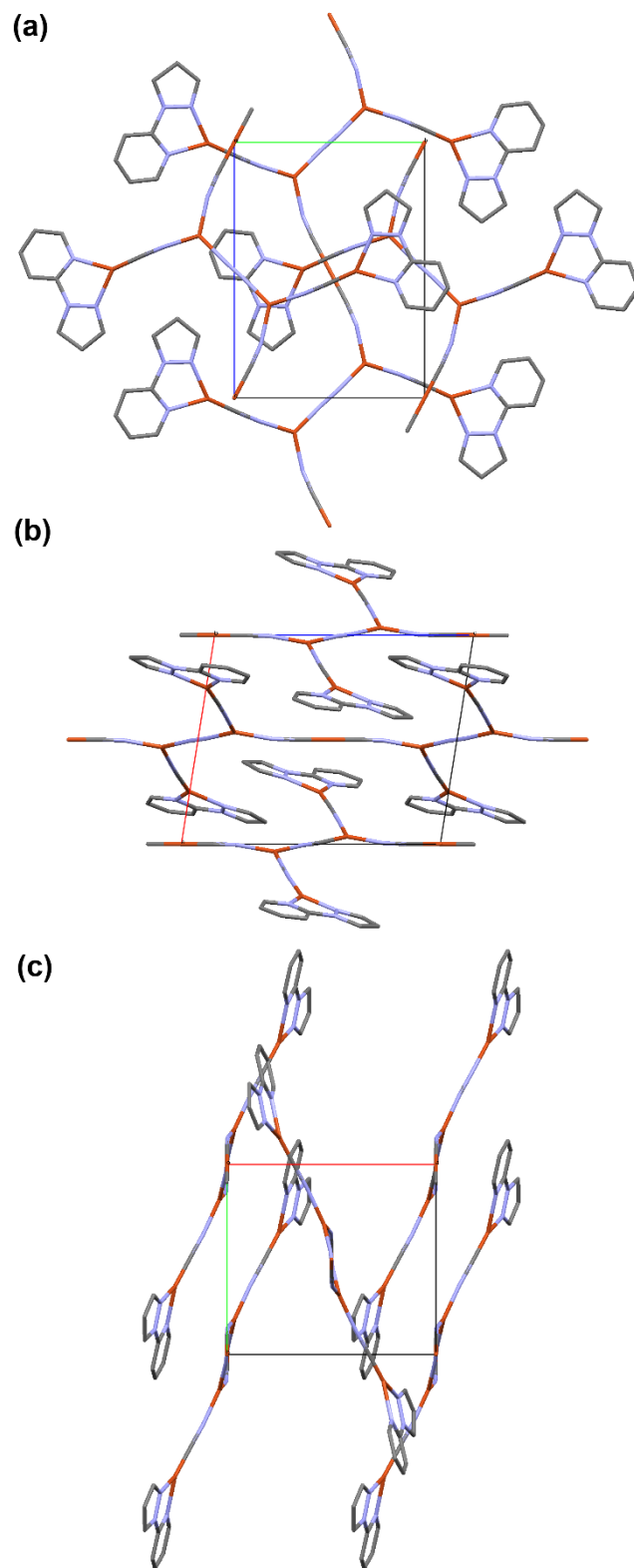


Figure C.4.5. Packing diagram of $[\text{Cu}^{\text{I}}(\text{pyIpy})_2(\text{CN})_5]_n$ viewed along the *a* (a), *b* (b), and *c* (c) axes. Hydrogen atoms have been omitted for clarity.

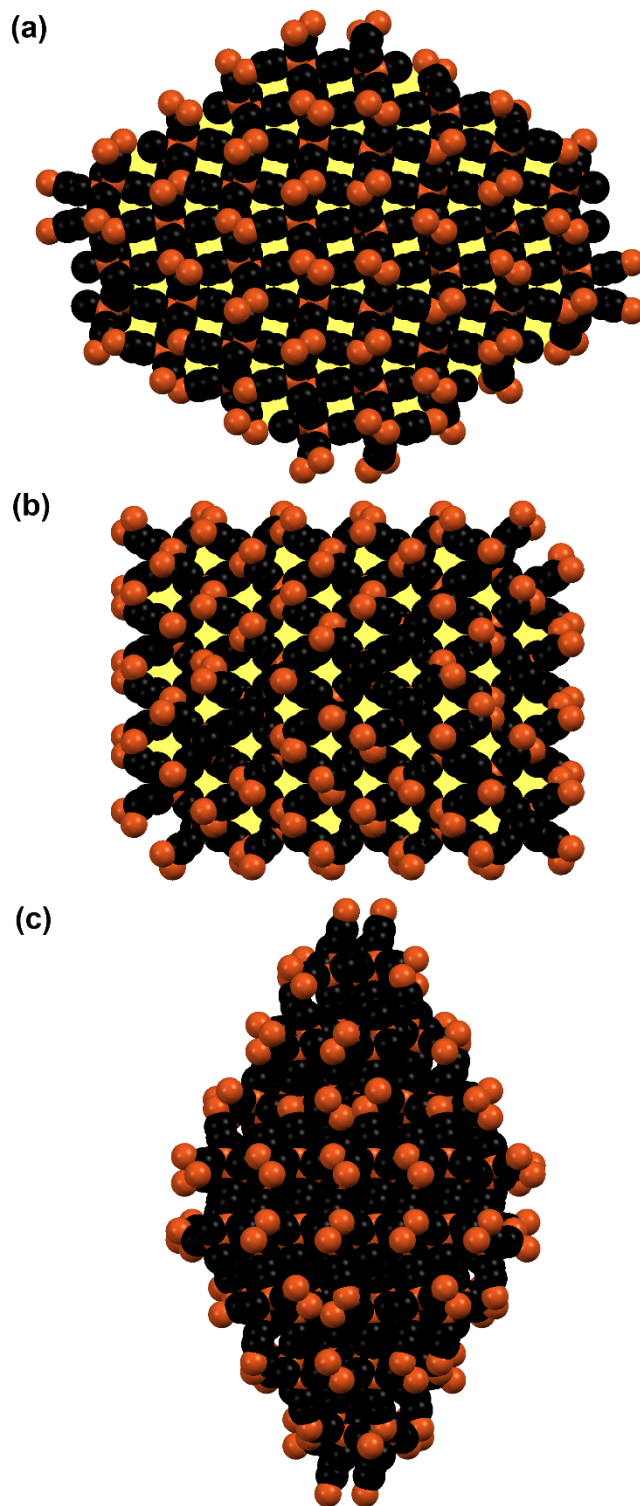


Figure C.4.6. Space filling model of $[\text{Cu}_2(\text{CN})_3 \cdot 0.5\text{TMEDA-H}_2]_n$ viewed along the a (a), b (b), and c (c) axes. Guest TMEDA molecules have been removed from clarity. Voids along the a and b axes are shown in yellow. Black=C or N, orange=Cu.

Appendix D.

Table D.1. Crystallographic Tables for $[\text{Cu}_4\text{CN}_6(\text{dbzpip-H}_2)]_n$ and $[\text{Cu}_2\text{CN}_3(\text{bdmpip-H})]_n$

	$[\text{Cu}_4\text{CN}_6(\text{dbzpip-H}_2)]_n$	$[\text{Cu}_2\text{CN}_3(\text{bdmpip-H})]_n$
Formula	$\text{C}_6\text{Cu}_4\text{N}_6 \cdot \text{C}_{18}\text{H}_{24}\text{N}_2$	$\text{C}_3\text{Cu}_2\text{N}_3 \cdot \text{C}_{30}\text{H}_{31}\text{N}_2$
Color	Colorless	Colorless
Shape	Plate	Plate
Formula Weight	678.71	624.73
Crystal System	Triclinic	Monoclinic
Space Group	P-1	P21/c
Temp (K)	180	180
Cell Constants		
a, Å	8.8904 (8)	8.8912 (5)
b, Å	10.8687 (9)	13.6294 (7)
c, Å	13.9640 (12)	24.5795 (14)
α, deg	86.545 (1)	90
β, deg	89.998 (1)	90.599 (4)
γ, deg	81.412 (1)	90
V, Å³	1331.7 (2)	2978.4 (3)
Formula units/unit cell	2	4
Dcal'd, gcm⁻³	1.693	1.393
Absorption coefficient, mm⁻¹	3.18	1.46
F(000)	680	1288
Diffractometer	Bruker Smart ApexII	Bruker Smart ApexII
Radiation, graphite monochr.	Mo K λ ($\lambda = 0.71073$ Å)	Mo K λ ($\lambda = 0.71073$ Å)
Crystal size, mm	0.13 × 0.13 × 0.06	0.25 × 0.05 × 0.03
θ range, deg	1.5 to 32.2	1.7 to 23.3
Range of h,k,l	±12, ±16, ±20	±9, ±15, ±27
Reflections collected/unique	17860/9053	28481/4281
Rint	0.025	0.154
Refinement Method	Full Matrix Least-Squares on F2	Full Matrix Least-Squares on F2
Data/Restraints/Parameters	9053/0/329	4281/0/361
GOF on F2	1.05	0.9
Final R indices [I>2σ(I)]	0.05	0.055
R indices (all data)	0.18	0.176
Max. Resid. Peaks (e⁻Å⁻³)	0.86 and -0.96	0.40 and -0.35

Table D.2. Crystallographic Tables for $[\text{Cu}_2\text{CN}_3(\text{Im-H})]_n$, $[\text{Cu}_3(\text{CN})_5(\text{PMDETA-H}_2)]_n$ and $[\text{Cu}_7\text{CN}_{12}(\text{Me}_6\text{TREN-H}_3)]_n$

	$[\text{Cu}_2\text{CN}_3(\text{Im-H})]_n$	$[\text{Cu}_3(\text{CN})_5(\text{PMDETA-H}_2)]_n$
Formula	$\text{C}_3\text{Cu}_2\text{N}_3 \cdot \text{C}_3\text{H}_5\text{N}_2$	$\text{C}_{15}\text{H}_{18}\text{CuN}_5$
Color	Colorless	Colorless
Shape	Cubic	Plate
Formula Weight	274.25	331.88
Crystal System	Monoclinic	Monoclinic
Space Group	<i>Cc</i>	<i>C2/c</i>
Temp (K)	298	180
Cell Constants		
a, Å	14.9610 (4)	22.8256(7)
b, Å	8.6661 (3)	8.5732(3) A
c, Å	7.1698 (2)	20.8377(7)
α, deg	90	90
β, deg	116.411 (2)	100.707(2)
γ, deg	90	90
V, Å³	832.56 (5)	4006.7(2)
Formula units/unit cell	4	8
Dcal'd, gcm⁻³	2.188	1.1
Absorption coefficient, mm⁻¹	5.06	1.091
F(000)	536	1376
Diffractometer	Bruker Smart ApexII	Bruker Smart ApexII
Radiation, graphite monochr.	Mo Kλ (λ = 0.71073 Å)	Mo Kλ (λ = 0.71073 Å)
Crystal size, mm	0.16 × 0.07 × 0.05	0.32 × 0.13 × 0.05
θ range, deg	2.8 to 27.5	1.82 to 26.17
Range of h,k,l	±9, ±11, ±19	±28, ±10, ±25
Reflections collected/unique	5714/1903	24304 / 3988
R_{int}	0.027	0.034
Refinement Method	Full Matrix Least-Squares on F ₂	Full Matrix Least-Squares on F ₂
Data/Restraints/Parameter s	1903/0/118	3988 / 0 / 231
GOF on F₂	0.81	1.04
Final R indices [I > 2σ(I)]	0.032	R1 = 0.0411, wR2 = 0.1087
R indices (all data)	0.105	R1 = 0.0556, wR2 = 0.1181
Max. Resid. Peaks (e*Å⁻³)	0.60 and -0.40	1.686 and -1.42

Table D.3. Crystallographic Tables for $[\text{Cu}_7\text{CN}_{12}(\text{Me}_6\text{TREN-H}_3)]_n$

	$[\text{Cu}_7\text{CN}_{12}(\text{Me}_6\text{TREN-H}_3)]_n$
Formula	$\text{C}_{12}\text{Cu}_7\text{N}_{12} \cdot 2(\text{C}_{12}\text{H}_{33}\text{N}_4)$
Color	Brown
Shape	
Formula Weight	1223.94
Crystal System	Monoclinic
Space Group	<i>P21/m</i>
Temp (K)	298
Cell Constants	
a, Å	8.5113 (4)
b, Å	32.9719 (14)
c, Å	9.5203 (4)
α, deg	90
β, deg	101.448 (3)
γ, deg	90
V, Å³	2618.6 (2)
Formula units/unit cell	2
Dcal'd, gcm⁻³	2.83
Absorption coefficient, mm⁻¹	1.552
F(000)	1250
Diffractometer	Bruker Smart ApexII
Radiation, graphite monochr.	Mo K λ ($\lambda = 0.71073$ Å)
Crystal size, mm	0.16 × 0.13 × 0.07
θ range, deg	1.2 to 24.5
Range of h,k,l	$\pm 10, \pm 11, \pm 38$
Reflections collected/unique	7879/3306
R_{int}	0.027
Refinement Method	Full Matrix Least-Squares on F ₂
Data/Restraints/Parameters	4521/0/304
GOF on F₂	1.01
Final R indices [I > 2σ(I)]	0.048
R indices (all data)	0.15
Max. Resid. Peaks (e[*]Å⁻³)	0.92 and -0.56

D.1 Infrared Spectrum of Two- and Three-Dimensional Copper Cyanide Coordination Polymer

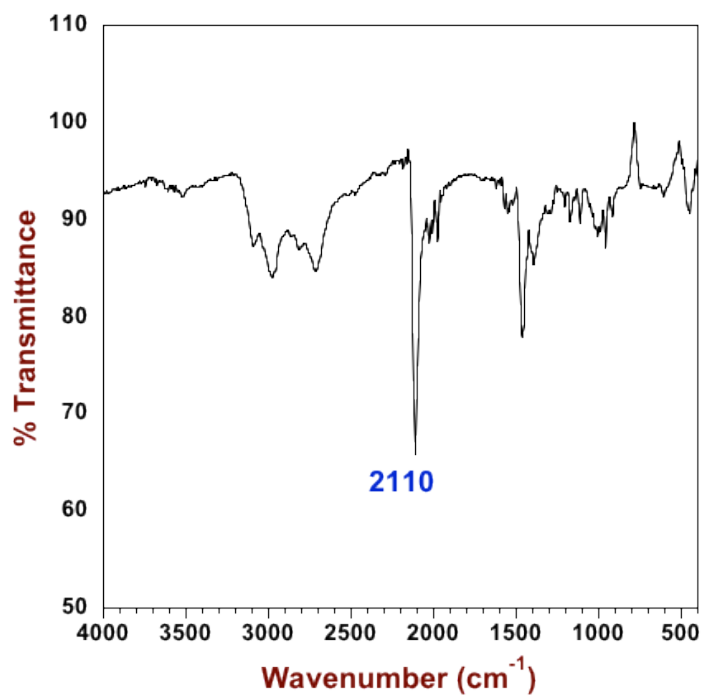


Figure D.1.1. Infrared spectrum of $[\text{Cu}_4\text{CN}_6(\text{dbzpip-H}_2)]_n$ (ATR, FT-IR)

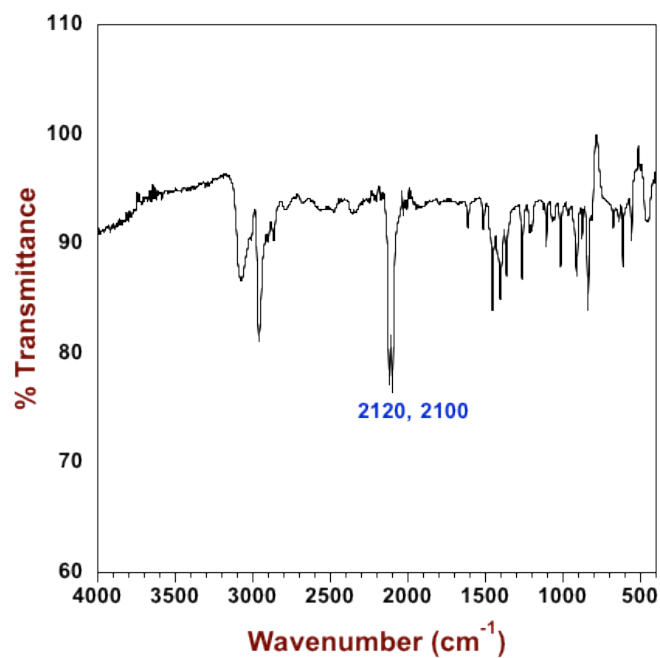


Figure D.1.2. Infrared spectrum of $[\text{Cu}_2\text{CN}_3(\text{bdpmpip-H})]_n$ (ATR, FT-IR)

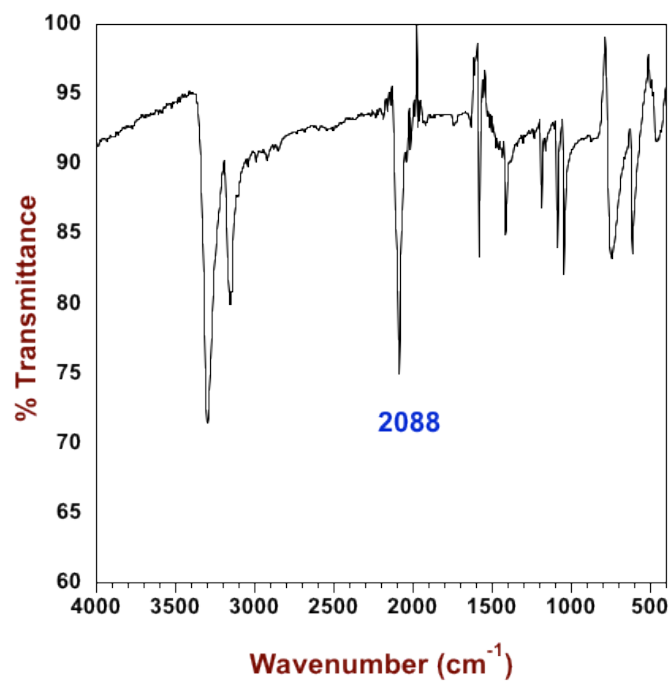


Figure D.1.3. Infrared spectrum of $[\text{Cu}_2\text{CN}_3(\text{Im-H})]_n$ (ATR, FT-IR)

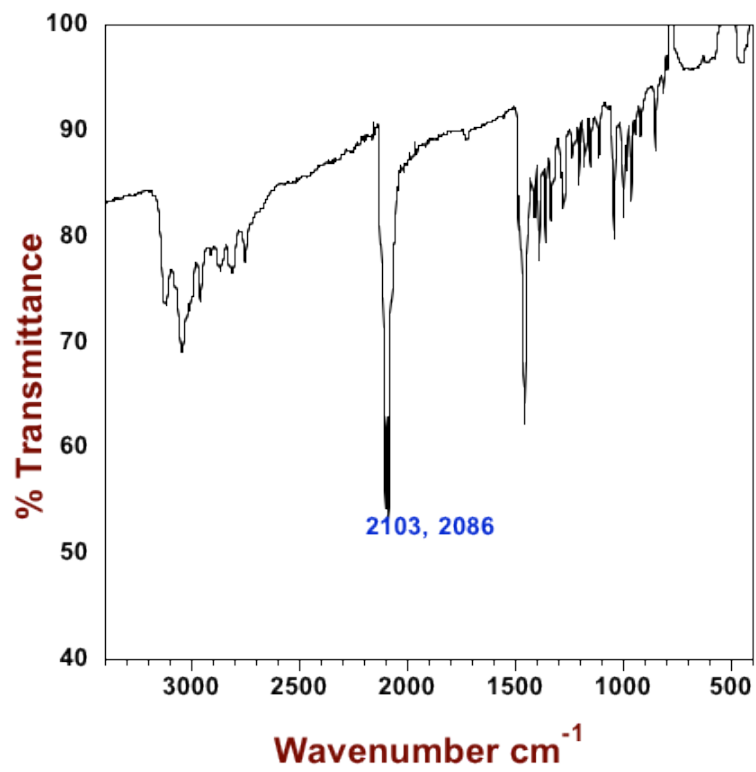


Figure D.1.4. Infrared spectrum of $[\text{Cu}_3(\text{CN})_5(\text{PMDETA-H}_2)]_n$ (ATR, FT-IR)

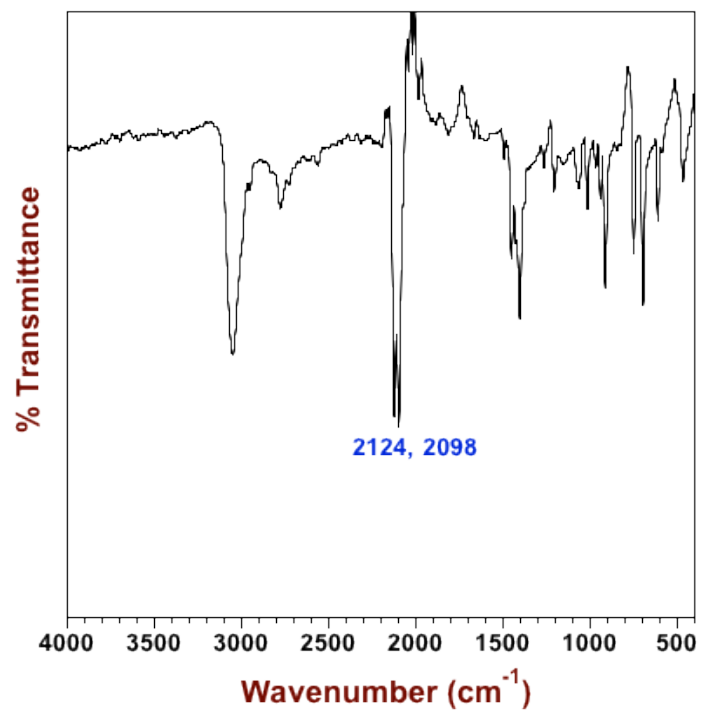


Figure D.1.5. Infrared spectrum of $[\text{Cu}_7\text{CN}_{12}(\text{Me}_6\text{TREN-H}_3)]_n$ (ATR, FT-IR)

D.2. Powder Diffraction Pattern of Two- and Three-dimensional Copper Cyanide Coordination Polymer.

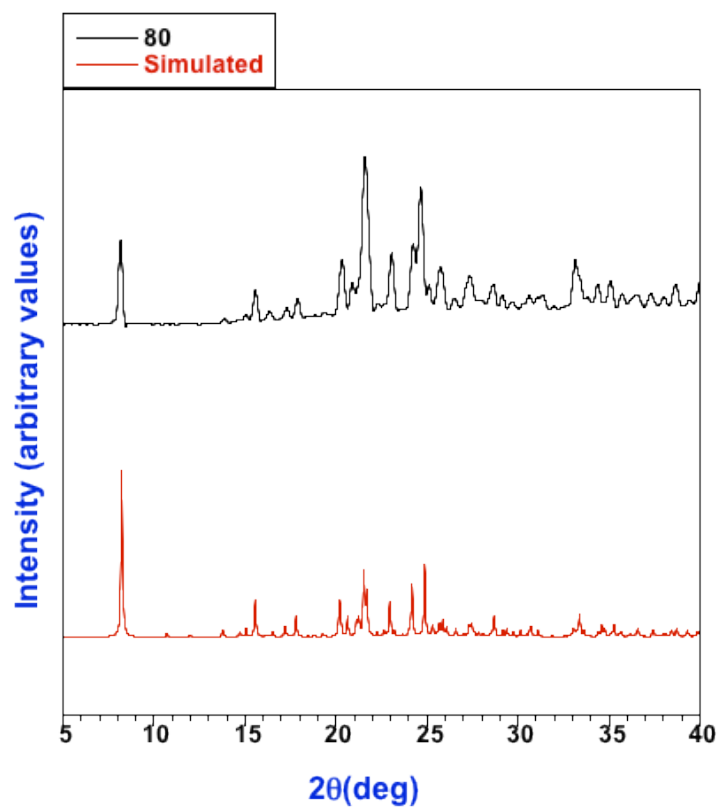


Figure D.2.1. Experimental and simulated powder X-ray diffraction pattern of $[\text{Cu}_4\text{CN}_6(\text{dbzpip-H}_2)]_n$ synthesized at 80°C .

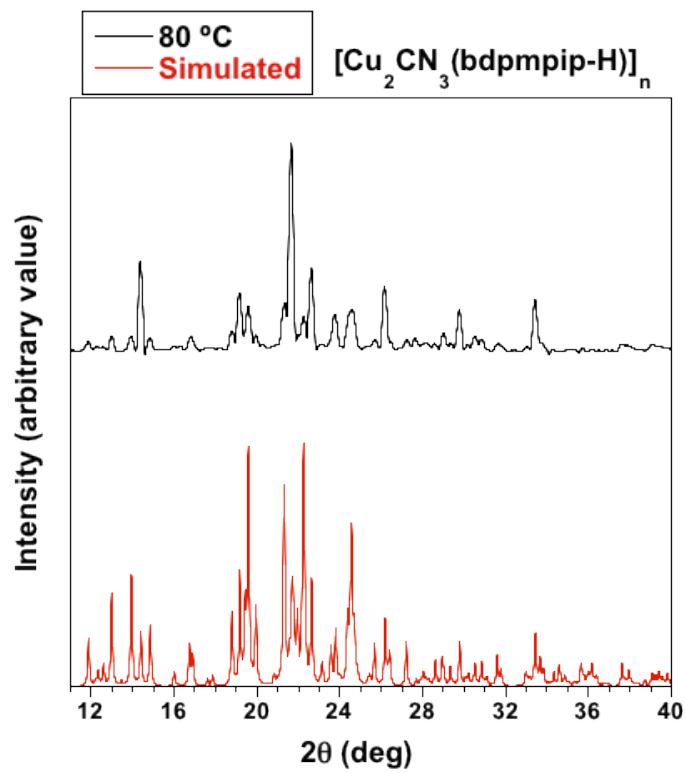


Figure D.2.2. Experimental and simulated powder X-ray diffraction pattern of $[\text{Cu}_2\text{CN}_3(\text{bdpmpip-H})]_n$ synthesized at 80 °C.

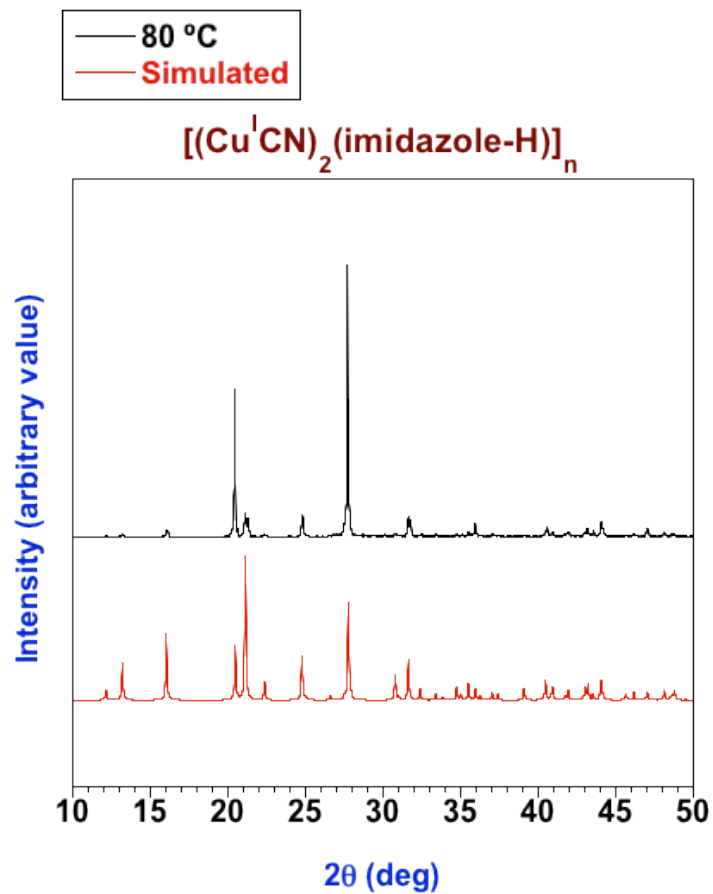


Figure D.2.3. Experimental and simulated powder X-ray diffraction pattern of $[\text{Cu}_2\text{CN}_3(\text{Im-H})]_n$ synthesized at 80 °C.

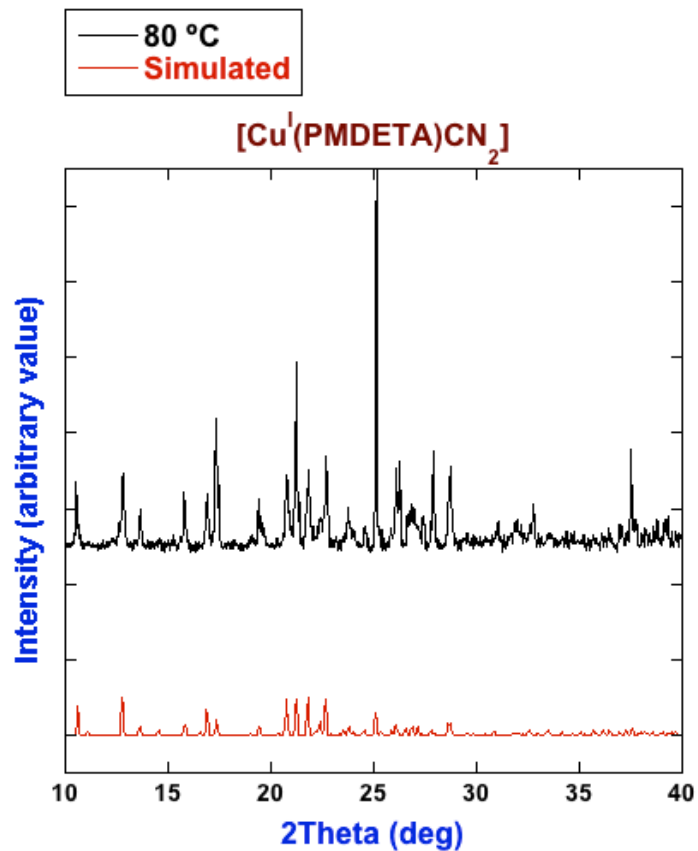


Figure D.2.4. Experimental and simulated powder X-ray diffraction pattern of $[\text{Cu}_3(\text{CN})_5(\text{PMDETA-H}_2)]_n$ synthesized at 80 °C.

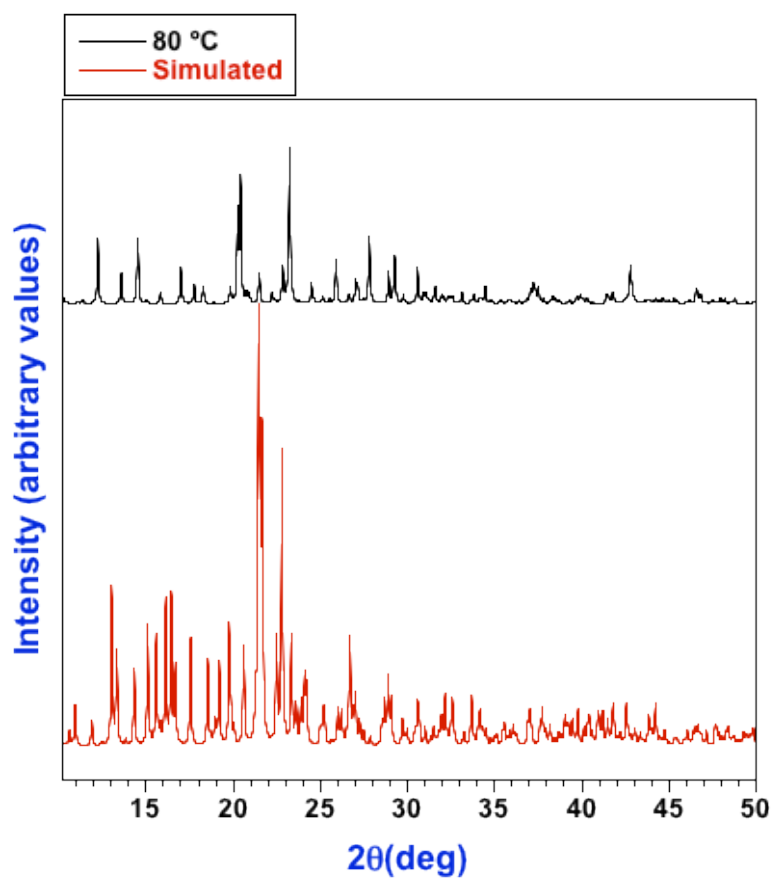


Figure D.2.5. Experimental and simulated powder X-ray diffraction pattern of $[\text{Cu}_7\text{CN}_{12}(\text{Me}_6\text{TREN-H}_3)]_n$ synthesized at 80 °C.

D.3 Fluorescence Spectrum of Copper(I) Cyanide Coordination Polymer

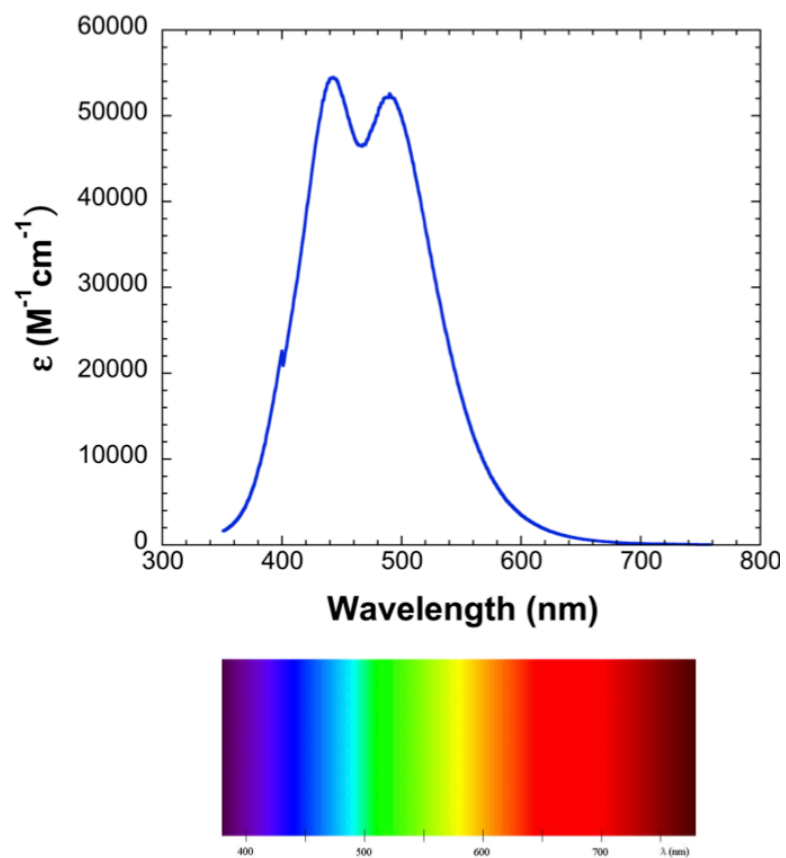
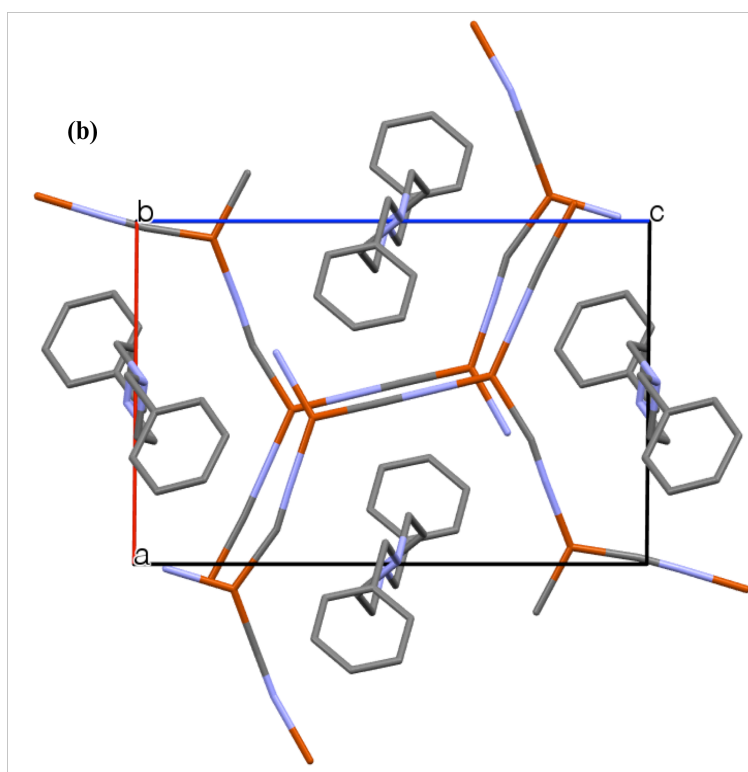
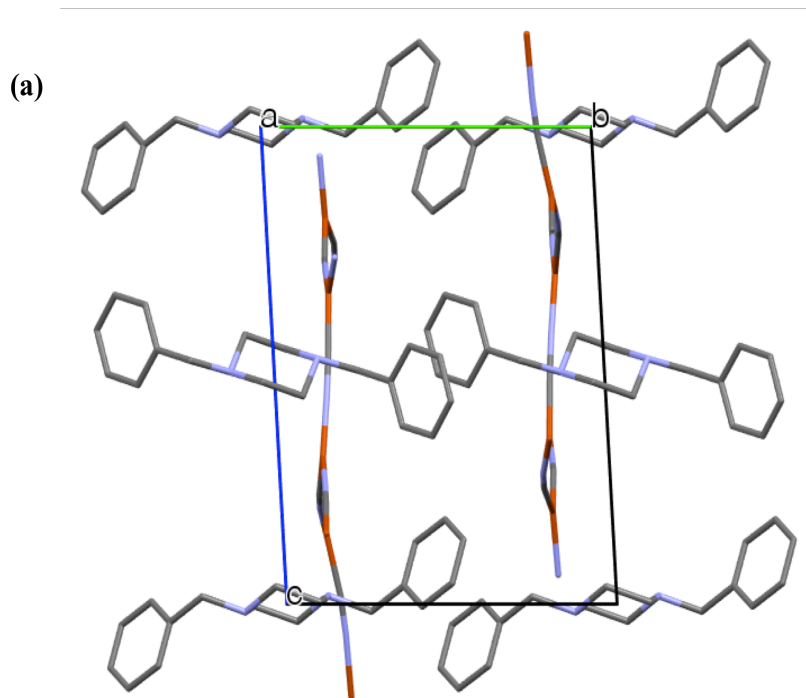


Figure D.3.1. Fluorescence spectrum of $[\text{Cu}_7\text{CN}_{12}(\text{Me}_6\text{TREN-H}_3)]_n$.

D.4. Crystal Packing Structure of Two- and Three-Dimensional Copper Cyanide Coordination Polymer



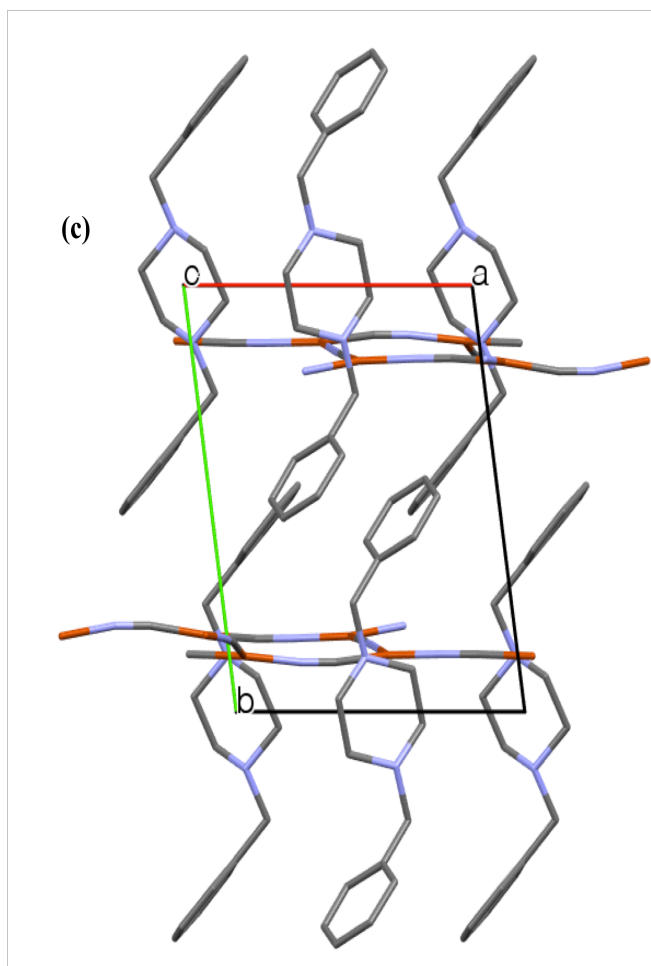
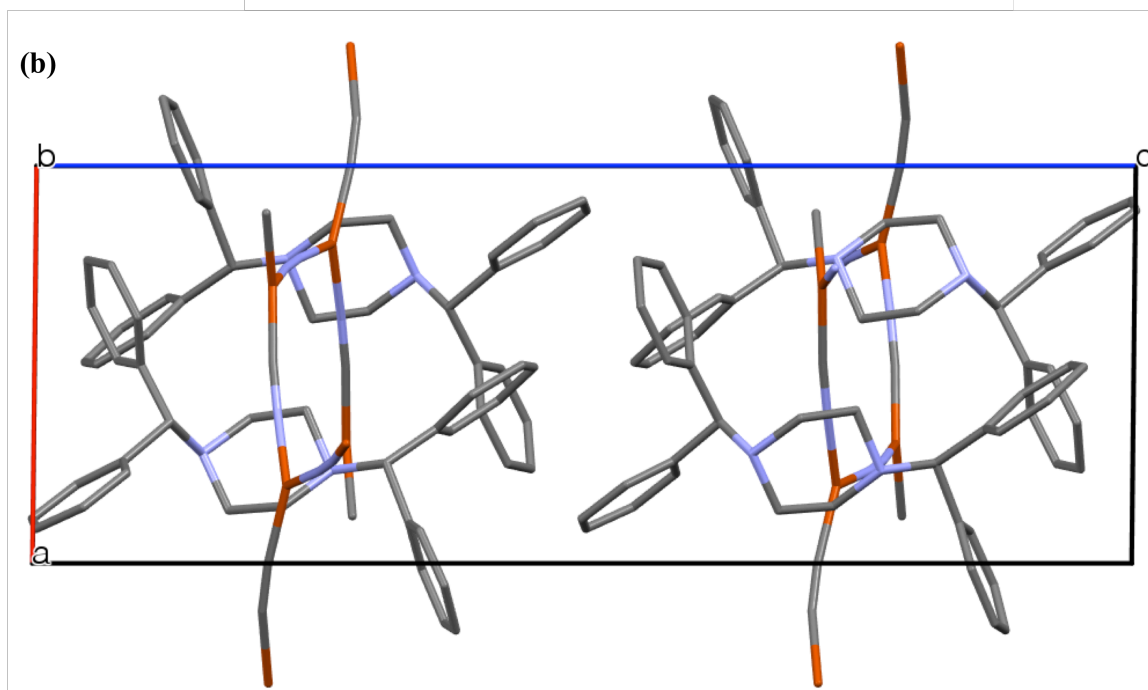
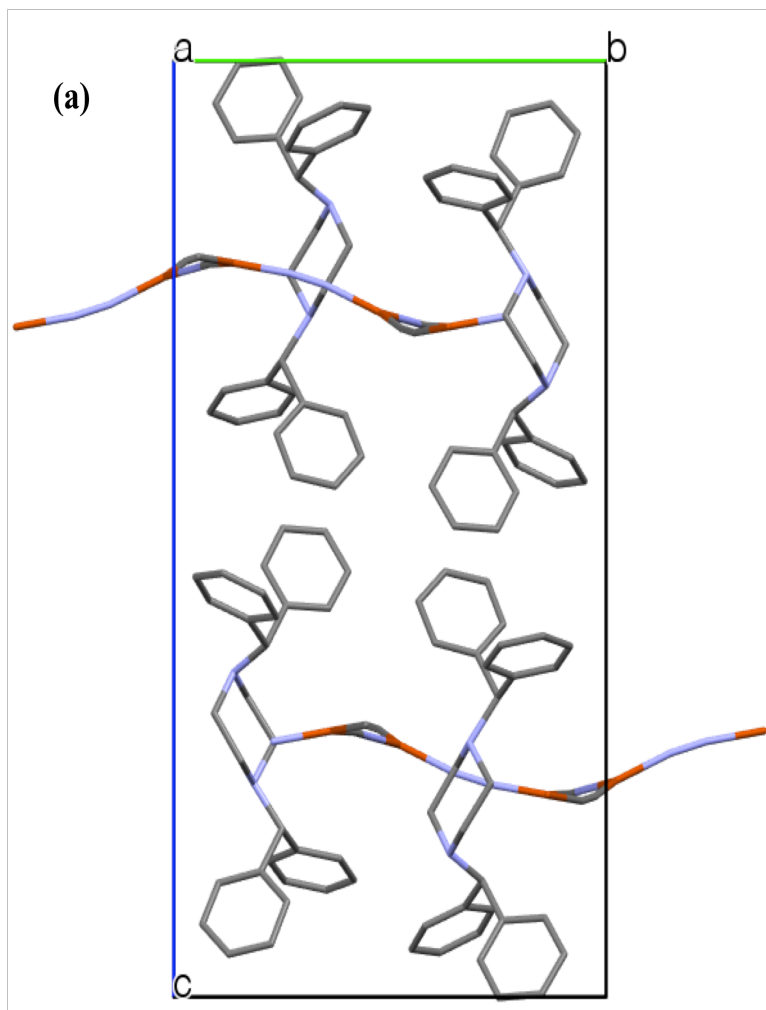


Figure D.4.1. Packing diagram of $[\text{Cu}_4\text{CN}_6(\text{dbzpip-H}_2)]_n$ viewed along the *a* (a), *b* (b), and *c* (c) axes. Hydrogen atoms have been omitted for clarity.



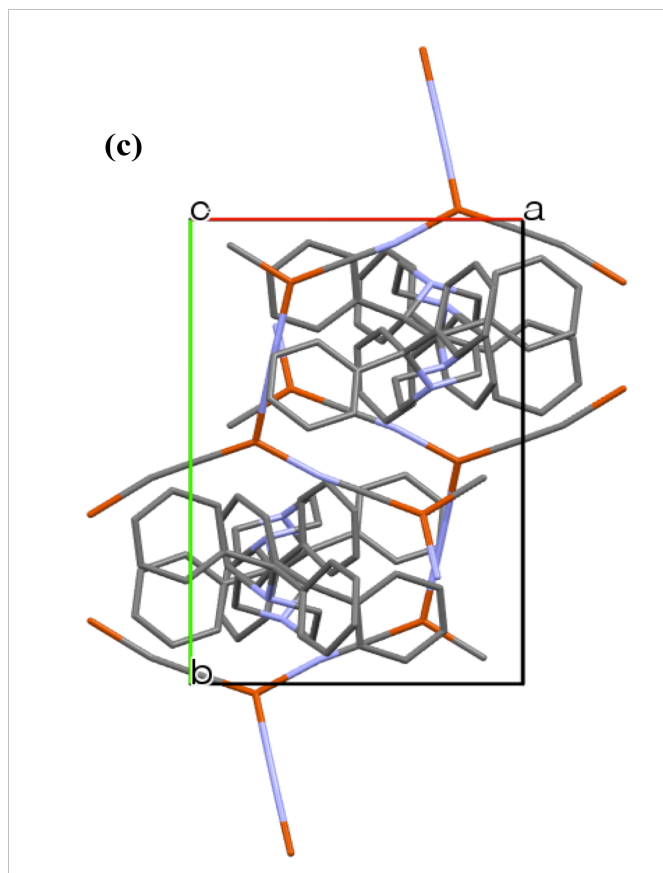
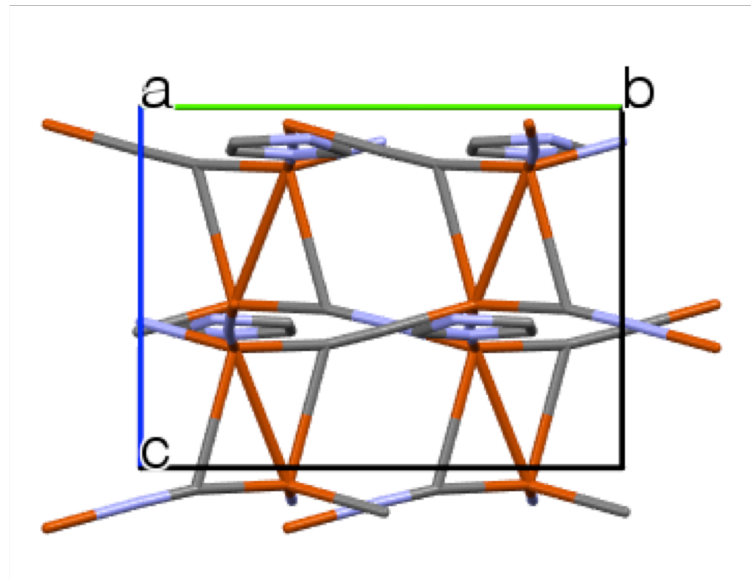
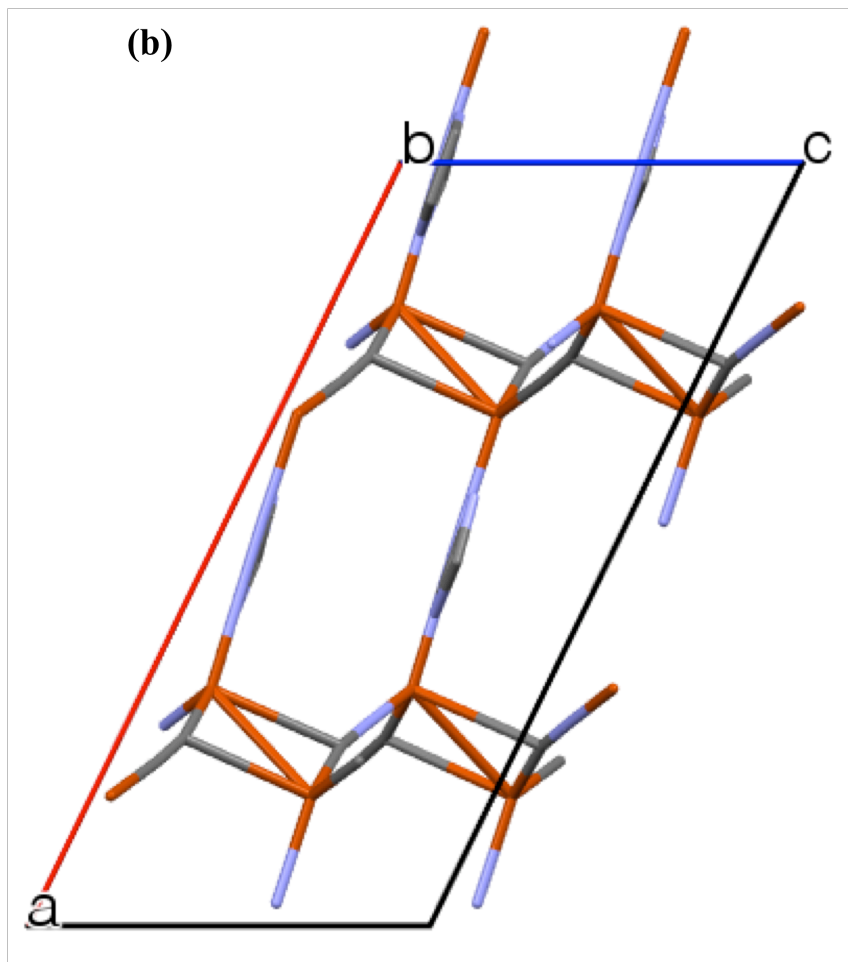


Figure D.4.2. Packing diagram of $[\text{Cu}_2\text{CN}_3(\text{bdpmpip-H})]_n$ viewed along the *a* (a), *b* (b), and *c* (c) axes. Hydrogen atoms have been omitted for clarity.

(a)



(b)



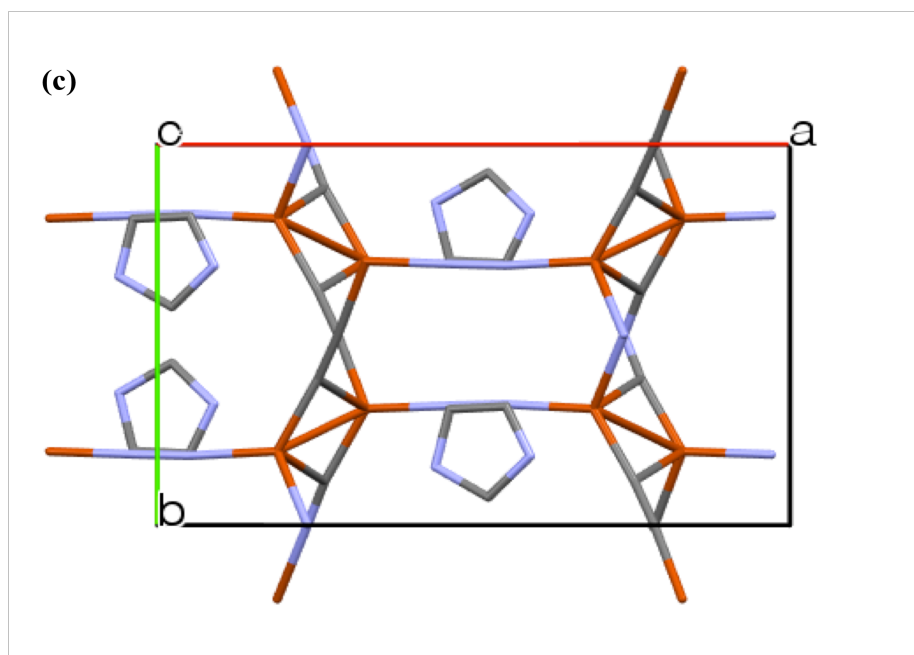
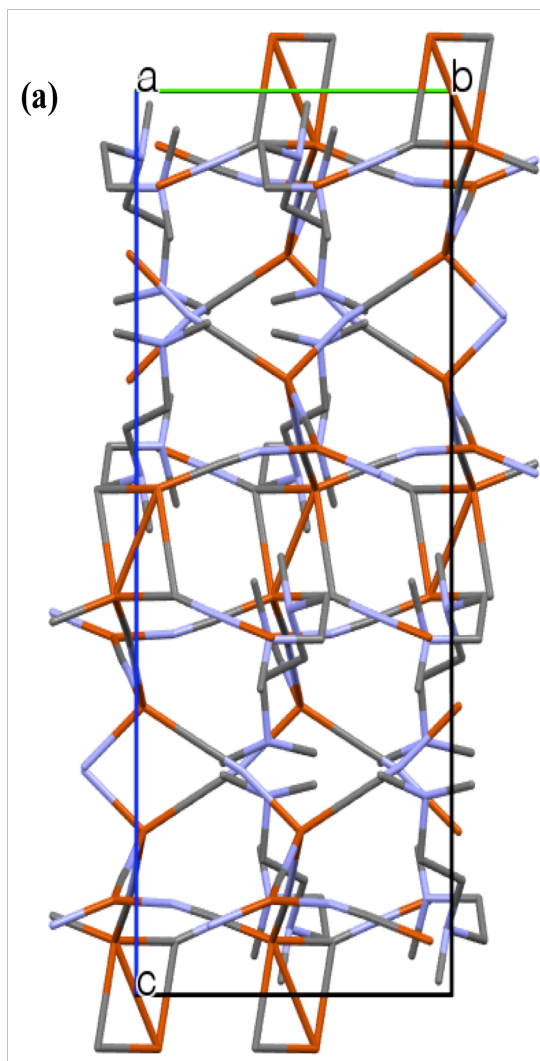


Figure D.4.3. Packing diagram of $[\text{Cu}_2\text{CN}_3(\text{Im-H})]_n$ viewed along the *a* (*a*), *b* (*b*), and *c* (*c*) axes. Hydrogen atoms have been omitted for clarity.



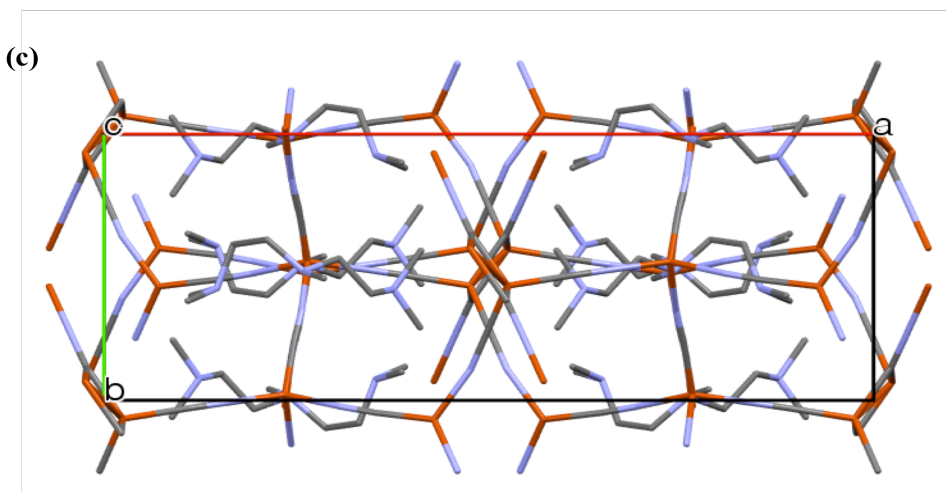
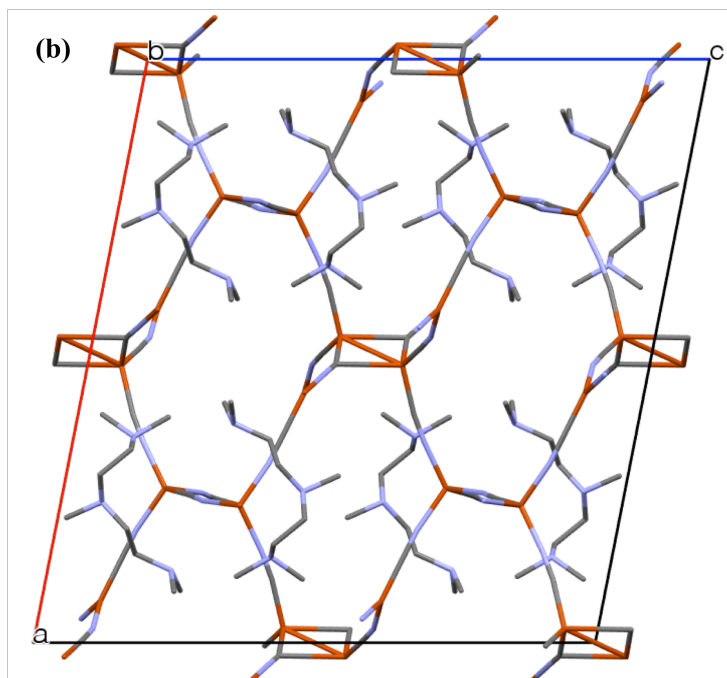
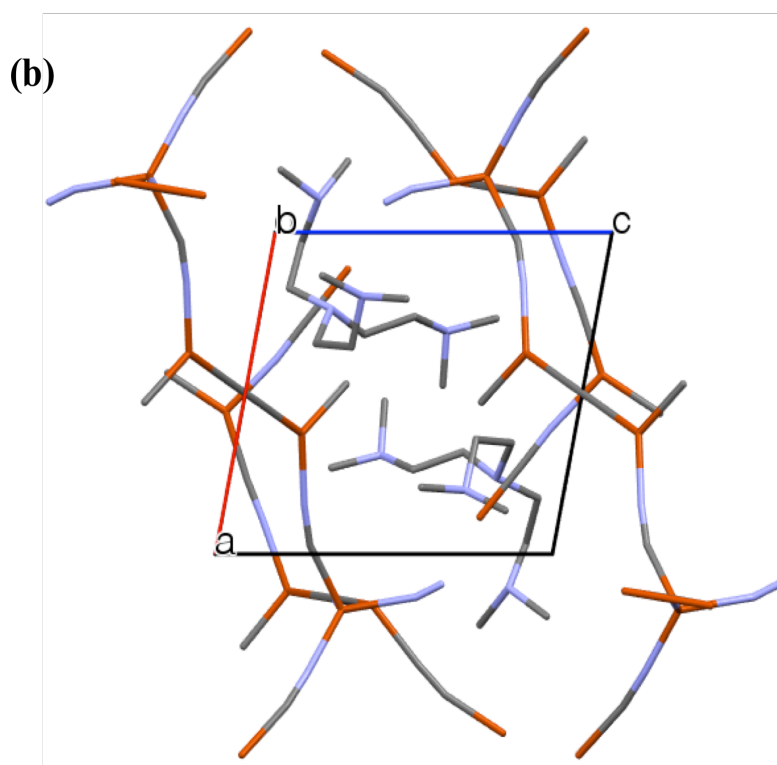
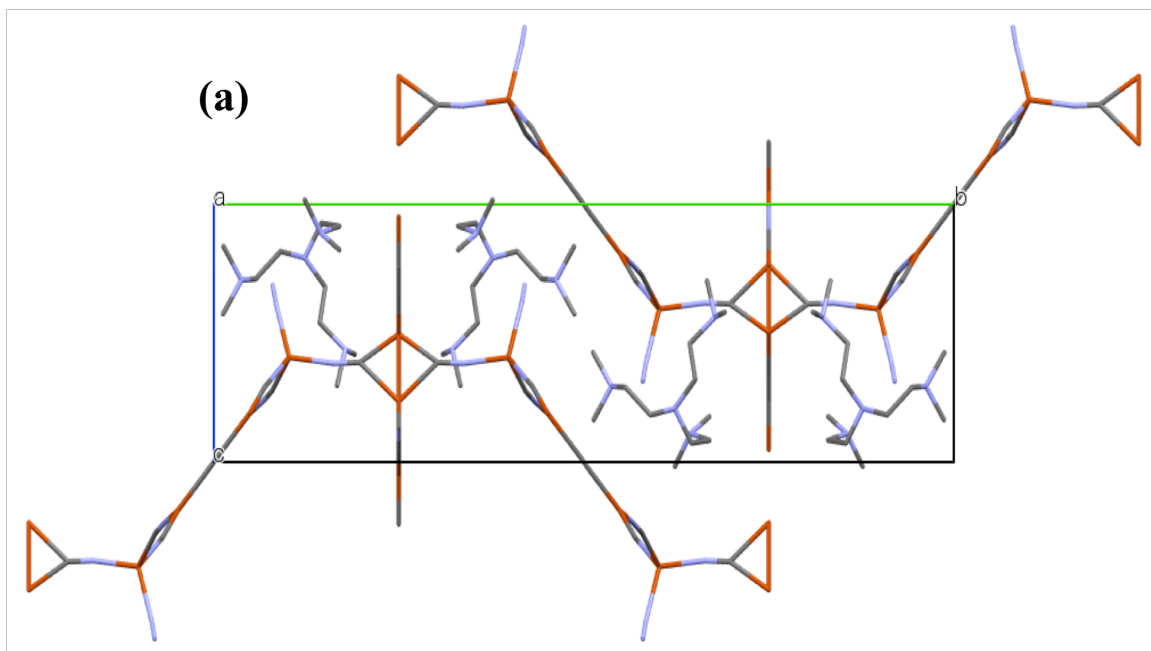


Figure D.4.4. Packing diagram of $[\text{Cu}_3(\text{CN})_5(\text{PMDETA-H}_2)]_n$ viewed along the *a* (a), *b* (b), and *c* (c) axes. Hydrogen atoms have been omitted for clarity.



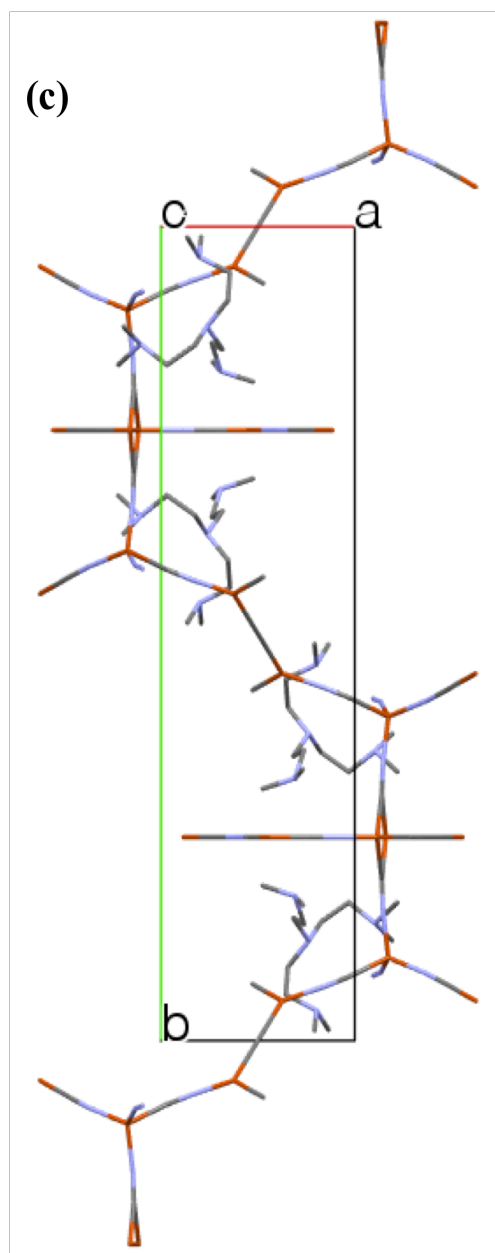


Figure D.4.5. Packing diagram of $[\text{Cu}_7\text{CN}_{12}(\text{Me}_6\text{TREN-H}_3)]_n$ viewed along the *a* (*a*), *b* (*b*), and *c* (*c*) axes. Hydrogen atoms have been omitted for clarity.